THE JOURNAL
OF
CHEMICAL PHYSICS

VOLUME 32, NUMBER 3 MARCH 1960

Analysis of the Solid-State Spectra of Trivalent Neodymium and Erbium

B. G. WYBOURNE

Physics Department, University of Canterbury, Christchurch, New Zealand

(Received September 8, 1959)

A term analysis of the solid-state spectra of trivalent neodymium and erbium has been made and this has allowed terms to be assigned to most of the observed levels of these ions. The complete spin-orbit matrices, with the addition of the electrostatic interaction energies, corresponding to the f^3 and f^{11} configurations have been diagonalized to calculate the energy level schemes for the neodymium and erbium ions, respectively. The appropriate parameters were calculated by a least-squares method.

INTRODUCTION

THE absorption spectra of neodymium[1–3] and erbium[4–6] salts have recently been studied in detail at low temperatures. Zeeman measurements and line counts have given the tentative assignment of J values to many line groups. However, the unequivocal assignment of LSJ numbers has been possible for only a few line groups. Satten[1] has analyzed the spectrum of $Nd(BrO_3)_3 \cdot 9H_2O$ using Russell-Saunders coupling with some success; however, the neglect of intermediate coupling is serious and can lead to incorrect assignments. Elliott, Judd, and Runciman[7] have shown how the spin-orbit interactions, with intermediate coupling, together with the electrostatic interactions of f^n configurations may be calculated using the methods of Racah.[8] The electrostatic interactions for the f^3 configuration have been calculated by Racah.[9] Judd and Loudon[10] have recently published the complete spin-orbit matrices for f^3. The electrostatic interactions will be unchanged for the f^{11} configuration, while the elements of the f^3 spin-orbit matrices require only a change in sign for f^{11}. With these calculations completed it is now possible to calculate, with the inclusion of intermediate coupling effects, the energy level schemes of the $4f^3$ and $4f^{11}$ configurations which correspond to the trivalent neodymium and erbium ions, respectively.

ENERGY LEVEL CALCULATION

For the purpose of this paper the electrostatic interaction energies were expressed in terms of the parameters E^1, E^2, and E^3, being the linear combinations of the Slater radial integrals defined by Racah[8] and the spin-orbit interaction in terms of the spin-orbit coupling constant ξ. The values of these parameters were obtained by a least-squares method as outlined previously.[11]

The parameters used to calculate the energy levels of the Nd^{3+} and Er^{3+} ions are given in Table I. The correspondence between the calculated energy level schemes and the experimentally observed levels was close enough to allow a clear assignment of LSJ terms to most of the known levels of the Nd^{3+} and Er^{3+} ions. These two ions will be discussed separately.

NEODYMIUM

The calculated energy levels are listed in Table II together with the positions of the principal line groups found by Dieke and Heroux for the $(Nd+La)Cl_3 \cdot 7H_2O$ salt and the components of the ^4I multiplet found by Carlson and Dieke.[12] A graphical comparison of the calculated energy level scheme with the experimentally known levels is given in Fig. 1. The letters labeling

[1] R. A. Satten, J. Chem. Phys. **21**, 637 (1952).
[2] G. H. Dieke and L. Heroux, U. S. Atomic Energy Comm. Report NYO-3977 (1955).
[3] G. H. Dieke and L. Heroux, Phys. Rev. **103**, 1227 (1956).
[4] H. Severin, Ann. Physik (6) **1**, 41 (1947).
[5] H. Severin, Z. Physik **125**, 445 (1948).
[6] H. G. Kahle, Z. Physik **145**, 361 (1956).
[7] Elliott, Judd, and Runciman, Proc. Roy. Soc. (London) **A240**, 509 (1957).
[8] G. Racah, Phys. Rev. **76**, 1352 (1949).
[9] G. Racah, Phys. Rev. **62**, 438 (1942).
[10] B. R. Judd and R. Loudon, Proc. Roy. Soc. (London) **A251**, 127 (1959).
[11] W. A. Runciman and B. G. Wybourne, J. Chem. Phys. **29**, 1149 (1959).
[12] E. Carlson and G. H. Dieke, J. Chem. Phys. **29**, 229 (1958).

Copyright © 1960 by the American Institute of Physics

TABLE I. Parameters in units of cm^{-1} derived by the least-squares method.

	E^1	E^2	E^3	ξ
Nd^{3+}	4 988	24.51	493.9	906
Er^{3+}	6 683	31.19	642.7	2471

the line groups are as given by Dieke and Heroux.[3] It is convenient to discuss the analysis under the separate groups.

^4I Components

The predicted positions of the $^4I_{11/2}$ and $^4I_{13/2}$ levels agree closely with the levels found by Dieke and Carlson[12] and the $^4I_{15/2}$ level is predicted to exist at $\sim$6000 cm^{-1}.

Groups *R*, *B*, and *C*

These groups are clearly due to the $^4F_{3/2}$ and $^4F_{9/2}$ and $^2H_{11/2}$ levels, respectively. These assignments are supported by Judd's and Wong's[13] analysis of neodymium double nitrate, Zeeman splittings, and line counts.

TABLE II. Energy levels for Nd^{3+}.

Term	Calculated Energy cm^{-1}	Spectral Group	Experimental Energy cm^{-1}
$^4I_{9/2}$	0		0
$^4I_{11/2}$	1 928		2 028
$^4I_{13/2}$	3 976		3 990
$^4I_{15/2}$	6 099		
$^4F_{3/2}$	11 524	R	11 525
$^4F_{5/2}$	12 607	*S*	12 572
$^2H_{9/2}$	12 612		
$^4S_{3/2}$	13 454	*A*	13 553
$^4F_{7/2}$	13 611		
$^4F_{9/2}$	14 903	*B*	14 807
$^2H_{11/2}$	15 985	*C*	15 997
$^2G_{7/2}$	17 354	*D*	17 321
$^4G_{5/2}$	17 356		
$^2K_{13/2}$	18 978		
$^4G_{7/2}$	19 320	*E*	19 151
$^4G_{9/2}$	19 720	*F*	19 564
$^2K_{15/2}$	21 027		
$^2D_{3/2}$	21 247	*G–H*	
$^2G_{9/2}$	21 255		
$^4G_{11/2}$	21 826		
$^2P_{1/2}$	23 147	I_1	23 338
$^2D_{5/2}$	23 880	I_2, I_3	23 874
$^2P_{3/2}$	26 348	*K*	26 234
$^4D_{3/2}$	28 641	*L*	28 179
$^2I_{11/2}$	28 694		
$^4D_{5/2}$	28 836		
$^4D_{1/2}$	29 276		
$^2L_{15/2}$	29 413		
$^2I_{13/2}$	30 070		
$^2L_{17/2}$	30 932		
$^4D_{7/2}$	31 004		
$^2H_{9/2}$	32 729		
$^2D_{3/2}$	33 771		
$^2H_{11/2}$	34 119		
$^2D_{5/2}$	34 970		
$^2F_{5/2}$	39 665		
$^2F_{7/2}$	41 114		
$^2G_{9/2}$	48 153		
$^2G_{7/2}$	49 066		
$^2F_{7/2}$	68 693		
$^2F_{5/2}$	69 874		

Group *S*

This is a composite group of the $^4F_{5/2}$ and $^2H_{9/2}$ states. A total of 8 levels is predicted and this agrees with Dieke's and Heroux's[2] $Nd(BrO_3)_3 \cdot 9H_2O$ data.

Group *A*

This group is a mixture of the $^4F_{7/2}$ and $^4S_{3/2}$ states. Six levels are predicted and six observed. Judd and Wong[13] have shown that the A_5 and A_6 levels, which are the close pair in this group, belong to the $^4S_{3/2}$ state and the remaining levels to the $^4F_{7/2}$ state.

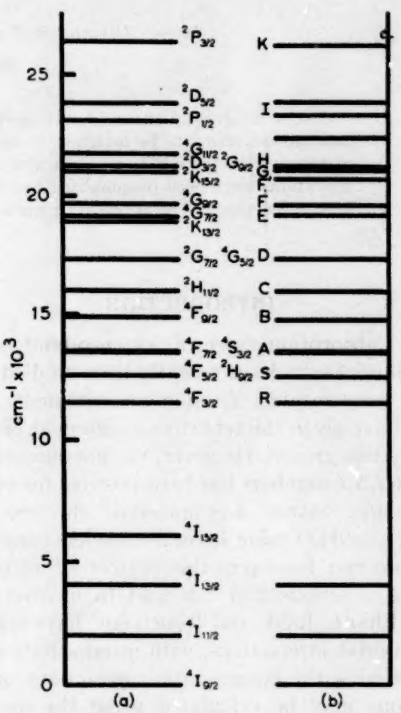

FIG. 1. (a) Calculated energy levels of Nd^{3+}; (b) Experimental energy levels of Nd^{3+}.

Group *D*

The *D* group appears to be a close mixture of the $^4G_{5/2}$ and $^2G_{7/2}$ states. Seven levels are predicted and observed. Judd and Wong[13] suggest $^4G_{7/2}$, however, with the inclusion of intermediate coupling the $^4G_{7/2}$ level occurs $\sim$1900 cm^{-1} above the *D* group. Therefore this assignment now appears unreasonable and $^2G_{7/2}$ is to be preferred.

[13] B. R. Judd and E. Wong, J. Chem. Phys. 28, 1097 (1958).

Groups *E* and *F*

The states $^2K_{13/2}$, $^4G_{7/2}$, $^4G_{9/2}$ are predicted to occur in the vicinity of these two line groups. Dieke and Heroux[2] give 4 sharp lines for *E* suggesting $J=\frac{7}{2}$ and 5 sharp lines for *F* suggesting $J=\frac{9}{2}$. This agrees with the predicted energy level scheme and it seems reasonable to assign $^4G_{7/2}$ to group *E* and $^4G_{9/2}$ to group *F*. Additional weak diffuse levels are reported in this region and are probably due to the $^2K_{13/2}$ state.

Group *F'*

Dieke and Heroux[2] report two strong lines in the neodymium ethylsulphate spectrum suggesting $J=\frac{3}{2}$. The nearest calculated line group with $J=\frac{3}{2}$ is the $^2D_{3/2}$ state. Judd and Loudon[10] have also made this assignment. Until Zeeman data are available for the components of the *F'* group this assignment must be regarded as tentative.

Groups *G* and *H*

The interpretation of these groups of lines is complicated by the occurrence of 4 states in a region of $\sim$1000 cm^{-1}. Crystal field mixing will be by no means negligible. The calculated energy level scheme does not allow a clear assignment to be made to the observed lines though it would appear that the upper levels could be attributed to the $^4G_{11/2}$ state and the lower levels to a mixture of the $^2G_{9/2}$ and $^2K_{15/2}$ states. The final interpretation must await further experimental data.

TABLE III. Energy levels for Er^{3+}.

Term	Calculated energy cm^{-1}	Spectral group	Experimental energy cm^{-1}
$^4I_{15/2}$	0		0
$^4I_{13/2}$	6 775		
$^4I_{11/2}$	10 415	*A*	10 191
$^4F_{9/2}$	12 496	*B*	12 511
$^4I_{9/2}$	15 449	*D*	15 290
$^4S_{3/2}$	18 525	*E*	18 475
$^2H_{11/2}$	19 407	*F*	19 182
$^4F_{7/2}$	20 717	*G*	20 513
$^4F_{5/2}$	22 321	*H*	22 228
$^4F_{3/2}$	22 701	*J*	22 587
$^2G_{9/2}$	24 893	*K*	24 622
$^4G_{11/2}$	26 889		
$^2K_{15/2}$	27 408		
$^4G_{9/2}$	27 940		
$^4G_{7/2}$	28 357		
$^2D_{3/2}$	32 061		
$^2K_{13/2}$	32 857		
$^2P_{1/2}$	33 623		
$^4G_{5/2}$	33 974		
$^2G_{7/2}$	34 656		
$^2D_{5/2}$	34 910		
$^2H_{9/2}$	37 317		
$^4D_{5/2}$	39 151		
$^4D_{7/2}$	39 679		
$^2I_{11/2}$	40 426		
$^2L_{17/2}$	40 737		
$^4D_{3/2}$	42 832		
$^2I_{13/2}$	43 341		
$^2P_{3/2}$	43 626		

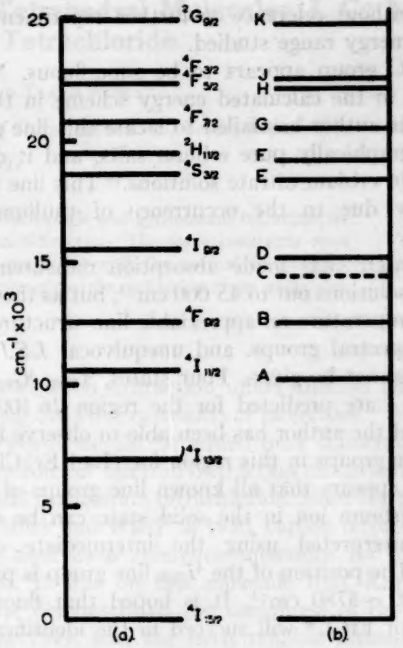

FIG. 2. (a) Calculated energy levels for Er^{3+}; (b) Experimental energy levels for Er^{3+}.

Groups *I* and *K*

The calculated energy level scheme shows clearly that the I_1 level is attributable to the $^2P_{1/2}$ state and the two upper levels I_2 and I_3 are components of the $^2D_{5/2}$ state. The two levels of the *K* group belong to the $^2P_{3/2}$ state. These assignments are supported by the Zeeman data of Dieke and Heroux[3] and agree with those given by Judd and Loudon.[10]

Other Levels

The positions of all the levels corresponding to the Nd^{3+} ion have been predicted. Many of these should be observable in the ultraviolet and their measurement would aid in the further analysis of this spectrum.

ERBIUM

The analysis of the Er^{3+} spectrum is considerably simpler than that of the Nd^{3+}. The individual line groups are well separated from each other and the complexity of overlapping states does not arise. This is primarily due to the large spin-orbit coupling constant and the pronounced effects of intermediate coupling in separating the individual states. Levels that coincide in the Russell-Saunders approximation are found to be separated by up to 3000 cm^{-1} when intermediate coupling is included.

The calculated energy level scheme and the line groups observed by Severin[4,5] are listed in Table III. The calculated and experimental levels are compared graphically in Fig. 2. As will be seen from the graph all the line groups except *C* can be readily assigned *LSJ*

terms without reference to further experimental data in the energy range studied.

The C group appears to be superfluous. No level appears in the calculated energy scheme in this position. The author has failed to locate this line group in spectrographically pure erbium salts, and it does not appear in erbium nitrate solutions.[14] This line group is probably due to the occurrence of thulium as an impurity.

Jørgensen[15] has made absorption measurements of erbium solutions out to 45 000 cm^{-1}, but as these are at room temperature no appreciable line structure occurs in the spectral groups, and unequivocal LSJ assignments cannot be given. Four states, $^4G_{7/2}$, $^4G_{9/2}$, $^2K_{15/2}$, and $^4G_{11/2}$ are predicted for the region 26 400–27 500 cm^{-1} and the author has been able to observe four distinct line groups in this region for $(La+Er)Cl_3 \cdot 7H_2O$. Thus it appears that all known line groups of the trivalent erbium ion in the solid state can be satisfactorily interpreted using the intermediate coupling model. The position of the $^4I_{13/2}$ line group is predicted to be at $\sim$5780 cm^{-1}. It is hoped that fluorescence studies of $ErCl_3$[16] will succeed in the identification of this state.

[14] J. Hoogschagen and C. J. Gorter, Physica **14**, 197 (1948).
[15] C. K. Jørgensen, Acta. Chem. Scand. **11**, 981 (1957).
[16] G. H. Dieke (private communication).

CONCLUSION

By the use of an intermediate coupling model most of the known spectral line groups of the neodymium and erbium ions can be satisfactorily assigned LSJ terms. Further experimental investigations of the spectra of neodymium salts must be made before the analysis of their spectra can be profitably extended. In particular, there is a need for more extensive Zeeman data for line groups, E, F, G, H, and F', in salts of high symmetry. There are no available Zeeman data on erbium salts and such data would be useful for an independent check on the LSJ assignments that have been made in this paper. The complete determination of the fluorescence spectra of the anhydrous trichlorides should allow the positions of all the components of the ground multiplets to be found.

ACKNOWLEDGMENTS

The author wishes to express his thanks to Mr. W. A. Runciman for suggesting the problem and for numerous helpful discussions; and to the staff at Sydney University who diagonalized the matrices using the Silliac computer.

The author acknowledges the award of a New Zealand University Research Fund Fellowship.

Mean Square Amplitudes and Force Constants of Tetrahedral Molecules. I. Carbon Tetrachloride and Germanium Tetrachloride

YONEZO MORINO, YASUSHI NAKAMURA, AND TAKAO IIJIMA

Department of Chemistry, Faculty of Science, The University of Tokyo, Bunkyo-ku, Tokyo, Japan

(Received September 11, 1959)

The atomic distances and mean square amplitudes of carbon tetrachloride and germanium tetrachloride were measured by the sector-microphotometer method of electron diffraction. The force constants were calculated by use of the mean square amplitudes thus obtained, combined with the normal frequencies. The results indicate that a force field of the Urey-Bradley type is approximately realized in these molecules.

INTRODUCTION

THE forces acting between atoms in a molecule hav usually been obtained by the analysis of vibra tional spectra. The number of frequencies observed is, in general, not enough to determine all the force constants in general quadratic form of potential energy: for example, even for such a simple molecule as carbon tetrachloride, which has T_d symmetry, three force constants are necessary for the F_2 type vibrations, but we have only two frequencies of this class. Thus, in molecular spectroscopy, some special form is tentatively assumed for the force field to reduce the number of unknown parameters. The simplest one is the so-called valence force system, in which only the forces along the valence bonds and those against the deformation of valence angles are taken into account. This assumption is, however, too simple to have actual significance. The first improvement to be made in this assumption is to add force constants which represent the interaction between nonbonded atoms. The result is a force field of the Urey-Bradley type[1] which has been applied to many molecules and proven to be successful by Mizushima, Shimanouchi, and others.[2]

In this situation any phenomenon can be used to fill up the deficiency of the data mentioned above, if it has a close connection with the force field of the molecule. In fact, isotopic shifts of vibrational spectra,[3] Coriolis coupling constants in rotation-vibration spectra,[4] and centrifugal distortion constants in microwave spectra,[5,6] etc. have been used heretofore. It is the purpose of this article to show that the mean square amplitude obtained by electron diffraction offers another basis for determining the force constants of molecules.

A few words should be added here concerning the previous studies of electron diffraction on carbon tetrachloride and germanium tetrachloride. Since the pioneer work by Mark and Wierl[7] in 1930, carbon tetrachloride has been used as a reference substance for electron diffraction. It was on this molecule that Karle and Karle[8] first demonstrated the usefulness of the sector method in 1949, and the most reliable measurement at present by the sector-microphotometer method must be that by Bartell, Brockway, and Schwendeman[9] on the same substance. Morino and Kuchitsu[10] used the substance for a test of their new sector apparatus. The reason why the same substance was again investigated was to get the most reliable values of the mean square amplitudes, by focusing attention upon their determination.

The molecular structure of germanium tetrachloride was studied by Pauling and Brockway[11] in 1935 by the visual method with the result Ge–Cl$=2.08\pm0.02$ A.

EXPERIMENTAL

The diffraction apparatus used is the same as that reported in the previous paper by Morino and Kuchitsu.[10] An r^3 sector was used with the shorter camera length, 11.8 cm, and an r^2 sector with the longer camera length, 27.9 cm. The accelerating voltage was about 45 kv, the fluctuation and the drift of the voltage being automatically regulated within 0.1%. A pure sample of germanium tetrachloride was kindly provided by Mr. H. Oikawa, of the Coal Research Institute of Mitsui Chemical Industrial Company, Ltd. About 10 cc of the sample was consumed in this work. The gaseous sample was kept in a 1-liter glass bulb at a pressure of 30 to 35 mm Hg and was led to the diffraction camera through a fine nozzle. The pressure decrease of the sample holder during exposure, 2 to 4

[1] H. C. Urey and C. A. Bradley, Phys. Rev. **28**, 1969 (1939).
[2] T. Shimanouchi, J. Chem. Phys. **17**, 245, 734, 848 (1949); S. Mizushima and T. Shimanouchi, *ibid.* **17**, 1102 (1949); J. Am. Chem. Soc. **71**, 1320 (1949); I. Nakagawa, J. Chem. Soc. Japan **76**, 813 (1955); **77**, 1030 (1956); T. Miyazawa, *ibid.* **77**, 366 (1956), etc.
[3] Cf. G. Herzberg, *Molecular Spectra and Molecular Structure* (D. Van Nostrand, Princeton New Jersey, 1945).
[4] J. H. Meal and S. R. Polo, J. Chem. Phys. **24**, 1119, 1126 (1956).
[5] D. Kivelson and E. B. Wilson, Jr., J. Chem. Phys. **20**, 1575 (1952); **21**, 1229 (1953); D. Kivelson, *ibid.* **22**, 904 (1954); L. Pierce, *ibid.* **24**, 139 (1956); P. H. Verdier and E. B. Wilson, Jr., *ibid.* **30**, 1372 (1959).
[6] Y. Morino and E. Hirota, Bull. Chem. Soc. Japan **31**, 423 (1958).
[7] H. Mark and R. Wierl, Naturwiss. **18**, 205 (1930).
[8] I. L. Karle and J. Karle, J. Chem. Phys. **17**, 1052 (1949).
[9] Bartell, Brockway, and Schwendeman, J. Chem. Phys. **23**, 1854 (1955).
[10] Y. Morino and K. Kuchitsu, J. Chem. Phys. **28**, 175 (1958).
[11] L. Pauling and L. O. Brockway, J. Am. Chem. Soc. **57**, 2684 (1935).

min., was a few mm Hg. The diffraction pattern was recorded on Fuji Process Plates which were developed with FD-131 developer at 20°C. The wavelength of the primary electron beam was calibrated by a transmission pattern of gold foil.

Microphotometer tracing was carried out either with a Riken B type microphotometer using a photographic recording system or with a Rigaku Denki MP-3 microphotometer using a pen-recording system. They are both equipped with a rotating disk on which the diffraction photograph is mounted and spun rapidly in order to average out irregularities in the photographic plate. Both types of photometers gave results consistent with each other. Six pairs of diffraction photographs including two pairs for small-angle region (q=8–30) were selected from about 40 plates and analyzed by the procedure described below.

In order to avoid difficulties in the density-intensity calibration,[12,13] the plates of optical densities less than 0.5 were used for the analysis. Having been well established by experiment, a linear relation was assumed between the density and intensity in the above region. The molecular intensities were obtained by drawing a smooth background line which was iteratively corrected with the criterion of minimum ghost in the radial distribution curve.

ANALYTICAL PROCEDURE

In order to obtain mean square amplitudes accurately enough to allow a useful determination of the force field, every possible correction should be taken into consideration. The errors involved in the measurement of mean amplitudes were thoroughly criticized by Kuchitsu.[14] He concluded that the largest error had its origin in the finite gas spread at the diffraction center. He found a method for estimating the distribution of gas molecules by the measurement of the deviation of the slope of the background curve from the theoretical one. Another source of uncertainty is the failure of the Born approximation which was first pointed out by Schomaker and Glauber.[15] We can roughly correct it by using Ibers and Hoerni's table.[16] Anharmonicity of intramolecular vibration of atoms and the displacements of atoms perpendicular to the bond direction provide serious difficulties in the determination of equilibrium distances and mean square amplitudes. In this section the procedure of the analysis shall be presented, with an attempt to eliminate as many uncertainties as possible.

1. Molecular Intensity

As was shown by Morino and Hirota,[17] the intensity of the coherent beam diffracted by a tetrahedral molecule is given by

$$sM(s)=\sum_{i,j}\frac{|\,F_i^e(s)\,||\,F_j^e(s)\,|}{I_B}\cos\Delta\eta\,\frac{\exp(-as^2)}{r_e}$$
$$\cdot\{\sin sr_e-(s/r_e)[\langle\Delta z^2\rangle-\tfrac{1}{2}(\langle\Delta x^2\rangle+\langle\Delta y^2\rangle)]\cos sr_e\},\quad(1)$$

where s has the usual meaning of $(4\pi/\lambda)\cdot\sin\theta/2$ and I_B is the sum of coherent and incoherent atomic scattering. $F_i^e(s)$ denotes the atomic structure factor of the ith atom for electron beam,* and $\cos\Delta\eta$ is due to the imaginary part of $F_i^e(s)F_j^e(s)$, that is, to the failure of Born approximation. Here $2a=\langle\Delta z^2\rangle$ is the mean square amplitude parallel to the equilibrium direction of the distance r_e, and $\langle\Delta x^2\rangle$ and $\langle\Delta y^2\rangle$ are the mean square amplitudes of the atomic displacements perpendicular to the equilibrium direction. This formula was derived based on the probability function $P_h(r)$ of the distance r, for which the intramolecular potential is assumed to be harmonic,

$$P_h(r)=(1/4\pi a)^{\frac{1}{2}}[1+\gamma(r-r_e)]\exp[-(r-r_e)^2/4a],\quad(2)$$

where

$$\gamma=(1/r_e)\cdot[(\langle\Delta x^2\rangle+\langle\Delta y^2\rangle)/2\langle\Delta z^2\rangle].$$

Now, considering the fact that $s\langle\Delta z^2\rangle(1-\gamma r_e)/r_e$ is much less than unity in the region $s\leqq 30$, we have a simple form of

$$sM(s)=\sum_{i,j}(|\,F_i^e(s)\,||\,F_j^e(s)\,|/I_B)\cos\Delta\eta$$
$$\cdot\exp(-as^2)(1/r_e)\sin sr_a,\quad(3)$$

where the apparent distance r_a is related to r_e by the relation of

$$r_a=r_e-2a/r_e+2\gamma a,\quad(4)$$

and the background intensity I_B can be given by the equation,[18–20]

$$I_B=\sum_i|\,F_i^e(s)\,|^2+\sum_i S_i(s).\quad(5)$$

2. Anharmonicity of Vibration

The effect of anharmonicity of vibration upon $M(s)$ was discussed by Bartell[21] for the ground state of a diatomic molecule, and was calculated by Reitan for H_2, H_2O, and CO_2 molecules.[22] For an atom in a polyatomic molecule the following expression of the distribution function seems to be adequate:

$$P_a(r)=[1+\beta_1(r-r_e)+\beta_2(r-r_e)^2+\beta_3(r-r_e)^3]P_h(r),\quad(6)$$

[12] J. Karle and I. L. Karle, J. Chem. Phys. **18**, 957 (1950).
[13] L. S. Bartell and L. O. Brockway, J. Appl. Phys. **24**, 656 (1953).
[14] K. Kuchitsu, Bull. Chem. Soc. Japan **32**, 748 (1959).
[15] V. Schomaker and R. Glauber, Nature **170**, 290 (1952).
[16] J. A. Ibers and J. A. Hoerni, Acta Cryst. **7**, 405 (1954).
[17] Y. Morino and E. Hirota, J. Chem. Phys. **23**, 737 (1955).

* $F_i^e(s)=Z_i-f_i(s)$ for the first Born approximation.
[18] L. H. Thomas and K. Umeda, J. Chem. Phys. **26**, 293 (1957).
[19] H. Viervoll and O. Ögrim, Acta Cryst. **2**, 277 (1949).
[20] L. Bewilogua, Physik Z. **32**, 740 (1931).
[21] L. S. Bartell, J. Chem. Phys. **23**, 1219 (1955).
[22] A. Reitan, Acta Chem. Scand. **12**, 131, 785 (1958).

where $P_h(r)$ designates the distribution function of a harmonic case given by Eq. (2). A manipulation similar to that carried out in the case of a harmonic potential provides an expression for the molecular intensity corresponding to Eq. (3),

$$sM(s)=\sum_{i,j}(|F_i^0(s)||F_j^0(s)|/I_B)\cos\Delta\eta \cdot\exp(-a's^2)(1/r_e)\sin s(r_a-\kappa s^2). \quad (7)$$

where

$$r_a=r_e-2a'/r_e+2(\beta_1+\gamma)a'+12(\beta_3+\gamma\beta_2)a'^2, \quad (8)$$

$$a'=a+4a^2(\beta_2+\gamma\beta_1), \quad (9)$$

and

$$\kappa=8a'^3(\beta_2+\gamma\beta_2). \quad (10)$$

The information obtained by the analysis of the intensity curve is r_a and a', and, if a precise measurement is performed, one more parameter κ shall be obtained. In order to get r_e, the values of β_1, β_2, β_3, and γ are required. Although γ can be calculated from spectroscopic data,[17] other parameters cannot be estimated without precise expressions of them. Similarly, the correction term of the mean square amplitude, $4(\beta_2+\gamma\beta_1)a^2$, is left out of the measurement.

In this connection it may be mentioned that

$$r_g=\int_0^\infty rP_a(r)dr \Big/ \int_0^\infty P_a(r)dr,$$

$$=r_e+2(\beta_1+\gamma)a'+12(\beta_3+\gamma\beta_2)a'^2. \quad (11)$$

Therefore, comparing it with Eq. (8), we have

$$r_g=r_a+2a'/r_e, \quad (12)$$

that is, r_g,† the mean of the distance with regard to the anharmonic probability function, is given in a straightforward way by r_a and a'; it is independent of the β's which are necessary for calculating r_e.

It would be worthwhile to consider here the precise meaning of the mean square amplitude. In particular, for the anharmonic case we must consider the effect of anharmonicity on the mean square amplitude. Since $2a=\langle\Delta z^2\rangle$ is the mean of the square of the deviation of the atomic distance from the equilibrium position, averaged with regard to the distribution function for a harmonic potential function, we find

$$2a=\langle\Delta z^2\rangle=\int_0^\infty(r-r_e)^2P_h(r)dr \Big/ \int_0^\infty P_h(r)dr.‡ \quad (13)$$

However, as was pointed out by Reitan[22] and discussed by Kuchitsu,[14] there are a number of slightly different definitions of the mean square amplitude, for example,

$$l_e^2=\int_0^\infty(r-r_e)^2P_a(r)dr \Big/ \int_0^\infty P_a(r)dr, \quad (14)$$

and

$$l_g^2=\int_0^\infty(r-r_g)^2P_a(r)dr \Big/ \int_0^\infty P_a(r)dr, \quad (15)$$

where l_e^2 is the mean of the deviation from the equilibrium position of the atom pair, l_g^2 that from the distance corresponding to the center of gravity of the distribution function, both being averaged with respect to the distribution function for the actual anharmonic potential function. The definition of l_g^2 is quite analogous with $\langle\Delta z^2\rangle$, the difference being only in the respect that the mean is made with regard to the anharmonic, rather than the harmonic probability function. If we assume Eq. (6) for $P_a(r)$, they are easily calculated as follows:

$$l_e^2=2a+8a^2(\beta_2+\gamma\beta_1), \quad (16)$$

and

$$l_g^2=l_e^2-4a^2(\beta_1+\gamma)^2. \quad (17)$$

Comparison of Eq. (16) with Eq. (9) reveals that

$$l_e^2=2a'. \quad (18)$$

Thus it is l_e that is obtained by the analysis of the intensity curve, because, as will be described in the following section, a' is treated as a parameter to be determined by least squares calculation. This is in sharp contrast to the fact that for the equilibrium distance, r_g is directly obtained by the measurement, whereas r_e is too difficult to be calculated.

3. Method of Least Squares

The least squares method has the advantage that it is not influenced by the termination effect which is encountered in the radial distribution method. At the same time it makes it possible to get the most reasonable values of the parameters with their standard errors. The procedure applied here is essentially the same as that reported by Bastiansen, Hedberg, and Hedberg.[23] The observed values of molecular intensity $qM(q)$ at each q value,§ denoted by F_0, are fitted by F_c, the theoretically calculated values of $qM(q)$, so as to reduce the square sum of residuals as much as possible, by changing the molecular parameters which specify the F_c.

For the analysis of the diffraction data of $GeCl_4$ and CCl_4, the following formula corresponding to Eq. (7) is assumed for F_c:

$$F_c=i\{C_1(1/r_{a1})\exp(-a_1's^2)\sin s(r_{a1}-\kappa_1s^2) +C_2(1/r_{a2})\exp(-a_2's^2)\sin s(r_{a2}-\kappa_2s^2)\}, \quad (19)$$

in which the subscript 1 designates the Ge–Cl or C–Cl pair and 2 the Cl–Cl pair. The r_a's in the denominators

† r_g is the same as $r_g(0)$ defined by Bartell (reference 21).

‡ Exactly speaking, $\langle\Delta z^2\rangle$ is the mean of $(z-z_e)^2$, but it coincides with $\langle(r-r_e)^2\rangle$ in the first approximation.

[22] O. Bastiansen, K. Hedberg, and L. Hedberg, J. Chem. Phys. 27, 1311 (1957).

§ The analysis in this article was carried out by use of the q scale ($q=10s/\pi$) though the description of the article is presented by the term s.

TABLE I. Results of the least squares analysis of the molecular intensity curves of $GeCl_4$ at 23°C.

	With five unknown parameters	With seven unknown parameters
i	$0.97_4 \pm 0.02_3$ A	$0.97_4 \pm 0.02_3$ A
r_{a1}(Ge—Cl)	$2.112_1 \pm 0.001_1$	$2.110_9 \pm 0.001_6$
r_{a2}(Cl—Cl)	$3.440_9 \pm 0.004_0$	$3.443_2 \pm 0.006_5$
$(2a_1')^{\frac{1}{2}}$(Ge—Cl)	$0.048_6 \pm 0.002_0$	$0.048_6 \pm 0.002_0$
$(2a_2')^{\frac{1}{2}}$(Cl—Cl)	$0.099_6 \pm 0.003_3$	$0.099_6 \pm 0.003_3$
κ_1(Ge—Cl)$\times 10^5$	...	-0.53 ± 0.50
κ_2(Cl—Cl)$\times 10^5$	...	1.86 ± 3.1

in Eq. (7) were safely approximated by r_a's. The coefficients

$$C_1(s) = \frac{8 \mid F_{Ge}^e(s) \mid\mid F_{Cl}^e(s) \mid}{\sum_i \mid F_i^e(s) \mid^2 + \sum_i S_i(S)} \cos\Delta\eta, \quad (20)$$

and

$$C_2(s) = \frac{12 \mid F_{Cl}^e(s) \mid^2}{\sum_i \mid F_i^e(s) \mid^2 + \sum_i S_i(s)}, \quad (21)$$

are numerically calculated at each q by use of a number of tables[16,18,19,20] and inserted into Eq. (19). The parameters to be determined by least squares are r_a, a', and κ for each atom pair and the index of resolution i. The preliminary values of the parameters for the starting model of least squares are given by the analysis of the radial distribution curve. The result of the radial distribution curve was so close to the final one that only one trial was necessary to get well-converged values. As for the weight to be multiplied to the difference of $F_0 - F_c$ at every q in the calculation of least squares, we have no exact knowledge except that it decreases at both ends of large and small q values. An approximate form was tentatively assumed for each case so as to realize the damping feature of the observed curves. All the numerical computations were carried out by the use of the parametron digital computer PC-1, at the Department of Physics.

4. Radial Distribution Function

The modified radial distribution function which offers the starting model is provided by the Fourier transformation of the ideal molecular intensity with an artificial damping factor $\exp(-bs^2)$, that is,

$$f(r) = \int_0^\infty sM^i(s) \exp(-bs^2) \cdot \sin sr ds. \quad (22)$$

The ideal molecular intensity $sM^i(s)$ is that of a fictitious model which has constant scattering factors instead of the true atomic structural factors depending on s,

$$sM^i(s) = \sum_{i,j} \frac{Z_i Z_j}{\sum_i Z_i(Z_i+1)} \cdot \frac{\sin sr_a}{r_a} \exp[-(B+a')s^2]. \quad (23)$$

This is the very function that was introduced by Bartell, Brockway, and Schwendeman,[9] except for a term $\exp(-Bs^2)$ which expresses the phase shift due to the failure of Born approximation. The factor B can be properly assumed[14] by the condition that the function $\exp(-Bs^2)$ expresses the term $\cos\Delta\eta$ with minimum deviation in the required range of s,

$$\int_0^{s\,\max} [\cos\Delta\eta(s) - \exp(-Bs^2)] \exp[-(a'+b)s^2] ds = 0, \quad (24)$$

where b is an artificial temperature factor for eliminating the termination effect. The value of B was estimated to be 0.464×10^{-3} for the Ge–Cl pair, by the value of $\cos\Delta\eta$ obtained from the table of Ibers and Hoerni and corrected for the accelerating voltage 45 kv by the use of their transformation formula.

The correction of $sM(s)$ to $sM^i(s)$ was made by the procedure proposed by Brockway, Bartell, and Schwendeman,[9] that is, the difference between $M^i(s)$ and $M(s)$ is calculated for an approximate model, the difference $\Delta M(s) = M^i(s) - M(s)$ is added to the observed molecular intensity, and the structural parameters of the model are successively corrected with the result of the analysis of the radial distribution curve which is obtained by the Fourier transformation of the $sM^{obs}(s) + s\Delta M(s)$.

RESULTS AND DISCUSSION

$GeCl_4$

Four curves of the observed molecular intensity were separately analyzed by the method described in the preceding. They gave results sufficiently consistent with one another, the average of which are listed in Table I with the standard deviations. The weight function $w(q)$ in the least squares was tentatively chosen as

$$w(q) = N_1 q \exp(-\alpha_1 q^2) \quad \text{for} \quad 8 \leqq q \leqq 25,$$
$$w(q) = 1 \quad \text{for} \quad 25 \leqq q \leqq 43,$$
$$w(q) = N_2 q \exp(-\alpha_2 q^2) \quad \text{for} \quad 43 \leqq q \leqq 97, \quad (25)$$

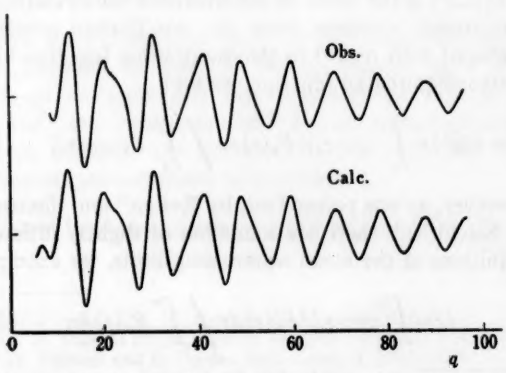

FIG. 1. Calculated and observed molecular intensity curves of $GeCl_4$.

where $\alpha_1=8.00\times10^{-4}$ and $\alpha_2=2.70\times10^{-4}$. Normalization coefficients N_1 and N_2 are taken so that the weight function $w(q)$ is continuous at $q=25$ and 43. The least squares treatment was applied to the molecular intensity curves, first with five unknown parameters, i, a_1', a_2', r_{a1}, and r_{a2}, neglecting the parameters κ_1 and κ_2, and then with seven parameters including κ_1 and κ_2. Equation (19) shows that the anharmonicity of vibration produces a phase shift $-\kappa s^2$, in the molecular intensity curve, so that it seems better to carry out the calculation with seven parameters. It was revealed, however, that the values of the mean amplitudes obtained with seven parameters were almost the same as those obtained with five parameters and the distances were only slightly affected within the magnitude of the standard error. In addition, as the standard error of the phase shift parameter κ is of comparable order with the value of κ itself, the values of κ obtained

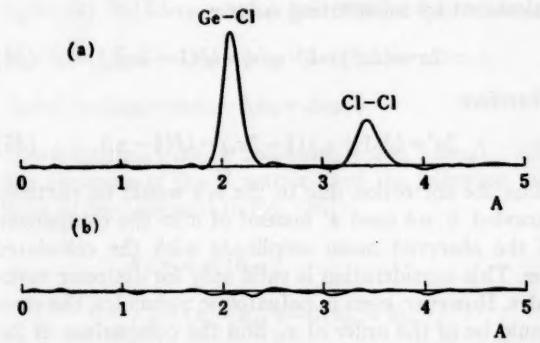

FIG. 2. Radial distribution curve of $GeCl_4$. Curve B indicates the difference between the experimental RD (curve a) and synthetic RD for the final model.

are meaningless. Thus there is no substantial difference whether the analysis is performed with five or with seven parameters.

The calculated molecular intensity curve is compared with the observed one in Fig. 1, and the experimental radial distribution curve $f(r)$ is shown in Fig. 2. It is well fitted by Gaussian peaks computed with the molecular parameters determined by the least squares. The difference between the experimental and the calculated $f(r)$ is plotted in Fig. 2. The maximum difference is about 3% of the height of the Ge–Cl peak; it is comparable to the level of the ghost signals.

The observed background line is compared with the theoretical one in Fig. 3. The theoretical background intensity for an r^3 sector was calculated by the equation

$$I(q)=(1/q)(1-\delta(q))\{\sum_i F_i^2(q)^2+\sum_i S_i(q)\}, \quad (26)$$

where

$$\delta(q)=(3/3200)\lambda^2q^2,$$

a constant coefficient beimg omitted. Equation (26) was derived by taking into account the intensity of

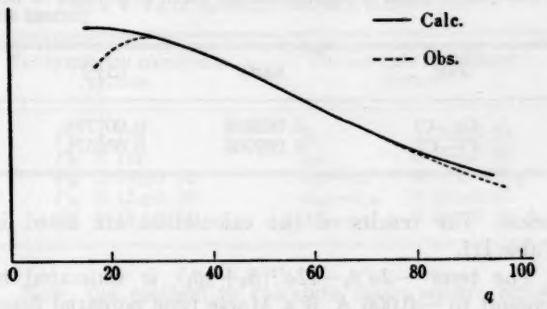

FIG. 3. Background line of $GeCl_4$. The deviation beyond $q=70$ is due to the finite spread of gas molecules at the nozzle.

scattered electrons which hit a unit area of a plate placed at right angles to the primary beam.

The distribution of gas molecules around the nozzle was estimated by the discrepancy of the slope of the observed background line from the theoretical one, in the region of q larger than 70 as shown in Fig. 3, and the corresponding corrections of the root mean square amplitudes were found to be −0.0013 A for the Ge–Cl and −0.0016 A for the Cl–Cl pair, respectively.

In Table II the final results of the analysis are tabulated, in which the distance parameters r_g were computed by Eq. (12) and the mean amplitudes were corrected for the finite sample size. The standard errors were determined by considering the standard deviations of the least squares as well as other possible systematic errors. The effect of uncertainty in the values of $\cos\Delta\eta$ for the Ge–Cl pair was assumed to be about 2%.

1. Equilibrium Distance

In order to obtain the equilibrium distance r_e, we have to have the correction terms in the expression of

$$r_e=r_a+2a'/r_e-2\gamma a'-2\beta_1a'-12a'^2(\beta_3+\gamma\beta_2). \quad (8')$$

As for γ, the perpendicular amplitudes $\langle\Delta x^2\rangle$ and $\langle\Delta y^2\rangle$ must be evaluated, in addition to the parallel amplitude $\langle\Delta z^2\rangle$. They are easily obtained by the relation[17]

$$\langle(x_i-x_j)^2\rangle=[\mathbf{D}_{ij}{}^x(\mathbf{M}^{-1}\mathbf{B}')]'\mathbf{U}'(\mathfrak{L}^{-1})'\langle\mathbf{Q}^2\rangle\mathfrak{L}^{-1}\mathbf{U}\cdot[\mathbf{D}_{ij}{}^x(\mathbf{M}^{-1}\mathbf{B}')], \quad (27)$$

The $\mathfrak{L}$ matrix elements were calculated with the force constants obtained by the consideration described

TABLE II. Final result for the molecular parameters of $GeCl_4$ at 23°C.

	Ge—Cl	Cl—Cl
r_g	2.113±0.003 A	3.444±0.006 A
l_e	0.047_4±0.003	0.097_9±0.003

TABLE III. Parallel and perpendicular mean amplitudes of $GeCl_4$ in A computed by the use of the force constants obtained by the present study (at 296°K).

Pair	$\langle\Delta z^2\rangle$	$\langle\Delta y^2\rangle$	$\langle\Delta x^2\rangle$	r	$2a/r$	$2\gamma a$
Ge—Cl	0.002028	0.007798	0.009790	2.113	0.00096	0.00416
Cl—Cl	0.009708	0.003571	0.010711	3.444	0.00282	0.00207

below. The results of the calculation are listed in Table III.

The term $-2a'\beta_1-12a'^2(\beta_3+\gamma\beta_2)$ is estimated to amount to -0.006 A, if a Morse type potential function is assumed

$$V(r)=D\{1-\exp[-\mathfrak{a}(r-r_e)]\}^2, \tag{28}$$

with $\mathfrak{a}=2.0$ A^{-1}. The correction is comparable to the term of $2\gamma a'$, or rather larger than that. For the present as the exact values of the anharmonicity parameters are not available, it is impossible to get the r_e with sufficient accuracy.

2. Mean Square Amplitude

As mentioned in the preceding section, the mean square amplitude obtained by the experiment is a', whereas the quantity obtained by the theoretical calculation is $2a=\langle\Delta z^2\rangle$, that for the harmonic potential. In order to obtain the mean square amplitude which may be compared with the experimental result, we must make a correction for the anharmonicity of the potential function, which is expressed by the term $4a^2(\beta_2+\gamma\beta_1)$ in Eq. (9). To make the argument simple, a case of diatomic molecules is taken as an example. In this case $\gamma=0$, and β_2 has the following relation to the Morse function parameters:

$$\beta_2=\mathfrak{a}^2/2, \tag{29}$$

$$\mathfrak{a}=2\pi\nu_e(\mu/2D_e)^{\frac{1}{2}}, \tag{30}$$

and

$$x_e=h\nu_e/4D_e. \tag{31}$$

For the calculation of the correction term, $4a\beta_2$, an approximate relation,

$$2a=h/8\pi^2\mu\nu_e, \tag{32}$$

which holds exactly only in the ground state, can be safely used, and the result is

$$l_e^2=2a'=2a(1+4a\beta_2)=2a(1+x_e). \tag{33}$$

Therefore, the correction is of the order of x_e. In fact, Reitan[22] calculated the effect for a number of diatomic molecules and arrived at a similar conclusion that root mean square amplitude must be corrected by an increase of about 1%.

In this connection it must be mentioned that the theoretical calculation should be performed by the use of the frequencies ν_e but the actual frequencies we have for $GeCl_4$ and CCl_4 are ν_0's: we have no means of securing the anharmonicity factor of these molecules. As the mean square amplitude is approximately inversely proportional to the frequency, as indicated by Eq. (32), the true mean amplitude is obtained by multiplying the factor ν_0/ν_e to apparent mean amplitude l_0^2 which was calculated by substituting ν_0 for ν_e,

$$2a=\langle\Delta z^2\rangle=l_0^2\cdot\nu_0/\nu_e=l_0^2(1-2x_e). \tag{34}$$

Therefore

$$2a'=l_0^2(1+x_e)(1-2x_e)=l_0^2(1-x_e). \tag{35}$$

Thus the correction due to the ν_0's would be partially canceled if we used a' instead of a in the comparison of the observed mean amplitude with the calculated one. This consideration is valid only for diatomic molecules. However, even in polyatomic molecules, the error would be of the order of x_e, and the comparison of $2a'$ with l_0^2 would have the smallest deviation. Considering the accuracy of the measurement of mean square amplitude by electron diffraction at present, we can safely neglect the correction and directly compare $2a'$, the factor obtained by electron diffraction, with the values calculated by the use of fundamental frequencies ν_0.

3. Force Constants

The general quadratic form of potential energy expression of a tetrahedral molecule is given by

$$\begin{aligned}2V=&\sum k_r(\Delta r_i)^2+\sum 2k_{rr}(\Delta r_i)(\Delta r_j)+\sum k_\alpha(r_e\Delta\alpha_{ij})^2\\&+\sum 2k_{r\alpha}(r_e\Delta\alpha_{ij})(r_e\Delta\alpha_{jk})+\sum 2k_{\alpha\alpha}(r_e\Delta\alpha_{ij})(r_e\Delta\alpha_{kl})\\&+\sum 2k_{r\alpha}'\Delta r_i(r_e\Delta\alpha_{ij})+\sum 2k_{r\alpha}'\Delta r_i(r_e\Delta\alpha_{jk}),\end{aligned} \tag{36}$$

where Δr denotes the displacement of bond distances and $\Delta\alpha$ the change of valency angles. This equation has seven force constants, but the symmetry of the molecule T_d reduces the number to five:

$$\begin{aligned}2V=&F_{11}S_1^2+F_{22}(S_{2a}^2+S_{2b}^2)+F_{33}(S_{3a}^2+S_{3b}^2+S_{3c}^2)\\&+2F_{34}(S_{3a}S_{4a}+S_{3b}S_{4b}+S_{3c}S_{4c})\\&+F_{44}(S_{4a}^2+S_{4b}^2+S_{4c}^2),\end{aligned} \tag{37}$$

TABLE IV. Fundamental frequencies ν_0 of $GeCl_4$ in cm^{-1}.

$\nu_1(A)$	$\nu_2(E)$	$\nu_3(F_2)$	$\nu_4(F_2)$
396	132	453	172

where

$$S_1=2^{-1}(\Delta r_1+\Delta r_2+\Delta r_3+\Delta r_4),$$

$$S_{2a}=(12)^{-\frac{1}{2}}r_e(2\Delta\alpha_{12}-\Delta\alpha_{23}-\Delta\alpha_{13}-\Delta\alpha_{14}-\Delta\alpha_{34}+2\Delta\alpha_{34}),$$

$$S_{2b}=2^{-1}r_e(\Delta\alpha_{23}-\Delta\alpha_{13}+\Delta\alpha_{14}-\Delta\alpha_{24}),$$

$$S_{3a}=6^{-\frac{1}{2}}(\Delta r_1+\Delta r_2-2\Delta r_3),$$

$$S_{3b}=(12)^{-\frac{1}{2}}(\Delta r_1+\Delta r_2+\Delta r_3-3\Delta r_4),$$

$$S_{3c}=2^{-\frac{1}{2}}(-\Delta r_1+\Delta r_3),$$

$$S_{4a}=(12)^{-\frac{1}{2}}r_e(2\Delta\alpha_{12}-\Delta\alpha_{23}-\Delta\alpha_{13}+\Delta\alpha_{14}+\Delta\alpha_{24}-2\Delta\alpha_{34}),$$

$$S_{4b}=6^{-\frac{1}{2}}r_e(\Delta\alpha_{12}+\Delta\alpha_{23}+\Delta\alpha_{13}-\Delta\alpha_{14}-\Delta\alpha_{24}-\Delta\alpha_{34}),$$

$$S_{4c}=2^{-1}r_e(\Delta\alpha_{23}-\Delta\alpha_{13}-\Delta\alpha_{14}+\Delta\alpha_{24}),$$

$$S_5=6^{-\frac{1}{2}}r_e(\Delta\alpha_{12}+\Delta\alpha_{23}+\Delta\alpha_{13}+\Delta\alpha_{14}+\Delta\alpha_{24}+\Delta\alpha_{34}). \quad (38)$$

The elements of the F matrix have the following relations to the constants in Eq. (36):

$$F_{11}=k_r+3k_{rr},$$

$$F_{22}=(k_\alpha-k_{\alpha\alpha}')-2(k_{\alpha\alpha}-k_{\alpha\alpha}'),$$

$$F_{33}=k_r-k_{rr},$$

$$F_{34}=\sqrt{2}(k_{r\alpha}-k_{r\alpha}'),$$

$$F_{44}=k_\alpha-k_{\alpha\alpha}'. \quad (39)$$

The symmetry coordinates relate to the normal coordinates by the transformation matrix L,

$$\mathbf{S}=\mathbf{LQ}. \quad (40)$$

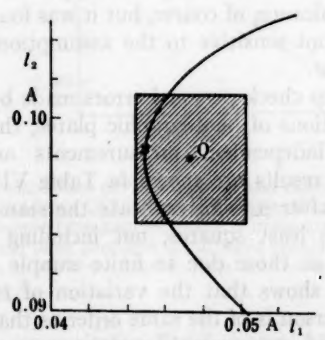

FIG. 4. Correlation curve of l_1(Ge—Cl) and l_2(Cl—Cl) of $GeCl_4$. The shaded area indicates the observed values. The boundary lines are drawn to show the standard errors. The cross corresponds to the Urey-Bradley force field.

TABLE V. Force constants of $GeCl_4$ in millidyne/A.

For symmetry coordinate system		For internal coordinate system	
F_{11}	3.276	k_r	2.79±0.23
F_{22}	0.121	k_{rr}	0.16±0.08
F_{33}	2.63±0.30	$k_\alpha-k_{\alpha\alpha}'$	0.18±0.01
F_{34}	0.12±0.20	$k_{\alpha\alpha}-k_{\alpha\alpha}'$	0.03±0.01
F_{44}	0.18±0.01	$k_{r\alpha}-k_{r\alpha}'$	0.09±0.14

Now, the method to calculate mean square amplitudes was previously presented by Morino *et al.*[24]; the mean amplitude of the vibration of a pair of the atoms whose displacements are given by the matrix relation

$$\Delta\mathbf{R}=\mathbf{AS},$$

is given by

$$\langle\Delta\mathbf{R}^2\rangle=\mathbf{A'L}\langle\mathbf{Q}^2\rangle\mathbf{L'A}, \quad (41)$$

where $\langle\mathbf{Q}^2\rangle$ is a diagonal matrix having the elements of

$$\langle Q^2\rangle_{ii}=(h/8\pi^2\nu_i)\coth(h\nu_i/2kT). \quad (42)$$

For a tetrahedral molecule Eq. (41) provides the following equations:

$$l_1^2(\text{Ge–Cl})=\tfrac{1}{4}G_{11}\langle Q_1^2\rangle+\tfrac{3}{4}L_{33}^2\langle Q_3^2\rangle+\tfrac{3}{4}L_{34}^2\langle Q_4^2\rangle, \quad (43)$$

$$l_2^2(\text{Cl–Cl})=\tfrac{2}{3}G_{11}\langle Q_1^2\rangle+\tfrac{1}{6}G_{22}\langle Q_2^2\rangle+\tfrac{1}{6}(2L_{33}+L_{43})^2\langle Q_3^2\rangle+\tfrac{1}{6}(2L_{34}+L_{44})^2\langle Q_4^2\rangle, \quad (44)$$

where the G_{ij}'s are the elements of the well-known Wilson G matrix and are given by the masses of the atoms and the geometry of the molecule. L_{33}, L_{43}, and L_{44} are calculated for every set of F_{33}, F_{34}, and F_{44} which satisfy the two observed frequencies, ν_3 and ν_4, through the secular equation $|\mathbf{GF}-\lambda\mathbf{E}|=0$. As infinite sets of force constants are allowed to express the λ_3 and λ_4, there must be a correlation between the values of l_1 and l_2 which satisfy the two frequencies. They were calculated by the use of the fundamental frequencies measured by the Raman effect (Table IV).[25] The result is shown in Fig. 4, where the observed values of the root mean square amplitudes are indicated by the

TABLE VI. F matrix elements of $GeCl_4$ in millidyne/A calculated with the assumption of Urey-Bradley force field.

	I[a]	II[b]	Present experiment
F_{33}	2.656	2.639	2.63±0.30
F_{34}	0.116	0.106	0.12±0.20
F_{44}	0.173	0.174	0.18±0.01

[a] With an assumption of $H'=0$.
[b] With an assumption of $F'=-F/10$.

[24] Morino, Kuchitsu, and Shimanouchi, J. Chem. Phys. **20**, 726 (1952).
[25] Delwaulle *et al.*, J. Phys. radium **15**, 206 (1954).

TABLE VII. Results of the least squares analysis of molecular intensity curves of CCl_4 at 22°C.

Observer	r_{a1}(C—Cl)	r_{a2}(Cl—Cl)	$(2a_1')^{\frac{1}{2}}$(C—Cl)	$(2a_2')^{\frac{1}{2}}$(Cl—Cl)	κ_1(C—Cl)$\times10^5$	κ_2(Cl—Cl)$\times10^5$	i
N	1.769±0.0031	2.888±0.0016	0.0531±0.0020	0.0736±0.0011	−5.7±3.1	−1.2±1.9	99.9±1.5
N	1.768±0.0031	2.887±0.0019	0.0499±0.0022	0.0723±0.0012	−4.7±4.4	−4.8±2.6	93.7±1.6
N	1.759±0.0033	2.882±0.0013	0.0497±0.0024	0.0697±0.0013	3.1±3.5	0.9±2.1	99.4±1.7
I	1.769±0.0062	2.899±0.0031	0.0503±0.0042	0.0737±0.0022	2.8±6.2	1.5±3.8	94.5±3.1
M	1.763±0.0036	2.888±0.0018	0.0525±0.0024	0.0718±0.0013	−3.0±3.6	3.9±2.2	95.5±1.8
Mean	1.765_3±0.002_0	2.886_4±0.002_1	0.0513±0.0014	0.0721_4±0.000_7	-2.1_2±2.6_5	0.1_6±1.4_0	97.0_7±1.3_3

TABLE VIII. Final results for the molecular parameters of CCl_4 at 22°C.

	Present measurement		Bartell, Brockway, and Schwendeman	
	C—Cl	Cl—Cl	C—Cl	Cl—Cl
r_a	1.765_3±0.002_0	2.886_4±0.002_1	r_{RD}=1.769±0.003	r_{RD}=2.887±0.004
$2a/r$	0.0014	0.0017		
r_g	1.766_7±0.003	2.888_1±0.003	$r_{RD}°$=1.766±0.003	...
$(2a')^{\frac{1}{2}}$	0.0513±0.001	0.0721_4±0.000_7		
Δl	−0.0012	−0.0025		
l_g	0.0505±0.002	0.0696±0.001	0.058±0.005	0.068±0.003

shaded area, the boundaries being drawn by the standard errors. The values of the **F** matrix elements corresponding to the line belonging to this area are shown in Table V. It should be noted that each of the force constants listed in Table V is not independent but must have a mutual correlation by the restriction that the set of force constants is consistent with the observed fundamental frequencies.

The values of force constants in the usual potential energy expression of Eq. (36) were calculated by Eq. (39) and are listed in Table V.

The Urey-Bradley force field

$$2V=\sum K(\Delta r_i)^2+\sum H(r_e\Delta\alpha_{ij})^2+\sum F(\Delta q_{ij})^2 +\sum 2H'r_e^2\Delta\alpha_{ij}+\sum 2F'q_e(\Delta q_{ij}), \quad (45)$$

has the following relations to the **F** matrix expression:

$$\begin{aligned} F_{11}&=K+4F,\\ F_{22}&=H+\tfrac{1}{3}F-\tfrac{1}{3}F'+[1/(8)^{\frac{1}{2}}]H',\\ F_{33}&=K+\tfrac{4}{3}F+\tfrac{4}{3}F',\\ F_{34}&=\tfrac{2}{3}(F+F'),\\ F_{44}&=H+\tfrac{1}{3}F-\tfrac{5}{3}F'-[3/(8)^{\frac{1}{2}}]H'. \end{aligned} \quad (46)$$

The **F** matrix elements corresponding to the Urey-Bradley field which satisfy the observed frequencies are listed in Table VI, one with the assumption $H'=0$,[26] and the other with $F'=-F/10$.[27] Both sets of mean amplitudes which were calculated with these constants are indicated by the cross in Fig. 4. Thus it can be concluded that the molecular field of germanium tetrachloride is very close to the Urey-Bradley force field. It should be mentioned that Cyvin[28] also arrived at the same conclusion, using his new secular equation method for calculating mean square amplitudes.

CCl_4

The same treatment was applied for carbon tetrachloride. The least squares calculation was carried out with seven unknown parameters. The weight factor for the measurement was assumed to have a similar form to that for $GeCl_4$, with the slight modification that the weight was assumed to be unity from $q=21$ to 60, both sides of which were spliced by two Gaussian functions:

$$\begin{aligned} w(q)&=\exp[-0.040(q-21)^2], &&\text{for}\quad 19\leqq q\leqq 21,\\ w(q)&=1, &&\text{for}\quad 21\leqq q\leqq 60,\\ w(q)&=\exp[-0.002(q-60)^2], &&\text{for}\quad 60\leqq q\leqq 95. \end{aligned} \quad (47)$$

This function is somewhat arbitrary and of no particular significance, of course, but it was found that the result was not sensitive to the assumption about the weight factor.

In order to check personal errors made by observers and fluctuations of photographic plates, three persons performed independent measurements on different plates. The results are shown in Table VII, in which the figures after ± signs indicate the standard deviations in the least squares, not including systematic errors such as those due to finite sample size. Table VII clearly shows that the variation of results from person to person is of the same order as that arising in the course of one person's measurement and of the order of the standard error. Judging from the magnitude

[26] T. Shimanouchi, J. Chem. Phys. **17**, 245 (1949).
[27] T. Shimanouchi, J. Chem. Soc. Japan **74**, 28 (1953).
[28] S. Cyvin (private communication).

of the standard deviations, the values of κ are meaningless, just as in the case of $GeCl_4$. The mean values listed on the lowest line are the weighted mean of the five observations, by taking into account their standard deviations obtained by least squares.

The distribution of gas molecules around the nozzle was found to require a correction of -0.0012 A for the root mean square amplitude of the C–Cl pair and -0.0025 A for that of the Cl—Cl pair. The error in the measurement of the scale factor which might give a direct influence on the atomic distance was estimated to be about 0.1%. It gives to the mean amplitudes an error of the same order but it is negligible compared with the standard errors.

The final values corrected for the finite sample size are shown in Table VIII. It is noted that the results are in excellent agreement with those of Bartell, Brockway, and Schwendeman,[9] except the root mean square amplitude of C–Cl: 0.0505 ± 0.002 A is definitely smaller than their value, 0.058 ± 0.005 A.||

As for the calculation of the force constants, the same procedure as that applied to $GeCl_4$ was found to give the result shown by curve A in Fig. 5. In this calculation the frequencies observed by the Raman effect in the gaseous state[29] were adopted for the frequencies of the normal vibrations (Table IX). It is well-known that the ν_3 is perturbed by a Fermi resonance with $\nu_1+\nu_4$ to yield a doublet, 751.1 and 790.6 cm^{-1}. The frequency of the stronger line, 790.6 cm^{-1} was used as the frequency of ν_3. It will be recognized that the shaded square for the observed values cuts the theoretical curve A only with an edge. It seems likely that one of the reasons for this discrepancy comes from the ambiguity of the frequencies due to the Fermi resonance and other causes. If small deviations are allowed

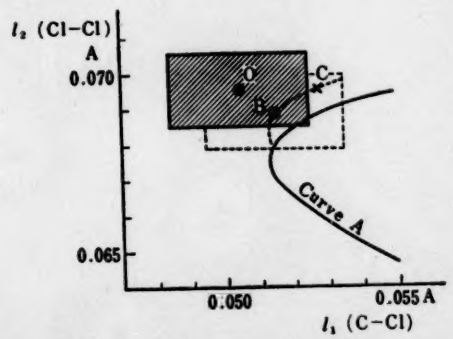

FIG. 5. Comparison of the observed and calculated root mean square amplitudes of CCl_4. Curve A indicates the calculated values with the observed frequencies, point B designates the calculated values for the most probable set of force constants, and cross C corresponds to the Urey-Bradley force field for the set of frequencies of point B.

TABLE IX. Comparison of the frequencies and root mean square amplitudes of CCl_4 at 295°K.

	Observed	Calculated	Difference
$\nu_1(A)$	455.7 cm^{-1}	454.0 cm^{-1}	+0.4%
$\nu_2(E)$	213.5	211.2	+1.1%
$\nu_3(F_2)$	790.6	794.9	−0.5%
$\nu_4(F_2)$	309.7	304.4	+1.7%
l_1(C—Cl)	0.0505 A	0.0515 A	−1.8%
l_2(Cl—Cl)	0.0696	0.0688	+1.2%

for the frequencies as well as for the mean square amplitudes, it might be interesting to select a set of force constants which represent both the frequencies and the root mean square amplitudes with the smallest deviations in the sense that

$$\sum[(\nu_i^{obs}-\nu_i^{calc})/\nu_i^{obs}]^2+\sum[(l_i^{obs}-l_i^{calc})/l_i^{obs}]^2 = \text{min}, \quad (48)$$

where equal weight is tentatively assumed for ν_i and l_i.¶ The best set of the root mean square amplitudes and the frequencies thus obtained are compared with the observed ones in Table IX, and the elements of the F matrix corresponding to this choice are tabulated in Table X. In the latter the figures after the $\pm$ signs indicate the ranges of the force constants found only when the root mean square amplitudes have deviations which are the same as the observed standard errors. Point B in Fig. 5 designates this best choice. Though it does not coincide exactly with the observed point O, it is positively within the shaded area of the standard errors of the observation.

The force constants in the usual potential expression (36) in terms of the displacements of bond distances and bond angles were calculated from the F matrix elements thus obtained; the result is listed in Table X. They compare well with those of germanium tetrachloride shown in Table VI.

One of the main objects of this study is to examine the availability of the Urey-Bradley force field, as already mentioned. The mean amplitudes of the force set of the Urey-Bradley type** which satisfies the four frequencies of the best set is indicated by cross C in Fig. 5. It does not fall in the shaded area of the observed point O, but it is located very close to the borderline of the area, and it is surely within the same range from the point B of the best set, which is shown by dotted lines. Judging from the nature of the estimated errors, this point can not be excluded as an unreasonable choice, but rather it may be preferable to say that the Urey-Bradley field is approximately

|| Private communication. Bartell obtained 0.058 A in place of 0.060 A. which he reported in reference 9, by recalculating the correction for the failure of the Born approximation.

[29] Morino, Watanabe, and Mizushima, Sci. Papers Inst. Phys. Chem. Research, 39, 348 (1942).

¶ It may be most reasonable to assume the weight of each quantity to be proportional to its accuracy, but the accuracy of the frequencies can not be evaluated because of the Fermi resonance and other unavoidable causes.

** With the assumption of $F'=-F/10$.

TABLE X. Force constants of CCl_4 in millidyne/A.

For symmetry coordinate system	For internal coordinate system		For Urey-Bradley force system		
			Present authors		Shimanouchi
F_{11} 4.305	k_r	3.59±0.56	K	2.32±0.86	1.81
F_{22} 0.311	k_{rr}	0.24±0.19	H	0.34±0.20	0.10
F_{33} 3.35±0.75	$k_\alpha - k_{\alpha\alpha'}$	0.38±0.03	F	0.50±0.22	0.64
F_{34} 0.52±0.21	$k_{\alpha\alpha} - k_{\alpha\alpha'}$	0.03±0.01	F'	0.28±0.38	−0.06
F_{44} 0.38±0.03	$k_{r\alpha} - k_{r\alpha'}$	0.36±0.15	H'	−0.31±0.37	−0.03

realized. The conclusion is also supported by the following comparison: the values of the constants, K, H, F, F', and H' of Eq. (45) are calculated by use of the relations (46) from the **F** matrix elements obtained above, without any restriction imposed upon F' or H'. The values thus obtained, which are listed in Table X, are compatible with the assumption of $F'=-F/10$ or $H'=0$, which has frequently been assumed for the usual Urey-Bradley type of force field. The set of force constants obtained by Shimanouchi,[27] though they were adjusted to the frequencies of liquid carbon tetrachloride, are also included in the range of errors.

Looking at Table IX, it will be noticed easily that the discrepancies of the frequencies are not confined to the ν_3 which suffers a perturbation by Fermi resonance but they are equally distributed over all the frequencies. Thus it seems likely that the discrepancies are not only due to the Fermi resonance but also due to the anharmonicity of the frequencies. In fact, in a tetrahedral molecule three fundamental frequencies are degenerate so that the effect of anharmonicity would be exaggerated two or three times. Moreover, the location of curve B corresponding to given values of ν_3 and ν_4, is sensitive to the frequency of the ν_2. In this sense it would be most indispensable to get exact values of ν_e, the frequencies of normal vibrations, not the ν_0 of the fundamental frequencies.

In this connection it is supposed that the anharmonicity is more serious in CCl_4 than in $GeCl_4$, because the calculated values of the mean square amplitudes are closer to the observed ones in $GeCl_4$ than in CCl_4. It is likely that the compact packing of chlorine atoms in the carbon tetrachloride molecule would produce a force field with high anharmonicity, whereas in germanium tetrachloride larger atomic distances would bring the molecular field to a more regular one.

ACKNOWLEDGMENTS

The authors wish to express their gratitude to Professor H. Takahashi and his co-workers, in the Department of Physics, for the use of the PC-1 computer, and to Mr. H. Oikawa, of the Coal Research Institute of Mitsui Chemical Industrial Company, Ltd., for his kind offer of germanium tetrachloride. They wish also to thank Mr. Y. Murata for reading one of the microphotometer tracings. They are indebted to the Ministry of Education of Japan for the research grant.

Detonation Pressure of Liquid TNT*

W. B. GARN

Los Alamos Scientific Laboratory, Los Alamos, New Mexico

(Received August 3, 1959)

The plane steady-state detonation pressure behind the reaction zone of liquid TNT is reported. This pressure of 171.8 kilobars was established by measuring free-surface velocity as a function of plate thickness for 2024 aluminum plates placed in contact with the detonating explosive. The zero thickness metal shock pressure, obtained by extrapolating the free-surface velocity data, is corrected to the corresponding detonation pressure by an impedance matching calculation. Recording was done by a sweeping-image camera technique.

INTRODUCTION

THE Hugoniot pressure-volume relationship for undetonated liquid TNT (trinitrotoluene) was previously reported.[1] This work is extended in the present paper to a determination of the detonation pressure for a plane steady-state detonation in liquid TNT.

Experimental data for TNT are of particular interest because this material can be readily investigated in both the solid and liquid states, thereby making available data for significant variations of both initial density and initial internal energy. Specifically, Deal[2] and Campbell *et al.*[3] have reported results, respectively, on the detonation pressure and the detonation velocity of the normal density solid. Current investigations by James *et al.*[4] and by Seely[5] will give detonation velocity dependence on initial density for both the solid and the liquid.

In light of the substantial shock pressures supported without detonation,[1] it was not clear, when present work was begun, that liquid TNT could be initiated without overdrive of the steady-state detonation pressure. Contemporary work by Seely, however, suggested that this could be done, and his initiation scheme has been used in the present program. The possibility of consistent errors due to overdrive has also been investigated by experimentation reported here.

The author is further indebted to Seely for his value of the detonation velocity of 92°C liquid TNT. His value of the detonation velocity is combined here with results of present experimentation to determine the desired detonation pressure.

EXPERIMENTAL METHOD

An optical technique used by Deal[2] was applied to measurements on detonating liquid TNT. A typical assembly is illustrated as Fig. 1(a). Initiation was by means of an 8-inch diameter plane-wave exposive system, consisting of a lens and 2 inches of Composition *B*. The 8-inch diameter TNT sample was detonated through a 1¼-inch Micarta shock attenuator plate. A carefully controlled oil heating bath surrounding the test sample maintained the liquid TNT, a solid at ordinary temperatures, in the liquid state at 92°C. Both the heating bath and the liquid sample were rapidly stirred before and during detonation in order to assure temperature uniformity.

The explosive pressure was obtained by measurement of free-surface velocity as a function of plate thickness for metal plates placed in contact with the TNT surface. Recording was by means of a sweeping-image camera technique.[1,2] Light for the record is produced when the 0.003-inch argon gaps under the slits [Fig. 1(b)] are closed by shock arrival at the plate surface and by the aluminum free-surface arrival at the Plexiglas step. A typical record is reproduced as Fig. 2. The offset between the surface and free-run traces gives the free-surface time of flight. Dividing the Plexiglas step depth by this time determines the desired free-surface velocity.

DATA AND RESULTS

The 2024 aluminum free-surface velocities for 12-inch charge lengths and various aluminum thicknesses are listed in Table I and plotted in Fig. 3. These data are extrapolated to zero metal thickness to remove effects of the rarefaction (Taylor wave) on the detonation pressure. Actually, the use of very thin aluminum plates should reveal shock strengths which are substantially above the shock strength indicated by the present extrapolation. This well-known effect is attributable to the explosive reaction zone. Measurements by Duff and Houston[6] for solid Composition *B* show the reaction zone affecting about the first millimeter of metal. Concurrent investigations[7] suggest that the effect is much less extensive for liquid explosives. The 2024 aluminum thickness in the present experiments was varied from 24.4 mm down to 3.81 mm and the extrapolated free-surface velocity corresponding to zero metal

* Work done under auspices of the U. S. Atomic Energy Commission.

[1] W. B. Garn, J. Chem. Phys. **30**, 819 (1959).
[2] W. E. Deal, J. Chem. Phys. **27**, 796 (1957).
[3] Campbell, Malin, Boyd, and Hull, Rev. Sci. Instr. **27**, 567 (1956).
[4] James, Smith and Urizar (to be published).
[5] L. B. Seely (to be published).
[6] R. E. Duff and E. Houston, J. Chem. Phys. **23**, 1268 (1955).
[7] A. W. Campbell and W. C. Davis (private communication).

thickness is 2.427 km/sec. This free-surface velocity corresponds, by using available data for 2024 aluminum,[8] to a metal shock pressure P_m of 234.5 kb and a shock-wave velocity U_s of 6.977 km/sec. Then, by applying the successive approximation Eqs. (1) through (6)[2] for the Chapman-Jouguet condition and assuming the use of these equations for the plane steady-state detonation does not introduce significant errors, the pressure can be evaluated from the zero thickness 2024 aluminum free-surface velocity and the constants of the explosive and aluminum.[2]

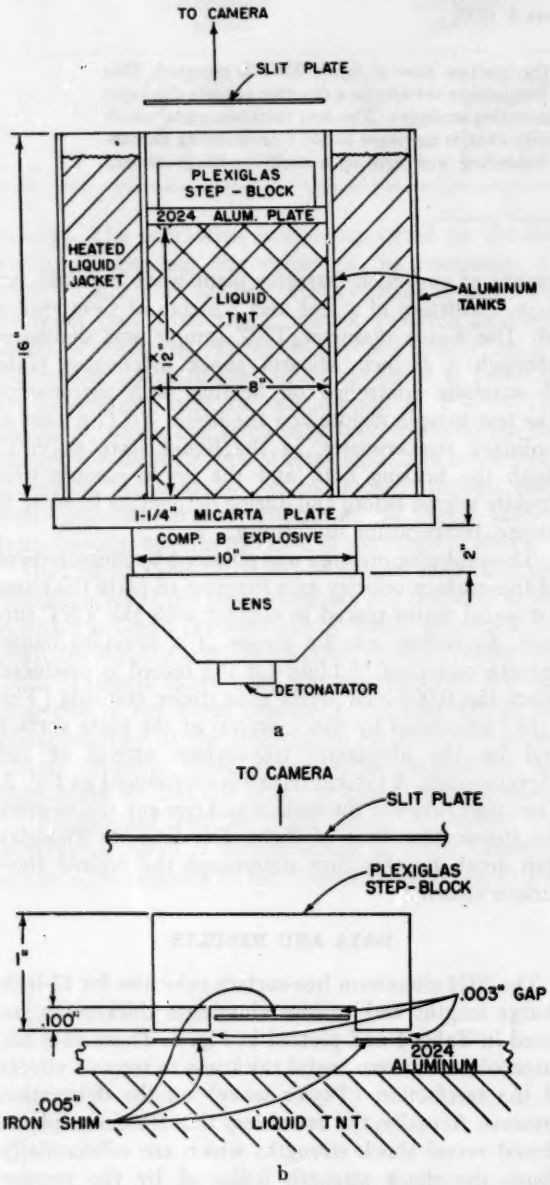

FIG. 1(a). Cross section of complete assembly showing explosive, heating liquid tank, liquid TNT, and 2024 aluminum test plate with Plexiglas step-blocks and slit plate. (b). Detail of Plexiglas step-block assembly under slits. Seven slits parallel to the plane of the figure were used giving seven simultaneous measurements. Sweep direction of camera is perpendicular to the slits.

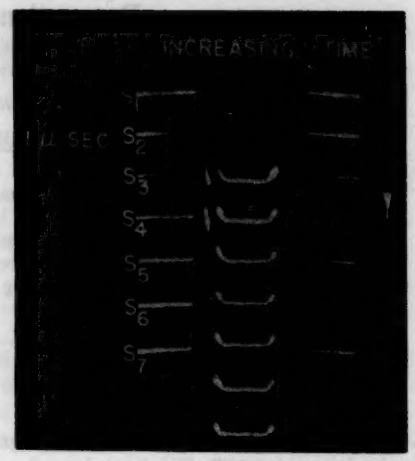

FIG. 2. A typical record obtained from the assembly illustrated in Fig. 1 used for determining 2024 aluminum free-surface velocity. Seven slits (S_1 through S_7) are used giving seven data points.

$$P_{cj}=P_m[1+R(\rho_{0x}D_x/\rho_{0m}U_s)]/(1+R), \quad (1)$$

where

$$R=D_r/(D_x-U_{cj}), \quad (2)$$

$$D_r=\{[P_m^2-2P_mP_{cj}/(\gamma+1)-P_{cj}^2(\gamma-1)/(\gamma+1)]/[2(P_m-P_{cj})\rho_{cj}/(\gamma+1)]\}^{\frac{1}{2}}, \quad (3)$$

$$\gamma=(\rho_{0x}D_x^2/P_{cj})-1, \quad (4)$$

$$U_{cj}=D_x/(\gamma+1)=C\text{-}J \text{ particle velocity}, \quad (5)$$

$$\rho_{cj}=\rho_{0x}(\gamma+1)/\gamma=C\text{-}J \text{ density}, \quad (6)$$

P_m = induced shock pressure in metal,
P_{cj} = Chapman-Jouguet explosive detonation pressure,
ρ_{0m} = initial density of metal,
ρ_{0x} = initial density of explosive (liquid TNT),
D_x = detonation velocity in explosive,[4]
U_s = induced shock velocity in metal.

TABLE I. Experimental free-surface velocities for various thicknesses of 2024 aluminum in contact with 8-inch diameter liquid TNT charges. Errors indicated are standard deviations of the averages. $V_0=0.687$ cc/g, $T_0=92.0\pm1.0$ deg C.

X Al thickness (mm)	TNT Sample depth (inches)	U_{fs} (km/sec)	Number of data points
3.81	12	2.398±0.017	5
3.81	9	2.402±0.010	7
3.81	24	2.397±0.029	5
6.35	12	2.375±0.004	6
12.70	12	2.355±0.005	7
25.40	12	2.254±0.009	6

[8] Walsh, Rice, McQueen, and Yarger, Phys. Rev. **108**, 196 (1957).

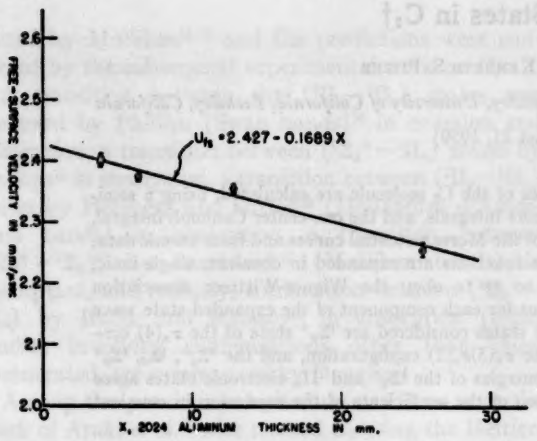

FIG. 3. Free-surface velocity data resulting from 2024 aluminum plates in contact with detonated liquid TNT. The straight line is a linear least-squares fit to data. Error flags signify standard deviation of the averages.

This calculation established the plane steady-state detonation pressure for 92°C liquid TNT as 171.8±1.4 kb. The detonation pressure and other pertinent explosive and 2024 aluminum constants and data are listed in Table II.

Several additional experiments serve as a check on the foregoing results. In one series of shots, charge length was varied with 2024 aluminum plate thickness held constant at 3.81 mm. One shot each for charge lengths of 9 inches and 24 inches were both well within one per cent, in 2024 aluminum free-surface velocity, of results reported herein for the 12-inch charges. These results are listed in Table I. The 12-inch charge results are accordingly thought to be free from the pressure attenuation which would accompany an overdriven detonation wave. It should be noted that the first attempt to determine the liquid TNT detonation pressure was done using 3-inch charge lengths and a 1-inch thick (instead of 1¼-inch) Micarta attenuator. The consequent extrapolated zero-thickness aluminum free-surface velocity was 1.2 % higher than that quoted for the given geometry. This work, compared with results cited previously in this paper, does suggest a slight overdrive. Work with the 3-inch charge lengths was discontinued when attempts to significantly increase Micarta thickness, in order to test the overdrive hypothesis, lead to curved detonation fronts and erratic results.

TABLE II. Input data and results obtained by application of Eqs. 1 through 6.

Explosive density ρ_{0e} at 92°C	=1.455±0.002 g/cc
Detonation velocity D_e[5] at 92°C	=6.600±0.006 km/sec
2024 aluminum density ρ_{0m}	=2.790±0.003 g/cc
2024 aluminum free-surface velocity U_{fs} for $X=0$	=2.427±0.017 km/sec
2024 aluminum shock velocity U_s for $X=0$	=6.977±0.017 km/sec
2024 aluminum pressure P_m for $X=0$	=234.5±2.7 kilobars
Plane detonation pressure P	=171.8±1.4 kilobars
Plane detonation particle velocity	=1.791±0.015 km/sec

TABLE III. Experimental free-surface velocities for 2024 aluminum plates in contact with 5.750-inch diameter pressed TNT charges. Errors indicated are standard deviations of the averages. V_0=0.687 cc/g.

X Al thickness (mm)	TNT Sample depth (inches)	U_{fs} (km/sec)
3.81	10.75	2.340±0.005
3.81	10.75	2.323±0.005
3.81	22.38	2.309±0.010
3.81	7.75	2.353±0.010
25.40	10.75	2.133±0.006

One shot was fired using a 3.81-mm thick magnesium plate instead of aluminum. The small correction (approximately 1 % needed in free-surface velocity) needed to extrapolate to zero plate thickness was estimated theoretically. The resulting free-surface velocity, 3.271±0.011 km/sec, indicates a liquid TNT detonation pressure of 171.1 kb, in good agreement with results obtained with the 2024 aluminum plates.

Additional experiments were done by using low-density pressed solid TNT samples. An elementary thermodynamic calculation (using $(1/V)(\partial E/\partial P)_s \approx 1.0$) indicates a slightly lower (about 3 kb) detonation pressure for the solid when pressed to liquid density (1.455 g/cc). The lower pressure is due to the lower initial internal energy. Data for five solid TNT shots are listed in Table III. These results indicate a detonation pressure for the solid, at density 1.455 g/cc, of 168±3.4 kb. The wide error limits are attributed to small but finite density variations within the charges, and the use of a simple over-all density in the analysis. The results are of interest because they demonstrate consistency between the liquid and solid detonation pressures. Also, solid TNT is sufficiently sensitive that initiation could be accomplished without risking overdrive. Actual initiation was accomplished with Baratol, an explosive of approximately 138 kb detonation pressure and higher shock impedance than TNT, so that the possibility of overdrive may be excluded.

The present results can also be compared with previously published data on solid TNT. Deal[2] reports a Chapman-Jouguet pressure of 189.1±1.0 kb for solid TNT of density 1.637±0.003 g/cc. This pressure determination utilizes an accepted detonation velocity[3] of 6.942±0.016 km/sec.

ACKNOWLEDGMENTS

This work was made possible only by the close cooperation of several people in GMX-6 and in the GMX-Division of Los Alamos Scientific Laboratory.

Low Excited States in C_2†

ENRICO CLEMENTI AND KENNETH S. PITZER

Lawrence Radiation Laboratory and Department of Chemistry, University of California, Berkeley, California

(Received August 21, 1959)

In this paper the energies of the low electronic states of the C_2 molecule are calculated, using a semiempirical approach. In the calculation, the two-center core integrals, and the one-center Coulomb integral, are empirical parameters which are obtained by fitting of the Morse potential curves and from atomic data, respectively. The standard ASMO—LCAO state wave functions are expanded in covalent, single ionic, and double ionic components, which are constructed so as to obey the Wigner-Wittmer dissociation rules at infinite internuclear distances. The contributions for each component of the expanded state wave functions are obtained by the variational method. The states considered are $^1\Sigma_g^+$ state of the $\pi_u(4)$ configuration (of $2p$ orbitals), the $^3\Pi_u$ and $^1\Pi_u$ states of the $\pi_u(3)\sigma_g(1)$ configuration, and the $^3\Sigma_g^-$, $^1\Delta_g$, $^1\Sigma_g^+$ states of the $\pi_u(2)\sigma_g(2)$ configuration. The calculated energies of the $^1\Sigma_g^+$ and $^1\Pi_u$ electronic states agree well with experiment. Finally, a critical analysis is given of the coefficients of the expansion in covalent and ionic structures.

1. INTRODUCTION

RECENTLY a new family of molecules, the C_n carbon polymers, were the subject of experimental[1–3] and theoretical[4] studies. The status of spectroscopic information for the smallest species, namely diatomic carbon C_2, is relatively well established when compared with that for C_3 and the larger polymeric forms. The latter are not known from spectroscopic data although the existence of C_5 is known from mass spectroscopic data. A band system of the C_3 molecule has been found in emission and has been assigned to a $^1\Sigma_g^+ - {}^1\Pi_u$ transition.[5–8]

Our interest in these larger molecules makes further theoretical study of C_2 desirable. At least two points deserve comment about C_2. Among the low excited states, the $^1\Sigma_g^+$ and the $^1\Delta_g$ states of the $\cdots\pi_u(2)\sigma_g(2)$ configuration are not experimentally known. In addition no transition has been observed between a triplet and a singlet state. For these reasons it appears to be of current interest to present a calculation which will give the amount of splitting between singlet and triplet states and attempt to predict the location of the previously mentioned $^1\Sigma_g^+$ and $^1\Delta_g$ states. The present calculation employs a semiempirical method in which one uses a convenient variational expansion of the molecular orbital wave function such as to ensure the correct dissociation energies, without introducing full configuration interaction. The method will be tested against the experimental thermodynamic data of Hicks.[9]

In Hicks' work evidence is given for a splitting of 1.38 ev at the equilibrium distances for the two electronic states, $^3\Pi_u$, the ground state, $^1\Pi_u$ and the lowest excited state. This is derived from measurements of the temperature coefficients of the Swan band[10] ($^3\Pi_u - {}^3\Pi_g$) and Phillips band[11] ($^1\Sigma_g^+ - {}^1\Pi_u$) which showed the lowest $^1\Sigma_g^+$ state to be 8 kcal (0.39 ev) above the ground state.[12] From Hicks, the derived dissociation energy D_0 is 6.04 ev; additional evidence for this dissociation energy of C_2 is given in our earlier paper.[4] The uncertainties of approximately 0.2 ev are inherent in the Hicks result in view of his experimental method.

The molecular orbitals for the C_2 molecule, given in order of increasing energy, are K, K, $\sigma_g(2s)$, $\sigma_u(2s)$, $\pi_u(2p_\pi)$, $\sigma_g'(2p_\sigma)$, $\pi_g(2p_\pi)$, $\sigma_u'(2p_\sigma)\cdots$. The $\pi_u(2p_\pi)$ and the $\pi_g(2p_\sigma)$ orbitals are nearly equal in energy at the equilibrium internuclear distance (see our earlier paper[4] for a semiquantitative diagram). The lowest configurations which may be constructed with these molecular orbitals, and the corresponding electronic states (which are constructed in accordance with the vector model and Pauli principle) are

$$\left.\begin{array}{lll} \text{(a)} & \sigma_g(2)\sigma_u(2)\pi_u(4) & :{}^1\Sigma_g^+ \\ \text{(b)} & \sigma_g(2)\sigma_u(2)\pi_u(3)\sigma_g'(1) & :{}^3\Pi_u,\ {}^1\Pi_u \\ \text{(c)} & \sigma_g(2)\sigma_u(2)\pi_u(2)\sigma_g'(2) & :{}^3\Sigma_g^-,\ {}^1\Delta_g,\ {}^1\Sigma_g^+ \end{array}\right\}. \quad (1.1)$$

The approximate location of these states was pre-

† This work was partially presented at the Conference of Molecular Quantum Mechanics, Boulder, Colorado, June, 1959.

[1] H. A. Chupka and M. G. Inghram, J. Chem. Phys. **22**, 1472 (1954).

[2] R. E. Honing, J. Chem. Phys. **22**, 126 (1954).

[3] H. A. Chupka and M. G. Inghram, J. Phys. Chem. **59**, 100 (1955).

[4] K. S. Pitzer and E. Clementi, J. Am. Chem. Soc. (to be published); presented at the Annual Meeting of the National Academy of Sciences, April, 1959, Washington, D. C.

[5] N. H. Kiess and P. H. Broida, Can. J. Phys. **34**, 1971 (1956).

[6] K. Clusius and A. E. Douglas, Can. J. Phys. **32**, 319 (1954).

[7] A. E. Douglas, Astrophys. J. **114**, 466 (1951).

[8] G. Herzberg, Mém. Soc. Roy. Sci. Liége **15**, 291 (1955).

[9] W. T. Hicks, "Spectroscopy of high temperature systems" (thesis), UCRL-3696 (February, 1957).

[10] J. G. Phillips, Astrophys. J. **108**, 434 (1948).

[11] J. G. Phillips, Astrophys. J. **107**, 489 (1948).

[12] When this work was already completed, we were informed by Dr. D. A. Ramsey that the $^1\Sigma_g^+$ state may be the ground state of the C_2 molecule, in contrast with the Hicks findings. The evidence given by Dr. Ramsey is based on a still incomplete analysis of the perturbations which appear in the rotational spectrum of the $^3\Sigma_g^-$ state and which suggest that the $^1\Sigma_g^+$ state lies ~0.07 ev below the $^3\Pi_u$.

dicted by Mulliken[13,14] and the predictions were confirmed by the subsequent experimental work on C_2.

A transition between the $(^3\Pi_g - ^1\Pi_g)$ states was observed by Phillips (Swan bands)[10] in emission and absorption, a transition between $(^1\Sigma_g^+ - ^1\Pi_u)$ states by Phillips[11] in absorption, a transition between $(^1\Pi_g - ^1\Pi_u)$ states by Herzberg and Sutton[15] (Deslandres d'Azambuja bands) in absorption, a transition between $(^1\Sigma_g^+ - ^1\Sigma_u^+)$ by Landsverk[16] (Mulliken bands) in absorption, and recently, a transition between $(^3\Sigma_g^- - ^3\Pi_u)$ by Ballik and Ramsey[17] in absorption (other studies involving configurations other than those enumerated, are summarized by Douglas[7]).

Among the previous calculations on C_2 we note the work of Araki *et al.*[18] who treated C_2 using the Heitler-London method, considering C_2 as a four-electron problem they obtained a binding energy of 19.42 ev for the $^1\Sigma_g^+$ state, whereas this state became repulsive when they considered C_2 as an eight-electron problem. A very high binding energy was also obtained by Wolfsberg[19] with an eight-electron calculation. Finally M. Ignatia Frye[20] treated C_2 with the Rothaan SCF-MO method using 4, 8, and 12 electrons with resulting binding energies (for $^3\Pi_u$) of 10.0 ev, 2.1 ev, and -0.2 ev, respectively. The absence of configuration interaction is presumably the reason for the large deviation from the observed dissociation energy.

2. SIMPLE ASMO SEMIEMPIRICAL CALCULATION

In the present work we will consider the states which belong to the configurations (a), (b), (c), in Eq. (1.1), given in the previous section. The state wave functions are built up according to the ASMO–LCAO approximation. The $D_{\infty h}$ symmetry for the homonuclear diatomic molecules and the adoption of a spin-independent Hamiltonian allows the use of the reflection $(+$ or $-)$ and the inverstion (u or g) symmetry operators and the S^2, S_z, Λ momentum operators as commutators.

The state wave functions are then constructed to be simultaneous eigenfunctions of these commuting operators. The $1s$ and $2s$ electrons are considered as core electrons, the $2p_\pi$ and $2p_\sigma$ as valence electrons. This choice does not imply that there is no hybridization between the $2s$ and $2p_\sigma$ electrons, but only that we may do without taking it into account in view of the subsequent adoption of semiempirical parameters. The molecular orbitals of interest are then given by the following expressions:

$$\begin{aligned}
\pi_u^+ &= [2(1+S_\pi)]^{-\frac{1}{2}}(\pi_A^+ + \pi_B^+) \\
&= \tfrac{1}{2}(1+S_\pi)^{-\frac{1}{2}}[(x_A+x_B)+i(y_A+y_B)], \\
\pi_u^- &= [2(1+S_\pi)]^{-\frac{1}{2}}(\pi_A^- + \pi_B^-) \\
&= \tfrac{1}{2}(1+S_\pi)^{-\frac{1}{2}}[(x_A+x_B)-i(y_A+y_B)], \\
\sigma_g &= [2(1+S_\sigma)]^{-\frac{1}{2}}(z_A+z_B), \qquad (2.1)
\end{aligned}$$

where x, y, z denote $2p_\pi(x)$, $2p_\pi(y)$ and $2p_\sigma(z)$ atomic orbitals, the subscripts A and B denote the two carbon atoms and S_π, S_σ are the overlap integrals for $2p_\pi$ and $2p_\sigma$ orbitals, respectively. The coefficients reduce to $\frac{1}{2}$ or $2^{-\frac{1}{2}}$ in the zero overlapping approximation, which we adopt following Pariser, Fumi, and Parr,[21,22] among others.

Sample state wave functions related to the configurations (a), (b), and (c) in Eq. (1.1) are given below:

$$\begin{aligned}
&\Psi(^3\Pi_u, b) = 2^{-\frac{1}{2}}(\pi_u^+\bar{\pi}_u^+\pi_u^-\bar{\sigma}_g + \pi_u^+\bar{\pi}_u^+\bar{\pi}_u^-\sigma_g), \\
&\Psi(^1\Pi_u, b) = 2^{-\frac{1}{2}}(\pi_u^+\bar{\pi}_u^+\pi_u^-\bar{\sigma}_g - \pi_u^+\bar{\pi}_u^+\bar{\pi}_u^-\sigma_g), \\
&\Psi(^1\Sigma_g^+, a) = \pi_u^+\bar{\pi}_u^+\pi_u^-\bar{\pi}_u^-, \\
&\Psi(^3\Sigma_g^-, c) = 2^{-\frac{1}{2}}(\pi_u^+\bar{\pi}_u^-\sigma_g\bar{\sigma}_g + \bar{\pi}_u^+\pi_u^-\sigma_g\bar{\sigma}_g), \\
&\Psi(^1\Delta_g, c) = \pi_u^+\bar{\pi}_u^+\sigma_g\bar{\sigma}_g, \\
&\Psi(^1\Sigma_g^+, c) = 2^{-\frac{1}{2}}(\pi_u^+\bar{\pi}_u^-\sigma_g\bar{\sigma}_g - \bar{\pi}_u^+\pi_u^-\sigma_g\bar{\sigma}_g), \qquad (2.2)
\end{aligned}$$

where we associate the upper bar with β spin and the absence of the upper bar with α spin. Clearly there are three wave functions for every triplet state considered with total spin momentum $+1$, 0, -1, but the use of a spin-independent Hamiltonian makes the three degenerate. Likewise $+$ and $-$ degeneracy exists for Π and Δ states. The energies for these states are expressed in terms of core integrals I, Coulomb repulsion integrals J, and Coulomb exchange integrals K over the molecular orbitals given by Eqs. (2.1). The coefficients of these terms in the energy are given in Table I.

The approximation of zero differential overlap is used in the reduction of the molecular integrals. This approximation[21] states (for the electron repulsion terms) that

$$\int r_{iA} r_{jB} d\tau = 0 \qquad (2.3)$$

for any atomic orbitals r_{iA} on one carbon atom and any r_{jB} on the other carbon atom.

The one-center integrals of the Coulomb type are obtained semiempirically from the electron affinity

[13] R. S. Mulliken, Phys. Rev. **56**, 778 (1939).
[14] R. S. Mulliken, Revs. Modern Phys. **4**, 66 (1932).
[15] G. Herzberg and R. B. Sutton, Can. J. Research **A18**, 74 (1940).
[16] O. G. Landsverk, Phys. Rev. **56**, 769 (1939).
[17] E. A. Ballik and D. A. Ramsey, J. Chem. Phys. **29**, 1418 (1958).
[18] (a) Araki, Tutihasi, and Watari, Progr. Theoret. Phys. (Japan) **6**, 135 (1951); (b) G. Araki and W. Watari, *ibid.* **6**, 945, 961 (1951).
[19] M. Wolfsberg, J. Chem. Phys. **21**, 2166 (1953).
[20] M. Ignatia Frye (Doctoral dissertation, Catholic University of America, Washington, D. C., 1955).
[21] R. Pariser and R. G. Parr, J. Chem. Phys. **21**, 466 (1953).
[22] F. Fumi and R. G. Parr, J. Chem. Phys. **21**, 1864 (1953).

TABLE I. State energies expressed in terms of molecular integrals.[a]

	$I(\pi_u)$	$I(\sigma_g)$	$J(\pi_u^+, \pi_u^+)$	$J(\pi_u^+, \sigma_g)$	$J(\sigma_g, \sigma_g)$	$K(\pi_u^+, \pi_u^-)$	$K(\pi_u^-, \sigma_g)$	$(\pi_u^+\pi_u^+ \mid \pi_u^-\pi_u^-)$
$^3\Pi_u, b$	3	1	3	3	0	−1	−2	0
$^1\Pi_u, b$	3	1	3	3	0	−1	0	0
$^1\Sigma_g^+, a$	4	0	6	0	0	−2	0	0
$^3\Sigma_g^-, c$	2	2	1	4	1	0	−2	−1
$^1\Delta_g, c$	2	2	1	4	1	0	−2	0
$^1\Sigma_g^+, c$	2	2	1	4	1	0	−2	+1

[a] Definitions of integrals are:

$$I(p) = \int p^* H_{\text{core}} p\, d\tau,$$
$$J(p_i, p_j) = \int p_i^*(1)\, p_j^*(2)\, (e^2/r_{12})\, p_i(1)\, p_j(2)\, d\tau,$$
$$K(p_i, p_j) = \int p_i^*(1)\, p_j^*(2)\, (e^2/r_{12})\, p_i(2)\, p_j(1)\, d\tau,$$
$$(p_i p_i \mid p_j p_j) = \int p_i^*(1)\, p_i^*(2)\, (e^2/r_{12})\, p_j(1)\, p_j(2)\, d\tau.$$

and ionization potential of the atom,[23] because the corresponding computed values[24] are unrealistically high.[21,25] In addition the following relations were used for one-center repulsion integrals[26]:

$$Jx_Ax_A = Jy_Ay_A = Jz_Az_A = J_3 + \tfrac{4}{3}K_3,$$
$$Jx_Ay_A = Jx_Az_A = Jy_Az_A = J_3 - \tfrac{2}{3}K_3, \qquad (2.4)$$

where J_3 and K_3 are Coulomb repulsion and exchange atomic integrals given by the following relation (the Roothaan notation[26,27] is preserved):

$$J_3 = (2p, 2p; S \mid 2p, 2p; S),$$
$$K_3 = (2p, 2p; D\Pi \mid 2p, 2p; D\Pi).$$

The value for the one-center integral Jx_Ax_A is 10.93 ev and for Jx_Ay_A it is 9.68 ev and K_3 is 0.623 ev.[28]

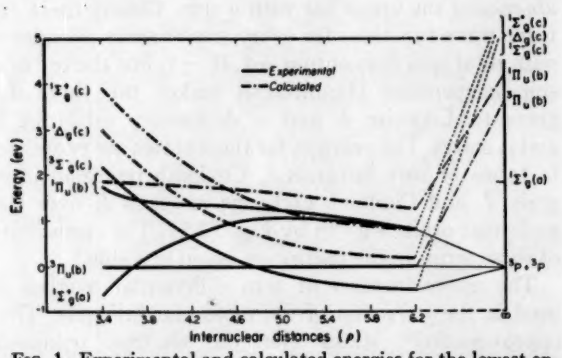

FIG. 1. Experimental and calculated energies for the lowest excited states in C_2. The calculated energies for the $^1\Sigma_g^+(a)$ state do not appear in the diagram because they fall below the bottom of the figure (at the equilibrium distance the energy is 6.3 ev below the $^3\Pi_u$ state). The calculated dissociation energies are given at the right side.

[23] R. S. Mulliken, J. Chem. Phys. **2**, 782 (1934).
[24] R. G. Parr and B. L. Crawford, J. Chem. Phys. **16**, 1049 (1948).
[25] R. Pariser and R. G. Parr, J. Chem. Phys. **21**, 767 (1953).
[26] G. G. J. Roothaan (Technical report, Laboratory of Molecular Structure and Spectra, Department of Physics, University of Chicago, Chicago, Illinois, 1955).
[27] G. G. J. Roothaan, J. Chem. Phys. **19**, 1445 (1951).
[28] J. M. Parks (thesis, Carnegie Institute of Technology, Pittsburgh, 1956).

The two-center integrals are tabulated by several authors and we have used the Roothaan table[29] with 3.25 for effective Z. The core integrals are obtained by fitting the $^3\Pi_u(b)$ and $^3\Sigma_g^-(c)$ states with the experimental values. The results are given diagrammatically in Fig. 1, where the $^3\Pi_u$ state is taken as zero and the internuclear distances are given in terms of $\rho = \zeta R = (Z_{eff}/2)R$ where R is in Bohr radii. The experimental values are calculated from the Morse potential curves of the form:

$$U(r) = D[1 - \exp(-2\beta\xi)]^2,$$

where $\xi = (r - r_e)/r_e$ with r_e the equilibrium internuclear distance, and where $\beta = \omega/4(BD)^{\frac{1}{2}}$. The parameters which enter in this equation are obtained from the literature given in the first section and are summarized in Table II. From Fig. 1 we see that even when semi-empirical one-center Coulomb integrals and semi-empirical values for the core integrals are used, still there is a serious discrepancy between calculated and experimental values for the $^1\Pi_u$ and $^1\Sigma_g^+(a)$ states. There are no experimental values for the $^1\Delta_g(c)$ state and the $^1\Sigma_g^+(c)$ state.

Another serious discrepancy is at the dissociation limits. The expected dissociation products, according to the Wigner-Wittmer rules[30,31] are $^3P + ^3P$ but the wave functions (2.2) give higher values, which correspond to some combination of atomic and ionic dissociation products. Let us consider this point in more

TABLE II. Molecular constants for the electronic states in C_2.

State	B (cm^{-1})	ω (cm^{-1})	D (ev)	r_e (A)
$^3\Pi_u$ (b)	1.6362	1641.35	6.04	1.312
$^1\Pi_u$ (b)	1.6170	1608.33	4.66	1.318
$^1\Sigma_g^+$ (a)	1.8205	1855.63	5.70	1.242
$^3\Sigma_g^-$ (c)	1.4031	1470.57	5.34	1.410

[29] G. G. J. Roothaan, *Tables of Two-Center Coulomb Integrals* (Department of Physics, University of Chicago, Chicago, Illinois, 1955).
[30] E. Wigner and E. E. Wittmer, Z. Physik **51**, 859 (1928).
[31] F. Hundt, Z. Physik **63**, 722 (1930).

detail. A carbon atom in its lowest configuration $1s(2)2s(2)2p(2)$ may be in the ^3P, ^1D, or ^1S atomic state. (The spin-orbital and magnetic splittings are unimportant in the present calculation in view of the type of Hamiltonian we have used.)

The energy of these terms may be expressed in terms of Coulombic integrals J and exchange integrals K. If we neglect the kinetic energy integrals, the nuclear potential energy integrals, and the K and J integrals involving $1s$ and $2s$ orbitals (since they are the same in each state), we obtain for the energy of those terms the following expressions:

$$\begin{aligned} &^3P: \quad J_3-\tfrac{5}{3}K_3, \\ &^1D: \quad J_3+\tfrac{1}{3}K_3, \\ &^1S: \quad J_3+\tfrac{10}{3}K_3, \end{aligned} \tag{2.5}$$

[see Eqs. (2.4)].

If we consider explicitly the $2p$ electrons in the C_2 molecule, and if we leave the $1s$ and $2s$ electrons in the core, we expect to have as dissociation energy $2J_3-10/3K_3$ (plus core contribution) for the states which dissociate as $^3P+^3P$. Instead the MO wave functions (2.2) give dissociation energy substantially higher than those expected. For example, the $^3\Pi_u$ state dissociates with energy $2\frac{1}{2}J_3-2\frac{1}{6}K_3$, and the $^1\Pi_u$ dissociates with energy $2\frac{1}{2}J_3-1\frac{1}{6}K_3$, that is, about 3.7 ev and 4.3 ev above the dissociation limits.

The ASMO–LCAO wave functions have included component wave functions corresponding to several covalent and ionic functions. These components are weighted in an arbitrary way, whereas one assumes that the best weight is that given by the variational theorem. The ASMO–LCAO wave functions may be expanded in order to show explicitly that the covalent and ionic type wave functions have the same coefficient for a given internuclear distance (at least in the zero overlap approximation). From such wave functions we have to expect a dissociation product energy higher than the correct one.

One familiar method for the removal of excessive ionic contributions to the wave function is the introduction of configuration interaction. But for the C_2 molecule the number of interacting states of a given symmetry is so high that very extensive calculations would be required if all configurations were to be included up to the energy of the important antibonding states. Instead we have tried to obtain the adjustment among the important covalent and ionic components of the bonding wave functions by a simple variational calculation described in the next section.

3. MODIFIED SEMIEMPIRICAL CALCULATION

In order to keep the computation at a reasonable level of complexity, we have used combinations of Slater determinants which are obtained by simple expansion of the ASMO–LCAO wave functions using the Wigner-Wittmer rules as a criterion to select the linear combinations. Thus the component wave functions of the expansion give the expected dissociation products, and the individual contributions are calculated by the use of the variational theorem. We have further simplified the treatment by expanding in a complete way only the components which give the lowest dissociation products, and grouping the single ionic structures and double ionic structures in common functions. (The only reason for doing so is to simplify the calculation.) This method bears some analogy to the valence bond method as far as the use of linear combination of wave functions corresponding to different covalent and ionic structures is concerned. An alternative way would be to start with a linear combination of molecular wave functions built up in such a way as to lead to all the dissociation products acceptable on the basis of Wigner and Wittmer's rule, without making direct reference to the MO wave function as we did.

The expanded state wave function for the configurations (a), (b), (c) in Eq. (1.1) is given in the following. The Slater determinants, which occur in the expansion of the state wave functions, are given in Table III. A and B refer to atomic orbitals centered on atom A and B, respectively, the subscripts $+$, 0, $-$ indicate $2p_{+1}$, $2p_0$, $2p_{-1}$ atomic orbitals, respectively, the absence and presence of upper bar indicates α and β, spin, respectively.

In the expanded wave functions, the ϕ_i are the Slater determinants which appear in the (a) configuration, the λ_i are Slater determinants which appear in

TABLE III. Slater determinants which occur in the expansion of the state wave functions.

$\phi_1=A_+\bar{B}_+A_-\bar{B}_-$	$\phi_2=A_+\bar{A}_+B_-\bar{B}_-$	$\phi_3=A_+\bar{B}_+B_-\bar{A}_-$	$\phi_4=A_+\bar{A}_+A_-\bar{B}_-$
$\phi_5=A_+\bar{A}_+B_-\bar{A}_-$	$\phi_6=A_+\bar{B}_+A_-\bar{A}_-$	$\phi_7=B_+\bar{A}_+A_-\bar{A}_-$	$\phi_8=A_+\bar{A}_+A_-\bar{A}_-$
$\lambda_1=A_+\bar{B}_+\bar{B}_-A_0$	$\lambda_2=A_+\bar{B}_+A_-\bar{B}_0$	$\lambda_3=A_+\bar{A}_+B_-\bar{B}_0$	$\lambda_4=A_+\bar{A}_+\bar{B}_-B_0$
$\lambda_5=A_+\bar{B}_+B_-\bar{A}_0$	$\lambda_6=A_+\bar{B}_+\bar{A}_-B_0$	$\lambda_7=A_+\bar{A}_+A_-\bar{B}_0$	$\lambda_8=A_+\bar{A}_+B_-\bar{A}_0$
$\lambda_9=A_+\bar{B}_+A_-\bar{A}_0$	$\lambda_{10}=B_+\bar{A}_+A_-\bar{A}_0$	$\lambda_{11}=A_+\bar{A}_+\bar{A}_-B_0$	$\lambda_{12}=A_+\bar{A}_+\bar{B}_-A_0$
$\lambda_{13}=A_+\bar{B}_+\bar{A}_-A_0$	$\lambda_{14}=B_+\bar{A}_+\bar{A}_-A_0$	$\lambda_{15}=A_+\bar{A}_+A_-\bar{A}_0$	$\lambda_{16}=A_+\bar{A}_+\bar{A}_-A_0$
$\xi_1=A_+\bar{B}_-A_0\bar{B}_0$	$\xi_2=\bar{A}_+B_-B_0\bar{A}_0$	$\xi_3=\bar{A}_+B_-A_0\bar{B}_0$	$\xi_4=A_+\bar{A}_-B_0\bar{B}_0$
$\xi_5=A_+\bar{B}_-B_0\bar{A}_0$	$\xi_6=\bar{A}_+A_-B_0\bar{B}_0$	$\xi_7=A_+\bar{A}_-A_0\bar{B}_0$	$\xi_8=A_+\bar{A}_-B_0\bar{A}_0$
$\xi_9=A_+\bar{B}_-A_0\bar{A}_0$	$\xi_{10}=B_+\bar{A}_-A_0\bar{A}_0$	$\xi_{11}=\bar{A}_+A_-A_0\bar{B}_0$	$\xi_{12}=\bar{A}_+A_-B_0\bar{A}_0$
$\xi_{13}=\bar{A}_+B_-A_0\bar{A}_0$	$\xi_{14}=\bar{B}_+A_-A_0\bar{A}_0$	$\xi_{15}=A_+\bar{A}_-A_0\bar{A}_0$	$\xi_{16}=\bar{A}_+A_-A_0\bar{A}_0$

the (b) configuration and the ξ_i are Slater determinants which appear in the (c) configuration. In addition the determinants $\bar{\phi}_i$, $\bar{\lambda}_i$, and $\bar{\xi}_i$ indicate the corresponding determinants ϕ_i, λ_i and ξ_i when A and B are interchanged.

With this convention about notation the state wave functions for the configurations (a), (b), and (c) are:

$$\Psi(^3\Pi_u, b) = a_1/\sqrt{2}[\lambda_1-\bar{\lambda}_1]+a_2/\sqrt{2}[-\lambda_2+\bar{\lambda}_2]$$
$$+a_3/2[-\lambda_3+\bar{\lambda}_3-\lambda_4+\bar{\lambda}_4]+a_4/2[\lambda_5-\bar{\lambda}_5-\lambda_6+\bar{\lambda}_6]$$
$$+a_5/4[-\lambda_7+\lambda_8+\lambda_9+\lambda_{10}+\bar{\lambda}_7-\bar{\lambda}_8-\bar{\lambda}_9-\bar{\lambda}_{10}-\lambda_{11}$$
$$+\lambda_{12}+\lambda_{13}+\lambda_{14}+\bar{\lambda}_{11}-\lambda_{12}-\bar{\lambda}_{13}-\bar{\lambda}_{14}]$$
$$+a_6/2[\lambda_{15}-\bar{\lambda}_{15}+\lambda_{16}-\bar{\lambda}_{16}], \quad (3.1a)$$

$$\Psi(^1\Pi_u, b) = b_1/\sqrt{2}[-\lambda_1+\bar{\lambda}_1]+b_2/\sqrt{2}[-\lambda_2+\bar{\lambda}_2]$$
$$+b_3/2[-\lambda_3+\bar{\lambda}_3+\lambda_4-\bar{\lambda}_4]+b_4/2[\lambda_5-\bar{\lambda}_5+\lambda_6-\bar{\lambda}_6]$$
$$+b_5/4[-\lambda_7+\lambda_8+\lambda_9+\lambda_{10}+\bar{\lambda}_7-\bar{\lambda}_8-\bar{\lambda}_9-\bar{\lambda}_{10}+\lambda_{11}$$
$$-\lambda_{12}-\lambda_{13}-\lambda_{14}-\bar{\lambda}_{11}+\bar{\lambda}_{12}+\bar{\lambda}_{13}+\bar{\lambda}_{14}]$$
$$+b_6/2[\lambda_{15}-\bar{\lambda}_{15}-\lambda_{16}+\bar{\lambda}_{16}], \quad (3.1b)$$

$$\Psi(^1\Sigma_g^+, a) = c_1/\sqrt{2}[\phi_1+\bar{\phi}_1]+c_2/\sqrt{2}[\phi_2+\bar{\phi}_2]$$
$$+c_3/\sqrt{2}[\phi_3+\bar{\phi}_3]$$
$$+c_4/2\sqrt{2}[\phi_4+\phi_5+\phi_6+\phi_7+\bar{\phi}_4+\bar{\phi}_5+\bar{\phi}_6+\bar{\phi}_7]$$
$$+c_5/\sqrt{2}[\phi_8+\bar{\phi}_8], \quad (3.1c)$$

$$\Psi(^3\Sigma_g^-, c) = d_1/\sqrt{2}[-\xi_1-\bar{\xi}_1]+d_2/\sqrt{2}[-\xi_2-\bar{\xi}_2]$$
$$+d_3/\sqrt{8}[-\xi_3-\bar{\xi}_3+\xi_4+\bar{\xi}_4-\xi_5-\bar{\xi}_5+\xi_6+\bar{\xi}_6]$$
$$+d_4/4[-\xi_7-\xi_8+\xi_9+\xi_{10}-\bar{\xi}_7-\bar{\xi}_8+\bar{\xi}_9+\bar{\xi}_{10}$$
$$-\xi_{11}-\xi_{12}+\xi_{13}+\xi_{14}-\bar{\xi}_{11}-\bar{\xi}_{12}+\bar{\xi}_{13}+\bar{\xi}_{14}]$$
$$+d_5/2[\xi_{15}+\bar{\xi}_{15}+\xi_{16}+\bar{\xi}_{16}],$$

$$\Psi(^1\Delta_g, c) = e_1/\sqrt{2}[-\xi_1-\bar{\xi}_1]+e_2/2[\xi_4-\bar{\xi}_4-\xi_5+\bar{\xi}_5]$$
$$+e_3/\sqrt{8}[-\xi_7-\bar{\xi}_8+\xi_9+\bar{\xi}_{10}-\bar{\xi}_7-\xi_8+\bar{\xi}_9+\xi_{10}]$$
$$+e_4/\sqrt{2}[\xi_{15}+\bar{\xi}_{15}], \quad (3.1d)$$

$$\Psi(^1\Sigma_g^+, c) = f_1/\sqrt{2}[-\xi_1-\bar{\xi}_1]+f_2/\sqrt{2}[\xi_2+\bar{\xi}_2]$$
$$+f_3/\sqrt{8}[\xi_3+\bar{\xi}_3+\xi_4+\bar{\xi}_4+\xi_5+\bar{\xi}_5-\xi_6-\bar{\xi}_6]$$
$$+f_4/4[-\xi_7-\xi_8+\xi_9+\xi_{10}-\bar{\xi}_7-\bar{\xi}_8+\bar{\xi}_9+\bar{\xi}_{10}+\xi_{11}$$
$$+\xi_{12}-\xi_{13}-\xi_{14}+\bar{\xi}_{11}+\bar{\xi}_{12}-\bar{\xi}_{13}-\bar{\xi}_{14}]$$
$$+d_5/2[\xi_{15}+\bar{\xi}_{15}-\xi_{16}-\bar{\xi}_{16}]. \quad (3.1e)$$

The dissociation products for the above component of the expanded wave functions are presented in Table IV, with the convention that the first set of dissociation products corresponds to the first component of the state in consideration, the second to the second, etc.

The rest of the calculation of the energy of an electronic state is carried on in the standard way. The one-center Coulomb integrals and the two-center Coulomb integrals are obtained as in the previous section. The one-center core integrals are obtained following Goeppert-Mayer and Sklar[22] or Parr and Crawford[23] among others. The two-center core integrals

$$\beta_\pi = \int 2p_\pi^* H_{core} 2p_\pi d\tau$$

and

$$\beta_\sigma = \int 2p_\sigma^* H_{core} 2p_\sigma d\tau$$

are obtained semiempirically by fitting the $^3\Pi_u(b)$ and the $^3\Sigma_g^-(c)$ states (these integrals appear in the secular equation as off-diagonal elements). The solution of the secular equation was performed on an IBM 701.

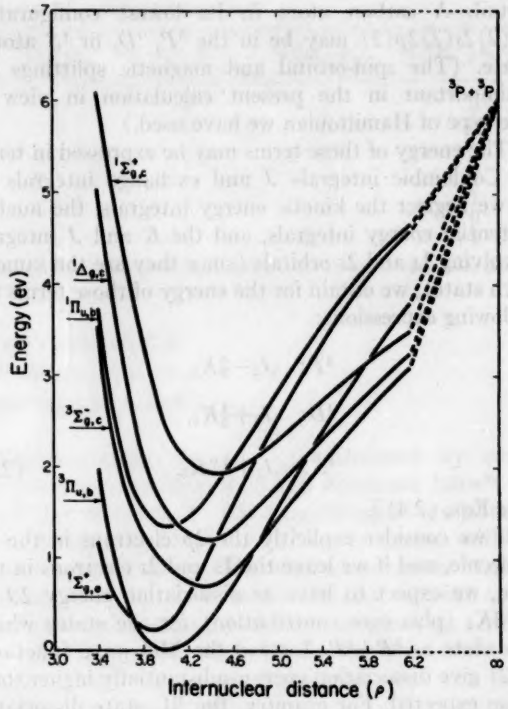

FIG. 2. Calculated energies for the lowest excited states of C_3 molecule.

The resulting energies for the electronic states at several internuclear distances are given in Table V. The coefficients for covalent, single ionic, and double ionic components are presented diagrammatically in Fig. 3.

The agreement for the calculated energies for the $^1\Pi_u(b)$ state is satisfactory indeed, when compared with Hicks' data. The three electronic states of configuration (c) are split by an amount which substantially confirms the previous predictions. The $^1\Sigma_g^+(a)$

[22] M. Goeppert-Mayer and A. L. Sklar, J. Chem. Phys. 6, 645 (1938).

TABLE IV. Dissociation products for the component wave functions of the C_2 electronic states.

$^3\Pi_u(b)$	$^1\Pi_u(b)$	$^1\Sigma_g^+(a)$	$^3\Sigma_g^-(c)$	$^1\Sigma_g^+(c)$	$^1\Delta_g(c)$
$^3P+^3P$	$^3P+^3P$	$^3P+^3P$	$^3P+^3P$	$^3P+^3P$	$^3P+^3P$
$^3P+^3P$	$^3P+^3P$	$^1D+^1D$	$^3P+^3P$	$^3P+^3P$	other covalent
$^3P+^1D$	$^1D+^1D$	$^1D+^1D$	other covalent	other covalent	single ionic
other covalent	other covalent	single ionic	single ionic	single ionic	double ionic
single ionic	single ionic	double ionic	double ionic	double ionic	
double ionic	double ionic				

TABLE V. Experimental and calculated energies for C_2 electronic states at different internuclear distances (ev).

	Internuclear distances ρ	3.4	4.2	4.6	5.4	6.2	∞
	Internuclear distances A	1.11	1.37	1.50	1.76	2.02	∞
$^3\Pi_u(b)$	Exptl.	1.99	0.09	0.67	2.39	3.79	6.04
	Calc.	(1.99)	(0.09)	(0.67)	(2.39)	(3.79)	(6.04)
$^1\Pi_u(b)$	Exptl.	3.76	1.44	2.02	3.52	4.53	6.04
	Calc.	3.75	1.45	2.04	3.54	4.66	6.04
$^1\Sigma_g^+(a)$	Exptl.	1.34	0.72	1.67	3.44	4.62	6.04
	Calc.	1.19	0.59	1.56	3.37	4.59	6.04
$^3\Sigma_g^-(c)$	Exptl.	4.20	0.74	0.83	2.01	3.03	6.04
	Calc.	(4.20)	(0.74)	(0.83)	(2.01)	(3.03)	(6.04)
$^1\Delta_g(c)$	Exptl.	...	...	...	...	...	...
	Calc.	5.05	1.27	1.27	2.31	3.21	6.04
$^1\Sigma_g^+(c)$	Exptl.	...	...	...	...	...	...
	Calc.	6.10	2.05	1.94	2.74	3.49	6.04

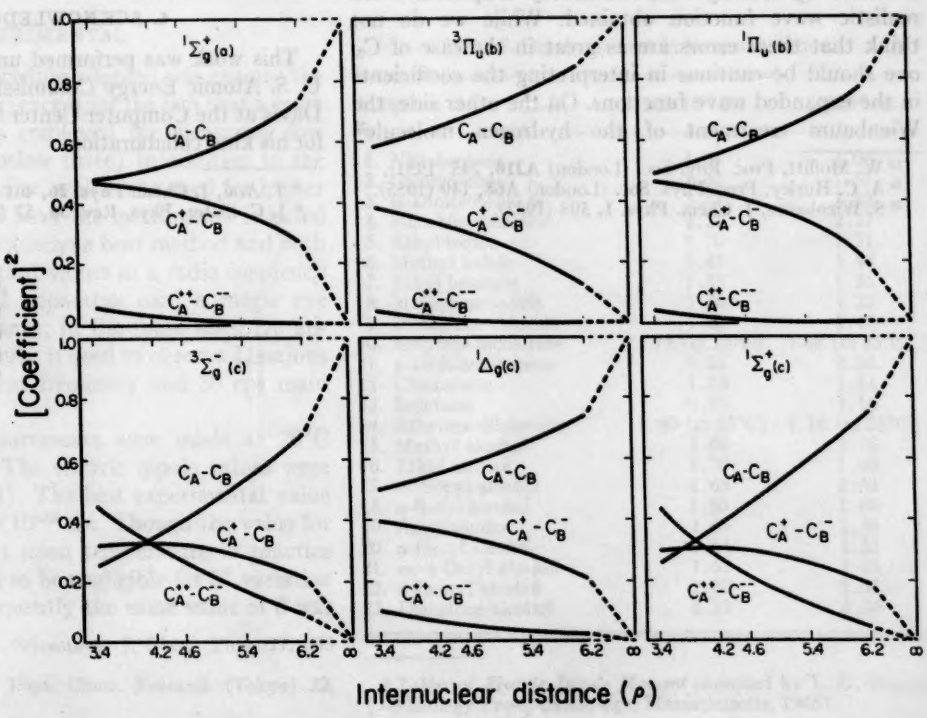

FIG. 3. Coefficients of the covalent, single ionic and double ionic structures for the lowest states of C_2 molecule, at different internuclear distances.

is also in satisfactory agreement with Hicks' data. (See, however, reference 12.)

Some critical comments are needed at this point to characterize the values obtained for the energies as well as the coefficients of the wave functions. The eigenvalues and eigenvectors are chiefly dependent on the assumptions regarding the core and the effective Z for the valence electrons.

The core integrals are here assumed to be the same for covalent and ionic structures. This assumption is quite a crude one, because it is clear that the valence electrons are correlated to the core electrons in addition to the correlation among themselves. Now, this correlation is expected to be different in covalent and ionic structure. (Such effect was taken into account by Parks in its formaldehyde calculation.[28]) The other problem directly related to polarization effects is the choice of the effective charge Z. The value adopted in this work is 3.25 for all the components (covalent and ionic) of the expanded wave function. Let us consider this point in some detail.

On the one side we know that the method of Moffitt[33] of "atoms in molecules" gives unsatisfactory results, if one disregards the difference in effective charges. This is clearly exemplified by the atoms in molecules calculation for H_2, made by Hurley.[34] The use of a common screening constant led to a completely ionic structure H^+-H^- for the equilibrium nuclear distances, with no contribution from covalent structure. This was due to a gross overestimate of the interaction between ions. It is interesting to note that the energy values obtained by Hurley are satisfactory despite the unrealistic wave function obtained. While we do not think that these errors are as great in the case of C_2, one should be cautious in interpreting the coefficients in the expanded wave functions. On the other side, the Wienbaum treatment of the hydrogen molecule[35] shows that one obtains the best results when the effective charges of both the neutral and ionic structure of H_2 are set equal to 1.193 instead of 1 for the isolated H atom and 0.687 for the H^- ion. The advantages of the use of common effective charges were recently stressed also by Arai[36] in his method of deformed atoms in molecules. Our choice of an effective charge Z of 3.25, following Slater's results[37] is certainly crude. In fact, the variational values for the effective charge Z for the $2p$ electrons in the ^3P, ^1D, and ^1S atomic states are 3.137, 3.072, and 2.974, respectively.[26] On the contrary, those effective Z values for the carbon atom lose their reliability when two atoms interact in the formation of the C_2 molecule. For this reason, we feel that the use of the 3.25 value is about as good as any manipulation of the preceding variational effective Z values. In addition, the use of empirical parameters should take care of the deformation of the atom in the molecule without making it necessary to introduce this correction explicitly.

In conclusion, we recognize the need of a more refined calculation with differentiation in the effective charges and explicit introduction of polarization corrections. On the other hand, the use of semiempirical parameters should take care in substantial degree of the crude approximations made. In addition, the present existence of experimental uncertainty for the dissociation energies and singlet-triplet splitting, make a more refined treatment of the C_2 molecule not very justified at this point because the semiempirical parameters cannot be evaluated accurately.

[33] W. Moffitt, Proc. Roy. Soc. (London) **A210**, 245 (1951).
[34] A. C. Hurley, Proc. Phys. Soc. (London) **A68**, 149 (1955).
[35] S. Wienbaum, J. Chem. Phys. **1**, 593 (1933).

4. ACKNOWLEDGMENTS

This work was performed under the auspices of the U. S. Atomic Energy Commission. We thank Mr. Lou Davis at the Computer Center in the Berkeley Campus for his kind collaboration.

[36] T. Arai, J. Chem. Phys. **26**, 431 (1957).
[37] J. C. Slater, Phys. Rev. **36**, 57 (1930).

Experimental and Theoretical Aspects of Higasi's Equation for a Quick Determination of Electric Dipole Moment in Solution

BAL KRISHNA AND K. K. SRIVASTAVA

Laboratory of Physical Chemistry, University of Allahabad, Allahabad, India

(Received March 23, 1959)

In the present investigation the authors have determined the electric dipole values for twenty-three organic solutes according to Higasi's method. Except for two substances, *viz.*, iodoform and ethylene dibromide, the dipole values so obtained agree fairly well with those obtained by usual methods. A reassessment of Higasi's equation has been made on theoretical grounds and a more general equation has been obtained.

INTRODUCTION

IN a previous publication[1] the authors have discussed the range of validity of Higasi's equation[2] for a quick determination of electric dipole moment in solution. The dipole values were calculated from the equation

$$\mu=\beta(d\epsilon_{12}/df_2)^{\frac{1}{2}}, \qquad (1)$$

where μ represents the electric dipole moment of the solute molecule dissolved in a nonpolar solvent, β is a constant, and $(d\epsilon_{12}/df_2)$ denotes the initial slope of the curve obtained on plotting ϵ_{12}, the dielectric values of the solution, against f_2, the mole fraction of the solute. Of the six organic solutes examined, two substances, *viz.*, ethylene dichloride and ethylene dibromide, gave anomalous results. All these results were rechecked and in addition, seventeen other organic solutes dissolved in benzene were examined to test the general applicability of Eq. (1).

EXPERIMENTAL

The experimental procedure adopted was exactly the same as described earlier[2] except for the fact that a more precise instrument was employed for measuring low dielectric values (i.e., below three) in addition to the apparatus employed earlier, which was used for higher ranges. The working of both the instruments is based upon the principle of heterodyne beat method and both measure dielectric constant values at a radio frequency of 10^6 cps. The original apparatus used a magic eye tube to indicate resonance; in the more sensitive apparatus a cathode ray tube is used to observe Lissajous figures produced by beat frequency and 50 cps main frequency.

Some of these measurements were made at 20°C while others at 25°C. The electric dipole values were calculated from Eq. (1). The best experimental value for β at 20°C is 0.282×10^{-18} esu. Though the value for β is slightly dependent upon temperature in practice this difference is found to be negligible for 5° variation in temperature. Consequently the same value of β was employed for both the temperatures. The results obtained are recorded in Table I where μ_H represents the value of electric dipole moment calculated according to Eq. (1) while μ_S is the value taken from standard tables[3] for the solute molecule dissolved in benzene.

In addition to the measurement of dielectric constant an accurate determination of density of solutions was also carried out. These were required for theoretical discussion. A special pycnometer was devised which consists of a thin Pyrex bulb (about 20 ml capacity) the neck of which consists of two uniform and calibrated capillaries (about 0.5 mm in diameter). Special precautions were taken to maintain the temperature at a constant value during density measurements.

An examination of Table I shows that with the exception of ethylene dibromide and iodoform the values for μ_H agree fairly well with those for μ_S, more so because the values for μ_S reported by different

TABLE I. Dipole moment in benzene solution.

Substance	$\mu_s\times10^{18}$ esu	$\mu_H\times10^{18}$ esu
1. Nitrobenzene	4.05	4.06
2. Chlorobenzene	1.57	1.57
3. *m*-Dinitrobenzene	3.81	3.82
4. *o*-Dichlorobenzene	2.26	2.27
5. Ethyl iodide	1.70	1.71
6. Methyl iodide	1.41	1.43
7. Ethyl bromide	1.88	1.85
8. Methylene iodide	1.10	1.22
9. Methylene chloride	1.50	1.47
10. Ethylene dichloride	1.75 (at 25°C)	1.68 (at 25°C)
11. *p*-Dichlorobenzene	0.23	0.36
12. Chloroform	1.10	1.11
13. Iodoform	0.99	1.16
14. Ethylene dibromide	1.40 (at 25°C)	1.16 (at 25°C)
15. Methyl alcohol	1.69	1.78
16. Ethyl alcohol	1.70	1.68
17. *n*-Propyl alcohol	1.65	1.63
18. *n*-Butyl alcohol	1.66	1.60
19. Amyl alcohol	1.65	1.59
20. *n*-Hexyl alcohol	1.64	1.55
21. *sec-n*-Octyl alcohol	1.62	1.65
22. *n*-Lauryl alcohol	1.62	1.52
23. Diacetone alcohol	3.35	3.24

[1] B. Krishna and K. K. Srivastava, J. Chem. Phys. **27**, 835 (1957).

[2] K. Higasi, Bull. Inst. Phys. Chem. Research (Tokyo) **22**, 805 (1943).

[3] *Tables of Electric Dipole Moment* compiled by L. G. Wessen (Technology Press, Cambridge, Massachusetts, 1948).

TABLE II. Magnitude of $(L+R)$.

Substance	$(d\epsilon_{12}/df_2)\cdot[3/\rho_1(\epsilon_1+2)^2]$	L	R	$(L+R)$
Ethyl iodide	0.8097	0.3400	−0.3399	+0.0001
Ethyl bromide	0.9421	0.1866	−0.2090	−0.0224
Ethylene dichloride	0.7768	0.1121	−0.1523	−0.0402
Methyl iodide	0.5633	0.3688	−0.3459	+0.0229
Chloroform	0.3400	0.2084	−0.2296	−0.0212
Methylene iodide	0.4040	0.8145	−0.7213	+0.0932
Methylene chloride	0.5949	0.1121	−0.2287	−0.1166
Iodoform	0.3733	1.2920	−1.1110	+0.1810
Ethylene dibromide	0.3730	0.8919	−0.4577	+0.4442

authors[3] show quite significant differences in the second decimal place. The value for diacetone alcohol was not available in the literature. This was determined by us according to the method of Halverstadt and Kumler.[4]

It was reported earlier[1] that in case of ethylene dichloride along with ethylene dibromide the agreement between μ_H and μ_S was not good. From Table I we find, however, that in case of ethylene dichloride at least the difference between μ_H and μ_S is not more than four percent. Consequently the suggestion made earlier, *viz.*, that Eq. (1) is not applicable to molecules subject to restricted rotation, is not valid.

DISCUSSION

Higasi[2] has given a simple proof for his equation but many assumptions are involved which can not be justified in each case where Eq. (1) gives correct dipole values. The following derivation more clearly brings forth the exact nature of the approximations involved.

For one gram of a solution of a polar solute in a nonpolar solvent, the Debye equation can be written in the form

$$[(\epsilon_{12}-1)/(\epsilon_{12}+2)]\cdot(1/\rho_{12})=(1-\omega_2)p_1+w_2p_2, \qquad (2)$$

where ρ_{12} represents the density of the solution, ω_2 refers to the weight fraction of the solute, while p_1 and p_2 are specific dielectric polarizations of solvent and solute respectively. Let Y and Z represent the left- and right-hand sides of Eq. (2). On differentiating Y with respect to ω_2 one obtains for infinite dilution

$$dY/d\omega_2=\{(d\epsilon_{12}/d\omega_2)\cdot[3/\rho_1(\epsilon_1+2)^2]\}-\{(d\rho_{12}/d\omega_2)\cdot[(\epsilon_1-1)/\rho_1^2(\epsilon_1+2)]\}. \qquad (3)$$

Similarly differentiating Z with respect to ω_2 and noting the fact that in case of nonpolar solvent p_1 represents the specific electronic polarization of the solvent while p_2 represents the sum of electronic and orientation polarizations of the solute, one obtains at infinite dilution

$$dZ/d\omega_2=(1/\rho_2)\cdot[(n_2^2-1)/(n_2^2+2)]-\{(1/\rho_1)\cdot[(\epsilon_1-1)/(\epsilon_1+2)]\}+0p_{2\infty}, \qquad (4)$$

[4] I. F. Halverstadt and W. O. Kumler, J. Am. Chem. Soc. **64**, 2988 (1942).

where n_2 represents the refractive index of the solute extrapolated to infinite wave length. Here $0p_{2\infty}$ represents the specific electronic polarization of the solute at infinite dilution. By comparing Eqs. (3) and (4) and changing over to mole fraction instead of weight fraction, we obtain

$$\{(d\epsilon_{12}/df_2)\cdot[3/\rho_1(\epsilon_1+2)^2]\}-\{(d\rho_{12}/df_2)\cdot(1/\rho_1^2)\cdot[(\epsilon_1-1)/(\epsilon_1+2)]\}=\frac{M_2}{M_1}\left\{\left[\frac{(n_2^2-1)}{(n_2^2+2)}\cdot\frac{1}{\rho_2}\right]-\left[\frac{(\epsilon_1-1)}{(\epsilon_1+2)}\cdot\frac{1}{\rho_1}\right]+0p_{2\infty}\right\}, \qquad (5)$$

where M_2 and M_1 represent the molecular weights of solute and solvent, respectively. Here $0p_{2\infty}$ is defined by

$$0p_{2\infty}=4\pi N\mu^2/9kTM_2, \qquad (6)$$

where k is the Boltzmann constant and N is the Avogadro number. From Eqs. (5) and (6) we obtain

$$\mu=\left[\frac{9kTM_1}{4\pi N}\left\{\left[\frac{d\epsilon_{12}}{df_2}\cdot\frac{3}{\rho_1(\epsilon_1+2)^2}\right]-(L+R)\right\}\right]^{\frac{1}{2}}, \qquad (7)$$

where L and R are given by

$$L=(d\rho_{12}/df_2)\cdot[(\epsilon_1-1)/\rho_1^2(\epsilon_1+2)], \qquad (8)$$

and

$$R=\frac{M_2}{M_1}\left\{\left(\frac{(n_2^2-1)}{(n_2^2+2)}\frac{1}{\rho_2}\right)-\left(\frac{(\epsilon_1-1)}{(\epsilon_1+2)}\cdot\frac{1}{\rho_1}\right)\right\}. \qquad (9)$$

If L and R are individually equal to zero or if their magnitudes are equal and opposite in sign, the quantity $(L+R)$ will be equal to zero. In such cases Eq. (7) reduces to Eq. (1) where β will be given by

$$\beta=[1/2(\epsilon_1+2)]\cdot(27kTM_1/\pi N\rho_1)^{\frac{1}{2}}. \qquad (10)$$

The values of L and R will be separately equal to zero if the magnitude of $(d\epsilon_{12}/df_2)$ is large as compared to that of $(d\rho_{12}/df_2)$ and if the electronic polarization of the solute is approximately equal to that of the solvent.[2] Where these approximations are not valid, the value of L is approximately equal to that of R and opposite in sign (see Table II) so that the sum $(L+R)$ approximates to zero.

A perusal of Table II shows that, with the exception of iodoform and ethylene dibromide the quantity $L+R)$ is negligible as compared to

$$(d\epsilon_{12}/df_2)[3/\rho_1(\epsilon_1+2)^2].$$

This fortuitous circumstance greatly enhances the generality of Eq. (1).

The authors are indebted to the Government of Uttar Pradesh for financing this project.

Dielectric Relaxation of Dilute Solutions in the Millimeter Wave Region*

JÜRGEN SCHNEIDER†

Department of Physics, Duke University, Durham, North Carolina

(Received August 17, 1959)

The dielectric losses of benzophenone, diphenylether, diphenylamine, chlorobenzene, and aniline, measured at 12.33, 6.19, 3.08, and 2.47 mm wavelength in dilute benzene solutions, have been found to fit Debye type relaxation curves within the limits of experimental error. The distinctly lower relaxation time of diphenylether and of diphenylamine, compared to the one for benzophenone, can be explained by a high internal mobility of the phenyl rings in these two molecules. Similarly, the mobility of the amino group in aniline results in a decrease of the relaxation time, compared to the rigid chlorobenzene molecule.

INTRODUCTION

THE occurence of internal mobilities in a dipolar molecule may result in a dielectric relaxation time which is considerably shorter than the one for a rigid molecule of comparable molecular dimensions. A striking example of this effect is the unusually short relaxation time of diphenylether and of diphenylamine, first reported by Fischer.[1,2] To obtain the relaxation curves of these molecules, it was necessary to extend dielectric loss measurements into the shorter millimeter wave region.

APPARATUS

Since absolute absorption measurements become increasingly difficult in the shorter mm region, mainly due to the small size of the waveguide components, we have performed only relative measurements of the dielectric loss ϵ'' and calibrated the data by means of standard substances. Benzophenone and chlorobenzene are suitable for this procedure.

A. Reflection Method

At wavelengths of 12 and 6 mm, dielectric losses were measured by means of a reflection method. A schematic diagram of the apparatus is given in Fig. 1. Microwave power was generated by a 2K33 *K*-band klystron and fed into a frequency multiplier M. After passing a crystal detector D and a tapered transition section T, the wave entered the absorption cell C, a vertical section of *K*-band waveguide shorted at the bottom by a metal plate. The height of the liquid in the cell could be changed with an accuracy of at least 1/1000 mm by immersing a micrometer plunger P into a second vessel, V, connected to the cell. The micrometer vessel and the cell were surrounded by a thermostat jacket, which kept the temperature constant within 1/10°C. The detector signal, modulated by applying a 200 cps audio voltage to the klystron reflector, was fed into a sensitive amplifier (gain 100 000) and measured with a vacuum tube voltmeter.

As the height of the liquid in the cell is changed, the detector voltage passes through maxima and sharp minima, similar to a standing wave pattern. When a dipolar substance is added to the nonpolar solvent, both the real and the imaginary part of the dielectric constant of the liquid are increased, and this results in a shift and in a broadening of the nodes in the standing wave pattern. For sufficiently low losses, the position of the node is only dependent on the real part, and its width only on the imaginary part of the dielectric constant. Thus, the complex dielectric constant can be determined by measuring the width and position of a node, as a function of the height of the liquid. Compared with the usual method, in which the height of the dielectric material is kept constant and the detector is moved along the waveguide to measure the shape of the standing wave, the above method has the advantage of great simplicity, since no complicated driving device for the detector probe is required.[3] To obtain a quantity proportional to the loss of the dipole substance, the node width obtained for the pure solvent was subtracted from that for the solution, and this difference was found to vary linearly with the concentration. In this work, only the imaginary part ϵ'' of the dielectric constant has been measured.

Microwave power for measurements at 6-mm wavelength was produced by a crossed multiplier, containing a slotted 1*N*26 crystal. A crystal of this type was also used for detection. At 12-mm wavelength the fundamental power of the klystron was used.

B. Transmission Method

At higher frequencies, where the microwave power available is comparatively small and unstable, the reflection method becomes inaccurate. Therefore, a transmission method was used to measure the dielectric loss at 3 and 2.5 mm wavelength. The absorption cell was a piece of *K*-band waveguide, closed at its ends by

* This research was supported by the United States Air Force through the Air Force Office of Scientific Research of the Air Research and Development Command. Reproduction in whole or in part is permitted for any purpose of the United States Government.

† Present address: Institut für Elektrowerkstoffe, Freiburg-Br., Hebelstr. 38, Germany.

[1] E. Fischer, Z. Naturforsch. **4a**, 707 (1949).

[2] E. Fischer, Naturwissenschaften **43**, 153 (1956).

[3] J. Schneider, Diplomarbeit, Freiburg-Br. (unpublished, 1955).

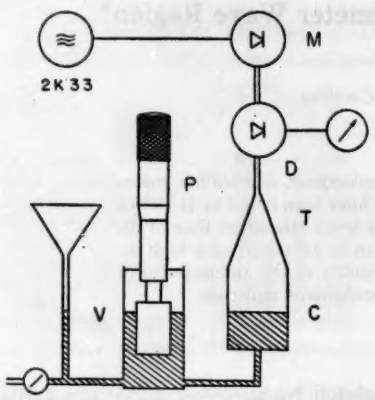

FIG. 1. Schematic diagram of the reflection arrangement.

two Teflon windows, and was located between a multiplier and a detector, of the type described by King and Gordy.[4] Two cells of length 181 and 55 mm were used for measurements at 3 and 2.5 mm wavelength, respectively. The attenuation, in db, of the microwave was found to vary linearly with the concentration of the solutions.

The measurements at 3 mm wavelength were carried out with a detector which responded to the fourth and all higher harmonics of the klystron. To eliminate these higher harmonics, whose intensity was not negligibly small, a 120-cm long absorption cell filled with OCS gas was introduced between the multiplier and the liquid cell. The 0→1 rotational transition of this linear molecule has a frequency of 12.163 kMc/sec. Owing to centrifugal distortion effects, the higher rotational transitions do not occur at exactly integral multiples of the fundamental frequency.[5] Therefore, when the detector output was displayed on an oscilloscope, a whole spectrum of absorption lines appeared, each one representing the intensity of a particular harmonic, generated by the multiplier. For instance, the fourth harmonic of the 2K33 klystron at 97 kMc/sec was represented by the 7→8 transition of the OCS molecule. By proper adjustment of the detector and multiplier tuning plungers, it was possible to cancel out almost completely all harmonics above the fourth. In a similar way, the measurements at 2.5 mm wavelength were carried out with a fifth harmonic detector.

For rough absorption measurements, it is also possible to take the intensity decrease of the rotational lines as a direct measure of the attenuation of the harmonics in an absorbing medium, located between the gas cell and the detector. By this method, absorption measurements at many frequencies can be carried out simultaneously.

TABLE I. Dielectric loss relative to benzophenone.

Wavelength (mm)	12.33	6.19	3.08	2.47
Frequency (kMc/sec)	24.32	48.46	97.30	121.65
benzophenone[a]	1.000	1.000	1.000	1.000
diphenylether[b]	0.173	0.348	0.473	0.510
diphenylamine[c]	0.117	0.174	0.196	0.221
chlorobenzene[d]	0.426	0.483	0.545	0.575
aniline[e]	0.302	0.473	0.573	0.642

[a] Melting point 48°C.
[b] Melting point 28°C.
[c] Melting point 53°C.
[d] Boiling point 132.5°C.
[e] Boiling point 182°C.

[4] W. C. King and W. Gordy, Phys. Rev. **93**, 407 (1954).
[5] Gordy, Smith, and Trambarulo, *Microwave Spectroscopy* (John Wiley & Sons, Inc., New York, 1953), p. 93.

TABLE II. Dielectric relaxation times τ, increments a_0-a_∞ and dipole moments μ at 25°C.

	τ (10^{-11} sec)	a_0-a_∞	μ[a] (Debye)
benzophenone	1.85	12.9	2.95
diphenylether	0.41	1.58	1.04
diphenylamine	0.60	0.96	0.81
chlorobenzene	0.91	3.52	1.55
aniline	0.54	2.48	1.30
benzophenone[b]	1.87	12.1	2.91
chlorobenzene[b]	0.95	3.30	1.50
diphenylether[c]	0.37	2.06	1.20

[a] Calculated from Eq. (3).
[b] Values obtained by Bergmann, see reference 7.
[c] Values obtained by Maier, see reference 8.

RESULTS

Benzophenone, diphenylether, diphenylamine, chlorobenzene, and aniline have been measured in dilute benzene solutions at 12.33 and 6.19 mm by the reflection method and at 3.08 and 2.47 mm by the transmission method. The temperature was 25±0.1°C. The molar fraction m of the solutions ranged from about 0.001 to 0.01. The dielectric losses of these substances, represented by quantities proportional to ϵ''/m, are listed in Table I. The values for benzophenone have been taken equal to unity for all wavelengths, since this molecule has been used to calibrate the dielectric losses of the other substances on an absolute

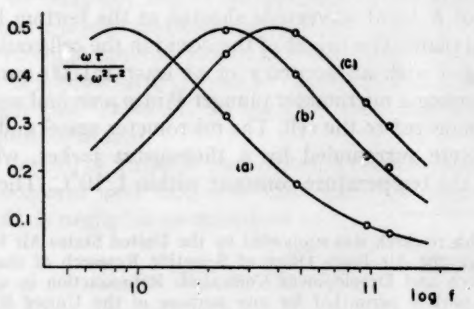

FIG. 2. Dielectric losses, in normalized units, of benzophenone (a), diphenylamine (b), and diphenylether (c) measured in dilute benzene solutions at 25°C. The solid lines are Debye curves, calculated from the values given in Table II.

scale. The experimental error is about 1 to 2% for the measurements at 12.33 and 6.19 mm and 2 to 4% for those at 3.08 and 2.47 mm.

DISCUSSION

The dielectric loss of a Debye-type relaxation process, characterized by a single relaxation time τ, is represented by the formula

$$\epsilon''=m(a_0-a_\infty)[\omega\tau/(1+\omega^2\tau^2)] \qquad (1)$$

where m is the molar fraction of the solution and ω the circular frequency of the electric field. The quantity ma_0 is the static dielectric constant and ma_∞ that at very high frequencies, usually the far infrared, where only the electronic and the atomic polarizability contribute to the total polarization. Rigid molecules whose structure deviates not too much from a spherical shape, are usually found to be in fair agreement with Eq. (1). Therefore, it can be expected that this is also true for the two calibration substances measured in this work, benzophenone and chlorobenzene.

The conversion of the relative values of the dielectric loss, as given by Table I, to absolute units was done in the following way: Assuming benzophenone and chlorobenzene to be in agreement with Eq. (1), a value for the relaxation time τ was chosen for benzophenone, so that the dielectric loss of chlorobenzene, now calibrated by that of benzophenone, also gave a good fit to a Debye curve. In this way, the values 1.85×10^{-11} sec and 0.91×10^{-11} sec were obtained for the relaxation times of benzophenone and chlorobenzene, respectively. In general, this method is only applicable, if the relaxation times of the two calibration substances differ sufficiently, as in the above case.

The dielectric increment a_0-a_∞ is related to μ, the dipole moment in solution, by

$$a_0-a_\infty=(4\pi/27kT)(L/M)\rho(\epsilon+2)^2\mu^2, \qquad (2)$$

where k is Boltzmann's constant, T the absolute temperature, L Avogadro's number, and ρ, ϵ, M are, respectively, the density, dielectric constant, and molecular weight of the solvent. For benzene solutions at 25°C, this equation becomes

$$a_0-a_\infty=1.469\mu^2, \qquad (3)$$

where μ is measured in debyes. The dipole moment of benzophenone is 2.95 debye,[6] this gives $a_0-a_\infty=12.9$. The dielectric losses of diphenylether, diphenylamine, and aniline, now calibrated by that of benzophenone, were found to be also in fair agreement with the assumption of a single relaxation time, see Table II.

The dispersion of the dielectric losses of these substances, in normalized units $\omega\tau/1+\omega^2\tau^2$ is shown in Figs. 2 and 3 as a function of the logarithm of the frequency f. The values for μ and τ are in fair agreement with those obtained by Bergmann[7] from ϵ' and ϵ'' measurements at 1, 3, and 14 cm wavelength and at 22°C. Measurements of the dielectric relaxation of diphenylether in dilute benzene solutions and at cm wavelengths have been recently reported by Maier.[8] His data also confirm the assumption of a single relaxation time, which is in rough agreement with the value given in Table II. However, his value for the dipole moment differs considerably from the one obtained in this work.

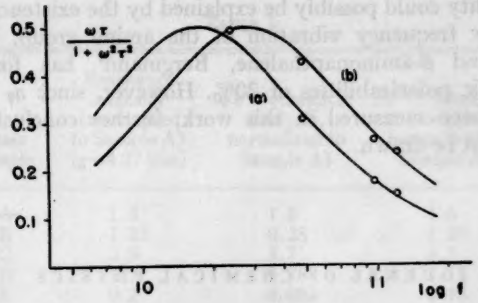

FIG. 3. Dielectric losses, in normalized units, of chlorobenzene (a) and aniline (b) measured in dilute benzene solutions at 25°C. The solid lines are Debye curves, calculated from the values given in Table II.

To explain the unusually short relaxation time of diphenylether, Maier[8] has proposed the following explanation: The whole dipole moment of this molecule can be reversed in direction by an internal motion around the molecular axis of greatest length. During this motion, the orientation of the two phenyl rings changes by considerably less than 180°, so that the orientation of the dipole moment will be associated with a relaxation time much shorter than that for a rigid molecule of comparable molecular dimensions. The same effect may be expected to occur in diphenylamine. In contrast, the longer relaxation time of benzophenone indicates a strong ridigity of the phenyl rings, probably due to conjugation between the rings and the CO double bond.

An internal mobility of the amino group in aniline is revealed by the distinctly shorter relaxation time, compared to chlorobenzene, a rigid molecule of similar dimensions. The same effect has been reported by Maier[8] for anisole, due to the mobility of the methoxy group. The dipole moment of aniline, 1.30 debye, as determined in this work, is considerably lower than that reported in the literature,[6] 1.52 debye. The latter was obtained from a static measurement of a_0 in benzene solution, with the assumption that the atomic polarizability does not exceed the electronic polarizability by much more than 10%. If, however, the atomic polarizability were unusually large, the dipole moment obtained by this method would be too high. A large atomic polar-

[6] L. G. Wesson, *Tables of Electric Dipole Moments* (Technology Press, Cambridge, Massachusetts, 1948).

[7] K. Bergmann, Dissertation, Freiburg-Br. (unpublished, 1957).

[8] W. Maier, Arch. Sci. (Geneva) **12**, 20 (1959).

izability could possibly be explained by the existence of a low frequency vibration of the amino group. For α- and β-aminonapthalene, Bergmann[7] has found atomic polarizabilities of 20%. However, since a_0 has not been measured in this work, further conclusions cannot be drawn.

ACKNOWLEDGMENTS

Thanks are due to Dr. Walter Gordy for his interest and for generously making equipment available. The author also wishes to thank Dr. D. W. Ovenall for reading the manuscript and Dr. M. J. Cowan for his assistance in some parts of the experimental work.

THE JOURNAL OF CHEMICAL PHYSICS VOLUME 32, NUMBER 3 MARCH, 1960

Note on the Paramagnetic Resonance of Iron in Glass*

THEODORE CASTNER, JR.,† GEORGE S. NEWELL,‡ W. C. HOLTON, AND C. P. SLICHTER§

Department of Physics, University of Illinois, Urbana, Illinois

(Received October 27, 1959)

Fe^{+++} and Fe^{++} ions in glass have been studied by means of paramagnetic resonance. The correlation of the Fe^{+++} concentration with an intense resonance at $g=4.27$ shows the resonance is due to Fe^{+++}. A theory is proposed explaining the observed g value and the implications for the atomic surroundings of Fe^{+++} are discussed. It is also proposed that the $g=6$ resonance observed in glass by Sands is due to Fe^{+++}.

I. INTRODUCTION

THE striking success of electron spin resonance in determining the structure of numerous paramagnetic centers leads one to wonder whether it could not be applied to the study of the structure of glasses. A pioneering resonance study of glasses has been reported by Sands.[1] In the course of his work, he discovered resonances of unknown origin. They could be characterized by giving their apparent g values, the g value being defined by

$$g\beta H = h\nu, \tag{1}$$

where β is the Bohr magneton, h is Planck's constant, and H is the static magnitic field for resonance in an applied alternating field of frequency ν. For a free electron spin, $g=2$. With ions such as copper, surrounding atoms "quench" the orbital angular momentum, giving one in a first approximation a free spin, but the spin-orbit coupling induces sufficient orbital moment to increase g by 10 to 20% above the spin-only value 2. Sands' "unknown" resonances had $g=4.2$ and $g=6$.

In cooperation with Dr. Scott Anderson of the Anderson Physical Laboratory who was interested in checking an optical method for determining the iron content of glasses, we have studied five samples of plate glasses containing differing amounts of Fe^{++} and Fe^{+++} ions, all other paramagnetic ingredients being present in much smaller amounts. In this paper we report our results. The ultimate objective of such a study would be to determine the detailed atomic surroundings of iron in both states of ionization. For example, is Fe^{+++} a so-called network former (i.e., does it occupy sites similar to a silicon) or is it a network modifier, like sodium? In practice one hopes to determine the parameters of what is called the spin Hamiltonian which describes the coupling of the spin to its surroundings, i.e., the extent to which the spin is not free. Although one can determine the spin Hamiltonian uniquely from knowledge of the atomic surroundings, the converse is not true. But from the spin Hamiltonian one can learn a great deal about the symmetry of the surroundings and can often test possible atomic models.

In Sec. II we describe our experimental results (which lead to the conclusion that the $g=4.2$ resonance comes from Fe^{+++} ions). In Sec. III we propose a spin Hamiltonian which gives the observed g value, and comment on the implications concerning the atomic surroundings. We also propose an explanation of the $g=6$ line, which we believe also results from Fe^{+++}. It is apparent that much work needs to be done involving studies of a variety of glasses, and it is our hope that this paper will stimulate such work.

II. EXPERIMENTAL RESULTS

The resonance studies were on five different samples. Their basic composition was identical (by weight 71% SiO_2, 13% Na_2O, 12% CaO, 4% other) but they differed in the relative concentrations of Fe^{++} and Fe^{+++}. The total iron was in all samples about 0.1%

* This research was supported in part by a grant from the Alfred P. Sloan Foundation.

† Now at the General Electric Research Laboratory, Schenectady, New York.

‡ Now at the Department of Physics, Purdue University, Lafayette, Indiana.

§ Alfred P. Sloan Fellow.

[1] R. H. Sands, Phys. Rev. 99, 1222 (1955).

by weight (in terms of Fe_2O_3). Runs were made at room temperature using an X-band "double bolometer" spectrometer. One sample was run at various temperatures in the liquid nitrogen-liquid helium range using an X-band superheterodyne spectrometer.

The Fe^{++} ion has an integral spin. In ordinary paramagnetic salts its resonance is not seen at room temperature, and sometimes not even in the liquid helium region. (The reasons are that the crystalline electric fields may split the spin states by too large an amount to be observed, or that the spin-lattice relaxation may be so short that the resonance becomes broad and correspondingly weak.) As with the salts[2] we did not anticipate a resonance from Fe^{++} at room temperature.

Since Fe^{+++} has zero orbital angular momentum in the free atom, we expected a line at the free-spin value $g=2$, with perhaps some crystalline splittings observable (perhaps as a broadening of the line) as is usually observed in paramagnetic salts containing Fe^{+++}.[2]

Instead we found a broad smear extending from $g\cong 10$ at low fields to above $g=1$ at high fields, with an intense and sharp resonance (60 gauss between peaks of the derivatives) at $g=4.27$. Except for intensity, the sharp resonance was identical in all five glass samples.

The intensities of the resonances were measured by comparing the amplitude of the derivative signals since the resonances were otherwise identical. An absolute intensity measurement was also made by integrating a derivative curve twice and comparing with a resonance of copper sulfate.

In Table I we list the relative intensity of the $g=4.27$ resonance (normalized to equal sample size) together with the relative concentration of Fe^{++} and Fe^{+++}. The correlation of the resonance intensity with the Fe^{+++} concentration indicates that

(1) The resonance arises from Fe^{+++}; (2) although Fe^{+++} might occupy several types of sites only some of which would contribute to a resonance at $g=4.27$, the fraction of Fe^{+++} in the sample contributing to the resonance is identical in all five samples (we shall discuss this point further in Sec. III);

(3) as far as the resonance can detect, the Fe^{+++} has the same sort of surroundings in all five samples.

If points 2 and 3 were not substantially true, we would not observe the excellent correlation of intensity with Fe^{+++} concentration even though the resonance were due to Fe^{+++} ions.

We therefore conclude that the glass resonance at $g=4.2$ is due to Fe^{+++} ions. As we shall discuss in Sec. III, we believe that $g=6$ resonance is also due to Fe^{+++} ions, the surroundings of which differ from those of the Fe^{+++} in our samples.

[2] See, for example, D. J. E. Ingram, *Spectroscopy at Radio and Microwave Frequencies* (Butterworths Scientific Publications, London, 1955), p. 169.

TABLE I.

Glass sample	Resonance intensity (normalized to Sample A) ($g=4.27$ line)	Fe^{++} (chemical analysis, normalized to Sample A)	Fe^{+++} (chemical analysis, normalized to Sample A)
A	1.0	1.0	1.0
B	1.25	0.28	1.29
C	3.8	3.7	3.7
D	1.5	0.78	1.18
E	0.2	0.083	0.18

III. THEORETICAL

The results of Sec. II appear to be rather clearly established on the basis of the intensity correlations, independently of any postulate as to the cause of a $g=4.27$ resonance. In Sec. III we shall make some theoretical speculations. We are at least able to propose theoretical models giving rise to the observed g values, and suggesting possible local atomic surroundings of the iron.

There are two reasons[3] that a g value may differ from the free-spin value of 2: (a) The orbital motion may contribute to the total magnetic moment. In free atoms, it is the vector combination of orbital and spin which gives rise to the famous Landé g factor. In solids, the orbital moment is often nearly "quenched."[4] That is, the average orbital moment is zero. It does not therefore couple effectively to the external magnetic field, and we get an apparent spin-only coupling. A residual unquenching (via spin-orbit coupling) may cause g to deviate from 2. (b) Even in the absence of a static magnetic field, the spin may prefer to align itself parallel to certain crystal directions. Such an effect may arise from spin-orbit effects, or from the dipole-dipole coupling between spins of the paramagnetic ion if the electron cloud of the ion is not spherically symmetric (just as a pair of magnets like to line up along the line between their centers). If the spins prefer some crystalline direction, they no longer precess freely in a static field, and there results an apparent g value different from 2.

We believe it is effect (b) which accounts for the g values in glass.

The complete explanation of a resonance would be given in principle by solving a Hamiltonian which included the paramagnetic ion and its couplings to its neighbors. Such a precedure is very complicated. It is therefore customary to start by a phenomenological description in terms of the so-called spin Hamiltonian.[3]

The spin Hamiltonian contains the magnetic interaction with the static field and terms describing the

[3] For a particularly clearly written discussion of the fundamentals of paramagnetic resonance, see B. Bleaney and K. W. H. Stevens, Repts. Progr. Phys. 16, 108 (1953).

[4] J. H. Van Vleck, *Theory of Electric and Magnetic Susceptibilities* (Clarendon Press, Oxford, 1935), pp. 273 and 287–297.

preference of the spin to line up along particular crystalline directions. The latter terms are customarily expressed phenomenologically in a power series in the spin coordinates. We shall consider the most general Hamiltonian[3] which does not involve powers higher than the second:

$$\mathcal{H}=g_0\beta HS_{z'}+DS_z^2+E(S_x^2-S_y^2), \qquad (2)$$

where D and E are constants, S_x, S_y, S_z are components of spin along three mutually perpendicular crystalline axes x, y, and z (chosen so that no terms such as S_xS_y occur in $\mathcal{H}$), z' is the axis of the static field H, and g_0 is the g value we would observe *if* D and E were zero. Here g_0 would be the free spin value of 2, except for the effects (a) in the foregoing. (Strictly speaking, when $g_0\neq 2$, it is a second rank tensor.) Effects of type (b) give rise to the terms D and E. We note as usual that there are no terms linear in S_x, S_y, or S_z other than the first term, expressing the fact that the crystalline electric fields cannot produce a preferred sense of magnetization, such as "up," but rather only a direction "up" or "down" of equal preference. We neglect higher terms in the spin although such terms are no doubt present to some extent.

For Fe^{+++}, the orbital angular momentum of the free ion is zero, so that we may take $g_0=2$. The total spin is 5/2.

The first point we note is that if the crystalline terms (i.e., D and E) are small, we may treat them by perturbation theory. The six levels produced by the magnetic field (of energy $2\beta mH$, $m=5/2$, $3/2$, etc.) are then shifted, but it is easy to prove that the frequency of the $m=-1/2$ and $m-+1/2$ transition is not shifted in first order. (This remark is not restricted to the particular form of crystalline terms we assume. An analogous theorem is well known in nuclear resonance: an electric quadrupole coupling does not change the $m=\frac{1}{2}$, $m=-\frac{1}{2}$ splitting in first order.) Consequently this transition is unperturbed and we will see a $g=2$ line if the crystal fields are weak. *The absence of a* $g=2$ *resonance proves that the crystal electric field terms are not weak.* If the crystal field terms are comparable to the magnetic term, we can make no simple prediction other than that in a glass the variety of orientations of "crystal" axes with respect to H will lead to a very messy situation with no well-defined frequencies. Part of the intensity of our observed broad background resonance may originate in just such a way. It is highly unlikely that the sharp $g=4.27$ resonance could result from such a case.

We therefore seek to solve Eq. (2) on the assumption that the crystalline effects dominate with $2\beta H\ll D$ or $2\beta H\ll E$. We may therefore solve Eq. (2) with $H=0$, and then treat H by perturbation theory. We shall first illustrate with an example, then describe the more general case.

Suppose $E=0$. Then the Hamiltonian is

$$\mathcal{H}=2\beta HS_z'+DS_z^2. \qquad (3)$$

Taking $H=0$, we quantize the spins along the z axis, getting for the energy, W, in zero field

$$W=Dm^2, \qquad m=\pm\tfrac{5}{2},\pm\tfrac{3}{2},\pm\tfrac{1}{2}. \qquad (4)$$

We note that since the plus and minus m values are degenerate, we have three groups of states, each doubly degenerate.

Application of a magnetic field parallel to the z axis[5] gives one a simple problem since the quantization according to the crystal z axis is still correct, and we get

$$W=2\beta Hm+Dm^2. \qquad (5)$$

Each of the degenerate m states now is split, the splitting being proportional to H. If D is sufficiently large, the oscillator of the resonance apparatus will not have a high enough frequency to induce transitions between states of different crystalline field energy, i.e., different values of $|m|$. Moreover, all transitions except that between $m=-\frac{1}{2}$ and $m=\frac{1}{2}$ are forbidden by the selection rule of $\Delta m=\pm 1$ for the alternating magnetic field perpendicular to H. The frequency of this transition would fit Eq. (1) with $g=2$.

If the magnetic field is perpendicular to the z axis, there is no first order splitting of the $\pm\frac{5}{2}$ or $\pm\frac{3}{2}$ states, but the $\pm\frac{1}{2}$ states are split according to Eq. (1) with $g=6$. This fact is easy to show by solving the two-by-two Hamiltonian matrix of the $m=\frac{1}{2}$, $m=-\frac{1}{2}$ levels. (One might suppose that there would be zero splitting since the diagonal matrix elements for both the $m=+\frac{1}{2}$ and the $m=-\frac{1}{2}$ states vanish. But there is an off-diagonal matrix element between them which must be included since they are degenerate.)

In a powder, one gets all orientations of magnetic field, hence resonances extending from the lowest field, which occurs at $g=6$, to the highest field at $g=2$. Since there is a strong possibility of H being perpendicular to the z axis, the resonance peaks at $g=6$.

Such an effect has been observed for Fe^{+++} in hemoglobin by Bennett, Gibson, and Ingram[6] and has been explained by Griffith.[7] For hemoglobin they believe the constant D is about 10 cm^{-1}. When they first observed the resonance in a paste, they saw only the peak at $g=6$. Griffith proposed the explanation and subsequent studies using single crystals showed the full dependence of g on orientation.

In general, if one has a spin, S, other than $\frac{5}{2}$ and the Hamiltonian of Eq. (3), it is easy to show the $\pm\frac{1}{2}$ level will have a g value lying between 2 for z' parallel to z and $2S+1$ for z' perpendicular to z. We feel there is little doubt that the $g=6$ resonance reported by Sands

[5] Of course in a substance such as a glass the crystalline axes of a paramagnetic ion are randomly oriented with respect to an applied field. We may consider what happens for each orientation of H relative to the crystal axes, and then average the results over their relative orientation.

[6] Bennett, Gibson, and Ingram, Proc. Roy. Soc. (London) **A240**, 67 (1957).

[7] J. S. Griffith, Proc. Roy. Soc. (London) **A235**, 23 (1956).

comes from an $S=\frac{5}{2}$ ion, presumably Fe^{+++}, with the Hamiltonian of Eq. (3).

Suppose we go back now to the general case in which both the D and E terms are present.

With $H=0$, the six spin states will be grouped into three degenerate pairs. Application of the magnetic field will cause a removal of the degeneracy, the splitting of each degenerate pair being proportional to H since the splitting occurs in first-order perturbation. Moreover, the splitting produced by any given field will depend on the orientation of the magnetic field with respect to the crystalline axes, as we saw in the foregoing. Each degenerate pair will then be described by a splitting which will vary with the orientation of the z' (magnetic field) axis. If the spacing between the three pairs of states is large in zero magnetic field, the oscillator frequency will not be high enough to induce transitions between them. It will, however, be able to produce transitions between states which are degenerate in zero magnetic field (providing such transitions are not forbidden by a selection rule) by applying the proper value of H. Each degenerate pair will be split an amount in energy ΔW given by

$$\Delta W = g\beta H,$$

where the value of g will depend on the orientation of the field with the crystalline axes. There will be a g tensor with the x, y, and z axes as principal axes. But there will *not* be any favored g value as was 6 in the foregoing example, and only a moderately uniform smear will result.

If, however, we have only the terms $S_x^2-S_y^2$ (i.e., $D=0$) another simple case results. The analysis is given in Appendix A. (In Appendix B we analyze the effect of a small additional S_z^2 term.) The levels are once again split into three degenerate pairs in zero magnetic field with energies $W=0$, $\pm 2(7)^{\frac{1}{2}}E$. The magnetic field splits the pairs.

The splitting of the $W=0$ pair is characterized by $g=30/7=4.286$ independent of the orientation of the field with respect to the crystalline axes. This is to be compared with the experimental value of $4.266\pm.002$. The agreement is so striking that we feel it must be taken seriously. [Actually there is some ambiguity in the g value. The value $4.266\pm.002$ corresponds to the point of zero derivative. Since there appears to be a broad background resonance, we do not know exactly where the peak of the $g=4.2$ line occurs. The points of maximum and minimum derivatives are $g=4.38$ and $g=4.20$ (see Fig. 1).] Moreover, an isotropic g value is just what is needed to explain the sharpness and approximate symmetry of the resonance (the $g=6$ resonance is, on the other hand, lopsided).

The upper and lower pairs have strongly anisotropic g values. The three principal values are 9.678, 0.857, 0.607.

Figure 1 reproduces a derivative spectrum obtained at 300°K. In addition to the $g=4.27$ resonance there is

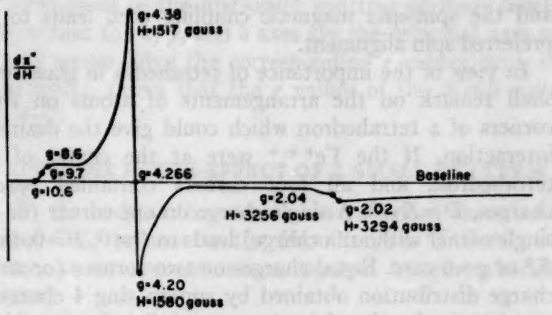

FIG. 1. Field sweep of the derivative of the absorption for glass sample. The vertical axis is the derivative of the absorption. The horizontal axis is generated by sweeping the magnet in time. Within 15% it is linear in field. Various points on the spectrum are labelled either in terms of their g value or the magnetic field they represent. (Field values were calibrated using a proton magnetic resonance.)

a broad background starting at low field near $g\cong 10$ and gradually decreasing to zero at fields corresponding to $g=\frac{1}{2}$ to 1. It is interesting to note that this rather abrupt onset at the low-field end is centered on $g=9.7$.

In an attempt to verify further the model and to determine roughly the magnitude of E, we studied the intensity of the resonance as a function of temperature at 77, 2, and 1.3°K. The features of the room temperature spectrum are preserved except for an increase in the asymmetry of the $g=4.27$ line and a distinct decrease ($\sim 3:1$) in its intensity relative to the $g=9.7$ shoulder and to an internal $CuSO_4\cdot 5H_2O$ standard. Defining a temperature Θ by $\Delta W=2(7)^{\frac{1}{2}}E=k\Theta$, our results are consistent with $\Theta=2.6$°K, and in any case require Θ to be in the range $1°K<\Theta<3°K$.

Since $h\nu/k$ is about 0.5°K, it is clear that we are on the borderline in treating the magnetic interaction as a perturbation. The approximations fail badly for analyzing the high field features of the spectrum. Since a substantially larger value of W would lead to an exponential decrease of intensity with inverse temperature, we may conclude that E is very much smaller than is D for hemoglobin.

Taking our explanation of the $g=4.27$ resonance to be correct (i.e., that the spins experience a coupling $S_x^2-S_y^2$ due to neighboring atoms) we might ask for the implications concerning the local atomic surroundings of the iron.

First we should mention that the existence of the results on hemoglobin proves that it is possible to get large terms D or E with Fe^{+++} ions. Although $E=0$ for hemoglobin, that is simply because of the symmetry of the surroundings. A different arrangement of nearby charges would make $D=0$, $E\neq 0$. Probably the neighbors which are responsible for the splittings are not as close in the glass as in hemoglobin, as evidenced by the smaller crystalline splitting in the glass. One guess at the physical mechanism of the splitting is that the electric fields of neighbors distort the orbit of the $3d$ electrons from their over-all spherical symmetry,

and the spin-spin magnetic coupling then leads to a preferred spin alignment.

In view of the importance of tetrahedra in glass, we shall remark on the arrangements of atoms on the corners of a tetrahedron which could give the desired interaction. If the Fe^{+++} were at the center of a tetrahedron, and all four corners contained *equal* charges, $D=E=0$. A single charge on one corner (or a single corner without a charge) leads to $D\neq 0$, $E=0$, the S_z^2 or $g=6$ case. Equal charges on two corners (or any charge distribution obtained by superposing 4 charges equal to each other but not necessarily equal to the first two) give the $S_z^2-S_y^2$ or $g=4.28$ case.[8]

For example, if Fe^{+++} is surrounded tetrahedrally by oxygen ions (as in a network forming position) the oxygen atoms would not contribute to either D or E. A single extra positive ion would give the S_z^2 or $g=6$ case. Perhaps the $g=6$ glasses are ones in which the iron is in a network forming site with a single extra positive charge in the immediate neighborhood. (The effect of the neighboring charges is found by expanding their electrostatic potential V in the vicinity of the Fe^{+++} ion. The effect of the potential is then found by means of perturbation theory. The dominant terms in giving D or E are probably from the second-order spherical harmonics of V. Since these fall off with the cube of the distance of the charge from the iron, we expect we may neglect the more distant oxygen and silicon atoms). If two positive charges came as close to the iron as the oxygen atoms would permit, they would be located on the corners of a tetrahedron (not, of course, the same tetrahedron occupied by the oxygen atoms.) The positives would then produce the $S_z^2-S_y^2$ or $g=4.28$ case.

If an iron atom were in a network modifying position (i.e., in the interstices of the glass structure rather in the center of an oxygen tetrahedron), we expect both D and E to be important. The resonance pattern would then be a broad smear. It is possible that some or all of the observed broad background resonance may arise in such a manner. *We do not expect to see sharp, well-defined lines such as occur at $g=4.28$ or $g=6$ from iron in network modifying positions.*

As we have remarked, the near absence of a $g=2$ line in our samples indicates that *essentially all* of the Fe^{+++} ions experience strong crystalline splittings.

It is interesting to speculate on the intensity of our resonance. Our measurements indicate that about $\frac{1}{4}$ to $\frac{1}{2}$ of all the Fe^{+++} is in a $g=4.28$ site. For the glasses we report on, the average number of nonbridging[9] oxygen atoms per silicon tetrahedron is about $\frac{1}{3}$. That is, about $\frac{1}{3}$ of the silicon tetrahedra have an isolated neighboring positive charge. If we assume that Fe^{+++} ions are all in network forming sites, they should have a strong probability of attracting a single positive charge to make then equivalent to the Si^{4+} ion. They should then give a $g=6$ resonance. By analogy with Si^{4+} about $\frac{1}{3}$ of the Fe^{+++} should have a nonbridging oxygen, thereby attracting a second positive ion. This is just what is needed for the $g=4.28$ site, and fits our high intensity determination. The question then arises why do we not see a $g=6$ resonance from those Fe^{+++} ions which have just a single neighboring positive. One might expect about $\frac{2}{3}$ of the iron to be in such a site on the basis of the argument that about $\frac{2}{3}$ of the silicon tetrahedra have all their oxygens shared with other tetrahedra. However, the fact that the $g=6$ line actually extends from $g=6$ to $g=2$ means that it is broad and comparitively weak. Its intensity at $g=6$ is diminished below the $g=4.28$ line in approximately the ratio $(\Delta H/2000)^3$ where ΔH is the breadth the resonance would have apart from the spread from $g=2$ to 6. (We assume the same ΔH for both $g=6$ and $g=4.28$ lines.) This ratio is about one-tenth, not enough by itself to surpress the $g=6$ resonance. Possibly the two resonances have different ΔH, or perhaps the iron is less likely to have a $g=6$ surrounding than we estimate.

The hypothesis that the $g=6$ resonance comes from Fe^{+++} could be checked by experiments similar to our own on one of the "$g=6$" glasses listed by Sands. A test of our speculations on the atomic surroundings of the iron would be a systematic study of the relative intensities of the $g=4.28$ and $g=6$ resonances as a function of the composition of the glass. One would expect the $g=4.28$ resonance to be relatively stronger in glasses where the probability of having two neighboring positives is quite high.

It is a pleasure to acknowledge that our studies on iron in glass are the direct result of the stimulus of Dr. Scott Anderson, who in addition also provided the samples and their analysis, and who has been most helpful in introducing us to the complexities of the physics of glasses. We also gratefully acknowledge the support given by the Alfred P. Sloan Foundation through a grant to one of us.

APPENDIX A: Eigenstates of $E(S_z^2-S_y^2)$

We outline here the determination of the eigenstates of the Hamiltonian $E(S_z^2-S_y^2)$. We note that rotating the x into the y axis changes the sign of the Hamiltonian. As a result we can show that the energy levels occur in pairs of equal but opposite energy. We define the operator R (and its inverse R^{-1}) which rotates x

[8] There are ways of getting the $S_z^2-S_y^2$ coupling from atomic arrangements based on symmetries other than that of a tetrahedron. For example, suppose the iron had six identical neighbors all the *same* distance away. Let four be on the corners of a rectangle with the iron at the center, and let the other two be above and below the rectangle on the line through the iron perpendicular to the plane of the rectangle. Denoting the angle between the diagonals of the rectangle as θ, we have $D=0$ and E is proportional to $\cos\theta$. (Thus, if the rectangle is a square, $\theta=90°$, and both D and E vanish.) Tinkham [Proc. Roy. Soc. (London) **A236**, 535 (1956)] has observed this case for Mn^{++} (which is isoelectronic with Fe^{+++}) in the ZnF_2 lattice. He found $D\cong 0$, $E\cong 120$ gauss.

[9] A bridging oxygen is one which is shared by two silicon atoms. That is, it is common to two silicon tetrahedra.

into y and y into $-x$, by the equations

$$RS_xR^{-1}=S_y$$

$$RS_yR^{-1}=-S_x$$

$$RR^{-1}=1.$$

Thus consider any eigenfunction u_1 of energy W_1

$$E(S_x^2-S_y^2)u_1=W_1u_1$$

$$=E(S_x^2-S_y^2)R^{-1}Ru_1.$$

Operating on both sides from the left by R we get

$$ER(S_x^2-S_y^2)R^{-1}(Ru_1)=W_1Ru_1$$

$$=E(S_y^2-S_x^2)(Ru_1).$$

Therefore

$$E(S_x^2-S_y^2)(Ru_1)=-W_1(Ru_1)$$

so that (Ru_1) is an eigenfunction of energy $-W_1$. Therefore, the energies occur in pairs (unless $W_1=0$).

We note also that

$$E(S_x^2-S_y^2)=(E/4)(S_+^2+S_-^2),$$

where $S_\pm=S_x\pm iS_y$. Therefore, in the S_z representation, all diagonal elements of $\mathcal{H}$ are zero, and the off-diagonal ones connect states of $|\Delta m|=2$.

For spin $\frac{5}{2}$ this means the 6×6 matrix factors into two 3×3's, one involving the states $m=\frac{5}{2}, \frac{1}{2}, -\frac{3}{2}$, the other $m=\frac{3}{2}, -\frac{1}{2}, -\frac{5}{2}$. Since the states must occur in *pairs* of energies $\pm W$, the roots must be $\pm W_0$, and 0. The 3×3, therefore, can be reduced to a 1×1 and a 2×2, and the roots are easily solved. The eigenfunctions and energies are:

Energy	*Eigenfunctions (normalized)*
$W=0$	$\psi_1=(9/14)^{\frac{1}{2}}[\Phi_{5/2}-(5/9)^{\frac{1}{2}}\Phi_{-3/2}]$
	$\psi_2=(9/14)^{\frac{1}{2}}[\Phi_{-5/2}-(5/9)^{\frac{1}{2}}\Phi_{3/2}]$
$W=2(7E)^{\frac{1}{2}}$	$\psi_3=(5/28)^{\frac{1}{2}}[\Phi_{3/2}+(14/5)^{\frac{1}{2}}\Phi_{1/2}+(9/5)^{\frac{1}{2}}\Phi_{-3/2}]$
	$\psi_4=(5/28)^{\frac{1}{2}}[\Phi_{-3/2}+(14/5)^{\frac{1}{2}}\Phi_{-1/2}+(9/5)^{\frac{1}{2}}\Phi_{3/2}]$
$W=-2(7E)^{\frac{1}{2}}$	$\psi_5=(5/28)^{\frac{1}{2}}[\Phi_{5/2}-(14/5)^{\frac{1}{2}}\Phi_{1/2}+(9/5)^{\frac{1}{2}}\Phi_{-3/2}]$
	$\psi_6=(5/28)^{\frac{1}{2}}[\Phi_{-5/2}-(14/5)^{\frac{1}{2}}\Phi_{-\frac{1}{2}}+(9/5)^{\frac{1}{2}}\Phi_{3/2}]$

Calculations of the first-order splitting of these levels show that the x, y, and z axes are the principal axes of the g tensor, give the corresponding g values, and, in particular, prove that the g values of the $W=0$ state is 30/7.

APPENDIX B: THE EFFECT OF A SMALL DS_z^2 TERM

In the body of the text we have assumed there is no term DS_z^2 present in the Hamiltonian. If $D\neq0$, we may, as an approximation, treat it by perturbation theory.

In the first-order perturbation, a term DS_z^2 shifts the levels but it does not remove the twofold degeneracy. Moreover, since in the first-order theory there is no change in the wave function, the g values are unchanged.

In second-order perturbation theory, the wave functions ψ_1 and ψ_2 are changed to new ones ψ_1' and ψ_2' given by

$$\psi_1'=\psi_1-[3(5)^{\frac{1}{2}}/7(7)^{\frac{1}{2}}](D/E)\Phi_{1/2}$$

$$\psi_2'=\psi_2-[3(5)^{\frac{1}{2}}/7(7)^{\frac{1}{2}}](D/E)\Phi_{-1/2}.$$

The new g values are readily shown to be

$$g_x=(30/7)-(120D/49E)$$

$$g_y=(30/7)+(120D/49E)$$

$$g_z=30/7 \text{ (unchanged)}.$$

The center of the resonance line is not shifted, but the line is broadened, the shape depending on the distribution in g values (i.e., of D/E) among various sites of the iron ions. The resonance line would be symmetrical about its center. If we use the peak heights of the derivatives as a measure of the line breadth, the corresponding g values are 4.20 and 4.38. Thus if the line breadth were due to a DS_z^2 term, a typical value of D/E would be

$$120D/49E)\cong0.10$$

or

$$D/E\cong0.05.$$

As a matter of fact, the breadth of the resonance is about what one expects from the magnetic dipole coupling between the iron ions. Consequently the figure for D/E given in the foregoing may be looked upon as an upper limit.

Light Scattering by Anisotropic Inhomogeneities in Thin Polymer Films under Strain. I. Simple Elongation*

HARI L. BHATNAGAR

National Chemical Laboratory, Poona-8, India

(Received October 27, 1959)

Inhomogeneities in thin polymer films are assumed to have two different polarizabilities, one longitudinal and the other transverse. A distribution function for orientation of these anisotropic inhomogeneities is obtained as a function of degree of strain and utilized to obtain average scattered intensity. Expressions for differential cross sections of scattering which have been defined are derived.

I. INTRODUCTION

THE scattering of light by thin polymer films under one-dimensional strain has been investigated by Stein and co-workers.[1] They have interpreted their data in the light of modified Debye-Bueche[2] theory assuming that the inhomogeneities are anisotropic and that the electric field of the incident light is not distorted on entering the particle (Rayleigh-Gans-Born approximation). Under these conditions, according to Norris and Stein[1a] (this paper will be referred to as NS), the expression for the Rayleigh ratio is

$$R_p(\psi,\omega)=(\pi^{5/2}/\lambda_0^4)\,\langle\eta^2(\psi,\omega)\rangle(abc)^{\frac{1}{2}}p(\psi,\omega),$$

where ψ is the angle of scattering with respect to the incident beam; ω characterizes the orientation about the axis of the incident beam; λ_0 is the wavelength of light in vacuum; $\langle\eta^2(\psi,\omega)\rangle$ is the mean-square dielectric constant fluctuation which is dependent on the state of polarization of the observed light; a, b, c are the three parameters characterizing the extension of an inhomogeneity in three directions, and $p(\psi,\omega)$ is the interference factor. The expressions in NS for $\langle\eta^2(\psi,\omega)\rangle$ are obtained in terms of functions of an angle ϵ which gives one particular orientation of an inhomogeneity with respect to the direction of stretch. They mention that for a distribution of orientations, the average value of the appropriate function of ϵ should be used. In their treatment Stein and Norris[1e] obtain the average values of $\cos^2\epsilon$ and $\cos^4\epsilon$ by manipulating the experimental data obtained using other techniques. Only through these functions do the expressions for Rayleigh ratios become dependent on the degree of strain.

In the present note, we retain the model proposed by Stein and co-workers,[1] but introduce the dependence of Rayleigh ratios on the degree of strain directly. Each inhomogeneity is treated as a spheroid, "a" being its semi-major axis and "b" its semi-minor axis. The principal polarizability $\alpha_{||}$ is assumed to be along "a" and $\alpha_\perp$ along "b". Each spheroid is treated as a Rayleigh scatterer, all the spheroids being identical as regards their optical properties. It is further assumed that no new crystalline nuclei are formed and that the dimensions of a spheroid do not suffer change due to strain. It will be pointed out later that the possibility of alteration in the dimensions can be adequately accommodated in the present treatment. In calculating the intensity of scattered light, multiple scattering due to individual spheroids is neglected, so that the resultant scattering is obtained as the statistical average emitted by the dipoles induced by the incident wave in the individual spheroids which are oriented spatially in accordance with a derived distribution function. Expressions for the scattering cross sections for the various states of polarizations so obtained will have to be multiplied by the $p(\psi,\omega)$ factor obtained by NS to take into account the interference arising due to the extension of an inhomogeneity comparable with the wavelength of light. A similar treatment of the effect of anisotropy on light scattering by streaming freely flexible linear macromolecules has been given by Stevenson and Bhatnagar.[3]

Distribution function for orientation of spheroids.—Let an elastic film containing crystalline inhomogeneities lie in the YZ plane of a right-handed cartesian system, the positive X axis being the direction of incident light ($\mathbf{S}_0$). Here an inhomogeneity is essentially a crystalline region which is connected to another inhomogeneity by means of flexible chains. When the film is stretched in a direction, say, parallel to the Z axis, a spheroid (inhomogeneity) suffering a displacement also changes its orientation. Let the vectors $\mathbf{r}_1$ and $\mathbf{r}_2$ specify the orientation of the spheroid, and X_1, Y_1, Z_1 and X_2, Y_2, Z_2 be the coordinates of its center before and after stretching. Then,

$$X_2=\lambda_1X_1, \qquad Y_2=\lambda_2Y_1, \qquad \text{and} \qquad Z_2=\lambda_3Z_1,$$

where λ_1, λ_2, and λ_3 are the extension ratios.

* Contribution No. 607 from the National Chemical Laboratory, Poona.

[1] (a) F. H. Norris and R. S. Stein, J. Polymer Sci. **27**, 87 (1958); (b) Plaza, Norris, and Stein, J. Polymer Sci. **24**, 455 (1957); (c) Keane, Norris, and Stein, J. Polymer Sci. **20**, 209 (1956); (d) J. J. Keane and R. S. Stein, *ibid.* **20**, 321 (1956); (e) R. S. Stein and J. J. Keane, *ibid.* **17**, 21 (1955); (f) J. J. Keane and R. S. Stein, Rev. Sci. Instr. **25**, 892 (1954); (g) R. S. Stein and F. H. Norris, J. Polymer Sci. **21**, 381 (1956).

[2] P. Debye and A. M. Bueche, Paper presented before the American Physical Society, Chicago, November, 1950; J. Appl. Phys. **20**, 518 (1949).

[3] A. F. Stevenson and H. L. Bhatnagar, J. Chem. Phys. **29**, 1336 (1958).

If one imposes the condition that

$$\lambda_1\lambda_2\lambda_3=1, \tag{1}$$

one obtains

$$\lambda_1=\lambda_2=1/\lambda^{\frac{1}{2}} \quad \text{and} \quad \lambda_3=\lambda$$

for a one-dimensional extension parallel to the Z axis. The probability that the axis of an unoriented spheroid will lie between θ and $\theta+d\theta$ and ϕ and $\phi+d\phi$ is given by $1/4\pi \sin\theta d\theta d\phi$. The probability $f(\theta', \phi')d\theta' d\phi'$ that after extension the major axis would lie between θ' and $\theta'+d\theta'$ and ϕ' and $\phi'+d\phi'$ is then given by

$$f(\theta', \phi')d\theta' d\phi' = (1-\kappa^2)/4\pi \sin\theta\cdot(1-\kappa^2 \sin^2\theta)^{-\frac{1}{2}}d\theta d\phi, \tag{2}$$

where $\kappa^2=1-1/\lambda^3$ and $1/4\pi$ is determined by the normalizing condition

$$A\int_{\theta=0}^{\pi}\int_{\phi=0}^{2\pi} f(\theta', \phi')d\theta' d\phi'=1. \tag{3}$$

Calculation of the differential cross sections.—We now calculate the intensity of scattered light by a spheroidal scatterer which is uniaxially isotropic with polarizabilities $\alpha_{||}$ and $\alpha_\perp$, respectively, parallel and perpendicular to its major axis, whose orientation is specified by θ' and ϕ'. Let α', β', and γ' be the direction cosines of $\mathbf{S}$, the direction of observation with respect to $\mathbf{S}_0$ ($\mathbf{S}_0$ being the direction of incidence, in this case the positive X axis). The plane of scattering is defined as usual as the plane containing $\mathbf{S}$ and $\mathbf{S}_0$.

Let $\mathbf{p}$ be the induced electric moment per unit amplitude of the electric vector $\mathbf{E}^0$ of the incident wave. Then one obtains for the components of the induced electric moment, per unit amplitude of the electric vector of the incident wave and for the two states of polarization of the incident wave, the following expressions:

parallel polarization:

$$\left.\begin{aligned} p_{x||} &= (\alpha_{||}-\alpha_\perp)(l_1m_1\mu+l_1n_1\nu) \\ p_{y||} &= (\alpha_{||}-\alpha_\perp)(m_1^2\mu+m_1n_1\nu)+\alpha_\perp\mu \\ p_{z||} &= (\alpha_{||}-\alpha_\perp)(m_1n_1\mu+n_1^2\nu)+\alpha_\perp\nu \end{aligned}\right\}; \tag{7}$$

perpendicular polarization:

$$\begin{aligned} p_{x\perp} &= (\alpha_{||}-\alpha_\perp)(l_1n_1\mu-l_1m_1\nu) \\ p_{y\perp} &= (\alpha_{||}-\alpha_\perp)(m_1n_1\mu-m_1^2\nu)-\alpha_\perp\nu \\ p_{z\perp} &= (\alpha_{||}-\alpha_\perp)(n_1^2\mu-m_1n_1\nu)+\alpha_\perp\mu, \end{aligned} \tag{8}$$

where

$$l_1=\sin\theta\cos\phi, \qquad m_1=\sin\theta\sin\phi, \qquad n_1=\cos\theta,$$

and

$$\mu=\cos\omega, \qquad \nu=\sin\omega, \tag{9}$$

ω being the angle that the scattering plane makes with the XY plane.

The radiation scattered by a dipole of moment $\mathbf{p}$ is given by $k^2\mathbf{S}\times(\mathbf{p}\times\mathbf{S})$, where the propagation factor $(1/r)\exp[-i\cdot k(r-ct)]$ is omitted and $k=2\pi/\lambda'$, λ' being the wavelength of light in the medium. The scattered amplitudes in the directions parallel and perpendicular to the plane of scattering are given by the following expressions:

$$E_{||}=k^2[-p_x\sin\psi+p_y\cos\psi\cos\omega+p_z\cos\psi\sin\omega], \tag{10}$$

$$E_\perp=k^2[-p_y\sin\omega+p_z\cos\omega]. \tag{11}$$

Substitution of (7) and (8) in (10) and (11) gives the scattered amplitudes, $E_{||\to||}$, $E_{||\to\perp}$, etc. Thus,

$$\begin{aligned} E_{||\to||} &= k^2[(\alpha_{||}-\alpha_\perp)(m_1\cos\omega+n_1\sin\omega) \\ &\cdot\{-l_1\sin\psi+m_1\cos\psi\cos\omega+n_1\cos\psi\sin\omega\}+\alpha_\perp\cos\psi], \end{aligned} \tag{12}$$

$$\begin{aligned} E_{\perp\to||} &= k^2[(\alpha_{||}-\alpha_\perp)(n_1\cos\omega-m_1\sin\omega) \\ &\cdot(-l_1\sin\psi+m_1\cos\psi\cos\omega+n_1\cos\psi\sin\omega)], \end{aligned} \tag{13}$$

$$\begin{aligned} E_{||\to\perp} &= k^2[(\alpha_{||}-\alpha_\perp)(m_1\cos\omega+n_1\sin\omega) \\ &\cdot(n_1\cos\omega-m_1\sin\omega)], \end{aligned} \tag{14}$$

and

$$E_{\perp\to\perp}=k^2[(\alpha_{||}-\alpha_\perp)(n_1\cos\omega-m_1\sin\omega)^2+\alpha_\perp]. \tag{15}$$

The corresponding differential cross sections for scattering, $\sigma_{||\to||}$, $\sigma_{\perp\to||}$, $\sigma_{||\to\perp}$, and $\sigma_{\perp\to\perp}$ are obtained by averaging the squares of Eqs. (12)–(15), respectively, and multiplying by $p(\psi, \omega)$, the interference factor. Thus,

$$\sigma_{||\to||}=p(\psi,\omega)\int_{\theta=0}^{\pi}\int_{\phi=0}^{2\pi} E^2_{||\to||}f(\theta', \phi')d\theta' d\phi',$$

where

$$\begin{aligned} p(\psi, \omega) = (ab^2/\pi^3)^{\frac{1}{2}}\exp[-(\pi a/\lambda')^2\{&p^2(1-\cos\psi)^2 \\ &+p^2\sin^2\psi\cos^2\omega+\sin^2\psi\sin^2\omega\}] \end{aligned}$$

and

$$p=b/a, \tag{16}$$

and respective equations hold for the rest of the differential cross sections for scattering. Here $\sigma_{||\to||}$ denotes the differential cross section for scattering by the inhomogeneity when the incident light is polarized with its electric vector parallel to the plane of scattering and the component of the scattered light whose electric vector is polarized parallel to the plane of scattering is observed, with similar meaning for the rest of the differential cross sections.

For the case of one-dimensional extension, one obtains the following expression:

$$\sigma_{||\to||}=k^4(1-\kappa^2)[\alpha_\perp^2\cos^2\psi/(1-\kappa^2)+\tfrac{1}{4}(\alpha_{||}-\alpha_\perp)^2 \cdot\{I_4\cos^2\psi\cos^2 2\omega+\tfrac{1}{2}(I_1+I_5-\tfrac{5}{8}\cdot I_3)\cos^2\psi\sin^2 2\omega +\sin^2\psi(I_3/4\cdot\cos^2\omega+I_4\sin^2\omega)\}]p(\psi,\omega), \quad (17)$$

$$\sigma_{\perp\to||}=k^4(1-\kappa^2)(\alpha_{||}-\alpha_\perp)^2(\tfrac{1}{4})[\{I_4\cos^2\omega +(I_3/4)\sin^2\omega\}\sin^2\psi+\{I_4\cos^2 2\omega +\tfrac{1}{2}(\tfrac{11}{8}I_3-I_1+I_5)\sin^2 2\omega\}\cos^2\psi]p(\psi,\omega), \quad (18)$$

$$\sigma_{||\to\perp}=k^4(\alpha_{||}-\alpha_\perp)^2(1-\kappa^2)(\tfrac{1}{4})[I_4\cos^2 2\omega +(\tfrac{1}{2})(\tfrac{11}{8}I_3-I_1+I_5)\sin^2 2\omega]p(\psi,\omega), \quad (19)$$

$$\sigma_{\perp\to\perp}=k^4(1-\kappa^2)[\alpha_\perp^2/(1-\kappa^2)+(\tfrac{1}{2})[\alpha_{||}-\alpha_\perp)^2 \cdot\{I_5\cos^4\omega+(\tfrac{3}{8})I_3\sin^4\omega+3I_4\sin^2\omega\cos^2\omega\} +(\tfrac{1}{2})\alpha_\perp(\alpha_{||}-\alpha_\perp)(I_1\sin^2\omega+2I_2\cos^2\omega)]p(\psi,\omega), \quad (20)$$

where

$$I_1=(2\,|\,\kappa^2)\{1/(1-\kappa^2)-(1/2\kappa)\ln[(1+\kappa)/(1-\kappa)]\}, \quad (21a)$$

$$I_2=(2\,|\,\kappa^2)\{(1/2\kappa)\ln[(1+\kappa)/(1-\kappa)]-1\}, \quad (21b)$$

$$I_3=(2/\kappa^4)\{1/(1-\kappa^2)+\tfrac{1}{2} -[(3+\kappa^2)/4\kappa]\ln[(1+\kappa)/(1-\kappa)]\}, \quad (21c)$$

$$I_4=I_1-I_3, \quad (21d)$$

$$I_5=-(1/\kappa^4)\{(3/2\kappa)(1-\kappa^2)\ln[(1+\kappa)/(1-\kappa)] -3+2\kappa^2\}. \quad (21e)$$

Equations for $\alpha_\perp$ and $(\alpha_{||}-\alpha_\perp)$ in terms of the dimensions of inhomogeneity.—Rayleigh[4] has shown that for a prolate spheroid with axial ratio $p=b/a$, $(0\leq p\leq 1)$

$$\alpha_\perp=\frac{(\frac{2}{3})(m^2-1)a^3}{[2/p^2+(m^2-1)I_a]}, \quad (22)$$

and

$$(\alpha_{||}-\alpha_\perp)=(\tfrac{2}{3})(m^2-1)a^3\{[(m^2-1)I_b+2/p^2]^{-1} -[(m^2-1)I_a+2/p^2]^{-1}\}, \quad (23)$$

[4] Lord Rayleigh, Phil. Mag. **114**, 28 (1897).

where

$$I_a=\{1/p^2(1-p^2)\}-[2(1-p^2)^{3/2}]^{-1}\ln\frac{1+(1-p^2)^{\frac{1}{2}}}{1-(1-p^2)^{\frac{1}{2}}} \quad (24)$$

and

$$I_b=[1/p^2-I_a], \quad (25)$$

where "a" is the semi-major axis of cross section of a spheroid.

The formulas (22)–(25) are applicable to oblate as well as prolate spheroids, provided for the case of oblate spheroids, (i) "a" is replaced by "pa"; (ii) p is replaced by $1/p$ in all formulas; and (iii) I_a is defined as

$$I_a=-p^4/(1-p^2)+[p^3/(1-p^2)^{3/2}]\cos^{-1}p. \quad (26)$$

DISCUSSION

The limit of applicability of Eqs. (17)–(20) is governed by the factor $\lambda'/(m-1)$, m being the ratio of the refractive index of the crystalline region to that of amorphous regions. Obviously, for polymer films, $(m-1)\ll 1$ and consequently the value of "a" can be much larger than in cases where $(m-1)$ is not very much less than unity.

For greater strain, the dimensions of the inhomogeneity as well as its orientation may change. Under such circumstances it is reasonable to assume that $a=a_0+C'\lambda$, where C' is a constant and the axial ratio p remains unaltered. However, it is advisable to work at low extensions to avoid contribution from amorphous regions whose polarizing properties may also undergo substantial change at high elongations.

Another important factor to be taken into account is the decrease in the number of inhomogeneities in the irradiated volume due to applied strain. If N is the number of such inhomogenities per unit volume before elongation, then after elongation the number would decrease by a factor $(1/\lambda^3)$. This would enable one to extrapolate for zero concentration of the inhomogeneities per unit volume so that specific scattering factors can be obtained.

ACKNOWLEDGMENT

I wish to thank Dr. A. S. Apte for many interesting and valuable discussions and to Professor A. F. Stevenson for going through the manuscript.

Some Considerations of Unimolecular Rate Theory*†

FRANK P. BUFF AND DAVID J. WILSON
Department of Chemistry, University of Rochester, Rochester, New York

(Received June 10, 1958; revised manuscript received August 21, 1959)

It is the purpose of this paper to examine the pressure dependence of the rate constant k of unimolecular decompositions within the framework of the generalized Lindemann mechanism. For trace amounts of reactive polyatomic molecules possessing very small equilibrium fractions of reactive states, the observed k may be identified with the lowest eigenvalue of the relaxation spectrum. After an examination of the Kassel and Slater microscopic decomposition frequencies (m.d.f.'s), this approach is applied to the strong collision mechanism which is a common feature of both theories. Finally, the lowest eigenvalue is calculated for the inefficient stepwise activation mechanism in combination with the simple Kassel m.d.f. The pressure dependence of k on a reduced basis is found to be relatively insensitive to the details of the activation mechanism employed. The effect of less efficient processes in the intermolecular energy transfer and of anharmonicities in the intramolecular energy transfer tend to broaden the transition range of k between the high- and low-pressure limits.

I

At present a number of simple polyatomic molecules are recognized to undergo homogeneous gas phase decompositions according to unimolecular mechanisms.[1] When small amounts of these reactants A decompose in a large excess of inert gas M, the observed kinetic behavior is first order. The observed pseudo first-order rate constant k is found to possess the following properties: (1) in the high-pressure limit k attains the constant value k_∞ independent of the nature of added gas; (2) in the low-pressure limit, k is proportional to the concentration of inert gas M, i.e., $k=k_0[\mathrm{M}]$: (3) k_0 depends on the nature of M; and (4) the pressure dependence of k in the extended intermediate region is specific with regard to the nature of both A and M. Subject to the availability of data, the value of k may be conveniently exhibited in terms of the limiting constants k_∞ and k_0 and the mutual dependence of the reduced variables k/k_∞ and $k_0[\mathrm{M}]/k_\infty$.

The accepted qualitative explanation of unimolecular decomposition was proposed by Christiansen[2] and Lindemann.[3] According to their mechanism, reactant molecules are activated by collision with other gas molecules to an activated state possessing sufficient vibrational energy to decompose. This activated state subsequently either decomposes or is collisionally deactivated. In this two-level system, the mechanism thus takes the form

$$\mathrm{A}_0+\mathrm{M}\underset{k_{-1}}{\overset{k_1}{\rightleftarrows}}\mathrm{A}_1^*+\mathrm{M} \qquad (1)$$

$$\mathrm{A}_1^*\xrightarrow{\nu_1}\text{products}.$$

The concentrations corresponding to the nonreactive state A_0 and the activated state A_1^*, are then governed by the rate equations

$$d[\mathrm{A}_0]/dt=-k_{-1}[\mathrm{M}]\{\exp(-\beta\epsilon^*)[\mathrm{A}_0]-[\mathrm{A}_1^*]\} \qquad (2)$$

$$d[\mathrm{A}_1^*]/dt=-k_{-1}[\mathrm{M}]\{[\mathrm{A}_1^*]-\exp(-\beta\epsilon^*)[\mathrm{A}_0]\}-\nu_1[\mathrm{A}_1^*]. \qquad (3)$$

The Boltzmann factor for the energy separation ϵ^* of A_1^* and A_0 arises from microscopic reversibility. In the usual treatment of these rate equations it is assumed that (1) the total concentration $[\mathrm{A}(t)]$ of the reactive gas follows the observed rate law, $[\mathrm{A}(t)]=[\mathrm{A}(0)]e^{-kt}$; and (2) the fraction of excited molecules may be obtained from Eq. (3) by employing the steady-state hypothesis and assigning the equilibrium distribution to the fraction of nonreactive molecules. This leads to the following expressions for the pressure dependence and limiting values of the pseudo first-order rate constant

$$\frac{k}{k_\infty}=\frac{1}{1+x}; \qquad x=\frac{k_\infty}{k_0[\mathrm{M}]} \qquad (4)$$

where

$$k_0=\frac{k_{-1}\exp(-\beta\epsilon^*)}{1+\exp(-\beta\epsilon^*)}; \qquad k_\infty=\frac{\nu_1\exp(-\beta\epsilon^*)}{1+\exp(-\beta\epsilon^*)}. \qquad (5)$$

In preparation for our subsequent treatment, it will now be convenient to observe that, for trace amounts of A, the constant coefficient differential Eqs. (2) and (3) may be easily integrated. For the experimental conditions of an initial equilibrium distribution of reactant, the evolution of A is given by

$$\frac{[\mathrm{A}(t)]}{[\mathrm{A}(0)]}=\sigma_-\exp(-\lambda_- t)+\sigma_+\exp(-\lambda_+ t),$$

* Presented at the Symposium on Absolute Reaction Rates, Madison, Wisconsin, March 30–April 1, 1959.

† This work was supported by the National Science Foundation under Grant 3056.

[1] For a review, see A. F. Trotman-Dickenson, *Gas Kinetics* (Butterworths Scientific Publications, London, 1955).

[2] J. A. Christiansen, Thesis: Reaktionkinetiske Studier, Copenhagen (1921), pp. 50–51.

[3] F. A. Lindemann, Trans. Faraday Soc. 17, 598 (1922).

where

$$\sigma_{\pm}=\pm\frac{\lambda_{-}([\mathrm{M}]=\infty)-\lambda_{\pm}}{\lambda_{+}-\lambda_{-}} \tag{6}$$

$$\lambda_{\pm}=\tfrac{1}{2}\{k_{-1}[1+\exp(-\beta\epsilon^{*})][\mathrm{M}]+\nu_{1}$$
$$\pm[\{\nu_{1}+k_{-1}[1+\exp(-\beta\epsilon^{*})][\mathrm{M}]\}^{2}$$
$$-4[\mathrm{M}]\nu_{1}k_{-1}\exp(-\beta\epsilon^{*})]^{\frac{1}{2}}\}.$$

It is of interest to observe that, despite the apparent complexity of this result, in the usual cases in which the equilibrium fraction of activated states is very small, to within negligible error $\sigma_{-}=1$ and λ_{-} is identical with the rate constant k of Eqs. (4) and (5). Furthermore in the present case of

$$\exp(-\beta\epsilon^{*})\ll 1, \qquad \lambda_{+}\approx\exp(+\beta\epsilon^{*})\,(k_{\infty}+k_{0}[\mathrm{M}])$$

which implies that $\lambda_{+}\gg\lambda_{-}$. These results show that (1) the second transient of Eq. (6) dies out immediately, (2) the approximations used in obtaining Eqs. (4) and (5) are very good, and (3) the observed rate constant may be identified with the lowest eigenvalue of the relaxation equations. This lowest eigenvalue is the perturbation, arising from the chemical sink, to the lowest (vanishing) eigenvalue in the absence of reaction.

It is the purpose of this investigation to examine the pseudo first-order rate constant k within the framework of generalizations of the Lindemann mechanism. We shall examine the limiting cases of very efficient and inefficient collisional mechanisms, and the salient features of the Kassel[4] and Slater[5] microscopic decomposition frequencies. These factors constitute, respectively, the generalizations of k_{-1} and ν_1 in Eqs. (2) and (3). In the next section we shall critically examine the Slater and Kassel theories which both employ the efficient collisional energy transfer mechanism and thus employ a Lorentz type collisional term. In Sec. III we shall examine the inefficient collisional mechanism corresponding to stepwise activation among neighboring vibrational states. This mechanism leads to a Fokker-Planck type collisional term. In both these limiting cases k may again be identified with the well separated lowest eigenvalue of the relaxation spectrum and may be obtained from a simple variational principle. The comparison of the two limiting activation mechanisms with a common Kassel sink is presented in Sec. IV. It is found that the pressure dependence of k on a reduced basis is quite insensitive to the intermolecular energy transfer mechanism selected. This relative insensitivity of k arises from the smoothing effect over many molecular states. Alternatively, it may be ascribed to the common variational origin of k. It is concluded in this investigation that an inefficient intermolecular energy transfer process as well as the influence of anharmonicities in intramolecular energy transfer both lead to a more gradual pressure dependence of k on a reduced basis. Measurements of k_0 provide the best criterion for bracketing the collisional mechanism.

[4] L. S. Kassel, *Kinetics of Homogeneous Gas Reactions* (Chemical Catalog Company, New York, 1932).
[5] N. B. Slater, Phil. Trans. Roy. Soc. (London) **A246**, 57 (1953).

II

We now turn to the available extensions of the simple Lindemann mechanism. Here it is again[6] assumed that reactant molecules are activated to reactive states by collisions with other gas molecules. The reactive states subsequently either decompose into products or are again deactivated. Thus, the general mechanism for a unimolecular reaction involving an inert gas and trace quantities of reactant is

$$\mathrm{A}_m+\mathrm{M}_k\rightleftarrows\mathrm{A}_n+\mathrm{M}_l$$
$$\mathrm{A}_n^{*}\xrightarrow{\nu_n}\text{products}. \tag{7}$$

A_n is a reactant molecule in an energy state represented by the set of quantum numbers $\{n\}$ (the superscript* will designate reactive states), M_l is an inert gas molecule in an energy state $\{l\}$, and ν_n is the microscopic decomposition frequency (m.d.f.) for the state $\{n\}$ and is assumed to be vanishingly small for nonreactive states. In order for this theory to take into account subsequent refinement, the m.d.f. should also be weakly pressure dependent. This arises, for example in Slater's theory[7] of "nonrandom gaps" and in the effect of anharmonicities in the intramolecular energy transfer that we shall examine briefly. The mechanism, Eq. (7), implies that the concentrations of reactants in the various states $\{n\}$ are determined by

$$(\partial f_n/\partial t)=(\partial f_n/\partial t)_{\mathrm{coll}}-\nu_n f_n^{*}$$
$$f_n(t)=[\mathrm{A}_n(t)]/[\mathrm{A}(0)];$$
$$[\mathrm{A}(t)]=\sum_n[\mathrm{A}_n(t)]. \tag{8}$$

Under heat bath conditions of M, the collisional contribution takes the form

$$(\partial f_n/\partial t)_{\mathrm{coll}}=-\sum_m a_{nm}[(f_n/P_n)-(f_m/P_m)]$$
$$a_{nm}=a_{mn} \tag{9}$$

where ρ_n is the normalized equilibrium distribution for the state $\{n\}$. Summation of Eq. (8) over all states, with use of the symmetry of the transition probabilities a_{nm}, determines the rate of change of the macroscopic concentration of reactant

$$\{-1/[\mathrm{A}]\}\{d[\mathrm{A}]/dt\}=\sum_{\substack{\text{reactive}\\ \text{states}\\ \text{only}}}\nu_n\rho_n^{*} \qquad \rho_n=[\mathrm{A}_n]/[\mathrm{A}]. \tag{10}$$

[6] See, for example, H. S. Johnston, J. Chem. Phys. **20**, 1103 (1952).
[7] N. B. Slater, J. Chem. Phys. **24**, 1256 (1956).

The theories of Kassel and Slater employ Eq. (10) as a common starting point. In both treatments the states $\{n\}$ are treated explicitly in the harmonic approximation. By analogy with the conventional solution of the classical theory: (1) the l.h.s. of Eq. (10) is identified with the experimentally observed k, (2) the fraction ρ_n corresponding to a nonreactive state $\{n\}$ is approximated by the equilibrium distribution P_n; and (3) the steady-state hypothesis is invoked for reactive states. The collisional term for reactive states is further assumed to have contributions only from the nonreactive states. This strong collision assumption then leads to a Lorentz type collision term,

$$\{1/[\mathrm{A}]\}\{d[\mathrm{A}_n^*]/dt\}=-[(\rho_n^*-P_n^*)/\tau_n]-\nu_n\rho_n^*=0;$$
$$\tau_n^{-1}=\sum_{\substack{\text{nonreactive}\\ m}} a_{nm}/P_n^*. \tag{11}$$

In actual application it is assumed that there is complete deactivation upon every collision so that the relaxation times τ_n are taken as constant and are represented in terms of the kinetic collision constant.[6]

$$\tau=1/[\mathrm{M}]b; \qquad b=(8\pi/\beta\mu)^{\frac{1}{2}}\sigma^2. \tag{12}$$

The specificity of the rate constant with respect to the nature of the inert gas M is here adjusted by the arbitrary assignment of variable collision diameters.

The main difference between the earlier theory of Kassel and that of Slater lies in the molecular detail inserted into the m.d.f. The former depends only on the total energy of the oscillators while the latter involves all their action variables. Despite this distinction Kassel's theory and Slater's classical treatment lead to the same type of temperature independent pre-exponential factor for k_∞ as appears in Eq. (5), in which equation the Boltzmann factor in the denominator should be justifiably deleted.

In Kassel's treatment the reactive molecular states are represented by s weakly coupled oscillators with common angular frequency ω. The m.f.d. for states with total energy $n\hbar\omega$ is assumed to be proportional to the probability that a particular oscillator, say n_1, possesses at least n^* quanta. The probability is computed by assuming a microcanonical distribution for the basic states belonging to n.

$$\nu_n=\bar{\nu}_K\langle u(n_1-n^*)\rangle_n=\bar{\nu}_K[g_s(n-n^*)/g_s(n)]u(n-n^*)$$
$$u(t)=0 \quad t<0$$
$$=1 \quad t\geq 0 \tag{13}$$
$$g_s(m)=(m+s-1)!/m!(s-1)!.$$

These specifications lead to the following expression for the pressure dependence of Kassel's k:

$$k/k_\infty=(1-e^{-\theta})^s\sum_{n=0}^{\infty}\frac{g_s(n)e^{-n\theta}}{1+[\bar{\nu}_K\tau g_s(n)/g_s(n+n^*)]}$$
$$\theta=\beta\hbar\omega, \tag{14}$$

while the high-pressure limit is given by

$$\kappa_\infty=\nu_K\exp(-\beta\epsilon_K^*)$$
$$\epsilon_K^*=n^*\hbar\omega. \tag{15}$$

The high-pressure pre-exponential factor $\bar{\nu}_K$ and activation energy ϵ_K^* are evaluated from the experimental k_∞. Since θ and s, the number of effective oscillators, are adjustable parameters, the theory is frequently only utilized in the semiclassical limit, so that the m.d.f. simplifies to

$$\nu(\epsilon)=\bar{\nu}_K[g_s(\epsilon-\epsilon_K^*)/g_s(\epsilon)]u(\epsilon-\epsilon_K^*)$$
$$g_s(n)=n^{s-1}/(s-1)! \tag{16}$$

which leaves the temperature dependence of k_∞ unchanged.

Slater's theory leads to a smaller number of adjustable parameters and is based on transition state criteria. He considers a particular reaction coordinate q_1, which is expressed in terms of the normal modes of the molecule. His m.d.f. is then assumed to be given by the frequency with which q_1 exceeds the critical value q_0. For the subsequent discussion it will be convenient to simplify the formulation in terms of the Dirac delta function, $\delta(q)$. The number of times the value q_0 is attained by q_1 in time τ is then given by

$$\sum\int\delta(q_1-q_0)dq_1=\int_0^\tau\delta(q_1-q_0)|\,q_1'\,|\,dt.$$

Upon only admitting positive extensions of q_1 and using the "random gap" approximation,[7] the desired m.d.f. is then taken as the infinite time average

$$c_n=L=\lim_{\tau\to\infty}\tau^{-1}\int_0^\tau\nu(P_1\ q_1)dt$$
$$\nu(P_1\ q_1)=[\delta(q_1-q_0)/2]\cdot|\,q_1'\,|. \tag{17}$$

This infinite time average is then computed in terms of a suitable phase average, where it is convenient to perform a contact transformation to the angle and action variables ψ, J of the normal modes. In the classical limit the proper average[8] is obtained by taking random phases and specified action variables

$$L(\{J_i\},\{\Delta\psi_i\})=\int\cdots\int\nu(p_1',q_1')\prod_{i=1}^{m'}\delta(J_i'-J_i)dJ_i'd\psi_i', \tag{18}$$

where m' is the number of nondegenerate modes contributing to q_1. The Fourier integral representation for $\nu(p_1, q_1)$ then immediately leads to Slater's explicit m.d.f., to which the interested reader is referred.[5] The k_∞ that arises in the classical limit from Eq. (18) takes the simple form

$$k_\infty=\bar{\nu}_e\exp(-\beta\epsilon_e^*). \tag{19}$$

[8] M. Kac, Am. J. Math. 65, 609 (1943).

Here $\bar{\nu}_s$ and the minimum energy required for dissociation ϵ_s^* are formally available from the frequencies and m amplitude factors contributing to q_1.

It is, however, of importance to recognize that in unimolecular rates two competing time scales appear in the theory. One involves the time between collisions and the other measures the time of intramolecular energy transfer. Since the former increases with decreasing pressure, one expects the anharmonic interactions to wash out some of the initial conditions, contained in Eq. (18), as the low-pressure limit is approached. Although the calculations of Fermi, Pasta, and Ulam[9] on the effect of anharmonicities for a small number of oscillators indicate that under certain conditions this may not arise, their work is as yet not applicable to the complicated anharmonic interactions in real molecules. The limiting form of smoothed out initial conditions is obtained by use of a microcanonical average in Eq. (18). The desired result is most easily obtained from the inverse Laplace transform of Eq. (19) and yields a Kassel type classical m.d.f.

$$\langle L\rangle=\frac{\int\cdots\int\nu(p_1', q_1')\delta(\epsilon'-\epsilon)\prod_{i=1}^{m}dJ_i'd\psi_i'}{g_m(\epsilon)}$$

$$=\bar{\nu}_s g_m(\epsilon-\epsilon_s^*)U(\epsilon-\epsilon_s^*)/g_m(\epsilon). \tag{20}$$

We now turn to the interpretation of this result. Although the m.d.f.'s, Eqs. (16) and (18), lead to different k_0's, in the classical limit the reduced pressure dependences are strikingly similar.

$$k/k_\infty=[1/\Gamma(t)]\int_0^\infty\frac{z^{t-1}e^{-z}dz}{1+[xz^{t-1}\alpha/\Gamma(t)]}$$

$$x=k_\infty/k_0[\mathrm{M}], \tag{21}$$

where in Kassel's theory

$$t=s$$

and

$$\alpha=\frac{\Gamma(s)e_{s-1}(\beta\epsilon_K^*)}{(z+\beta\epsilon_K^*)^{s-1}}$$

$$\approx\frac{1}{[1+(z/\beta\epsilon_K^*)]^{s-1}\{1-[(s-1)/\beta\epsilon_K^*]\}}, \tag{22}$$

while by Slater's theorem[5] t is molecularly specified,

$$t=\tfrac{1}{2}(m'+1)$$

and

$$\alpha=1. \tag{23}$$

It is now of interest to observe that an increase of t leads to a more gradual pressure falloff for k. Since by comparison of Eqs. (20) and (23), $t_{\mathrm{anharm}}>t_{\mathrm{harm}}$, within the framework of the transition state criterion (17) the implicit inclusion of anharmonic interactions leads to a more gradual falloff. The extent to which this trend occurs cannot be established at present.

Since the frequencies in molecular vibrations must be quantized, Slater[10] has more recently proposed a quantum formulation. He retains all the earlier assumptions of his classical treatment including the m.d.f., Eq. (17), but simply replaces the normalized classical equilibrium distribution in the final Eq. (21) by the equilibrium Wigner[11] function for the oscillators. This procedure leads to revised expressions for k_0 and k_∞, but yields the same pressure dependence for k/k_∞ on a reduced basis. By contrast Kassel's theory on a reduced basis depends strongly on the quantum spacing θ.

We shall explore Slater's extension by examining, for illustrative purposes, the case of only one oscillator. Here the Wigner phase space function, recognized to be real but not positive definite, is defined for the nth pure state as

$$W_n(p, q)=(\pi\hbar)^{-1}\int_\infty^\infty\psi_n(q+y)\psi_n^*(q-y)$$

$$\times\exp(2ipy/\hbar)dy. \tag{24}$$

Upon inserting the normalized oscillator wave function ψ_n into Eq. (24) and using a standard formula[12] one finds that W_n can be expressed in terms of the Laguerre polynomial

$$W_n=(-1)^n\exp-(2H/\hbar\omega)L_n(4H/\hbar\omega)$$

$$\sim\delta[(J/h)-n]/h$$

$$H=(p^2/2m)+(m\omega^2q^2/2). \tag{25}$$

Although the Wigner function is recognized to yield correct expectation values only for sum functions of noncommuting variables,[13] its simple use implies the following quantum m.d.f.

$$\nu_n=\iint\delta(q-q_0)\mid p/m\mid W_n(p, q)dpdq$$

$$=\int_0^\infty\nu_{\mathrm{class}}(J)W_n(J)dJ. \tag{26}$$

The classical configurational criterion underlying the theory thus also leads to contributions from the nonreactive states. Upon introduction of the generating function

$$P(J)=\sum_{n=0}^{\infty}\rho_nW_n(J),$$

$$\rho_n=h\int_0^\infty W_n(J)P(J)dJ \tag{27}$$

[9] Fermi, Pasta, and Ulam, Los Alamos Scientific Laboratory Rept. 1940 (1955).

[10] N. B. Slater, Proc. Roy. Soc. Edinburgh **A164**, 61 (1955).

[11] E. Wigner, Phys. Rev. **40**, 749 (1932).

[12] A. Erdelyi, *Tables of Integral Transforms* (McGraw-Hill Book Company, New York, 1954), Vol. II, p. 292.

[13] A. O. Barut, Phys. Rev. **108**, 565 (1957).

the rate constant k with use of Eqs. (10) and (26), indeed takes Slater's final form

$$k=\sum_{n=0}^{\infty}\nu_n\rho_n=\int_0^{\infty}\nu_{class}(J)P(J)dJ. \quad (28)$$

In the high-pressure limit $P(J)$ corresponds to equilibrium so that

$$k_\infty=\nu\exp(-\beta^\dagger\epsilon_s^*)$$
$$\beta^\dagger=(2/\hbar\omega)\tanh(\theta/2). \quad (29)$$

The calculation of $P(J)$ at lower pressures is more complex. It is obtained by summing Eq. (11) with use of the definition (27). Upon carrying out this operation it is found that Slater's surmise

$$P(J)=P_{eq}(J)/(1+\nu_{class}\tau), \quad (30)$$

is subject to two approximations. The first is the relatively good estimate

$$W_n(H'/\hbar\omega)W_n(H/\hbar\omega)$$
$$=W_n(H'/\hbar\omega)(\delta[(H'-H)/\hbar\omega]/h).$$

The second is the implicit assumption that the Lorentz collision term also applies to the nonreactive states, a condition which now implies that

$$(\partial[\mathrm{A}]/\partial t)_{coll}\neq 0.$$

Thus Slater's application of the Wigner function to noncommuting variables and his surmise Eq. (30), leave his quantum extension on less secure ground than his important classical theory.

III

We now turn to that solution of the basic equation (8) which is the extension of Eq. (6). It is here convenient to introduce a function which measures deviations from equilibrium. The desired relation determining the evolution of molecular states now reads

$$P_n(\partial G_n/\partial t)=-\sum_m a_{nm}(G_n-G_m)-\nu_nP_nG_n^*;$$
$$G_n=f_n/P_n. \quad (31)$$

It will be noted that the formal inclusion in a_{nm} of anharmonic contributions to the intramolecular process would lead to a higher effective pressure and thus to a more gradual pressure dependence. The general solution of Eq. (31) immediately follows when one recognizes that its r.h.s. involves a self-adjoint operator. With the usual experimental condition of an initial equilibrium distribution, the macroscopic concentration of reactant species then takes the simple form

$$[\mathrm{A}(t)]/[\mathrm{A}(0)]=\sum_\alpha\sigma_\alpha\exp(-\lambda_\alpha t) \quad (32)$$

where

$$\sigma_\alpha=[\sum_n P_nG_n^{(\alpha)}]^2/\sum_n P_nG_n^{(\alpha)2}.$$

The eigenvectors and eigenvalues appearing in Eq. (32) are related by

$$\lambda_\alpha P_nG_n^{(\alpha)}=\sum_m a_{nm}(G_n^{(\alpha)}-G_m^{(\alpha)})+\nu_nP_nG_n^{*(\alpha)}, \quad (33)$$

and thus follow from the variation criterion

$$\delta\lambda=0$$

where

$$\lambda=\tfrac{1}{2}[\sum_{n,m}a_{nm}(G_n-G_m)^2+\sum_n\nu_nP_nG_n^{*2}]/\sum_n P_nG_n^2. \quad (34)$$

In those representative systems whose reactive states correspond to a very small initial fraction, the leading term σ_0 in Eq. (32) again differs only negligibly from unity. The associated lowest eigenvalue is well separated from the higher ones and may be identified with the experimentally observed pseudo first-order rate constant k. These consequences of the mechanism, Eq. (7), thus account for the observed time evolution of the system. Since in the high-pressure limit an equilibrium distribution is attained, $G_m^{(0)}=1$ in this limit, so that

$$k_\infty=\lambda_0([\mathrm{M}]=\infty)=\sum\nu_nP_n^*. \quad (35)$$

By using the familiar inequality satisfied by the lowest eigenvalue

$$\lambda_0(G_n^0)\leq\lambda_0(G_n=1)$$

it follows that

$$k\leq k_\infty, \quad (36)$$

which qualitatively accounts for the pressure falloff of the rate constant.

The assertion that the lowest eigenvalue λ_0 is well separated from λ_1 follows from Courant's theorem.[14] We designate the lowest nonvanishing eigenvalue in the absence of the chemical sink by λ_1^0 and note that the quadratic form associated with the chemical sink alone is positive definite. The theorem then ensures that $\lambda_1>\lambda_1^0$. Furthermore, the separation between λ_1 and λ_0 is least in the low-pressure limit. Here

$$\lambda_0\approx P_{n^*}\lambda_1^0,$$

when P_{n^*}, the equilibrium fraction for the least energetic state leading to dissociation, is very small. Thus, we finally obtain the result $\lambda_1\gg\lambda_0$.

These considerations will now be applied to the earlier case of the strong activation mechanism. Here, we again only consider transitions to reactive states from the nonreactive states distributed at equilibrium. With use of the previous notation, the lowest eigenvalue then takes the simple form

$$\lambda_0=\frac{\sum_{\substack{\text{reactive}\\ \text{states}}}(P_n/\tau_n)(G_n^{(0)}-1)^2+\nu_nP_nG_n^{(0)2}}{\sum_n P_nG_n^{(0)2}}. \quad (37)$$

[14] R. Courant and D. Hilbert, *Methoden der Mathematischen Physik* (Julius-Springer, Berlin, 1931), p. 28.

The distribution of reactive states follows from the condition $\delta\lambda_0=0$, so that

$$G_n^{(0)}=[1+\tau_n(\nu_n-\lambda_0)]^{-1}. \tag{38}$$

Since in general $\lambda_0 \ll \min \nu_n$, the substitution of Eq. (38) into Eq. (37) finally yields

$$k=\lambda_0=\sum_{\substack{\text{reactive}\\ \text{states}}}[P_n\nu_n/(1+\nu_n\tau_n)]. \tag{39}$$

Relation (39) is identical with the result obtained from the steady-state hypothesis Eq. (11), and the assumption that the l.h.s. of Eq. (10) may be equated to k.

We shall now examine in greater detail the transitions that would be induced in A by collision with M. Since the very low-lying nonreactive states can be adequately treated in the harmonic approximation, one here takes transitions among neighboring vibrational states as dominant. The relevant transition probabilities for this case were introduced by Landau and Teller[15] in their investigation of sound dispersion. This theory has been subsequently refined by Shuler[16,17] for closed systems of one-oscillators. As the reactive states are approached, due to the increasing contribution of anharmonicity, centrifugal stretching, etc., broader transitions and larger transfers of intermolecular energy become of increasing importance. The example of strong collisions considered in the foregoing is the limiting case for the efficient transfer of energy. In the remainder of this paper we shall calculate k for polyatomic molecules, employing the other limiting case of an inefficient collisional operator corresponding to the transfer of small amounts of energy and transitions only between adjacent vibrational states of the reactant molecule. It is to be expected that the actual collisional contribution is bracketed by these extremes.

This treatment is carried out within the framework of the generalized Lindemann mechanism and again ignores the effect of possible low-lying excited electronic states.

The present case of a set of oscillators, weakly coupled to the heat bath environment, implies that Eq. (9) is an example of the Pauli equation whose foundation has been critically analyzed by van Hove.[18] In order to study the pressure dependence of k for this essentially quantal activation process, we adopt the Kassel model of s effective degenerate oscillators and an m.d.f. dependent only on total energy. Although this model possesses too many adjustable parameters, its use facilitates explicit calculations, and leads to a temperature dependence for k_∞ consistent with experiment. The discussion of Sec. II reviews that with proper choice of the parameter t the pressure dependence of k is comparatively insensitive to the m.d.f. selected. Since both the initial equilibrium conditions and the m.d.f., Eq. (13), are functions of the total quantum number n, it suffices to take those G's in the variational formulation (34) as dependent only on n. Use of the familiar Landau-Teller transition probabilities for the individual oscillators and summation over all quantum numbers except that corresponding to the total energy immediately leads to the following expression for λ:

$$\lambda=[\sum_{n=0}^{\infty}\zeta(n+s)P_n(G_{n+1}-G_n)^2+\sum_{n=n^*}^{\infty}\nu_nP_nG_n^2]/\sum_{n=0}^{\infty}P_nG_n^2 \tag{40}$$

$$P_n=g_s(n)(1-e^{-\theta})^s e^{-n\theta}$$

$$\zeta=e^{-\theta}P_{10}^{ell}b[\mathrm{M}],$$

where the Kassel ν_n is given by Eq. (13). P_{10}^{ell} designates the "effective" Landau-Teller transition probability per collision for the transition 1 to 0 of a representative oscillator and is recognized to depend on the nature of the inert gas M.

The desired relaxation spectrum is obtained from the condition $\delta\lambda=0$, which yields the basic relation

$$(\lambda/\zeta)P_nG_n=(n+s-1)P_{n-1}(G_n-G_{n-1})u(n-1)$$
$$-(n+s)P_n(G_{n+1}-G_n)+(\nu_nP_nG_n/\zeta)u(n-n^*). \tag{41}$$

IV

In preparation for the calculation of the lowest eigenvalue of Eq. (41), it will be instructive to consider a related mechanism which utilizes the foregoing stepwise process for the degenerate oscillators but employs an energy dependent m.d.f. that leads to the Slater type k of Eq. (29). Since the differential equation that arises resembles formally the semiclassical limit of Eq. (41), it leads rather easily to the main physical conclusions inherent in the difference equation. This procedure will also provide a simple route for obtaining λ_m^0, the eigenvalues in the absence of a sink. We again use the Wigner function for the oscillators, Eq. (25), and note that in the present degenerate case we only require the function defined by

$$W_n=[g_s(n)]^{-1}\sum_{\{n_i\}}\prod_{i=1}^{s}W_{n_i}(H_i/\hbar\omega). \tag{42}$$

$$\sum n_i=n. \tag{42}$$

With the use of the addition theorem for Laguerre polynomials,[19] W_n may be expressed in terms of associated Laguerre polynomials and the total Hamiltonian of the oscillators:

$$W_n=\frac{(-1)^n\exp-(2H/\hbar\omega)L_n^{s-1}(4H/\hbar\omega)}{g_s(n)(\pi\hbar)^s}. \tag{43}$$

[15] L. Landau and E. Teller, Physik. Z. Sowjetunion **10**, 34 (1936).
[16] R. J. Rubin and K. E. Shuler, J. Chem. Phys. **25**, 59 (1956).
[17] E. W. Montroll and K. E. Shuler, J. Chem. Phys. **26**, 454 (1957).
[18] L. van Hove, Physica **23**, 441 (1957).
[19] W. Magnus and F. Oberhettinger, *Formulas and Theorems for the Functions of Mathematical Physics* (Chelsea Publishing Company, New York, 1954), p. 85.

We again construct the generating function

$$F(H)=[H^{s-1}/(s-1)!]\sum_{n=0}^{\infty}P_nG_nW_n(H);$$

$$G_n=e^{n\vartheta}(1-e^{-\vartheta})^{-s}h^s\int_0^{\infty}F(H)W_n(H)dH. \qquad (44)$$

At equilibrium where $G_n=1$, $F(H)$ reduces[20] to the normalized Wigner function $P(y)$

$$F_{eq}(H)=P(y)=[y^{s-1}/(s-1)!]\beta^{\dagger}e^{-y};$$
$$y=\beta^{\dagger}H. \qquad (45)$$

We next substitute the collisional part of Eq. (41) into Eq. (44) and find, with use of recursion formulas for Laguerre polynomials, that the desired relation for the mechanism leading to a

$$k_{\infty}=\bar{\nu}\exp(-\beta^{\dagger}\epsilon^*)$$

is given by

$$\lambda P(y)G(y)=-(d/dy)[\zeta^{\dagger}yP(y)(dG/dy)]$$
$$+\bar{\nu}[1-(y^*/y)]^{s-1}P(y)G(y)U(y-y^*), \qquad (46)$$

where

$$G(y)=F(y)/P(y); \qquad y^*=\beta^{\dagger}\epsilon^*;$$
$$\zeta^{\dagger}=(1-e^{-\vartheta})P_{10}^{s+1}[\mathrm{M}]b.$$

The collisional contribution to Eq. (46) is seen to possess the expected Fokker-Planck form[21] with "friction constant" $\zeta^{\dagger}$. Equation (46) must be solved subject to vanishing of current at the end points and continuity of function and current at $y=y^*$. This yields the conditions

$$\lim_{y\to 0}y^se^{-y}(dG/dy)=0;$$

$$\lim_{y\to\infty}y^se^{-y}(dG/dy)=0;$$

$$(d\log G/dy)\text{ continuous at }y=y^*. \qquad (47)$$

From the derivation of Eq. (46) it follows that in the absence of a sink Eqs. (41) and (46) are equivalent. The solution of Eq. (46) with $\bar{\nu}=0$ subject to the conditions (47) is readily seen to be

$$G_m=L_m^{s-1}(y),$$

so that the spectrum of Eq. (41) in the absence of reaction is given by

$$\lambda_m^0=m\zeta^{\dagger}. \qquad (48)$$

This result and application of Courant's[14] and Weyl's[22] theorems then provides a convenient bound for the spectrum resulting from stepwise activation and Kassel's m.d.f.

$$\text{larger of } m\zeta^{\dagger} \text{ or } \nu_n\leq\lambda_m\leq m\zeta^{\dagger}+\bar{\nu}_K. \qquad (49)$$

We now return to the study of the lowest eigenvalue of Eq. (46). For $y\leq y^*$ the solution satisfying the boundary condition at the origin is given by the confluent hypergeometric function[23]

$$G_-=a\Phi[(-\lambda/\zeta^{\dagger}),s,y]. \qquad (50)$$

For the case considered here of $P_n^*\ll 1$, it is sufficient to retain only linear terms in λ_0.

$$\Phi[-(\lambda_0/\zeta^{\dagger}),s,y]=1-(\lambda_0/\zeta^{\dagger})h(y), \qquad (51)$$

where

$$h(y)=(s-1)!\int_0^y\{[e^y-e_{s-1}(y)]/y^s\}dy.$$

On the basis of this result, the low-pressure limit can be calculated since here $G_-(y^*)=0$. For the present illustrative model, $\lambda_0([\mathrm{M}]\to 0)$ takes the form[24]

$$k_0[\mathrm{M}]=\zeta^{\dagger}/h(y^*)$$

$$h(y)\sim\frac{(s-1)!e^y}{y^{s-1}(y-s)}\{1+[s/(y-s)^2]+\cdots\}. \qquad (52)$$

For the desired pressure dependence of k solutions of Eq. (46) must also be obtained for values of y larger than that of the "classical turning point" y^*. Although for $s=1$ and 2, the solution is again in terms of confluent hypergometric functions, the general case is most readily handled by alternative techniques. The use of the trial function $G\propto 1-\alpha h(y)$ for $y\leq y^*$ and $G\propto\exp(1-\delta)y/2$ for $y\geq y^*$ in the variational formulation of Eq. (46) leads to results indistinguishable from those obtained by machine calculation if s is very small. k/k_{∞} may then be expressed as a function of $k_0[M]/k_{\infty}$ by the parametric equations

$$k_0[\mathrm{M}]/k_{\infty}=\frac{4\{(s+2)\delta+s\}}{\delta^{s-1}(\delta^2-1)(3\delta+1)},$$

$$k/k_{\infty}=\frac{4\{(s+2)\delta^2+\delta-(s-1)\}}{\delta^s(\delta+1)^2(3\delta+1)}. \qquad (53)$$

For arbitrary s available asymptotic techniques are sufficient to map out the pressure dependence of k in the low and high pressure regions. The procedure is straightforward in the low-pressure region[25] while in the high-pressure region an extension of Langer's method[26] leads to modified Bessel functions of the third

[20] A. Erdelyi, *Higher Transcendental Functions* (McGraw-Hill Book Company, Inc., New York, 1953), Vol. II, p. 189.
[21] R. W. Zwanzig, J. Chem. Phys. **28**, 365 (1958).
[22] H. Weyl, Math. Ann. **71**, 441 (1912).
[23] Reference 20, Vol. I, p. 248.
[24] Reference 20, Vol. II, p. 140.
[25] A. Erdelyi, *Asymptotic Expansions* (Dover Publications, Inc., New York, 1956), p. 83.
[26] Reference 25, p. 93.

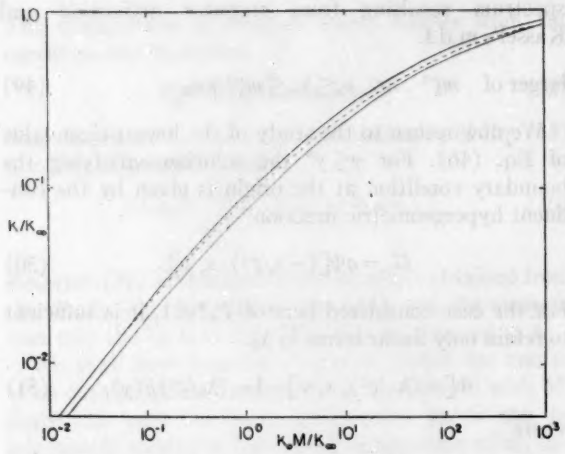

FIG. 1. k/k_∞ *versus* $k_0[M]/k_\infty$. $e^{-\beta}=0.6$. Solid lines are curves calculated with the present theory for $s=9$ (bottom) and 8 (top); dashed line is that given by Kassel theory for $s=10$.

kind. With neglect of terms $0(1/y^*)$ the result of these calculation may be easily summarized:

$$k/k_\infty \sim 1-\{k_\infty/k_0[M]\}[(2s)!/(s!)^2]+\cdots$$

$$k/k_0[M] \sim 1-c[M]^{1/(s+1)}. \qquad (54)$$

This result is to be contrasted with the analogous pressure dependence that is derived from the strong collision mechanism and the classical Kassel model, Eq. (21). Here it is found that

$$k/k_\infty \sim 1-\{k_\infty/k_0[M]\}[(2s-2)!/(s-1)!^2]$$

$$k/k_0[M] \sim 1-c'[M]^{1/(s-1)}. \qquad (55)$$

It is thus seen that our approximation to the difference equation describing the stepwise activation process leads to a pressure dependence for k, on a reduced basis very similar to that of the semiclassical strong collision Kassel theory. The present mechanism requires 1 less Kassel oscillator at high pressures and 2 fewer Kassel oscillators at low pressures. The same insensitivity to activation mechanism and the identical oscillator rule

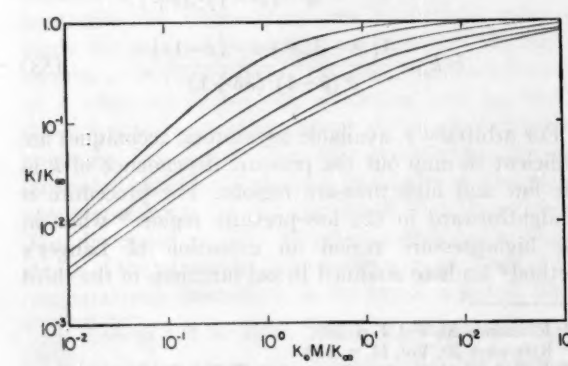

FIG. 2. k/k_∞ *versus* $k_0[M]/k_\infty$. Variation with s. $e^{-\beta}=0.6$; $s=1, 3, 5, 7, 9, 10$ (from top to bottom).

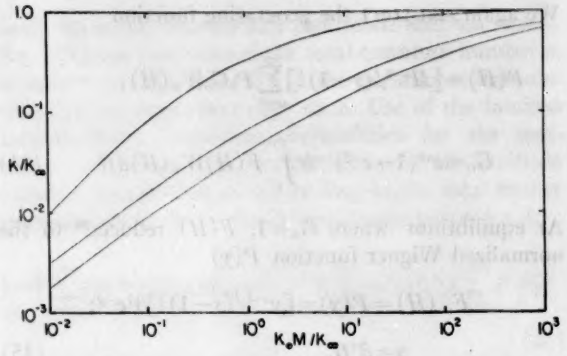

FIG. 3. k/k_∞ *versus* $k_0[M]/k_\infty$. Variation with $e^{-\beta}$. $s=10$; $e^{-\beta}=0.1, 0.6, 0.8$ (from top to bottom).

hold for the solutions of the difference equation, Eq. (41), which we shall now examine.

Here we designate the solutions of Eq. (41) by G^- for n below n^* and by G^+ for n above n^*. The equation for the nonreactive states is conveniently solved by double summation of Eq. (41) to yield the discrete analog of an integral equation

$$G_n^- - G_0^- = -(\lambda/\zeta)\sum_{l=0}^{n-1}\sum_{m=0}^{l}[P_m G_m^-/(l+s)P_l]. \qquad (56)$$

This equation may be solved in terms of a power series in λ by iteration. For the present case of $P_{n^*} \ll 1$, calculation shows that for the evaluation of λ_0, a linear perturbation is sufficient, so that

$$G_n^- = G_0^-[1-(\lambda_0/\zeta)h_n] \qquad (57)$$

where

$$h_n = \sum_{l=0}^{n-1}\sum_{m=0}^{l}\frac{g_s(m)\,e^{(l-m)\theta}}{(l+1)g_s(l+1)}. \qquad (58)$$

For large values of n, h_n may be approximated with high

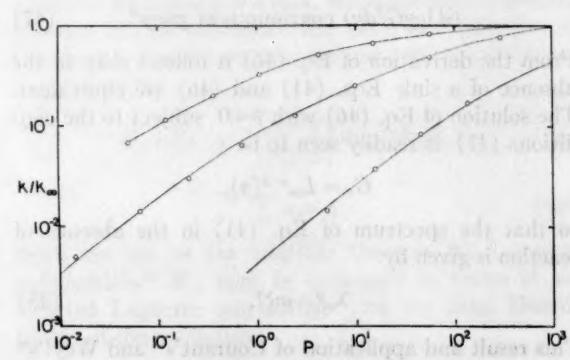

FIG. 4. k/k_∞ *versus* pressure. Comparison of theory with experiment. The horizontal scale has been shifted for the various curves to permit convenient display. From top to bottom; cyclopropane (0.8, 8), nitrogen pentoxide (0.6, 10), nitrous oxide (0.8, 3). Circles indicate theoretical values computed using the values of $e^{-\beta}$ and s given in the parentheses. Experimental data were taken from reference 1.

precision by the discrete analog of the Blanch expansion[24]

$$h_n \sim \frac{e^{(n-1)\theta}}{n g_s(n)(1-e^{-\theta})^{s+1}\{1-[se^{-\theta}/(n-1)(1-e^{-\theta})]\}}. \quad (59)$$

By means of the quantities h_n one can compute the degree of depletion of the states below n^* due to chemical reaction for any value of (λ_0/ζ). Due to the exponential dependence on n of h_n, deviations from equilibrium for $n<n^*$ are negligible except in the vicinity of n^*. The deviation is a maximum in the low-pressure limit since here the activated states are completely depleted by chemical reaction, so that $G_{n^*}=0$. Thus in the low pressure limit, with use of Eqs. (57) and (59), one obtains

$$k_0[M] \approx \zeta g_s(n^*)(1-e^{-\theta})^s \exp(-n^*\theta)[n^*(e^\theta-1)-s]$$
$$= P_{n^*}\zeta^\dagger\{n^*-[s/(e^\theta-1)]\} \quad (60)$$

where $\zeta^\dagger$ is explicitly given in Eq. (46). In the high-pressure limit, $G_n^0=1$, so that by summation of Eq. (41) over all states we obtain

$$k_\infty = \bar{\nu}_k \exp(-\beta\epsilon_k^*);$$
$$\epsilon_k^* = n^*\hbar\omega. \quad (61)$$

In the intermediate pressure range, solutions of Eq. (41) are required for all n. Equation (57) and the matching conditions

$$G_{n^*-1}^- = G_{n^*-1}^+$$

and

$$G_{n^*}^- = G_{n^*}^+$$

lead to the desired relation of (k/k_∞) as a function of $x=k_\infty/k_0M$,

$$k/k_\infty = (1/x)\frac{G_{n^*-1}^+ - G_{n^*}^+}{[G_{n^*-1}^+ - G_{n^*}^+(h_{n^*-1}/h_{n^*})]}. \quad (62)$$

Since $\lambda_0 \ll \nu_{n^*}$, the G^+'s are determined by the relation

$$n\epsilon^\theta(G_n^+ - G_{n-1}^+) + (n+s)(G_n^+ - G_{n+1}^+) + \frac{xg_s(n-n^*)G_n^+}{\exp(-n^*\theta)h_{n^*}g_s(n)} = 0. \quad (63)$$

Equation (62) was evaluated on the IBM 650 computer of the University of Rochester Computing Center.[27] h_{n^*} and h_{n^*-1} were calculated from Eq. (58). Because of the strongly divergent nature of the inadmissible solution of Eq. (63), it was found, for the parameters selected for evaluation, that the solutions at n^* were completely insensitive to reasonable starting values for $G_{n\dagger}$, $n^\dagger \geq 2n^*$. The results of these calculations computed for $n^*\theta=38.4$, are summarized in the figures.

Figure 1 is a representative comparison of the present stepwise activation mechanism with the original strong collision process, Eq. (14), both with a Kassel m.d.f. It is seen that the pressure dependence on a reduced basis is strikingly similar and is in agreement with the oscillator rule established in the continuum case. The less efficient intermolecular energy transfer process for the same assignment of s leads to a more gradual pressure dependence than the efficient process. Figures 2 and 3 illustrate, for the stepwise model, the variation with the "effective oscillator parameter" s for fixed energy level spacing θ, and the variation with spacing for fixed s. As in the familiar Kassel theory, an increase in s leads to a broader transition, while a larger quantum spacing narrows the transition range. Due to the flexibility of the Kassel m.d.f., the theory can account for the observed reduced pressure dependence of k with realistic assignment of parameters. This comparison between theory and experiment is illustrated in Fig. 4 for cyclopropane, nitrogen pentoxide, and nitrous oxide, for which reliable data are available over a wide pressure range.

TABLE I.

Reactant	T°K	$\epsilon^{-\theta}$	s	P_{10}^{eff}	$(2P_{10}^{eff}n^*/s)$
N_2O	880	0.6	4	6.3×10^{-3}	1.1×10^{-1}
NO_2Cl	475	0.6	5	1.6×10^{-2}	3.8×10^{-2}
N_2O_5	300	0.6	10	6.3×10^{-3}	8.7×10^{-2}
		$b=10^{-13.9}$ cc/mole sec			

The oscillator rule, illustrated in Fig. 1 brackets the pressure dependence of k for the two limiting activation mechanisms. The actual applicability to polyatomic molecules of the limiting case of small collisional energy transfer may be examined by a comparison of k_0 (theoretical), given by Eq. (60), and k_0 (experimental). Table I summarizes this comparison for selected molecules for which reliable values of k_0 are available. k_0 (experimental) for N_2O and N_2O_5 has been taken from reference 1 and that for NO_2Cl from the work of Volpe and Johnston.[28] The values of P_{10}^{eff} listed in the table are those that would lead to agreement between theory and experiment. The last column lists the energy transfer efficiency, per oscillator for those high-lying states that no longer contribute to the value of k. The mean values of P_{10}^{eff} thus obtained for the high-lying states of these molecules are not inconsistent with known large experimental P_{10}'s for very low-lying states. Nevertheless, due to the unavoidable arbitrary assignment of parameters this result does not warrant any definite conclusions as to the extent of applicability of this mechanism to polyatomic molecules.

We are indebted to Shuler for recently bringing our attention his paper[29] on the low-pressure limit for diatomic molecules which also employs stepwise activation. Our expression for this quantity is obtained by setting $s=1$ in Eq. (60) and is in complete agreement with the criteria adopted by Montroll and Shuler.

[27] We are indebted to Dr. Patricia Eberlein for help in programing this problem.

[28] M. Volpe and H. S. Johnston, J. Am. Chem. Soc. 78, 3910 (1956).

[29] E. W. Montroll and K. E. Shuler, *Advances in Chemical Physics* (Interscience Publishers, Inc., New York, 1958), Vol. I, p. 361.

Microwave Absorption in Compressed Oxygen

A. A. MARYOTT AND G. BIRNBAUM*
National Bureau of Standards, Washington, D. C.
(Received July 23, 1959)

Precise measurements of the absorption in oxygen resulting from the small magnetic dipole moment are reported at frequencies near 2, 3, 9, and 23 kMc and at pressures in the range from 3 to 70 atmos. Up to 10 atmospheres the resonant contribution agrees with the Van Vleck-Weisskopf theory and the line width increases in proportion to the pressure. The line width (relaxation frequency) for the nonresonant contribution also increases in proportion to the pressure, but is only about one-third as large as the resonant line width. Above 20 atmospheres the resonant absorption shows anomalous behavior resembling that previously noted in the case of the inversion spectra of NH_3 and ND_3. In particular, the resonant frequency appears to decrease rapidly while the line width changes much less rapidly than the pressure.

INTRODUCTION

IN its ground electronic state, $^3\Sigma$, the oxygen molecule has two unpaired electrons, and the permanent magnetic dipole moment gives rise to absorption at microwave frequencies. As shown by Van Vleck,[1] this absorption is divided into two distinct spectra, one resonant and the other nonresonant.

Since oxygen is the principal gaseous constituent of the atmosphere that absorbs microwave radiation, both spectra are of considerable practical as well as theoretical interest. The resonant spectrum, consisting of many lines in the vicinity of 60 kMc, has been very extensively studied at low pressures and high resolution.[2]

Some observations have also been made of the unresolved envelope of these lines under atmospheric conditions.[2b,3a] Measurements at the higher pressures and lower frequencies, needed to determine the characteristics of the nonresonant contribution, have not been reported previously. In computations of the atmospheric attenuation due to oxygen, it has been generally assumed that the line widths for the resonant and nonresonant contributions are the same.

Measurements of the resonant absorption at higher pressures, where the line width becomes comparable to or greater than the resonant frequency, are also of particular interest in connection with the line-shape theory of pressure broadening. The resonant spectrum of oxygen, like the inversion spectra of NH_3 and ND_3, is especially suited for such studies, since it is confined to a rather narrow region of frequency and the widths of the individual lines at low pressures are known. At higher pressures, where the widths become substantially greater than the separation between lines, the entire spectrum may be approximated by a single line having the same integrated intensity. Previous data on NH_3[4] and ND_3[5] show pronounced changes in this region. In particular, the data can be reconciled with the Van Vleck-Weisskopf theory only if both the resonant frequency and the line-width parameter decrease rapidly with increasing pressure. Eventually, the absorption becomes indistinguishable from that of a purely nonresonant, or zero-frequency, spectrum. The transition occurs well below atmospheric pressure in the case of ND_3.

In this investigation the absorption in oxygen has been measured at pressures up to 70 atmos at frequencies near 9 and 23 kMc and up to 8 atmos at 2.3 kMc.[6] The latter conditions permit an accurate determination of the parameters characterizing the nonresonant spectrum without serious overlap from the resonant lines. At the higher frequencies and pressures the resonant and nonresonant terms both make substantial contributions to the observed loss. The general behavior of the resonant spectrum can be readily deduced and it is found to resemble, at least superficially, that observed in the ammonias.

THEORETICAL RELATIONS

The resonant spectrum consists of a number of lines which, with one minor exception that will be neglected hereafter, lie near 60 kMc. These involve transitions between the multiplet levels of each rotational state and are governed by the selection rules $\Delta J=\pm 1$, $\Delta N=0$, J and N being the quantum numbers for the total and the end-over-end angular momenta, respectively. Selection rules for the nonresonant absorption are $\Delta J=0$.

The total absorption in oxygen, expressed in terms of the loss tangent, is given by

$$\tan\delta=(2\pi N_0\mu^2/3kT)\cdot\sum_N f_N\{[N(2N+3)S_+/3(N+1)(2N+1)]+[(N+1)(2N-1)S_-/3N(2N+1)]+[(N^2+N+1)S_0/3N(N+1)]\}, \quad (1)$$

* Present address: Research Laboratories, Hughes Aircraft Company, Culver City, California.

[1] J. H. Van Vleck, Phys. Rev. **71**, 413 (1947).

[2] (a) R. M. Hill and W. Gordy, Phys. Rev. **93**, 1019 (1954); (b) J. O. Artman and J. P. Gordon, *ibid.* **96**, 1237 (1954); (c) M. Tinkham and M. W. P. Strandberg, *ibid.* **99**, 537 (1955); (d) M. Mizushima and R. M. Hill, *ibid.* **93**, 745 (1945).

[3] (a) R. Beringer, Phys. Rev. **70**, 53 (1946); (b) Strandberg, Meng, and Ingersoll, *ibid.* **75**, 1524 (1949).

[4] B. Bleaney and J. H. N. Loubser, Proc. Phys. Soc. (London) **A63**, 483 (1950).

[5] G. Birnbaum and A. A. Maryott, Phys. Rev. **92**, 270 (1953).

[6] A brief preliminary report of results over a more limited range of pressures was given previously (Phys. Rev. **99**, 1886 (1955)).

where N_0 is the molecular density, μ the dipole moment ($\mu^2=8\mu_0^2$ where $\mu_0=1$ Bohr magneton$=0.927\times10^{-20}$ erg gauss^{-1}), and f_N is the fractional number of molecules in the rotational state designated by the quantum number N. The summation extends only over odd values of N, as states with even values are excluded because of symmetry. The shape factors are designated by S, and the subscripts $+$, $-$, and 0 refer, respectively, to the transitions

$$J=N+1\leftarrow N,$$

$$J=N-1\leftarrow N,$$

and

$$J=\begin{cases}N+1\leftarrow N+1,\\ N\leftarrow N,\\ N-1\leftarrow N-1.\end{cases}$$

From the Van Vleck-Weisskopf theory,[7] we find

$$S_\pm=\{\nu\Delta\nu_\pm/[(\Delta\nu_\pm)^2+(\nu-\nu_\pm)^2]\}+\{\nu\Delta\nu_\pm/[(\Delta\nu_\pm)^2+(\nu+\nu_\pm)^2]\}$$

where ν is the applied frequency, $\Delta\nu_\pm$ is the line width, and $\nu_\pm$ is the resonant frequency. The factor S_0 pertains to transitions between degenerate states for which the resonant frequency is zero. For this case, $S_\pm$ reduces to

$$S_0=2\nu\Delta\nu_0/(\Delta\nu_0^2+\nu^2).$$

Hereafter, $\Delta\nu_0$ will be referred to as the relaxation frequency in order to distinguish it from the resonant line width, $\Delta\nu_\pm$.

Although more exact matrix elements than the above have been given by Tinkham and Strandberg,[8] the difference is too small to be of consequence in the present application. Equation (1) also involves other slight approximations which have negligible importance when the dielectric constant and magnetic permeability are close to unity.

If S_0 does not depend on the state N, the summation involving the last term of Eq. (1) reduces to $S_0/3$. The resonant part may also be simplified. Recent measurements of the individual line widths[2] indicate little if any variation from line to line. Also the lines are much too broad to be resolved at the pressures with which we are concerned and we may, to a close approximation, replace the $\nu_\pm$ by a single frequency corresponding to the center of the band. Then, for $T=298°$K, Eq. (1) becomes

$$\tan\delta=8.60\times10^{-7}(p/Z)(S_0/3+2S_\pm/3), \qquad (2)$$

where p is in atmospheres and Z is the compressibility factor. Data on the static magnetic susceptibility show that the suceptibility per molecule decreases slightly with increasing pressure and indicate a tendency to form weak, diamagnetic complexes.[9] The change in susceptibility per unit of pressure, however, is essentially constant for the pressures in question. Consequently, in the following analysis, we shall use Eq. (2) and simply let Z equal unity.

TABLE I. List of cavities used to measure the dielectric loss in compressed oxygen.

Cavity mode	Frequency (kMc)	Loaded Q (approx)	Pressure range (atmos)
TE_{011}	2.30	48 000	3–8
TE_{012}	9.07	28 000	8–38
TE_{112}	9.07	10 000	21–68
TE_{013}	23.34	15 000	8–40
TE_{114}	23.34	6 500	21–68

EXPERIMENTAL

The method of measuring the absorption in gases, specifically the loss tangent, using tunable, transmission-type cavities is described in another paper.[10] A number of different cavities were used. The characteristics of the cavities are given in Table I.

The loss tangents were obtained from the changes in transmitted power at resonance and the loaded Q, when the cavity was filled first with oxygen and then with a reference gas having the same refractive index and negligible loss. Argon was used for the reference gas because it has practically the same refractive index as oxygen at a given pressure. Use of argon minimizes the errors that might result from changes in transmitted power or in the Q of the cavity because of pressure distortion.

Samples of oxygen from several commercial sources, including one of high purity used previously for precise measurements of the dielectric constant, were measured and no significant differences in the loss tangent were obtained. Water vapor was a likely contaminant in some of the samples and an estimate of its effect on the loss tangent was made, assuming maximum contamination (saturation). The computed loss is at least two orders of magnitude smaller than any observable effect.

Measurements were made at a temperature of 25± 1°C. Pressures were determined with calibrated Bourdon test gauges; to precision of ±0.5%.

RESULTS

The data obtained at 2.30 kMc are summarized in Table II. The second series of measurements was made after a lapse of more than a year and with a different experimental assembly. The agreement between the two sets is quite satisfactory.

The data for 9.07 and 23.34 kMc are shown graphically in Fig. 1. The values of $\tan\delta/p$, interpolated from

[7] J. H. Van Vleck and V. F. Weisskopf, Revs. Modern Phys. 17, 227 (1945).
[8] M. Tinkham and M. P. W. Strandberg, Phys. Rev. 97, 932 (1955).
[9] Woltjer, Copoolse, and Wiersma, Communs. Phys. Lab. Univ. Leiden 201d; Proc. Acad. Sci. Amsterdam 32, 1329 (1929).
[10] A. A. Maryott and G. Birnbaum, J. Chem. Phys. 24, 1022 (1956).

TABLE II. Loss tangent for oxygen at 2.30 kMc.

Run 1		Run 2	
p (atmos)	tan δ/p	p (atmos)	tan δ/p
3.05	$2.8_2\times10^{-7}$	2.97	$2.8_9\times10^{-7}$
4.09	2.9_5	3.98	2.9_7
5.10	2.8_8	5.00	2.9_3
6.08	2.8_1	6.01	2.8_9
7.12	2.6_7	7.05	2.6_4
7.80	2.5_8	8.06	2.5_0

these curves at intervals of 10 atmos, are given in Table III. At the intermediate pressures, where measurements with the TE_{01} and TE_{11} cavities overlap, the agreement is good. The result obtained with the TE_{11} cavities average about 2% higher at both frequencies.

ANALYSIS

(a) Data at 2.30 kMc

A superficial examination of the data at 2.30 kMc (Table II) shows that the loss in this region is of the nonresonant type and any overlap from the resonant part is minor. It is evident from Eq. (2) that as the pressure, and consequently the relaxation frequency $\Delta\nu_0$, increases, the quantity tan δ/p (nonres) should rise to a maximum value of 2.87×10^{-7} when $\Delta\nu_0=\nu$ and then decline as the pressure is further increased. The observed maximum value occurs in the neighborhood of 4 atmos and is close to this theoretical limit.

Before we evaluate the parameters characterizing the nonresonant spectrum, we shall examine the resonant contribution in more detail. For the case where the line width and the applied frequency are both small compared to the resonant frequency, the resonant term

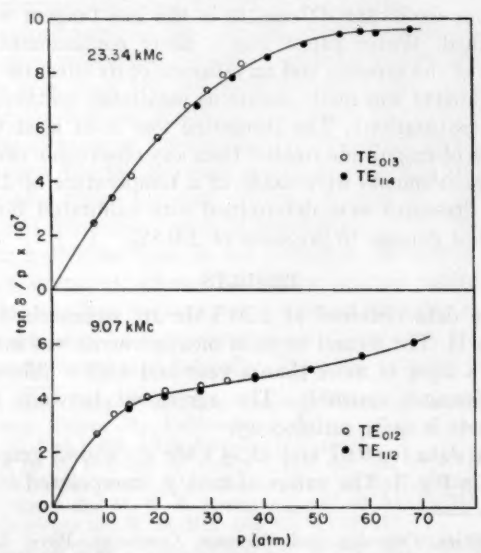

FIG. 1. Plot of the loss tangent per atmosphere for oxygen as a function of the pressure at 23.34 and 9.07 kMc.

TABLE III. Interpolated values of the loss tangent per atmosphere at 9.07 and 23.34 kMc.

p (atmos)	tan δ/p	
	9.07 kMc	23.34 kMc
10	3.05×10^{-7}	2.94×10^{-7}
20	4.07	5.42
30	4.42	7.24
40	4.79	8.47
50	5.18	9.22
60	5.60	9.59
68.4	6.03	9.64

in Eq. (2) reduces to

$$\tan\delta/p(\text{res})=11.5\times10^{-7}\nu\Delta\nu_{\pm}/\nu_{\pm}^2. \quad (3)$$

The centroid frequency, $\nu_{\pm}$, may be taken as 60 kMc and the line width parameter as $\Delta\nu_{\pm}/p=1.95$ Mc per mm Hg.[2] Subsequent analysis of our data at the higher frequencies will justify the use of this line width relation at the much higher pressures now under consideration. The resonant loss tangent computed from Eq. (3) amounts to 1 to 3% of the measured loss at 0.0765 cm^{-1}. Allowance for the small resonant contribution was made in obtaining the parameters characterizing the nonresonant absorption.

The parameters for the nonresonant absorption were obtained from the data as plotted in Fig. 2, in the manner described previously.[10] A straight line results if the relaxation frequency is the same for molecules in all states and if this frequency increases in proportion to the pressure. The experimental data show a random scatter of 1 to 2% about a straight line. The characteristic parameters are

$$\Delta\nu_0/p=0.018\text{cm}^{-1}\text{ atmos}^{-1}$$

and

$$(\tan\delta/p)_{max}=2.93\times10^{-7}\text{ atmos}^{-1}.$$

The maximum value of $\tan\delta/p$ is about 2% higher than the theoretical limit. The close agreement confirms the existence of a single relaxation frequency parameter. If there were a distribution of relaxation frequencies associated with molecules in different rotational states, the experimental value should be lower than the theoretical value.

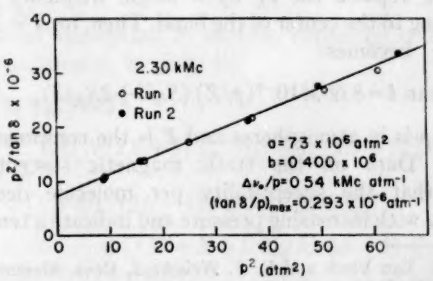

FIG. 2. Plot for obtaining the parameters characterizing the nonresonant loss in oxygen below 10 atmospheres.

(b) Data at 9.07 and 23.34 kMc

At the higher frequencies the resonant and nonresonant terms in Eq. (2) both make substantial contributions to the measured loss. If we compute the loss with the assumption that $\Delta\nu_\pm$ and $\Delta\nu_0$ are proportional to the pressure, we obtain curve 2 of Fig. 3. At 10 atmos the agreement between the computed and the observed values (curve 1) is rather close, the computed values being about 4% lower at both frequencies. At this pressure there is little uncertainty in computing the nonresonant part. Since the nonresonant term accounts for about 83 and 43% of the total loss near 9 and 23 kMc, respectively, it is evident that the data near 23 kMc are more indicative of the behavior of the resonant absorption. The agreement between the measured and

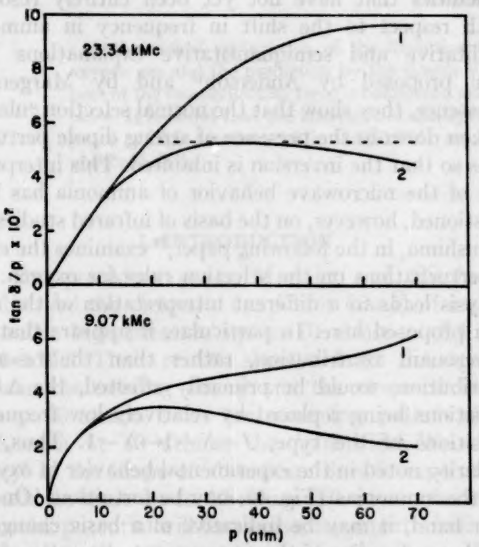

FIG. 3. Comparison of the experimental values of the loss tangent with the values computed from the Van Vleck-Weisskopf relation: experimental data (curve 1), values computed with the low-pressure relaxation frequency and line width parameters (curve 2), and with these parameters adjusted to give the maximum loss (dashed curve).

computed values suggests that the Van Vleck-Weisskopf line-shape theory is adequate and that the line width is essentially a linear function of the pressure for pressures below 10 atmos.

At pressures greater than 10 atmos very significant discrepancies appear. At 68 atmos and 23 kMc the observed loss is twice the calculated value, and at 9 kMc the discrepancy is nearly threefold. This discrepancy cannot be explained solely on the basis that $\Delta\nu_0$ and $\Delta\nu_\pm$ are no longer linear functions of the pressure. Even if $\Delta\nu_0$ and $\Delta\nu_\pm$ are chosen arbitrarily to give the maximum loss at each pressure, the computed values are still too small for pressures above 20 atmos. The upper limit in the computed values for this arbitrary choice of line width and relaxation frequency at 23 kMc is shown by the dashed line in Fig. 3. It is

TABLE IV. Selected values of the relaxation frequency ($\Delta\nu_0$), the resonant line width ($\Delta\nu_\pm$), and the resonant frequency ($\nu_\pm$) that fit the experimental data on oxygen.

p (atmos)	$\Delta\nu_0$ (kMc)	$\Delta\nu_\pm$ (kMc)	$\nu_\pm$ (kMc)	tan δ (obs) / tan δ (calc) 9.07 kMc	23.34 kMc
10	5.4	14.7	57.0	0.98	1.02
20	10.2	27.0	48.0	1.06	1.00
30	13.8	33.0	33.0	1.04	0.99
40	16.8	31.5	21.0	1.02	1.02
50	18.9	25.5	16.5	1.00	1.01
60	20.1	22.5	13.5	1.01	1.01
68.4	21.0	21.0	10.5	1.03	1.02

apparent that the primary difficulty is not due to the uncertainty in these parameters at higher pressures.

If we are to interpret the data with the Van Vleck-Weisskopf relation, it is necessary to assume that the resonant frequency, $\nu_\pm$, decreases rapidly as the pressure increases. In addition, the data at the highest pressures require quite narrow line widths, not very much larger than the value at 10 atmos. Hence, in order to avoid the unrealistic situation of having $\Delta\nu_0$ eventually become larger than $\Delta\nu_\pm$, it is also necessary to let $\Delta\nu_0$ increase somewhat less rapidly than the pressure.

We thus have three unknowns $\Delta\nu_0$, $\Delta\nu_\pm$, and $\nu_\pm$ to determine at each pressure and the present measurements at only two frequencies are insufficient to determine uniquely these values. Nevertheless, the form of the shape factors is such as to restrict very severely the permissible range of values for these parameters. A trial and error analysis is therefore useful in providing at least semiquantitative information regarding trends and magnitudes. Table IV lists a selection of values that represent the experimental data quite well.

DISCUSSION

The behavior of the resonant absorption in oxygen resembles rather strikingly that previously noted for the inversion spectra of NH_3[4] and ND_3.[5] In each case the line width increases essentially in proportion to the pressure until it approaches in magnitude the resonant frequency. A transition then occurs in which the reson-

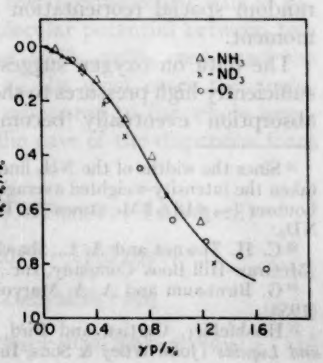

FIG. 4. Comparison of the relative shifts in resonant frequency for O_2, NH_3, and ND_3. $\nu_0'-\nu_0$ is the apparent shift in resonant frequency and γ_0 is the initial (low-pressure) line width parameter.

ant frequency appears to decrease quite rapidly and the line width no longer increases in porportion to the pressure.

In Fig. 4 the fractional shift in resonant frequency $(\nu_0-\nu_0')/\nu_0$ is plotted as a function of $\gamma_0 p/\nu_0$, γ_0 being the initial line width parameter.[11] The data for the three gases lie on essentially the same curve, although the data refer to widely different ranges of pressure. In fact, the transition in ND_3 occurs at 300-fold lower pressures than in oxygen. In the microwave region, according to collision theories of pressure broadening,[12] $\gamma_0 p$ is a measure of the frequency of molecular impacts that interrupt the radiation process by inducing changes in the quantum states. It is apparent from Fig. 4 that the transition region occurs at pressures where this collision frequency is of the same order as the initial resonant frequency.

The absorption in the ammonias at pressures above the transition region has a purely nonresonant character, in accord with the Van Vleck-Weisskopf line shape specialized to the limit of zero resonant frequency. The line width (relaxation frequency) again increases in proportion to the pressure, but the new collision cross section is only about one-third as large as in the limit of low pressure. It has been shown that this change in cross-section is real[5] and not an apparent change due to an effect of multiple collisions, as originally suggested.[4] The new cross sections are consistent with those obtained for other symmetric-top molecules,[13] where the inversion barrier is much higher than in ammonia so that the absorption is nonresonant irrespective of the pressure.

Since absorption in oxygen has a nonresonant as well as a resonant contribution, we can compare the corresponding collision cross sections directly at pressures below the transition region. The cross section, σ, is defined by the relation $\Delta\nu=Nv\sigma$, where v is the mean relative velocity. For the nonresonant case σ is 22 A^2, compared to about 60 A^2 for the resonant case. As in the ammonias, the nonresonant cross section is several times smaller than the resonant cross section. The nonresonant cross section is also smaller than the kinetic collision value, which is about 37 A^2.[14] Thus, collisions that effect a transfer of kinetic energy or linear momentum are not strong enough, on an average, to cause random spacial reorientation of the oxygen magnetic moment.

The data on oxygen suggest, but do not extend to sufficiently high pressures to show conclusively, that the absorption eventually becomes purely nonresonant. Figure 1 shows that $\tan\delta/p$ is reaching a maximum value, as would be true in the nonresonant case when $\Delta\nu_0=\nu$, but the numerical values are too large by about 10%. Thus, the loss still retains some resonant character, the apparent resonant frequency being in the neighborhood of 10 kMc. The line width reaches a maximum value in the vininity of 30 atmos and then begins to decrease, the width at 68 atmos being not much larger than at 10 atmos. The dependence on pressure is probably complicated somewhat by the inapplicability of the simple binary collision mechanism at these densities. However, the width at the highest pressures is of the order expected in the nonresonant limit.

The theoretical treatment of microwave pressure broadening and line shape at higher pressures presents difficulties that have not yet been entirely resolved. With respect to the shift in frequency in ammonia, qualitative and semiquantitative explanations have been proposed by Anderson[15] and by Margenau.[16] In essence, they show that the normal selection rules are broken down in the presence of strong dipole perturbations so that the inversion is inhibited. This interpretation of the microwave behavior of ammonia has been questioned, however, on the basis of infrared studies.[17,18] Mizushima, in the following paper,[19] examines the effect of perturbations on the selection rules for oxygen. His analysis leads to a different interpretation of the data than proposed here. In particular, it appears that the nonresonant contribution, rather than the resonant contribution, would be primarily affected, the $\Delta J=0$ transitions being replaced by relatively low frequency transitions of the type, $J=N+1\leftrightarrow N-1$. Thus, the similarity noted in the experimental behavior of oxygen and the ammonias (Fig. 4) may be fortuitious. On the other hand, it may be indicative of a basic change in line shape. In view of the nonresonant character of the dipolar absorption in the liquid state, it is evident that the resonant character of the absorption will disappear, in general, at sufficiently high densities.

It is assumed in the preceding analysis that the integrated dipolar intensity per molecule is independent of the pressure, except for the rather trivial change indicated by measurements of the magnetic susceptibility. At higher pressures significant microwave absorption can arise from electric dipoles induced by the force fields of neighboring molecules. Such absorption has been found in certain non-dipolar gases, notably CO_2,[20] and can be attributed primarily to small transient dipoles induced by the molecular quadrupole fields. The quadrupole moment of oxygen, however, is rela-

[11] Since the widths of the NH_3 lines vary considerably, we have taken the intensity-weighted average value given by Bleaney and Loubser ($\gamma_0=18.6$ kMc atmos^{-1}). The same value is assumed for ND_3.

[12] C. H. Townes and A. L. Shawlow, *Microwave Spectroscopy* (McGraw-Hill Book Company, Inc., New York, 1955).

[13] G. Birnbaum and A. A. Maryott, J. Chem. Phys. **29**, 1422 (1958).

[14] Hirshfelder, Curtiss, and Bird, *Molecular Theory of Gases and Liquids* (John Wiley & Sons, Inc., New York, 1954).

[15] P. W. Anderson, Phys. Rev. **75**, 1450 (1949).

[16] H. Margenau, Phys. Rev. **76**, 1423 (1949).

[17] A. H. Nethercot, Jr., and C. W. Peters, Phys. Rev. **79**, 225 (1950).

[18] Benedict, Plyler, and Tidwell, J. Research Natl. Bur. Standards U.S. **61**, 123 (1958).

[19] M. Mizushima, J. Chem. Phys. **32**, 691 (1960), this issue.

[20] Birnbaum, Maryott, and Wacker, J. Chem. Phys. **22**, 1782 (1954).

tively small.[21] Estimates of the pressure-induced absorption, based partly on the theoretical analysis of Buckingham and Pople,[22] indicate that this absorption should be negligibly small. Furthermore, no absorption was observed in nitrogen under comparable conditions of frequency and pressure, although the quadrupole moment is considerably larger than for oxygen. Consequently, it does not seem likely that the present data on oxygen are materially influenced by this effect.

[21] W. V. Smith and R. Howard, Phys. Rev. **79**, 132 (1950).
[22] A. D. Buckingham and J. A. Pople, Trans. Faraday Soc. **51**, 1029 (1956).

THE JOURNAL OF CHEMICAL PHYSICS VOLUME 32, NUMBER 3 MARCH, 1960

Theory of Microwave Absorption by Compressed Oxygen Gas*

MASATAKA MIZUSHIMA

Department of Physics, University of Colorado, Boulder, Colorado

(Received August 7, 1959)

A theoretical explanation of the deviation between observed microwave absorption by high-pressure oxygen gas and the prediction by the simple Van Vleck-Weisskopf theory is attempted. The nonspherical part of the intermolecular force is considered and the distortion of energy levels and wave functions is calculated. It is found that the nonresonant absorption vanishes and a low-frequency (~10 kMc) resonance appears at high pressure, while the 60 kMc resonance does not change much. This theory can explain the observed data.

I. INTRODUCTION

IN the preceding paper Maryott and Birnbaum[1] observed the dielectric loss factor ($\tan\delta$) of oxygen gas under high pressure up to 70 atmos at 9.1 and 23.34 kMc. Their results show a large discrepancy between the existing theory and the observed values even at 20 atmos. Since the mean free path is about 20 A even at 40 atmos, the Van Vleck-Weisskopf theory[2] of the shape of absorption lines is expected to be valid at least up to 40 atmos. However, the intermolecular potential will be a rather large perturbation in that region, since it can change the frequency of the microwave absorption by about 500 kMc or more at the intermolecular distance of about 10 A.

The same kind of phenomenon, the intermolecular perturbation on the microwave absorption, is observed for the ammonia molecule.[3] In that case the explanation has been made by considering the electric dipole-dipole interaction between molecules.[4]

In the case of the oxygen molecule the situation is somewhat different in the sense that the electric dipole moment does not exist. Since the microwave absorption is due to the change of angular momentum, we have to consider the rotation of molecules from the beginning, while in the case of the ammonia, it could be neglected in the first approximation.

* This research has been supported by National Science Foundation and U. S. Navy contract Nonr 1147(05).
[1] A. A. Maryott and G. Birnbaum, Phys. Rev. **99**, 1886 (1955); J. Chem. Phys. **32**, 686 (1960), this issue.
[2] J. H. Van Vleck and V. F. Weisskopf, Revs. Modern Phys. **17**, 227 (1945).
[3] B. Bleaney and J. H. N. Loubser, Nature **161**, 522 (L) (1948); Proc. Phys. Soc. (London) **63A**, 483 (1950); I. R. Weingarten, Columbia Radiation Lab. Report (May 1, 1948); G. Birnbaum and A. A. Maryott, Phys. Rev. **92**, 270 (1953).
[4] H. Margenau, Phys. Rev. **76**, 1423 (1949); P. W. Anderson, Phys. Rev. (Letters) **75**, 1450 (1949).

II. INTERMOLECULAR POTENTIAL

The intermolecular potential between oxygen molecules is due mainly to the dispersion force and the repulsive overlap force. The magnetic force due to the residual electronic spin is very small in comparison. Since both the dispersion force and the repulsive overlap force are due to the charge of the electrons, not their spin, they are expected to have the same symmetry as the electronic distribution of each molecule. In fact any intermolecular forces except the one due to the spin should be the same if we rotate one molecule by 180° around an axis perpendicular to the molecular axis, keeping all the other intermolecular coordinates the same. Thus, if the angles between the intermolecular axis and each molecular axis are θ_1 and θ_2, respectively, the intermolecular distance is r_{12}, and the relative azimuthal angle around the intermolecular axis is ϕ_{12}, then the electric intermolecular potential between two molecules is a function of $\cos^2\theta_1$, $\cos^2\theta_2$, $\cos\phi_{12}$ and the intermolecular distance r_{12}. In most cases the angle-dependent part is small compared to the whole intermolecular potential. In the case of the dispersion force we can easily obtain

$$V=-(\tfrac{3}{2}r^6)[9\alpha^2E+(\tfrac{3}{2})\alpha\gamma E(3\cos^2\theta_1+3\cos^2\theta_2-2)$$
$$+(\tfrac{3}{4})\gamma^2E\{(3\cos^2\theta_1-1)(3\cos^2\theta_2-1)$$
$$-9\sin\theta_1\cos\theta_1\sin\theta_2\cos\theta_2$$
$$\times\cos\phi_{12}+\sin^2\theta_1\sin^2\theta_2\cos^2\phi_{12}\}] \quad (1)$$

where

$$\alpha=(\tfrac{1}{3})(\alpha_{||}+2\alpha_{\perp}),$$

$$\gamma=(\alpha_{||}-\alpha_{\perp}),$$

and $\alpha_{||}$ is the polarizability along the molecular axis, $\alpha_{\perp}$ is the one perpendicular to it, and E is the ionization energy. In the case of the oxygen molecule[5]

$$\alpha_{||}=2.35\ \text{A}^3 \qquad \gamma=1.21\ \text{A}^3$$

so that the ratio of the angle-independent part to the dependent part is essentially $\gamma/\alpha=0.71$.

The electric quadrupole moment gives an angle-dependent intermolecular force, but, since this moment is known to be very small,[6] this contribution will also be small.

For the repulsive intermolecular force the van der Waals radius[7] gives 2.6 and 1.4 A as effective range to the direction of the molecular axis and perpendicular to it, respectively. Thus the nonsphericity can be expressed in the same way as in the polarizability terms, that is, $(2.6-1.4)/3^{-1}(2.6+2.8)=0.67$.

If the nonsphericity is small, we can, in general, expand the intermolecular force as

$$U=A(r_{12})+B_1(r_{12})P^{(2)}(\cos\theta_1)+B_2(r_{12})$$

$$\times P^{(2)}(\cos\theta_2)+C(r_{12})P^{(2)}(\cos\theta_1)P^{(2)}(\cos\theta_2)+\cdots \quad (2)$$

where the first term is the angle-independent part and the next two terms are the interaction between the spherical part of one molecule and the nonspherical part of the other molecule. $P^{(2)}$ is the second-order Legendre function. The last term gives the interaction between nonspherical parts. The ratio of B to C is approximately 1 to 0.7 in the case of the dispersion force and the repulsive force.

Since the repulsive potential is larger at $\theta=0$ than at $\theta=\pi/2$, this potential contributes a positive quantity to the B and C terms, while the dispersion potential will contribute a negative quantity to them as can be seen in Eq. (1).

III. ENERGY LEVELS UNDER STRONG PERTURBATION

The rotational energy of the oxygen molecule is now well known both experimentally[8,9] and theoretically.[9,10] According to these results each end-over-end rotational level, which is designated by the quantum number N, is a triplet due to the coupling between the end-over-end rotational angular momentum **N** and the electronic spin **S** ($S=1$). The separation among each triplet is much smaller than the separation between different N levels. (N is not an exact quantum number, but it is a good quantum number.[9,10])

The perturbation due to a colliding molecule does have matrix elements between different N states as well as among triplet states, but, since the energy difference between different N states is very large, we neglect the corresponding nondiagonal matrix elements and consider only matrix elements which connect the triplet states among themselves (See Appendix I).

It can be immediately seen that the angle-independent A term of the intermolecular potential (2) just gives a constant diagonal matrix element and does not change the relative energy of rotational levels. Thus, we can neglect it and first consider only

$$V=BP^{(2)}(\cos\theta) \qquad (30)$$

as a perturbation, where B gives the strength of the perturbation. The value of B can be either positive or negative, as is explained at the end of the last section.

The wave function of each state is $(NSJM\,|$ but since $S=1$, the triplet states we consider are represented by $(N1N+1M\,|$, $(N1NM\,|$, and $(N1N-1M\,|$. If $(N1JM\,|\,V\,|\,N1JM)$ is abreviated as V_J, the secular equation is

$$\begin{vmatrix} W_0+V_N-E & (N1NM\,|\,V\,|\,N1N+1M) & (N1NM\,|\,V\,|\,N1N-1M) \\ & W_++V_{N+1}-E & (N1N+1M\,|\,V\,|\,N1N-1M) \\ \text{symmetric} & & W_-+V_{N-1}-E \end{vmatrix}=0, \qquad (4)$$

where W_0, W_+, W_- are the unperturbed energy of the $(N1N\,|$, $(N1N+1\,|$, $(N1N-1\,|$ states, respectively. By

[5] See, for example, Hirschfelder, Curtiss, and Bird, *Molecular Theory of Gases and Liquids* (John Wiley & Sons, Inc., New York, 1954), p. 950.
[6] Anderson, Smith, and Gordy, Phys. Rev. **82**, 264 (1951).
[7] L. Pauling, *Nature of the Chemical Bond* (Cornell University Press, Ithaca, New York, 1945), p. 189.
[8] Burkhalter, Anderson, Smith, and Gordy, Phys. Rev. **79**, 651 (1950).
[9] M. Mizushima and R. M. Hill, Phys. Rev. **93**, 745 (1954).
[10] R. Schlapp, Phys. Rev. **51**, 342 (1937); S. L. Miller and C. H. Townes, Phys. Rev. **90**, 537 (1953); M. Tinkham and M. W. P. Strandberg, Phys. Rev. **97**, 937 (1955).

using Racah's formulas[11] we easily obtain

$$V_J=(N1JM\mid V\mid N1JM)=-\frac{B[3X(X-1)-4N(N+1)J(J+1)][3M^2-J(J+1)]}{2(2J-1)(2J+3)J(J+1)(2N-1)(2N+3)N}$$

$$(N1NM\mid V\mid N1N+1M)=-\frac{3BM[(N+M+1)(N-M+1)]^{\frac{1}{2}}}{(2N+3)(N+1)N(2N+1)}$$

$$(N1NM\mid V\mid N1N-1M)=\frac{3BM[(N-M)(N+M)]^{\frac{1}{2}}}{(2N-1)N(N+1)(2N+1)}$$

$$(N1N+1M\mid V\mid N1N-1M)=-\frac{3B[(N^2-M^2)\{(N+1)^2-M^2\}]^{\frac{1}{2}}}{(2N-1)(2N+1)(2N+3)N(N+1)} \tag{5}$$

where $X=N(N+1)+J(J+1)-2$.

In the foregoing formulas we took the intermolecular axis as the space-fixed axis along which the quantum number M is defined.

If we define

$$F_1(N)=\sum_M^N(N1NM\mid V\mid N1N+1M)^2/(2N+1)B^2,$$

$$F_2(N)=\sum_M^{N-1}(N1NM\mid V\mid N1N-1M)^2/(2N-1)B^2,$$

$$F_3(N)=\sum_M^{N-1}(N1N+1M\mid V\mid N1N-1M)^2/(2N-1)B^2, \tag{6}$$

we can easily see that

$$F_1(N)=(3/5)\frac{N+2}{(2N+3)(N+1)(2N+1)},$$

$$F_2(N)=(3/5)\frac{N-1}{(2N-1)N(2N+1)},$$

$$F_3(N)=(6/25)\frac{1}{(2N+1)(2N-1)(2N+3)}. \tag{7}$$

We see from Table I that

$$F_1(N)\simeq F_2(N)\gg F_3(N) \tag{8}$$

which shows that as an average the

$$(N1N-1M\mid V\mid N1N+1M)$$

matrix element can be neglected in Eq. (4).

The resulting secular equation is still a third-order one, and it is too tedious to solve it for each value of M. Since we are considering an averaged property anyway it will be simpler to take an averaged secular equation and solve it instead of taking an average of the solutions. Since the average of diagonal elements V_J over M is zero, we simply neglect all V_J's in this approximation, and obtain

$$\begin{vmatrix} W_0-E & \mp B(F_1)^{\frac{1}{2}} & \pm B(F_2)^{\frac{1}{2}} \\ \mp B(F_1)^{\frac{1}{2}} & W_+-E & 0 \\ \pm B(F_2)^{\frac{1}{2}} & 0 & W_--E \end{vmatrix}=0, \tag{9}$$

where double signs mean to take the upper one for $M>0$ and the lower one for $M<0$. We reserve this sign because it is important in calculating the transition probability. By solving this equation we obtain energy levels, as a function of the perturbation B. It will be easily seen that the solution E does not depend on the choice of the signs in nondiagonal matrix elements; thus it does not depend on the sign of B either.

We designate the energy of the highest energy state as E_α, that of the lowest state as E_β and the middle one E_γ. As B goes to zero

$$E_\alpha=W_0,$$
$$E_\beta\rightarrow W_+,$$
$$E_\gamma\rightarrow W_-, \tag{10}$$

if $N\geqq 7$. For $N=1, 3, 5$, $E_\beta\rightarrow W_-$, $E_\gamma\rightarrow W_+$ according to this definition.

A simplified theory can be obtained if one neglects

TABLE I. Values of $F_1(N)$, $F_2(N)$, and $F_3(N)$.

N	$(5/3)F_1(N)$	$(5/3)F_2(N)$	$(5/3)F_3(N)$
1	0.100	0	0.00889
3	0.0198	0.0267	0.00018
5	0.00816	0.00988	0.000028
7	0.00441	0.00507	0.0000080
9	0.00276	0.00308	0.0000031
11	0.00189	0.00206	
13	0.00137	0.00148	
15	0.00104	0.00111	
17	0.00082	0.00086	
19	0.00066	0.00069	
21	0.00054	0.00057	
23	0.00045	0.00047	

[11] G. Racah, Phys. Rev. 62, 438 (1942).

the difference between F_1 and F_2 and between W_+ and W_-. If we set

$$F_1=F_2=F,$$
$$W_+=W_-=0, \tag{11}$$

one can solve Eq. (9) immediately to obtain

Energy	Wave function
$E=\frac{1}{2}\{W_0+(W_0^2+8B^2F)^{\frac{1}{2}}\}$,	$x(N1NM\mid+(y/\sqrt{2})\{(N1N+1M\mid-(N1N-1M)\}$
$E=0$	$(1/\sqrt{2})\{(N1N+1M\mid+(N1N-1M\mid\}$
$E=\frac{1}{2}\{W_0-(W_0^2+8B^2F)^{\frac{1}{2}}\}$,	$y(N1NM\mid-(x/\sqrt{2})(N1N+1M\mid-(N1N-1M\mid.$ (12)

where the coefficients x and y are easily obtained from the corresponding value of E and $x^2+y^2=1$.

This approximation is not bad if $\mid B\mid \gg \mid W_+-W_-\mid$.

IV. TRANSITION PROBABILITY

The transition among our three states will take place through the spin magnetic moment. Thus we have to calculate the matrix element of the spin operator **S**. Suppose by solving the secular equation (9) we obtain an eigenfunction

$$a(N1N\mid+b(N1N+1\mid+c(N1N-1\mid$$

for one state and

$$a'(N1N\mid+b'(N1N+1\mid+c'(N1N-1\mid$$

for another, then the matrix element of **S** between them is

$$\begin{aligned}\langle\mathbf{S}\rangle=aa'(N1N\mid\mathbf{S}\mid N1N)+bb'(N1N+1\mid\mathbf{S}\mid N1N+1)\\+cc'(N1N-1\mid\mathbf{S}\mid N1N-1)\\+(ab'+a'b)(N1N\mid\mathbf{S}\mid N1N+1)\\+(ac'+a'c)(N1N\mid\mathbf{S}\mid N1N-1).\end{aligned}\tag{13}$$

The simplification made in Sec. III corresponds to assuming $\mid b\mid=\mid c\mid$. The matrix elements of S between $(N_1JM\mid$ states are given in Table II.

The transition probability is given essentially by

$$\sum_M\langle\mathbf{S}\rangle^2.$$

Exactly speaking a, b, and c are different for each M, but we calculated them, in the previous section, by taking an averaged secular equation to avoid complicated calculation. Here we need the average value of $\langle\mathbf{S}\rangle_{ij}^2$ over M where i and j are two states among α, β and γ. We calculate that by using the coefficient a, b, c obtained before and averaging each term over M for $J\geqq M\geqq -J$, that is,

$$\begin{aligned}&(N1N\mid\mathbf{S}\mid N1N)^2\to 1/3N(N+1),\\&(N1N+1\mid\mathbf{S}\mid N1N+1)^2\to(N+2)/3(N+1),\\&(N1N-1\mid\mathbf{S}\mid N1N-1)^2\to(N-1)/3N,\\&(N1N\mid\mathbf{S}\mid N1N+1)^2\to N(2N+3/3(N+1)(2N+1),\\&(N1N\mid\mathbf{S}\mid N1N-1)^2\to(N+1)(2N-1)/3N(2N+1),\\&(N1N\mid\mathbf{S}\mid N1N)(N1N+1\mid\mathbf{S}\mid N1N+1)\to 1/(3N+3),\\&(N1N\mid\mathbf{S}\mid N1N)(N1N-1\mid\mathbf{S}\mid N1N-1)\to-1/3N,\\&(N1N+1\mid\mathbf{S}\mid N1N+1)(N1N-1\mid\mathbf{S}\mid N1N-1)\to-\tfrac{1}{3},\\&(N1N\mid\mathbf{S}\mid N1N+1)(N1N\mid\mathbf{S}\mid N1N-1)\to\tfrac{1}{3},\end{aligned}\tag{14}$$

and other terms are zero.

This procedure, actually, produces an inconsistency for $\mid M\mid$ around J, but for large J such an effect is negligible. Thus simplifying (14) by assuming that N is large, we obtain

$$\begin{aligned}S^2=(2N+1)^{-1}\sum\langle\mathbf{S}\rangle^2\simeq&[(aa')^2/3N^2]\\&+\tfrac{1}{3}[(bb')^2+(cc')^2]+\{[2(aa'bb'-aa'cc')]/3N\}\\&-(2/3)bb'cc'+(1/3)\{(ab'+a'b)^2+(ac'+a'c)^2\\&+2(ab'+a'b)(ac'+a'c)\}\\=&(1/3)[\{a(b'+c')+a'(b+c)\}^2\\&+(bb'-cc'+aa'/N)^2.\end{aligned}\tag{15}$$

If one changes the sign of B, the sign of a (or a') will be changed but not those of b and c. One sees in (14), then, that the transition probability is the same for $+B$ and $-B$. Since it is already shown that the energy does not depend on the sign of B either, there is no difference at all for positive and negative B in this theory.

TABLE II. Matrix elements of the spin operator **S**.

$(N1NM\mid\mathbf{S}\mid N1NM)$	$=[M/N(N+1)]\mathbf{k}$
$(N1N+1M\mid\mathbf{S}\mid N1N+1M)$	$=[M/(N+1)]\mathbf{k}$
$(N1N-1M\mid\mathbf{S}\mid N1N-1M)$	$=-[M/N]\mathbf{k}$
$(N1NM\mid\mathbf{S}\mid N1N+1M)$	$=-[N\{(N+1)^2-M^2\}/(N+1)^2(2N+1)]^{\frac{1}{2}}\mathbf{k}$
$(N1NM\mid\mathbf{S}\mid N1N-1M)$	$=-[(N+1)(N^2-M^2)/N^2(2N+1)]^{\frac{1}{2}}\mathbf{k}$

k is the unit vector to the z direction.

TABLE III. Absorption frequencies and $\langle S^2\rangle (N=9)$.

B (kMc)	0	±100	±300	±500	±700	±700	±1100
$\nu_{\alpha\beta}$(kMc)	61	62	70	81	100	120	140
$\langle S_{\alpha\beta}{}^2\rangle$	0.33	0.26	0.03	0.01	0.00	0.00	0.00
$\nu_{\alpha\gamma}$(kMc)	58	59	64	70	0.80	90	100
$\langle S_{\alpha\gamma}{}^2\rangle$	0.33	0.40	0.61	0.62	0.60	0.59	0.57
$\nu_{\beta\gamma}$(kMc)	2.8	2.8	5.5	10.8	20	30	40
$S_{\beta\gamma}{}^2\rangle$	0.00	0.01	0.28	0.37	0.40	0.41	0.43
$\langle S^2\equiv\langle S_{\alpha\alpha}{}^2\rangle+\langle S_{\beta\beta}{}^2\rangle+\langle S_{\gamma\gamma}{}^2\rangle$	0.66	0.65	0.17	0.03	0.00	0.00	0.00

If we use the approximate result (12), we obtain

$$\langle S_{\alpha\gamma}{}^2\rangle=(1/3)(2x^2+y^2)$$
$$\langle S_{\beta\gamma}{}^2\rangle=(1/3)(x^2+2y^2)$$
$$\langle S_{\alpha\beta}{}^2\rangle=0$$
$$\langle S^2\rangle=\langle S_{\alpha\alpha}{}^2\rangle+\langle S_{\beta\beta}{}^2\rangle+\langle S_{\gamma\gamma}{}^2\rangle=0 \qquad (16)$$

One can see that a sum rule

$$\sum_{i,j}\langle S_{ij}{}^2\rangle=S(S+1)=2$$

is satisfied by the result (16).

In Table II we took $\Delta M=0$ transitions only, but due to the spectroscopic stability we do not have to calculate the other cases to obtain a quantity which is proportional to the transition probability. That is, the transition probability in general is proportional to formula (15) or (16).

V. NUMERICAL RESULTS

Since $|W_+-W_-|$ is about 1~4 kMc for most popular rotational states ($N=3\sim11$), the approximation (12) is not bad if $|B|$ is above 300 kMc or so. A typical case of $N=9$ is calculated without the above approximation. The result shown in Table III shows that above $|B|$ of 300 kMc it indeed approaches the simple results (12).

The main feature of the high-pressure situation (12) is that the absorption at 60 kMc stays essentially the sams as at low pressures, but the nonresonant (zero frequency) absorption changes into a low-frequency (~10 kMc) absorption.

The situation, however, is very complicated because the value of F is different for different N states. As a result the transition to the high-pressure situation represented by (12) occurs at different B value for different N states.

At a given pressure, that is, at the same B value, some states still have zero frequency absorption, while the other states have absorption at low frequencies instead of zero frequency. As a result the absorption in the low-frequency region is expected to be a smeared-out one which extends from zero to 20 or 30 kMc. Thus the absorption curve in the low-frequency region may be given by a Gaussian curve rather than by the Van Vleck-Weisskopf curve,[2] while the 60 kMc absorption may still be represented by the Van Vleck-Weisskopf curve.

At very high pressure, the peak of the Gaussian curve for the low-frequency region is expected to leave zero frequency and move towards higher frequency, since, eventually, the transition to the high-pressure situation whould take place for all existing N states.

VI. COMPARISON WITH EXPERIMENT

Although the present theory is just a qualitative one, it is interesting to see how one can explain the experimental data given by Maryott and Birnbaum.[1]

Suppose we assume that the 60 kMc resonance curve is given by the Van Vleck-Weisskopf theory with the half-width parameter

$$\Delta\nu=1.47p \text{ Mc/sec}, \quad p \text{ in atmos.} \qquad (17)$$

as obtained by many people including Maryott and Birnbaum[1] at low pressure. Subtracting this assumed 60 kMc contribution from the observed values of tan δ/p at each pressure and frequency we obtain a contribution by zero and low-frequency resonance as shown in Table IV. In this table these values are normalized such that the corresponding total absorption coefficient by zero and low-frequency resonances is one. This can be easily done since we know the theoretical value for the integrated value of tan δ/p. Thus if we take a Gaussian curve for the absorption curve, the tabulated value here should be expressed as

$$\frac{2\exp\{-(\nu-\nu_0)^2/\Delta\nu_0{}^2\}}{\nu_0(1+\Phi(\nu_0/\Delta\nu_0)}, \qquad (18)$$

where Φ is the error integral.

The last two columns give the parameters in the foregoing Gaussian function which reproduce the observed value with reasonable accuracy. It can be shown that the peak of the theoretical curve certainly starts with zero frequency and increases with pressure to

TABLE IV. Contribution from zero and low-frequency resonance to tanδ/P (normalized).

P (atmos)	9.07 kMc	23.34 kMc	ν_0	$\Delta\nu_0$ (kMc)
20	4.2×10^{-3}	1.5×10^{-3}	0	20
30	4.4	2.2	5	25
40	4.8	2.8	10	30
50	5.4	3.2	20	30
60	6.0	3.6	...	...
68.4	6.6	3.6	...	...

TABLE V. Matrix elements of V.

$$(N\ \ NM|\,V\,|N+2\ \ N+2M)=(-1)^N\ B\frac{3}{2(2N+3)}\left[\frac{N(N+3)\{(N+1)^2-M^2\}\{(N+2)^2-M^2\}}{(2N+1)(2N+5)(N+1)(N+2)}\right]^{\frac{1}{2}}$$

$$(N\ \ NM|\,V\,|N+2\ \ N+1M)=(-1)^{N+1}\ B\frac{3M[(N+1)^2-M^2]^{\frac{1}{2}}}{(2N+3)[(2N+1)N(N+1)(N+2)]^{\frac{1}{2}}}$$

$$(N\ \ N+1M|\,V\,|N+2\ \ N+3M)=(-1)^N\ B\frac{3}{2(2N+3)(2N+5)}\left[\frac{(N+1)\{(N+2)^2-M^2\}\{(N+3)^2-M^2\}}{N+3}\right]^{\frac{1}{2}}$$

$$(N\ \ N+1M|\,V\,|N+2\ \ N+2M)=(-1)^{N+1}\ B\frac{3M[(N+2)^2-M^2]^{\frac{1}{2}}}{(2N+3)[(N+1)(N+2)(N+3)(2N+5)]^{\frac{1}{2}}}$$

$$(N\ \ N+1M|\,V\,|N+2\ \ N+1M)=(-1)^N\ B\frac{3\{3M^2-(N+1)(N+2)\}}{(2N+1)(2N+3)(2N+5)[(N+1)(N+2)]^{\frac{1}{2}}}$$

$$(N\ \ N-1M|\,V\,|N+2\ \ N+1M)=(-1)^N\ B\frac{3}{2(2N+1)(2N+3)}\left[\frac{(N+2)[(N+1)^2-M^2](N^2-M^2)}{N}\right]^{\frac{1}{2}}$$

about 20 kMc. The corresponding half-width $\Delta\nu_0$ also increases with pressure, but not in a proportional way. This, however, does not exclude the possibility that individual absorption lines, which are presumably of the Van Vleck-Weisskopf type, have a half-width proportional to the pressure. At 60 atmos or higher pressure the foregoing simple idea does not work. The correction due to the transfer of part of the total intensity of the 60 kMc line into low-frequency resonance indicated in (12) is not enough to give a reasonable Gaussian curve. Probably at extremely high pressure the 60 kMc resonance can not be expressed as a single Van Vleck-Weisskopf curve with $\Delta\nu=1.47p$. This breakdown of the theory is expected since the assumption of two-body collisions should be not valid at such high pressure.

The mean free path of the oxygen molecule is about 20 A at 40 atmos and about 15 A at 60 atmos. The nonsperical part of the dispersion force, on the other hand, is

$$B\ (\text{dispersion force})=-9\alpha\gamma E/r^6 \qquad (19)$$

which gives -400 kMc for the parameter B at 7 A. Thus our interpretation is seen to be numerically reasonable; that is, the transition to the high-pressure situation occurs at around 40 atmos, and at 60 atmos, the Van Vleck-Weisskopf theory based on the two-body collision breaks down.

The present interpretation is rather successful, but is completely different from the one suggested by Maryott and Birnbaum, who associated the high-pressure effect with a change of the 60 kMc resonance, assuming no change in the intensity of the zero frequency (nonresonant) absorption.

Since we have data only at two frequencies, we can not tell which is better. Further experimental research should be done to test these theories.

APPENDIX I. INTERACTION BETWEEN DIFFERENT ROTATIONAL STATES

If the perturbation V becomes large, the interaction between different N states will become important too. It is very difficult to solve the problem of such interactions regorously since we now obtain an infinite matrix instead of the 3×3 matrix we discussed in the previous section. We therefore, treat the problem of interaction between rotational states as a perturbation.

Since, in the ordinary oxygen molecule, we have only odd integers for the rotational quantum number, the only nonzero matrix elements are those tabulated in Table V, which are obtained in the same way as in obtaining (5).

As in the previous section we make an approximation by taking the average over M in the matrix element rather than in the eigenvalue. If we do that, we find easily that all second-order contributions to the nondiagonal elements are exactly or approximately zero. The averaged contribution to the diagonal elements can be calculated from the results shown in Table VI.

TABLE VI. Mean square of some matrix elements.

$$\langle(N1NM|\,V\,|N+2\ \ N+2M)^2\rangle=(3/10)B^2[N(N+3)/(2N+1)(2N+3)]$$

$$\langle(N1NM|\,V\,|N+2\ \ 1N+1M)^2\rangle=(3/5)B^2/[(2N+1)(2N+3)]$$

$$\langle(N1N+1M|\,V\,|N+2\ \ 1N+3M)^2\rangle=(3/10)B^2[(N+1)(N+2)(2N+7)/(2N+3)^2(2N+5)]$$

$$\langle(N1N+1M|\,V\,|N+2\ \ 1N+2M)^2\rangle=(3/5)B^2/[(2N+3)^2]$$

$$\langle(N1N+1M|\,V\,|N+2\ \ 1N+1M)^2\rangle=(4/5)B^2/[(2N+1)(2N+5)(2N+3)^2]$$

$$\langle(N1N-1M|\,V\,|N+2\ \ 1N+1M)^2\rangle=(3/10)B^2[(N+1)(N+2)/(2N+1)(2N+3)]$$

We notice in Table VI that if $N \gg 1$, three of the mean squares are much larger than the other three.

The second-order perturbation due to the above matrix elements can be estimated in the following way.

We make a simplification by assuming

$$\langle (N1NM \mid V \mid N+2 \quad 1N+2M)^2 \rangle$$
$$= \langle (N1N+1M \mid V \mid N+2 \quad 1N+3M)^2 \rangle$$
$$= \langle (N1N-1M \mid V \mid N+2 \quad 1N-1M)^2 \rangle = (3/40)B^2$$

and that all the other matrix elements are zero. This simplification is not bad if N is very large as can be seen from Table VI.

The second-order perturbation on each energy level is now

$$E_{\alpha,N}^{(2)} = (3B^2/40)\left\{ \frac{(a_N a_{N-2}+b_N b_{N-2})^2}{E_{\alpha,N}-E_{\alpha,N-2}+2\beta(2N-1)} + \frac{(a_N b_{N-2}-b_N a_{N-2})^2}{E_{\alpha,N}-E_{\gamma,N-2}+2\beta(2N-1)} - \frac{(a_N a_{N+2}+b_N b_{N+2})^2}{E_{\alpha,N+2}-E_{\alpha,N}+2\beta(2N+3)} - \frac{(a_N b_{N+2}-b_N a_{N+2})^2}{E_{\alpha,N+2}-E_{\alpha,N}+2\beta(2N+3)} \right\} = E_{\gamma,N}^{(2)}$$

$$E_{\beta,N}^{(2)} = (3B^2/40)[E_{\beta,N}-E_{\beta,N-2}+2\beta(2N-1)]^{-1} - [E_{\beta,N+2}-E_{\beta,N}+2\beta(2N+3)]^{-1}.$$

Where β is the rotation constant, and it is assumed that the energy difference between different N states is given by the difference of the rotational energy. $E_{\alpha,N}$ etc. are eigenvalues obtained in Sec. III, by assuming $W_+=0$ for each N.

The effect calculated in this way, however, turns out to have only negligible contribution to values given in Table III.

It is worthwhile to note, however, that if the perturbation becomes extremely large, the mixing of rotational states is expected to occur. In such cases the quenching of the angular momentum N appears, that is, molecules are not rotating any more, and the spin S is expected to have finite diagonal matrix elements again.

APPENDIX II. EFFECT OF THE C TERM OF EQ. (2)

Since the ratio of B to C is expected to be about 1 to 0.7 as indicated in Sec. II, the effect of this C term, which gives a part of the interaction between nonspherical parts of two molecules, may not be negligible.

The calculation can be done by considering a system composed of two oxygen molecules. The simple product of two single molecule wave functions given in formula (12) can be easily seen to be an eigenfunction of this C term. The calculation of matrix elements can be done easily, and the results for large N is

$$(6/5)C(ab/N)(a'b'/N')$$

if molecule 1 is in state $N\alpha$ or $N\beta$, and molecule 2 is in state $N'\alpha$ or $N'\beta$. The matrix element is zero if one of the molecules is in the γ state. At very high pressure the product ab approaches its maximum of $\frac{1}{2}$, so that if $N=N'=9$, this term is $C/272$.

It can be easily seen that this term will split $\nu_{\beta\gamma}$ and $\nu_{\alpha\gamma}$ into doublets of frequencies $\nu_{\beta\gamma}$ and $\nu_{\beta\gamma}-C/272$, and $\nu_{\alpha\gamma}$ and $\nu_{\alpha\gamma}+C/272$, respectively.

If we take C/B to be 0.7, $C/272$ is about 2.6 kMc at $B=1000$ kMc. It can be seen from Table III, that such an effect can be neglected for the order of magnitude calculation.

Potential Energy Curves of Hydrogen Fluoride*

ROBERT J. FALLON, JOSEPH T. VANDERSLICE, AND EDWARD A. MASON

Institute for Molecular Physics, University of Maryland, College Park, Maryland

(Received November 2, 1959)

Potential energy curves for the $X\,^1\Sigma^+$ and $V\,^1\Sigma^+$ states of HF and DF have been calculated by the Rydberg-Klein-Rees method. The results calculated from the different sets of data for HF and DF are found to be in very good agreement. The theoretical results of Karo are compared to the experimental results obtained here.

INTRODUCTION

QUANTUM mechanical calculations on molecular systems are known to give reliable estimates of the total energy of such systems, but, in general, the values calculated for the binding energies of diatomic molecules are in poor agreement with experiment. The reason for this is that the error in the total energy, although small on a percentage basis, is often of the same order of magnitude as the binding energy. In relatively simple cases, such as H_2, the problem can be handled by brute force methods.[1] For more complicated systems containing a large number of electrons, such techniques are as yet out of the question. It would seem that approximation schemes are the most desirable at the present time if one wants to be able to calculate accurate potential energy curves for diatomic molecules.

In order to test the reliability of such approximation schemes, it is well to have reliable potential energy curves for diatomic systems against which the various schemes can be tested. Since a relatively large amount of effort has been expanded by theoreticians on the hydrogen fluoride molecule,[2–8] it was felt that it would be worthwhile to have an accurate potential curve for this system.

Recently, Johns and Barrow[9] have obtained some excellent spectroscopic data on HF and DF, and these, together with older data,[10–12] have enabled us to obtain experimental potential energy curves for the $X^1\Sigma^+$ and $V^1\Sigma^+$ states of these molecules over a range of internuclear distance. The actual curves were calculated by the Rydberg-Klein-Rees (RKR) method.[13–16]

The experimental curve for the $X^1\Sigma^+$ state was compared with a Morse curve and with one obtained theoretically by Karo.[7]

RYDBERG-KLEIN-REES METHOD AND SPECTROSCOPIC DATA

The RKR method is a semiclassical procedure for obtaining the potential energy curves for diatomic molecules. The curves obtained with this method are based directly on the measured vibrational and rotational energy levels of the molecule and do not depend on the assumption of any empirical potential form. The method has been adequately described in recent articles[15–16] so that we shall omit the details of the procedure. It suffices to say that the method is quite rapid and appears to give reliable results.

The spectroscopic data for the $X^1\Sigma^+$ states of HF and DF do not include all the vibrational levels from the lowest to the highest. Johns and Barrow[9] have obtained data for the higher levels, whereas Nielsen and co-workers,[10,12] and Naudé and Verleger[11] have obtained data on the lower. Johns and Barrow[9] have carried out what appears to be a reliable interpolation between the upper and the lower levels so that the intermediate levels could be inferred from the standard spectroscopic formulas. We have used the observed data plus results obtained by the interpolation method to calculate experimental curves for the $X^1\Sigma^+$ state of both systems.

RESULTS AND DISCUSSION

The results for the $X^1\Sigma^+$ and $V^1\Sigma^+$ states of HF and DF are listed in Tables I to IV and are shown as solid lines in Fig. 1. The corresponding curves for the two systems do not differ by more than ± 0.001 A. This indicates that the different sets of data and the inter-

* This research was supported in part by the National Aeronautics and Space Administration.

[1] W. Kolos and C. C. J. Roothaan, paper presented at the International Conference on Molecular Quantum Mechanics, Boulder, Colorado, June 7–15, 1959 (to be published in Revs. Modern Phys.).

[2] A. B. F. Duncan, J. Am. Chem. Soc. **77**, 2107 (1955).

[3] D. Kastler, J. chim. phys. **50**, 556 (1953).

[4] A. C. Hurley, Proc. Roy. Soc. (London) **A248**, 119 (1958).

[5] M. Krauss, J. Chem. Phys. **28**, 1021 (1958).

[6] A. M. Karo and L. C. Allen, J. Am. Chem. Soc. **80**, 4496 (1958).

[7] A. M. Karo, Quarterly Progress Report, Solid State and Molecular Theory Group, M. I. T., October 15, 1957, p. 16; A. M. Karo and L. C. Allen, J. Chem. Phys. **31**, 968 (1959).

[8] R. A. Ballinger, Mol. Phys. **2**, 139 (1959).

[9] J. W. C. Johns and R. F. Barrow, Proc. Roy. Soc. (London) **A251**, 504 (1959).

[10] Talley, Kaylor, and Nielsen, Phys. Rev. **77**, 529 (1950).

[11] S. M. Naudé and H. Verleger, Proc. Phys. Soc. (London) **A63**, 470 (1950).

[12] Kuipers, Smith, and Nielsen, J. Chem. Phys. **25**, 275 (1956).

[13] R. Rydberg, Z. Physik **73**, 376 (1931); **80**, 514 (1933).

[14] O. Klein, Z. Physik **76**, 226 (1932).

[15] A. L. G. Rees, Proc. Phys. Soc. (London) **59**, 998 (1947).

[16] Vanderslice, Mason, Maisch, and Lippincott, J. Mol. Spectroscopy **3**, 17 (1959); Vanderslice, Mason, and Lippincott, J. Chem. Phys. **30**, 129 (1959); Vanderslice, Mason, and Maisch, *ibid.* **31**, 738 (1959).

TABLE I. Potential energy of the $X\,^1\Sigma^+$ state of HF.[a]

v	V (cm^{-1})	V (ev)	r_{max} (A)	r_{min} (A)
0	2 047	0.2537	1.023	0.836
1	6 008	0.7448	1.115	0.786
2	9 798	1.215	1.187	0.755
3	13 419	1.663	1.253	0.733
4	16 878	2.092	1.317	0.716
5	(20 193)	(2.503)	1.379	0.701
6	(23 351)	(2.895)	1.441	0.689
7	(26 350)	(3.266)	1.503	0.679
8	(29 191)	(3.619)	1.567	0.670
9	(31 875)	(3.951)	1.633	0.662
10	34 335	4.256	1.701	0.656
11	36 705	4.550	1.772	0.650
12	38 921	4.825	1.847	0.644
13	40 973	5.079	1.928	0.639
14	42 850	5.312	2.018	0.633
15	44 543	5.522	2.121	0.630
16	46 031	5.706	2.244	0.626
17	47 292	5.862	2.397	0.623
18	48 294	5.987	2.604	0.621

[a] Numbers in parentheses are interpolated values.

TABLE II. Potential energy of the $X\,^1\Sigma^+$ state of DF.[a]

v	V (cm^{-1})	V (ev)	r_{max} (A)	r_{min} (A)
0	1 488	0.1845	1.005	0.847
1	4 395	0.5448	1.079	0.802
2	7 211	0.8938	1.137	0.774
3	(9 947)	(1.233)	1.188	0.753
4	(12 600)	(1.562)	1.236	0.737
5	(15 169)	(1.880)	1.283	0.723
6	(17 655)	(2.189)	1.328	0.711
7	(20 058)	(2.486)	1.373	0.701
8	(22 377)	(2.774)	1.418	0.692
9	(24 613)	(3.051)	1.462	0.684
10	(26 766)	(3.318)	1.508	0.677
11	(28 834)	(3.574)	1.554	0.670
12	(30 820)	(3.820)	1.601	0.664
13	(32 722)	(4.056)	1.649	0.659
14	(34 541)	(4.282)	1.699	0.654
15	(36 276)	(4.497)	1.750	0.650
16	37 815	4.688	1.803	0.646
17	39 385	4.882	1.858	0.642
18	40 866	5.066	1.918	0.638
19	42 257	5.238	1.982	0.635
20	43 552	5.399	2.051	0.632
21	44 746	5.547	2.129	0.630
22	45 832	5.681	2.216	0.627
23	46 799	5.801	2.315	0.624

[a] Numbers in parentheses are interpolated values.

TABLE III. Potential energy of the $V\,^1\Sigma^+$ state of HF.

v	V (cm^{-1})	V (ev)	T_e+V(ev)[a]	r_{max}(A)	r_{min}(A)
0	574.8	0.0713	10.5813	2.275	1.924
1	1699	0.2106	10.7206	2.426	1.811
2	2788	0.3456	10.8556	2.540	1.735
3	3844	0.4764	10.9864	2.641	1.675
4	4868	0.6035	11.1135	2.733	1.625
5	5862	0.7266	11.2366	2.822	1.580

[a] T_e is the energy difference between the bottom of the potential curve in question and the bottom of the curve for the $X\,^1\Sigma^+$ state. The value of T_e used is 10.5100 ev. The value appears to be uncertain to ±0.005 ev.

TABLE IV. Potential energy of the $V\,^1\Sigma^+$ state of DF.

v	V (cm^{-1})	V (ev)	T_e+V(ev)	r_{max}(A)	r_{min}(A)
0	417.4	0.0517	10.5617	2.244	1.946
1	1239	0.1536	10.6636	2.369	1.848
2	2042	0.2532	10.7632	2.462	1.782
3	2828	0.3506	10.8606	2.542	1.730

polations are consistent and also that the RKR method is capable of this precision.

The heavy dashed line in Fig. 1 represents a Morse curve with constants derived from the spectroscopic data. The agreement with the experimental curve is surprisingly good in view of the fact that the Morse curve is often a rather poor representation of the actual curves for the cases where it has been compared with the experimental curves.[16]

The light dashed line in Fig. 1 is the curve obtained by Karo for the $X^1\Sigma^+$ state using an LCAO—MO method which included a large amount of configuration interaction. Although the calculations of Karo are quite extensive, it can not be said that the results are in too good agreement with the actual experimental curve. Karo, of course, was aware of this in his original work.[7]

In view of the difficulties inherent in an *ab initio* calculation on many-electron systems, various approximation schemes have been suggested in the past[17]

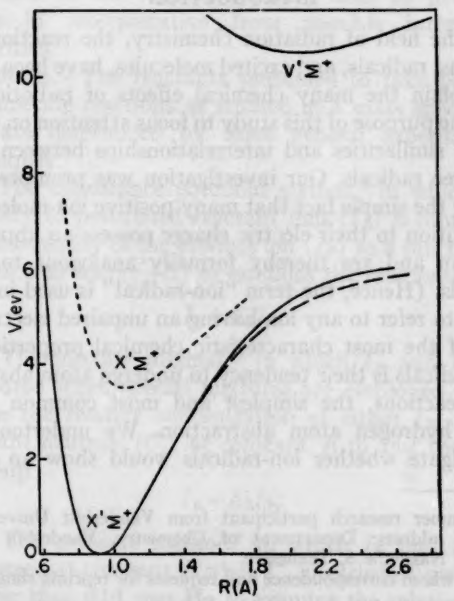

FIG. 1. Potential energy curves for HF and DF. The solid lines are curves derived directly from the spectroscopic data by the RKR method. The heavy dashed line represents a Morse curve and the light dashed line corresponds to the potential curve obtained theoretically by Karo.

[17] Eyring, Walter, and Kimball, *Quantum Chemistry* (John Wiley & Sons, Inc., New York, 1944).

for the calculation of interaction energies and undoubtedly others will be put forward in the future.[18] With a knowledge of the experimental curves for hydrogen fluoride, as well as for other systems,[15,16] it is now possible to check the adequacy of approximation schemes which may be proposed.

[18] H. Preuss, Technical Note No. 24 from the Quantum Chemistry Group, Uppsala University, Uppsala, Sweden, April 20, 1959.

ACKNOWLEDGMENT

The authors are grateful to Louis T. Ho for checking some of the calculations.

THE JOURNAL OF CHEMICAL PHYSICS VOLUME 32, NUMBER 3 MARCH, 1960

Hydrogen Atom Abstraction Reactions by Cyanide Ion-Radicals

T. W. MARTIN* AND C. E. MELTON†

Chemistry Division, Oak Ridge National Laboratory,‡ Oak Ridge, Tennessee

(Received August 24, 1959)

Ion-molecule reactions of low energy (0–0.15 ev) CHN^+ and CH_2N^+ are shown conclusively to follow a hydrogen atom abstraction mechanism of the type, $XH^+ + YH \rightarrow XH_2^+ + Y$. These reactions are presumably bimolecular being first order with respect to each reactant over the pressure range 10^{-7}–10^{-3} mm Hg. The rates of these reactions are markedly influenced by the molecular structure of both the cyanide ion and the hydrogen donor (YH). Ion-molecule reactions of this type are similar to the hydrogen atom abstraction processes of free radicals, but differ in having no appreciable temperature coefficients (in the range of 100–215°C), and in having much larger rate constants. On the basis of this study, chemical species having unpaired electrons whether charged (ion-radicals) or uncharged (free radicals) are shown to undergo similar types of reactions. Possible implications of these observations to the field of radiation chemistry are discussed.

INTRODUCTION

IN the field of radiation chemistry, the reactions of ions, radicals, and excited molecules, have been used to explain the many chemical effects of radiation.[1–5] It is the purpose of this study to focus attention on some of the similarities and interrelationships between ions and free radicals. Our investigation was prompted by noting the simple fact that many positive ion-molecules in addition to their electric charge possess an unpaired electron and are thereby formally analogous to free radicals. (Hence, the term "ion-radical" is used in this paper to refer to any ion having an unpaired electron.) One of the most characteristic chemical properties of free radicals is their tendency to undergo atom abstraction reactions, the simplest and most common type being hydrogen atom abstraction. We undertook to investigate whether ion-radicals would show an analogous chemical behavior so as to emphasize that the chemistry of ion-radicals can be better understood by recognizing both their charge and free radical characteristics.

Mnay ion-radical reactions are reported which involve possible hydrogen atom abstraction.[6–8] However, the results are complicated to interpret because there are at least four conceivable mechanisms involving singly charged ions which would explain the transfer of a hydrogen nucleus, namely,

(A) hydrogen atom transfer to ion (ion-radical abstraction),

$$XH^+ + YH \rightarrow XH_2^+ + Y,$$

(B) proton transfer,

$$XH^+ + YH \rightarrow X + YH_2^+$$

(C) hydride-ion transfer,[9]

$$XH^+ + YH \rightarrow XH_2 + Y^+,$$

and (D) hydrogen atom transfer to neutral

$$XH^+ + YH \rightarrow X^+ + YH_2,$$

* Summer research participant from Vanderbilt University; present address: Department of Chemistry, Vanderbilt University, Nashville 5, Tennessee.

† To whom correspondence and requests for reprints should be sent.

‡ Operated for the U. S. Atomic Energy Commission by The Union Carbide Corporation.

[1] C. E. Melton and G. A. Ropp, J. Am. Chem. Soc. **80**, 5573 (1958); P. S. Rudolph and C. E. Melton, J. Phys. Chem. **63**, 916 (1959).

[2] J. L. Magee and M. Burton, J. Am. Chem. Soc. **73**, 523 (1951).

[3] T. W. Martin and J. N. Pitts, Jr., J. Am. Chem. Soc. **77**, 5465 (1955).

[4] H. Essex, J. Phys. Chem. **58**, 42 (1954).

[5] C. J. Hochanadel, J. Phys. Chem. **56**, 587 (1952).

[6] Lampe, Field, and Franklin, J. Am. Chem. Soc. **79**, 6132 (1957); **80**, 5583 (1958).

[7] D. P. Stevenson, J. Phys. Chem. **61**, 1453 (1957).

[8] V. L. Tal'roze and A. K. Lyubimova, Doklady Akad. Nauk. S.S.S.R. **86**, 909 (1952).

[9] F. H. Field and F. W. Lampe, J. Am. Chem. Soc. **80**, 5587 (1958).

where X and Y represent any chemical group attached to a hydrogen nucleus. Mechanisms A and B form a set on the basis of their product ions which show a mass increase relative to their reactant precursor. Similarly, mechanisms C and D form another set where the product ions display a mass decrease. Hence, the two sets are easy to differentiate from each other, but it is not possible with present experimental techniques to distinguish between either A or B and between either C or D when any of the following limiting conditions interfere:

1. If XH=YH, as in studies of one component systems, mechanisms A and B or C and D are inherently indistinguishable because of charge transfer and possible rearrangement in the collision complex.

2. If the ionization potentials of XH and YH are nearly equal (within 1 ev), multiple ionic processes involving XH^+, YH^+ and perhaps other ions can take place concurrently to obscure the results. This condition cannot be circumvented by isotopic labeling with deuterium.

3. If neutral impurities from either contaminated reagents or subsequent spontaneous chemical reactions give rise to interfering ions.

In view of these three limiting conditions, we searched for a suitable chemical system which might allow a more definitive interpretation to be made between the hydrogen atom and proton transfer mechanisms A and B in order to test our hypothesis that ion-radicals should display similar reactions to those already well established for free radicals. The type of system finally chosen consisted of a binary mixture of an alkyl cyanide and some simple hydrogen donor (YH) like D_2, H_2, or CH_4. The use of such mixtures eliminated the problem of indistinguishability between mechanism A and B discussed under limiting condition 1. Alkyl cyanides were selected to furnish the ion-radicals for the following reasons: (a) The cyanide functional group is highly unsaturated and its alkyl ion-radical (XH^+) should be particularly susceptible to accept a hydrogen atom whereas the neutral cyanide (XH) might accept a proton so that the relative probabilities of mechanisms A and B could be estimated. (b) The ionization potentials of alkyl cyanides are significantly lower than the simple hydrogen donors used. This minimizes the uncertainty due to competing ionic reactions posed by limiting condition 2. (c) The cyanide and hydrogen donor mixtures studied did not appear to undergo spontaneous chemical reactions in the absence of the electron beam. This reduced the number of possible interferences mentioned under limiting condition 3. (d) Various alkyl cyanides are readily available to test the effect of structure on the reactivity of different ion-radicals.

Under these favorable experimental conditions it was possible to examine specific hydrogen transfer processes of cyanide ion-radicals to interpret their mechanism, to measure their relative and absolute rate constants, and to determine the influences of temperature, pressure, and molecular structure on the rate of reaction.

EXPERIMENTAL

Apparatus.—Our results were obtained with the 6-in. radius, 60°-sector research mass spectrometer and procedures described elsewhere.[10,11] The energy and intensity of the electrons from the thoria-iridium filament[12] were electronically controlled[13] in the energy range of 9–135 ev and at 0.5 μa trap current. The temperature in the ionization chamber was controlled at either 100° or 215° to ±1°. Pressures in the ionization chamber were measured by the technique previously developed[14] and are accurate to ±20%.

Reagents.—The hydrogen (Matheson, prepurified), deuterium (Stuart Oxygen Company), methane (Matheson, cp), methyl cyanide (Eastman, spectro grade) and monochloromethyl cyanide (Eastman, white label) were used in this study without further purification. The hydrogen cyanide was synthesized by Dr. P. S. Rudolph of this Laboratory and had a minimum purity of 99% as determined by the mass spectrometer. The ethyl and allyl cyanides (each Eastman practical grade) were studied to obtain only semiquantitative data and their purity was not carefully assessed. However, the mass spectrum of all the chemicals cited was examined at the highest pressure used to preclude errors in interpretation from possible interfering impurities.

Methods.—The reactants presumed to take part in ion-molecule reactions as studied in a mass spectrometer are determined by three general experimental techniques:

1. The appearance potential method,[6] in which the intensity of postulated reactant ions (I_R) is compared to the intensity of the product ion (I_P) as a function of the electron energy (E) to establish the relationship,

$$I_R = K_1 I_P.$$

2. The mixture method,[10] in which I_R and I_P are compared when special mixtures are employed to increase the relative concentration of either I_R or the reactant neutrals (C_n) at constant E to test the relationship

$$I_R = K_2 I_P.$$

3. The pressure method,[2] in which I_R and I_P are compared at constant E when C_n is varied at pressures greater than 0.01 mm Hg to examine the relationship,

$$I_R + I_P = K_3 C_n.$$

---

[10] C. E. Melton and P. S. Rudolph, J. Chem. Phys. (submitted for publication.)

[11] Melton, Ropp, and Rudolph, J. Chem. Phys. **29**, 968 (1958).

[12] C. E. Melton, Rev. Sci. Instr. **29**, 250 (1958).

[13] D. A. Hutchison and J. R. Wolff, Rev. Sci. Instr. **25**, 1083 (1954).

[14] G. F. Wells and C. E. Melton, Rev. Sci. Instr. **28**, 1065 (1957).

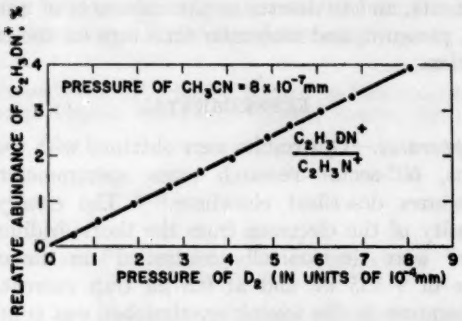

FIG. 1. Relative abundance of $C_2H_3DN^+$ *vs* the D_2 pressure.

Methods 1 and 2 were employed to establish the cyanide ion-radical reactions reported in this investigation. Proton transfer via mechanism B from possible proton donor ions (D_2^+, CH_4^+, H_2^+) to the cyanide neutrals was precluded by suitably adjusting the electron energy to produce only the cyanide parent ion.

The average kinetic energy of the reactant ions was estimated from the potential applied to the ion repeller and contact potentials[15] to be about 0.15 ev. The effect of the fringing field from the drawout potential is considered to be negligibly small because of the narrow exit slit of the ionization chamber.[1]

RESULTS

Evidence for deuterium atom abstraction by $C_2H_3N^+$ ion-radicals is presented graphically in Fig. 1. (The empirical formula notation is used for ions in this work.) These data were obtained by using a binary mixture of CH_3CN and D_2. The temperature in the ionization chamber was controlled at 100°, and the $C_2H_3N^+$ ion-radicals were produced by electrons having an indicated energy of 14.5 ev. Under these conditions $C_2H_3N^+$ was the only (99.9%) primary ion detected because D_2^+ and possible degradation ions, such as $C_2H_2N^+$, have significantly higher ionization potentials.[16,17] The absence of ions above mass 43 indicates that possible competing reactions of excited neutrals formed in the electron beam or at the wall are most unlikely. Thus, all the major limiting conditions are overcome and the product ion ($C_2H_3DN^+$) appears to be generated unequivocally by the atom abstraction reaction,

$$C_2H_3N^+ + D_2 \xrightarrow{k_1} C_2H_3DN^+ + D \qquad (1)$$

in accord with mechanism A. That the $C_2H_3DN^+$ ion is formed by a bimolecular reaction is shown by the linear pressure dependence of the $C_2H_3DN^+/C_2H_3N^+$ ratio. Further evidence in support of reaction (1) was obtained by the appearance potential studies which are presented in Fig. 2 where the energy scale is given in arbitrary units uncorrected for contact potential and other sources of systematic error. The virtually identical values for the appearance potentials of $C_2H_3N^+$ and $C_2H_3DN^+$ conclusively show the parent ion-radical is the precursor for $C_2H_3DN^+$. Furthermore, the fact that the slope of the $C_2H_3DN^+$ intensity curve does not change abruptly with the rapid increase in the D_2^+ intensity is strong evidence that the conceivable proton transfer reaction, $CH_3CN + D_2^+ \rightarrow C_2H_3DN^+ + D$, is not an efficient process.

The additional ion-radical reactions,

$$C_2H_3N^+ + H_2 \xrightarrow{k_2} C_2H_4N^+ + H \qquad (2)$$

$$C_2H_3N^+ + CH_4 \xrightarrow{k_3} C_2H_4N^+ + CH_3 \qquad (3)$$

$$CHN^+ + D_2 \xrightarrow{k_4} CHDN^+ + D, \qquad (4)$$

were confirmed by studies analogous to that described for reaction (1) using either $C_2H_3N^+$ or CHN^+ as the parent ion-radical together with a large excess of one of the neutral hydrogen atom donors D_2, H_2, or CH_4. These reactions, like (1), are unequivocal examples of the atom abstraction mechanism and demonstrate that the process is not limited to a single hydrogen donor. They are also convincing proof that proton transfer is an improbable process for these systems.

Specific rate constants for these reactions, calculated with the usual approximations,[6,7] are summarized in Table I together with rate constants for the well-known ion-radical reaction, $CH_4^+ + CH_4 \rightarrow CH_5^+ + CH_3$, which were measured to calibrate our method and apparatus (because of limiting conditions 1 and 2 the mechanism of this reference reaction is not implied or known). None of these reactions shows a discernable temperature dependence over the range 100–215°C; hence, they evidently have no appreciable activation energies. The ratio, $k_2/k_1 \simeq (\text{mass } D_2/\text{mass } H_2)^{\frac{1}{2}}$, which suggests the difference in these two rate constants is simply attributable to an isotope effect affecting their relative collision numbers. The fact that $k_3 > k_1$, shows that the

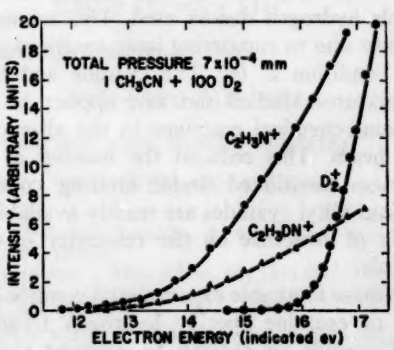

FIG. 2. Appearance potential study of the CH_3CN—D_2 mixture.

[15] J. A. Hipple, Phys. Rev. **71**, 594 (1947).
[16] G. Herzberg, *Spectra of Diatomic Molecules* (Van Nostrand Company, Inc., Princeton, New Jersey, 1950).
[17] C. A. McDowell and J. W. Warren, Trans. Faraday Soc. **48**, 1084 (1952).

chemical nature of the hydrogen donor can influence the rate of reaction. Similarly, since $k_4 > k_1$, the structure of the cyanide ion-radical plays an important role in the efficiency of the atom abstraction process.

This structural effect of the cyanide ion-radical was further tested in using binary mixtures of CH_2ClCN, CH_3CHCN, or CH_3CH_2CN with D_2. To our surprise, the parent ions of each of these cyanides failed (within our limits of detection) to abstract from D_2. Therefore, HCN and CH_3CN are quite unique in being the only cyanides investigated whose parent ion-radicals show a tendency for hydrogen atom abstraction from D_2. This result is more significant when contrasted with the observation that the parent ion-radicals of all the cyanides mentioned, without exception, will undergo hydrogen self-abstraction reactions in the pressure range $10^{-7}-10^{-3}$ mm Hg of the type,

$$RHCN^+ + RHCN \rightarrow RH_2CN^+ + (RCN)$$

where (RCN) may represent several uncharged species.

The self-abstraction reaction for the CH_3CN system was carefully studied with 14.5 ev electrons and found to be a bimolecular process with a $k = 3.5 \times 10^{-9}$ cc molecule^{-1} sec^{-1}. The $C_2H_4N^+/C_2H_3N^+$ ratio was directly proportional to the CH_3CN pressure and the absence of detectable ion masses greater than 42 precludes the possibility of degration products from possible intermediate ions[2,10] (such as $C_4H_6N^+$) to form the product ion $C_2H_4N^+$. Compared to the CH_3CN reaction, the relative rates of self-abstraction for the cyanides HCN, CH_2ClCN, CH_2CHCN, and CH_3CH_2CN are about 1, 0.04, 1, and 4, respectively. The interpretation of the chloromethyl cyanide self-abstraction process is complicated because of competing primary reactions to give a variety of product ions of higher mass, including some containing two chlorine atoms. The ethyl cyanide rate constant is uncertain because a second primary ion $C_3H_4N^+$, which may influence the $C_3H_6N^+/C_3H_5N^+$ ratio, is formed in greater abundance than the parent ion-radical $C_3H_5N^+$.

The fact that all of the cyanides investigated self-abstract, whereas only two of them undergo hydrogen atom abstraction from different hydrogen donors, suggests that there might be a different mechanism for self-abstraction, possibly proton transfer. Unfortunately, any discussion of detailed hydrogen transfer mechanisms for self-abstraction processes is sheer speculation because of limiting conditions 1 and 2.

DISCUSSION

We believe the results obtained in this investigation combined with other findings in this Laboratory adequately support our general contention that there are marked similarities and interrelationships between the behavior of certain ion-molecules and free radicals. At the outset, it is evident that all gaseous ions, like radicals, are in unusual valence states and must react to form more stable products. This has been confirmed

TABLE I. Hydrogen atom abstraction reactions by cyanide ion-radicals

Reaction	Electron energy (indicated ev)	$k \times 10^{9}$[a] (cc molecule^{-1} sec^{-1})
(1) $C_2H_3N^+ + D_2 \rightarrow C_2H_2DN^+ + D$	14.5	0.3$_9$
(2) $C_2H_3N^+ + H_2 \rightarrow C_2H_4N^+ + H$	13.8	0.5$_7$
(3) $C_2H_3N^+ + CH_4 \rightarrow C_2H_4N^+ + CH_3$	12.5	1.$_7$
(4) $CHN^+ + D_2 \rightarrow CHDN^+ + D$	14.5	2.$_0$
Reference Reaction: $CH_4^+ + CH_4 \rightarrow CH_5^+ + CH_3$	14.7	1.$_3$
	100	1.$_3$

[a] Comparative values for K_x were obtained using the following relationship:

$$K_x = K_{CH_4} \frac{(I_P/I_R)_x}{(I_P/I_R)_{CH_4}},$$

where the subscripts, x and CH_4, refer to the ion-radical abstraction and the reference reaction, respectively, with the ion current ratios taken under identical conditions.

in recent work[2,10,18] where all the observed primary ions were depleted in proportion to the enhancement of secondary and tertiary ions. Before discussing other similarities between ions and radicals, we feel that it is helpful to classify each chemical species, ion or free radical, as either "odd" or "even" according to their number of electrons. It then follows that any odd species obviously has an unpaired electron and is a radical, whereas most even species are presumed to have their electrons paired. However, the possibility that even species have unpaired electrons and hence are di-radicals must not be overlooked. Applying these terms we can discuss more easily three general positive ion-radical reactions similar to general processes known for free radicals. These processes have been verified in the mass spectrometric work cited in this paper; they are:

I. Ion-Radical Displacement:

$$\text{e.g., } \underset{\text{odd}_1}{XM^+} + \underset{\text{even}_1}{YN} \rightarrow \underset{\text{even}_2}{XMN^+} + \underset{\text{odd}_2}{Y}$$

II. Ion-Radical Addition:

$$\text{e.g., } \underset{\text{odd}_1}{XM^+} + \underset{\text{even}_1}{YN} \rightarrow \underset{\text{odd}_2}{XMYN^+}$$

III. Ion-Radical Decomposition:

$$\text{e.g., } \underset{\text{odd}_1}{XY^+} \rightarrow \underset{\text{even}_2}{X^+} + \underset{\text{odd}_2}{Y},$$

where the subscripts 1 and 2 refer to primary and secondary species, respectively.

Process I has been extensively studied and includes the atom abstraction reactions reported in this paper

[18] P. S. Rudolph and C. E. Melton, J. Chem. Phys. (submitted for publication).

as a special case. This process is perhaps the most striking example of both the similarities and interdependence of ions and free radicals in that *the ion-radical is always the precursor for a free radical*. Bimolecular rate constants for this process are of the order of 10^{-9} cc molecule^{-1} sec^{-1} compared with the usual values of 10^{-12} to 10^{-14} for similar free radical displacements which have appreciable activation energies and smaller steric factors. This analysis of the rate constants shows that ions undergo displacements from 10^3 to 10^5 times faster than free radicals; consequently, it would appear that ions play the dominant role in radiolytic reactions. However, the following factors must be carefully assessed before drawing any such conclusion: (1) the relative initial concentrations of radicals and ions formed in the energizing process, and (2) the subsequent forward and reverse reactions of secondary ions and radicals, including reactions of positive ions with radicals, electrons, or negative ions. Usually, little or nothing is known about either of these factors.

Process II has been shown to be very important in radiation polymerization reactions[2,10] and is very probable for both even and odd secondary ions. It is *unique* in perpetuating ion-radicals in the system and is analogous to the basic process in free radical polymerizations. The rate constants which are reported for ionic reactions of this type are about 10^2 to 10^5 times greater than methyl radical additions to olefins.[19]

[19] A. F. Trotman-Dickenson, *Gas Kinetics* (Academic Press, Inc., New York, 1955).

Process III is involved in rearrangement-decomposition reactions[20,21] and in the formation of many metastable ions observed in mass spectra. Ionic reactions of this type generate free radicals, ion-radicals or both. Hence, this process is another example of the direct connections between ions and radicals. Rate data for both the ionic and free radical processes of this type are not available for comparative purposes.

We have shown in this discussion that ions, particularly the ion-radicals, are both chemically similar to and directly inter-related to free radicals; ion-radicals undergo analogous general reaction types known for free radicals, some of which, actually *generate* free radicals as products. Therefore, it seems unreasonable to interpret chemical effects in radiation chemistry without considering both the similarities and interrelationships of ions and radicals. The mass spectrometer is the most definitive tool for the study of ionic reactions, but we believe that further correlations with free radical data will be increasingly important in achieving an understanding of these reactions.

ACKNOWLEDGMENT

The authors are indebted to Dr. R. Baldock, Dr. J. F. Burns, and Dr. C. J. Hochanadel for their helpful discussions and encouragement of this work.

[20] P. N. Rylander and S. Meyerson, J. Am. Chem. Soc. **78**, 5799 (1956).

[21] F. W. McLafferty, Appl. Spectroscopy **11**, 148 (1957).

Thermal Conductivity of Condensed Films: Methane*

JOHN T. CLARKE† AND RALPH GORDEN, JR.

National Bureau of Standards, Washington 25, D. C.

(Received October 16, 1959)

A new method of determining the thermal conductivity of condensed films at low temperature has been developed. It is based on determining the surface temperature of a film of known area and thickness by measuring its equilibrium vapor pressure. The thermal conductivity (K) of the film is calculated by measuring the increase in surface temperature as the film thickness is increased when a known heat flux is flowing across the film. For methane at 85°K, $K=3.5\times10^{-3}$ w/cm°K.

I. INTRODUCTION

IN condensing reactive species from the gas phase onto a surface cooled by a boiling refrigerant (liquid nitrogen, hydrogen, or helium), the surface temperature of the condensed film depends on the rate of deposition, the thickness of the film, and the thermal conductivity of the condensed film. The thermal conductivity of a film condensed from the vapor phase may differ from that obtained by solidification from a melt as a result of either a different crystal lattice or a less compact crystal. Because of this possible variation in the physical structure of the film and since thermal conductivities were not known within a factor of 10 or more, the experimental method was designed with the hope of obtaining an accuracy of ±10%.

The method used to measure thermal conductivity in these experiments was to determine the surface temperature of the film from the equilibrium vapor pressure of the condensed gas. The temperature difference across an increment of the film thickness was determined by observing the increase in surface temperature as the film thickness was increased with a known heat flux across the film. The heat flow was measured electrically and the film thickness was calculated from the known weight of gas condensed on the known surface area of the conductivity cell.

II. APPARATUS

The present apparatus is the result of the improvement of three earlier models based on the same principle. The first cell consisted of a single wire centrally located inside a Pyrex tube immersed in liquid nitrogen; a cold cathode pressure gauge was used to determine surface temperatures of Freon and ethane. The conductivity of the gas at $P=10^{-3}$ mm of Hg was so low that the temperature of the wire had to be increased above the cracking point of the gas before a measurable pressure increase could be observed with this apparatus. Analysis of the problem showed that the gas must have a pressure above 0.1 mm, the surface area of the heater should be a maximum, and the distance between the heater and the cold surface should be as short as possible and yet allow significant pressure measurements. The present appratus is shown in Fig. 1.

A. Heater

The heater ia a 100-watt cylindrical cartridge heater $\frac{5}{8}$ in. by 6 in. machine-fitted into a $\frac{1}{8}$-in. thick copper sheath. The copper sheath is gold-plated (to minimize radiation) and silver soldered to a copper-Pyrex seal. The electrical leads are brought out through tungsten seals and the inside, after having been evacuated, is sealed off with helium to improve heat transfer from the cartridge to the sheath. A copper-constantan thermocouple is soldered to the copper jacket and read by

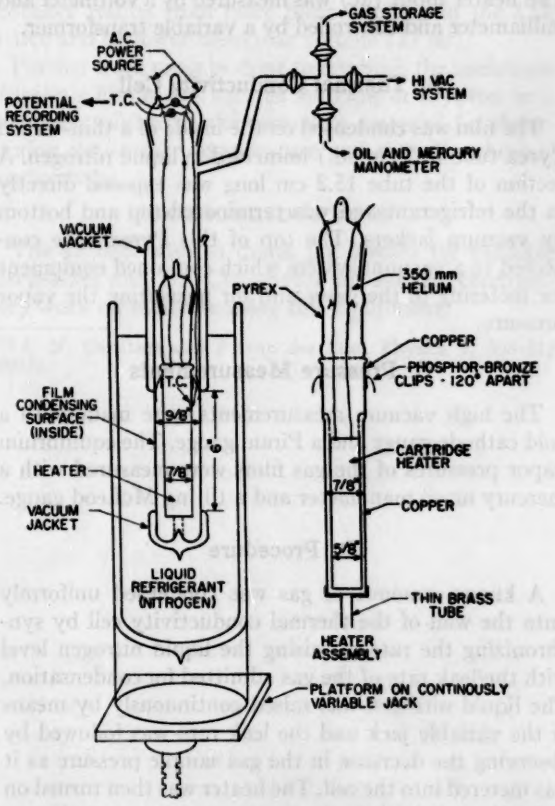

FIG. 1. Thermal conductivity apparatus.

* This research was performed under the National Bureau of Standards Free Radicals Research Program, supported by the Department of the Army.

† Guest scientist, Ethyl Corporation, Chemical Research and Development Division, Baton Rouge, Louisiana.

TABLE I.

Methane				
Volume liters (STP)	Film thickness cm	Heat applied watts	Press. mm	Temp. °K
1.5	0.0144	29.2	22.5	82.07
1.5	0.0144	22.6	20.0	81.40
1.5	0.0144	24.5	20.1	81.42
1.5	0.0144	23.5	20.2	81.45
1.5	0.0144	17.9	18.6	80.95
1.5	0.0144	14.6	17.1	80.45
1.5	0.0144	3.3	12.2	78.55
2.5	0.0249	39.8	34.7	84.61
2.5	0.0249	33.6	31.3	84.00
2.5	0.0249	28.4	27.4	83.27
2.5	0.0249	23.7	23.4	82.30
2.5	0.0249	18.7	20.4	81.49
4.5	0.0448	40.5	49.0	86.79
4.5	0.0448	35.3	40.6	85.58
4.5	0.0448	27.9	33.0	84.32
4.5	0.0448	17.4	21.9	81.77
4.5	0.0448	16.3	21.0	81.66
7.5	0.0746	41.4	66.8	88.80
7.5	0.0746	41.4	65.9	88.71
7.5	0.0746	36.0	53.0	87.30
7.5	0.0746	21.9	31.2	83.96
7.5	0.0746	12.5	23.0	82.20

means of a microvolt recorder. Part of the thermal emf was balanced with an auxiliary potentiometer. The heater input (ac) was measured by a voltmeter and milliameter and controlled by a variable transformer.

B. Thermal Conductivity Cell

The film was condensed on the inside of a thin-walled Pyrex tube (3.2 cm i.d.) immersed in liquid nitrogen. A section of the tube 15.2 cm long was exposed directly to the refrigerant and was terminated top and bottom by vacuum jackets. The top of this Pyrex tube connected to a vacuum system which contained equipment for metering in the gases and for measuring the vapor pressure.

C. Pressure Measurements

The high vacuum measurements were made with a cold cathode gauge and a Pirani gauge. The equilibrium vapor pressures of the gas films were measured with a mercury or oil manometer and a tilting McLeod gauge.

D. Procedure

A known amount of gas was condensed uniformly onto the wall of the thermal conductivity cell by synchronizing the rate of raising the liquid nitrogen level with the leak rate of the gas admitted for condensation. The liquid nitrogen was raised continuously by means of the variable jack and the leak rate was followed by observing the decrease in the gas sample pressure as it was metered into the cell. The heater was then turned on and adjusted until the heater temperature and the gas pressure reached constant values. Other steady states were obtained at different heat inputs. Additional determinations were made using increased quantities of condensed gas, thus giving increased film thicknesses.

III. EXPERIMENTAL RESULTS

A. Methane

The methane used was specially purified and had a purity of 99.8%. However, in addition it was condensed at liquid nitrogen temperature and sublimed until the vapor pressure was equal to that given in the NBS tables.[1] The experimental results with methane are summarized in Table I and Fig. 2.

Figure 2 shows that the increase in surface temperature for a given thickness of film is proportional to the heat applied. It is also seen that for a given heat input the temperature increases with increasing film thickness. To get an approximate value of the thermal conductivity, the temperatures for the different film thicknesses at 30 watts heat input are summarized in Table II.

From Table II it is seen that there appears to be a greater thermal gradient between 1.5 and 2.5 liters of gaseous methane (STP) than there is between 4.5 and 7.5 liters methane. This results from the unevenness of the film in the 1.5 liter deposit because of imperfections in the glass cell wall. The most reliable gradient to be

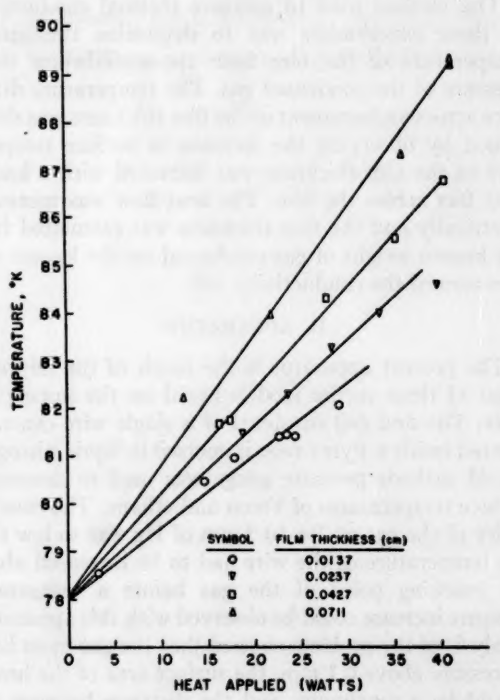

FIG. 2. Plot of the data used to determine the thermal conductivity of methane.

[1] *Selected Values of Properties of Hydrocarbons*, National Bureau of Standards Circ. No. C461.

TABLE II. Heat flow at 30 watts.

Methane layer				
Volume liters (STP)	Film thickness cm	Surface temp. °K at 30-w heat flux	Temp. difference	Temp. difference per cm of CH_4 film
1.5	0.0144	82.53		
			0.90	86
2.5	0.0249	83.43		
			1.10	55.3
4.5	0.0448	84.53		
			1.67	56.0
7.5	0.0746	86.20		

used for the thermal conductivity calculation is that between the 2.5 and 7.5 liters methane, namely, 55.7° per cm of methane in the film. The area of the cell is 153 cm². Thus, using the equation

$$\text{heat applied (watts)} = KA\Delta T/t$$

where K = thermal conductivity (w/cm°K), A = cell area (cm²), ΔT = temp. difference for incremental film of thickness t, t = incremental film thickness (cm), then $K = 3.5\times10^{-3}$ w/cm°K at 85°K.

This equation is valid if the heat flux is the same in both steady states. Moreover, in evaluating ΔT, it is necessary to take into account any difference of temperature of the refrigerant surrounding the cell during the two steady states.

It is difficult to determine the error with any degree of certainty, but the precision is estimated to be about 20%. There may be an absolute error of the order of 5% resulting from incomplete transfer of the heat to the film.

B. Krypton

Work with krypton has given $K = 2\times10^{-3}$ w/cm°K, but as a result of the lower vapor pressure of the gas the results are less accurate.

C. Carbon Dioxide

Considerable work was done using CO_2 with a layer of methane on top as a thermometric material. Increasing the amount of CO_2 from 100 ml to 4.6 liters and finally to 11.0 liters gave results which could not be explained in terms of a thermal conductivity coefficient. Whether this was because the thermal conductivity was too high for the apparatus to measure or because the film of CO_2 allowed methane to penetrate to the cold surface was not determined. The film appeared dense and it is believed that the conductivity of CO_2 is much higher than that of methane.

IV. DISCUSSION OF RESULTS

Gerritsen and van der Star[2] measured the thermal conductivity of methane using a solid section of CH_4 and found the value to be 1.2×10^{-3} w/cm°K at 20°K. The present value of 3.5×10^{-3} w/cm°K at 84°K is in reasonable agreement since one would expect the conductivity of a hydrocarbon to increase with temperature. The fact that the data obtained using the thermal conductivity cell yielded an approximately linear plot of temperature *vs* heat flux and thickness of the film indicates that the basic laws of thermal conduction are obeyed.

The results indicate that the thermal conductivity of condensed krypton is less than that of methane, although they have the same molecular volumes (39 ml) and the density of the condensed krypton is five times that of methane. Perhaps there is less interaction between molecules in a perfect gas crystal.

The apparently high thermal conductivity of CO_2 probably results from more polar bonding in the CO_2 lattice and its lower molecular volume (27 ml).

Further work must be done to establish the usefulness of using a film of gas such as methane or krypton on a substrate solid as a thermometric material for determining the surface temperature and thus the thermal conductivity.

ACKNOWLEDGMENTS

The authors wish to thank Dr. Broida for valuable discussions and Dr. Chatenever for further confirmatory work on methane using this equipment.

[2] A. N. Gerritsen and P. van der Star, Physica 9, 503–512 (1942).

Estimated Electron Affinities of the Light Elements*

GEORGE GLOCKLER

Department of Chemistry, Duke University, Durham, North Carolina

(Received July 20, 1959)

Estimates have been made of the electron affinities of the following elements: He(∼+0.), Li(0.5), Be(∼+0.), B(0.3), N(0.2), Ne(∼+0.), Na(0.7), Mg(∼+0.), Al(0.4), Si(1.9), P(0.8) ev. The known electron affinities of the other elements of the first two groups of the periodic table form the basis of the graphical method. It involves the variation of screening constants derived from the ionization potentials of isoelectronic sequences.

TWO groups of investigators[1,2] have lately been concerned with the problem of electron affinity (EA). An earlier quadratic extrapolation method[3] has now been refined by graphic means and yields the results shown in Figs. 1 and 2 and in Table I. It is assumed that the zeroth ionization potential of an atom (i.e., its electron affinity, EA) will vary with atomic number (Z) though not quite in the manner of the first and second ionization potentials (Fig. 2). The various ionization potentials of the n-electron systems are assumed to be given by the relation

$$I_{Z,n}=13.6(Z-s_{Z,n})^2, \tag{1}$$

where s is an arbitrary screening constant. Negative values of the electron affinities will not occur. The I_Z values were taken from a compilation of Moore.[4] Successive values of I_{Z+1}, I_Z etc. yield for a given n-electron system

$$s_{Z+1}=(Z+1)-(I_{Z+1}/13.6)^{\frac{1}{2}} \tag{2}$$
$$s_Z=Z-(I_Z/13.6)^{\frac{1}{2}}.$$

The differences $\Delta s(s_{Z+1}-s_Z)$ are shown in Fig. 1 as functions of atomic number (Z).

The electron affinity of the rare gas and other atoms in S states, such as the Group II elements must be very small although slightly positive.[5] These negative ions will show some stability due to an ion-induced dipole interaction between the electron and the polarizable neutral atom (+0., Table I). Evidence for this view is given by wave-mechanical calculations,[6] which indicate that the electron affinity of helium is either zero or slightly positive. Furthermore, the existence of helium negative ions has recently been reported.[7] They may be normal helium atoms (^1S) plus an electron, or a metastable helium atom (^3S) plus an electron.

Negative values of the electron affinity of an atom would mean that the corresponding ion would be unstable and could not exist in the gas phase.[8] Negative electron affinities are known for such ions as O^{--} which are said to occur in ionic crystal oxides. Their existence depends on the presence of positive ions so that the solid as a whole is stable.[9]

The extrapolation indicated in Fig. 1 would not be possible without knowledge of the electron affinities of some of the atoms involved. The following values were used: EA(C) = 1.13[5,10]; (O) = 1.48±0.1[11]; (F) =

TABLE I. Estimated electron affinities (ev).

Negative	Ion	Exptl.	G, M[g]	J, R[h]	$G.G.$[i]	ΔS[i]
H^-	$^1S_0$	0.715[a]	...	...	0.7[j]	−0.016
He^-	$^2S_{\frac{1}{2}}$	...	...	...	+0.	0.370
Li^-	$^1S_0$	...	...	...	0.5	0.374
Be^-	$^2P_{\frac{1}{2}}^0$	...	−0.12	...	+0.	0.219
B^-	$^3P_0$	...	0.56	0.82	0.3	0.240
C^-	$^4S_{\frac{3}{2}}^0$	1.13[b]	1.59	1.21	...	0.256
N^-	$^3P_2$	...	−0.10	0.54	0.2	0.130
O^-	$^2P_{\frac{3}{2}}^0$	1.48[c]	1.60	1.47	...	0.195
F^-	$^1S_0$	3.62[d]	...	3.62	...	0.257
Ne^-	$^2S_{\frac{1}{2}}$	...	...	...	+0.	0.358
Na^-	$^1S_0$	...	...	...	0.7	0.475
Mg^-	$^2P_{\frac{1}{2}}^0$	...	−0.56	...	+0.	0.337
Al^-	$^3P_0$	...	0.43	1.19	0.4	0.405
Si^-	$^4S_{\frac{3}{2}}^0$	...	1.63	...	1.90	0.475
P^-	$^3P_2$	...	0.7	1.33	0.8	0.365
S^-	$^2P_{\frac{3}{2}}^0$	2.07[e]	2.24	2.79	...	0.412
Cl^-	$^1S_0$	3.82[f]	...	3.84	...	0.453

[a] E. A. Hylleraas, Z. Physik **65**, 209 (1930).
[b] Reference 5, 10.
[c] Reference 11.
[d] Reference 12–14.
[e] L. M. Branscomb and S. J. Smith, J. Chem. Phys. **25**, 598 (1956).
[f] H. O. Pritchard, Chem. Revs. **52**, 529 (1953).
[g] Reference 1.
[h] Reference 2.
[i] Present work.
[j] G. Glockler, Phys. Rev. **41**, 685 (1932).

* This research is supported by the Office of Ordnance Research, U. S. Army under Contract No. DA-31-124-ORD-10-4.

[1] A. P. Ginsberg and J. M. Miller; J. Inorg. and Nuclear Chem. **7**, 351 (1958).
[2] H. R. Johnson and F. Rohrlich, J. Chem. Phys. **30**, 1608 (1959).
[3] G. Glockler, Phys. Rev. **46**, 111 (1934).
[4] Charlotte E. Moore, *Atomic Energy Levels*, Cir. 467 (U. S. Government Printing Office, Washington, D. C.), Vol. 1-3.
[5] L. M. Branscomb, Advances in Electronics and Electron Phys. **9**, 43 (1957).
[6] Hurst, Gray, Brigman, and Matsen, Mol. Phys. **1**, 189 (1958).
[7] Windham, Joseph, and Weinman, Phys. Rev. **109**, 1193 (1958).
[8] H. S. W. Massey, *Negative Ions* (Cambridge University Press, Cambridge, England, 1938).
[9] A. E. Van Arkel and J. H. de Boer, *Chemische Bindung als elektrostatische Erscheinung* (S. Hirzel, Leipzig, 1931).
[10] R. E. Honig, J. Chem. Phys. **22**, 126 (1954).
[11] L. M. Branscomb and S. J. Smith, Phys. Rev. **98**, 1127 (1955).

3.62[13–14]; (S) = 2.07±0.07[15]; and (Cl) = 3.82 ev.[14] A decided change of slope takes place in the curves shown in Fig. 1, which could only be found by the use of the known EA values just mentioned. This large change in curvature is caused by the greater difference in the radial change of the field near a neutral atom as compared with the Coulomb-field variation near a charged positive or negative ion.[1,16]

The curves in both figures show the separation of the sixteen electrons into six groups. In the case of the neutral atoms, they are: Li($^2S_{\frac{1}{2}}$) and Be($^1S_0$); B($^2P_{\frac{1}{2}}^0$), C($^3P_0$), and N($^4S_{\frac{3}{2}}^0$); O($^3P_2$), F($^2P_{\frac{3}{2}}^0$), and Ne($^1S_0$). In the second row of the periodic table, the corresponding groups with the same spectroscopic states are: Na and Mg; Al, Si, P; and S, Cl, A. The positive atomic ions with the same electron states are also grouped: Be^+ and B^+; C^+, N^+, and O^+; F^+, Ne^+, and Na^+; Mg^+ and Al^+; Si^+, P^+, and S^+; Cl^+, A^+, and K^+. Similarily, the negative atomic ions with the same number of electrons and the same states are arranged in an identical fashion: He^-, Li^-; Be^-, B^-, and C^-; N^-, O^-, and F^-; Ne^- and Na^-; Mg^-, Al^-, and Si^-; P^-, S^-, and Cl^-. This systematic arrangement was used in making the present estimates of the electron affinities. These groupings of atoms and ions are stressed by tie-lines in Figs. 1 and 2.

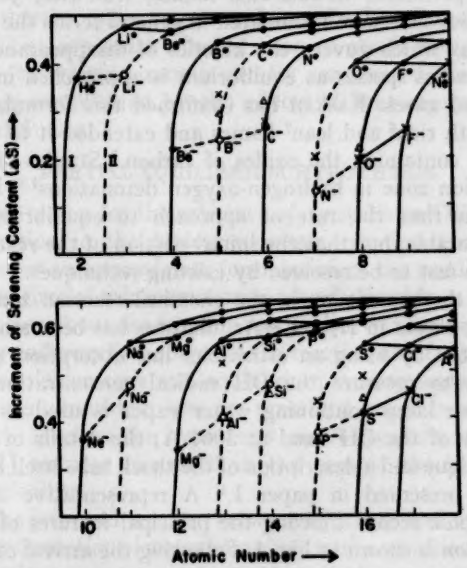

FIG. 1. Increment in screening constant as a function of atomic number. ● Experimental values; ○ Present estimates; Δ Reference 1, × Reference 2.

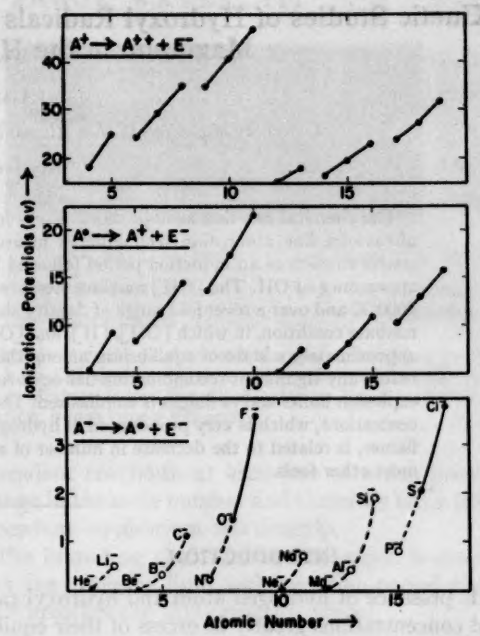

FIG. 2. Ionization potentials of positive ions, neutral and negative atoms as a function of atomic number. ● Experimental values, ○ Present estimates.

The unknown electron affinities (open circles) were found from the known ionization potentials and known electron affinities (black dots) in the following manner: The full curve (Fig. 1, I) (He^-, Li^0, Be^+ B^{++} etc.) was extended toward the abscissa by following the change of curvature from Li^0 to He^-. The next dotted line (Fig. 1, II) (Li^-, Be^0, B^+, etc.) was drawn with the same change in curvature as line I. The point of intersection of the vertical line ($Z=3$) and curve II gives $\Delta S[S(Be^0)-S(Li^-)]$. EA(Li) is then calculated from Eq.(1). It is assumed that the dotted lines have the same change of curvature as the full drawn curves. Since the tie lines (Li^0-Be^0), (B^0, C^0, N^0), etc., are straight lines, it was assumed that the tie lines for the negative ions should also be straight lines. Hence, the intersection of three lines determines a ΔS value uniquely.

[13] J. L. Margrave, J. Chem. Phys. 22, 636 (1954).
[14] T. L. Bailey, J. Chem. Phys. 28, 792 (1958).
[15] H. O. Pritchard, Chem. Revs. 52, 529 (1953).
[16] L. M. Branscomb and S. J. Smith, J. Chem. Phys. 25, 598 (1956).
[16] H. S. W. Massey, *Negative Ions* (Cambridge University Press, Cambridge, England, 1950).

Kinetic Studies of Hydroxyl Radicals in Shock Waves. III. The OH Concentration Maximum in the Hydrogen-Oxygen Reaction*

GARRY L. SCHOTT

University of California, Los Alamos Scientific Laboratory, Los Alamos, New Mexico

(Received October 9, 1959)

The chemical reaction zone in shock waves in H_2—O_2—Ar mixtures has been studied in detail using an ultraviolet line absorption technique to measure the OH radical concentration. The observed reaction course consists of an induction period followed by a sharp rise of [OH] to a maximum and then slow disappearance of OH. The [OH] maxima measured in rich, lean, and stoichiometric mixtures at $1000° \leqq T \leqq 2600°K$ and over a sevenfold range of density show that the reaction occurs in two distinct steps. The intermediate condition, in which [OH], [H], and [O] reach values greatly in excess of their equilibrium ones, is approximately a state of equilibrium among the three independent bimolecular reactions which is reached before any significant recombination has occurred. The relationship of these results to experiments near the explosion limits and in flames is emphasized. The occurrence of this overshoot in atom and free radical concentrations, which is very pronounced in hydrogen-oxygen flames but is not observed in many hydrocarbon flames, is related to the decrease in number of moles which occurs in the oxidation of hydrogen but not of most other fuels.

INTRODUCTION

THE presence of hydrogen atom and hydroxyl radical concentrations greatly in excess of their equilibrium values has been demonstrated in hydrogen-oxygen flames in several ways over the past thirty years.[1] Considerable knowledge of the mechanism of the reaction of hydrogen and oxygen has been gained from studies of the explosion limits[2] and of the induction period in the explosive reaction near the lower explosion limit.[3] The mechanism during the early stages of the explosive reaction is a branching chain process, and the qualitative way in which this mechanism leads to excess quantities of free radicals has been pointed out by Semenov.[4] Recent progress in understanding the mechanism of the later stages of the reaction has come from studies of hydrogen-oxygen flames. On the basis of experiments in fuel rich flames, Bulewicz, James, and Sugden[5] have formulated in general terms the conditions which govern the kinetics of disappearance of the excess species as equilibrium is approached in the burned gases. Kaskan has confirmed this formulation in both rich[6] and lean[7] flames and extended it to mixtures containing the oxides of carbon.[8] Studies of the reaction zone in hydrogen-oxygen detonations[9,10] have shown that the rate of approach to equilibrium is measurable, but that the initial portion of the reaction is too fast to be resolved by existing techniques.

In the present work, the chemical reaction zone in shock waves in H_2-O_2-Ar mixtures has been studied in detail by using an ultraviolet line absorption technique to measure the OH radical concentration.[11,12] A flash lamp containing water vapor is used as the source of the OH band at 3064 A; the details of this technique and a description of the shock tube itself have been presented in paper I.[11] A representative oscillographic record showing the principal features of the reaction is shown in Fig. 1. Following the arrival of the shock wave, which suddenly heats the experimental mixture from room temperature to one at which homogeneous gaseous reaction can proceed rapidly, the following sequence of events is observed. First, there is an induction period during which OH is not detectable. At the end of the induction period, the light absorption by OH exhibits a sharp S-shaped rise to a maximum and then slowly decreases. A quantitative study of the

* Work performed under the auspices of the U. S. Atomic Energy Commission. This paper and related material were presented as paper No. 87, Division of Physical Chemistry, 135th Meeting, American Chemical Society, Boston, Massachusetts, April, 1959.

[1] Some early reports include: (a) direct observation of OH by absorption spectroscopy; L. I. Avramenko and V. N. Kondratiev, Acta Physicochim. U.R.S.S. **7**, 567 (1937); L. I. Avramenko, *ibid.* **17**, 197 (1942). (b) H atoms inferred from rate of $H+H_2$ exchange; F. Goldmann, Z. physik. Chem. **B5**, 305 (1929), discussed by W. Jost, *Explosion and Combustion Processes in Gases*, translated by H. O. Croft (McGraw-Hill Book Company, Inc., New York, 1946), p. 321. (c) H atoms detected by thermocouples which catalyze $2\,H \rightarrow H_2 + 103$ kcal; H. Kondratieva and V. N. Kondratiev, Acta Physicochim. U.R.S.S. **21**, 1, 629 (1946). W. T. David and J. Mann, Nature **160**, 229 (1947). More recent work is presented and cited in references 5–8 and 20.

[2] B. Lewis and G. v. Elbe, *Combustion, Flames, and Explosions* (Academic Press, Inc., New York, 1951), Chaps. I and II.

[3] N. Semenov, Acta Physicochim. U.R.S.S. **20**, 291 (1945). Karmilova, Nalbandjan, and Semenov, Zhur. Fiz. Khim. **32**, 1193 (1958). The Russian work on the hydrogen-oxygen reaction is reviewed by N. Semenov, *Some Problems in Chemical Kinetics and Reactivity*, translated by M. Boudart (Princeton University Press, Princeton, New Jersey, 1959), Chap. X.

[4] N. Semenov, Izvest. Akad. Nauk S.S.S.R., Otdel. Khim. Nauk **3**, 210 (1945). English translation can be found in: Basseches, Beckett, and Johnston, Tech. Int. Report No. F-TR-2265-IA-2 (Part of ATI-83 148), Ohio State University Cryogenics Laboratory, 1949, Appendix IX.

[5] Bulewicz, James, and Sugden, Proc. Roy. Soc. (London) **A235**, 89 (1956).

[6] W. E. Kaskan, Combustion and Flame **2**, 229 (1958).

[7] W. E. Kaskan, Combustion and Flame **2**, 286 (1958).

[8] W. E. Kaskan, Combustion and Flame **3**, 39, 49 (1959).

[9] J. C. Chesick and G. B. Kistiakowsky, J. Chem. Phys. **28**, 956 (1958). G. B. Kistiakowsky and P. H. Kydd, *ibid.* **25**, 824 (1956).

[10] T. Just and H. Wagner, Z. physik. Chem. (Frankfurt) **13**, 241 (1957).

[11] Bauer, Schott, and Duff, J. Chem. Phys. **28**, 1089 (1958).

[12] G. L. Schott and J. L. Kinsey, J. Chem. Phys. **29**, 1177 (1958).

length of the induction period has been reported in paper II.[12] The present paper presents experimental measurements and a quantitative interpretation of the maximum OH concentration which occurs in this reaction.

Shock wave experiments in which the reactants are carried in an excess of inert gas have several advantages over flames and detonations for studies of the chemical kinetics of exothermic reactions. The conditions in the reaction zone are determined primarily by the shock strength in the carrier gas so that they are not closely tied to the nature or the progress of the chemical reaction. This allows one to vary the reaction temperature and the mixture composition nearly independently, and to cover much greater ranges of both. Better resolution of the reaction zone can be achieved also, for the following reasons. Practical detonation experiments require fairly high densities of reactants, but in driven shock waves one can use lower densities of reactants and thereby make reactions slower. In flames, the flow velocities are much smaller than in shock waves, so that the reaction zone is greatly compressed in space and is complicated by the effects of heat conduction and diffusion.

PARTIAL EQUILIBRIUM HYPOTHESIS

The reason for the existence of a maximum OH concentration in the hydrogen-oxygen reaction and the basis for an approximate formulation of the conditions at the time of this maximum can be deduced from what is known about the reaction mechanism during the very early and very late stages of the reaction and from general stoichiometric and equilibrium requirements. The pertinent considerations are presented below in a way which develops the hypothesis which accounts for the [OH] maxima measured in the present shock wave experiments.

The principal reaction between hydrogen and oxygen is the formation of water according to the stoichiometric equation

$$2H_2+O_2=2H_2O. \qquad (1)$$

In the equilibrium mixtures at high temperatures and in the homogeneous reaction mechanism, three additional species, H, O, and OH are known to be important.

The elementary processes which make up the reaction mechanism can be divided into two general classes,[5] those which increase or decrease the number of molecules in the system and those which do not. In this connection, it will be convenient throughout this paper to refer to the mole number n, which is here defined as the number of moles per gram of material, i.e., the reciprocal of the mean molecular weight. This parameter, rather than pressure or concentration, is used because we shall consider systems in which the temperature and density change with reaction.

Equilibrium considerations require that among the six species H_2, O_2, H_2O, OH, H, and O there be four independent reactions, at least one of which involves a change in the mole number and therefore has a pressure dependent equilibrium relationship.

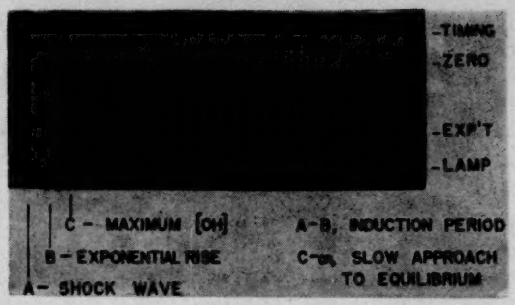

FIG. 1. Experimental record showing absorption in 3064 A band by OH during reaction of H_2—O_2—Ar mixture in shock wave. Mixture E (see Fig. 2), $P_0=10$ cm Hg, $T=1300°K$ before reaction, sweep time = 500 μsec.

The branching chain mechanism which is associated with the explosion limit and induction period phenomena[12] involves the three reaction steps:

$$H+O_2 \xrightarrow{k_2} OH+O \qquad (2)$$

$$O+H_2 \xrightarrow{k_3} OH+H \qquad (3)$$

$$OH+H_2 \xrightarrow{k_4} H_2O+H. \qquad (4)$$

All these reactions preserve the mole number and hence are not sufficient to accomplish the stoichiometry (1) or lead to complete equilibrium among the six species. Thus some independent process for combining species must be involved in any complete mechanism.

In the realm of slow reaction at temperatures below the explosion limits, recombination keeps pace with the chain reaction so that chain branching is kept in check and reaction proceeds stoichiometrically according to (1) with small steady-state amounts of the intermediates. But the characteristic of the branching chain reaction above the explosion limits is that atoms and OH radicals are produced through reactions (2)–(4) faster than they can be removed by recombination processes. This time lag in the recombination process necessarily produces a stepwise reaction in which the quantities of the intermediate species overshoot their subsequent equilibrium values.[4]

The reaction conditions in the shock wave experiments are far removed from the explosion limits and during the induction period[12] the chain branching by reactions (2)–(4) is very much faster than chain breaking by recombination reactions. Since reactions (3) and (4) are significantly faster than (2), O and OH are consumed substantially as fast as they are formed and the stoichiometry which results is approximately (2) plus (3) plus twice (4), which yields:

$$3H_2+O_2=2H_2O+2H. \qquad (5)$$

The reaction rate increases exponentially with time according to

$$d[H]/dt = 2k_2[O_2][H]. \quad (6)$$

The concentrations of O and OH are related to [H] by the kinetic steady-state relationships:

$$[OH]/[H] = 2k_2[O_2]/k_4[H_2] \quad (7)$$

and

$$[O]/[H] = k_2[O_2]/k_3[H_2]. \quad (8)$$

This reaction course cannot continue indefinitely, but like any autocatalytic process it must be terminated by depletion of the reactants if by no other mechanism. However, there are two other important processes which become operative when appreciable quantities of H_2O, OH, H, and O have been formed, namely back reactions and recombination reactions. The effect of recombination reactions is to reduce the mole number so that the stoichiometry tends toward (1). However, as will be emphasized in the following, recombination reactions in this system are relatively slow and it is appropriate to consider the effect of back reactions alone. As back reactions become important, the forward and reverse rates of the individual steps (2)–(4) tend to be equilibrated. The relationships among the various concentrations are no longer the steady-state conditions, Eqs. (7) and (8), but instead approach the equilibrium conditions of reactions (2)–(4). The stoichiometry which then results is a mixture, or reactions (5), (9), and (10).

$$H_2 + O_2 = H_2O + O \quad (9)$$

$$H_2 + O_2 = 2OH. \quad (10)$$

These reactions represent, respectively, the stoichiometric formation of H, O, and OH from the original reactants. Since they are linear combinations of the kinetic steps (2)–(4), they reach their respective equilibria through the equilibration of (2)–(4). Under such conditions, reaction (5), which is exothermic by 11 kcal, is the dominant stoichiometric process, as it was during the induction period. However, the contributions of the slightly endothermic processes (9) and (10) are also significant. Thus the amounts of atoms and OH radicals formed in this system in the absence or extreme slowness of recombination reactions represent sizable fractions of the original reactants.

As the experiments in flames have shown,[5–7] recombination is truly the rate determining step in the late stages of the reaction. Equilibration of forward and reverse rates of the bimolecular processes (2)–(4) is relatively rapid and keeps pace with the progress of recombination.

The separation of the characteristic rates of equilibration of the bimolecular reactions of the type (2)–(4), which conserve the mole number, and recombination reactions, which reduce the mole number, comes about in this system from a combination of two factors. First, recombination reactions among simple gaseous species require the participation of a third body and are kinetically third-order processes at pressures near or below one atmosphere, whereas the bimolecular processes are second order. Second, the bimolecular reactions in this system involve small activation energies which while significant at lower temperatures are no real deterrent to fast reaction at high temperatures. Recombination rates, on the other hand, generally decrease slightly with increasing temperature. Thus high temperatures and low pressures favor the separation of the rates of equilibration of these two kinds of reactions.

The limiting case of separation of characteristic rates of the two kinds of kinetic processes is one in which the bimolecular reactions essentially reach equilibrium before any significant recombination has occurred. The intermediate state to which the system tends under these circumstances is one of partial equilibrium with no change in the mole number. This state is completely described by (a) the three independent equilibrium conditions of reactions (2)–(4), and (b) the stoichiometric condition:

$$(n_0 - n)\rho = \tfrac{1}{2}([H_2O] - (\rho/\rho_0)[H_2O]_0 - [H] - [O]) = 0. \quad (11)$$

Here, ρ is the density, n is the mole number defined above, and the subscript zero refers to conditions before any reaction. This equation states simply that the change in the mole number, which can be expressed as half the difference in the amounts of triatomic and monatomic species formed from diatomic reactants, is zero. H and O atoms are assumed to be absent initially and H_2O present initially has been taken into account. The detailed course of the autocatalytic reaction during the induction period and the mechanism of of attainment of such a state of partial equilibrium, whether by reactions (2)–(4) or equivalent processes, are no longer important, since reactions (2)–(4) constitute a complete set of independent reactions in which the mole number does not change and all other such processes can be written as linear combinations of (2)–(4).

This hypothetical intermediate state, which will be referred to simply as the *partial equilibrium* state, is proposed as a good approximation to the conditions that obtain at the time of the observed maximum OH concentration in the shock wave induced combustion of hydrogen and oxygen at high temperatures and low densities.

For comparison of the measured [OH] maxima with those predicted by this hypothesis, the *partial equilibrium* conditions have been calculated for the experimental gas mixtures and shock wave conditions. This job was simplified by the fact that the *partial equilibrium* conditions are independent of pressure, so that calculations needed to be done for each mixture over the appropriate range of temperature, but the experi-

ments at different gas densities did not require separate treatment.

In performing these calculations, it has been possible to use a general solution of the equations of chemical equilibrium which is incorporated in an existing digital computer code for the solution of the Rankine-Hugoniot equations.[13] The special solution which satisfies the arbitrary stoichiometric condition (11) has been obtained at each of a series of temperatures by varying the value of the initial pressure in the calculation. This procedure is valid because any stoichiometrically possible mole number corresponds to equilibrium at one and only one pressure. The pressures which were considered in these calculations bear no relationship to the experimental pressures; but the results of interest, namely the mole fractions and the intensive shock wave parameters, are independent of pressure.

EXPERIMENTAL RESULTS

The experiments in which maximum OH radical concentrations have been measured have been described in detail in paper II.[12] These experiments cover the temperature range $1000°\leq T\leq 2600°K$ and involve four different H_2-O_2-Ar mixtures and observations in both incident and reflected shock waves, the latter at two optical path lengths. The experimental conditions are summarized in the legend to Fig. 2.

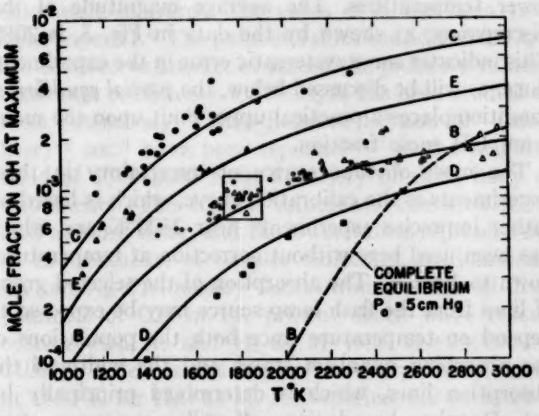

FIG. 2. OH mole fraction at maximum *vs* temperature for four experimental mixtures. Solid curves are for conditions of *partial equilibrium* with no recombination; the dashed curve is a sample curve for complete equilibrium. The points and mixtures are identified as follows:

Symbol	Mixture	$\%H_2$	$\%O_2$	Type of shock	Optical path (cm)
○	B	1.0	0.5	Incident	10.0
△	B	1.0	0.5	Reflected	10.0
□	B	1.0	0.5	Reflected	3.2
●	C	3.8	2.0	Incident	10.0
■	D	2.5	0.5	Incident	10.0
▲	E	1.0	2.0	Incident	10.0

[13] This code for the IBM 704 is due to R. E. Duff and incorporates W. Fickett's code of the Brinkley matrix method of solution of the chemical equilibria.

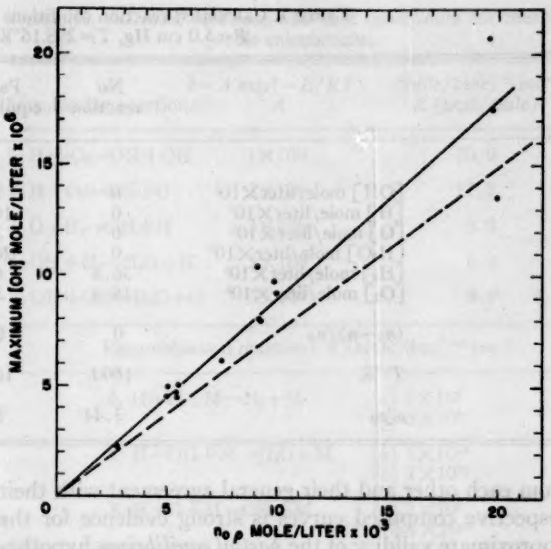

FIG. 3. Proportionality of maximum [OH] to gas density for mixture *B* near 1800°K. The points shown are those enclosed in the rectangle in Fig. 2. The solid line has the mean slope (mole fraction of OH) determined by the individual points; the dashed line represents the mole fraction computed by the *partial equilibrium* hypothesis.

The calibration curve relating fractional light transmission to OH concentration is an empirical one based on the equilibrium conditions attained in shock wave experiments near 2800°K. Such experiments were reported in paper I.[11] In the present work, those experiments and seven additional experiments in hydrogen-oxygen-argon mixtures have been recalculated using the currently favored value of $+9.27\pm0.3$ kcal/mole[14] for the standard heat of formation of OH at 0°K.

For comparison with the computed conditions of the hypothetical *partial equilibrium* state, it is convenient to consider the curve of OH mole fraction *vs* temperature for each mixture. The experimental OH concentrations deduced from the calibration curve have been converted to mole fractions and the temperature has been deduced from the measured shock velocity on the assumption that the temperature, density, and mole number of the shocked gas at the time of maximum light absorption are those computed for the *partial equilibrium* state. Since the gas is mostly argon, the changes in these quantities with reaction are small and no serious error is introduced by this procedure.

The results of this analysis of the [OH] maximum data are plotted in Fig. 2. Shown for comparison are the computed curves corresponding to the *partial equilibrium* state. In addition, one calculated curve is shown for complete equilibrium under a representative set of experimental conditions, incident shock waves in mixture *B* at an initial pressure of 5 cm Hg. The obvious separation of the four groups of experimental points

[14] R. F. Barrow, Arkiv Fysik **11**, 281 (1956); P. Brix and G. Herzberg, J. Chem. Phys. **21**, 2240 (1953).

TABLE I. Calculated reaction conditions for 4% H_2, 2% O_2 in Ar for initial conditions $P=5.0$ cm Hg, $T=298.16°K$, shock velocity $=1.263$ mm/μsec.

	No reaction	Partial equilibrium	At maximum [OH] (a) (b)	Equilibrium	Complete reaction
[OH] mole/liter$\times10^5$	0	2.00	1.99–1.89	0.11	0
[H] mole/liter$\times10^5$	0	16.3	15.2–12.1	0.015	0
[O] mole/liter$\times10^5$	0	3.8	3.6–2.8	0.004	0
[H_2O] mole/liter$\times10^5$	0	20.1	20.4–20.8	25.6	25.8
[H_2] mole/liter$\times10^5$	36.8	6.9	6.8–6.6	0.31	0
[O_2] mole/liter$\times10^5$	18.4	5.1	5.0–4.5	0.13	0
$(n_0-n)/n_0$	0	0	0.0009–0.0034	0.0197	0.0200
T °K	1600	1614	1628–1674	1938	1943
ρ/ρ_0	3.44	3.39	3.34–3.20	2.43	2.41

from each other and their general agreement with their respective computed curves is strong evidence for the approximate validity of the *partial equilibrium* hypothesis over a wide range of experimental conditions. The agreement among the three kinds of experiments with mixture *B* also supports the reliability of the experiments and their interpretation.

The proportionality of maximum OH concentration to density for a given mixture and temperature is implicit in the *partial equilibrium* hypothesis and in the plot of Fig. 2. This proportionality is shown explicitly in Fig. 3, where fifteen points for mixture *B* between 1740° and 1900°K (shown in the rectangle in Fig. 2) are plotted as OH concentration *vs* total gas concentration. For definiteness, the data have been adjusted to 1800°K using the temperature dependence of the calculated *partial equilibrium* curve. A sevenfold range of the density is covered in this group of experiments. The solid line is the average of the individual mole fractions, (after adjustment to 1800°K); the broken line represents the mole fraction given by the *partial equilibrium* hypothesis.

It may be noted that the *partial equilibrium* and total equilibrium curves of OH mole fraction *vs* temperature cross at a temperature between 2500° and 3000°K for the conditions of these experiments. This is exemplified by the sample curve for mixture *B* in Fig. 2. In this temperature range and at higher temperatures, no overshoot in [OH] is found experimentally, but rather the absorption rises sharply to a plateau and then no subsequent change is observed. The six experimental points shown in this region can as well be interpreted as representing complete equilibrium, which is reached rapidly because no slow recombination step is involved. At temperatures above that at which the two curves cross, the partial equilibrium curve of course does not represent the maximum OH mole fraction and probably does not represent any intermediate stage of the reaction. Below this temperature, however, the overshoot in OH concentration occurs and the [OH] maxima approximately follow the *partial equilibrium* curves, which are much less steeply dependent on temperature than the complete equilibrium curves.

As a detailed examination of Fig. 2 shows, the agreement between the observed [OH] maxima and the OH concentrations computed by the *partial equilibrium* hypothesis is not exact within the experimental scatter. For mixture *D*, the points are slightly below the computed curve, which is what might be expected if some recombination occurs while OH is still being formed. But for mixtures *B*, *C*, and *E*, the experimental points lie generally above the computed curves, especially at lower temperatures. The average magnitude of this discrepancy, as shown by the data in Fig. 3, is 20%. This indicates some systematic error in the experiments since, as will be discussed below, the *partial equilibrium* condition places a practical upper limit upon the maximum OH mole fraction.

The most obvious source of uncertainty in these experiments is the calibration curve, which is based on rather imprecise experiments near 2800°K and which has been used here without correction at temperatures down to 1000°K. The absorption of the selected group of lines from the flash lamp source may be expected to depend on temperature since both the populations of the absorbing quantum states and the width of the absorption lines, which is determined principally by the Doppler broadening effect,[15] are temperature dependent. In the absence of detailed knowledge of the emission spectrum of the lamp, these effects cannot be taken into account properly at the present time.

CALCULATED RESULTS

It is of interest to compare parameters calculated for various stages of the reaction under a representative set of experimental conditions. This is done in Table I. The first and fourth columns are for the limiting conditions of no reaction and total equilibrium, respectively. The second and fifth columns are for the hypothetical conditions of *partial equilibrium* with no recombination

[15] W. E. Kaskan, J. Chem. Phys. **28**, 729 (1958); **29**, 1420 (1958); T. Carrington, *ibid.* **31**, 1243 (1959).

and for complete burning of the hydrogen and oxygen to water. Complete rotational and vibrational equilibrium has been assumed in all these calculations. Comparison of columns 2 and 5 shows the magnitudes of the overshoots in the H, O, and OH concentrations and the dependence of the energy release, indicated by the temperature and density changes, on the recombination part of the reaction. Comparison of columns 4 and 5 shows that the equilibrium stoichiometry is very little different from Eq. (1).

The third column contains the estimated range of conditions at the time of the maximum OH concentration. These estimates were made by numerical calculations of the reaction profile for an assumed mechanism in which finite recombination rates were included. The details of these calculations have been described by Duff.[16] The system of reactions and rate coefficients considered is given in Table II. It should be emphasized that this mechanism is somewhat arbitrary and that the rate coefficients used do not necessarily best represent the available data in all cases. However, it is believed that this mechanism includes good estimates of the rates of the reactions which are most important in determining the OH concentration maximum. These are reaction (2), which is the rate determining step in the OH buildup mechanism, and the recombination reactions involving hydrogen atoms, reactions (6)–(8), which dominate the recombination mechanism in stoichiometric mixtures. The value of k_2 has been taken from paper II.[12] The pairs of values considered for k_6–k_8 are believed to bracket or exceed the probable values of these rate coefficients. Of these, k_8 has been studied the most extensively. Values between 10^9 and 10^{10} (mole/liter)$^{-2}$ sec^{-1} have been reported[5,6,17] in the neighborhood of 1500–2000°K in a variety of third body environments. The higher values are characteristic of H_2O as third body, and the lower values represent data in environments of simpler molecules, predominantly H_2 and N_2. Preliminary results from the rate of disappearance of OH in the present shock wave reaction system with Ar and H_2 as M yield $k_6=2\times10^9$ near 2100°K. Bulewicz and Sugden[17] have reported $k_7/k_6=24$ at 1650°K for H_2O as M. No experimental evidence on reaction 8 is available.

The results of these calculations using the low (a) and high (b) estimates of k_6–k_8 are shown in Table I as conditions at the time of the maximum OH concentration. The indication is that departure from the hypothetical *partial equilibrium* condition are at most a small fraction of the differences between the partial and total equilibrium conditions. The OH concentration maximum, which is the quantity measured in these experiments, is less sensitive to the finite progress of recombination than some of the other parameters.

Kinetic calculations have also been done considering only reactions (1)–(5) and excluding recombination processes. Since the mole number is fixed by this limited mechanism, the final state to which these calculations tend is the *partial equilibrium* state. It is found that slight concentration maxima are still possible for H atoms and also for OH as the system adjusts from the kinetic steady state of the branching chain mechanism to the conditions of equilibrium among the bimolecular reactions. However, these maxima are significant only in mixtures containing a large excess of O_2. In mixtures of near stoichiometric composition, the calculations described above indicate that recombination becomes important as the concentrations of recombinable species become large, so that maxima greater than given by the *partial equilibrium* calculation are not obtained. Thus the *partial equilibrium* condition represents a practical upper limit to the H, O, and OH concentration maxima.

Additional calculations were performed using the lower (a) values of k_6–k_8 and values of k_3–k_5 a factor of three smaller than those listed in Table II. The effect on the conditions at the OH concentration maximum was negligible, indicating that reaction (2) is indeed the rate determining step in the approach of the bimolecular processes to equilibrium. This is so even though, with these assumed rate coefficients, the approximation $k_2 \ll k_3$, k_4 is no longer a very good one, and the growth of the branching chain is slower than given by Eqs. (6)–(8). This makes the length of the induction period and the time to reach the [OH] maximum several percent longer than in the computations using the values of k_3–k_5 in Table II.

TABLE II. Assumed reactions and rate coefficients for reaction profile calculations.

Bimolecular reactions	$k=A\exp(-E/RT)$ A	(mole/liter)$^{-1}$ sec^{-1} E (kcal/mole)
1. $H_2+O_2\rightarrow OH+OH$	1×10^{11}	70.0
2. $H+O_2\rightarrow OH+O$	3×10^{11}	17.5
3. $O+H_2\rightarrow OH+H$	3×10^{11}	8.0
4. $OH+H_2\rightarrow H_2O+H$	3×10^{11}	6.0
5. $OH+OH\rightarrow H_2O+O$	3×10^{11}	6.0
Recombination reactions	**k (mole/liter)$^{-2}$ sec^{-1}**	
6. $H+H+M\rightarrow H_2+M$	(a) 1×10^9 (b) 5×10^9	
7. $H+OH+M\rightarrow H_2O+M$	(a) 1×10^{10} (b) 1×10^{11}	
8. $H+O+M\rightarrow OH+M$	(a) 1×10^9 (b) 1×10^{10}	
9. $O+O+M\rightarrow O_2+M$	3×10^8	

RELATION TO OTHER WORK

The branching chain mechanism of the autocatalytic initial portion of the reaction has been established from

[16] R. E. Duff, J. Chem. Phys. **28**, 1193 (1958).
[17] E. M. Bulewicz and T. M. Sugden, Trans. Faraday Soc. **54**, 1855 (1958).

its relationship to the explosion limit phenomena[2] and the induction period in the explosive reaction.[3,12] Semenov and co-workers[3,18] have analyzed the course of the explosive reaction beyond the end of the induction period by using a model which considered the effect of depletion of O_2 but did not consider the depletion of H_2 or the reversibility of the chain reaction steps. Using similar steady state considerations, Kondratiev and co-workers[19] have treated the super-equilibrium H and OH concentrations measured in flames. The present work and the recent work on flames[5–8] show that the equilibria approached by the chain reactions are of primary importance in determining the course of the reaction following the induction period. This is especially true at the temperatures encountered in flames and detonations. These temperatures are well above the explosion limits and the chain reactions are much faster than recombination processes so that large amounts of intermediates are accumulated.

The kinetics of disappearance of the excess atoms and OH radicals in the recombination zone in flames has been shown to indicate the approximate maintainment of equilibrium among the bimolecular reactions (2)–(4). However, the connection between the recombination zone and the primary reaction zone has been obscure.[5] The present results support and extend the description of the conditions in the recombination zone by showing clearly the source of the excess species and defining the starting point for the recombination phase of the reaction.

EXTENSION TO OTHER SYSTEMS

The overshoot in atom and free radical concentrations which is so pronounced in the hydrogen-oxygen reaction is the result of a rare combination of circumstances. First, the over-all reaction involves a decrease in the mole number, so that recombination is a necessary part of the mechanism. Such a reaction must be highly exothermic to proceed at high temperatures in spite of the decrease in entropy. Second, recombination occurs relatively slowly compared to the equilibration of bimolecular reactions which involve the atom and OH radical intermediates. The stepwise reaction in which the overshoot occurs is thus associated with the super-equilibrium mole number. This overshoot behavior is not a general characteristic of combustion of fuels with oxygen. Several hydrocarbon flames that have been examined under rich mixture conditions do not show this behavior.[20] A simple explanation is that only H_2 and a few other simple molecules can burn in oxygen with a decrease in mole number. Examples of these are CO, H_2S, CS_2, and C_2H_2, which in the presence of sufficient oxygen can burn to triatomic products with an overall decrease in mole number. The participation of CO in the overshoot phenomenon in H_2–CO–O_2 flames has been demonstrated by Kaskan.[8] Most hydrocarbons and other organic compounds, on the other hand, generally burn with either no change or an increase in the mole number. Hence the burning of these substances need not involve finite progress of recombination reactions in the mechanism. This does not mean that the burning of these substances cannot involve transient excesses of atoms and unstable radicals, since in general the combustion occurs by chain reactions. However, it does mean that large general overshoots associated with a super-equilibrium mole number need not occur, and in fact will not occur unless conditions are such that a great deal of bond breakage occurs in conjunction with an early stage of the reaction. This situation has been encountered in lean hydrocarbon flames, where oxidation of CO to CO_2 does not keep pace with the consumption of the hydrocarbon.[8,21]

ACKNOWLEDGMENTS

The author wishes to acknowledge the participation of Mr. John G. Williamson and Dr. J. L. Kinsey in the experimental work and Mr. Paul F. Bird in the analysis of data. It is also a pleasure to acknowledge helpful discussions with Dr. R. E. Duff, particularly in connection with the digital computer codes, and Professor Norman Davidson, whose stimulating questions ledthe author to the formulation of Eq. (11) and the *partial equilibrium* hypothesis.

[18] N. Semenov, Doklady Akad. Nauk S.S.S.R. **44**, 241 (1944).

[19] V. N. Kondratiev, *The Spectroscopic Investigation of Chemical Gas Reactions* (Academy of Sciences, Moscow, 1944); English translation of this monograph can be found in: Basseches, Beckett, and Johnston, Tech. Int. Report No. F-TR-2265-IA-2, (part of ATI-83 148), Ohio State University Cryogenics Laboratory, 1949, Appendix II.

[20] C. P. Fenimore and G. W. Jones, J. Phys. Chem. **62**, 693 (1958).

[21] Fristrom, Avery, and Grunfelder, *Seventh Symposium (International) on Combustion* (Butterworth's Scientific Publications, London, 1959), p. 304.

New Method for the Measurement of Microwave Integrated Line Intensities and Line Widths

A. DYMANUS,* H. A. DIJKERMAN, AND G. R. D. ZIJDERVELD

Fysisch Laboratorium der Rijksuniversiteit, Utrecht, Netherlands

(Received September 11, 1959)

A method is described for the measurement of microwave line widths and integrated intensities with Stark-modulation spectrometers. The method makes use of a property that the peak intensity $\alpha_{max,meas}$, measured at a given Stark field E, depends, under certain conditions, only on the half-width a and the peak intensity α_{max}. In the present investigation, the method has been used with a Stark cavity spectrometer employing "antimodulation" techniques which were described in an earlier paper. Experimental procedure, and the possibilities of the method are illustrated by measurements on two lines arising from the $J=1\rightarrow2$ rotational transition of the $^{16}O^{12}C^{32}S$ molecule in the ground state, and in the excited bending-vibrational state (l-doublet). The measured integrated intensity of the ground-state line of $(103\pm3.5)10^{-6}$ cm^{-1} sec^{-1} at 1 mm Hg agrees well with the theoretical value of $101.5\cdot10^{-6}$ cm^{-1} sec^{-1}. The half-width constant of the ground-state line and of the l-doublet line was found to be 6.27 ± 0.18 and 6.17 ± 0.23 Mc/mm Hg, respectively. From the measurements on the various mixtures of OCS and N_2, a value of 4.36 ± 0.12 Mc/mm Hg has been obtained for the collision broadening factor for OCS molecules with N_2 molecules.

The present method is applicable to sharp (also weak) lines of which the Stark splitting pattern is quantitatively known.

INTRODUCTION

MEASUREMENT of integrated line intensities is of primary importance in many applications of microwave spectroscopy, especially in chemical and isotopic analysis, and in the determination of various molecular quantities from line intensities. Although analysis with microwaves can be performed by peak intensities, the dependence of the latter on the composition of the sample makes this approach useful only in special cases.[1] It is well known that analysis by integrated intensities is not subject to this limitation. Various molecular quantities can be obtained from peak intensities only if the half-width of the line is known.

Generally, the integrated line intensity can be determined either: (1) by measuring the line intensity at a number of frequencies and by integrating the resulting curve of line intensity *vs* frequency, or (2) by measuring both peak intensity and half-width of the line (see below). The first method cannot be applied to weak or very sharp lines, while for strong and broad lines it is still subject to serious limitations.[1] The main difficulty of the second method stems from the fact that entirely different techniques are usually needed for the measurement of peak intensities and of line widths. Moreover, the ordinary techniques used for the determination of line widths[2] are difficult to apply for very sharp and weak lines.

A method, which largely eliminates the difficulties mentioned above forms the main subject of this paper. With this method, both the peak intensity and the half-width of the line are obtained from a single set of measurements on the line intensity. Although the method is thus intended primarily for the measurement of integrated intensities, it can also be used for the determination of line widths only. The method is applicable with Stark modulation spectrometers for all lines (also very sharp and weak ones) of which the Stark splitting pattern is quantitatively known. The present accuracy (~3% for line widths, and ~4% for integrated intensities) is largely determined by deficiencies of electronic equipment. Usefulness of the method and experimental procedure are illustrated by measurements on two lines arising from the $J=1\rightarrow2$ rotational transition of OCS near 24 kMc.

LINE INTENSITIES

The absorption intensity $\alpha(\nu)$ and the shape of a sharp absorption line broadened only by molecular collisions is given by[1]:

$$\alpha(\nu)=Cn(\nu^2/a)\{a^2/[(\nu-\nu_0)^2+a^2]\}\text{cm}^{-1}, \quad (1)$$

where ν, ν_0 = frequency of the incident radiation and the resonance frequency of the line, respectively; a = half-width of the line at half its maximum intensity (half-width in the following); n = number of molecules per cubic centimeter; C = constant depending on absolute temperature, structure of the molecule, and particular transition involved. For $\nu=\nu_0$, $\alpha(\nu)$ attains its maximum value

$$\alpha_{max}=Cn(\nu_0^2/a)\text{ cm}^{-1}, \quad (2)$$

which is the peak intensity of the line.

For a pure sample at a constant temperature, the half-width a is proportional to the pressure P in the absorption cell:

$$a=KP, \quad (3)$$

* Present address, Harvard University, Cruft Laboratory, Cambridge, Massachusetts.

[1] R. H. Hughes, Ann. N. Y. Acad. Sci. 55, 872 (1952).

[2] Gordy, Smith, and Trambarulo, *Microwave Spectroscopy* (John Wiley & Sons, Inc., New York, 1953), Sec. 1.5.

with the constant K called the half-width constant or the collision broadening factor for self-broadening. Since n is also proportional to P, α_{max} is thus independent of the pressure.

The peak intensity, $\alpha_{i,max}$, of a line originating from the ith constituent of a mixture is also given by Eq. (2) if n therein is replaced by n_i, the number of molecules of this constituent/cm^3, and a by a_i, the corresponding half-width. The last quantity can be written[1]:

$$a_i=\sum_j K_{ij}pj, \tag{3a}$$

with

$$K_{ii}\equiv K.$$

Herein, p_j is the partial pressure of the jth constituent of the mixture, and K_{ij} is the collision broadening factor of molecules of material j with molecules of material i. For a given composition of the mixture and at a given temperature both n_i and a_i are proportional to the total pressure. In this case, $\alpha_{i,max}$ is independent of the pressure in the absorption cell.

The collision broadening factors K_{ij} vary within wide limits for different molecules and are known only for few molecules. As a consequence, a_i and hence $\alpha_{i,max}$ depend on the composition of the mixture.

The integrated line intensity, α_{int}, is defined as

$$\alpha_{int}=\int_0^\infty \alpha(\nu)d\nu.$$

By integrating Eq. (1), one obtains for α_{int}:

$$\alpha_{int}=C\pi n\nu_0^2 \text{ cm}^{-1}\text{ sec}^{-1}. \tag{4}$$

The integrated intensity, $\alpha_{i,int}$, of the ith constituent of a mixture is also given by Eq. (4) if n is replaced by n_i.

As can be seen from Eq. (4), the integrated intensity is independent of the line width, and proportional to the number of absorbing molecules. For a given partial pressure p_i, the integrated intensity due to the ith constituent of a mixture is thus independent of the composition of the mixture and the pressure in the absorption cell.

By combining Eqs. (2) and (4), the expression for α_{int} reads:

$$\alpha_{int}=\pi a\alpha_{max} \text{ cm}^{-1}\text{ sec}^{-1}. \tag{5}$$

The integrated intensity can thus be obtained by measuring both α_{max} and a of the line.

METHOD

It is well known that the absorption intensity $\alpha(\nu_0, E)$ at the resonance frequency of a gas enclosed in a Stark absorption cell, and at the applied Stark field E is

$$\alpha(\nu_0, E)=\alpha_{max} \tag{6}$$

for $E=0$, and

$$\alpha(\nu_0, E)=\sum_M \alpha_M(\nu_0, E) \tag{7}$$

for $E\neq 0$.[3] Herein, $\alpha_M(\nu_0, E)$ is the absorption intensity by the Mth Stark component at the resonance frequency of the line, M being the magnetic quantum number. The sum in Eq. (7) is taken over all Stark components.

The peak intensity $\alpha_{max,meas}$ measured with an ideal (see last section of this paper) Stark spectrometer at the strength E of the modulating square-wave field is given [Eq. (6) and (7)] by

$$\alpha_{max,meas}=\alpha(\nu_0, E=0)-\alpha(\nu_0, E=E),$$

or

$$\alpha_{max,meas}=\alpha_{max}-\sum_M \alpha_M(\nu_0, E). \tag{8}$$

At pressures higher than approximately 0.02 mm Hg, the half-width of microwave absorption lines is determined mainly by molecular collisions. In a uniform Stark field, and in the absence of power saturation, it may be assumed that at these pressures the unsplit line and all of its Stark components have the same half-width and the same (Lorentzian) shape. The absorption intensity $\alpha_M(\nu_0, E)$ of the Mth Stark component can thus be written [see Eqs. (1) and (2)]:

$$\alpha_M(\nu_0, E)=\alpha_{M,max}(\nu_0^2/\nu_M^2)\left\{1+\left[\frac{\nu_0-\nu_M(E)}{a}\right]^2\right\}^{-1}. \tag{9}$$

Herein, $\alpha_{M,max}$ and $\nu_M(E)$ are the peak intensity and the center frequency of the Mth component, respectively.

From the principle of spectroscopic stability, and from the relation (5) applied to the unsplit line and to all its Stark components follows:

$$\alpha_{max}=\sum_M \alpha_{M,max} \tag{10}$$

or

$$\alpha_{M,max}=\alpha_{max}\cdot R_M,$$

with

$$\sum_M R_M=1.$$

The ratio $R_M(=\alpha_{M,max}/\alpha_{max})$ can readily be calculated for all microwave transitions from the well-known quantum-mechanical expressions.[4]

For lines possessing (in the usual approximation) a pure nth-order Stark effect ($n=1$ or 2 for the first or second order Stark effect, respectively) the frequency displacement of the Mth component from the unsplit line can be written[4]:

$$\nu_0-\nu_M(E)=K_M\cdot E^n. \tag{11}$$

The constant K_M depends on the strength of the molecular dipole moment and on the particular transi-

[3] A. Dymanus, "Intensity measurements in the microwave spectroscopy of gases," Thesis, Utrecht (1958), p. 26.

[4] C. H. Townes and A. L. Schawlow, *Microwave Spectroscopy* (McGraw-Hill Book Company, Inc., New York, 1955), Chap. 10.

tion involved. It can be calculated from known expressions for all microwave transitions in linear and symmetric-top molecules. For asymmetric-top molecules, K_M cannot be calculated in many cases. In these cases it is, however, not difficult to determine K_M experimentally with high accuracy.

By combining Eqs. (8)–(11), the expression (8) for $\alpha_{max,meas}$ becomes

$$\alpha_{max,meas}=\alpha_{max}\left(1-\sum_M \frac{R_M\nu_0^2/\nu_M^2}{1+K_M^2E^{2n}/a^{-2}}\right). \qquad (12)$$

The ratio ν_0^2/ν_M^2 differs from unity by less than 0.001 for the usual Stark splittings ($\nu_0-\nu_M(E)<12$ Mc at 24 kMc). The influence of this ratio on the Stark field dependence of $\alpha_{max,meas}$ and hence on the value of a is thus far below the accuracy of the present method and can be neglected.

Several methods can be followed to obtain the two unknown quantities, α_{max} and a, and hence α_{int}, from Eq. (12). In principle, they can be obtained from the values of $\alpha_{max,meas}$ at two different Stark fields. The accuracy is, however, considerably increased by measuring $\alpha_{max,meas}$ at a number of Stark fields, and by applying the method of least squares.[5] The values of α_{max} and a obtained from the values of $\alpha_{max,meas}$ at two fields are in this case used as preliminary values of these quantities.

A slightly different procedure suggests itself from the property [Eq. (12)]: $\alpha_{max,meas}\to\alpha_{max}$ for $E\to\infty$. Thus, if the available Stark field is strong enough to split the line completely, $\alpha_{max,meas}$ becomes a constant ($=\alpha_{max}$) at fields higher than a certain value. If the available field is not strong enough for a complete splitting, an extrapolation of $\alpha_{max,meas}$ values for $E\to\infty$ yields the desired α_{max}. With the known value of α_{max}, a is readily obtained from Eq. (12) by one of the methods mentioned above.

EXPERIMENTAL EQUIPMENT

The peak intensities $\alpha_{max,meas}$ were determined by the so-called antimodulation method described in detail elsewhere.[3,6] This method has been applied in the present investigation with a Stark cavity spectrometer utilizing Stark modulation at 400 cps, and superheterodyne detection at an IF of 30 Mc. By using the superheterodyne detection scheme, high spectrometer sensitivity could be obtained with low input powers to the cavity cell, which greatly minimize the danger of power saturation of the gas. Both signal and local oscillator klystrons were frequency stabilized by modified Pound-Zaffarano circuits.[3] The accuracy of the absolute value of $\alpha_{max,meas}$ was about 2%, while the variation of $\alpha_{max,meas}$ with the applied field could be determined with an accuracy of about 0.1%.

The absorption cell of the spectrometer was a pillbox shaped cylindrical Stark cavity oscillating in a TE_{0m1} mode ($4\lesssim m\lesssim 12$).[7] In this investigation the TE_{011} mode has been used almost exclusively. The modulating Stark voltage, a zero-biased square wave with an amplitude adjustable from zero to a maximum value of about 1200 v, was applied between the bottom and the plunger of the cavity. As the electric vectors of the Stark and microwave fields are perpendicular to each other, only transitions corresponding to $\Delta M=\pm 1$ are detected. Owing to the large diameter to length ratio (15–20), the resulting Stark field is very well homogeneous.

The pressure in the cavity cell was measured with a precision micromanometer with an accuracy of about 1.5%.

PROCEDURE AND RESULTS

The method has been applied to two lines arising from $J=1\to 2$ rotational transition of the $^{16}O^{12}C^{32}S$ molecule in the ground vibrational state (ground-state line in the following) and in the: $v_1=v_3=0$, $v_2=1_1^1$ bending vibrational state (lower-frequency component of the l-doublet, reference 4, Chap. 2). Extensive measurements have been performed only on the ground-state line, as for this line only was good comparison possible between theory and experiment. In the case of the l-doublet, there exists a discrepancy, thus far unexplained, between the measured and the calculated peak intensities.[6] The measurements on the l-doublet line were intended primarily for the determination of the half-width constant K of this line, and as an illustration of the usefulness of the present method also in the case of difficult lines.

(a) The Ground-State Line

The Stark effect of the ground-state line is of the second order with R_M and K_M for the $\Delta M=\pm 1$ transitions given by[8] (see also reference 3, Chap. 2):

$$R_M=1/20(2\pm M)(3\pm M),$$
$$K_M=-4.98\cdot 10^{-8}[63M^2-5(M\pm 1)^2-32]\text{Mc(v/cm)}^{-2}, \qquad (13)$$

where M refers to the lower state of the transition, and the upper (+) sign and the lower (−) sign correspond with the $\Delta M=+1$ and $\Delta M=-1$ transitions, respectively. Since $J=1$, M in Eq. (13) obviously takes the values −1, 0, +1. The line is thus split into three components. The strongest component ($R_M=0.6$) is also the nearest to the unsplit line ($K_M=0.55$ Mc at $E=1000$ v/cm).

By substituting the above values of R_M and K_M into Eq. (12), an explicit expression for $\alpha_{max,meas}$ in terms of α_{max}, a, and E is obtained. At fields and

[5] H. Margenau and G. M. Murphy, *The Mathematics of Physics and Chemistry* (D. Van Nostrand Company, Inc., Princeton, New Jersey, 1947), p. 500.
[6] A. Dymanus, Physica **25**, 859 (1959).
[7] A. Dymanus, Rev. Sci. Instr. **30**, 191 (1959).
[8] Dymanus, Dijkerman, and Zijderveld (to be published).

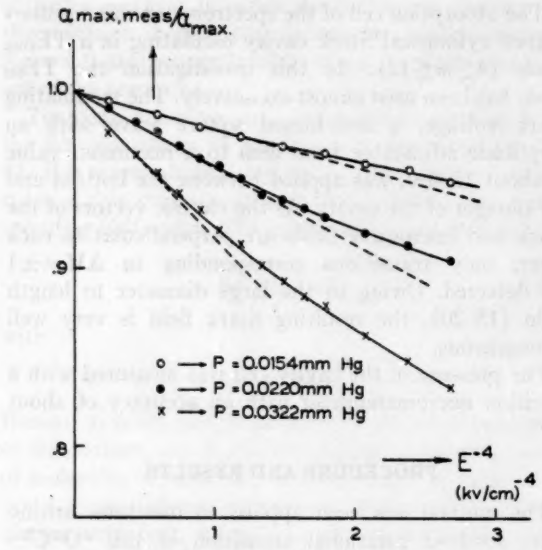

FIG. 1. The peak-intensity ratio $\alpha_{max,meas}/\alpha_{max}$ of the ground-state line of $^{16}O^{12}C^{32}S$ as a function of E^{-4} at three pressures in a cavity absorption cell. The dashed lines are the tangent lines to the corresponding $\alpha_{max,meas}/\alpha_{max}$ curves at $E^{-4}=0$.

pressures at which $E^4/a^{-2}>2\cdot10^{12}$ this expression can be approximated (to within 1%) by the expression,

$$\alpha_{max,meas}=\alpha_{max}\left(1-\frac{0.64}{1+3.02\cdot10^{-13}E^4a^{-2}}\right), \qquad (14)$$

which is suitable for the application of the least square method. Moreover, as can be seen from Eq. (14), the relation between $\alpha_{max,meas}$ and E^{-4} becomes (practically) a linear one:

$$\alpha_{max,meas}\simeq\alpha_{max}(1-2.12\cdot10^{12}a^2E^{-4}), \qquad (15)$$

at fields and pressures at which $3.02\cdot10^{-13}E^4a^{-2}\gg1$. The desired quantities, α_{max} and a, can thus be obtained from the intersection of the curve $\alpha_{max,meas}$ *vs.* E^{-4} with the line $E^{-4}=0$ and from the slope of this curve at $E^{-4}=0$, respectively.

Three curves of $\alpha_{max,meas}/\alpha_{max}$ *vs.* E^{-4} are given in Fig. 1 for the ground-state line at pressures of 0.0154, 0.0220, and 0.0322 mm Hg. Each point in this figure is a mean value of at least three measurements at a temperature of about 296°K. As can be seen from Fig. 1, the lowest field strength at which Eq. (15) is still a good approximation of Eq. (14) increases rapidly with increasing pressure in the cell; it is ~950 v/cm at a pressure of 0.0154, and increases to ~1450 v/cm at a pressure of 0.0322 mm Hg.

The mean value of K obtained from the slopes of the $\alpha_{max,meas}/\alpha_{max}$ *vs.* E^{-4} curves in Fig. 1 is ~6.4 Mc/mm Hg. This value agrees well with the value of 6.46 and 6.16±0.35 Mc/mm Hg obtained by Feeny *et al.*,[9] and by Johnson and Slager,[10] respectively. A consideration of Fig. 1 reveals, however, at once, that the value of K obtained from the slopes is not very accurate, especially at higher pressures.

The dependence of a, α_{max}, and α_{int} of a pure OCS sample on the pressure in the absorption cell is shown in Fig. 2 for pressures between 0.015 and 0.035 mm Hg. The experimental points in this figure (and also in the following ones) have been obtained from Eq. (14) by the methods explained above. In agreement with Eqs. (2)–(4), α_{max} in Fig. 2 is independent of the pressure, and both a and α_{int} are proportional to the pressure. From the appropriate curves the following values are obtained for K, α_{max}, and α_{int} at a temperature $T\simeq296$°K:

$$K=6.25\pm0.18 \text{ Mc/mm Hg}$$

$$\alpha_{max}=(5.14\pm0.10)\ 10^{-5}\text{ cm}^{-1}$$

$$\alpha_{int}=(103\pm3.5)\ 10^{-5}\text{ cm}^{-1}\text{ sec}^{-1}\text{ at 1 mm Hg.}$$

The value of K given above lies between the values of Johnson and Slager, and of Feeny *et al.* The value of α_{max} agrees well with the value (5.13±0.12) 10^{-5} cm^{-1} reported previously.[6] The integrated intensity obtained from the present measurements is close to the theo-

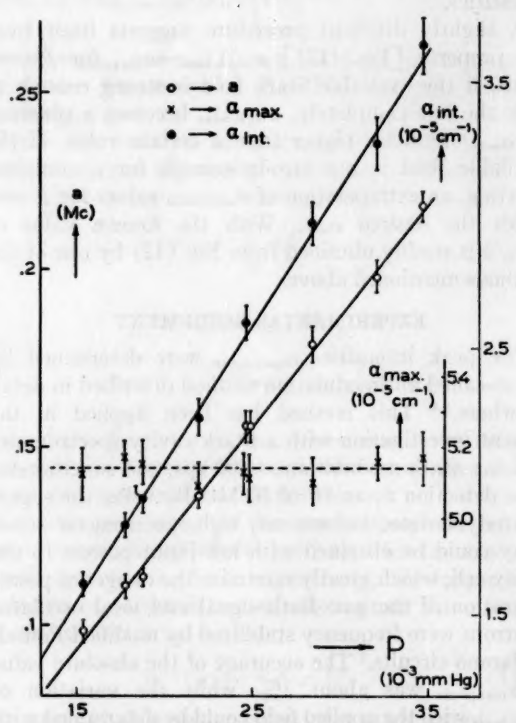

FIG. 2. The pressure dependence of the peak-intensity α_{max}, of the integrated intensity α_{int}, and of the half-width a of the ground-state line of OCS for a pure OCS sample.

[9] Feeny, Lackner, Moser, and Smith, J. Chem. Phys. **22**, 79 (1954).

[10] C. M. Johnson and D. M. Slager, Phys. Rev. **87**, 677 (1952).

retical value of $101.5\cdot10^{-6}$ cm^{-1} sec^{-1} at 1 mm Hg (reference 3, Sec. 6.2.3, and reference 6).

The results of extensive measurements on mixtures of carbonyl sulfide and nitrogen (N_2) are summarized in Figs. 3 and 4. In these measurements the pressure of OCS has been kept constant (0.0178 mm Hg in Fig. 3, and 0.0247 mm Hg in Fig. 4), and the pressure of N_2 varied from zero to about 0.015 mm Hg. Larger admixtures of N_2 have not been used because of difficulties in measuring accurately partial pressures of N_2 higher than 0.015 mm Hg.

A consideration of Figs. 3 and 4 indicates good agreement between experimental results and predictions of the theory. At both partial pressures p(COS), of OCS, α_{int} is proportional to p(COS) and independent of the partial pressure $p(N_2)$ of N_2, and hence of the mixture composition [Eq. (4)]. The mean values of α_{int}: $1.80\cdot10^{-6}$ cm^{-1} sec^{-1} at p(COS) = 0.0178 mm Hg, and $2.55\cdot10^{-6}$ cm^{-1} sec^{-1} at p(COS) = 0.0247 mm Hg agree well with the values of $1.83\cdot10^{-6}$ and $2.54\cdot10^{-6}$ cm^{-1} sec^{-1} obtained with a pure OCS sample [Fig. (2)], and with the calculated values of $1.82\cdot10^{-6}$ and $2.53\cdot10^{-6}$ cm^{-1} sec^{-1} for $T=296$°K. All quantities in Figs. 3 and 4 have been measured at temperatures close to 295°K.

At both partial pressures of OCS, the half-width of the line increased linearly with increasing $p(N_2)$ according to Eq. (3a). The mean value of the collision broadening factor K_{COS,N_2} for collisions of OCS molecules with N_2 molecules obtained from the slope of the a *vs* $p(N_2)$ curves in Figs. 3 and 4 is

$$K_{COS,N_2}=4.36\pm0.12 \text{ Mc/mm Hg}.$$

No previous measurement of this factor is known to us.

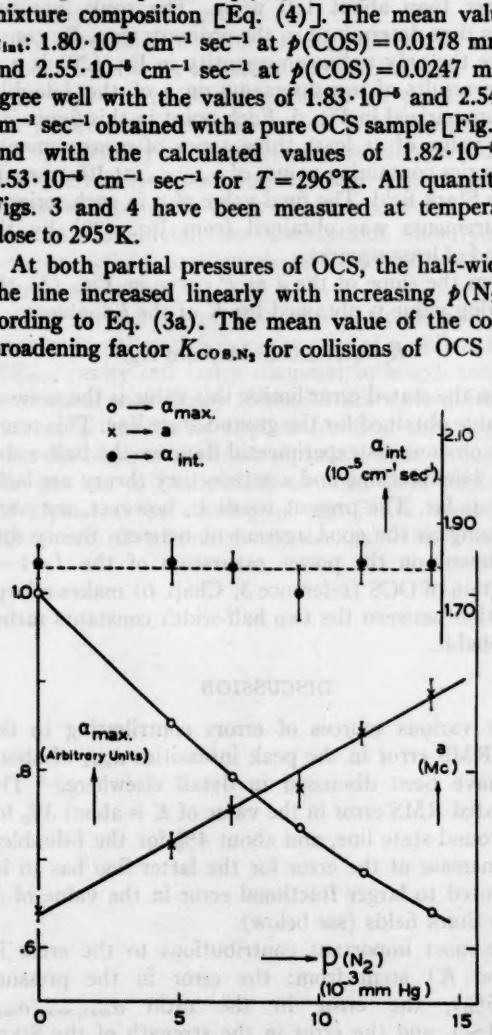

FIG. 3. The dependence of the peak intensity α_{max} (measured in units of the peak intensity of a pure OCS sample), the half-width a, and the integrated intensity α_{int} of the ground-state line on the partial pressure $p(N_2)$ of N_2 in a mixture of OCS and N_2. The partial pressure of OCS was 0.0178 mm Hg.

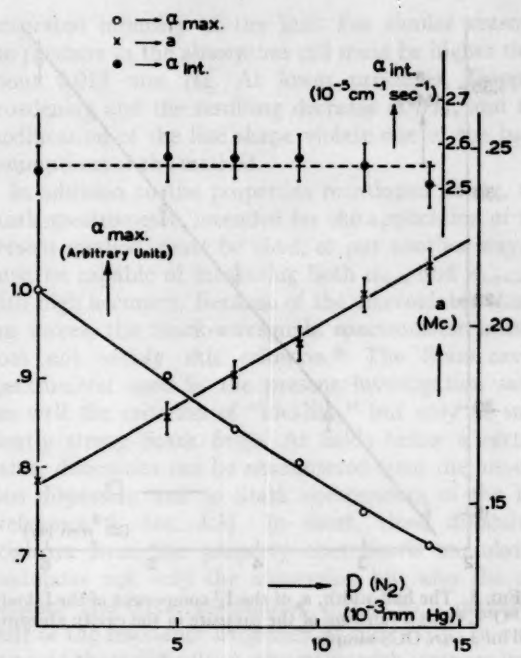

FIG. 4. The same as Fig. 3, but at the partial pressure of OCS of 0.0247 mm Hg.

The decrease of the peak intensity α_{max} with increasing $p(N_2)$ (Figs. 3 and 4) is in good (~2%) agreement with the relation:

$$\frac{\alpha_{max}(p(N_2)\neq0)}{\alpha_{max}(p(N_2)=0)}=\frac{K\cdot p(\text{COS})}{K\cdot p(\text{COS})+K_{COS,N_2}\cdot p(N_2)}, \quad (16)$$

using the K_{COS,N_2} value given above. The relation (16) follows from Eqs. (2)–(3a). An investigation of Figs. (3) and (4) indicates that for a given molar fraction of N_2, α_{max} is (within ~1)% the same at the two partial pressures of OCS. For a given composition of a binary mixture, α_{max} is thus independent of the total pressure in the cell.

(b) The *l*-Doublet Line

The Stark effect of the $J=1\rightarrow2$, $\Delta M=\pm1$ rotational transition of OCS in the excited bending degenerate vibration (l-doublet) is treated in details elsewhere.[8] For the lower (1_1^1) component of the doublet, the frequency displacement $\nu_0-\nu_M(E)$ of the Mth Stark component from the unsplit line, and the ratio R_M are:

$$\nu_0-\nu_M(E)=[368+34.5(M\pm1)^2\,10^{-4}E^2]^{\frac{1}{2}}$$
$$-[40.9+310\cdot10^{-4}M^2E^2]^{\frac{1}{2}}-12.78 \text{ Mc},$$
$$R_M=\tfrac{1}{20}(2\pm M)(3\pm M). \quad (17)$$

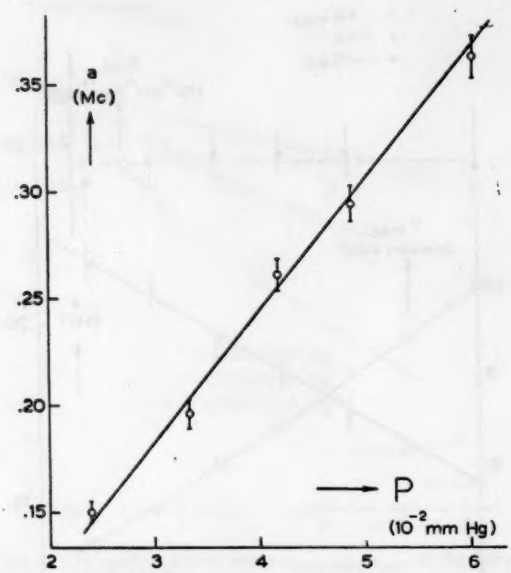

FIG. 5. The half-width, a, of the $1_1{}^1$ component of the l-doublet of $^{16}O^{12}C^{32}S$ as a function of the pressure in the cavity absorption cell for a pure OCS sample.

Herein, the $\pm$ sign convention is the same as used in Eq. (13).

The line is thus split into three components having relative intensities of 0.6, 0.3, and 0.1. The order of the Stark effect changes uniformly from second at low fields ($\lesssim$10 v/cm) to first at high fields ($\gg$100 v/cm). At all fields the frequency displacement, $\nu_0-\nu_M(E)$, of the components with $R_M=0.6$ and 0.1 is 7–10 times larger than the displacement of the $R_M=0.3$ component. A complete splitting of the line is readily obtained at fields stronger than $\sim$150 v/cm.

By combining Eqs. (8)–(10), and (17), an expression is obtained for $\alpha_{max,meas}$ in terms of E, a, and α_{max}, from which the last two quantities can be determined by the methods explained previously. The resulting expression for $\alpha_{meas,max}$ is however, quite complicated and not suitable for the application of the least square method. Several procedures seem possible to simplify this expression. The one followed in this investigation was the following.

The Stark-field dependence of $\alpha_{max,meas}$ was measured at fields between 50 and 100 v/cm. It can be readily shown from Eq. (17) that at these fields; (i) the frequency displacement $\nu_0-\nu_M(E)$ of the $R_{M=0}=0.3$ component can be written (error $<1\%$) as:

$$\nu_0-\nu_M(E)\equiv A_{M=0}=9.00\cdot10^{-5}E^2(1-473\cdot10^{-8}E^2)^{\frac{1}{2}}; \quad (18)$$

(ii) the contribution of the $R_M=0.1$ component to the sum in Eq. (8) is negligible at these fields if the pressure is less than $\sim$0.1 mm Hg; (iii) the contribution β to the sum in Eq. (8) of the $R_M=0.6$ component is given by:

$$\beta\simeq qR_{M=0}(1+A_{M=0}{}^2a^{-2})^{-1}, \quad (19)$$

where $A_{M=0}$ is given by Eq. (18), and q by the equation:

$$q\simeq0.005+\tfrac{1}{3}P,$$

which can be obtained by numerical computation from Eqs. (7), (9), and (17), assuming for K a reasonable value of 6.3 Mc/mm Hg.

With these considerations in mind, the following expression is obtained for $\alpha_{max,meas}$ from Eqs. (8)–(10), (18), and (19):

$$\alpha_{max,meas}=\alpha_{max}\left[1-\frac{R_{M=0}(1+q)}{1+A_{M=0}{}^2a^{-2}}\right]. \quad (20)$$

This expression can be rearranged to yield a in terms of the remaining quantities. It should be noted [Eq. (17)] that the line is easily split completely by fields stronger than about 150 v/cm. The peak intensity α_{max} is thus determined in the ordinary way. By consequence the only unknown quantity in Eq. (20) is a.

The results of measurements on a of the l-doublet are summarized in Fig. 5. Each point in this figure is a mean value of at least three series of measurements, each series containing values of $\alpha_{max,meas}$ at 10 strengths of the Stark field. The final value of a in each series of measurements was obtained from Eq. (20) by the method of least squares.

From the slope of the a *vs* P curve in Fig. (5) the following value is obtained for K of the l-doublet:

$$K=6.17\pm0.23 \text{ Mc/mm Hg}.$$

Within the stated error limits, this value is the same as the value obtained for the ground-state line. This result is not obvious, as experimental data on the half-width of the l-doublet line and a satisfactory theory are lacking thus far. The present result is, however, not very surprising as the good agreement between theory and experiment on the power saturation of the $J=1\rightarrow2$ transition of OCS (reference 3, Chap. 6) makes a large deviation between the two half-width constants rather improbable.

DISCUSSION

The various sources of errors contributing to the total RMS error in the peak intensities α_{max} of about 2% have been discussed in detail elsewhere.[3,8] The estimated RMS error in the value of K is about 3% for the ground-state line, and about 4% for the l-doublet. The increase of the error for the latter line has to be attributed to larger fractional error in the value of E at low Stark fields (see below).

The most important contributions to the error in a (and K) stem from: the error in the pressure ($\sim$1.5%), the error in the ratio $\alpha_{max,meas}/\alpha_{max}$ ($\sim$0.1$\sim$), and the error in the strength of the Stark field ($\sim$1$\sim$ at high fields; $\sim$15% at low fields). The error due to the pressure drift was eliminated by the method described in reference 3 (Sec. 6.1.3). It should be noted, that although the error in $\alpha_{max,meas}/\alpha_{max}$ is very

small, its influence on the error in a is not negligible. This comes from the fact that not the error in $\alpha_{max,meas}/\alpha_{max}$ but (roughly: see Eqs. (14) and (20)) the error in $[1-\alpha_{max,meas}/\alpha_{max}]^{\frac{1}{2}}$ contributes to the error in a. Altogether, this contribution was about 1.5% in the present investigation.

The contribution of the Stark field inhomogeneity to the error in E is negligibly small in the TE_{0m1} Stark-cavity cell. The error in E is thus completely determined by instability of the square-wave generator, sag of the square wave, amplitude dependent "zero" biasing, and by the error (including reading error) in measuring the peak value of the square-wave voltage. The fractional error due to improper zero-biasing was larger at low fields than at high ones. As a is roughly proportional to E^{-2}, the error in E becomes the largest contribution to the error in a.

By combining the errors in α_{max} and a, the standard error in α_{int} can be estimated to be about 4%.

In view of the results obtained on the OCS lines, the present method looks useful. With some improvement, especially of the electronic circuitry, a reduction of the error in a, and α_{int} to 2 and 3%, respectively, seems well possible. However, it is useful to consider here in more detail the assumptions underlying the present method, particularly in connection with experimental apparatus.

The obvious assumption of high Stark field homogeneity is well satisfied in the case of a pillbox shaped TE_{0m1} cavity cell (large diameter to length ratio). In the case of an ordinary X-band Stark wave-guide cell a correction has to be applied for field inhomogeneity near the edges of the Stark septum. Power saturation of the gas has to be carefully avoided as it results in a M-dependent broadening of the Stark components. Moreover, it affects both the half-width and the integrated intensity of the line. For similar reasons, the pressure in the absorption cell must be higher than about 0.015 mm Hg. At lower pressures, Doppler broadening and the resulting decrease of α_{max} and the modification of the line shape violate one of the basic assumptions of the method.

In addition to the properties mentioned above, the Stark spectrometer, intended for the application of the present method, must be ideal, or put another way, it must be capable of measuring both α_{max} and $\alpha_{max,meas}$ with high accuracy. Because of the unavoidable standing waves, the Stark-waveguide spectrometer usually does not satisfy this criterion.[11] The Stark-cavity spectrometer used in the present investigation satisfies well the criterion of "ideality," but only at sufficiently strong Stark fields. At fields below a certain value, difficulties can be encountered from the anomalous dispersion due to Stark components of the line (reference 3, Sec. 3.3). In short, these difficulties originate from the property that Stark modulation modulates not only the absorption but also the dispersion. The latter modulation results in a periodical shift of the resonance frequency of the cavity. In order to avoid these difficulties, especially with stronger lines, the Stark field must be sufficiently strong to make $\alpha_{max,meas}/\alpha_{max}>0.5$.

ACKNOWLEDGMENTS

This investigation is part of the research program of the "Stichting voor Fundamenteel Onderzoek der Materie," and was made possible by financial support from the "Nederlandse Organisatie voor Zuiver Wetenschappelijk Onderzoek."

The authors are greatly indebted to Dr. J. C. Kluyver for his careful reading of the manuscript.

[11] D. H. Baird and G. R. Bird, Rev. Sci. Instr. **25**, 324 (1954).

Proton Magnetic Resonance Studies of Some Silicones*

HAZIME KUSUMOTO,† IAN J. LAWRENSON, AND H. S. GUTOWSKY
Noyes Chemical Laboratory, University of Illinois, Urbana, Illinois

(Received September 29, 1959)

Proton magnetic resonance techniques have been used to study the molecular motions occurring in some dimethyl silicones. The substances investigated were cured Silastic 80, 400 Gum, and 200 Fluid (viscosity grade 20 centistokes at 25°C). Measurements were made of the absorption line shape from 77°K to room temperature, and of the spin-lattice relaxation time, T_1, from 160°K to 415°K. Evidence is found for the existence of methyl group reorientation about the triad axis, segmental motions about the Si—O bonds and a form of intramolecular "spiral" motion of the $(CH_3)_2Si$ groups. The relation of the latter motion to the difference in macroscopic properties of natural and silicone rubbers is discussed.

1. INTRODUCTION

THE silicones studied here have the molecular structure

$$CH_3-\left[\begin{array}{c}CH_3\\|\\Si-O\\|\\CH_3\end{array}\right]_n-\begin{array}{c}CH_3\\|\\Si-CH_3.\\|\\CH_3\end{array}$$

It is known that many such substances retain their characteristic elastic properties down to temperatures of the order of −100°C, and this has been attributed to ease of rotation about the Si—O bonds.[1] Previous measurements down to −50°C,[1] by the methods of nuclear magnetic resonance, revealed a very narrow proton absorption line and indicated the presence of relatively free molecular motions. The present investigation was undertaken to characterize in more detail the nature of these motions.

2. EXPERIMENTAL DETAIL

The proton absorption line shape was studied from liquid nitrogen temperature upwards for three substances: cured Silastic 80 rubber, 400 Gum, and 200 Fluid. The grade of 200 Fluid used had a viscosity of 20 centistokes at 25°C. In addition, the proton spin-lattice relaxation time was measured for the 400 Gum and 200 Fluid between approximately 160°K and 415°K. The samples of all three silicones were supplied by the Dow Corning Corporation. The Silastic 80 was cured for 24 hours at a temperature of 250°C prior to investigation.

The apparatus used has been described previously. The line-shape studies were made with a regenerative spectrometer,[2] operating at a frequency of 26.5 Mc/sec, corresponding to a magnetic field of 6300 gauss. Measurements of the spin-lattice relaxation time were made with a "spin-echo" type apparatus,[3] similar to that described by Hahn.[4] These measurements were made at 22.1 Mc/sec and a field of 5190 gauss. All the relaxation time measurements were made by the method of two 90° pulses.[5]

Two cryostats were used. The line-shape measurements were made using a variable heat-leak cryostat[2]; the measurements of relaxation time used a gas-flow system.[6] In all cases, the samples were contained in 9-mm Pyrex tubes, with a thermocouple inserted in a well in the side of the tube.

3. RESULTS AND DISCUSSION

A. Line-Shape Studies

Throughout the entire temperature range studied, the proton absorption lines for all three samples were simple bell-shaped curves without appreciable structure. Since we record the first derivative of the absorption line,[2] the line width is defined, for convenience, as the separation in gauss between points of maximum and minimum slope. Measured values for the three silicones are shown as a function of temperature in Figs. 1 and 2. The three curves are of approximately the same form. At the lowest temperature observed (77°K) the absorption lines were about the same width, 4.5 gauss, for all three substances. The 400 Gum and the 200 Fluid, Fig. 1, show evidence of a small, but real, narrowing of the line, starting at about 90°K. This is not found in the case of the Silastic 80, Fig. 2. In the temperature range between approximately 150°K and 180°K, all three absorption lines narrow rapidly and considerably, the 200 Fluid at temperatures about 10° below the 400 Gum and Silastic 80. The line widths continue to decrease slightly as the temperature is raised and, above about 220°K are very narrow; at room temperature the 200 Fluid has an absorption line only about 2 cps wide, observed at resonance frequencies of 16.7 and 40 Mc/sec.

* Assisted in part by the U. S. Office of Naval Research and by Grants-in-Aid from the Goodyear Tire and Rubber Company and the National Science Foundation.

† Now at the Institute of Scientific and Industrial Research, Osaka University, Japan.

[1] Honnold, McCaffrey, and Mrowca, J. Appl. Phys. **25**, 1219 (1954).

[2] Gutowsky, Meyer, and McClure, Rev. Sci. Instr. **24**, 644 (1953).

[3] Buchta, Gutowsky, and Woessner, Rev. Sci. Instr. **29**, 55 (1958).

[4] E. L. Hahn, Phys. Rev. **80**, 580 (1950).

[5] E. L. Hahn, Phys. Today **6**, No. 11, 4 (1953).

[6] E. R. Andrew and R. G. Eades, Proc. Roy. Soc. (London) **A216**, 398 (1953).

The second moments of the absorption lines were calculated from the observed line shapes. They exhibit a temperature dependence similar to that shown by the line widths. The mean values found in the region of 77°K were 8.4, 8.4, and 7.8 gauss^2 for the cured Silastic 80, 400 Gum, and 200 Fluid, respectively. These values are small compared to those found for other elastomers. For instance, the proton resonance in natural rubber[7] has a line width of about 9.5 gauss, and a second moment of about 18.5 gauss^2 at liquid nitrogen temperature. This suggests that considerably more molecular motion is occurring in the silicones than in other elastomers. The proton second moment in natural rubber at liquid nitrogen temperatures corresponds to that predicted for a "rigid lattice." The smaller value in the silicones may be ascribed to rotation of the methyl groups about their C_3 axes.

A single, rigid methyl group will contribute 21.4 gauss^2 to the second moment, assuming tetrahedral angles, and a C—H bond length of 1.10 A[8] with the corresponding inter-proton separation of 1.796 A. Rotation of the group about the triad axis would reduce this value by a factor of four,[9] giving a contribution of 5.4 gauss.^{2} The contributions arising from the interactions between protons in different methyl groups, and between protons in different molecules cannot be evaluated exactly. However, the results for substituted methanes having $(CH_3)_2C$ groups, and the absence of structure in the low-temperature line shapes indicate[10] that the 2 to 3 gauss^2 required for agreement with experiment is reasonable for the inter-CH_3 group broadening when C_3 rotation of the CH_3 groups occurs in the silicones. Further support of this interpretation results from the likelihood that the barriers to CH_3 group rotation will be smaller in the silicones than in the substituted methanes. The Si—C bonds are longer than the C—C, so there is less interaction between the methyl groups in $(CH_3)_2Si$ than in $(CH_3)_2C$. The barriers in substituted methanes having the latter

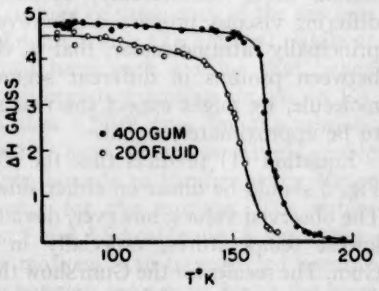

FIG. 1. Line width of the proton absorption as a function of temperature for 200 Fluid and 400 Gum.

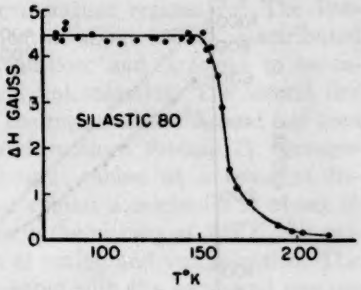

FIG. 2. Line width of the proton absorption as a function of temperature for Silastic 80.

group are barely large enough,[11] ~4 kcal, to prevent CH_3 group rotation from narrowing the proton resonance at liquid nitrogen temperature and, therefore, such narrowing is probable in the silicones.

There is evidence of at least two additional types of molecular motion, corresponding to the narrowing of the line at 90°K and near 160°K. The two most likely mechanisms are rotation of the $Si(CH_3)_2$ groups about the Si—O bonds, and some form of translational motion. We might expect this rotation to affect the resonance line in much the same way for all three substances. On the other hand, the translational motion should, presumably, decrease in importance as we proceed from the Fluid, through the Gum to the Silastic. It is tempting, therefore, to ascribe the slight narrowing at 90°K to translational motion, and the major narrowing near 160°K to the onset of rotation about the Si—O bonds. The measurements of the spin-lattice relaxation time confirm this hypothesis.

B. Spin-Lattice Relaxation Studies

The proton spin-lattice relaxation time T_1 was measured for the 400 Gum and the 200 Fluid, and the values observed up to room temperature are shown in Fig. 3. A few measurements were made at higher temperatures, up to about 415°K on both Gum and Fluid; the observed values fitted closely the extension towards higher temperatures of the linear portions of Fig. 3. In the figure, the measured values are plotted against the reciprocal of the absolute temperature. The relaxation time of the Gum shows a minimum which is not observed for the Fluid. The lowest temperatures at which measurements were made were 160°K for the Gum and 180°K for the Fluid. Measurements at temperatures lower than this are made difficult by the increased line width. In the case of the Fluid, the induction decay following the 90° pulse changed shape at temperatures below 180°K, indicating a change in line shape.

The most interesting feature of this study is the T_1 minimum value of 135 msec observed at 190°K for the 400 Gum. Neither CH_3 group reorientation nor random molecular tumbling of the CH_3 group can account for the value found. A strong argument against CH_3

[7] H. S. Gutowsky and L. H. Meyer, J. Chem. Phys. **21**, 2122 (1953).
[8] G. E. Hansen and D. M. Dennison, J. Chem. Phys. **20**, 313 (1952).
[9] H. S. Gutowsky and G. E. Pake, J. Chem. Phys. **18**, 162 (1950).
[10] J. G. Powles and H. S. Gutowsky, J. Chem. Phys. **21**, 1695 (1953).
[11] Stejskal, Woessner, Farrar, and Gutowsky, J. Chem. Phys. **31**, 55 (1959).

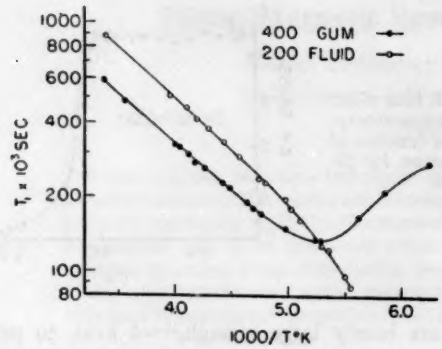

FIG. 3. The proton spin-lattice relaxation time, T_1, as a function of the reciprocal temperature, $10^3/T$, for 400 Gum and 200 Fluid.

group reorientation is that it is fast enough at 77°K to produce the characteristic $\frac{1}{2}$ reduction in second moment, so it would be much too fast at 190°K to contribute to T_1. A quantitative argument is provided by the expression for the spin-lattice relaxation caused by this motion.[12] Assuming any tumbling of the molecule as a whole occurs so slowly as to be negligible, the relation is[13]

$$(1/T_1)=(9\gamma^4\hbar^2/40)\sum_j r_j^{-6}\{[\tau_c/(1+\omega_0^2\tau_c^2)]+[4\tau_c/(1+4\omega_0^2\tau_c^2)]\}, \quad (1)$$

where τ_c is the correlation time for the CH_3 reorientation, ω_0 is the angular resonant frequency, r_j is the interproton separation, and γ is the proton gyromagnetic ratio.

This expression has a minimum value when $\omega_0\tau_c=0.6158$, the minimum value of T_1 then being given by

$$(1/T_1)_{\min}=0.3206(\gamma^4\hbar^2/\omega_0)\sum_j r_j^{-6}. \quad (2)$$

If we insert the interproton distances calculated above for the methyl group, this leads to a T_1 minimum of 12.8 msec,[14] much less than the observed value of 135 msec. Moreover, in at least two cases, *t*-butyl chloride and methyl chloroform, where there is independent evidence that CH_3 group reorientation should dominate the proton T_1, minima of about 7.5 and 15 msec have been reported,[11] in good agreement with the predictions. Reorientation of the methyl groups cannot, therefore, be the dominant relaxation process for the minimum observed in the 400 Gum. Nor can the latter arise from random tumbling of the CH_3 groups, because the predicted T_1 minimum is also much too small, being only $\frac{4}{9}$ the value for C_3 reorientation.[11,12] Rotation of the $(CH_3)_2Si$ groups about the Si—O bonds is also unlikely to produce the minimum. This is a special type of molecular tumbling; the principal interproton distances would again be those within the methyl group, leading to a value for the minimum much smaller than that observed.

Some form of "translational" motion is the most likely mechanism. Here the important interproton distances are greater and the effective amplitudes of motion smaller, making this an inherently weaker relaxation process. Indeed, this type of motion may give minima of the order of seconds.[11] The exact nature of the "translational" relaxation mechanism is rather indeterminate. It will probably be mainly intramolecular and involve movement relative to one another of protons in different segments of the same molecule with some contribution from interactions between protons in different molecules. Such an intramolecular process is reasonable. It is known that the silicone molecules are very flexible,[15] and at rest assume a coiled form, temperature changes making the molecule coil more tightly or straighten out slightly. The process would then consist of a thermally activated extension and contraction of the molecular chain similar to the oscillations of a spring. Besides the translational motions of the $(CH_3)_2Si$ groups there would be a rotational component similar to a torsional oscillation of large amplitude. The individual $(CH_3)_2Si$ groups experience an approximation to a spiral motion.

The straight-line portions of the T_1 *vs* $1/T$ curves in Fig. 3 correspond to Arrhenius plots of rate constants.[9,11] Assuming only one significant thermally activated relaxation process, we obtain the activation energy of the process from the slope of the line. In this manner values of 1.8 and 1.9 kcal/mole are found for the Gum and Fluid, respectively. The fact that these values are so similar is interesting and informative. If the relaxation were produced mainly by interactions between molecules, then the values for the Gum and the Fluid should differ considerably, because of their widely differing viscous properties. However, if the effect is principally intramolecular, that is, due to interactions between protons in different segments of the same molecule, we might expect the two activation energies to be approximately equal.

Equation (1) predicts that the T_1 curves shown in Fig. 3 should be linear on either side of the minimum. The observed values, however, deviate from this at the lowest temperatures, especially in the case of the Gum. The results for the Gum show that, in this temperature range, the methyl group reorientation is becoming slow enough to have a significant effect on the relaxation.

C. General Comments

A comparison of the line width and T_1 data provides further evidence about the nature of the motions and

[12] E. O. Stejskal and H. S. Gutowsky, J. Chem. Phys. **28**, 388 (1958).

[13] In reference 11, the left-hand side of Eq. (5) should be $1/\tau_{c1}$ instead of τ_{c1}.

[14] In reference 11, on p. 58, the value predicted for the T_1 minimum in *t*-butyl chloride should be 11.5 msec rather than 23 msec as given.

[15] R. R. McGregor, Ind. Eng. Chem. **46**, 2323 (1954).

their dependence upon molecular structure. It may easily be shown that the spiral motion postulated is not responsible for the rapid narrowing of the lines at about 160°K. From the T_1 minimum in the curve for the Gum, using Eq. (1), we obtain a value of 4.4×10^{-6} sec for the correlation time of the motion at 190°K, the temperature of the minimum. This leads to a correlation frequency, ν_c, of 1.6×10^7 cps at 160°K. If we use the criterion that the absorption line is narrowed, when the correlation frequency is of the order of the line width[9] (2.2×10^4 cps), we see that this mechanism should narrow the line at a much lower temperature. In fact we should expect the narrowing to begin at about 80°K, which is close to the temperature at which the slight narrowing is observed (90°K). We may, therefore, attribute the narrowing of the line in this region to the spiral motion.

We might, rather naively, expect such motion to decrease in importance as we proceed from the Fluid to the Gum to the Silastic, and this is observed. Indeed, there is no evidence of any narrowing of the absorption line of the Silastic 80 between 80°K and 150°K, other than that produced by the methyl group reorientation. Moreover, the line width differences have their counterpart in the T_1 data. The line width for the Fluid narrows by a greater amount and at lower temperatures, in the 80° to 150°K region, than for the Gum. In a similar manner, the T_1 data in Fig. 3 for the Fluid show that it has a T_1 minimum which is both smaller and at a lower temperature than for the Gum. The conclusion is that the amplitude of the rotational or torsional oscillation component of the spiral motion is greater in the Fluid than in the Gum, which is reasonable.

The principal narrowing of the line at about 160°K may be ascribed to random motions of chain segments and rotation of the $Si(CH_3)_2$ groups about the Si—O bonds. However, there is no evidence that these motions are significant proton relaxation mechanisms even at temperatures as high as 400°K. In order for this to be so, both the frequency factor and the activation energy for the motions must be rather small. We know that at 160°K, the correlation frequency of the motions is of the order of the line width (2×10^4 cps), while at about 400°K it must have such a value that, when inserted into the appropriate equation similar to Eq. (1), it is still too slow ($\lesssim 10^7$ cps) for the motions to shorten the relaxation time. These two criteria enable us to establish upper bounds to the frequency factor and activation energy for the motions. The values obtained are 10^9 sec^{-1} and 3.5 kcal/mole. A low activation energy for the motions is to be expected because of the wide spacing between segments, due to the large bond lengths and the presence of the oxygen atoms. The low-frequency factor probably reflects the necessity for the chain segments to have fairly specific configurations before they can tumble about.

The results obtained here for the dimethyl silicones may be compared to those obtained for natural rubber.[1,7,16,17] In general, the line width for rubber is narrowed in two temperature regions.[1,7,16] The low-temperature narrowing, at about 150°K, is attributed to CH_3 group reorientation, and is found to be inhibited by curing and vulcanization. The second line narrowing occurs in the region of 220°K, and has been assigned to segmental motion. Proton T_1 measurements[17] made on natural rubber at a resonant frequency of 20 Mc/sec exhibit a minimum of about 20 msec at temperatures in the vicinity of 300°K, depending upon the extent of curing and vulcanization. This T_1 minimum is associated with the segmental motions which produce the high temperature line narrowing. There is no evidence of a contribution to T_1 or to the line narrowing from motions other than C_3 rotation of the CH_3 groups and random tumbling motions of the chain segments. Moreover, for the segmental motions, the frequency factors and activation energies obtained from the T_1 measurements are significantly greater for natural rubber than those for the silicones. For the former, the frequency factors range from 10^{12} to 10^{15} sec^{-1} and the activation energies from 5.1 to 7.8 kcal/mole.

A comparison of the NMR results for natural rubber with those for the silicones supports the interpretation given here for the latter. The discussion of T_1 in Sec. 3B assumes that each type of motion is described by a single correlation time. If there were a distribution of correlation times, say for the CH_3 group reorientation, the resultant T_1 minimum would be larger than otherwise predicted.[17] However, a very broad distribution of correlation times is needed to explain the 135 msec T_1 minimum observed for the 400 Gum, and this does not seem to be very likely. In natural rubber, the CH_3 groups and chain segments have less mobility than in the silicones and, consequently, one would expect any distribution of correlation times to be broader. Instead, the T_1 minimum in natural rubber is very nearly that predicted for a single correlation time.

The structure of polyisobutylene is similar to that of the silicones in that alternate carbon atoms along the molecular chain each support two methyl groups. We might expect, therefore, a corresponding similarity in the molecular motions. However, line-shape[18] studies have indicated considerable differences. Severe interlocking of the methyl groups in polyisobutylene inhibits their reorientation. But there is a gradual narrowing of the proton absorption at temperature above 90°K which indicates the presence of random motions of the chain segments and of the methylene groups. At about 260°K, the line is narrowed fairly suddenly, showing considerable motion of the chains, corresponding to the glass to rubber transition. The silicones are similar to

[16] Holroyd, Codrington, Mrowca, and Guth, J. Appl. Phys. **22**, 696 (1951).
[17] Gutowsky, Saika, Takeda, and Woessner, J. Chem. Phys. **27**, 534 (1957).
[18] J. G. Powles, Proc. Phys. Soc. (London) **B69**, 281 (1956).

polyisobutylene in that the line width change assigned to motions of the chain segments occurs at temperatures very near to the second order transition temperatures, about 150°K, found in thermal expansion studies of the silicones.[19]

Relaxation time data for polyisobutylene[20] indicate the presence of two relaxation processes, one with a correlation frequency much greater than that of the other. The last process is associated with motion of a small number of links in the molecular chain; the slow process arises from movement of larger segments, and the nuclear magnetic interaction here is mainly external to the molecule. Both of these relaxation processes show a considerable distribution of correlation frequencies. However, the arguments given in the second paragraph above and the relatively sharp T_1 minimum found for the 400 Gum suggest that a single correlation time is sufficient in the silicone.

The relation to the macroscopic properties, of these differences in the dynamic behavior on a molecular level of natural rubber and of the silicones and polyisobutylene, is a question meriting further study. Also, additional NMR studies of the silicones are required to learn whether the spiral motions postulated here are generally present in silicones and how they are affected by the structure of the silicones. An attractive possibility is that such spiral motions in the silicones are associated with self-diffusion and can account for the ability of the Gum to flow very slowly under constant stress yet exhibit elastic properties upon sharp impact.

[19] C. E. Weir, W. H. Leser, and L. A. Wood, J. Research Natl. Bur. Standards **44**, 367 (1950).
[20] J. G. Powles and K. Luszczynski, Physica **25**, 455 (1959).

THE JOURNAL OF CHEMICAL PHYSICS VOLUME 32, NUMBER 3 MARCH, 1960

Infrared Spectrum and Dipole Moment Function of Lithium Hydride

THOMAS C. JAMES,* WILFRED G. NORRIS,† AND WILLIAM KLEMPERER‡
Department of Chemistry, Harvard University, Cambridge 38, Massachusetts

(Received September 30, 1959)

Line intensities in the 0–1 and 1–2 rotation-vibration bands of lithium hydride at 7 μ have been measured. The ratio of the dipole moment to the dipole derivative is $u_e/(\partial u/\partial r)_{r_e} r_e = 1.8 \pm 0.3$. It is shown that the dipole moment of a diatomic molecule approaches the united atom limit as the third power of the internuclear separation.

INTRODUCTION

IN recent years, there has been an increasing interest in the determination of absolute infrared absorption intensities. In diatomic molecules, the measured intensities permit the evaluation of the derivative of the molecular dipole moment with respect to the internuclear distance. The general problem of the theoretical interpretation of dipole derivatives has by no means been solved. The difficulties inherent in a realistic calculation of this quantity were pointed out long ago by Robinson[1] in an examination of the hydrogen halides. Since that time, development in the computational techniques of molecular quantum chemistry has progressed to a point where the calculation of the dipole derivative for simple systems appears to be feasible. It is, therefore, important to attempt experimental measurement of the dipole derivatives of such simple systems.

Lithium hydride is the simplest stable heteronuclear diatomic molecule, and has received a considerable amount of theoretical attention.[2–4] In view of the difficulties inherent in the construction of exact wave functions for even such a simple system as lithium hydride, it is felt that experimental data for observables other than the energy will be exceedingly welcome since such quantities provide a much more severe test of the correctness of the wave functions than the energy itself. One such useful quantity is the aforementioned dipole moment derivative. Another quantity, which is perhaps equally useful for comparison with theoretical calculations and which is probably subject to less experimental error, is the ratio of the dipole moment to the dipole derivative.

In this paper, we will be concerned with the experimental determination of this ratio in lithium hydride. Our instrumentation has been improved since an earlier report.[5] As will be pointed out in the following section, it is possible to obtain this ratio from a study of the *relative* intensities of the rotational fine structure of the

* Standard Oil of California Fellow.
† Present address: Department of Physics, Juniata College, Huntingdon, Pennsylvania.
‡ Alfred P. Sloan Fellow.
[1] D. Z. Robinson, J. Chem. Phys. **17**, 1022 (1949); see also C. A. Coulson, *Valence* (Oxford University Press, New York, 1952), pp. 207 ff.
[2] A. M. Karo and A. R. Olson, J. Chem. Phys. **30**, 1232, 1241 (1959).
[3] Miller, Friedman, Hurst, and Matsen, J. Chem. Phys. **27**, 1385 (1957); Hurst, Miller and Matsen, J. Chem. Phys. **26**, 1092 (1957).
[4] J. K. Knipp, J. Chem. Phys. **4**, 300 (1936).
[5] W. G. Norris and W. Klemperer, J. Chem. Phys. **28**, 749 (1958).

rotation-vibration band. One particular advantage, which results from this measurement, is that an algebraic sign is determined whereas in the usual absolute intensity measurements only the magnitude of the dipole derivative is determined. Furthermore, it is considerably easier to obtain relative line strengths rather than absolute line strengths for lithium hydride.

In the case of lithium hydride, it is necessary to work at temperatures in the region of 1000°C in order to obtain appreciable absorption. This is made evident by a consideration of Table I, which gives the vapor pressure of lithium hydride in equilibrium with metallic lithium and hydrogen vapors. The vibration frequency of LiH is $\omega_e=1406$ cm^{-1}, and the bands observable in this region extend from approximately 1600 to 1100 cm^{-1}. The difficulties in obtaining windows for this region, which are capable of withstanding the elevated temperatures and the chemical reactivity of lithium, appear to the authors to preclude the use of standard absolute absorption intensity techniques.[6] Since techniques useful for obtaining absorption frequencies at high temperatures[7] involve the use of a poorly defined path length, absolute intensity measurements of reasonable accuracy do not seem possible. For this reason, we have had to turn to relative intensity measurements in order to derive meaningful experimental data.

A secondary objective in this work has been to develop techniques which may permit the measurement of dipole moment data for molecular species which are thermodynamically unstable at room temperature and moderate pressure. Lithium hydride clearly fulfills this requirement, and it is hoped that the technique used in this study will prove useful in the study of similar systems.

THEORY

Herman, Wallis, and Rubin[8] have considered in detail the line strengths in a vibration-rotation band of a $^1\Sigma$ diatomic molecule and their dependence on the potential energy function and dipole moment function. These line strengths are shown to depend on the influence of rotation-vibration interaction as a result of the dependence of the dipole moment on the internuclear distance. Herman and Wallis show that the square of the vibrational matrix element can be written as

$$|M_v^{v'}(m)|^2=|R_v^{v'}|^2F_v^{v'}(m), \qquad (1)$$

where $R_v^{v'}$ is a vibrational matrix element for the nonrotating oscillator and $F_v^{v'}(m)$ is a correction factor which takes into account the effect of rotation-vibration interaction. Correspondingly, the intensity of an absorption line $vJ\rightarrow v'J'$ is given by

$$I_v^{v'}(m)=\frac{8\pi^3N_{v,J}\nu_v^{v'}}{3hc(2J+1)}|m||R_v^{v'}|^2F_v^{v'}(m), \qquad (2)$$

where m is $-J$ and $J+1$ for the P and R branches, respectively. To first order, using a harmonic oscillator potential and a linear dipole moment expansion the quantity $F_v^{v'}(m)$ is given by§

$$F(m)\simeq[1-2\theta\gamma m]^2,$$

where $\gamma=2B_e/\omega_e$ and $\theta=\mu_e/(\partial\mu/\partial r)_{r_e}r_e$ with μ=dipole moment. From a comparison of the relative line intensities in the P and R branches, a value of the sign and magnitude of θ can be determined. The ratio of F factors for lines in the P and R branch originating from the same J level is given by

$$F_v^{v'}(P)/F_v^{v'}(R)=[I(P)/I(R)][(J+1)/(J)][\nu_J(R)/\nu_J(P)]. \qquad (3)$$

In this expression, it is not necessary to know the number of absorbers. It is necessary, however, to know the temperature approximately since the correction for induced emission is not negligible at the relatively high temperatures and low transition frequencies encountered in this work.

[6] Overend, Youngquist, Curtis, and Crawford, Jr., J. Chem. Phys. **30**, 532 (1959).

[7] W. Klemperer and S. A. Rice, J. Chem. Phys. **26**, 618 (1957).

[8] R. Herman and R. F. Wallis, J. Chem. Phys. **23**, 637 (1955); Herman, Rothery, and Rubin, J. Mol. Spectroscopy **2**, 369 (1958).

§ Herman and Wallis give, for this F factor,

$$(F)^{\frac{1}{2}}=\{1-2\theta\gamma m[1+(15/2)b\gamma^{\frac{1}{2}}+3\gamma-\tfrac{3}{8}(b\gamma^{\frac{1}{2}}/\theta)+\tfrac{3}{4}(b\gamma^{\frac{1}{2}}/\theta)(m-1)+(3/8)(\gamma/\theta)(m-1)]\}.$$

The term $\frac{1}{2}\gamma^2m(m-1)=\frac{1}{2}\gamma^2J(J+1)$ arises from the increase in internuclear distance with rotational state and is present even in the harmonic oscillator approximation. The other terms arise by treating the anharmonicity and the cubic term in the expansion of the rotation-vibration interaction term $-J(J+1)/r^2$ as a perturbation $H'=hc\omega_eb_J\alpha^3u^3$

where

$$\alpha=(1/\gamma)r_e^{-1}; \qquad \gamma=(2B_e/\omega_e); \qquad u=r-r_e$$

and

$$b_J=b[1-2(\gamma^{\frac{1}{2}}/b)J(J+1)]$$

b is $k'/hc\omega_e\alpha^3$, k' being the coefficient of the cubic term in the expansion of the vibrational potential $U(r)$. The perturbation is carried out to obtain first order wave functions in the parameter b. In the subsequent evaluation of dipole moment matrix elements, terms to order γ^3 are kept. The quantity b can be related to γ by the relation $b=(a_1/2)\gamma^{\frac{1}{2}}$, where a_1 is defined by the expansion $U(r)=hca_0\xi^2(1+a_1\xi+\cdots)$ with $\xi=(r-r_e)/r_e$. For most molecules a_1 is of the same order of magnitude as 2, so that b is of order $\gamma^{\frac{1}{2}}$. Therefore, it appears that a first order perturbation treatment in b does not yield an expression which will be correct to order γ^2. To obtain an expression correct to order γ^2, it is necessary to go to a higher order perturbation in b, at which point additional terms in the perturbing Hamiltonian should also be considered. In view of this uncertainty of the expression when terms of order γ^2 are included, we have decided to use the expression known to be correct to first order in γ: $(F)^{\frac{1}{2}}=1-2\theta\gamma m$. There is no real justification for omitting the term $\frac{1}{2}\gamma^2J(J+1)$ since it appears even before the perturbation is applied. For the J's employed in this experiment, ($J\sim10$) this introduces only a few percent error in θ, which is much smaller than the experimental uncertainty. The effect of neglecting all of the γ^2 terms introduces some uncertainty into the result, but this is very likely smaller than our quoted error.

TABLE I. Equilibrium pressure of lithium hydride at 1 atmos total pressure.

Temp °K	[a] P_{Li} (atmos)	K	P_{LiH} (atmos)
1000	1.41×10^{-3}	1.57×10^{-1}	2.2×10^{-4}
1200	2.4×10^{-2}	9.92×10^{-2}	2.35×10^{-3}
1293	6.6×10^{-2}	8.54×10^{-2}	5.35×10^{-3}
1400	1.69×10^{-1}	7.35×10^{-2}	1.13×10^{-2}
1600	7.94×10^{-1}	5.78×10^{-2}	2.08×10^{-2}

K is given for $Li(g)+\frac{1}{2}H_2(g)=LiH(g)$

[a] Vapor pressure of Li from L. Brewer, "Chemistry and metallurgy of miscellaneous materials," *Thermodynamics*, edited by L. L. Quill (McGraw-Hill Book Company, Inc., New York, 1950), p. 30. Constants used

LiH [b] $D_0°=2.4288$ ev; [c] $\omega_e=1405.6$ cm^{-1}; [c] $B_e=7.513$ cm^{-1}

H_2 [c] $D_0°=4.476$ ev; $\omega_e=4395.6$ cm^{-1}; $B_e=60.81$ cm^{-1}

[b] R. Velasco, Can. J. Phys. **35**, 1204 (1957).

[c] G. Herzberg, *Spectra of Diatomic Molecules* (D. Van Nostrand Company, Inc., Princeton, New Jersey, 1950).

EXPERIMENTAL

The general technique used to obtain the spectrograms has been described.[7] For the present work several modifications are necessary. In order to obtain meaningful intensity measurements on individual lines it is necessary to use an instrument of higher resolving power than obtainable with prisms. A Perkin-Elmer Model 12 spectrometer was converted in the standard manner[9] for use with a Bausch and Lomb 65×65 mm 1800 line/in. replica grating. Order separation was achieved by use of an Eastman Kodak 240 infrared filter. Residual false energy was measured with a lithium fluoride shutter. The R branch of the lithium hydride spectrum is somewhat overlapped by the 1600 cm^{-1} atmospheric water absorption. The intensity of this background was decreased sufficiently by intense flushing with dry nitrogen. Lines in the fundamental R branch above $J=11$ could not be measured with sufficient accuracy because of their weakness and the residual atmospheric absorption.

The cell is a 5-cm diam, 100 cm long stainless steel tube heated by a 46-cm Kanthal wound alundum core furnace. Lithium metal is contained in a nickel boat located in the central section of the heated tube. Hydrogen is admitted and maintained at a total pressure of one atmos. The hydrogen also serves as a buffer gas preventing deposition of solids on the potassium bromide windows which are at room temperature. Temperatures were measured at the center, and 10 cm from one end of the annular space between the furnace and steel cell with chromel P-Alumel thermocouples. In a typical run, the temperature is 1055°C at the center and 970°C 10 cm from the end. The cell is heated until the bands are developed to the desired intensity, then allowed to stabilize for a period of two hours before spectra are recorded. In order to use slit widths of 0.5 to 1 cm^{-1}, the spectrum is scanned at 12 min/100 cm^{-1}.

The frequencies of the lines were measured only roughly (i.e. to 0.2 cm^{-1}), but it was noted that the line positions did not agree well with the calculated positions using the much more accurate spectroscopic constants of Crawford and Jorgensen.[10] In particular if the 0–1 band is used for calibration, the lines of the 1–2 band are displaced from their calculated position by ~0.5 cm^{-1} on the average. This seems to indicate a slight error in one of the anharmonic constants given by Crawford and Jorgensen.

RESULTS AND DISCUSSION[11]

The spectrum of lithium hydride is shown in Fig. 1. The resolved lines of the 1–2 and some lines of the 2–3 band are clearly evident as would be expected from the relatively high temperature and low vibration frequency involved. The path length is estimated to be 26 cm and a LiH pressure of 4.1 mm is calculated using an average temperature of 1020°C.

The equivalent widths obtained from a typical spectrum are given in the first column of Table II. These were obtained from the measurement of line areas with a planar planimeter. The shapes of the *recorded* lines are certainly determined by the instrument since the slits are an order of magnitude greater than the true line widths which are estimated to be about 0.06 cm^{-1}. Due to the large slit widths employed compared to the true line widths, wing corrections are considered to be negligible.

Two corrections to the equivalent widths are necessary before relative line strengths are known. The first is due to the fact that many of the lines are not well approximated by a linear absorption law. The second correction is for induced emission since this quantity does vary somewhat with the individual transitions.

Since the true shape of a line in the present instance is determined primarily by pressure broadening there is little doubt that the line shape is well approximated as Lorentzian. The relation then between equivalent width and the actual line strength is given by the well known Ladenburg-Reiche absorption law[12]:

$$W=2\pi\gamma f(Sl/2\pi\gamma)$$

$$f(x)=x\exp(-x)[I_0(x)+I_1(x)], \qquad (4)$$

where W = equivalent width, S = line strength, γ = line width, and l = path length. I_0 and I_1 are modified Bessel functions of the first kind. By using the tables of

[9] R. C. Lord and T. K. McCubbin, Jr., J. Opt. Soc. Am. **47**, 689 (1957).

[10] F. H. Crawford and T. Jorgensen, Phys. Rev. **47**, 932 (1935).

[11] An excellent discussion of the problems involved in the reduction of a spectrogram to line strengths can be found in papers by Benedict, Herman, Moore, and Silverman, Can. J. Phys. **34**, 830, 850 (1956); J. Chem. Phys. **26**, 1671 (1959).

[12] R. Ladenburg and F. Reiche, Ann. Physik **42**, 181 (1913).

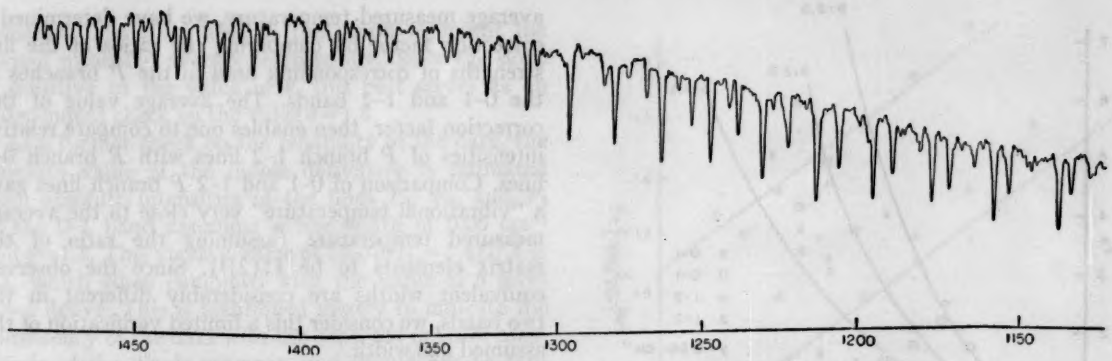

FIG. 1. Infrared absorption spectrum of lithium hydride. $T=1293°K$, pressure $=4.1$ mm, path length ~ 26 cm.

$f(x)$ given by Kaplan and Eggers,[13] values of Sl can be obtained from a given equivalent width W provided that the line widths are known.

The modern theory of pressure broadening of lines in the microwave and infrared regions is due to Foley[14] and Anderson.[15] A complete calculation of line widths by means of this theory is a laborious procedure requiring a detailed knowledge of the structure of the molecules comprising the system. For hydrogen, which is the main broadener in these experiments, a complete set of the relevant structural parameters is known. On the other hand, little is known of lithium hydride. It is possible, however, to obtain a reasonable estimate of the line width by considering only the LiH dipole—H_2 quadrupole interaction as being responsible for all of the broadening. The line width is then given by[16,17]

$$2\gamma=(n/c)(\mu Q/\hbar)^{\frac{1}{2}}(\bar{v})^{\frac{1}{2}}(0.84), \qquad (5)$$

where n=number of molecules, $\bar{v}$=average relative velocity, u=dipole moment of radiating molecule, Q=quadrupole moment of broadener, and c=velocity of light. For LiH at 1293°K broadened by one atmos of hydrogen, a value of $\gamma=0.05$ cm^{-1} obtains, using a dipole moment of $4D$ for LiH as will be discussed later. The "effective quadrupole moment" of hydrogen[18] is 0.6×10^{-26} esu cm^2.

These calculations determine an approximate value of the line width. In order to convert our equivalent widths to line strengths, we have used the tables of Kaplan and Eggers and calculated values of Sl for assumed line widths from 0.04 to 0.1 cm^{-1}. The results of these calculations after corrections for induced emission are given in the remaining columns of Table II.

The corrections for induced emission are made after the line strengths are obtained from the Ladenberg-Reiche absorption law. At the temperature employed in these experiments ($kT\sim900$ cm^{-1}), there is an appreciable fraction of molecules in the final state so that the intensity is not simply proportional to $N_{v,J}$ but instead to $N_{v,J}-(d_J/d_{J'})N_{v',J'}$. Therefore, even though we will compare line strengths of lines originating from the same J level, it is necessary to make a correction for induced emission since there is a significant difference in the population of the final states in the P and

TABLE II. Equivalent widths and line strengths of lithium hydride.

$P_{LiH}=4.1$ mm $T=1293°K$ 1 atmos total pressure					
		Line strength cm^{-1}			
Line 0—1 band	Equivalent width cm^{-1}	$\gamma=0.04$	$\gamma=0.06$	$\gamma=0.08$	$\gamma=0.10$ cm^{-1}
P_{13}	0.265	0.720	0.577	0.512	0.484
P_{12}	0.242	0.623	0.520	0.454	0.428
P_{11}	0.233	0.581	0.474	0.428	0.406
P_{10}	0.278	0.780	0.609	0.538	0.503
P_9	0.284	0.806	0.627	0.554	0.516
P_8	0.200	0.884	0.680	0.595	0.553
P_7	0.299	0.879	0.677	0.592	0.550
P_6	0.232	0.573	0.465	0.422	0.400
P_5	0.238	0.602	0.489	0.442	0.416
P_4	0.214	0.514	0.426	0.390	0.372
P_3	0.154	0.348	0.309	0.291	0.280
P_2	0.111	0.228	0.210	0.187	0.197
R_1	0.086	0.119	0.111	0.109	0.105
R_2	0.223	0.450	0.370	0.335	0.319
R_3	0.160	0.277	0.242	0.227	0.218
R_4	0.193	0.366	0.310	0.286	0.274
R_5	0.192	0.365	0.308	0.286	0.274
R_6	0.198	0.383	0.322	0.297	0.272
R_7	0.124	0.199	0.179	0.171	0.167
R_8	0.220	0.450	0.372	0.338	0.322
R_9	0.134	0.220	0.197	0.186	0.182
R_{10}	0.122	0.194	0.175	0.168	0.163
R_{11}	0.081	0.117	0.110	0.107	0.106
R_{12}					
R_{13}	0.050	0.068	0.064	0.063	0.063
1—2 band					
P_{10}	0.140	0.278	0.248	0.234	0.228
P_9	0.148	0.298	0.262	0.248	0.240
P_8	0.152	0.308	0.272	0.256	0.248
P_7	0.214	0.513	0.425	0.405	0.370
P_6	0.137	0.270	0.241	0.228	0.222
P_5	0.131	0.254	0.228	0.218	0.211
P_4	0.099	0.180	0.167	0.161	0.157

[13] L. D. Kaplan and D. F. Eggers, Jr., J. Chem. Phys. **25**, 876 (1956).
[14] H. M. Foley, Phys. Rev. **69**, 616 (1946).
[15] P. W. Anderson, Phys. Rev. **76**, 647 (1949).
[16] W. V. Smith, J. Chem. Phys. **25**, 510 (1949).
[17] L. J. Keiffer and A. V. Bushkovitch, J. Mol. Spectroscopy **2**, 558 (1958).
[18] Hirschfelder, Curtiss, and Bird, *Molecular Theory of Gases and Liquids* (John Wiley & Sons, Inc., New York, 1954), p. 1028.

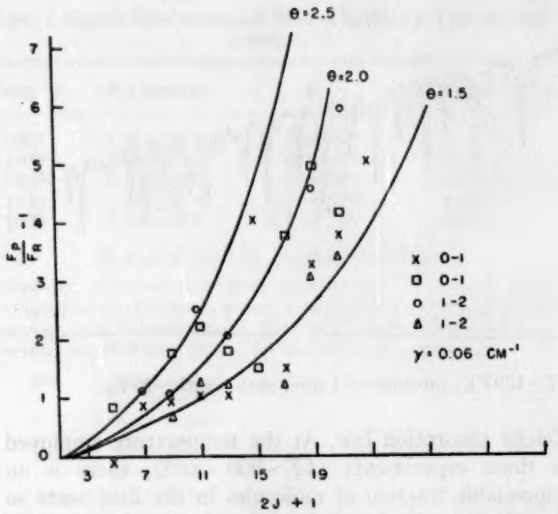

FIG. 2. Ratio of F factors minus 1 *vs* $2J+1$. × and ⊖ refer to data for the 0–1 and 1–2 bands given in Table II. □ and Δ refer to an average of several other 0–1 and 1–2 bands not included in Table II. The solid lines refer to the theoretical curves for different values of θ.

R branches. If S is the line strength that is measured, then the strength $\bar{S}$ which would be measured if there were no induced emission is given by

$$\bar{S}=S/[1-(d_i/d_j)\exp(-\Delta E/kT)], \qquad (6)$$

where d_i and d_j are the degeneracies of the initial and final states and ΔE is the difference in energy of the initial and final state.

This correction requires a knowledge of the temperature in the cell. This is not a constant throughout the cell, but an average temperature for the cell is sufficient as the ratio of the induced emission correction for lines in the P and R branches is not extremely temperature sensitive.

The quantity of interest is $\theta=\mu_e/(\partial\mu/\partial r)_{r_e}r_e$. Figure 2 shows the experimentally determined ratios of the F factors in addition to the theoretical curves for different values of θ. These ratios are computed from the line strengths given in Table II (and additional line strengths not included in that table) and Eq. (3). The data comes from several runs and is indicative of the experimental scatter. In this plot, the line widths are assumed to be 0.06 cm^{-1}. Since the lines comprising the R branch of the 1–2 "hot" band are extremely weak, their equivalent widths are subject to considerable uncertainty. Therefore, these lines were not used but instead lines in the P branch of the 1–2 band are compared with lines of the same initial J level in the R branch of the 0–1 band. In order to make this comparison, it is necessary to correct for the difference in population of the ground and first excited vibrational levels, and for the approximate factor of two difference in the square of the vibrational matrix element. Instead of using a "vibrational temperature," which is the average measured temperature, we have determined a correction factor by comparing the ratios of the line strengths of corresponding lines in the P branches of the 0–1 and 1–2 bands. The average value of this correction factor, then enables one to compare relative intensities of P branch 1–2 lines with R branch 0–1 lines. Comparison of 0–1 and 1–2 P branch lines gave a "vibrational temperature" very close to the average measured temperature (assuming the ratio of the matrix elements to be $1:(2)^{\frac{1}{2}}$). Since the observed equivalent widths are considerably different in the two bands, we consider this a limited verification of the assumed line width.

From the plot shown in Fig. 2 we estimate a value for θ of $+1.8\pm0.3$. This is on the basis of a line width of $\gamma=0.06$ cm^{-1}. The effect of the uncertainty in line widths on θ is shown for the data in Table I in Fig. 3. The limits of the lines correspond to the variation in the ratio of the F factors as the line widths are allowed to vary from 0.04 to 0.1 cm^{-1}.

In order to check the reliability of the data, we show in Fig. 4 a plot for the determination of P and R branch temperatures in the 0–1 band and P branch temperatures in the 1–2 band. Combining all the J dependent terms in the intensity of a line, this intensity is related to these terms as follows:

$$I\propto[N_{v,J}/(2J+1)]\nu\,|\,m\,|\,F(m)$$

or, since

$$N_{v,J}\sim N_v(hcB/kT)(2J+1)\exp[-BJ(J+1)/kT],$$

$$I\propto\nu\,|\,m\,|\,F(m)\exp-[BJ(J+1)/kT]. \qquad (7)$$

Therefore, a plot of $\log_{10}(\nu\,|\,m\,|\,F(m)/I)$ *vs* $J(J+1)$ should have slope $B/2.3kT$. Since only the slope of the lines through the experimental points is significant, we plot $\log_{10}(\nu\,|\,m\,|\,F(m)/I)+C$ where C is an arbitrary

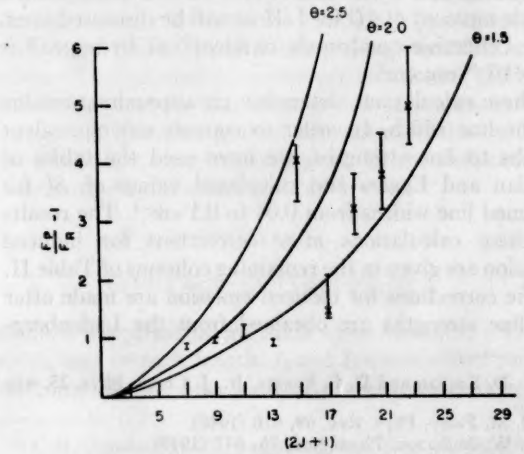

FIG. 3. Ratio of F factors minus 1 *vs* $2J+1$ for line widths from 0.04 to 0.1 cm^{-1}. The vertical lines indicate the variation in the ordinate as the line width varies from 0.04 to 0.1 cm^{-1}. The points × refer to the 0–1 values given in Table II.

constant. The solid lines in the graph represent the correct measured average temperature. Since the slope is sensitive to the value of θ, this plot serves as an independent check on the value $\theta=1.8$.

As a further check on the reliability of the data, the absolute value of the dipole derivative is estimated from absolute intensities of the lines P_4, P_6, and P_9 of the 0–1 band assuming a line width of 0.06 cm^{-1} and $\theta=1.8$. This yields a value of $(\partial\mu/\partial r)_{r_e}=1.4D/A\pm 0.1$, which when combined with the value of θ gives $\mu_e=4$ debye. This is mentioned merely to indicate the consistency of the data with the expected order of magnitude of the dipole moment, and should not be considered as a determination of the dipole moment. The considerable uncertainty introduced into the dipole moment and its derivative as a result of uncertainties in the absolute intensity measurements have been discussed earlier.

CHEMICAL CONSIDERATIONS

In this section, the dipole moment function calculated from several models of chemical bonding in LiH will be compared with the observed equilibrium value of the logarithmic derivative of the dipole moment. We shall also show that a general functional restriction exists for the dipole moment of a molecule.

The simplest model for LiH capable of predicting dipole moment behaviour is the classical ionic model considered in detail by Rittner.[19] In this model, the dipole derivative can be approximated as,

$$\partial\mu/\partial r=3e-(2\mu/r),$$

so that

$$\theta=[(3er/\mu)-2]^{-1}.$$

Since generally $\mu<er$, then,

$$0<\theta<1.$$

Thus, the dipole moment function of lithium hydride near the equilibrium internuclear distance is not well described by an ionic model. Agreement with experiment can be forced by considering the polarizability of the ions to be strong functions of the internuclear separation. This is not necessary in fitting the observed variation of the dipole moment with internuclear distance of the alkali halides, and would detract greatly from the simplicity and utility of the classical ionic model.

Recent work by Karo and Olson[2] is representative of the modern valence bond and molecular orbital treatments of lithium hydride. Their calculations of energy and dipole moment extend over a wide range of internuclear separation, and thus permit immediate comparison with experiment. The calculated value of θ is +4.5. The quality of the calculation is indicated by the fact that their binding energy is 66% of the observed value (based on a *calculated* energy of the lithium atom).

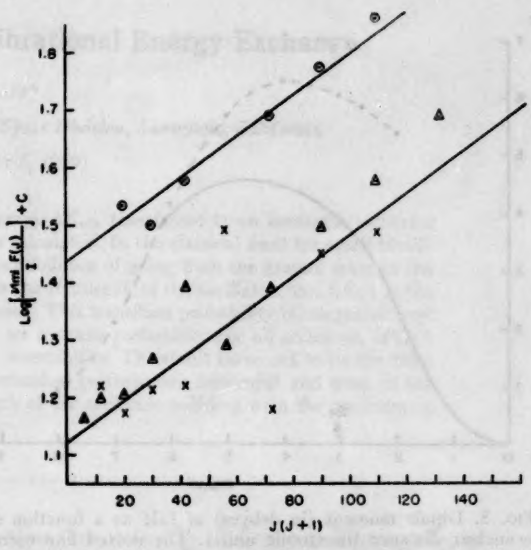

FIG. 4. Plot of log $[\nu\,|\,m\,|\,F(m)/I]+C$ *vs* $J(J+1)$. The solid lines correspond to the measured temperature. The data is taken from Table II. △ refers to the 0–1 *P* branch, × to the 0–1 *R* branch, and ⊙ to the 1–2 *P* branch lines.

In order to indicate reasons for the divergence from experiment, we now consider the general functional form of the dipole moment near the united atom limit. The matrix elements of the energy of a molecular system in a united atom representation are given by Bingel,[20] and we shall refer to his paper and equation numbering. In the coordinate system used by Bingel, the separated nuclei have zero dipole moment. To first order the dipole moment of a molecular state derived from the united atom state Φ_0 is

$$\mu=2\sum_a[V_{0a}/(E_0-E_a)]\int\Phi_0 ez\Phi_a d\tau, \qquad (8)$$

where V_{0a} is an element of the perturbation Hamiltonian and z is the coordinate of the electrons along the internuclear axis. It is well known that the dipole moment operator only connects states differing by unit angular momentum. Bingel has shown [see his Eq. (18b)] that the lowest order term in internuclear separation for a matrix element involving unit change in angular momentum is||

$$V_{0a}=R^3\frac{Z_a^2Z_b-Z_aZ_b^2}{(Z_a+Z_b)^2}\left\{\frac{3}{10}\rho_{1,0}^{0a}(0)-\int_0^\infty\rho_{3,0}^{0,a}(r)\,dr\right\}. \qquad (9)$$

The quantities $\rho_{1,0}^{0a}(r=0)$ and $\rho_{3,0}^{0a}(r)$ are related to the first order transition density matrix and Z_a and Z_b are the nuclear charges. Equations (8) and (9) show that the dipole moment of a molecule approaches the united atom limit of zero as the third power of the

[19] E. S. Rittner, J. Chem. Phys. **19**, 1030 (1951).

[20] W. A. Bingel, J. Chem. Phys. **30**, 1250 (1959).

|| For a system whose united atom limit is an *S* state $\rho_{3,0}^{0a}(r)=0$.

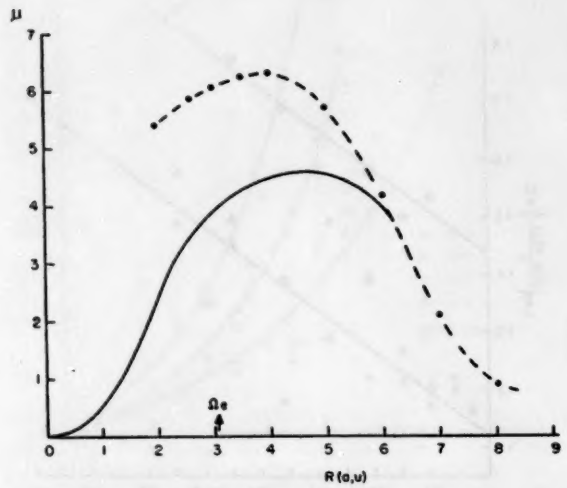

FIG. 5. Dipole moment (in debyes) of LiH as a function of internuclear distance (in atomic units). The dotted line corresponds to the calculations of Karo and Olsen.[2] The solid line is our estimated curve.

internuclear separation. The value of $\rho_{1,0}^{0,a}(0)$ for LiH will depend strongly upon the exact choice of beryllium wave functions, and thus will not be evaluated here.[21]

In Fig. 5 is shown the calculated dipole moment function of Karo and Olsen together with our estimate of this curve. It seems likely that the dipole moment at the equilibrium internuclear distance is less than $6D$, the value calculated by several groups, because of the experimental value of θ, and also because of the demand that the origin be approached as R^3. We have fitted the height of our curve to the dipole moment of $4D$, which we obtained from absolute intensity measurements but strongly urge caution in regarding this as determined experimentally.

[21] E. U. Condon and G. H. Shortley, *Theory of Atomic Spectra* (Cambridge University Press, New York, 1935), pp. 148 for a related example.

CONCLUSIONS

This problem was undertaken in order to evaluate the present status of theoretical calculations of dipole moment functions. The results indicate that wave functions obtained by applying the variational method give qualitative agreement with experiment for an observable as sensitive as the dipole derivative. It is apparent, however, that a quantitative calculation of the dipole moment function of a molecule will be an exceedingly complex problem if minimization of the energy of the system is the only criterion for choice of wave functions. It should be emphasized that the calculations of Karo and Olsen were *ab initio*. It will be interesting to compare more semiempirical techniques when they are applied to lithium hydride. The bearing that this work has upon the interpretation of experimental dipole derivatives in more complex systems is, of course, a subjective question. It does seem apparent, though, that the dipole moment function is indeed a subtly determined molecular property.

As far as the problem of obtaining the dipole moment function of a system over the entire range of internuclear coordinates is concerned, it appears that perturbation calculations around the united atom and separated atom limits should be capable of good accuracy. These calculations, when supplemented by observations in the limited accessible region around the equilibrium configuration, should permit construction of a realistic molecular dipole moment function.

ACKNOWLEDGMENT

This work was made possible by grants from the Research Corporation and the National Science Foundation.

Complete Classical Theory of Vibrational Energy Exchange

DONALD RAPP*

Lockheed Aircraft Corporation, Missiles and Space Division, Sunnyvale, California

(Received October 5, 1959)

By using purely classical mechanics, the amount of energy $\Delta E_{v\,ib}$ transferred to an harmonic oscillator molecule in a head-on molecular collision of velocity v_0 is calculated. In the classical limit for small transition probabilities, the quantum-mechanical probability per collision of going from the ground state to the first excited state is given by $P_{0\to1}=(\Delta E_{v\,ib}/\hbar\omega)$, where ω is the frequency of the oscillator, and $\Delta E_{v\,ib}$ is the energy classically transferred to the oscillator in one collision. This transition probability is integrated over a normalized distribution of collision velocities to give an average probability for all collisions $\langle P_{0\to1}\rangle$. Finally, $\langle P_{1\to0}\rangle$ is calculated from the law of microscopic reversibility. The result turns out to be the same as that obtained by Herzfeld,[1] who used a quantum-mechanical perturbation treatment and went to the classical limit by assuming that the de Broglie wavelength of the molecule colliding with the oscillator is small compared to the range of the intermolecular forces.

I. INTRODUCTION

THIS paper uses essentially the method of Landau and Teller.[2] The purpose of the paper is to show that the classical method of calculating energy transfer to a vibrating system gives the same result as the quantum-mechanical method when all factors are included. Herzfeld's discussion[1] of Landau-Teller theory is not complete, and the discrepancy he finds between classical and quantum theories is eliminated in the discussion presented here.

II. COLLISIONAL MODEL

A head-on collision model is adopted; oblique collisions can be accounted for at the end by a "steric factor'" as Herzfeld has done. A molecule A collides with an atom B of the oscillator BC, and the relative velocity of collision at infinite separation is v_0. The vibrational amplitude coordinate is y, and the distance between the centers of mass is x, as illustrated in Fig. 1.

As Herzfeld points out, the intermolecular potential must be a function of y (for, if it were a function of x only, the collision would be effectively between point masses and no vibrational energy exchange would occur). In fact, the probability of vibrational energy transfer is intimately related to the dependence of the repulsive potential on coordinate y. Since it is well known from relaxation measurements that transition probabilities $(0\to1)$ for most diatomic molecules are very low, we may conclude that the intermolecular potential is only slightly dependent on y. We therefore assume a repulsive potential between molecule A and atom B which is exponential in the distance between the center of mass of A and atom B. This distance is $x-[m_c/(m_B+m_C)]y$, and the repulsive energy is

$$V(x,y)=E_0\exp\left\{\frac{-1}{L}\left[x-\left(\frac{m_C}{m_B+m_C}\right)y-\sigma_{AB}\right]\right\}, \quad (1)$$

where

$$E_0=\tfrac{1}{2}\tilde{m}v_0^2, \qquad \tilde{m}=\left\{\frac{m_A(m_B+m_C)}{m_A+m_B+m_C}\right\},$$

and σ_{AB} is the distance between A and B at the turning point, and L is a parameter which characterizes the steepness of the exponential potential. Since

$$\sigma_{AB}=x_T-\left(\frac{m_C}{m_B+m_C}\right)y_T,$$

where the subscript T denotes the turning point, Eq. (1) becomes

$$V(X,Y)=E_0\exp(-X/L)\exp\{[m_C/(m_B+m_C)]Y/L\}, \quad (2)$$

where $X=x-x_T$ and $Y=y-y_T$. The condition that the potential is only weakly dependent on Y can be obtained by assuming the vibrational amplitude is small compared to parameter L, so that the exponential can be expanded,

$$V(X,Y)=E_0\exp(-X/L)\left\{1-\left(\frac{m_C}{m_B+m_C}\right)\frac{Y}{L}\right\}. \quad (3)$$

The attractive part of the potential is accounted for later on by using a modified velocity distribution.

If the assumption that $|Y|\ll L$ is fulfilled, then the effect of vibrations of BC on the collision trajectory is small, and the transition probability is also small. Thus, for purposes of finding the trajectory, the potential neglecting vibrations can be used as a good approximation,

$$V(X)\cong E_0\exp(-X/L). \quad (4)$$

* Work performed at the University of California, Department of Chemistry.

[2] L. Landau and E. Teller, Physik. Z. Sowjetunion 11, 18 (1936).

[1] K. F. Herzfeld, "Relaxation phenomena in gases," in *Thermodynamics and Physics of Matter* (Princeton University Press, Princeton, New Jersey, 1955).

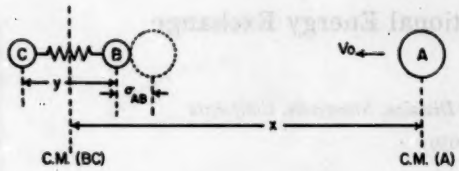

FIG. 1. Collision coordinates.

Figure 2 illustrates this assumption qualitatively. The classical equation of motion,

$$dX/dt=(2/\tilde{m}\{E_0-V(X)\})^{\frac{1}{2}}, \tag{5}$$

can then be integrated between limits $X=0$ at $t=0$ and X, t by using Eq. (4) for the potential energy. The result is

$$\exp(-X/L)=\operatorname{sech}^2(v_0t/2L). \tag{6}$$

Since the effect of vibrations on this trajectory is small, Eq. (6) can be substituted in Eq. (3) to obtain an approximate potential energy as a function of Y and time during the collision, yielding

$$V(Y,t)=E_0\left\{1+\left(\frac{m_C}{m_B+m_C}\right)\frac{Y}{L}\right\}\operatorname{sech}^2(v_0t/2L). \tag{7}$$

III. ENERGY TRANSFERRED TO THE OSCILLATOR

We can now regard the oscillator as driven by a force

$$F(t)=-(\partial/\partial Y)\{V(Y,t)\}. \tag{8}$$

Substituting Eq. (7) into Eq. (8), one obtains

$$F(t)=(E_0/L)[m_C/(m_B+m_C)]\operatorname{sech}^2(v_0t/2L). \tag{9}$$

The problem is now simply that of a harmonic oscillator of reduced mass $\mu=[m_Bm_C/(m_B+m_C)]$ and frequency $\omega=2\pi\nu$, driven by a transient force depending only on time. Green's method[3] can be applied to such a force to give

$$Y(t')-Y(-\infty)=\int_{-\infty}^{t'}[F(t)/\mu\omega]\exp(i\omega t)dt. \tag{10}$$

The net amount of vibrational energy transferred to the oscillator is given by

$$\Delta E_{\text{vib}}=\tfrac{1}{2}\mu\omega^2\{|\,Y(\infty)\,|^2-|\,Y(-\infty)\,|^2\}. \tag{11}$$

$|\,Y(-\infty)\,|=0$, because the oscillator was not excited originally. Therefore,

$$\Delta E_{\text{vib}}=(1/2\mu)\left|\int_{-\infty}^{+\infty}F(t)\exp(i\omega t)dt\right|^2. \tag{12}$$

The integral in Eq. (12) can be evaluated using Eq. (9) for the force, giving

$$\Delta E_{\text{vib}}=(E_0/L)^2\left(\frac{m_C}{m_B+m_C}\right)^2(1/2\mu)\cdot\{[4\pi\omega L^2/v_0^2/\sinh(\pi\omega L/v_0)]\}^2. \tag{13}$$

If there are many vibrations during the course of a collision, $(\pi\omega L/v_0)\gg1$, and Eq. (13) becomes

$$\Delta E_{\text{vib}}=8\pi^2\omega^2L^2(\tilde{m}^2/\mu)\left(\frac{m_C}{m_B+m_C}\right)^2\exp(-2\pi\omega L/v_0). \tag{14}$$

In classical mechanics, one would say that the amount of energy given by Eq. (14) is transferred in every collision with relative velocity v_0. Since this quantity of energy is much smaller than a vibrational quantum, the quantum-mechanical equivalent of this statement is that a whole quantum is transferred in only relatively few collisions, and it is physically impossible to identify the individual collisions which result in an energy exchange. However, for a large number of quantum-mechanical collisions, a transition probability can be defined per collision by the expression

$$P_{0\to1}=\Delta E_{\text{vib}}/\hbar\omega. \tag{15}$$

This expression must be integrated over a normalized distribution of relative collision velocities along the line of centers. The usual Maxwellian distribution is modified since the approaching molecules are speeded up in a potential well of depth ϵ. The resulting distribution is

$$dN/N_0=(\tilde{m}/KT)v_0\exp(-\tilde{m}v_0^2/2KT)\exp(\epsilon/KT). \tag{16}$$

The resulting average transition probability for all collisions is

$$\langle P_{0\to1}\rangle=\left[\frac{8\pi^2\omega L^2\tilde{m}^2}{\hbar\mu}\right]\left[\frac{m_C}{m_B+m_C}\right]^2\left[\frac{2\pi\omega LKT}{\tilde{m}}\right]^{\frac{1}{2}}\left[\frac{2\pi KT}{3\tilde{m}}\right]^{\frac{1}{2}}\cdot\exp\{-\tfrac{3}{2}(\theta'/T)^{\frac{1}{3}}-(\theta/2T)+(\epsilon/KT)\}, \tag{17}$$

where $\theta=\hbar\omega/K$ and $\theta'=(2\pi\omega L)^2(\tilde{m}/K)$. In this equation, we have replaced v_0 by an average of velocities

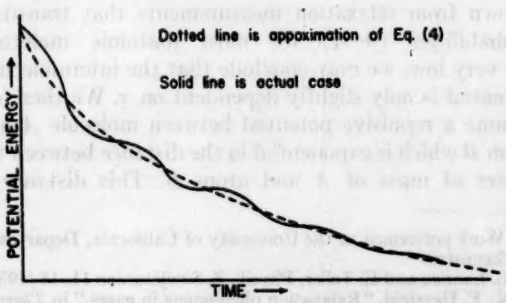

FIG. 2. Potential energy *vs* time in a molecular collision.

[3] J. C. Slater and N. H. Frank, *Mechanics* (McGraw-Hill Book Company, Inc., New York, 1947).

before and after collision such that the two translational energies at infinite separation differ by the vibrational quantum. By assuming $\frac{1}{2}\tilde{m}v_0^2 \gg h\nu$, the factor $-\theta/2T$ in the exponential is obtained. Now using $\langle P_{1\to 0}\rangle = \langle P_{0\to 1}\rangle \exp(\theta/T)$, and replacing m_C/m_B by $\frac{1}{2}\{(m_B/m_C)+(m_C/m_B)\}$ to account for the possibility of collision of A with C, we obtain

$$\langle P_{1\to 0}\rangle = 2(2\pi/3)^{\frac{1}{2}}(\theta'/\theta)(\theta'/T)^{1/6} \cdot\left[\frac{m_A(m_B^2+m_C^2)}{2m_Bm_C(m_A+m_B+m_C)}\right] \cdot\exp\{-\tfrac{3}{2}(\theta'/T)^{\frac{1}{3}}+(\theta/2T)+(\epsilon/KT)\}, \quad (18)$$

which is identical with the quantum result of Herzfeld after he went to the classical limit. Landau and Teller made only an approximate calculation and obtained

$$\langle P_{1\to 0}\rangle \propto \exp[-\tfrac{3}{2}(\theta'/T)^{\frac{1}{3}}]. \quad (19)$$

Both the quantum and classical theories assume: (1) that there are many vibrations during the course of a collision; (2) that the quantum of vibrational energy transferred is small compared to the relative kinetic energy of collision; (3) that the vibrational amplitude is small compared to the range of intermolecular forces. In addition, the quantum theory reduces to the classical result when one assumes, as Herzfeld did, that the de Broglie wavelength for the collision is small compared to $4\pi^2 L$. Since it turns out in many actual cases that this fourth assumption is better than the other three, it may be concluded that it should be more fruitful to extend existing treatments to additional potentials using the classical method, because it is simpler and gives better insight into the assumptions involved.

The same result obtained in Eq. (18) could have been obtained by a very simple time-dependent perturbation treatment. If a quantum-mechanical oscillator is initially in the first excited state and has only a slight transition probability of going to adjacent states, then the usual theory of time-dependent perturbations shows the translation probability to be proportional to the square of the ω-Fourier component of the perturbation energy, analogous to Eq. (12). By using Eq. (7) to obtain the perturbation energy, one obtains the result that the perturbation energy is proportional to the Y-matrix element between initial and final states of the harmonic oscillator. This shows that to the approximation that the potential is linear in Y only transitions to adjacent states are allowed, in the same manner that dipole emission selection rules are derived. The method very briefly is as follows. Since initially the oscillator is in its first excited state, the initial wave function for the oscillator is Ψ_1. After collision, the wave function is $\Psi_f = \Sigma a_n \Psi_n$, and, in our case, $\Psi_f \approx \Psi_1 + a_0\Psi_0$. Then

$$P_{1\to 0} = |a_0|^2 = |(-i/\hbar)\int H_{10}' \exp(i\omega t)\,dt|^2 \quad (20)$$

and

$$H_{10}' = (E_0/L)\{\operatorname{sech}^2(v_0t/2L)\}\left(\frac{m_C}{m_B+m_C}\right)\int_0^\infty \Psi_1 Y \Psi_0\, dY. \quad (21)$$

The net result of the integration, keeping all the proportionality factors, is Eq. (18).

Ultraviolet Resonance Spectrum of the Iodine Molecule*

R. D. VERMA

Laboratory of Molecular Structure and Spectra, Department of Physics, The University of Chicago, Chicago 37, Illinois

(Received October 2, 1959)

The ultraviolet resonance spectrum of I_2 observed in electric discharges in the region 1830–2370 A has been photographed at high resolution with a 21-ft vacuum grating spectrograph, and a thorough and complete analysis of the data in this region is given. The five doublet resonance series are shown to be excited from five rotational levels of vibrational level $v''=0$ of the ground state of I_2 to three vibrational levels $(v_n', v_{n+3}', v_{n+4}')$ of an upper electronic state by a single iodine atomic line 1830.4 A. The rotational constants for the ground state of I_2 may be represented:

$$B_v=0.03734-0.0001208\,(v+\tfrac{1}{2})+0.444\times10^{-6}(v+\tfrac{1}{2})^2-1.839\times10^{-8}(v+\tfrac{1}{2})^3-0.057\times10^{-10}(v+\tfrac{1}{2})^4 \quad (1)$$

$$D_v=1.99\times10^{-9}+1.236\times10^{-10}(v+\tfrac{1}{2}). \quad (2)$$

The ground-state $\Delta G(v+\frac{1}{2})$ values have been obtained from $v''=0$ up to the dissociation limit. A precise value of the dissociation energy of I_2, has been found to be 12 452.5±1.5 cm^{-1} as against the previous value of 12439±8 cm^{-1}.

The potential energy curve of $X\ ^1\Sigma_g^+$ has been computed by using the Rydberg-Klein-Rees method after modifying its final expressions, right up to the dissociation limit, and certain curious features in the neighbourhood of the dissociation limit are pointed out. The curve follows the van der Waals force law c/r^6 between $r=4.6$ A and $r=6.4$ A with $c=3.7\times10^6$. Various possibilities for the nature of the upper electronic state are discussed.

INTRODUCTION

OLDENBERG[1] studied the fluorescence spectrum of I_2 in the ultraviolet region, excited by various atomic lines, and discussed the results in a qualitative way. From the work of Asagoe,[2] and Kimura and Tonomura[3] it has been known for a long time that in the same region as that studied by Oldenberg, a series of I_2 resonance lines, excited by iodine atom emission lines, are observed in electric discharges through iodine vapor. Kimura and Tonomura gave an analysis of this spectrum after photographing it in the region 2050–2370 A with a Hilger E_1 quartz spectrograph and reported this resonance spectrum as excited by the iodine atomic lines 1830.4 A and 1844.5 A. They also photographed the spectrum down to 1783 A with a small fluorite spectrograph and indicated in the published spectrum short and weak resonance series excited by iodine atomic lines 1782.9, 1799.2, and 1876.4 A, together with the extension of those excited by 1830.4 and 1844.5 A. No data were given below 2050 A. The process of excitation could not be decided uniquely. The present author also repeated the experiment in India by using a Hilger E_1 quartz spectrograph. The preliminary analysis of the spectrum showed that the analysis could be improved and further definite knowledge about the ground electronic state of I_2 could be obtained, if the spectrum were photographed with a high resolution instrument down to 1700 A. Hence the study of this spectrum was continued in this laboratory and the results are discussed in this paper.

EXPERIMENTAL

Various conditions of the discharge were tried to excite this resonance spectrum and a high-frequency (2450 Mc/sec) discharge was found to be an efficient method. The source of iodine vapor was kept at 0°C and the vapor was pumped off continuously by a mechanical pump during the exposure time and the discharge tube was cooled with a fan. The exposure time ranged from 10 to 90 minutes. Ilford Q_2 photographic plates were used. The spectrum was photographed in the region 1700–2060 A in the third order of a 21-ft vacuum grating spectrograph having a grating with 30 000 lines/inch. The Ge atomic spectrum[4] was used as the standard for the measurements. The region 2000–2400 A was photographed in the 2nd order of the same instrument and copper and iron atomic lines were used as reference spectra for measurements. The measurements were made with an SIP comparator. The accuracy for sharp lines was ±1 mA, but for the weak lines and for those which were overlapped by other lines, the error ranged from ±3 mA to ±6 mA. The wavelengths measured were vacuum wavelengrhs (λ_{vac}); λ_{vac} values for the standard lines above 2000 A were obtained with the help of Edlen's table.[5] The wave numbers of the resonance lines, along with their analysis, are given in Tables I to IV.

* This work was assisted by the Geophysics Research Directorate of the Air Force Cambridge Research Center under Contract No. AF 19(604)-3478 with the University of Chicago, and the preliminary work by the Council of Scientific and Industrial Research, Government of India, under the research scheme sanctioned to Dr. P. Venkateswarlu at the Muslim University, Aligarh, India.

[1] O. Oldenberg, Z. Physik **18**, 1 (1923).

[2] K. Asagoe, Sci. Repts. Tokyo Burnika Daigaku **2**, 9 (1935).

[3] M. Kimura and K. Tonomura, *Pieter Zeeman* (Martinus Nijhoff, The Hague, Netherlands, 1935), p. 241.

[4] Meissner, Van Veld, and Wilkinson, J. Opt. Soc. Am. **48**, 1001 (1958).

[5] B. Edlen (private distribution, 1952).

RESULTS

The spectrum consists of groups of sharp lines which are repeated at intervals from 1830 A to 2370 A. On the lower frequency side, the spectrum converges to a sharp limit [Fig. 1(g)] followed by a maze of lines. Each group of lines consists of doublets which form doublet resonance series. The intervals between the members of the individual series correspond to the vibrational quanta of the ground electronic state of iodine molecule. In all, five doublet series are found to be excited. In individual resonance series, a number of the members are very weak or missing in accordance with the wave-mechanical formulation of the Franck-Condon principle. It is found that these resonance series involve the ground state of I_2 for their lower electronic state. The resonance doublets in some of the series, could be identified up to the vibrational level $v''=84$ of the ground state without any difficulty. Though the resonance series extend up to the dissociation limit of the ground state, v'' values could not be independently identified above $v''=84$ because of the overlapping of the various series and also because of larger gaps due to missing doublets in the series.

Microphotometric traces of the resonance doublets for certain v'' values are given in Fig. 1. The five doublet series are marked I, II, III, IVa, and IVb. The P line of series II and the R line of series III overlap each other for lower v'' values and could be resolved only after $v''=42$. Thus below $v''=43$ the doublets of series II and III together give the appearance of triplets. A similar kind of overlap is observed for the

TABLE I. Doublet series I.[a]

v''	$R(86)$ cm^{-1}	$P(88)$ cm^{-1}	$\Delta\nu_{obs}$	$\Delta\nu_{calc}$
0	54 632.93[b]	54 619.23	13.70	13.04
2	54 209.30	54 196.55	12.75	12.95
4	53 790.97	53 778.10	12.87	12.87
5	53 583.50	53 570.76	12.74	12.83
6	53 377.29	53 364.58	12.71	12.79
8	52 968.82	52 955.92	12.90	12.70
9	52 766.16	52 753.47	12.69	12.66
10	52 565.43	52 552.47	12.96	12.62
11	52 365.78	52 353.06	12.72	12.58
12	52 166.31	52 153.63	12.68	12.53
13	51 970.30	51 957.61	12.69	12.49
15	51 580.21	51 567.74	12.47	12.41
17	51 195.47	51 183.36	12.11	12.32
19	50 816.52	50 804.39	12.13	12.23
21	50 443.30	50 431.19	12.11	12.14
24	49 894.17	49 882.10	12.07	12.01
26	49 534.87	49 523.07	11.80	11.91
28	49 182.37	49 170.35	12.02	11.81
30	48 836.42	48 824.88	11.54	11.71
31	48 665.78	48 654.08	11.70	11.66
33	48 329.16	48 317.90	11.26	11.55
35	47 999.69	47 998.28	11.41	11.44
36	47 837.25	47 826.02	11.23	11.39
38	47 517.86	47 506.68	11.18	11.27
40	47 206.02	47 194.70	11.32	11.15
41	47 052.54	47 041.38	11.16	11.08
43	46 751.65	46 740.77	10.88	10.95
44	46 604.10	46 593.24	10.86	10.89
46	46 315.32	46 304.61	10.71	10.75
49	45 897.25	45 886.80	10.45	10.53
50	45 762.36	45 751.81	10.55	10.45
52	45 498.72	45 488.46	10.26	10.29
55	45 120.97	45 110.92	10.05	10.04
56	44 999.48	44 989.84	9.64	9.96
58	44 765.08	44 755.49	9.59	9.78
59	44 651.59	44 641.76	9.83	9.68
62	44 326.95	44 317.52	9.43	9.39
63	44 224.19	44 214.76	9.43	9.29
66	43 932.89	43 923.92	8.97	8.97
67	43 841.59	43 832.64	8.95	8.86
71	43 505.78	43 497.36	8.42	8.39
75	43 218.10	43 210.25	7.85	7.88
76	43 154.21	43 146.63	7.58	7.74
77	43 093.10	43 085.64	7.46	7.60
83	42 789.32	42 783.02	6.30	6.72
84	42 749.26	42 742.79	6.47	6.56

[a] For explanation of the missing lines, see the text.
[b] Exciting line.

TABLE II. Doublet series II.

v''	$R(45)$ cm^{-1}	$P(47)$ cm^{-1}	$\Delta\nu_{obs}$	$\Delta\nu_{calc}$
0	54 640.09	54 632.93[b]	7.16	6.93
2	a	54 208.12[c]		
4	53 795.14	53 788.31[c]	6.83	6.84
6	53 380.37	53 373.53	6.84	6.80
7	53 174.92	53 167.90	7.02	6.78
8	52 970.54	52 963.77[c]	6.77	6.76
10	52 565.43	52 558.96[c]	6.47	6.71
11	52 365.45	52 358.60[c]	6.85	6.69
12	52 166.31	52 159.93	6.38	6.67
13	51 968.68	51 962.20[c]	6.48	6.64
15	51 577.60	51 570.80[c]	6.80	6.60
17	51 191.32	51 184.77[c]	6.55	6.55
19	50 810.84	50 804.39[c]	6.45	6.51
21	50 436.17	50 429.86[c]	6.31	6.46
23	50 067.14	50 060.80[c]	6.34	6.41
24	49 884.77	49 878.35[c]	6.42	6.39
26	49 524.02	49 517.75[c]	6.27	6.34
28	49 170.35	49 164.16[c]	6.19	6.29
30	48 822.50	48 816.30[c]	6.20	6.23
31	48 650.93	48 644.92[c]	6.01	6.20
33	48 312.96	48 306.86[c]	6.10	6.15
35	47 981.42	47 975.53[c]	5.89	6.09
36	47 818.31	47 812.39[c]	5.92	6.06
38	47 497.03	47 491.09[c]	5.94	6.00
40	47 183.10	47 177.31[c]	5.79	5.93
41	47 028.90	47 023.09[c]	5.81	5.90
43	46 726.16	46 720.37	5.79	5.83
46	46 286.74	46 280.96	5.78	5.72
48	46 003.70	45 998.12	5.58	5.65
49	45 865.42	45 859.84	5.58	5.61
51	45 595.23	45 589.66	5.57	5.53
52	45 463.47	45 457.89	5.58	5.48
54	45 206.40	45 201.30	5.10	5.40
55	45 081.98	45 076.64	5.34	5.35
58	44 722.08	44 716.84	5.24	5.21
61	44 385.07	44 379.95	5.12	5.06
62	44 278.00	44 272.94	5.06	5.01
65	43 973.17	43 968.41	4.76	4.85
66	43 877.32	43 872.50	4.82	4.79
69	43 606.52	43 601.90	4.62	4.61
70	43 522.22	43 517.62	4.60	4.55
74	43 214.56	43 210.25	4.31	4.29
75	43 145.16	43 141.05	4.11	4.22
76	43 078.75	43 074.56	4.19	4.15
80	42 842.88	42 838.88	4.00	3.86
81	42 791.24	42 787.45	3.79	3.78
82	42 742.79	42 738.92	3.87	3.70

[a] This line is masked by the atomic line 1844.5 A.
[b] Exciting line (iodine atomic line 1830.4 A).
[c] These lines are blended with those as marked * in series III.

TABLE III. Doublet series III.

v''	$R(48)$ cm^{-1}	$P(50)$ cm^{-1}	$\Delta\nu_{obs}$	$\Delta\nu_{calc}$
0	54 632.93*	54 625.76	7.17	7.38
2	54 208.12*	54 200.84	7.28	7.33
4	53 788.31*	53 781.05	7.26	7.29
8	52 963.77*	52 956.45	7.32	7.19
9	52 760.68	52 753.47	7.21	7.17
10	52 558.96*	52 551.73	7.23	7.14
11	52 358.60*	52 351.36	7.24	7.12
13	51 962.20*	51 955.02	7.18	7.07
15	51 570.80*	51 563.80	7.00	7.03
17	51 184.77*	51 177.83	6.94	6.98
19	50 804.39*	50 797.44	6.95	6.93
21	50 429.86*	50 422.97	6.89	6.88
23	50 060.80*	50 054.06	6.74	6.83
24	49 878.35*	49 871.78	6.57	6.80
26	49 517.75*	49 511.18	6.57	6.75
28	49 164.16*	49 158.02	6.14	6.69
30	48 816.30*	48 809.82	6.48	6.64
31	48 644.92*	48 638.32	6.60	6.61
33	48 306.86*	48 300.52	6.34	6.55
35	47 975.53*	47 969.32	6.21	6.48
36	47 812.39*	47 806.13	6.26	6.45
38	47 491.09*	47 485.28	5.81	6.39
40	47 177.31*	47 171.10	6.21	6.32
41	47 023.09*	47 017.09	6.00	6.28
43	46 720.89	46 714.67	6.22	6.21
46	46 281.51	46 275.47	6.04	6.10
48	45 998.65	45 992.66	5.99	6.02
49	45 860.43	45 854.54	5.89	5.97
51	45 590.30	45 584.38	5.92	5.89
52	45 458.60	45 452.73	5.87	5.84
54	45 202.03	45 196.31	5.72	5.75
55	45 077.37	45 071.52	5.85	5.71
58	44 717.58	44 711.96	5.62	5.56
61	44 380.77	44 375.36	5.41	5.40
62	44 273.84	44 268.43	5.41	5.35
65	43 969.27	43 964.12	5.15	5.17
66	43 873.47	43 868.42	5.05	5.11
69	43 603.04	43 598.18	4.86	4.93
70	43 518.79	43 513.94	4.85	4.86
74	43 211.48	43 207.00	4.48	4.59
75	43 142.24	43 137.62	4.62	4.52
76	43 075.97	43 071.63	4.34	4.44
80	42 840.77	42 836.57	4.20	4.14
81	42 789.32	42 785.33	3.99	4.05
82	42 740.67	42 736.80	3.87	3.97

* Exciting line.

other two doublet series IVa and IVb which could be resolved only for the last member identified ($v''=74$). The separation between the P line of series II and the R line of series III is found to increase slowly with v''. This feature together with the fact that the P line of II and the R line of III coincide for the lower values of v'', shows that the doublet series II and III are excited to the same vibrational level of the upper electronic state by monochromatic radiation which coincides with the P line of II and the R line of III for a certain low v'' value. A similar conclusion is valid for the doublet series IVa and IVb. According to the analysis it was found that all the five doublet series are excited by the single iodine atomic line 1830.4 A which is the resonance line of the iodine atom and is strongly excited in electric discharges. The 1830.4 A atomic line excites the five doublet series from five rotational levels of the vibrational level $v''=0$ to the rotational levels of three different vibrational levels (v_n', v_{n+1}', v_{n+4}') of the upper electronic state. Unfortunately the resonance doublets at 1830.4 and 1844.5 A are overrun by the Rowland ghosts of these atomic lines of the iodine atom and hence only a few resonance series lines could be measured in this region and others were masked by the ghosts.

The process of excitation is explained in the energy level diagram (Fig. 2). This process of excitation requires that the following relations hold good:

$$F''(24)-F''(23)=F'(25)-F'(22)$$

or

$$48\,B_0''=144B_n'$$

$$F''(48)-F''(47)=F'(49)-F'(46)$$

or

$$96B_0''=288B_{n+1}'=288B_n'.$$

(The effect of α' falls within the width of the exciting line) and

$$F''(47)-F''(23)=\omega_n'-(\omega x)_n'+F'(46)-F'(22)$$

$$F''(86)-F''(48)=\{4\omega_n'-16(\omega x)_n'+F'(87)\}-\{\omega_n'-(\omega x)_n'+F'(49)\}.$$

TABLE IV. Doublet series IVa and IVb.

v''	$R(21)$ cm^{-1}	$\Delta\nu_{RP}$	$P(23)$ $R(24)$ cm^{-1}	$\Delta\nu_{RP}$	$P(26)$ cm^{-1}
2	54 211.21	3.09	54 208.12	4.05	54 204.07
4	53 790.97	3.35	53 787.62	3.79	53 783.83
6	53 375.75	3.30	53 372.45	3.76	53 368.69
7	...		53 166.83	3.79	53 163.04
8	52 965.48	3.31	52 962.17	3.70	52 958.47
11	52 359.87	3.41	52 356.46	3.65	52 352.81
12	52 160.49	3.16	52 157.33	3.70	52 153.63
15	51 570.80	3.06	51 567.74	3.89	51 563.85
17	51 184.77	3.35	51 181.42	3.59	51 177.83
19	50 803.56	3.10	50 800.46	3.61	50 796.85
21	50 428.52	3.18	50 425.34	3.43	50 421.91
23	50 059.02	3.11	50 055.91		
24	49 876.41	2.94	49 873.47	3.33	49 870.14
26	49 515.44	2.99	49 512.45	3.28	49 509.17
28	49 161.21	3.12	49 158.09	3.16	49 154.93
30	48 812.73	2.91	48 809.82	3.36	48 806.46
33	48 302.42	2.90	48 299.52	3.27	48 296.25
35	47 970.58	2.85	47 967.73	3.20	47 964.53
36	47 807.27	3.04	47 804.23	3.17	47 801.06
38	47 485.28	2.73	47 482.55	3.23	47 479.32
40	47 171.10	3.02	47 168.08	3.05	47 165.03
41	47 016.39	2.74	47 013.65	3.10	47 010.55
43	46 713.12	2.74	46 710.38	3.10	46 707.28
46	46 275.47	2.74	46 272.73	2.78	46 269.95
48	45 989.23	2.70	45 986.53	2.92	45 983.61
49	45 850.53	2.65	45 847.88	2.94	45 844.94
51	45 579.60	2.66	45 576.94	2.74	45 574.20
54	45 190.02	2.41	45 187.61	2.72	45 184.89
55	45 064.84	2.46	45 062.38	2.68	45 059.70
58	44 703.73	2.36	44 701.37	2.60	44 698.77
61	44 365.55	2.30	44 363.25	2.56	44 360.69
62	44 257.93	2.41	44 255.52	2.35	44 253.17
65	43 951.87	2.28	43 949.59	2.39	43 947.20
69	43 583.09	2.13	43 580.96	2.16	43 578.80
74	43 188.00	2.19	43 185.81		
			43 186.58	2.42	43 184.16

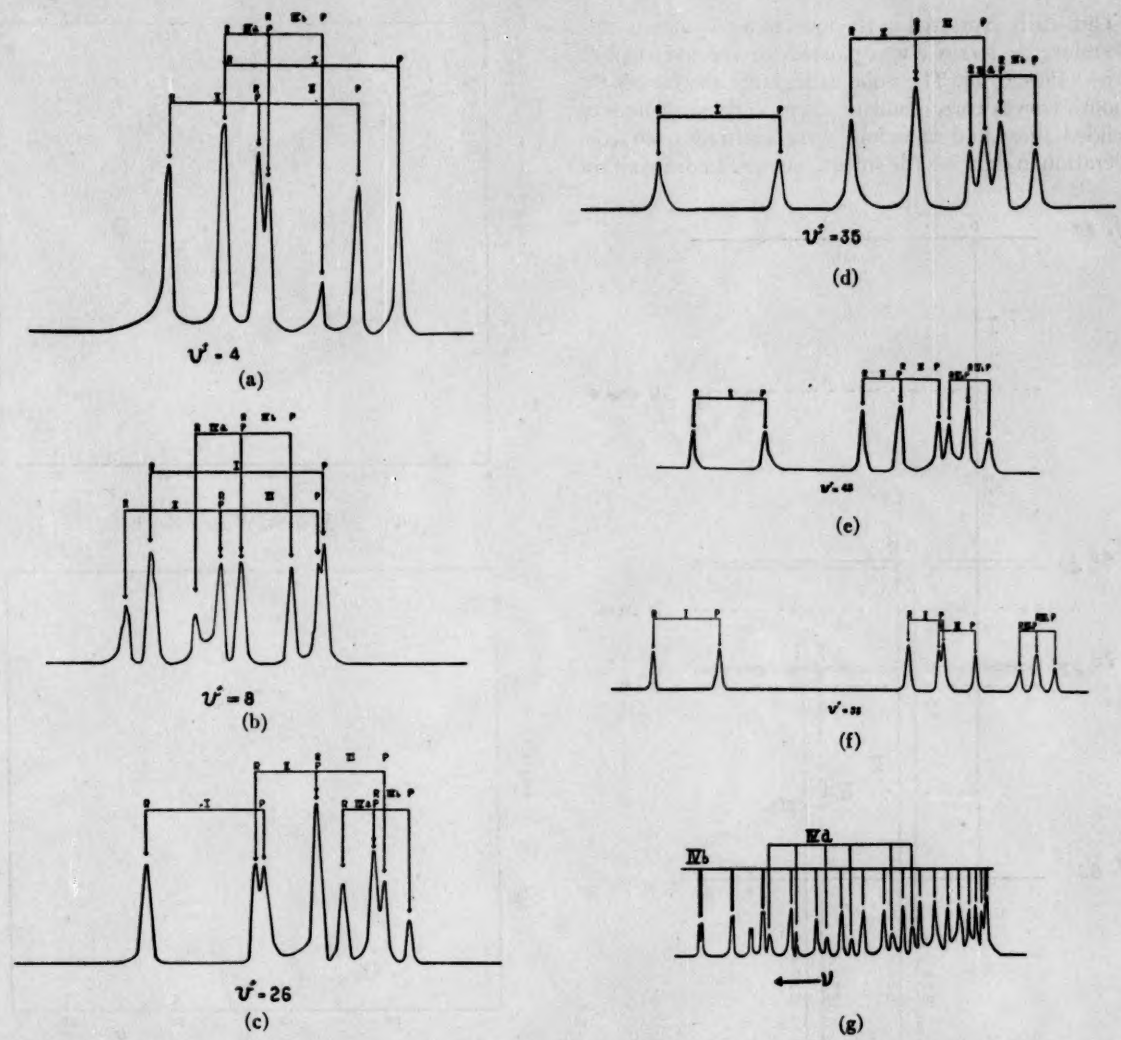

FIG. 1. (a)–(f). Microphotometric traces for the five resonance doublets at certain v'' values. (g) The resonance series IVb near the convergence limit.

Thus a single line is able to excite the molecule from five rotational levels of $v''=0$.

It may be pointed out that according to Kimura and Tonomura the doublet series I is excited by the 1830.4 A atomic line and II, III, IVa, and IVb are excited by the 1844.5 A atomic line. However, it may be noted that according to the present analysis the R line of II at $v''=2$ falls very close to the 1844.5 A atomic line, giving rise to the probability of one mistaking 1844.5 A as the exciting line, especially in a low dispersion spectrum. The calculations are based on the following theory.

The doublet separation $\Delta\nu$ in a doublet series can be shown to be given by

$$\Delta\nu=(4J_r+2)[B_v''-(2J_r^2+2J_r+2)D_v''] \quad (1)$$

where J_r is the rotational quantum number of the level excited in the upper state. B_v'' and D_v'' are the rotational constants of the lower state (ground state in this case) and are functions of the vibrational quantum number v''. Expressing B_v'' and D_v'' in a polynomial in v'' and dropping off the primes, one gets

$$B_v=B_e-\alpha_e(v+\tfrac{1}{2})+\gamma_e(v+\tfrac{1}{2})^2+\delta_e(v+\tfrac{1}{2})^3+\phi_e(v+\tfrac{1}{2})^4, \quad (2)$$

$$D_v=D_e+\beta_e(v+\tfrac{1}{2}). \quad (3)$$

On substitution in Eq. (1),

$$\begin{aligned}\Delta\nu=(4J_r+2)[&B_e-\tfrac{1}{2}\alpha_e+\tfrac{1}{4}\gamma_e+\tfrac{1}{8}\delta_e+\tfrac{1}{16}\phi_e\\&-(2J_r^2+2J_r+2)(D_e+\tfrac{1}{2}\beta_e)]\\&-(4J_r+2)[\alpha_e-\gamma_e-\tfrac{3}{4}\delta_e-\tfrac{1}{2}\phi_e+(2J_r^2+2J_r+2)\beta_e]v\\&+(4J_r+2)[\gamma_e+\tfrac{3}{2}\delta_e+\tfrac{3}{2}\phi_e]v^2\\&+(4J_r+2)[\delta_e+2\phi_e]v^3+(4J_r+2)\phi_e v^4. \quad (1')\end{aligned}$$

Thus $\Delta\nu$ is expressed in the form of a polynomial in v. Therefore $\Delta\nu$ *versus* v was plotted for the five doublet series (Figs. 3–7). The points which are too far off the smooth curves correspond to either very weak lines or blended lines and therefore were omitted from consideration in drawing the smooth curves. In drawing the

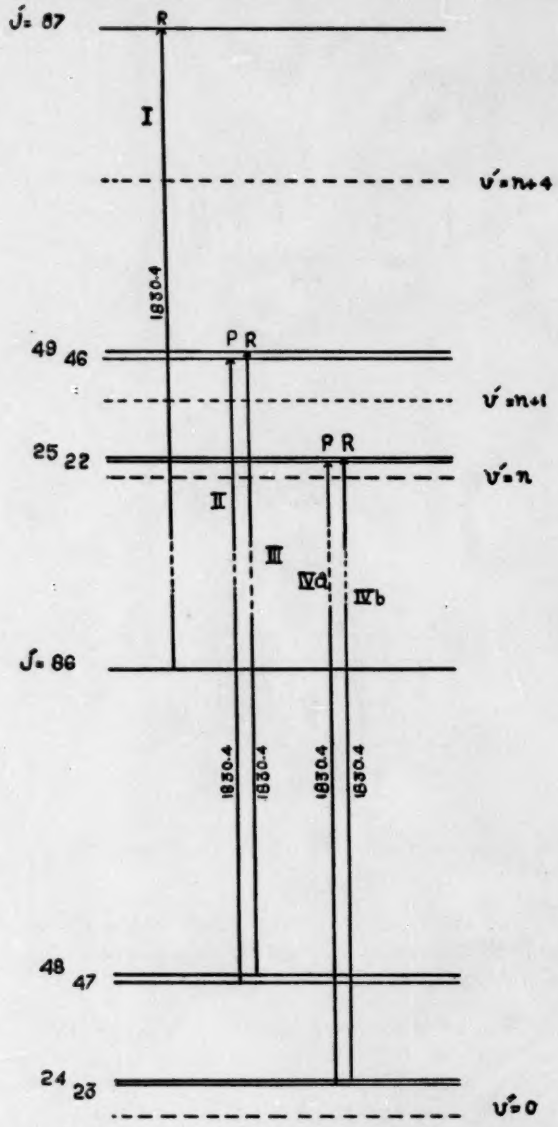

FIG. 2. Energy level diagram showing the process of excitation by a single iodine atomic line 1830.4 A.

smooth curves for II and III, emphasis was given to the points below $v''=20$ and above $v''=42$. The points between are found to lie below the smooth curve, as is expected according to the analysis. The *P* line of *II* and the *R* line of III coincide for low v'' values and for higher v'' values they begin to separate out. But they could not be resolved by the instrument used

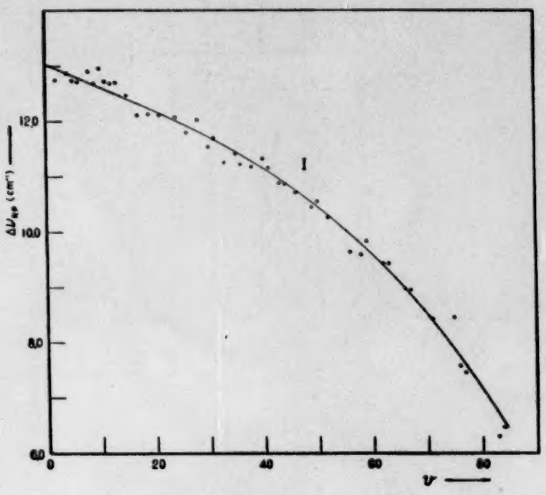

FIG. 3. $\Delta\nu$ *versus* v'' for series I.

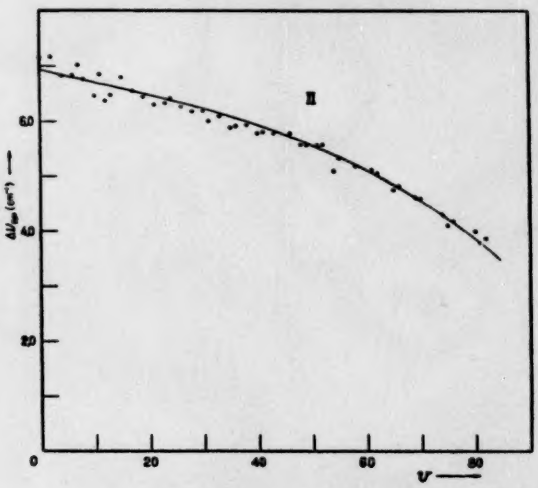

FIG. 4. $\Delta\nu$ *versus* v'' for series II.

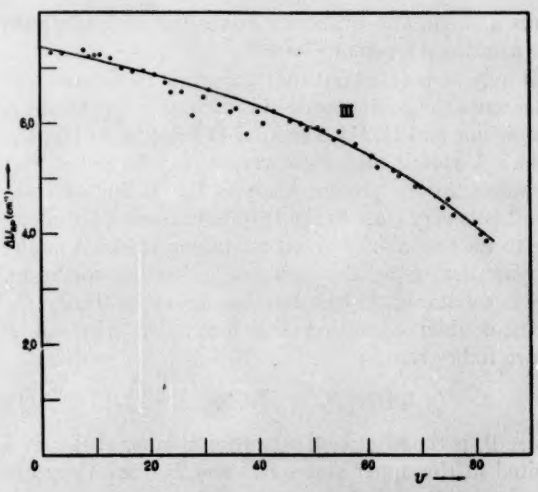

FIG. 5. $\Delta\nu$ *versus* v'' for series III.

below $v''=43$ and the measurements correspond to the mean of the positions of the two lines and hence this mean is larger than the true value of the P line of II and less than the true value of the R line of III. Thus $\Delta\nu$ for the two doublet series II and III falls below the true curves for the points below $v''=43$. The empirical equations developed for the three curves are given in the following:

For I,

$$\Delta\nu=13.037-0.0428v+1.52\times10^{-4}v^2-6.5\times10^{-6}v^3 -0.20\times10^{-8}v^4. \quad (4)$$

For II,

$$\Delta\nu=6.932-2.25\times10^{-2}v+0.756\times10^{-4}v^2-3.43\times10^{-6}v^3. \quad (5)$$

For III,

$$\Delta\nu=7.380-2.40\times10^{-2}v+0.81\times10^{-4}v^2-3.60\times10^{-6}v^3. \quad (6)$$

On comparing the coefficients of equations (1′) and (4) and on elimination one gets from series I,

$$(4J_r+2)[B_e-(2J_r^2+2J_r+2)D_e]=13.0584 \quad (7)$$

$$(4J_r+2)[\alpha_e+(2J_r^2+2J_r+2)\beta_e]=0.042937 \quad (8)$$

$$\left.\begin{aligned}(4J_r+2)\gamma_e&=1.61947\times10^{-4}\\(4J_r+2)\delta_e&=6.496\times10^{-6}\\(4J_r+2)\phi_e&=0.20\times10^{-8}.\end{aligned}\right\} \quad (9)$$

B_e is known precisely from the interferometric work on the resonance spectrum in the visible region by Rank and Baldwin.[6] Neglecting the term D_e in Eq. (7) and putting $B_e=0.037364$ give

$$4J_r+2\simeq349.5$$
$$J_r\simeq86.9$$
$$=87 \quad (\text{as } J_r \text{ has to be integer}).$$

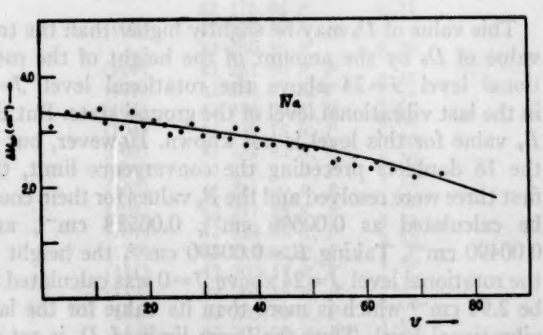

FIG. 6. $\Delta\nu$ *versus* v'' for series IVa.

[6] D. H. Rank and W. M. Baldwin, J. Chem. Phys. 19, 1210 (1951).

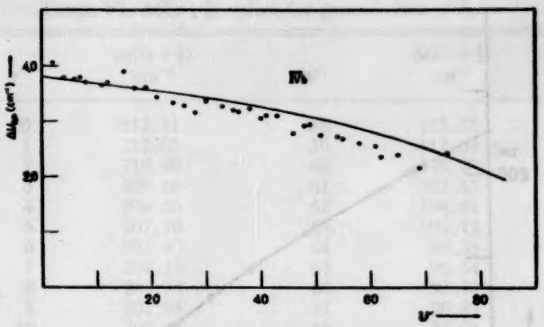

FIG. 7. $\Delta\nu$ *versus* v'' for series IVb.

It has been checked that neglect of the term D_e in the above calculation does not cause any error in J_r, and also any uncertainty in the last two figures of B_e are insignificant in the calculation of J_r. Having thus decided J_r, one could calculate γ_e, δ_e and ϕ_e directly from Eqs. (9). Equations (7) and (8) then reduce to the following:

$$B_e-15314D_e=0.037309797 \quad (7')$$

$$\alpha_e+15314\beta_e=0.000122677. \quad (8')$$

Similar calculations were followed for series II and III and the equations corresponding to (7′) and (8′) are obtained in the following:

For II,

$$\left.\begin{aligned}B_e-4326D_e&=0.03732933 \quad (7'')\\\alpha_e+4326\beta_e&=0.000121239 \quad (8'')\end{aligned}\right\}$$

For III,

$$\left.\begin{aligned}B_e-4902D_e&=0.03733362 \quad (7''')\\\alpha_e+4902\beta_e&=0.000121483. \quad (8''')\end{aligned}\right\}$$

The J_r values for II and III are found to be 46 and 49, respectively. γ_e and δ_e for these two series were calculated as for I. Equations (7′), (7″), and (7‴) were solved by the least squares method and B_e and D_e were found. Similarly α_e and β_e were calculated. The average values of these constants are represented by the following two equations:

$$B_v=0.03734-0.0001208(v+\tfrac{1}{2})+0.444\times10^{-6}(v+\tfrac{1}{2})^2 -1.839\times10^{-8}(v+\tfrac{1}{2})^3-0.057\times10^{-10}(v+\tfrac{1}{2})^4 \quad (10)$$

$$D_v=1.99\times10^{-9}+1.236\times10^{-10}(v+\tfrac{1}{2}). \quad (11)$$

For the series IVa and IVb, the J_r values are calculated to be 22 and 25 and the solid curves IVa and IVb were drawn by using the following equations:

For IVa,

$$\Delta\nu=3.355-1.083\times10^{-2}v+3.751\times10^{-5}v^2 -1.641\times10^{-6}v^3 \quad (12)$$

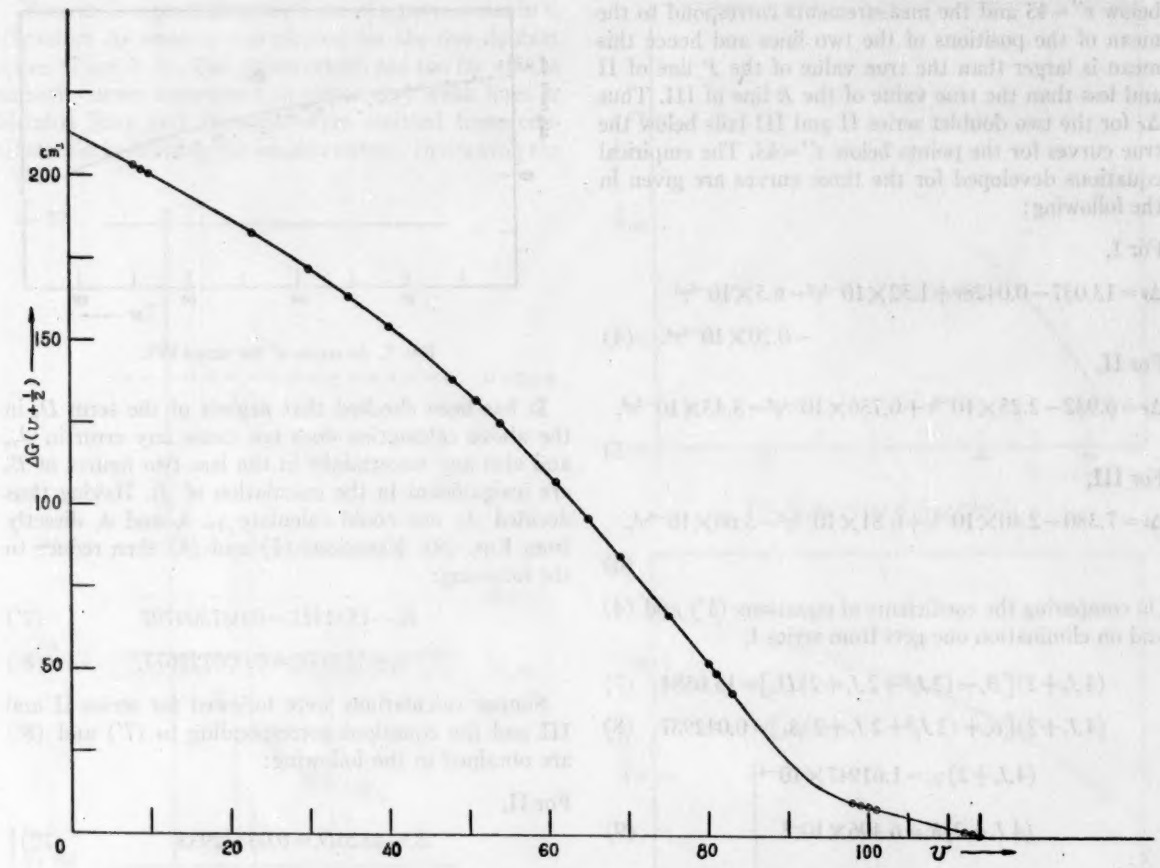

FIG. 8. $\Delta G(v+\frac{1}{2})$ *versus* v for the ground state of I_2. For description see the text.

and

for IVb

$$\Delta\nu = 3.805 - 1.226\times10^{-2}v + 4.251\times10^{-5}v^2 - 1.859\times10^{-6}v^3. \quad (13)$$

These equations were developed from the constants given in Eqs. (10) and (11). The smooth curves so drawn represent the points for low v'' values as well as for the last point, for which the overlapping lines of the two doublets are resolved. The in-between points are below these curves in accordance with the reasons given for II and III.

Since three different vibrational levels are excited in the upper state as shown in Fig. 2, it was possible to calculate the vibrational and rotational constants of the upper state at those vibrational levels and the values found are given in the following:

$$\omega_n' = 43.13 \text{ cm}^{-1}$$

$$(\omega x)_n' = 0.19 \text{ cm}^{-1}$$

$$B_n' = 0.01243 \text{ cm}^{-1}$$

where n is unknown.

The series IVb is found to converge at 42201.41 cm^{-1} [Fig. 1(g)]. Therefore the dissociation energy of the ground electronic state of I_2 could be calculated as follows:

$$D_0 = \text{exciting line } (\text{cm}^{-1}) - 42201.4 + F''(24) \text{ (for } v''=0)$$
$$= 54632.9 - 42201.4 + 22.4$$
$$= 12453.9 \text{ cm}^{-1}.$$

This value of D_0 may be slightly higher than the true value of D_0 by the amount of the height of the rotational level $J=24$ above the rotational level $J=0$ in the last vibrational level of the ground state. But the B_v value for this level is not known. However, out of the 18 doublets preceding the convergence limit, the first three were resolved and the B_v values for them could be calculated as 0.00696 cm^{-1}, 0.00588 cm^{-1}, and 0.00490 cm^{-1}. Taking $B_v = 0.00490$ cm^{-1}, the height of the rotational level $J=24$ above $J=0$ was calculated to be 2.94 cm^{-1} which is more than its value for the last vibrational level. Thus the lower limit of D_0 is set at 12451.0 cm^{-1} and the higher limit at 12453.9 cm^{-1}, i.e., $D_0 = 12452.5 \pm 1.5$ cm^{-1}. This value of D_0 can be contrasted with the previous value of 12439 ± 8 cm^{-1}

determined from the convergence limit[7] of the visible absorption bands.

The separation between successive R lines or P lines in a series is equal to the separation between two successive vibrational levels of the lower electronic state (ground state in this case) for a constant J value. Denoting this by $\Delta E^J(v+\frac{1}{2})$ it can be shown that

$$\Delta G''(v+\tfrac{1}{2})=\Delta E^J(v+\tfrac{1}{2})+J(J+1)(B_v''-B_{v+1}'') - J^2(J+1)^2(D_v''-D_{v+1}''). \quad (15)$$

The contribution by the last term is negligible, and therefore Eq. (15) reduces to

$$\Delta G''(v+\tfrac{1}{2})=\Delta E^J(v+\tfrac{1}{2})+J(J+1)(B_v''-B_{v+1}''). \quad (15')$$

Thus it was possible to calculate the $\Delta G(v+\frac{1}{2})$ values for the ground electronic state of I_2. The P lines of series III were chosen to obtain $\Delta E^J(v+\frac{1}{2})$. Missing lines were obtained from the graph plotted between ν_p and v''. The $\Delta G''(v+\frac{1}{2})$ values were then calculated up to $v''=83$ using Eq. (15'). B_v'' in Eq. (15') was calculated from Eq. (10). The $\Delta G''(v+\frac{1}{2})$ values thus obtained are plotted against v'' (Fig. 8) and are shown by a smooth curve. The points marked in Fig. 8 are those for which the $\Delta E^J(v+\frac{1}{2})$ values were obtained directly. The $\Delta E^J(v+\frac{1}{2})$ values for the last 17 vibrational quanta were obtained from series IVb which converges to a sharp limit, but vibrational quantum numbers for them could not be identified independently. The doublet separation could be resolved only in the first three members as pointed out earlier. Therefore the B_v values for other members could not be found and hence the $\Delta G(v+\frac{1}{2})$ values for these vibrational levels could not be calculated according to Eq. (15'). However, taking the B_v values for the first three members out of 18, the $\Delta G(v+\frac{1}{2})$ values were calculated for the first four vibrational levels. The last three $\Delta E^J(v+\frac{1}{2})$ values were taken equal to the $\Delta G(v+\frac{1}{2})$ values which holds fairly well in the neighborhood of the dissociation limit. With the help of these seven $\Delta G(v+\frac{1}{2})$ values and the D_0 value calculated earlier, the curve after $v''=83$ could be adjusted without any difficulty and the v'' values for these 18 members

TABLE V. Doublet series IVb at convergence limit.

v''	ν_{vac} cm^{-1}	$\Delta E^J(v+\frac{1}{2})$ cm^{-1}
(98)	42 289.41 R	9.87
	42 288.70 P	
(99)	42 279.54 R	
	42 278.94 P	9.24
(100)	42 270.30 R	
	42 269.80 P	8.70
(101)	42 261.60 R, P	
(102)	42 253.37 R, P	8.23
(103)	42 246.00 R, P	7.37
(104)	42 239.18 R, P	6.82
(105)	42 232.92 R, P	6.26
(106)	42 227.22 R, P	5.70
(107)	42 221.99 R, P	5.23
(108)	42 217.55 R, P	4.44
(109)	42 213.44 R, P	4.11
(110)	42 210.12 R, P	3.32
(111)	42 207.13 R, P	2.99
(112)	42 204.85 R, P	2.28
(113)	42 203.19 R, P	1.66
(114)	42 202.02 R, P	1.07
(115)	42 201.41 R, P	0.61

TABLE VI. $\Delta G(v+\frac{1}{2})$ values for ground state of I_2.

v''	$\Delta G(v+\frac{1}{2})$ cm^{-1}	v''	$\Delta G(v+\frac{1}{2})$ cm^{-1}
0	213.31	58	115.28
1	212.05	59	112.69
2	210.80	60	110.09
3	209.66	61	107.47
4	208.50	62	104.81
5	207.20	63	102.12
6	205.80	64	99.35
7	204.55	65	96.54
8	203.18	66	93.71
9	201.93	67	90.87
10	200.68	68	88.01
11	199.30	69	85.11
12	198.05	70	82.25
13	196.73	71	79.28
14	195.36	72	76.16
15	194.06	73	73.18
16	192.73	74	70.07
17	191.31	75	67.04
18	189.96	76	64.12
19	188.47	77	61.16
20	187.07	78	58.21
21	185.71	79	55.25
22	184.21	80	52.33
23	182.74	81	49.43
24	181.34	82	46.60
25	179.85	83	43.70
26	178.28	84	40.50
27	176.78	85	37.4
28	175.23	86	34.3
29	173.62	87	31.5
30	172.05	88	28.5
31	170.43	89	25.6
32	168.76	90	23.0
33	167.15	91	20.6
34	165.45	92	18.4
35	163.79	93	16.4
36	162.05	94	14.8
37	160.23	95	13.5
38	158.44	96	12.4
39	156.57	97	11.4
40	154.62	98	10.5
41	152.72	99	9.8
42	150.85	100	9.0
43	148.98	101	8.5
44	147.00	102	8.0
45	145.10	103	7.4
46	143.02	104	6.7
47	141.03	105	6.2
48	138.87	106	5.5
49	136.80	107	5.0
50	134.65	108	4.5
51	132.33	109	3.9
52	130.01	110	3.3
53	127.67	111	2.6
54	125.24	112	2.0
55	122.71	113	1.4
56	120.27	114	0.5
57	117.86		

[7] W. G. Brown, Phys. Rev. 38, 709 (1931).

TABLE VII. Results of calculations for potential energy curve for ground state of I_2.

v	$U(r)$ cm^{-1}	r_{min} A	r_{max} A
0	102.08	2.621	2.717
2	527.44	2.564	2.790
6	1 363.60	2.510	2.874
10	2 179.06	2.474	2.940
14	2 973.82	2.446	3.001
18	3 747.28	2.423	3.056
22	4 498.49	2.403	3.111
26	5 226.63	2.386	3.164
30	5 930.54	2.371	3.217
34	6 608.93	2.358	3.273
38	7 260.45	2.346	3.329
42	7 882.80	2.336	3.389
46	8 474.73	2.328	3.451
50	9 034.45	2.321	3.517
54	9 559.11	2.315	3.591
58	10 045.19	2.309	3.671
62	10 490.72	2.305	3.760
66	10 893.54	2.301	3.861
70	11 251.24	2.298	3.973
74	11 562.11	2.296	4.108
78	11 824.50	2.294	4.263
82	12 039.72	2.292	4.448
85	12 170.52	2.291	4.628
89	12 302.32	2.290	4.942
91	12 352.32	2.290	5.133
93	12 393.42	2.289	5.354
95	12 427.12	2.289	5.563
97	12 454.62	2.289	5.778
99	12 476.92	2.288	6.010
101	12 495.02	2.288	6.263
103	12 509.82	2.288	6.522
105	12 522.32	2.288	6.823
107	12 532.22	2.288	7.236
112	12 547.52	2.288	8.814

of IVb, thus identified, are shown in Table V. After adjusting the curve, the $\Delta G(v+\frac{1}{2})$ values were read off and all the values are collected in Table VI. The ω_e value for the ground state of I_2 according to these $\Delta G(v+\frac{1}{2})$ values is 214.52 cm^{-1}. It may be pointed out that the ω_e value of 214.248 cm^{-1} as given by Rank and Baldwin for I_2 has been calculated wrongly from their empirical equation[8] and it should be 214.518 cm^{-1} which agrees very well with the present value.

POTENTIAL ENERGY CURVE

Since this work provides data for the positions of all the vibrational levels of the ground electronic state and for the values of the rotational constants, an attempt has been made to compute the potential energy curve right up to the dissociation limit by the Rydberg-Klein-Rees method.[9,10] However, the final forms of the expressions for the computations of the RKR method have been changed into more convenient forms as discussed in the following

[8] The author examined the data which Professor Rank kindly sent to him and this mistake has been confirmed by private communication.

[9] A. L. G. Rees, Proc. Phys. Soc. (London) **59**, 998 (1947).

[10] Vanderslice, Mason, and Maisch, J. Mol. Spectroscopy **3**, 17 (1959). (It is to be noted that a factor of $\frac{1}{4}$ in the expression for g should read 2. This has been confirmed by private communication with the authors.)

The auxiliary function S as defined in earlier work,[9,10] is

$$S(U,k)=(2\pi^2\mu)^{-\frac{1}{2}}\int_0^{I'}[U-E(I,k)]^{\frac{1}{2}}dI \qquad (16)$$

where at $I=I'$, $U=E$ and $I=h(v+\frac{1}{2})$, $k=J(J+1)/b$, $b=8\pi^2\mu/h^2$. Substituting the value of

$$E(I,\ k)=\omega_e(v+\tfrac{1}{2})-\omega_e x_e(v+\tfrac{1}{2})^2+B_eJ(J+1)$$
$$-D_eJ^2(J+1)^2-\alpha_eJ(J+1)(v+\tfrac{1}{2})$$

in Eq. (16) and introducing the variables I and k, we have

$$S(U,k)=q\int_0^{I'}(A-lI+mI^2)^{\frac{1}{2}}dI \qquad (16')$$

where

$$1/q=(2\pi^2\mu h)^{\frac{1}{2}},$$
$$A=h[U-B_eJ(J+1)+D_eJ^2(J+1)^2],$$
$$l=\omega_e-\alpha_eJ(J+1),$$
$$m=\omega_e x_e/h.$$

Differentiating with respect to U and k under the integral sign, and then performing the integration, leads to the following expressions for f and g:

$$f=qh/2m^{\frac{1}{2}}\ln\{(l-2mI')/[l-(4mA)^{\frac{1}{2}}]\} \qquad (17)$$

$$g=qb/2(m^3)^{\frac{1}{2}}[\alpha_e(4mA)^{\frac{1}{2}}+2mB_eh+4mD_ehbk-\alpha_el]$$
$$\cdot\ln\{[l-2mI')]/[l-(4mA)^{\frac{1}{2}}]\}. \qquad (18)$$

For the rotationless state ($J=0$), applying the condition $U=E$ at $I=I'$ one gets

$$l-2mI'=\omega_e-2\omega_e x_e(v+\tfrac{1}{2})$$
$$=\Delta G(v+\tfrac{1}{2})+\omega_e x_e \qquad (19)$$

and

$$(4mA)^{\frac{1}{2}}=[4\omega_e x_e\{\omega_e(v+\tfrac{1}{2})-\omega_e x_e(v+\tfrac{1}{2})^2\}]^{\frac{1}{2}}$$
$$=[\omega_e^2-\{\Delta G(v+\tfrac{1}{2})+\omega_e x_e\}^2]^{\frac{1}{2}}=\chi^{\frac{1}{2}}.$$

Therefore

$$f=(8\pi^2\mu c/h)^{-\frac{1}{2}}\ln W/(\omega_e x_e)^{\frac{1}{2}}$$
$$g=(2\pi^2\mu c/h)^{\frac{1}{2}}[(\alpha_e/(\omega_e x_e)^{\frac{1}{2}}\cdot\chi^{\frac{1}{2}}+(2B_e-\alpha_e\omega_e/\omega_e x_e)$$
$$\cdot\ln W/(\omega_e x_e)^{\frac{1}{2}}]$$

where

$$W=(\Delta G(v+\tfrac{1}{2})+\omega_e x_e)/(\omega_e-\chi^{\frac{1}{2}})$$
$$\chi=\omega_e^2-[\Delta G(v+\tfrac{1}{2})+\omega_e x_e]^2.$$

However, when a series of quadratics in the form of $E(I\cdot k)$ are chosen to represent the entire experimental range, the auxiliary function S can be put in the

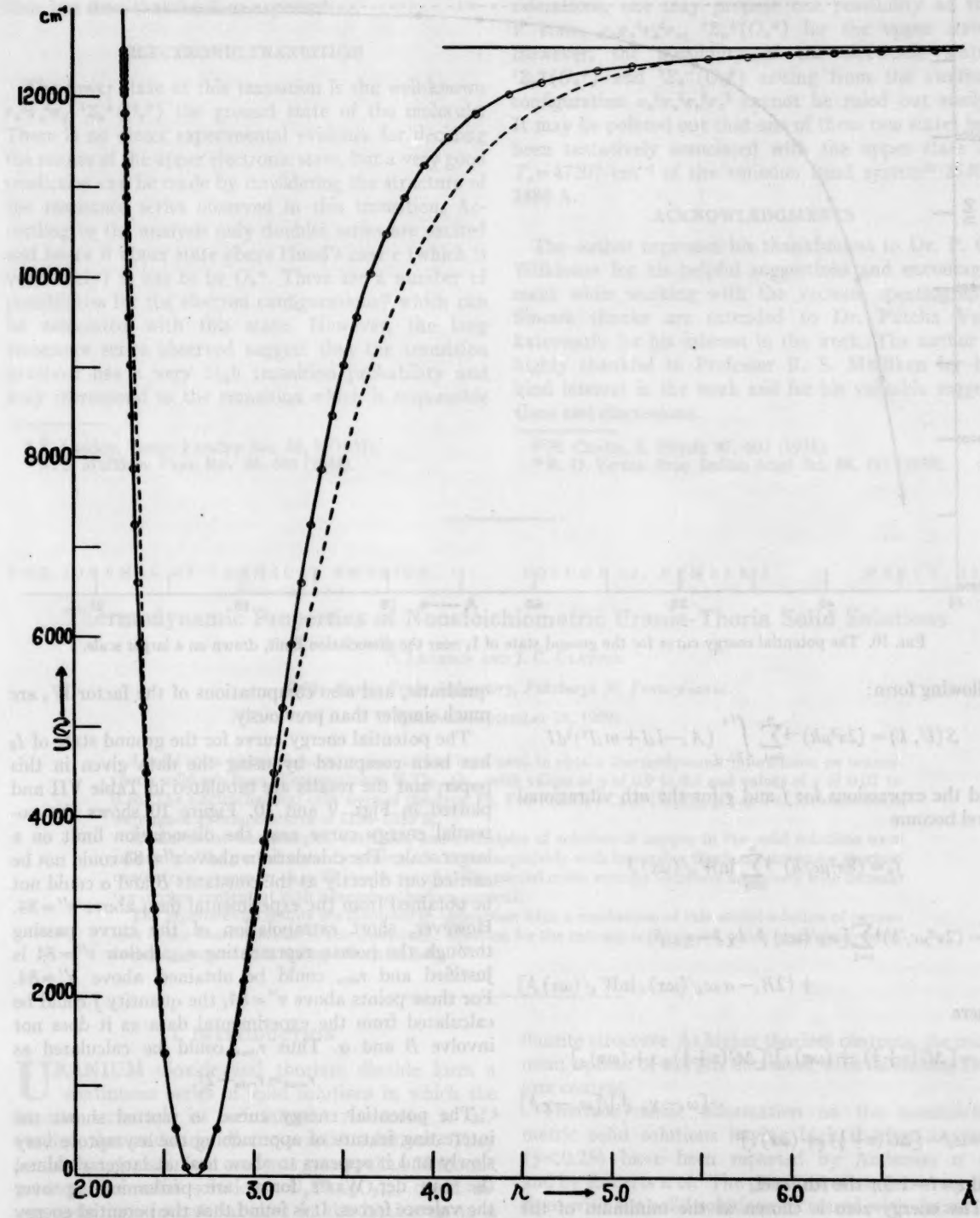

FIG. 9. The potential energy curve for the ground state of I_2 as computed by the RKR method. The dotted curve is the Morse curve.

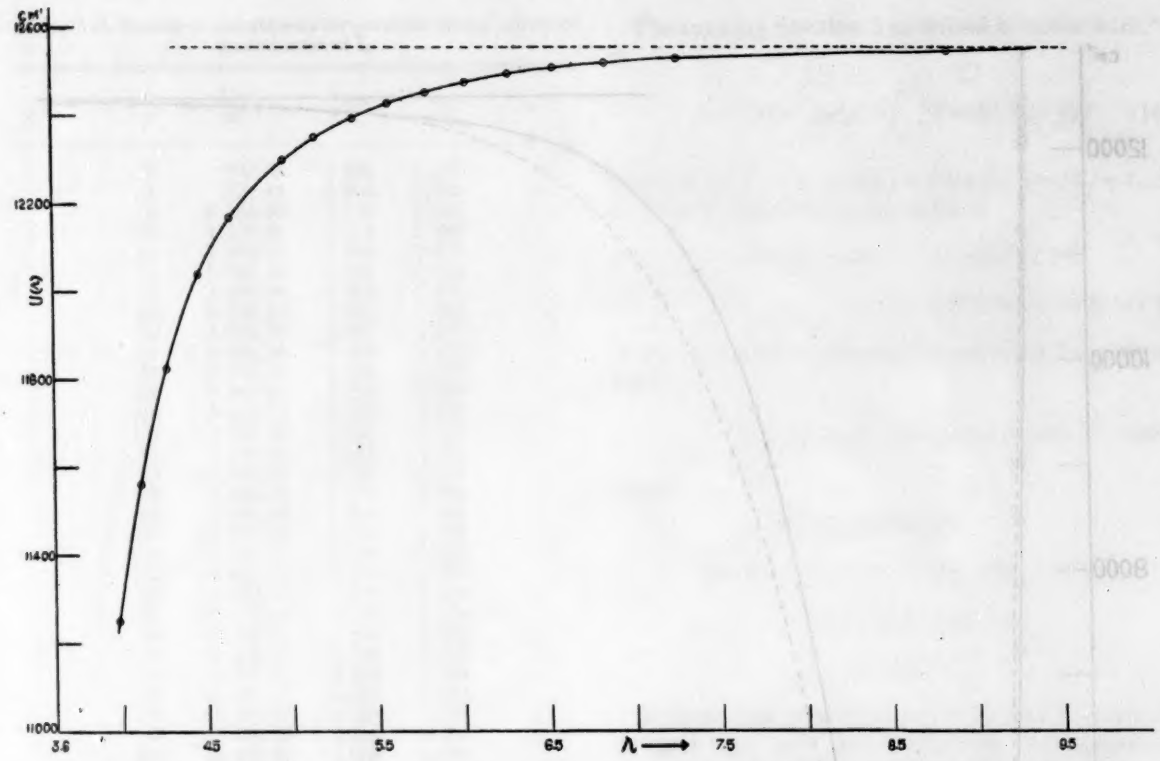

FIG. 10. The potential energy curve for the ground state of I_2 near the dissociation limit, drawn on a larger scale.

following form:

$$S(U,k)=(2\pi^2\mu h)^{-\frac{1}{2}}\sum_{i=1}^{n}\int_{I_{i-1}}^{I_i}(A_i-l_iI+m_iI^2)^{\frac{1}{2}}dI$$

and the expressions for f and g for the nth vibrational level become

$$f_n=(8\pi^2\mu c/h)^{-\frac{1}{2}}\sum_{i=1}^{n}\ln W_i/(\omega x)_i^{\frac{1}{2}}$$

$$g_n=(2\pi^2\mu c/h)^{\frac{1}{2}}\sum_{i=1}^{n}[\alpha_i/(\omega x)_i^{\frac{1}{2}}\cdot(\chi_i^{\frac{1}{2}}-\chi_{i-1}^{\frac{1}{2}})+(2B_i-\alpha_i\omega_i/(\omega x)_i\ln W_i/(\omega x)_i^{\frac{1}{2}}]$$

where

$$W_i=[\Delta G(v+\tfrac{1}{2})_i+(\omega x)_i]/[\Delta G(v+\tfrac{1}{2})_{i-1}+(\omega x)_i]\cdot[\omega_i-\chi_{i-1}^{\frac{1}{2}}]/[\omega_i-\chi_i^{\frac{1}{2}}]$$

$$\chi_i=\omega_i^2-[\Delta G(v+\tfrac{1}{2})_i+(\omega x)_i]^2$$

and $v=i-1$ for the ith level.

The energy zero is chosen as the minimum of the $U(r)$ curve (i.e., $U_0=0$). Therefore $\chi_0=0$ and $\Delta G(v+\frac{1}{2})_0+(\omega x)_1=\omega_1$. The constants ω, ωx, B, and α are allowed to vary from quadratic to quadratic. This form involves the $\Delta G(v+\frac{1}{2})$ instead of U and hence avoids the confusion about zero reference point for each quadratic, and also computations of the factor W_i are much simpler than previously.

The potential energy curve for the ground state of I_2 has been computed by using the data given in this paper, and the results are tabulated in Table VII and plotted in Figs. 9 and 10. Figure 10 shows the potential energy curve near the dissociation limit on a larger scale. The calculations above $v''=84$ could not be carried out directly as the constants B and α could not be obtained from the experimental data above $v''=84$. However, short extrapolation of the curve passing through the points representing r_{min} below $v''=84$ is justified and r_{min} could be obtained above $v''=84$. For these points above $v''=84$, the quantity f could be calculated from the experimental data as it does not involve B and α. Thus r_{max} could be calculated as

$$r_{max}=r_{min}+2f.$$

The potential energy curve so plotted shows the interesting feature of approaching the asymptote very slowly and it appears to show that at larger r values, the van der Waals forces are predominating over the valence forces. It is found that the potential energy curve follows the c/r^6 force law between $r=4.6$ A and $r=6.4$ A. The van der Waals force constant c was calculated to be 3.7×10^6, if $U(r)$ and r are in cm^{-1} and A respectively. The curve could be fitted within ±3 cm^{-1}. It may be pointed out that the theoretical

value[11] of 'c' for the HI molecule is 2.24×10^6 and is a little less than that for I_2 as expected.

ELECTRONIC TRANSITION

The lower state of this transition is the well-known $\sigma_g^2\pi_u^4\pi_g^4\,{}^1\Sigma_g^+(O_g^+)$ the ground state of the molecule. There is no direct experimental evidence for deciding the nature of the upper electronic state, but a very good prediction can be made by considering the structure of the resonance series observed in this transition. According to the analysis only doublet series are excited and hence if upper state obeys Hund's case c (which is very likely) it has to be O_u^+. There are a number of possibilities for the electron configurations[12] which can be associated with this state. However, the long resonance series observed suggest that the transition involved has a very high transition probability and may correspond to the transition which is responsible for the Cordes[13] absorption bands. From these considerations, one may propose one possibility as the V state, $\sigma_g\pi_u^4\pi_g^4\sigma_u$, ${}^1\Sigma_u^+(O_u^+)$ for the upper state. However, the possibility of the electronic states ${}^1\Sigma_u^+(O_u^+)$ and ${}^3\Sigma_u^-(O_u^+)$ arising from the electron configuration $\sigma_g^2\pi_u^3\pi_g^3\sigma_u^2$ cannot be ruled out easily. It may be pointed out that one of these two states has been tentatively associated with the upper state at $T_v=47207$ cm^{-1} of the emission band system[14] 2730–2486 A.

ACKNOWLEDGMENTS

The author expresses his thankfulness to Dr. P. G. Wilkinson for his helpful suggestions and encouragement while working with the vacuum spectrograph. Sincere thanks are extended to Dr. Putcha Venkateswarlu for his interest in the work. The author is highly thankful to Professor R. S. Mulliken for his kind interest in the work and for his valuable suggestions and discussions.

[11] F. London, Trans. Faraday Soc. 33, 8 (1937).
[12] R. S. Mulliken, Phys. Rev. 46, 549 (1934).
[13] H. Cordes, Z. Physik 97, 603 (1935).
[14] R. D. Verma. Proc. Indian Acad. Sci. 48, 197 (1958).

THE JOURNAL OF CHEMICAL PHYSICS VOLUME 32, NUMBER 3 MARCH, 1960

Thermodynamic Properties of Nonstoichiometric Urania-Thoria Solid Solutions

S. Aronson and J. C. Clayton
Bettis Atomic Power Laboratory, Pittsburgh 30, Pennsylvania

(Received September 28, 1959)

A solid state electrochemical technique has been used to obtain thermodynamic information on urania-thoria solid solutions of compositions $U_yTh_{1-y}O_{2+x}$ with values of y of 0.9 to 0.3 and values of x of 0.02 to 0.16. The electrochemical cells were of the type Fe, FeO | (ZrO_2+CaO) | $U_yTh_{1-y}O_{2+x}$, Pt. Measurements were made at temperatures of 1150–1350°K.

Partial molar free energies, entropies, and enthalpies of solution of oxygen in the solid solutions were calculated. The partial molar free energy decreases negatively with increasing thorium content for thorium concentrations greater than 30 atomic percent. The partial molar entropy increases negatively with increasing oxygen content or with increasing thorium content.

The experimental results are discussed in connection with a mechanism of interstitial solution of oxygen ions in the fluorite lattice. A thermodynamic equation for the entropy is developed which gives semiquantitative agreement with the experimental data.

I. INTRODUCTION

URANIUM dioxide and thorium dioxide form a continuous series of solid solutions in which the fluorite structure is maintained.[1] Anderson *et al.*[2] studied the oxidation of these solid solutions. They found that, for uranium contents greater than 50 atomic percent, the solid solutions, $U_yTh_{1-y}O_{2+x}$, could incorporate into interstitial sites in the lattice up to a value of x equal to 0.32–0.34 without destroying the fluorite structure. At higher thorium contents, the maximum uptake of oxygen decreased with increasing thorium content.

Thermodynamic information on the nonstoichiometric solid solutions having high thorium contents ($y<0.25$) have been reported by Anderson *et al.*[2] and by Roberts *et al.*[3] The pressures of oxygen in equilibrium with the solid solutions increased with decreasing uranium content.[2] The partial molar heats of solution of oxygen in the solid decreased negatively with de-

[1] W. Trzebiatowski and P. W. Selwood, J. Am. Chem. Soc. 72, 4504 (1950).
[2] Anderson, Edgington, Roberts, and Wait, J. Chem. Soc. 1954, 3324.
[3] Roberts, Russell, Adwick, Walter and Rand, "Proceedings of the Second United Nations International Conference on the Peaceful Uses of Atomic Energy," Geneva, September 1–13, 1958, Vol. 28, p. 215.

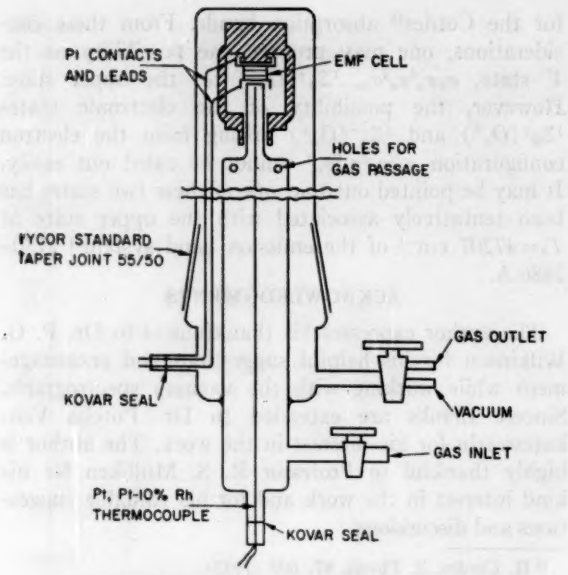

FIG. 1. Apparatus for emf measurements of the cells Fe, FeO | (ZrO_2+CaO) | $U_yTh_{1-y}O_{2+x}$, Pt.

creasing uranium content.[3] These data indicate an increasing resistance to oxidation of the U^{4+} ions as the uranium content of the solid solution decreases.

In the present study, a solid state electrochemical technique was used to obtain thermodynamic data on urania-thoria solid solutions of compositions $U_yTh_{1-y}O_{2+x}$ with y values of 0.9 to 0.3 and values of x of 0.02 to 0.16. The results are compared with the data obtained in a similar study on nonstoichiometric uranium dioxide.[4] The effect of the presence of thorium on the thermodynamic properties of the uranium dioxide lattice is discussed in the light of current theories of nonstoichiometry in ionic solids.

II. EXPERIMENTAL

The experimental procedures have been discussed in some detail in a previous paper[4] on nonstoichiometric uranium dioxide. The discussion in this section is, therefore, limited to additional information and modifications of the apparatus.

The electrochemical cells were of the type Fe, FeO | (ZrO_2+CaO) | $U_yTh_{1-y}O_{2+x}$, Pt. The solid electrolyte was a solid solution of 15 mole percent CaO in ZrO_2. The apparatus used was a modified form of that described by Kiukkola and Wagner.[5] A schematic of the apparatus† is shown in Fig. 1. The three pellets comprising the cell were placed one upon the other and were held together by the weight of the upper quartz support. Electrical contact was made through two platinum wires welded to flat pieces of platinum foil sandwiched between the quartz and the pellet surfaces. The Pt, Pt−10% Rh thermocouple was positioned inside the quartz tube which supported the pellets from below. After insertion of the pellets, a quartz tube was fitted by a ground joint over the apparatus and the system was evacuated. An inert atmosphere was maintained around the pellets by flowing a slow stream of helium, dried over magnesium perchlorate, through the system. The gas entered the apparatus through the inlet stopcock, passed through the inner tube and through the holes below the pellets, and exited by way of the outer tube through a second stopcock. Heat was supplied by a tube furnace which was lowered over the apparatus.

The solid solutions of compositions $U_yTh_{1-y}O_2$, with y values of 0.90, 0.71, 0.52, and 0.29, were prepared from Fisher Certified thorium nitrate and uranyl nitrate. A solution of these salts was precipitated by ammonium hydroxide, dried at 100°C, decomposed in air at 600°C, and reduced in hydrogen at 1300°C for 24 hours. X-ray patterns of the material showed the presence of a single phase fluorite structure in all cases. Measurements of the lattice parameters were made and were in agreement, within ±0.003 A, with the work of Slowinski and Elliot,[6] indicating that homogeneous solid solutions were obtained. Controlled amounts of oxygen were added to the samples by controlled oxidation in oxygen at temperatures of 200–400°C. The oxi-

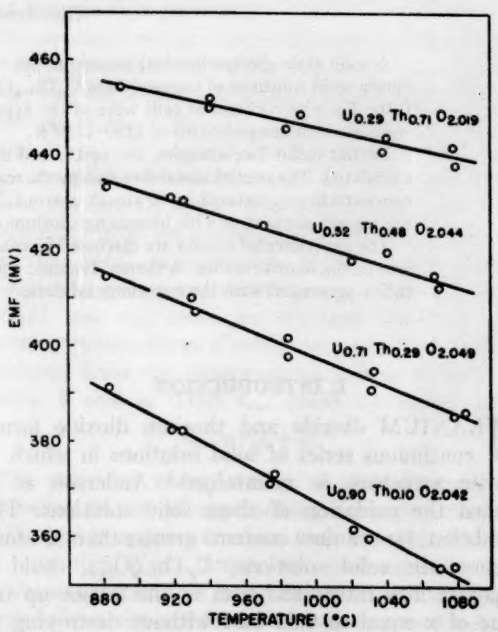

FIG. 2. Electromotive force of cells Fe, FeO | (ZrO_2+CaO) | $U_yTh_{1-y}O_{2+x}$, Pt.

* The information upon which this paper is based was presented at the 136th meeting of the American Chemical Society, Atlantic City, New Jersey, September 13, 1959.

[4] S. Aronson and J. Belle, J. Chem. Phys. **29**, 151 (1958).

[5] K. Kiukkola and C. Wagner, J. Electrochem. Soc. **104**, 379 (1957).

† The apparatus was designed by J. E. Rulli of this laboratory.

[6] E. Slowinski and N. Elliot, Acta Cryst. **5**, 768 (1952).

dized samples were annealed for a week at 800°C in vacuo to homogenize the oxygen. X-ray patterns of these materials showed fluorite structures with contracted lattices in agreement with Anderson *et al.*[2] The powders were pressed into pellets about 0.1-in. thick at about 60 tsi.

The oxygen contents of the $U_yTh_{1-y}O_{2+x}$ pellets were determined by the weight changes on reduction in hydrogen to $U_yTh_{1-y}O_2$ at 800°C. A spring balance made of Nispan C alloy was employed for the determinations. The method of analysis was checked in several cases by chemical analysis for uranium (IV) and uranium (VI). The estimated accuracy of the oxygen determinations is ± 0.01 in the value of x.

III. RESULTS

Figures 2 and 3 show plots of emf as a function of temperature for some selected compositions of $U_yTh_{1-y}O_{2+x}$. The variation of emf with temperature was approximately linear in all cases. The method of calculation of the partial molar free energies $\bar{F}_{O_2}$, entropies $\bar{S}_{O_2}$, and enthalpies H_{O_2} of solution of oxygen in the solid solutions and the pressures of oxygen in equilibrium with the solid solutions has been discussed in the previous paper on nonstoichiometric uranium dioxide.[4] The partial molar properties are defined as the changes in the properties of the system which occur when a mole of oxygen is transferred from the gas phase at 1 atmos pressure to a large amount of the solid.

The thermodynamic data for the $U_yTh_{1-y}O_{2+x}$ compositions and the data previously obtained for UO_{2+x} are presented in Table I. The free-energy values are given for a temperature of 1250°K which is approximately in the middle of the temperature range studied. Although there is considerable scatter in the entropy and enthalpy data in Table I, it can be seen that the

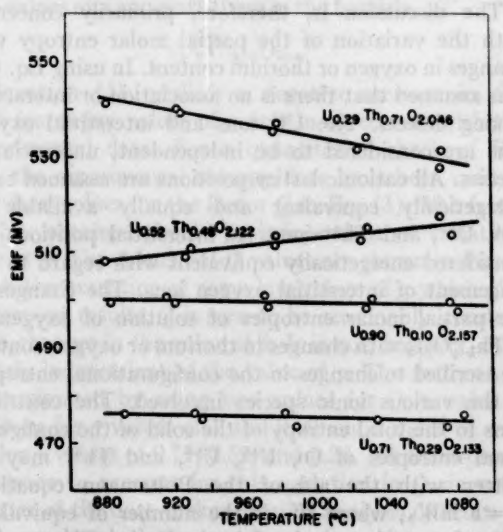

FIG. 3. Electromotive force of cells Fe, FeO | (ZrO_2+CaO) | $U_yTh_{1-y}O_{2+x}$, Pt.

TABLE I. Partial molar free energies, entropies and enthalpies of solution of oxygen in $U_yTh_{1-y}O_{2+x}$.

y[a]	x	$-\bar{F}_{O_2}$ (kcal/mole) 1250°K	$-\bar{S}_{O_2}$ (eu/mole)	$-\bar{H}_{O_2}$ (kcal/mole)
1	0.013	54.2	6.3	62
1	0.018	53.2	6.4	61
1	0.044	51.2	12.8	67
1	0.044	51.1	6.8	60
1	0.051	50.3	12.2	66
1	0.075	49.5	13.6	66
1	0.078	49.4	12.7	65
1	0.087	47.3	16.7	67
1	0.112	45.8	18.3	69
1	0.128	44.0	22.5	72
1	0.142	42.1	25.3	74
1	0.143	42.0	24.3	72
1	0.160	39.8	27.1	74
1	0.164	40.1	27.0	74
1	0.181	37.6	28.0	73
1	0.184	37.7	27.6	72
1	0.198	35.1	27.9	70
1	0.203	35.2	29.4	72
0.90	0.042	51.8	8	62
0.90	0.042	52.4	13	69
0.90	0.076	48.7	17	70
0.90	0.081	48.4	17	70
0.90	0.123	44.7	23	73
0.90	0.126	44.7	21	71
0.90	0.157	40.7	29	77
0.71	0.046	50.9	14	68
0.71	0.049	50.9	14	68
0.71	0.084	47.2	21	74
0.71	0.092	46.9	28	82
0.71	0.121	44.0	34	85
0.71	0.133	42.9	29	80
0.71	0.152	40.3	34	83
0.71	0.154	40.2	35	84
0.52	0.044	47.5	20	72
0.52	0.045	46.8	22	74
0.52	0.079	43.4	22	72
0.52	0.087	44.4	31	83
0.52	0.119	39.8	35	84
0.52	0.122	39.5	34	82
0.52	0.152	35.7	40	85
0.52	0.152	35.2	35	78
0.29	0.019	45.4	22	72
0.29	0.027	43.2	19	67
0.29	0.046	37.3	24	67
0.29	0.053	36.2	26	69
0.29	0.053	36.8	30	74
0.29	0.069	33.5	30	71
0.29	0.073	33.1	34	76

[a] The data for y values of 1 are taken from the work of S. Aronson and J. Belle.[4]

partial molar entropy increases negatively with increasing oxygen content or increasing thorium content and that there is some increase (negative) in the enthalpy values with increasing oxygen or thorium content. The partial molar free energies and, consequently, the oxygen pressures, are approximately the same for equal values of x in the range of y from 1 to 0.7. Plots of the log of the oxygen pressures *vs* oxygen contents for the various values of y are shown in Fig. 4 for a temperature of 1250°K.

IV. DISCUSSION

The oxidation of urania-thoria solid solutions is discussed on the basis of the following simple reaction

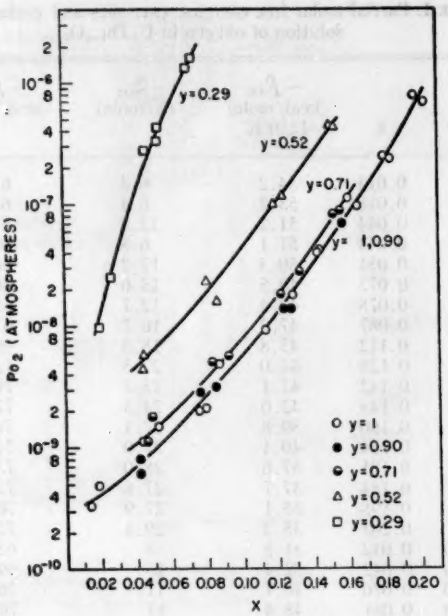

FIG. 4. Pressures of oxygen in equilibrium with $U_yTh_{1-y}O_{2+x}$ at 1250°K.

scheme:

$$O_2\,(\text{gas})+4U^{4+}+2\,\text{i.s.}=2O^{i}+4U^{5+}. \qquad (1)$$

The symbols i.s. and O^{i}, have the meanings, vacant interstitial sites and interstitial oxygen ions, respectively.

Equation (1) represents only one of several possible mechanisms. It would be well at this point to discuss the choice of Eq. (1) and some of the assumptions that are employed in its use. Equation (1) represents the oxidation reaction as the oxidation of U^{4+} ions by gaseous oxygen to form discrete U^{5+} ions and interstitial oxygen ions. An alternative approach would be to consider the reaction as one involving the removal of electrons from the valence band of the solid with the formation of positive holes. The choice between the two mechanisms depends upon the nature of the electronic structure of the solid. In the case of nonstoichiometry in TiO_2, for example, Buessem and Butler[7] have decided, on the basis of thermodynamic calculations, that an ionic representation is more suitable than a valence band picture. On the other hand, the band picture applies well in the case of ZnO.[8] Morin[9] has discussed the electronic structure of the 3*d* transition metal oxides and has concluded that, in the majority of cases, the 3*d* wave functions appear to be localized on the cations.

[7] W. R. Buessem and S. Butler, "Defect reactions in TiO_2," Conference on High Temperature Processes, Endicott House, Massachusetts Institute of Technology, June 23–27, 1958.
[8] D. G. Thomas, J. Phys. Chem. Solids **3**, 229 (1957).
[9] F. J. Morin in "*Semiconductors*," edited by N. B. Hannay (A.C.S. monograph, Reinhold Publishing Corporation, New York, 1959), Chap. 14.

The nature of the electronic structure of the uraniathoria solid solutions is not clear. Since the band picture is relatively complex, the simpler ionic picture has been chosen for discussion here. It is shown in the following discussion that this picture gives semiquantitative agreement with the thermodynamic data. In the previous paper on UO_{2+x},[4] the reaction was discussed in a superficial manner in terms of the valence band picture. As is seen below, the ionic mechanism is, at least, equally applicable in the case of UO_{2+x} and much easier to apply in the case of solid solutions.

The formation of U^{5+} ions rather than U^{6+} ions in Eq. (1) is assumed on the basis of the crystallographic data of Anderson *et al.*[2] on nonstoichiometric uraniathoria solid solutions. These workers found that the unit cell contracted as the average uranium valency increased from 4.0 to 5.0 and then began to expand. The results indicated that the U^{4+} ions were first transformed into discrete U^{5+} ions after which ionic groups, possible $(UO_2)^{++}$, were formed.

In applying Eq. (1), it would be convenient if a simple equilibrium relationship for an ideal solution could be written in which an equilibrium constant could be set equal to the product of the reaction product concentrations divided by the product of the reactant concentrations. A procedure of this type was adopted in the case of UO_{2+x}.[4] However, the use of such a procedure requires a constant partial-molar heat of solution, $\bar{H}_{O_2}$. The variation of $\bar{H}_{O_2}$ with changes in oxygen or thorium content, shown in Table I, appears to be real and outside the range of experimental error. An additional, related, factor which precludes the use of a simple equilibrium relationship is the relative constancy of the partial molar free energy $\bar{F}_{O_2}$ with changes in y for the range of y between 1 and 0.7. A larger variation of $\bar{F}_{O_2}$ with thorium content would be expected on the basis of a simple equilibrium relationship.

The discussion is, therefore, primarily concerned with the variation of the partial molar entropy with changes in oxygen or thorium content. In using Eq. (1), it is assumed that there is no association or interaction among defects. The U^{5+} ions and interstitial oxygen ions are considered to be independent, unassociated, species. All cationic lattice positions are assumed to be energetically equivalent and equally available to U^{4+}, U^{5+}, and Th^{4+} ions. All interstitial positions are considered energetically equivalent with regard to the placement of interstitial oxygen ions. The changes in the partial molar entropies of solution of oxygen in $U_yTh_{1-y}O_{2+x}$ with changes in thorium or oxygen content are ascribed to changes in the configurational entropies of the various ionic species involved. The contributions to the total entropy of the solid of the configurational entropies of O^{i}, U^{4+}, U^{5+}, and Th^{4+} may be written with the aid of the Boltzmann equation, $S_A=k\ \ln W_A$, where W_A is the number of equivalent ways of arranging species A in the lattice. The number of ways of arranging interstitial oxygen ions in the

interstitial positions in the lattice are $[N^i!/(N^i-N_{O^i})!N_{O^i}!]$. The number of ways of arranging the three cationic species in the cationic lattice positions are $[N^s!/N_{U^{5+}}!N_{U^{4+}}!N_{Th^{4+}}!]$. Here N^i is the number of interstitial sites; N_{O^i} is the number of interstitial oxygen ions; N^s is the number of cationic lattice positions; $N_{U^{5+}}$, $N_{U^{4+}}$ and $N_{Th^{4+}}$ are the number of U^{5+}, U^{4+} and Th^{4+} cations in the lattice. The contributions of the foregoing terms to the partial molar entropy of solution of oxygen in the solid $\bar{S}_{O_2}$ can be obtained by using Sterling's approximation and differentiating the entropy with respect to the number of gaseous oxygen molecules, N_{O_2}:

$$\bar{S}_{O_2}=-N(\partial S/\partial N_{O_2})=-N(\partial S/\partial N_{O^i})(dN_{O^i}/dN_{O_2})$$
$$-N(\partial S/\partial N_{U^{4+}})(dN_{U^{4+}}/dN_{O_2})+Q, \quad (2)$$

where

$$(\partial S/\partial N_{O^i})=-k\ln(N_{O^i}/N^i-N_{O^i}),$$
$$(\partial S/\partial N_{U^{4+}})=-k\ln(N_{U^{4+}}/N_{U^{5+}})$$

and

$$(dN_{O^i}/dN_{O_2})=-2, \quad (dN_{U^{4+}}/dN_{O_2})=4.$$

We have used the relationship $N_{U^{5+}}=N^s-N_{Th^{4+}}-N_{U^{4+}}$; S is the entropy of the system and N is Avogadro's number. The factor Q includes a term for the decrease in entropy which occurs upon removing one mole of oxygen from the gas phase and a term for the contribution to the vibrational entropy of the solid of the added interstitial oxygen ions. It seems reasonable to assume that Q does not vary greatly with changes in oxygen or uranium content. By using the fact that N^s is equal to N^i in the case of the fluorite structure, Eq. (2) can be easily changed into the form

$$\bar{S}_{O_2}=-2R\ln[x/(1-x)]-4R\ln[2x/(y-2x)]+Q. \quad (3)$$

The values of x and y are those in the formula,

$$U_yTh_{1-y}O_{2+x}.$$

Equation (3) predicts a negative increase in $\bar{S}_{O_2}$ with increasing values of x or y in agreement with the experimental data. For a quantitative check of Eq. (3), the experimental entropy data have been used to calculate values for the factor Q in Eq. (3). The factor Q thus obtained should be independent of variations in x or y. The calculated Q values are shown in Fig. 5. With the exception of some low values of x which give discrepant results, Q is seen to be reasonably constant with changes in the value of x. It is not, however, completely independent of the value of y. The data can be approximated by using two values for Q, a value of -38 eu for y values of 1 and 0.90 and a value of -43 eu for y values of 0.71, 0.52, and 0.28. No attempt will be made to account for this variation in Q since the scatter of the data makes detailed analysis difficult.

A rough calculation can be made to determine if Q values close to -40 eu, as obtained in the foregoing,

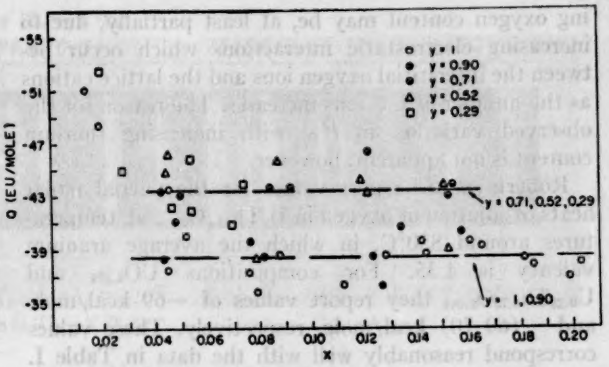

FIG. 5. Calculation of Q for $U_yTh_{1-y}O_{2+x}$ from Eq. (3).

are reasonable. It was noted that the factor Q consists primarily of two terms. The first term, the decrease in entropy which occurs upon removal of a mole of oxygen from the gas phase at one atmosphere pressure is the negative of the molar entropy of oxygen gas and has a value of -60 eu at 1250°K.[10] This leaves approximately 20 eu for the contribution to the vibrational entropy of the solid of 2 gram-atomic weights of interstitial oxygen ions. An estimate of the vibrational frequency of these ions can be obtained from the Einstein equation for the vibrational entropy,[8] assuming $3N$ degrees of freedom:

$$S=-3(2R)\left\{\ln[1-\exp(-h\nu/kT)]-(h\nu/kT)\left[\frac{\exp(-h\nu/kT)}{1-\exp(-h\nu/kT)}\right]\right\}.$$

From this equation, the calculated vibrational frequency at 1250°K is 1×10^{13} sec^{-1}. If it is assumed that the interstitial ions vibrate in phase with the lattice ions, the calculated frequency for the urania-thoria solid solutions can be compared to frequencies obtained for other crystalline solids. In the case of zinc oxide, Thomas has established that interstitial zinc ions vibrate in phase with the lattice ions.[8] A qualitative comparison with other crystalline solids[8,11] indicates that the calculated frequency, 1×10^{13} sec^{-1}, is reasonable. Quantitative comparison cannot be made, however, because of the lack of precise information on the values of the vibrational frequencies in urania and thoria and because of the approximate nature of the Einstein relationship.

The values obtained for the partial molar heats of solution $\bar{H}_{O_2}$ are now briefly considered. There is a negative increase in the partial molar heat of solution with increasing oxygen content although the variation is not regular. This negative increase in $\bar{H}_{O_2}$ with increas-

[10] L. Brewer in *The Chemistry and Metallurgy of Miscellaneous Materials: Thermodynamics*, edited by L. L. Quill (McGraw-Hill Book Company, Inc., New York, 1950), Paper 5.

[11] M. Born and K. Huang, *Dynamical Theory of Crystal Lattices* (Oxford University Press, New York, 1954), Chap. 2.

ing oxygen content may be, at least partially, due to increasing electrostatic interactions which occur between the interstitial oxygen ions and the lattice cations as the number of U^{5+} ions increases. The reason for the observed variation in $\bar{H}_{O_2}$ with increasing thorium content is not apparent, however.

Roberts *et al.*[3] report values for the partial molar heats of solution of oxygen in $U_yTh_{1-y}O_{2+x}$, at temperatures around 850°C, in which the average uranium valency is 4.35. For compositions $UO_{2.175}$ and $U_{0.25}Th_{0.75}O_{2.044}$ they report values of -69 kcal/mole and $-(60$–$70)$ kcal/mole, respectively. These values correspond reasonably well with the data in Table I. At higher thorium contents ($0.06>y>0.005$), the partial molar heats range from -44 kcal/mole to -14.5 kcal/mole. The reason for these low values is not apparent. The low values cannot be explained on the basis of the simple oxidation mechanism proposed in the foregoing.

In the preceeding discussion, nonstoichiometry in urania-thoria solid solutions has been treated in terms of simple solution theory. The fact that semiquantitative agreement with the thermodynamic data was obtained indicates that this approach has merit. However, the inability of the theory to account for some of the entropy and enthalpy data, as noted, indicates that considerable refinement of the theory and more precise data are required for a full understanding of the thermodynamic properties of these solid solutions.

ACKNOWLEDGMENTS

This work was performed under contract AT-11-1-GEN-14. The authors are grateful to the Atomic Energy Commission and the Westinghouse Electric Corporation for permission to publish this data.

The authors wish to acknowledge the able assistance of J. E. Rulli and F. C. Schrag in carrying out the experimental work.

THE JOURNAL OF CHEMICAL PHYSICS VOLUME 32, NUMBER 3 MARCH, 1960

New Emission Bands of Forbidden Systems of Nitrogen in the Vacuum Ultraviolet Region

M. OGAWA AND Y. TANAKA

Geophysics Research Directorate, Air Force Cambridge Research Center, Air Research and Development Command, Laurence G. Hanscom Field, Bedford, Massachusetts

(Received September 23, 1959)

Using a 2-m vacuum spectrograph and an ordinary transformer discharge through mixtures of N_2 with argon and xenon, we observed two new systems of N_2 emission bands, one for each mixture, in the region between 1550 and 2250 A. According to the vibrational analysis, the bands, which were excited in the mixture of (N_2+A), are due to the transition ($a'\,^1\Sigma_u^- - X\,^1\Sigma_g^+$), and the bands, which were excited in the mixture of (N_2+Xe), are due to the transition ($^3\Sigma_u^- - X\,^1\Sigma_g^+$). The present results are in good agreement with those of Wilkinson and Mulliken whose observations were made for the same systems of bands in absorption.

INTRODUCTION

ACCORDING to Mulliken's[1] recent calculation of the low-lying electronic states of N_2, there are four stable states, $^3\Delta_u$, $^3\Sigma_u^-$, $a'\,^1\Sigma_u^-$, and $w\,^1\Delta_u$, in addition to the well-known states, $A\,^3\Sigma_u^+$, $B\,^3\Pi_g$, and $a\,^1\Pi_g$, in the energy range from about 6 ev to 9 ev. Among these states, the $a'\,^1\Sigma_u^-$ is the common lower state of the fifth positive (or Van der Ziel) system ($x\,^1\Sigma_g^- - a'\,^1\Sigma_u^-$) and Kaplan's first system ($y\,^1\Pi_g - a'\,^1\Sigma_u^-$);[2] the $w\,^1\Delta_u$ state is the lower state of Kaplan's second system ($y\,^1\Pi_g - w\,^1\Delta_u$).[2] Recently, Kistiakowsky and his co-worker[3] observed a new system of emission bands in the near-infrared region in the afterglow of nitrogen at liquid nitrogen temperature, and they called them "Y bands." LeBlanc and his co-workers[4] also independently observed the same bands in their work on the afterglow of nitrogen at liquid nitrogen temperature, and they suggested that the upper state of the bands is either $^3\Sigma_u^-$ or $^3\Delta_u$, most probably the latter, the lower state being $B\,^3\Pi_g$. Shortly after the above findings, Wilkinson and Mulliken[5] observed three forbidden systems of N_2, ($A\,^3\Sigma_u^+ - X\,^1\Sigma_g^+$), ($^3\Sigma_u^- - X\,^1\Sigma_g^+$), and ($a'\,^1\Sigma_u^- - X\,^1\Sigma_g^+$), in absorption, and determined accurate molecular constants for the states involved in the transitions. Furthermore, according to their analysis, the upper state of the afterglow bands mentioned above is the $^3\Sigma_u^-$ rather than the $^3\Delta_u$. Independent of their work, we were attempting to observe possible

[1] R. S. Mulliken, Technical Report, Laboratory of Molecular Structure and Spectra, Univ. of Chicago (1956); *The Threshold of Space* (Pergamon Press, New York, 1956), p. 169.
[2] A. Lofthus and R. S. Mulliken, J. Chem. Phys. **26**, 1010 (1957).
[3] G. B. Kistiakowsky and P. Warneck, J. Chem. Phys. **27**, 1417 (1957).
[4] LeBlanc, Tanaka, and Jursa, J. Chem. Phys. **28**, 979 (1958).
[5] P. G. Wilkinson and R. S. Mulliken (to be published).

FIG. 1. $a'\,^1\Sigma_u^- - X\,^1\Sigma_g^+$

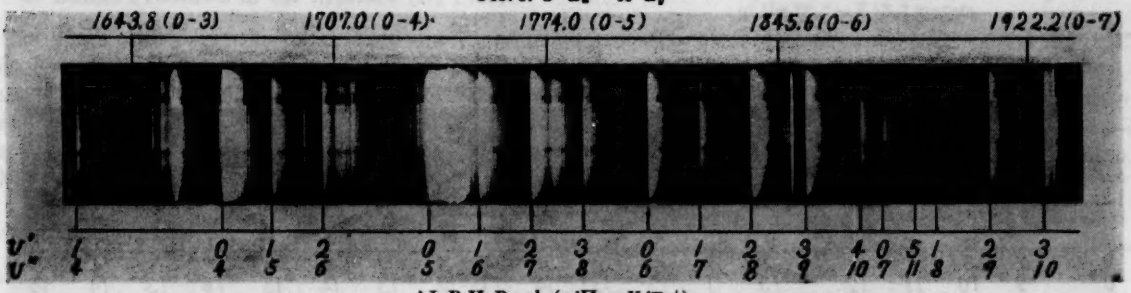

TABLE I. Wavelengths and wave numbers of the $a'\,^1\Sigma_u^- - X\,^1\Sigma_g^+$ system.

v', v''	I	λ_{obs}(A)	ν_{obs}(cm^{-1})	ν_{calc}(cm^{-1})	O—C	ΔG_{obs}	ΔG_{calc}[a]
0, 3	3	1643.84	60 832.4	60 828.7	+3.7		
						2250.1	2244.0
0, 4	4	1707.00	58 582.3	58 584.6	−2.3		
						2212.5	2215.3
0, 5	4	1774.00	56 369.8	56 369.4	+0.4		
						2188.1	2186.5
0, 6	3	1845.64	54 181.7	54 182.9	−1.2		
						2156.6	2157.6
0, 7	2	1922.15	52 025.1	52 025.3	−0.2		
						2129.1	2128.7
0, 8	1	2004.17	49 896.0	49 896.6	−0.6		

[a] Calculated by using Lofthus' values for vibration constants.

emission bands, which might be ascribed to the forbidden transitions between the ground state and the four states mentioned earlier, for the purpose of finding their exact excitation energies and of finding any contribution of these states to the production of the nitrogen afterglow. Consequently, at approximately the same time when Wilkinson and Mulliken observed their absorption bands, we observed the same bands due to the transitions ($^3\Sigma_u^- - X\,^1\Sigma_g^+$) and ($a'\,^1\Sigma_u^- - X\,^1\Sigma_g^+$)[6] in emission.

EXPERIMENTAL

A Hilger 2-m normal-incidence type vacuum spectrograph was used. A Π-shaped discharge tube, 5 mm in diam and 25 cm in length with a thin LiF window at one end, was filled with 2–4 mm Hg of pure N_2 and 1–5 cm Hg of argon or xenon. The tube was excited by a transformer, 15 kv 0.9 kva, with a primary current of about 7 amp. At the beginning of the discharge, the spectrum in the visible region showed the strong first and second positive bands. But with continuation of the discharge, the amount of N_2 decreased gradually while the rare gas pressure remained apparently unchanged. After about 20 hours operation the visual spectrum did not show any nitrogen bands. The bands of present interest usually appeared at that time during the discharge when the impurity of NO (γ bands) and CO (4th positive bands) disappeared, while there still remained in the tube a small amount of nitrogen with the rare gas being used. Because the present bands are extremely weak, 3–5 hours exposure time was necessary to photograph them with a 20-μ slit width and with SWR film.

RESULTS

Bands Produced in the Mixture (N_2+A)

Six new bands, all fitting very well into one progression, were observed in the region 1550–2250 A. They are reproduced in Fig. 1, from which you can see in that the individual bands showed almost no head but a clear shading toward the red with an intensity alternation. The measurement was made at the shortest wavelength edge for each band, and the values are listed in Table I. Since most of them were superimposed with the higher rotational lines of the Lyman-Birge-Hopfield bands ($a\,^1\Pi_g - X\,^1\Sigma_g^+$), which are very strong, the discharge tube was cooled with liquid nitrogen to remove the

TABLE II. Wavelengths of $v''=0$ progression of the $a'\,^1\Sigma_u^- - X\,^1\Sigma_g^+$ system.

	Wilkinson and Mulliken[a]		Present	
v', v''	ν_{obs}(cm^{-1})	λ_{obs}(A)	ν_{calc}(cm^{-1})	λ_{calc}(A)
0, 0			67 732	1476.4
1, 0	69 244.18	1444.16	69 236	1444.3
2, 0	70 727.87	1413.87	70 717	1414.1
3, 0			72 175	1385.5
4, 0	73 623.0	1358.27	73 610	1358.5
5, 0	75 034.82	1332.71	75 022	1332.9

[a] Their values are of the band origins.

[6] M. Ogawa and Y. Tanaka, J. Chem. Phys. 30, 1354 (1959).

FIG. 2. $^3\Sigma_u^- - X\,^1\Sigma_g^+$

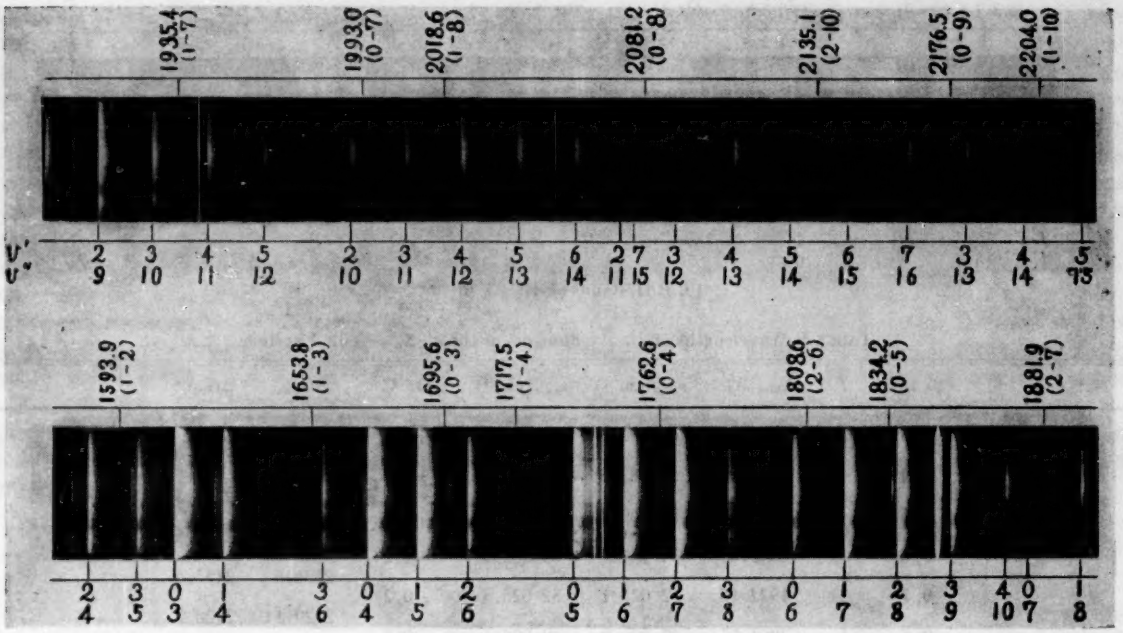

L.B.H. Bands ($a\,^1\Pi_g - X\,^1\Sigma_g^+$)

obscurity through a reduction of the rotational temperature.

The wave number differences of the consecutive bands agree very well with the calculated ΔG values of the ground state ($X\,^1\Sigma_g^+$) as is shown in Table I. This fact indicates that the present bands form a single progression produced by a transition from a single vibrational level of a certain upper state to the vibrational levels $v=3$, 4, 5, 6, 7, and 8 of the ground state. If one assumes that the upper vibrational level is $v=0$, the bands are expressed by the following equation:

$$\nu_{0v''}=68\,907.5-2358.07(v''+\tfrac{1}{2})+14.188(v''+\tfrac{1}{2})^2 +0.0124(v''+\tfrac{1}{2})^3. \quad (1)$$

where the vibration constants of $X\,^1\Sigma_g^+$ given by Lofthus[7] are adopted. The wave numbers of the corresponding bands calculated with this equation are shown in Table I, column 5, and are compared in column 6 with those of the observed values. The T_{00} of the upper state is 67732.0 cm^{-1} (8.398 ev), and this is fairly close to the value $T_{00}\sim$70 700 cm^{-1} of $^3\Sigma_u^-$ and $a'\,^1\Sigma_u^-$, which is theoretically estimated by Mulliken.[1] He also estimated the value $T_{00}\sim$ 60 500 cm^{-1} for $^3\Delta_u$ but this may be excluded from the present consideration because the value is too small to be compared with that of the present value. Gaydon[8] also estimated the value $Te=$ 60 000 cm^{-1} for $a'\,^1\Sigma_u^-$, which is about 1.33 ev smaller than Mulliken's value. As mentioned earlier, only a single branch, which is headless, was observed in the present bands, and among the electronic states mentioned earlier, only $a'\,^1\Sigma_u^-$ gives a single Q branch combining with the ground state. This strongly indicates that the upper state of the present bands is $a'\,^1\Sigma_u^-$.

At about the same time that we were looking for the forbidden bands of N_2 in the vacuum region in emission, Wilkinson and Mulliken[5] were working on the same bands in absorption, using a high order of their 6-m vacuum spectrograph. They observed, among others, four weak absorption bands due to the transition ($a'\,^1\Sigma_u^- - X\,^1\Sigma_g^+$), which are shown in Table II. They observed only the Q branch in the individual bands. This is compatible with our observation of the present bands, and their value of T_{00} for the $a'\,^1\Sigma_u^-$ state is 67 738.18 cm^{-1} (8.398 ev) which is also in good agreement with that of the upper state of the present bands. Calculations were made for their bands by using the present data combined with the constants of the $a'\,^1\Sigma_u^-$ state, listed in Herzberg's book,[9] and the results are shown in the last two columns of Table II. The average difference between the two is about 10 cm^{-1} (0.2 A), and we consider that the agreement is very good. We did not intend to make a rotational analysis of the bands because of insufficient resolution of the spectrograph used. However, the evidence stated above strongly supports the assumption that the present bands are due to the transition ($a'\,^1\Sigma_u^- - X\,^1\Sigma_g^+$).

[7] A. Lofthus, Can. J. Phys. **34**, 780 (1956).
[8] A. G. Gaydon, Proc. Roy. Soc. (London) **A182**, 286 (1944).
[9] G. Herzberg, *Spectra of Diatomic Molecules* (D. Van Nostrand Co., Inc., Princeton, New Jersey, 1950).

B. Bands Produced in the Mixture (N_2+Xe)

The bands observed in this mixture are reproduced in Fig. 2, and their wavelengths are shown in the upper part of the reproduction with the vibrational assignments. As one can see in the figure, the individual bands have double heads and shade toward the red. The observed wavelengths are listed in Table III. If

TABLE III. Wavelengths and wave numbers of the $^3\Sigma_u^- - X\,^1\Sigma_g^+$ system.

v', v''	I	λ_{obs}(A)	ν_{obs}(cm^{-1})	ν_{calc}(cm^{-1})	O−C
1, 2	1.0	1593.94	63 737.6		
	1.0	94.63	710.5	62 713.3	−2.8
1, 3	1.0	1653.82	60 466.1		
	1.0	54.48	442.0	60 440.7	+1.3
0, 3	1.0	1695.61	58 975.8		
	0.7	96.50	944.9	58 947.0	−2.1
1, 4	1.0	1717.47	59 225.2		
	0.5	18.36	195.0	58 196.7	−1.7
0, 4	1.5	1762.64	56 733.1		
	1.5	63.45	707.0	56 703.0	+4.0
2, 6	0.5	1808.57	55 292.3		
	0.5	09.31	269.7	55 266.7	+3.0
0, 5	1.5	1834.17	54 520.6		
	2.0	35.33	486.1	54 487.8	−1.7
2, 7	0.5	1881.93	53 136.9		
	0.5	83.01	106.5	53 109.1	−2.6
1, 7	0.5	1935.37	51 669.7		
	0.3	36.59	637.2	51 637.4	−0.2
0, 7	1.0	1993.01	50 175.4		
	0.8	94.30	142.9	50 143.7	−0.8
1, 8	0.8	2018.60	49 539.3		
	0.5	19.78	510.3	49 508.7	+1.6
0, 8	0.8	2081.23	48 048.5		
	0.5	82.54	018.3	48 015.0	+3.3
2, 10	1.0	2135.09	46 836.4		
	0.8	36.33	809.2	46 810.2	−1.0
0, 9	0.5	2176.47	45 946.0		
	0.2	78.06	912.4	45 915.3	−2.9
1, 10	1.0	2204.02	45 371.6		
	0.8	05.54	340.4	45 338.5	+1.9
2, 11	1.5	2232.18	44 799.3		
	1.0	33.68	769.2	44 768.7	+0.5

we assume the quantum assignment shown in the table, the ΔG values of the present lower state agree very well with those of the ground state, and the entire group of bands is expressed by the following equation,*

$$\nu_{v'v''} = 66\,270.8 + 1515.7(v'+\tfrac{1}{2}) - 11.00(v'+\tfrac{1}{2})^2 - 2358.07(v''+\tfrac{1}{2}) + 14.188(v''+\tfrac{1}{2})^2 + 0.0124(v''+\tfrac{1}{2})^3, \quad (2)$$

* In the equation, the values of the second head (the head at the longer wavelength) are used.

TABLE IV. Wavelengths and wave numbers of $v''=0$ progression of the $^3\Sigma_u^- - X\,^1\Sigma_g^+$ system.

	Present		Wilkinson's	
v', v''	ν_{calc}(cm^{-1})	λ_{calc}(A)	ν_{obs}(cm^{-1})[a]	λ_{obs}(A)[b]
0, 0	65 850.4	1518.6		1518.0
1, 0	67 344.1	1484.9	67 340.62	1484.6
2, 0	68 815.8	1453.2		1453.1
3, 0	70 265.5	1423.2		1423.3

[a] This value is of the band origin.
[b] These values show the location of the bands.

where again Lofthus' values[7] of the vibration constants of $X\,^1\Sigma_g^+$ are adopted for the lower state. As derived from Eq. (2), the value of T_{00} of the upper state is 65 850.4 cm^{-1} (8.164 ev), and there is no known state whose T_{00} is close to this value other than the two states $^3\Sigma_u^-$ and $^3\Delta_u$, either of which is suggested as the upper state of the near-infrared bands produced by the nitrogen afterglow at liquid nitrogen temperature. Mulliken's[1] estimated values of T_{00} for $^3\Sigma_u^-$ and $^3\Delta_u$ are 70 700 cm^{-1} and 60 500 cm^{-1} respectively. In his absorption work, Wilkinson[10] observed four bands at 1518.0, 1484.6, 1453.1, and 1423.3 A and made a rotational analysis of the band at 1484.6 A, and found it to be the (1, 0) band of the transition ($^3\Sigma_u^- - X\,^1\Sigma_g^+$). According to our vibrational assignment, none of the observed bands has $v''=0$ (see Table III). However, as shown in Table IV, the wavelength of the (1, 0) band calculated by Eq. (2) agrees very well with that of Wilkinson's value of the band origin indicating that the present bands are most probably due to the transition ($^3\Sigma_u^- - X\,^1\Sigma_g^+$). Regarding the observed two heads, the one which is situated at shorter wavelength is probably formed by the S branch and the other is formed by the Q branch.

As suggested by Wilkinson,[10] it seems more likely to be considered that the upper state of the near-infrared bands produced by the low temperature afterglow of nitrogen is the $^3\Sigma_u^-$ instead of the $^3\Delta_u$. A recalculation of the near-infrared bands was attempted by using the data obtained in the above analysis. In this calculation,

TABLE V. Wave numbers of near-infrared bands of N_2 afterglow.

v', v''	ν_{calc} (cm^{-1})	ν_{obs} (cm^{-1})	v', v''	ν_{calc} (cm^{-1})	ν_{obs} (cm^{-1})
0, 0	6 551		6, 1	13 447	13 447
1, 0	8 043		7, 1	14 998	14 997
2, 0	9 512		8, 1	16 126	16 125
3, 0	10 957		6, 2	11 771	11 771
4, 0	12 379	12 381	7, 2	13 122	13 122
5, 0	13 777	13 778	8, 2	14 450	14 450
6, 0	15 152	15 151	7, 3	11 475	11 475
7, 0	16 503	16 504	8, 3	12 803	12 803
8, 0	17 831		8, 4	11 185	11 184
5, 1	12 072	12 073			

[10] P. G. Wilkinson (to be published).

we assumed that the observed lowest vibrational level of the upper state of the afterglow bands is $v=4$. A small modification for the anharmonicity term was also made by combining the ΔG values observed in the present bands with the ΔG values of the afterglow bands. The resulting formula for the afterglow bands is the following:

$$\nu_{v'v''}=6659.1+1515.7(v'+\tfrac{1}{2})-11.75(v'+\tfrac{1}{2})^2 -1734.11(v''+\tfrac{1}{2})+14.47(v''+\tfrac{1}{2})^2, \quad (3)$$

where the constants of the lower state are the values listed in Herzberg's book[9] for $B\,^3\Pi_g$. In Table V, the calculated wave numbers are compared with those of the observed bands.

ACKNOWLEDGMENT

The authors are indebted to Dr. P. G. Wilkinson and Professor R. S. Mulliken for their discussion concerning this work, and for making available their manuscripts in advance of publication.

THE JOURNAL OF CHEMICAL PHYSICS VOLUME 32, NUMBER 3 MARCH, 1960

Measured Transition Probabilities for the Schumann-Runge System of Oxygen*

CHARLES E. TREANOR AND WALTER H. WURSTER

Cornell Aeronautical Laboratory, Inc., Buffalo, New York

(Received September 21, 1959)

Transition probabilities for the Schumann-Runge system of O_2 have been measured in absorption in the wavelength region 2650–3900 A. Oxygen was heated in a shock tube to temperatures up to 4500°K, thereby populating high vibrational and rotational levels. Absorption spectra were photographed using a high-speed flash lamp and a large Littrow quartz spectrograph. Transition probabilities for the bands of three sequences, associated with the zero, 1st, and 2nd vibrational levels of the excited electronic state, yield an f value of 0.048 ± 0.008 which, when corrected for wavelength dependence, is about $\frac{1}{3}$ that determined in the vacuum ultraviolet. This corresponds to a decrease in transition probability with increasing internuclear separation. Line-width variations with temperature and density have also been measured. The optical diameter for O_2-O_2 collisions was determined as 6 A and for O_2-O collisions as 10 A.

I. INTRODUCTION

THE experimental determination of transition probabilities for transitions between excited states of an atom or molecule requires both a measurement of the absorbed or emitted radiation from known transitions and the evaluation of the population of the excited energy states of the gas under measurement. Gas samples excited in the usual ways for spectroscopic studies are generally not in thermodynamic equilibrium and are not uniformly excited along the optical path. For such cases intensity measurements alone are not sufficient to determine the transition probabilities. As a result, few data on transition probabilities are available, although the subject has long been of interest to astrophysicists[1] and currently is being studied by those concerned with missile and satellite reentry.[2,3]

In recent years, the shock tube has been used as a device for heating gases uniformly to high temperatures. The gases can be brought to thermodynamic equilibrium and quantitative absorption[4] and emission[3,5] studies performed. This paper presents a discussion of the use of the shock tube for absorption studies of heated O_2 and the determination of transition probabilities and line-width variations for the Schumann-Runge system.

The testing time available for shock-tube experiments ($\sim$1 msec) is not, in general, adequate for high-resolution emission spectroscopy because of the limited intensity of the emitted light. This difficulty is circumvented in absorption studies, where a high-speed, high-intensity light source can be used to provide the necessary plate exposure. The testing time is more than sufficient to permit thermodynamic equilibrium to be established for simple gases. The temperatures available are many times greater than can be obtained with furnaces; they are sufficient to populate high molecular vibrational levels and even to produce complete dissociation of diatomic molecules. Thus, it is possible to perform quantitative absorption measurements of spectra that are usually observed only in emis-

* This paper is based on research supported by the U. S. Air Force through the Air Force Office of Scientific Research, ARDC, under Contract No. AF 49(638)-269. The Combustion Dynamics Division was the monitoring agency for this research.

[1] For a review of the data available as of 1955, see Trans. Intern. Astron. Union **IX**, 214 (1957).

[2] R. E. Meyerott, Lockheed Aircraft Corp., Rept. No. LMSD-2264 (November 8, 1957).

[3] Keck, Camm, and Kivel, J. Chem. Phys. **28**, 723 (1958).

[4] Wurster, Treanor, and Glick, J. Chem. Phys. **29**, 250 (1958).

[5] Keck, Camm, Kivel, and Wentink, Ann. Phys. (N. Y.) **7**, 1 (1959). J. G. Clouston and A. G. Gaydon, Nature **180**, 1342 (1957). W. H. Wurster and H. S. Glick, J. Chem. Phys. **27**, 1218 (1957).

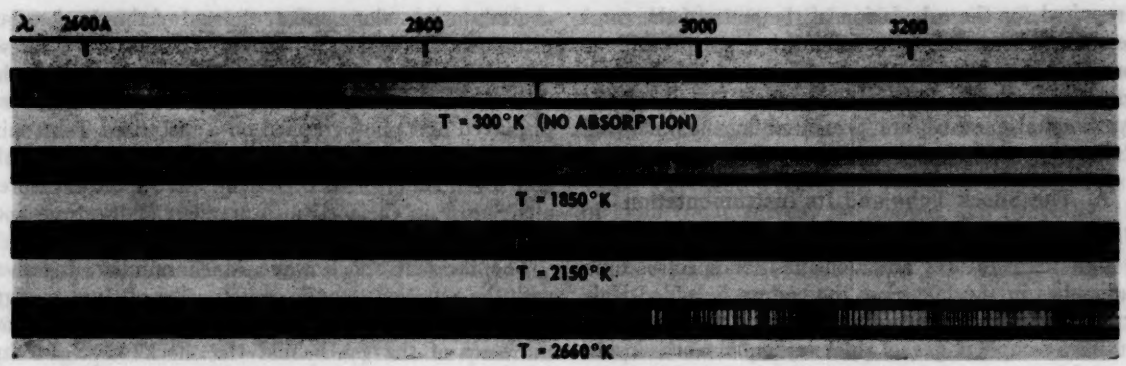

FIG. 1. Ultraviolet absorption spectra of oxygen at varying temperatures. Optical pathlength~50 cm-atmos. ($L=6.4$ cm, $\rho\sim 8\rho_0$).

sion. In the experiments described in this paper absorption was measured from as high as the 17th vibrational level of the ground state of O_2. Spectra obtained at various temperatures are shown in Figs. 1 and 2.

The present studies began with an investigation of the absorptive properties of air heated to temperatures up to about 5000°K. These experiments showed[4] that, in the ultraviolet region of the spectrum, molecular oxygen was the major absorbing constituent at these temperatures and that a separate study of the O_2 absorption was warranted. The experiments reported herein were performed with pure oxygen, and have employed an optical system capable of high wavelength resolution.

The study of spectral line widths for transitions between excited energy states is a second subject limited by the lack of knowledge of the state of the excited gas. The absolute magnitude of the collision broadening of lines cannot be determined theoretically in a reliable manner. This broadening is usually expressed in terms of the "optical cross section" of the colliding particles and the frequency of collision. Separate experimental study of line-width dependence on the temperature and density therefore yields the optical cross section and permits a discussion of the broad-band emission and absorption of radiation. The range of conditions available in the shock tube, as far as both temperature and density are concerned, admit of a considerable variation in the width of the spectral lines of O_2. With the spectrometer used in the present studies it was not possible to observe the Doppler broadening of the spectral lines ($\Delta\lambda<0.03$ A), but tests at high density (up to 8 atmos density at 3000°K) resulted in collision broadened lines up to 0.8 A in half-width. The half-widths of the absorption lines have been correlated with test conditions in the shock tube, and optical cross sections determined for O_2-O_2 and O_2-O collisions.

II. EXPERIMENTAL

All measurements were made on the photographed absorption spectrum of oxygen in the near ultraviolet. Continuum radiation from a flash-lamp light source was rendered parallel, sent through the heated gas sample, and refocused on the entrance slit of a large Littrow quartz spectrograph. The resultant absorption spectrum was photographed on standard spectrograph plates. The gas sample was contained in a shock tube which was suitably instrumented for synchronization of the optical system and for the accurate measurement of the incident shock wave velocity. This measurement

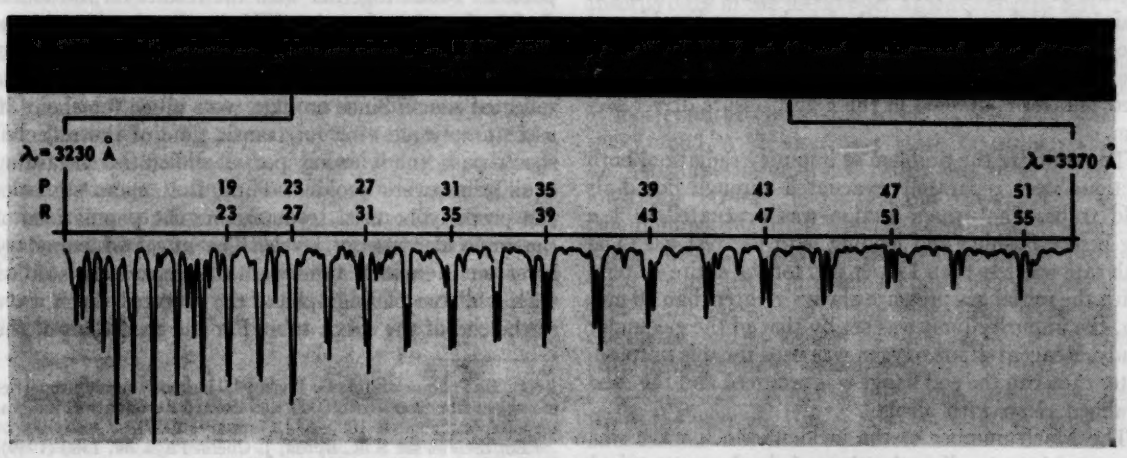

FIG. 2. Absorption spectrum of the (0, 13) band. $T=3410$ K, $\rho=3.6\rho_0$.

is required for the calculation of the state of the compressed and heated test gas. In addition, optical calibrations for slit width, wavelength, and emulsion response were recorded on each spectrum plate. Details of the experimental method are presented in the following sections.

A. The Shock Tube and Its Instrumentation

The advantage of using a shock tube to process gases to high temperatures and densities for spectroscopic studies lies in the fact that the energy is added uniformly and almost instantaneously to the gas. One obtains a sample of gas, of thickness equal to the inside dimension of the tube, whose thermodynamic state variables are known and which remains in equilibrium for a short interval of time.

Shock tubes consist primarily of two sections of tube separated by a diaphragm. The driver section contains gas at high pressures, which, upon diaphragm rupture, expands into the driven section and generates a shock wave through the test gas contained therein. This incident shock wave heats, compresses and accelerates the gas, and upon reflection at the closed end of the tube, processes the gas further by bringing it to rest at still higher temperatures and densities. The gas remains at these conditions (neglecting radiation loss and convective cooling) until further disturbances, resulting from interactions with the advancing driver gas, arrive at the end of the tube. For the studies reported here the oxygen temperatures ranged from 1500° to 5000°K and the densities from 0.5 to 8 times normal density, with testing times of 50 to 300 μsec.

The driver and driven sections of the shock tube used in this study were 3 and 14 ft long, respectively. They were constructed of steel, with a working pressure of several thousand psi and Kanigen- and chrome-plated internally for abrasion resistance and cleanliness. The driven section was $1\frac{1}{2}\times 2\frac{1}{2}$ in. in cross section and equipped with an observation section having quartz windows spanning the $2\frac{1}{2}$-in. dimension near the reflecting end of the shock tube. The diaphragms were made of stainless steel and were scribed to be near breaking at pre-set pressures. The runs were initiated by piercing the center of the scribed pattern with a solenoid operated plunger contained in the high-pressure driver section.

To minimize the problem of impurity radiation, both sections were separately evacuated through liquid-air cold traps. The driven section was evacuated to 1 μ Hg before flushing and loading with the test gas. The leak rate was less than 1 μ per min for the entire system. With the initial gas pressure always greater than 10 mm Hg, the impurity limit was set by that of the gas under study. Reagent-grade oxygen was used for this purpose. After each run the end flange was removed and the tube swabbed clean with alcohol.

The Mach number of the incident shock wave was measured by recording the time of shock wave arrival at five stations along and at the end of the shock tube, using thin film resistance gauges. The outputs of these gauges served to trigger multivibrator circuits which, upon differentiation, provided shaped signals that were displayed and photographed on a rasterized Tektronix 535 oscillscope. The gauge response was at the sub μsec level. An error of 1% in the wave speed measurement arose in the final measurement of the time and distance intervals.

The incident shock wave Mach number, together with the equations for the conservation of mass, energy and momentum across the shock, are used to determine the state of the gas behind the shock wave. In the case of the reflected shock, one makes use of the boundary condition of zero flow velocity behind the reflected shock at the end of the shock tube. The equation of state of the gas provides the necessary fourth equation for the solution. At higher temperatures it is important to include the effects of vibrational excitation and molecular dissociation. Tabulated thermodynamic properties for O_2 were used in this calculation.[6]

As a rough experimental check on these calculations, and also to monitor the duration of the constant equilibrium interval of the test gas, a high-frequency pressure transducer was placed in the end wall of the shock tube. Its output was recorded on a Tektronix 502 oscilloscope. The record resembles that of a step function, starting at the time of shock wave reflection, rising to an amplitude corresponding to the pressure behind the reflected shock wave and remaining constant for a period of between 50 and 300 μsec. Subsequent changes in output signal are due to pressure disturbances resulting from the interaction of the reflected shock and the driver gas. These changes mark the end of the time interval during which the state of the gas is known and during which all measurements on the gas must be made.

The question of the attainment of equilibrium was considered in detail. Several studies on the relaxation times of O_2 to dissociative equilibrium have been reported.[7] Taken together with the results on the vibrational relaxation times for O_2,[7] it is clear that, for the experiments reported here, complete equilibrium was attained in less than five μsec after the passage of the reflected shock. Since no data were taken for about 30 μsec (amply allowing for transit time of the reflected shock past the viewing ports) difficulties regarding equilibrium were avoided. Thus, Boltzmann statistics can properly be used to determine the populations of the molecular energy levels. The effect of boundary layer on the shock tube wall was separately studied with schlieren photographs of the reflected shock wave at the end of the shock tube. For the conditions of the

---

[6] C. E. Treanor and J. G. Logan, "Thermodynamic properties of oxygen from 2000°K to 5000°K," Cornell Aeronautical Laboratory Report No. BE-1007-A-4 (January, 1957).

[7] For reviews see S. R. Byron, J. Chem. Phys. **30**, 1380 (1959); D. L. Mathews, Phys. Fluids **2**, 170 (1959).

present experiments these effects can be neglected. Boundary layer effects behind reflected shock waves have recently been discussed in detail by Strehlow and Cohen.[8]

B. The Optical System

High demands were placed on the light source, which was the most critical part of the system. Because of the short testing time available it was desired that the lamp radiate for less than 20 μsec with an integrated intensity sufficient to exposure the spectrograph plate for 10- to 20-μ slit-width settings of the large Littrow (f/25) spectrograph. Further, it was required that the spectrum be continuous (over the wavelength region of interest) with few superimposed lines.

A suitable light source was developed to meet these criteria in the form of an argon-filled flash lamp. The lamp was made by sealing aluminum electrodes into each end of a quartz tube of 4 mm inside diameter and 1 mm wall thickness. The electrode spacing was about 4½ in. The lamp was evacuated and filled with 100 mm argon by means of a small hole drilled through one of the electrodes. A 0.5-mfd capacitor charged to 20 kv was used to pulse the lamp. An open spark gap was used as a switch, with an axially located teaser electrode across a pulse transformer serving to initiate the lamp flash. The output of a photomultiplier tube placed next to the collimating lens inside the spectrograph was used to monitor the total radiation time, and served as a cross check on the time at which the spectrum was recorded, relative to shock reflection at the end of the shock tube. The photomultiplier output was displayed by the second beam of the Tektronix 502 oscilloscope. In this manner a single record shows both the length of the equilibrium testing time and the time of the lamp flash, obtained independently from the pressure transducer and the photomultiplier tube.

It was found in the course of earlier studies[9] that the flash lamp output was not exactly reproducible. Small intensity differences between two flashes, one before and one during a given run, could not be reliably ascribed to absorption by the gas. The optical system described in reference 9 was therefore modified for the present experiments. Radiation from the flash lamp was directed in two separate beams to focus on different parts of the spectrograph slit. Two spectra were therefore obtained from the same flash, one containing the absorption by the gas sample and the second serving as a reference spectrum. Care was taken to have both beams view very nearly the same portion of the lamp and to focus exactly in the lamp axis since the spectra were found to vary markedly for different azimuthal directions about the capillary axis. The beams were focused with 3000 A light with the aid of an eyepiece equipped with a uranium glass window. The beam through the shock tube was about $\frac{3}{16}$ in. sq., and passed about ½ in. in front of the reflecting wall of the tube. The trigger signal for the light pulse was generated by a variable delay circuit actuated by the arrival of the shock wave at the reflecting wall. Any 20 μsec segment of time could thereby be chosen, during which the spectrum was recorded. Kodak type 103–0 spectroscopic plates with normal development were used exclusively.

After each experiment a series of exposures was made on the same plate, with calibrated filters placed in the sample beam. The flash lamp was used for these calibrations to preclude any reciprocity-failure problems. Since four flashes were made for each plate (one during the experiment, three through the plate-calibrating filters) twin-beam optics were particularly useful in correcting for small variations in intensity of the lamp. An iron arc furnished an accurate wavelength reference.

The optical system was arranged so that the emission originating in the gas was also focused on a portion of the spectrograph plate. It should be mentioned that for some high temperature tests the emission spectrum appeared, and indicated the presence of impurity radiators (i.e., diaphragm material). Time-resolved studies have shown this radiation to appear subsequent to the clean testing time. The radiation arises from the further heating by waves reflected from the advancing driver gas, and also from the appearance of matter, carried along by the driver gas, which becomes thermally excited in the region of the observation section. For these cases a capping shutter[10] was used to close off the entrance slit of the spectrograph. The shutter was electronically synchronized to close just after the lamp flash. The monitoring photomultiplier tube inside the spectrograph then served to check proper shutter operation.

C. Reduction of Data

It is well known that oxygen at room temperature absorbs only in the ultraviolet at wavelengths less than 2000 A, and gives rise to the so-called continuum vacuum-ultraviolet absorption. If the oxygen is strongly heated as in the present experiments, the population of molecules in vibrational levels as high as $v''=17$ of the ground $X\,^3\Sigma$ electronic state becomes sufficient for detectable numbers of transitions to occur to the low-lying (O−2) levels of the upper $B\,^3\Sigma$ state. One obtains thereby a large portion of the Schumann-Runge discrete band system in absorption. Further, since the oxygen is in thermal equilibrium the distribution of the population of the vibrational levels can be calculated and is known to be valid over the entire path through the gas sample.

The general features of the oxygen-absorption spectra in the near ultraviolet are shown in Fig. 1 for vari-

[8] R. A. Strehlow and A. Cohen, J. Chem. Phys. **30**, 257 (1959).
[9] Wurster, Glick, and Treanor, "Radiative properties of high-temperature air," Final Report, Cornell Aeronautical Laboratory Report No. QM-997-A-2, AFSWC TR 58-35 (September, 1958).
[10] W. H. Wurster, Rev. Sci. Instr. **28**, 1093 (1957).

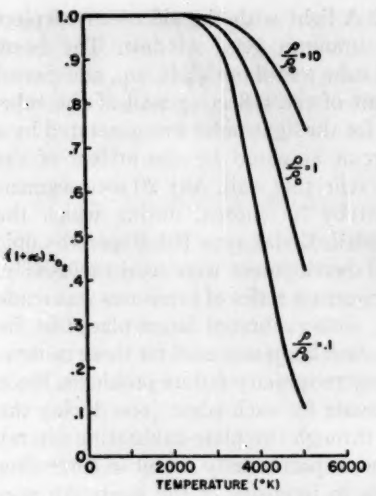

FIG. 3. Concentration of O_2 molecules in high-temperature oxygen.

ous temperatures of the absorbing gas. The effect of the increase in the population of vibrational levels with increasing temperature can be seen by comparing the absorption at a given wavelength. Since the density was constant for each of these spectra, the increased absorption relates directly to energy-level population. An enlarged section of the spectrum is shown in Fig. 2. In this case the oxygen was heated to 3410°K and compressed to a density of 3.6 normal. The vibrational bands in this region are well separated, and one can clearly see a large portion of the $V'=0$, $V''=13$ band. The tail of the 0,12 band can be seen at the left, and the bandhead of the 0,14 at about 3370 A near the right side of the photograph. For each band the Q branches and even-numbered rotational lines are missing, and since the triplet structure of each line is not resolved, there results the doublet-like structure shown in the photograph. More overlap of significant portions of bands occurs at other regions of the spectrum.

The absorption coefficient for the gas sample was determined from the Bouguer-Beer law,

$$I_\nu = I_{0\nu} \exp(-k_\nu n_{O_2} X), \qquad (1)$$

where $I_{0\nu}$ and I_ν are the intensities of radiation entering and leaving the sample. k_ν is the absorption coefficient at unit concentration, n_{O_2} is the number of O_2 molecules per cc divided by the number at STP, and X is the pathlength in the gas. For a discrete line absorption-spectrum, k_ν is a rapidly varying function of ν. To assure the necessary resolution, the instrumental slit width was kept less than $\frac{1}{3}$ the line widths by conducting the experiments with sufficiently collision-broadened lines. The line width is discussed in greater detail in Sec. IV.

A Jarrell-Ash recording microphotometer was used to analyze the spectrum plates. The scanning beam is adjustable in width to 1 μ, allowing line scans with no loss in resolution. The over-all resolution was thus determined by the Littrow spectrograph.

Density differences between the background level and the absorption lines can be directly related to the ratio of incident and transmitted intensities when the characteristic curve for the plate has been determined. This characteristic curve was obtained from the spectra of the flash lamp taken through the calibrated filters. With this information, the curve of k_ν *vs* ν can be constructed for the rotational lines. Finally, the integral $\int k_\nu d\nu$ was determined for the separate lines. These data were used to determine the transition probabilities as described in Sec. III.

III. ANALYSIS OF ABSORPTION MEASUREMENTS

The absorption coefficient defined in Eq. (1) can be related to fundamental constants of the O_2 molecule through the equation[11]

$$\int k_\nu d\nu = N_l h\nu (8\pi^3/3h^2c) \mid R_{n',v';n'',v''} \mid^2, \qquad (2)$$

where the integral is extended over both rotational lines (i.e., both $P_{K''}$ and $R_{K''}$) of a given rotational level from which the absorption occurs. $\mid R_{n',v';n'',v''} \mid^2$, the square of the matrix element of the dipole moment, is then independent of the rotational quantum numbers K' and K''. The temperature and density dependence of the integrated absorption is completely contained in the factor N_l, the number density of O_2 molecules in the lower vibrational-rotational level. For absorption by the Schumann-Runge system of O_2 this number density is given by,

$$N_l = (\rho/\rho_0)(1+\alpha)X_{O_2} L_0 [(2K''+1)/\tfrac{1}{3}Q] \times \exp[-(E_{K''}+E_{v''})/kT], \qquad (3)$$

where Q is the total internal partition function for O_2 (degeneracy of ground electronic state $=3$); $E_{K''}$, $E_{v''}$ are rotational and vibrational energies for the lower level, with rotational and vibrational quantum numbers K'', V''; ρ is the density of oxygen, $\rho_0 = 1.35\times10^{-3}$ g/cm^3 (STP density); X_{O_2} is the mole fraction of oxygen molecules; α is the degree of dissociation: $(1+\alpha)=$ total numbers of particles (atoms plus molecules) per original molecule of O_2; and $L_0=$Loschmidt number$=2.5468\times10^{19}$ molecules/cm^3. The quantities Q and $(1+\alpha)X_{O_2}$ are available[6] from statistical mechanics calculations. $(1+\alpha)X_{O_2}$ is the concentration of O_2, the ratio of the number of O_2 molecules present to the original number. A plot of the concentration *vs* temperature for various gas densities is shown in Fig. 3. As pointed out in Sec. II, separate experiments have verified that equilibrium was attained before the absorption spectrograms were photographed. Since the temperature and density can be calculated for each shock tube experiment, Eqs. (2) and (3) permit the determination of

[11] G. Herzberg, *Molecular Spectra and Molecular Structure. I. Spectra of Diatomic Molecules* (D. Van Nostrand Co. Inc., Princeton, New Jersey, 1950), second edition.

$|R_{n',v';n'',v''}|^2$ from a measurement of the integrated absorption coefficient.

The data obtained from the microphotometer were analyzed in the following way[11]: Values of the integrated absorption coefficient were measured for the separate rotational lines; the log of this quantity divided by $2K''+1$ was then plotted *vs* $E_{K''}$. From Eqs. (2) and (3), this plot should give a straight line for each vibrational band. The slope is $-1/kT$, and the intercept is proportional to $|R_{n',v';n'',v''}|^2$. A graph of this type is shown in Fig. 4 for a run at $T=3040°K$. The straight lines shown were drawn with a slope $-1/kT$, where T is the calculated temperature. It has not been possible to use these data to obtain an accurate measure of the "rotational temperature," the scatter of the points being sufficient to permit of about $\pm 10\%$ error in the temperature determined from the slope of the graph. In all cases, however, the calculated temperature gives a good line through the points.

Values of $|R_{n',v';n'',v''}|^2$ for each of 18 bands were determined from experiments at different temperatures and densities of the absorbing gas. Thus, Eqs. (2) and (3) provide an internal check of the over-all experiment. Results obtained from experiments at the various test conditions were consistent within the estimated accuracy of the data reduction process. The values determined experimentally are shown in Table I, along with the estimated errors.

Errors in the results are introduced from several sources. The measurement of the speed of the shock wave is accurate to $\pm 1\%$. This introduces an error of $\pm 1.5\%$ in the temperature and $\pm 1\%$ in the density, which reflects as an error of about 15% in the measured transition probability. Reduction of the data also requires an accurate calibration of the photographic plate. The slope of the characteristic curve was obtained to $\pm 10\%$, resulting in $\pm 10\%$ error in the transition probability. The actual measurement of the density of the photographic emulsion for the absorption spectrogram can also introduce an error, and as a result the accuracy of the determinations for the various bands

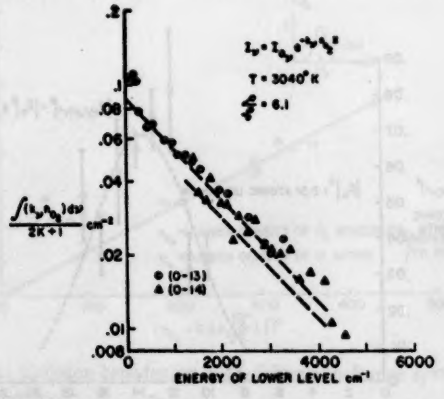

FIG. 4. Normalized absorption coefficient *vs* energy of the lower level of the transition.

TABLE I. Measured transition probability for 18 vibrational transitions of the Schumann-Runge system of O_2.

Transition v', v''	$\|R_{n',v';n'',v''}\|^2$ (atomic units)	
0, 10	0.033	+0.008, −0.005
0, 11	0.031	+0.010, −0.005
0, 12	0.081	±0.017
0, 13	0.073	±0.008
0, 14	0.065	±0.005
0, 15	0.059	+0.015, −0.005
0, 16	0.035	+0.010, −0.005
0, 17	0.052	±0.013
1, 9	0.042	±0.005
1, 10	~0.05	
1, 11	0.042	±0.010
1, 12	~0.04	
1, 16	0.028	±0.008
1, 17	0.045	±0.009
1, 18	~0.05	
2, 9	0.05	±0.02
2, 15	0.05	±0.02
2, 16	0.04	±0.02

depends on the number of rotational lines available in the band, free from overlap of other bands. In the best cases, (0–13), (0–14), from 15 to 25 lines are either free from overlap of known lines or can easily be corrected for small overlap. A few of these lines show consistently high absorption, and are probably overlapped with high rotational lines of other bands. The remaining lines were used to obtain a transition probability which should be accurate to within $\pm 25\%$. For some of the bands only 5 to 8 lines are available free from apparent overlap, and for these cases the estimated error is higher.

The quantity $|R_{n',v';n'',v''}|^2$ can be discussed further in terms of the vibrational overlap integral and the electronic transition moment with the relation,

$$|R_{n',v';n'',v''}|^2 = \left|\int \Psi_{n'v'}(e\mathbf{r}_e)\Psi_{n''v''}\,dr\,d\mathbf{r}_e\right|^2 = \left|\int R_e(r)\Psi_{v'}\Psi_{v''}\,dr\right|^2, \quad (4)$$

The average value of the electronic moment, $\bar{R}_e$, is known to depend on some extent on the vibrational levels V' and V'' involved in the transition. It has been shown by Fraser[12] and Nicholls[13,14] that $\bar{R}_e = R_e(\bar{r})$ where

$$\bar{r}_{v'v''} = \int \Psi_{v'} r \Psi_{v''}\,dr \Big/ \int \Psi_{v'}\Psi_{v''}\,dr \quad (5)$$

The function $\bar{R}_e^2$ varies slowly with $\bar{r}$ (i.e., it changes little from one vibrational band to another), and the main dependence of the absorption coefficient is on the

[12] P. A. Fraser, Can. J. Phys. **32**, 515 (1954).
[13] R. W. Nicholls, Proc. Phys. Soc. (London) **A69**, 741 (1956).
[14] R. W. Nicholls, *The Airglow and Aurorae* (Pergamon Press, London and New York, 1956).

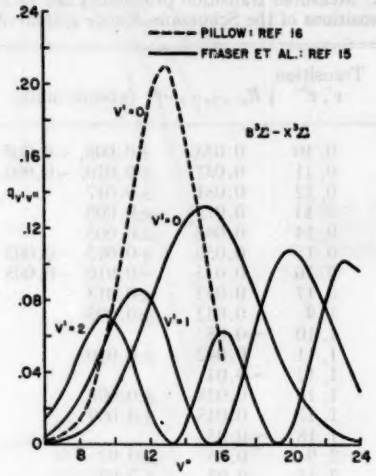

FIG. 5(a). Overlap integrals squared for three sequences of O_2.

overlap integral squared,

$$q_{v',v''}=\left[\int \Psi_{v'}\Psi_{v''}dr\right]^2. \tag{6}$$

These integrals have been calculated for the O_2 Schumann-Runge system by Fraser *et al.*[15] and by Pillow.[16] The calculated values from reference 15 for three sequences of importance herein are shown graphically in Fig. 5(a), and the $V'=0$ sequence as calculated in reference 16 is also shown. The experiments determine the product $R_e^2 q_{v'v''}$, and the experimental values for this product for the zero sequence are plotted in Fig. 5(b). Since $\bar{R}_e^2$ varies slowly with $\bar{r}$, the points in Fig. 5(b) should describe a curve similar to the zero-sequence curves in Fig. 5(a). The curve drawn through the experimental points is Fraser's curve shifted 1.5 quantum numbers to the left. Shifting the curves in this way permits a comparison of the experimental results for the $V'=0$, 1, and 2 sequences. The shift corresponds to a slight change (<0.01 A) in the relative position of the two electronic-potential curves that are involved. As would be required, it places the zeros of the $q_{1v''}$ and $q_{2v''}$ [Fig. 5(a)] curves at the transitions that have not been observed either in the present work by by Feast[17] or Lochte-Holtgreven and Dieke[18] in their emission studies. The positioning of the $V'=0$ curve as in Fig. 5(b) yields an $|\bar{R}_e|^2$ value of 0.51 atomic unit and is probably accurate to within ±0.10 atomic unit. With this shift a value of $|\bar{R}_e|^2=0.63$ gives best agreement with the experimental data for the $V'=1$ and 2 sequences, as can be seen from the results in Table I. Discrepancies of this order may be related to inaccuracies of both the overlap integral calculation and the experiments. Using a value of $|\bar{R}_e|^2=0.51$ atomic units and using the relation,[11]

$$f=(8\pi^2 mc\nu/3he^2)\,|\bar{R}_e|^2, \tag{7}$$

the f value for the Schumann-Runge system in this spectral region is equal to 0.048. Drawing a curve of $q_{v'v''}$ through the experimental points assumes that, within the experimental error, $R_e(\bar{r})$ is constant within the region investigated where r varies from ~1.45 A for (0, 9) to ~1.53 A for (0, 16). A comparison of the present results with other data for O_2 is given in Sec. V.

IV. LINE WIDTH

An additional item of interest in this work has been the effect of temperature and density on the width of the spectral lines. It is important for the accuracy of the measured absorption coefficients that the spectral line widths be reasonably larger than the slit function of the spectrograph. Further, changes in line width with the state of the gas can be related to physical properties of the oxygen molecule.

The Doppler broadening of the lines is too small to be observable with the large Littrow spectrograph. For example, at 5000°K the Doppler half-width is 0.03 A, which is about a fourth of the slit-function half-width. However, considerable broadening of the lines was observed, especially in experiments at high density. In some cases the observed half-width of the absorption lines was as large as 0.8 A. This was attributed to collision broadening of the lines.

The slit function for the spectrograph was obtained by photographing emission lines from a low-pressure mercury discharge tube. The lines were densitometered, and the data reduced to a plot of the relative intensity of the line *vs* wave number. The minimum half-width attainable was about 1.3 cm^{-1} (~0.12 A), which is also of the order of the triplet splitting of the oxygen lines.[18]

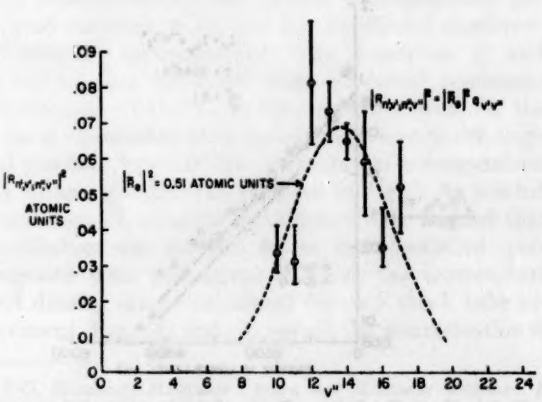

FIG. 5(b). Transition moments for V'=0 sequence.

[15] Fraser, Jarmain, and Nicholls, Astrophys. J. **119**, 286 (1954).
[16] M. E. Pillow, Proc. Phys. Soc. (London) **A63**, 940 (1950).
[17] M. W. Feast, Proc. Phys. Soc. (London) **A63**, 549 (1950); W. R. S. Garton and M. W. Feast, Nature **165**, 281 (1950).
[18] V. W. Lochte-Holtgreven and G. H. Dieke, Ann. Physik. **3**, 937 (1929).

A numerical investigation[19] shows that assuming reasonable shapes for the slit function and absorption coefficient curves a slit width of $\frac{1}{3}$ the line width leads to an error of less than 1% in integrated absorption coefficient, for absorption coefficients of the magnitude investigated here. Accordingly, the present data for integrated absorption coefficient were taken from experiments where the line width was at least three times the slit width and no corrections were required. However, the measurements of absorption line widths are more sensitive to the slit function, so that corrections were made for the observed line widths according to the calculations of reference 19. These corrections amount to about 6% for the broadest lines and 20% for the narrowest.

A general feature which is immediately noticeable is that the spectra taken at high density (up to ~8 atmos) show appreciably broadened lines. This is what one would expect for collision-broadened lines, with the line half-width (in cm^{-1}) increasing linearly with the number of collisions per sec suffered by any given O_2 molecule. However, experiments at high temperature with relatively low density, showed inordinately broad lines. This effect occurred in all cases where there was an appreciable number of dissociated oxygen molecules in the equilibrium mixture and indicates that the oxygen atoms are especially effective in broadening the molecular lines. All the data can, in fact, be accounted for on the basis of collision broadening if it is assumed that the optical cross section for molecule-atom collisions is 2.5 times that for molecule-molecule collisions. With this adjustment, the half-width of the spectral lines [the value of $\Delta\nu=(\nu_1-\nu_2)$ where $k(\nu_1)=k(\nu_2)=\frac{1}{2}k(\nu_0)$] plotted *vs* a coordinate proportional to the number of collisions per sec for a given oxygen molecule gives a straight line (Fig. 6). Since the optical cross section is related to the half-width by,

$$\Delta\nu=(\sqrt{2}/\pi c)(3R/M_{O_2})^{\frac{1}{2}}L_0 S_{O_2O_2}$$
$$\times[n_{O_2}+(S_{O_2O}/S_{O_2O_2})n_0(\tfrac{3}{2})^{\frac{1}{2}}](T)^{\frac{1}{2}}, \quad (8)$$

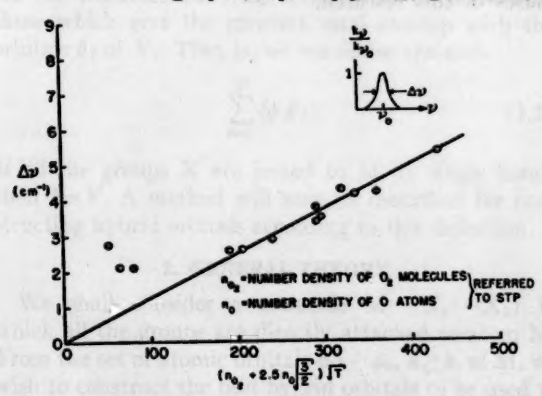

FIG. 6. Collision broadening in O_2 Schumann-Runge system.

[19] H. J. Kostkowski and A. M. Bass, J. Opt. Soc. Am. **46**, 1050 (1956).

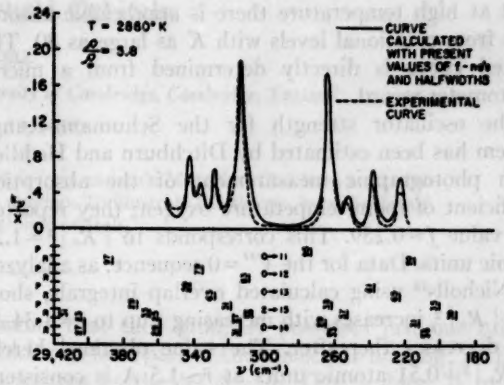

FIG. 7. Spectral absorption coefficient in the region of 3415 A.

the slope of the line is equal to,

$$(\sqrt{2}/\pi c)(3R/M_{O_2})L_0 S_{O_2O_2}.$$

In these relations, n_j=number density of particles of jth type referred to standard conditions of temperature and pressure, S_{ij}=collision cross section for collision of ith with jth type, M_{O_2}=molecular weight of O_2. From the slope, one obtains a value of 6 A for the O_2-O_2 optical collision diam and $(2.5)^{\frac{1}{2}}$ times that, 10 A, for O_2-O collisions. Since some of the experiments correspond to as much as 60% dissociation, the factor 2.5 can be determined to within ~20% by the criteron that all the experimental points lie along a straight line. The measurements were taken from various spectral lines which were chosen, according to the data of references 17 and 18, because they were either clearly separated from other lines or were directly superimposed on one other line. There was no noticeable dependence of line width on rotational quantum number.

V. COMPARISON OF RESULTS

The internal consistency of the present results can be tested by reconstructing a portion of the absorption spectrum from the transition probabilities given in Fig. 5(b) and the line width given in Fig. 6, and comparing this with absorption measurements. For this purpose a Cauchy line shape was used for the absorption coefficient,

$$k_\nu=(S/\pi)[\Delta\nu/2/(\nu-\nu_0)^2+(\Delta\nu/2)^2], \quad (9)$$

where ν_0 is the wave number of the line[17,18] and $\Delta\nu$ is the half-width obtained from Fig. 6. The quantity S is the integrated absorption for the line,

$$S=\int k_\nu d\nu, \quad (10)$$

and is obtained from Eq. (2). The absorption coefficient (or spectral emissivity) at any wave number is then a sum of the values of k_ν for all lines which contribute to the absorption at that wave number. A typical reconstruction is shown in Fig. 7, and it can be seen

that at high temperature there is appreciable absorption from rotational levels with K as large as 80. The dotted curve is directly determined from a microphotometer record.

The oscillator strength for the Schumann-Runge system has been estimated by Ditchburn and Heddle[20] from photographic measurement of the absorption coefficient of room-temperature oxygen; they reported the value $f=0.259$. This corresponds to $|R_e|^2 \approx 1.28$ atomic units. Data for the $V''=0$ sequence, as analyzed by Nicholls[13] using calculated overlap integrals, show that $|R_e|^2$ increases with increasing $\bar{r}$ up to $\bar{r}=1.34$ A. and decreases thereafter. The value obtained herein of $|R_e|^2=0.51$ atomic units at $\bar{r}\sim 1.5$ A is consistent with this decrease, but because of the large difference in internuclear separation at which the transition occurs, no quantitative comparison can be made. With photoelectric measurement of the absorption of cold O_2 Watanabe *et al.*[21] obtained $f=0.169$, or $|R_e|^2 \sim 0.836$. This lower value may be in part related to a lower resolution in the photoelectric experiment.

A more direct comparison of the present results can be made with recent measurements of the emission from shock-heated O_2. Keck *et al.*[3] have reported the measured emission at three 30-A wavelength bands in the ultraviolet for oxygen at 4100°K and densities of 0.19 and 0.022 atmos. By using the procedure described at the beginning of this section, the emissivity (equal to k_ν) can be calculated as a function of wavelength, and the net emission over a wavelength interval can be obtained. However, to compare with the results of reference 3 this detailed calculation is not required, since the emissivity is sufficiently small so that self-absorption effects may be neglected. For example, at a temperature of 4100°K, a density of 0.19 atmos and with a path-length of 3.8 cm, the maximum value of the emissivity in the wavelength region near 3400 A is ~ 0.5. For most of the emission the value is smaller, so that the approximate expression $(1-\exp -k_\nu X) \approx k_\nu X$ may be used and the average power emitted per steradian per micron per cm³ of gas in a direction perpendicular to the shock tube is given by,

$$I_{O_2}=[\Sigma S_{\nu K}/(\nu_2-\nu_1)]I_B, \qquad (11)$$

where the summation is over-all spectral lines within the region $(\nu_2-\nu_1)$ and I_B is the black body intensity in the normal direction at the wave number ν. To obtain the emission per molecule, Eq. (11) must be divided by the number of molecules per cm³, viz.,

$$\rho/\rho_0(1-\alpha)X_{O_2}L_0.$$

The radiation was calculated for the region near 3400 A and for a temperature of 4100° K, using $I_B=86.0$ w/cm² μ sterad. The I_{O_2} obtained, 3.32×10^{-19}, should be compared with 3.7×10^{-19}, given in reference 3. The value calculated here includes the effects of the 0→11, 0→12, 0→13, 0→14, and 2→15 bands. A similar calculation at 3850 A gives 0.62 of the value reported in reference 3. This is probably as close an agreement as can be expected for the two experiments.

Finally, the present results may be compared with data previously reported[4] for the ultraviolet absorption of shock heated air at a temperature of 4380°K and a density of 4 atmos. From the present results, molecular oxygen in the air under these conditions accounts for slightly more than half of the reported absorption. The remainder may be associated with absorption by NO in this spectral region. The effect of nitric oxide is presently being investigated.

VI. ACKNOWLEDGMENT

The authors wish to express their thanks to Miss Marcia Williams for her careful work in the reduction of the data and to Professor S. H. Bauer of Cornell University for helpful discussions concerning various phases of this research.

[20] R. W. Ditchburn and D. W. O. Heddle, Proc. Roy. Soc. (London) **A220**, 61 (1953); **A226**, 509 (1954).
[21] Watanabe, Inn, and Zelikoff, J. Chem. Phys. **21**, 1026 (1953).

THE JOURNAL OF CHEMICAL PHYSICS VOLUME 32, NUMBER 3 MARCH, 1960

Construction of Hybrid Orbitals

J. N. MURRELL

Department of Theoretical Chemistry, The University of Cambridge, Cambridge, England

(Received August 13, 1959)

A method is given for constructing the best hybrid orbitals for a molecule M—($X_1 \cdots X_k$) from a set of n atomic orbitals of M, based on the principle of maximum overlap. To illustrate the theory, hybrid orbitals for ClF_3 are constructed from the chlorine $3s$, $3p$, and $3d$ atomic orbitals.

1. INTRODUCTION

AN important first step in the quantum-mechanical description of the covalent bond is the construction of suitable hybrid orbitals for the atoms involved. For example, in a valence-bond description of the ground state of methane one pairs electrons in the hydrogen $1s$ orbitals with those occupying four equivalent hybrid orbitals obtained by taking suitable linear combinations of the carbon $2s$ and $2p$ atomic orbitals. These four orbitals point to the corners of a regular tetrahedron, and give the maximum overlap with the hydrogen orbitals.

The construction of hybrid orbitals is relatively simple for molecules which possess a high degree of symmetry, as does methane, since they can be obtained from the operations of the symmetry group of the molecule. (For a description of this technique see Eyring, Walter, and Kimball.[1]) In this paper the problem of constructing these orbitals for molecules which possess little or no symmetry will be considered. Under these conditions one must fall back entirely on the principle of maximum overlap: it is known that the strength of a bond is roughly proportional to the overlap of the orbitals involved; the stronger the bond the lower the energy of the molecule, hence by the variational principle, if we maximise the overlap we obtain the best wave functions for the molecule. With this principle in mind, the best hybrid orbitals ψ of M for the molecule M—($X_1 \cdots X_k$), will be defined as those which give the greatest total overlap with the orbitals θ_i of X_i. That is, we maximise the sum

$$\sum_{i=1}^{k'} \langle \psi_i \theta_i \rangle. \tag{1.1}$$

If all the groups X are joined to M by single bonds then $k=k'$. A method will now be described for constructing hybrid orbitals according to this definition.

2. GENERAL THEORY

We shall consider a molecule M—($X_1 \cdots X_k$) in which all the groups are directly attached to atom M. From the set of atomic orbitals $\phi_1 \cdots \phi_n$, $n \geq k$, of M, we wish to construct the best hybrid orbitals to be used to describe the wave function of the molecule. We shall assume that each group X possesses just one orbital which can take part in the molecular binding; let these be written as the set $\theta_1 \cdots \theta_k$. Our problem is to find linear combinations of the form

$$\psi_i = \sum_{j=1}^{n} a_{ij} \phi_j. \tag{2.1}$$

such that the sum of the overlap integrals,

$$\sum_{i=1}^{k} \langle \psi_i \theta_i \rangle \equiv \sum_{i=1}^{k} \sum_{j=1}^{n} a_{ij} \langle \phi_j \theta_i \rangle, \tag{2.2}$$

is a maximum. With matrix notation, if the overlap matrix between the orbitals θ_i and ϕ_j is written $\mathbf{R}$, and that between θ_i and the best hybrid orbitals as $\mathbf{S}$, then we wish to find a matrix $\mathbf{A}$ such that

$$\mathbf{AR} = \mathbf{S}, \tag{2.3}$$

where the trace of the $k \times k$ submatrix formed from the first k rows of $\mathbf{S}$ is a maximum, subject to the condition that the hybrid orbitals given by

$$\{\psi\} = \mathbf{A}\{\phi\}, \tag{2.4}$$

are orthonormal ($\{\psi\}$ and $\{\phi\}$ are column matrices).

We shall now prove two important theorems concerning the nature of the overlap matrix $\mathbf{S}$.

Theorem 1.—The submatrix formed from the last $n-k$ rows of $\mathbf{S}$ must be a zero matrix.

Suppose that we have found the best hybrid orbitals ψ_i. If ψ_r, $r>k$ has an overlap integral S_{1r} with the ligand orbital θ_1, then we can form a new orbital

$$\psi_1' = (1+\lambda^2)^{-\frac{1}{2}}(\psi_1 + \lambda\psi_r), \tag{2.5}$$

such that

$$\langle \psi_1' \theta_1 \rangle = (1+\lambda^2)^{-\frac{1}{2}}(S_{11} + \lambda S_{r1}). \tag{2.6}$$

Expanding $(1+\lambda^2)^{-\frac{1}{2}}$ for small values of λ, we find

$$\langle \psi_1' \theta_1 \rangle = (1 - \tfrac{1}{2}\lambda^2 + \cdots)(S_{11} + \lambda S_{r1}). \tag{2.7}$$

It follows that we can always choose λ small enough and of the correct sign such that ψ_1' will have a bigger overlap with θ_1 than had ψ_1, except when S_{r1} is zero. We therefore deduce that of our n hybrid orbitals, $n-k$ must be orthogonal to all the ligand orbitals.

[1] Eyring, Walter, and Kimball, *Quantum Chemistry* (John Wiley & Sons, Inc., New York, 1944), p. 226.

Theorem 2.—The submatrix formed from the first k rows of $\mathbf{S}$ must be symmetric.

If we replace the best hybrid orbitals ψ_i and ψ_j by the orthonormal pair of functions

$$\psi_i' = (1+\lambda^2)^{-\frac{1}{2}}(\psi_i+\lambda\psi_j), \tag{2.8}$$

and

$$\psi_j' = (1+\lambda^2)^{-\frac{1}{2}}(\psi_j-\lambda\psi_i), \tag{2.9}$$

the trace of our new overlap matrix minus the trace of the old is equal to

$$\lambda(S_{ii}-S_{ij})-\tfrac{1}{2}\lambda^2(S_{ii}+S_{jj})+\text{higher powers of }\lambda. \tag{2.10}$$

Again we can always choose λ small enough and of the correct sign such that 2.10 is positive unless $S_{ij}=S_{ji}$. We conclude that the overlap matrix between the best hybrid orbitals and the ligand orbitals must be symmetric.

As a first step in the construction of the hybrid orbitals we take linear combinations of atomic orbitals

$$\chi_i=\sum_{j=1}^{n} b_{ij}\phi_j \quad (\{\chi\}=\mathbf{B}\{\phi\}) \tag{2.11}$$

such that the χ_i are an orthonormal set, and $\chi_{k+1}\cdots\chi_n$ are orthogonal to all the orbitals $\theta_1\cdots\theta_k$. That is

$$\langle\chi_i\theta_t\rangle=\sum_{j=1}^{n} b_{ij}\langle\phi_j\theta_t\rangle=0, \tag{2.12}$$

for $i=k+1$ to n, and $t=1$ to k, and also

$$\sum_{j=1}^{n}(b_{ij}b_{i'j}-\delta_{ii'})=0. \tag{2.13}$$

We first of all construct orbitals χ_{k+1} to χ_n. There are $n(n-k)$ coefficients to be determined, and $(n-k)\cdot(n+k+1)/2$ equations of the type (2.12) and (2.13). It follows that there is considerable freedom in our choice of coefficients providing $n>k+1$. This is evident from the fact that if χ_a and χ_b satisfy the conditions (2.12) and (2.13), then any orthogonal combination of these functions also satisfies these conditions. However, a suitable set of χ's may be constructed as follows: we form χ_{k+1} by assigning arbitrary values to $n-k$ of the coefficients $b_{k+1,j}$ (providing that at least one is nonzero), solving the k equations

$$\sum_{j=1}^{n} b_{k+1,j}\langle\phi_j\theta_t\rangle, \tag{2.14}$$

to obtain the other k coefficients, and then normalizing our function by dividing throughout by

$$\Big(\sum_{j=1}^{n} b_{k+1,j}^2\Big)^{\frac{1}{2}}.$$

χ_{k+2} is now obtained by assigning arbitrary values to $n-k-1$ of the coefficients $b_{k+2,j}$ and solving the equations

$$\sum_{j=1}^{n} b_{k+2,j}\langle\phi_j\theta_t\rangle, \tag{2.15}$$

together with

$$\sum_{j=1}^{n} b_{k+1,j}b_{k+2,j}=0. \tag{2.16}$$

This process is continued until we have constructed χ_{k+1} to χ_n orthogonal to all the orbitals $\theta_1\cdots\theta_k$.

We now construct $\chi_1\cdots\chi_k$ orthogonal to $\chi_{k+1}\cdots\chi_n$ by the Schmidt process, thus:

$$\chi_k=N_k\{\phi_k-\sum_{i=k+1}^{n}\langle\chi_i\phi_k\rangle\chi_i\}, \tag{2.17}$$

$$\chi_{k-1}=N_{k-1}\{\phi_{k-1}-\sum_{i=k}^{n}\langle\chi_i\phi_{k-1}\rangle\chi_i\}, \tag{2.18}$$

the N's being normalizing constants.

We now have a set of orbitals $\chi_1\cdots\chi_k$ which have an overlap matrix $\mathbf{P}$ (say) with the functions $\theta_1\cdots\theta_k$, where

$$\mathbf{P}=\mathbf{B}_1\mathbf{R}. \tag{2.19}$$

$\mathbf{B}_1$ being the submatrix formed by the first k rows of $\mathbf{B}$. We have to find an orthogonal $k\times k$ matrix $\mathbf{C}$ such that

$$\mathbf{CP}=\mathbf{S}_1, \qquad (\mathbf{CC}'=\mathbf{I}), \tag{2.20}$$

and the trace of $\mathbf{S}_1$ is a maximum. $\mathbf{S}_1$ is the submatrix formed from the first k rows of $\mathbf{S}$. Our best hybrid orbitals are then given by

$$\{\psi\}=\mathbf{C}\{\chi\}=\mathbf{CB}_1\{\phi\}. \tag{2.21}$$

One could at this stage proceed to evaluate the matrix $\mathbf{C}$ under the condition that $tr\cdot\mathbf{S}_1$ is a maximum and that $\mathbf{C}$ is orthogonal. Following the Lagrange method of undetermined multipliers leads, however, to a set of simultaneous quadratic equations in the k^2 elements of $\mathbf{C}$, and these cannot be easily solved. An alternative solution will now be described in which we use the result of theorem 2 that $\mathbf{S}_1$ shall be a symmetric matrix. It will be shown that there are a limited number of solutions to Eq. (2.20) under this condition, and we shall easily be able to pick out the one which gives the maximum value to $tr\cdot\mathbf{S}_1$.

Since $\mathbf{S}_1$ is a symmetric matrix we can take the transpose of Eq. (2.20) and obtain

$$\mathbf{P}'\mathbf{C}'=\mathbf{CP}=\mathbf{S}_1. \tag{2.22}$$

Multiplying on the right by $\mathbf{C}$ then gives

$$\mathbf{P}'=\mathbf{CPC}, \tag{2.23}$$

since $\mathbf{CC}'=\mathbf{I}$. Multiplying (2.23) on the left by $\mathbf{P}$ gives

$$\mathbf{PP}'=\mathbf{PCPC}, \tag{2.24}$$

whence

$$\mathbf{PC}=(\mathbf{PP}')^{\frac{1}{2}}, \tag{2.25}$$

or

$$\mathbf{C}=\mathbf{P}^{-1}(\mathbf{PP}')^{\frac{1}{2}}, \tag{2.26}$$

from which we can calculate the required overlap matrix between the ligand orbitals and the best hybrid orbitals.

To find the square root of $\mathbf{PP}'$, we note that it is a symmetric matrix hence it can be diagonalized by an orthogonal matrix $\mathbf{U}$ (say), thus:

$$\mathbf{UPP}'\mathbf{U}'=\mathbf{D}(\alpha_1\cdots\alpha_k), \tag{2.27}$$

where $\mathbf{D}$ is a diagonal matrix with elements $\alpha_1\cdots\alpha_k$. It follows that

$$\mathbf{PP}'=\mathbf{UD}(\alpha_1\cdots\alpha_r)\mathbf{U}', \tag{2.28}$$

and

$$(\mathbf{PP}')^{\frac{1}{2}}=\mathbf{UD}[(\alpha_1)^{\frac{1}{2}}\cdots(\alpha_k)^{\frac{1}{2}}]\mathbf{U}'. \tag{2.29}$$

It is seen that there are various solutions of Eq. (2.23) corresponding to the (in general) 2^k square roots of the matrix $\mathbf{PP}'$ which arise from our choice of signs for the square roots of the diagonal elements of $\mathbf{D}$. It can be proved that the latent roots of $\mathbf{PP}'$ are all positive as follows: from (2.27) we have

$$\mathbf{D}=\mathbf{UPUU}'\mathbf{P}'\mathbf{U}'=\mathbf{QQ}', \tag{2.30}$$

where $\mathbf{Q}=\mathbf{UPU}$. However, the diagonal elements of any matrix $\mathbf{QQ}'$ ($\mathbf{Q}$ being real) are positive, hence $\alpha_1\cdots\alpha_k$ are positive and their square roots real.

It only remains to evaluate the matrix $\mathbf{C}$ from expression (2.26), and to choose the sign of the square roots so that $\mathbf{S}_1$ has the maximum trace. An example of the procedure described in this section will now be given.

3. HYBRID ORBITALS FOR ClF_3

ClF_3 is approximately a T shaped molecule as shown[2]:

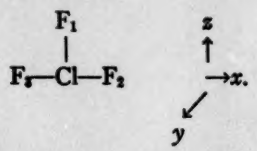

Chlorine possesses seven electrons outside a closed shell. Three of these are involved in the formation of the ClF bonds, and the other four are contained in two non-bonding orbitals. It follows that we require at least five orbitals of the chlorine atom to describe the electronic structure of the molecule; the $3s$ and $3p$ are not enough, it is necessary to use the $3d$ as well. We shall now find the best hybrid orbitals of the chlorine as determined by their overlap with the fluorine orbitals.

[2] D. F. Smith, J. Chem. Phys. **21**, 609 (1953).

The following set of atomic orbitals will be used:

$$\begin{aligned}
&3s=R_s && 3d_{z^2}=(5/4)^{\frac{1}{2}}(3\cos^2\theta-1)R_d\\
&3p_x=\sqrt{3}\cos\theta R_p && 3d_{xz}=15^{\frac{1}{2}}\sin\theta\cos\theta\cos\phi R_d\\
&3p_z=\sqrt{3}\sin\theta\cos\phi R_p && 3d_{yz}=15^{\frac{1}{2}}\sin\theta\cos\theta\sin\phi R_d\\
&3p_y=\sqrt{3}\sin\theta\sin\phi\ R_p && 3d_{x^2-y^2}=(15/4)^{\frac{1}{2}}\sin\theta\cos 2\phi R_d\\
& && 3d_{xy}=(15/4)^{\frac{1}{2}}\sin\theta\sin 2\phi R_d.
\end{aligned}$$

The R's are normalized radial functions divided by $2(\pi)^{\frac{1}{2}}$.

To simplify the calculation it will be assumed that the overlap integrals between the above orbitals and the fluorine orbitals are just proportional to the projection of the angular part of the chlorine orbitals along the three Cl—F bonds. With this assumption we construct the following overlap matrix:

$$\mathbf{R}=\begin{array}{c|ccc}
 & \phi_1 & \phi_2 & \phi_3\\
s & 1 & 1 & 1\\
p_x & \sqrt{3} & 0 & 0\\
p_z & 0 & \sqrt{3} & -\sqrt{3}\\
d_{z^2} & 5^{\frac{1}{2}} & -5^{\frac{1}{2}}/2 & -5/^{\frac{1}{2}}2\\
d_{x^2-y^2} & 0 & 15^{\frac{1}{2}}/2 & 15^{\frac{1}{2}}/2\\
p_y & 0 & 0 & 0\\
d_{xz} & 0 & 0 & 0\\
d_{yz} & 0 & 0 & 0\\
d_{xy} & 0 & 0 & 0
\end{array}. \tag{3.1}$$

We already have four orbitals which are orthogonal to all the fluorine orbitals, we have to construct two more from the first five functions in the column to the left of (3.1). Following the procedure given in Sec. 2, it can be seen that the following orbitals satisfy this condition:

$$\begin{aligned}
\chi_4&=(1/3)[(5)^{\frac{1}{2}}s-d_{z^2}-\sqrt{3}d_{x^2-y^2}).\\
\chi_5&=[1/(207)^{\frac{1}{2}}][2(5)^{\frac{1}{2}}s-3(15)^{\frac{1}{2}}p_x+7d_{z^2}+\sqrt{3}d_{x^2-y^2}].
\end{aligned} \tag{3.2}$$

We now have to form linear combinations of s, p_x, p_z, d_{xz}, and $d_{x^2-y^2}$, which are orthogonal to χ_4 and χ_5. By the Schmidt process we construct the following functions:

$$\begin{aligned}
\chi_1&=p,\\
\chi_2&=(1/12)(2/23)^{\frac{1}{2}}(24s+10\sqrt{3}p_x\\
&\qquad +3(5)^{\frac{1}{2}}d_{z^2}+7(15)^{\frac{1}{2}}d_{x^2-y^2}),\\
\chi_3&=(1/12)(2/5)^{\frac{1}{2}}[2(15)^{\frac{1}{2}}s+15d_{z^2}-5\sqrt{3}d_{x^2-y^2}).
\end{aligned} \tag{3.3}$$

It now remains to find linear combinations of χ_1, χ_2, and χ_3 which have the maximum overlap with the

ligand orbitals. The overlap matrix between the χ's and ϕ's, which is represented by the **P** matrix in Eq. (2.19) is as follows:

$$\mathbf{P}=\begin{array}{c} \\ \chi_1 \\ \chi_2 \\ \chi_3 \end{array}\begin{array}{c} \begin{array}{ccc} \phi_1 & \phi_2 & \phi_3 \end{array} \\ \begin{pmatrix} 0 & \sqrt{3} & -\sqrt{3} \\ (23/8)^{\frac{1}{2}} & (23/8)^{\frac{1}{2}} & (23/8)^{\frac{1}{2}} \\ 7/(8)^{\frac{1}{2}} & -5/(8)^{\frac{1}{2}} & -5/(8)^{\frac{1}{2}} \end{pmatrix} \end{array}. \quad (3.4)$$

We then have

$$\mathbf{PP'}=\begin{pmatrix} 6 & 0 & 0 \\ 0 & 69/8 & -3(23)^{\frac{1}{2}}/8 \\ 0 & -3(23)^{\frac{1}{2}}/8 & 99/8 \end{pmatrix}. \quad (3.5)$$

The latent roots of this matrix are 6, and $[21(27)^{\frac{1}{2}}]/2$, from which we deduce

$$\mathbf{PP'}=\begin{pmatrix} 1 & 0 & 0 \\ 0 & 0.928 & 0.373 \\ 0 & 0.373 & -0.928 \end{pmatrix}\begin{pmatrix} 6 & 0 & 0 \\ 0 & 7.90 & 0 \\ 0 & 0 & 13.10 \end{pmatrix}\begin{pmatrix} 1 & 0 & 0 \\ 0 & 0.928 & 0.373 \\ 0 & 0.373 & -0.928 \end{pmatrix}, \quad (3.6)$$

and hence

$$(\mathbf{PP'})^{\frac{1}{2}}=\begin{pmatrix} a & 0 & 0 \\ 0 & 0.861b+0.139c & 0.346(b-c) \\ 0 & 0.346(b-c) & 0.139b+0.861c \end{pmatrix}, \quad (3.7)$$

where $a=\pm(6)^{\frac{1}{2}}$, $b=\pm(7.90)^{\frac{1}{2}}$, and $c=\pm(13.10)^{\frac{1}{2}}$. It can then be shown that

$$\mathbf{S}_1=\mathbf{P}^{-1}(\mathbf{PP'})^{\frac{1}{2}}\mathbf{P}=\begin{pmatrix} 0.790b+0.211c & 0.290(b-c) & 0.290(b-c) \\ 0.290(b-c) & 0.501a+0.103b+0.396c & -0.501a+0.103b+0.396c \\ 0.290(b-c) & -0.501a+0.103b+0.396c & 0.501a+0.103b+0.396c \end{pmatrix}. \quad (3.8)$$

The trace of (3.8) is evidently a maximum when a, b, and c are all positive. Inserting the values for these parameters in (3.8) we obtain the overlap integrals between our best hybrid orbitals and the fluorine orbitals as follows:

$$\mathbf{S}_1=\begin{pmatrix} 2.98 & -0.23 & -0.23 \\ -0.23 & 2.95 & 0.50 \\ -0.23 & 0.50 & 2.95 \end{pmatrix}. \quad (3.9)$$

The hybrid orbitals themselves are obtained from (3.3) and the expression for $\mathbf{P}^{-1}(\mathbf{PP'})^{\frac{1}{2}}$.

$$\begin{pmatrix} 0 & 0.385 & 0.588 & 0.708 & 0.089 \\ 0.708 & 0.316 & 0.039 & -0.278 & 0.568 \\ -0.708 & 0.316 & 0.039 & -0.278 & 0.568 \end{pmatrix}\begin{pmatrix} p_z \\ s \\ p_x \\ d_z \\ d_{x^2-y^2} \end{pmatrix}. \quad (3.10)$$

To complete the preliminary stages in obtaining the wave function of ClF_3 we require orbitals to contain the nonbonding electrons. It is probable that these point towards the remaining two vertices of the trigonal bipyramid (three being picked out by the Cl—F bonds). The best lone pair orbitals could be expressed as some linear combination of our nonbonding orbitals p_y, d_{xy}, d_{xz}, d_{yz}, χ_4, and χ_5, using a similar technique to that described in Sec. 2.

Finally it might be added that the calculations on the ClF_3 molecule could have been extended by allowing the chlorine s, p, and d orbitals to have different radial functions, and by calculating their overlap with the fluorine orbitals exactly. Once the initial overlap matrix **R** has been written down, the calculation becomes no more complicated than that illustrated above.

Crystalline Transitions and Mechanical Resonance Dispersion in Vinyl and Ethyl Stearate*

EDWIN R. FITZGERALD

Department of Physics, The Pennsylvania State University, University Park, Pennsylvania

(Received September 11, 1959)

Dynamic shear compliance measurements on vinyl and ethyl stearate yield results depending critically on the particular crystalline modification in which these materials exist at the time of measurement. When first crystallized from the melt the materials are in a metastable state and only a few very small resonance dispersions are found in the range 50 to 5000 cps. At later times many large resonances occur; the largest is in the vicinity of 300 cps for both vinyl and ethyl stearate. While vinyl stearate is in its metastable state (about 60 days) a reversible transition takes place at $24.8_5 \pm 1_0$°C such that above this temperature there are no resonances from 50 to 600 cps, but below the transition point the large resonance near 300 cps always appears. A break in the slope of density-temperature curves for vinyl stearate occurs between 25 and 24°C indicating that a transition occurs in the vinyl stearate while in its β form (with the molecules tilted with respect to the planes formed by the terminal groups). X-ray powder diffraction photographs show no changes in the long spacing between planes so the transition must involve alterations in cross-sectional packing of the chains or a change from a monoclinic to triclinic unit cell rather than a variation in angle of tilt. While the details of the crystalline modification at 24–25°C are not as yet sufficiently clear to define a specific mechanism for the resonance phenomena, the results do prove conclusively that the dispersions are intimately connected with the crystalline state of the material. Eventually a kind of mechanical spectroscopy may be evolved yielding information on the actual crystalline state of solids in much the same way that electromagnetic spectra now aid in determinations of molecular structures.

I. INTRODUCTION

SHARP mechanical resonance dispersions in the audio-frequency range have been found in previous measurements of the dynamic shear compliance ($J^* = J' - iJ''$) of polycrystalline metals,[1] crystalline polymers,[2,3] single crystals of quartz[4] and fused quartz,[4] and single crystals of sodium chloride, copper sulfate, and Rochelle Salt.[5] The resonances were found to be independent of sample dimensions,[2–4] but to depend on the static stress and thermal histories of the samples. Resonances observed in highly crystalline (~90%) polyvinyl stearate were much larger than those observed in other materials and this fact suggested that measurements on the monomer, vinyl stearate, would be of interest. The long side chains present in polyvinyl stearate must make a high degree of order in the polymer possible only if there is side chain crystallinity, i.e., it is difficult to conceive of the main polymer chains lining up in any regular fashion without a regular side chain structure. Hence the crystal structures of the polymer and monomer might be similar and the same type of mechanical behavior found.

Another consideration was that long chain hydrocarbon compounds such as vinyl and ethyl stearate are known to exist in a variety of crystalline modifications[6–11] so that changes in the mechanical resonance spectra could be expected to occur with changes in crystal form. A correlation between known changes in crystalline form and the resonances could then possibly lead to an explanation of these puzzling phenomena.

Measurements of the storage compliance J' and the loss compliance J'' made at closely spaced frequency intervals in the range 100 to 5000 cps and at temperatures and times corresponding to different crystalline forms are described. The results in part bear out the expectations previously cited.

II. MATERIALS STUDIED

The vinyl stearate and ethyl stearate used were furnished by the United States Department of Agriculture, Agricultural Research Service. The ethyl stearate contained less than 0.3% stearic acid and had a saponification value of 180.0 (theoretical value 179.5).[12] Vinyl stearate was prepared commercially from purified stearic acid by direct vinylation and crystallized from three volumes of acetone. Its iodine number was 80.0 (theoretical value 81.7). In both cases the sample material was received in the form of a fine, white powder as precipitated from solution; samples were prepared by heating to 60°C and casting in a stainless steel mold to give pairs of small discs for testing. Freezing temperatures were found to be 30.5 and 30.9°C for vinyl and ethyl stearate, respectively, when cooled from the melt. Samples of vinyl stearate cooled slowly from the melt to temperatures above 25°C were found to "explode" out of the mold in the form of a white, granular ma-

* This is a report of work done under contract with the U. S. Department of Agriculture and authorized by the Research and Marketing Act of 1946. The contract is being supervised by the Eastern Utilization Research and Development Division of the Agricultural Research Service.

[1] E. R. Fitzgerald, Phys. Rev. **108**, 690 (1957).
[2] E. R. Fitzgerald, J. Chem. Phys. **27**, 1180 (1957).
[3] E. R. Fitzgerald, J. Appl. Phys. **29**, 1442 (1958).
[4] E. R. Fitzgerald, Phys. Rev. **112**, 765 (1958).
[5] E. R. Fitzgerald, Phys. Rev. **112**, 1073 (1958).
[6] T. Malkin, J. Chem. Soc. **1931**, 2796.
[7] J. C. Smith, J. Chem. Soc. **1931**, 802.
[8] J. W. C. Phillips and S. A. Mumford, J. Chem. Soc. **1931**, 1732.
[9] R. Buckingham, Trans. Faraday Soc. **30**, 377 (1934).
[10] V. Vand, Acta Cryst. **1**, 697 (1954).
[11] E. S. Lutton, J. Am. Oil Chemists' Soc. **35**, 11 (1958).
[12] The samples were prepared by W. S. Port of the Eastern Utilization Research Branch of the Agricultural Research Service of the U. S. Department of Agriculture, Philadelphia, Pennsylvania.

TABLE I. Sample dimensions.

Material	Vinyl stearate (A)	Vinyl stearate (B)	Ethyl stearate
Sample No.	42	45	47
Dimensions			
Diameter (in.)	0.500	0.375	0.375
Thickness (in.)	0.125	0.200_1	0.188_3
			0.187_8
Sample coefficient[a] (cm)	7.98	2.80	2.98
Weight (g)	0.387_0	0.346_0	0.319_8
	0.382_8	0.347_0	0.316_1

[a] $A_1/h_1+A_2/h_2\cong 2A/h$ where A is the cross-sectional area and h the thickness of each sample.

terial full of cavities, not suitable for mechanical tests. However if the liquid vinyl stearate was quenched by cooling from 60 to 15°C within 5 minutes a compact, semitranslucent, waxy material was obtained which was suitable for dynamic measurements. After a long time at room temperature (~25°C) these samples become increasingly opaque with white regions visible throughout their generally cloudy volume. These observations naturally lead to the conclusion that at least two (and perhaps more) crystalline forms are possible.

The behavior of the ethyl stearate upon freezing was in agreement with previous observations,[6,7,8,13] i.e., at 30.9°C the liquid became a soft, transparent solid which changed instantly to a white, opaque (and less plastic) solid at 25.5°C. The change observed at 25.5°C was not reversible. This particular transition has been attributed to a tilt of the stearate chain with respect to the crystal planes formed by the terminal groups in the lower (β) form while the chains are vertical to these planes in the high temperature (α) form. A corresponding difference is found in the long spacing from x-ray diffraction[6] as the distance between planes is 28.6 A for the α form and 25.5 A in the β form.

A summary of sample dimensions is given in Table I.

III. EXPERIMENTAL METHODS

1. Volume Expansion and Cooling Curves

In order to locate transition points several cooling curves were obtained for both vinyl and ethyl stearate. The method consisted of placing about 3 cc of liquid sample (at 50°C) in a 5-cc test tube with a two-junction iron-constantan thermocouple (No. 30 B and S gauge wire) in the center. The test tube was placed in an insulated container and immersed in a water bath which was regulated so that the ambient temperature in the air space surrounding the test tube dropped at the rate of approximately 0.2°C per minute. A Rubicon[14] potentiometer and pointerlite galvanometer were used to determine the emf between the junctions in the sample and reference junctions kept at 0°C. By comparison with a standard thermocouple calibrated by the National Bureau of Standards the thermocouple was found to be within ±0.1°C (equal to the precision of measurement). Temperature readings of the samples were taken every minute and the ambient temperature read (by means of a second thermocouple) every two or three minutes.

A mercury dilatometer[15] was used to determine the density of vinyl stearate at various temperatures between 50 and 15°C. The dilatometer bulb was immersed in water in an unsilvered Dewar flask so that the appearance of the sample could be noted; a mercury thermometer with scale divisions of 0.1°C was placed in the Dewar near the dilatometer bulb and used to indicate the sample temperature under equilibrium conditions. The sample was put in the dilatometer in liquid form and thoroughly degassed by alternately freezing and melting it under a vacuum (10^{-3} mm Hg) to remove all dissolved air or other gases. Degassed, clean mercury was then added and the dilatometer bulb connected to a 2-mm precision bore capillary in which the height of the mercury column could be read to within 0.01 mm by means of a cathetometer. For vinyl stearate this meant that changes in density of the order of 5×10^{-4} g/cc could easily be determined within ±2%. All readings were taken under equilibrium conditions, i.e., a series of cathetometer readings was taken at each temperature until two readings taken from one to two hours apart were the same. At the freezing point, for example, twenty-five hours were required for an equilibrium height to be reached.

2. Shear Compliance Measurements

Complex shear compliance measurements were made by means of an electromagnetic transducer apparatus previously described.[1,16] In this apparatus a pair of samples is clamped between metal surfaces and sheared by a sinusoidally varying stress in a direction perpendicular to the static clamping stress. Readings of resistance and capacitance of an electrical bridge circuit at balance are used to calculate the storage compliance J' (defined as the amplitude of the strain component in phase with the stress divided by the amplitude of the stress) and the loss compliance J'' (defined as the amplitude of the strain component 90° out of phase with the stress divided by the stress amplitude) with a precision of ±3%. J' is a measure of the elastic response or energy stored per cycle while J'' is proportional to the viscous part of the response or energy loss per cycle. The ratio J''/J' is proportional to the reciprocal Q or logarithmic decrement obtained in internal friction

[13] W. O. Baker and C. P. Smyth, J. Am. Chem. Soc. **60**, 1229 (1938).

[14] Rubicon Company, Philadelphia, Pennsylvania.

[15] The dilatometer was provided through the courtesy of W. Webb and R. R. Nelson. A description of it is given in the thesis of R. R. Nelson submitted in January 1959 in partial fulfillment of the requirements for the Ph.D. degree at The Pennsylvania State University.

[16] E. R. Fitzgerald and J. D. Ferry, J. Colloid Sci. **8**, 1 (1953).

measurements. Static clamping stresses vary from 10^6 to 10^7 dynes/cm² (~15 to 150 psi) while the dynamic stress amplitudes are always less than 5×10^3 dynes/cm² (~0.08 psi) resulting in strain amplitudes of 10^{-5} to 10^{-7} depending on the sample dimensions and properties. All of the results were for strains small enough so that compliance changes with strain amplitude were less than 0.1% over a twofold range in strain.

Sample temperatures are determined by a two-junction copper-constantan thermocouple located within 0.025 in. of the samples. The precision of temperature readings is ±0.05°C; comparison of the thermocouple with one calibrated by the National Bureau of Standards revealed no differences greater than 0.1°C.

IV. EXPERIMENTAL RESULTS

1. Cooling and Heating Curves

Typical cooling curves for vinyl and ethyl stearate are shown in Fig. 1. Vinyl stearate exhibited a small bump in its cooling curve at 32.6–33.1°C for four different sets of measurements so that some sort of liquid-liquid transition may take place in this region. At this temperature the sample also changed from a clear to a cloudy liquid. The freezing point, represented by the temperature at which the long plateau occurs,

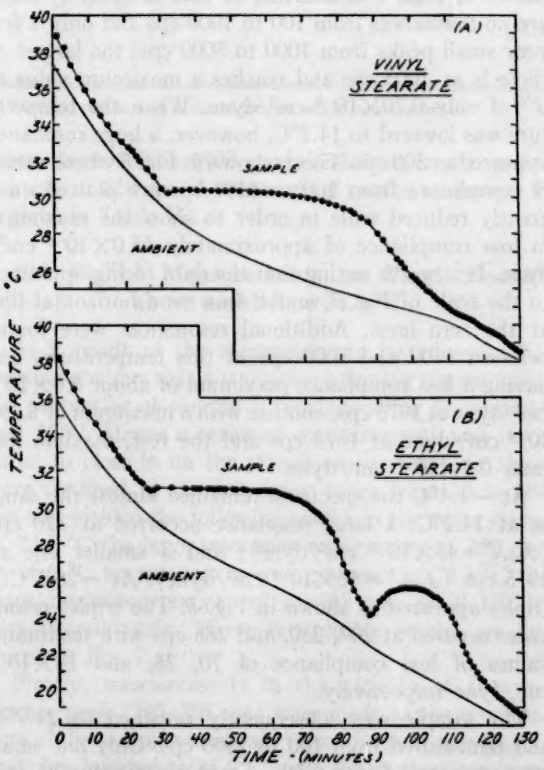

FIG. 1. Cooling curves: (A) vinyl stearate; crystallization point 30.5°C, no evidence of a solid-solid transition; (B) ethyl stearate; crystallization point 30.9°C, $\alpha-\beta$ transition at 25.5°C.

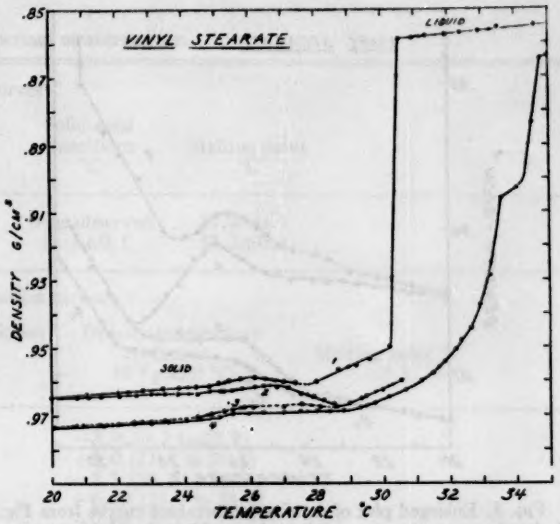

FIG. 2. Temperature dependence of density for vinyl stearate; crystallization point 30.5°C. Descending temperatures, curves 1 and 3; ascending temperatures, curves 2 and 4.

was found to be 30.5±0.1°C in each case. At this temperature the sample changed from a milky or cloudy liquid to a white, opaque solid. Heating curves for vinyl stearate revealed a more gradual transition from solid to liquid giving a melting point between 31.2 and 33.2°C.

Two cooling curves were obtained for the sample of ethyl stearate giving a freezing point of 30.9°C in each case. No change in the slope or appearance was noted while the sample was a liquid. From 30.9 to 25.5°C a clear, transparent solid was present but at 25.5°C a change to a white, opaque material was noted. This corresponds to a small plateau (preceded by supercooling to 24.1°C) observed in the cooling curves [see Fig. 1(B)]. A heating curve from 16 to 45°C showed no solid-solid transition but only a long plateau from which a melting point of 33.2°C was obtained. The results for ethyl stearate are in substantial agreement with those reported by previous investigators[6–8]; the cooling curve plateau at 25.5°C corresponds to the irreversible α, β transition previously mentioned.

2. Temperature Dependence of Density

Cooling curves do not yield information on second-order transitions or first-order transitions which occur very slowly. In order to search for possible transitions in vinyl stearate not revealed by the cooling or heating curves equilibrium measurements of density—temperature were carried out as described in Part III. A portion of the density temperature curve for vinyl stearate is shown in Fig. 2. Measurements were started with the vinyl stearate in the form of a clear liquid at 40°C and continued down to 15°C (curve 1). At 32–33°C the liquid became cloudy and at 30.5°C began to crystallize. The temperature was held at 30.25°C for twenty-five

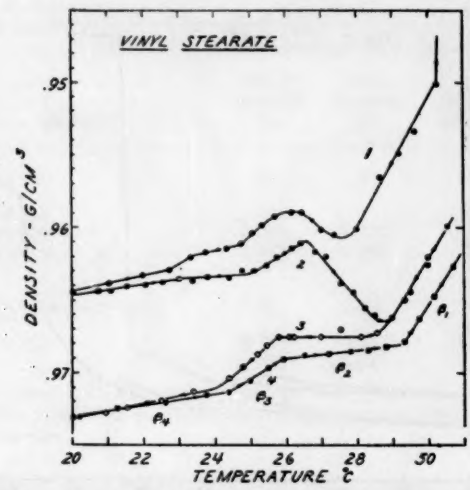

FIG. 3. Enlarged plot of density-temperature curves from Fig. 2 showing second order solid-solid transitions in vinyl stearate. Curve 4: β_4, β_3 at 24.4°C; β_3, β_2 at 25.9°C; β_2, β_1 at 29.2°C.

hours before the crystallization was complete and the dialatometer readings became constant with time. Below 30.25 five different slopes were observed with transition temperatures of 27.7, 26.1, 24.7, and 23.0°C. Measurements with increasing temperature from 15 to 30.5°C again revealed five slopes (curve 2) with transitions at 23.0, 24.9, 26.5, and 28.7°C. A third, descending run (curve 3) from 30.5 to 17.0°C gave four slopes with transitions at 28.7, 25.8, and 24.1°C. A final, ascending run showed four different slopes in the solid state with transitions at 24.3, 25.9, and 29.2°C. An additional set of measurements with rising and falling temperatures taken before curve 4 fell between curves 3 and 4. The existence of different crystalline forms in the solid state is also evidenced by the density changes occuring in remelting. The first melting occurs between 31.3 and 33.6°C (corresponding closely to the heating curve results mentioned in part 1 of this section). A second melting then occurs between 34.2 and 34.8°C, while a third transition (not shown in Fig. 2) occurs at 36.7°C. The vinyl stearate appeared to be a grayish solid or semisolid between 31.3 and 34.8°C but above this temperature portions of clear liquid were visible. The entire sample became clear at about 40°C.

The solid-solid transitions are shown more clearly in the enlarged plot of Fig. 3 where the four slopes finally obtained are identified with possible β_1, β_2, β_3, and β_4 crystalline states. The entire set of density measurements extended over a period of 51 days. A summary of the results of both cooling curve and density measurements is given in Table II.

3. Frequency Dependence of Compliance for Vinyl Stearate

Measurements of shear compliance on sample A of vinyl stearate at 25.7°C made from 100 to 5000 cps within 2 to 100 hr after formation from the melt showed only one substantial resonance, at 3070 cps. At 19.1°C measurements from 100 to 4000 cps revealed no change in the 3070 cps resonance but a few additional, small resonances were more noticeable than at 25.7°C. The sample was kept in the apparatus at temperatures between 24.5 and 27.5°C for 1504 hr (about 62 days) and then remeasured at 25.5°C. A huge resonance was now found at 360 cps. Values of J'' increased from about 0.02×10^{-9} cm²/dyne off resonance to 95.0×10^{-9} cm²/dyne at the resonant frequency. Additional, smaller resonances were found at nine other frequencies between 500 and 4000 cps. As the temperature was lowered to 13.5, −1.3, and −27.8°C the large resonance broke up into a triplet so that at −27.8°C, for example, there were resonances at 300, 340, 435 cps with maximum values of loss compliance (J'') of 224, 27, and 7.0×10^{-9} cm²/dyne, respectively. The number of additional resonances between 1400 and 4000 cps increased from seven at 24.5°C to ten at −28.3°C and various changes in magnitude occured as well. These results are summarized in Table III.

A second set of samples (B) of vinyl stearate was prepared in the same manner as A but instead of waiting a long time at room temperature the temperature was lowered to 14, −1.4, and −28°C within 800 hr after the samples were formed. Some of the results are shown in Figs. 4–8. Starting at 25.1°C (Fig. 4) there are no resonances from 100 to 1000 cps and only a few very small peaks from 1000 to 5000 cps; the largest of these is at 1005 cps and reaches a maximum value of J'' of only 0.70×10^{-9} cm²/dyne. When the temperature was lowered to 14.2°C, however, a huge resonance appeared at 300 cps. This is shown in Fig. 5 where values of compliance from 100 to 1400 cps are plotted on a greatly reduced scale in order to show the maximum in loss compliance of approximately 65.0×10^{-9} cm²/dyne. It is worth noting that the data of Fig. 4 plotted to the scale of Fig. 5 would show as a horizontal line at the zero level. Additional resonances were found between 1400 and 5000 cps at this temperature, one having a loss compliance maximum of about 8.0×10^{-9} cm²/dyne at 1975 cps, another with a maximum of 1.3×10^{-9} cm²/dyne at 1675 cps and the rest, maxima less than 0.5×10^{-9} cm²/dyne.

At −1.4°C the spectrum remained almost the same as at 14.2°C; a large resonance occurred at 320 cps ($J_{max}''=45\times10^{-9}$ cm²/dyne); and a smaller one at 1975 cps ($J_{max}''=16\times10^{-9}$ cm²/dyne). At −28.4°C a triplet appeared as shown in Fig. 5. The triplet resonances occured at 200, 230, and 285 cps with maximum values of loss compliance of 70, 28, and 18×10^{-9} cm²/dyne respectively.

The sample was subsequently returned to 24.9°C and remeasured from 100 to 1400 cps. Only one small resonance was found with a maximum value of loss compliance of 1.0×10^{-9} cm²/dyne at 970 cps. The temperature was again lowered to 14.0°C and measure-

TABLE II. Summary of thermal measurements.

Material	Freezing point °C	Solid-solid transitions °C	Melting point °C
Cooling curves[a]			
Vinyl stearate	30.5±0.1	none observed	31.2–33.2
Ethyl stearate	30.9±0.1	25.5±0.1	33.2±0.1

Vinyl stearate	Freezing point °C ±0.1	Solid-solid transitions °C ±0.1	Density-temperature coefficient 10^{-3} g/cm³ °C	Melting point °C ±0.1
Density-temperature curves				
Descending (1)	30.5	27.7	−3.9(30.2 to 27.7)	
			+2.0 (27.7 to 26.1)	
		26.1	−2.1 (26.1 to 24.7)	
		24.7	−0.70 (24.7 to 23.0)	
		23.0	−0.60 (23.0 to 15.0)	
Ascending (2)		28.7	−3.9 (30.6 to 28.7)	
			+2.8 (28.7 to 26.5)	
		26.5	−1.4 (26.5 to 24.9)	
		24.9	−0.21 (24.9 to 23.0)	
		23.0	−0.40 (23.0 to 15.0)	
Descending (3)		28.7	−3.9 (30.5 to 28.7)	
			−0.0 (28.7 to 25.8)	
		25.8	−2.0 (25.8 to 24.1)	
		24.1	−0.46 (24.1 to 20.0)	
Ascending (4)		29.2	−3.9 (30.7 to 29.2)	31.3–33.6
			−0.30 (29.2 to 25.9)	
		25.9	−0.92 (25.9 to 24.3)	34.2–34.8
		24.3	−0.42 (24.3 to 20.0)	36.7

[a] Identical results were obtained for two sets of measurements.

ments from 100 to 1400 cps revealed an enormous resonance at 310 cps. A summary of results on sample B is given in Table IV.

4. Compliance Measurements on Vinyl Stearate above and below 24.8$_5$°C

As a result of the measurements just described it became obvious that a transition affecting the mechanical properties of sample B was occurring between 14 and 25°C. Hence a series of measurements was instituted to close in on the transition temperature; these were confined to the frequency range from 50 to 600 cps and yielded the following results in the order given: at 23.8$_3$°C the large resonance was present at 300 cps; at 25.0$_7$°C no resonances were present; at 24.3$_0$°C the large resonance reappeared at 305 cps; at 25.1$_0$°C it disappeared again. These remarkable results are adduced in Fig. 7.

Finally, measurements in the vicinity of the resonance peak (295–305 cps) were made as the temperature of the sample was slowly raised from 24.6 to 25.2°C and then lowered to 24.6°C again. From these measurements a transition temperature between 24.7$_1$ and 25.0$_0$ was deduced; the mean value was set at 24.8$_5$°C as shown in Fig. 8.

5. Changes in the Compliance of Vinyl Stearate with Time

It has already been pointed out that after 1677 hr at room temperature sample A of vinyl stearate showed a very large resonance at 360 cps. (Sec. 3 and Table III). Since no measurements were made on sample A between 173 and 1677 hr the exact time at which this resonance appeared could not be determined. Sample B was measured at 25.1°C at 1415 hr after forming from the melt and had no resonance between 50 and 600 cps. At 1462 hours, however, the same resonance (305 cps) previously found only below 24.8$_5$°C was now found at 25.1°C in sample B. Measurements at 1606 and 1773 hr at 25.3 and 25.4°C confirmed the continued existence of the resonance. Thus it appeared that the state of the sample occurring initially only below 24.8$_5$°C was also attained with time at higher temperatures, and was the final or stable state at room temperature. (see Table IV). The results on B are therefore in essential agreement with those on A.

6. Effect of Static Stress on Compliance Spectrum of Vinyl Stearate

Previous measurements on polyvinyl stearate[3] demonstrated that the positions and magnitudes of me-

TABLE III. Summary of mechanical resonances in sample A of vinyl stearate at various times and temperatures.

Time after crystallization from melt (hr)	Temp °C	Resonant frequencies (cps)	Loss compliance maxima, J_{max}'' 10^{-9} cm²/dyne	Range (cps)
2–100	25.7	1520	0.10	100–5000
		3070	4.4	
		3240	0.10	
122–173	19.1	1540	0.45	100–4000
		2840	0.32	
		3070	4.	
		3670	0.20	
1677–1853	25.5	360	95.0	100–1400
		550	2.5	
		625	2.5	
	24.5	1510	1.2	1400–4000
		1895	1.3	
		2040	2.1	
		2315	0.60	
		2930	0.65	
		3325	0.30	
		3840	0.25	
	13.5	420	200	50–1400
		475	32	
		615	1.6	
	14.5	1515	1.6	1400–4000
		1835	3.8	
		1955	2.9	
		2465	0.30	
		2890	0.15	
		3285	1.3	
		3870	0.60	
2330–2356	−1.3	350	~200	50–1400
		405	18	
		510	3.5	
		1340	0.20	
	−2.2	1510	1.45	1400–4500
		1620	0.50	
		1750	4.5	
		1860	0.55	
		1940	0.35	
		1970	0.25	
		2245	0.60	
		3250	1.4	
		3900	0.50	
2691–2832	−27.8	300	224	50–1400
		340	27	
		435	7.0	
		1340	0.30	
	−28.3	1510	2.25	1400–4000
		1640	2.9	
		1695	3.0	
		1770	0.90	
		1970	0.15	
		2110	0.35	
		3160	0.65	
		3220	0.65	
		3670	0.20	
		3890	0.50	

chanical resonances were altered by changes in static clamping stresses. Therefore a very slight increase in static stress (corresponding to one-quarter turn of the sample holder screw[1]) was applied to sample B at the conclusion of the measurements described in the previous section. With the increased pressure only one resonance was observed in the 100 to 4000 cps region; at 2940 cps. The peak value of loss compliance at this frequency was about 1.8×10^{-9} cm²/dyne. The spectrum everywhere else was absolutely flat. Subsequently the static pressure was reduced to approximately its initial value and with this a large resonance reappeared, now at 195 cps with a loss compliance maximum of 100×10^{-9} cm²/dyne, and accompanied by a smaller reso-

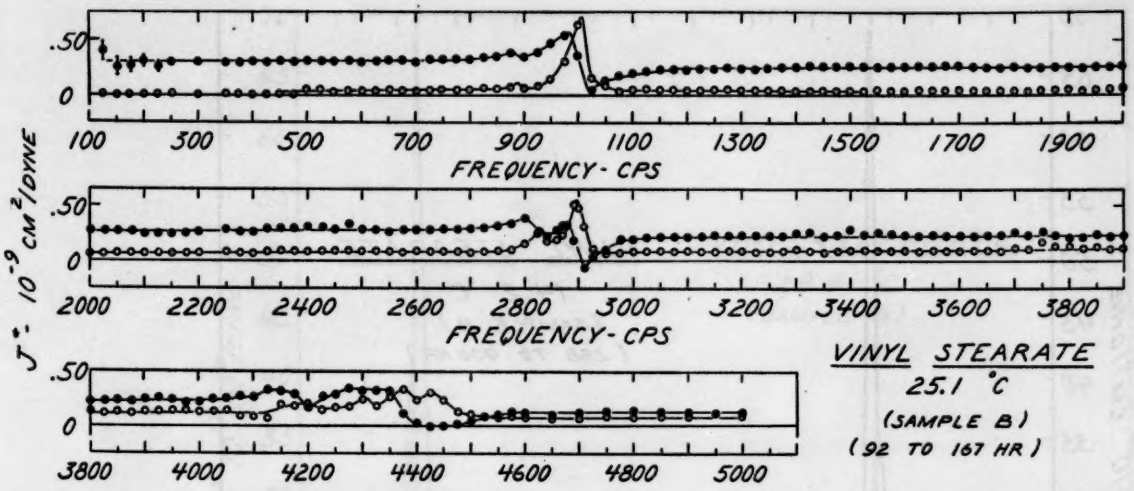

FIG. 4. Variation of complex shear compliance ($J^*=J'-iJ''$) with frequency for vinyl stearate (sample B) at 25.1°C and 92 to 167 hours after crystallization from the melt. Solid points, J'; open points, J''.

nance at 325 cps ($J_{max}''=10\times10^{-9}$ cm²/dyne). With increasing time the resonance moved to higher frequencies and decreased in magnitude. A summary of these measurements (confined to the 50 to 600 cps region) is given in Table V.

7. Compliance Measurements on Ethyl Stearate

Samples of ethyl stearate quenched to 15°C from the melt and then warmed to 24.2°C were measured within a few hours after formation (2.2 to 10.8 hr) and found to have only one very small resonance at 1100 cps ($J_{max}''=0.516\times10^{-9}$ cm²/dyne) in the frequency range from 50 to 1200 cps. From 1200 to 2560 cps no resonances were found but between 29.5 and 69.2 hours the levels of J' and J'' increased. That is, values of compliance at 2175 cps at 29.5 hr were 0.270 and 0.030×10^{-9} cm²/dyne for J' and J'' respectively but at 69.2 hr were 0.335 and 0.055×10^{-9} cm²/dyne at the same frequency! Subsequently at 172.2 to 195.5 hr values of compliance from 50 to 1400 cps were obtained revealing resonances at 275, 320, and 420 cps with maximum values of loss compliance of 80, 5.5, and 1.0×10^{-9} cm²/dyne, respectively. The results at 2.2 and 172.2 hr are compared in Fig. 9. Measurements from 50 to 600 cps made at later times (up to 1200 hr) showed that the resonance first observed at 172.2 hr remained at practically the same frequency, but the level of J_{max}'' at 275 cps rose to around 100×10^{-9} cm²/dyne while the maximum value of loss compliance of the third resonance rose from 1.0 to 3.0×10^{-9} cm²/dyne. Resonances were also found at 1500, 1705, 1845, and 2990 cps. The results are summarized in Table VI. It should be pointed out that results at 26.8°C were the same as those at 24.2°C. It was originally intended to drop the temperature to 15°C as was done for sample B of vinyl stearate but the appearance of resonances in ethyl stearate occured before initial meaurements at room temperature could be completed, (i.e., after 69 instead of 1462 hr).

V. DISCUSSION

1. Crystalline Modifications in Long-Chain Hydrocarbon Compounds

The main features of the polymorphism of long chain hydrocarbon compounds can be summarized briefly as follows[6–11]: the compounds crystallize with their end groups in planes and with the hydrocarbon chains either perpendicular (α form) or tilted with respect to the planes (β form).[6] The α and β forms can be distinguished by their long x-ray spacings which are smaller in the β than in the α form and by the fact that the α form is generally transparent and the β form is opaque. The α forms (perpendicular chains) can be further classified according to the cross-sectional arrangement of the chains in hexagonal or rectangular arrays. The β forms (tilted chains) can be subdivided, in turn, according to the angle of tilt, or the cross-sectional spacings of the chains. Thus in the α form hexagonal or orthorhombic unit cells are possible while in the β form various monoclinic or triclinic forms can exist. A further distinction is made according to the relative orientation of the planar zigzag carbon chains with respect to each other. These may be randomly oriented (freely rotating, e.g., in the α hexagonal form), alternate rows may be parallel, or all zigzag planes may be lined up in the same direction. Classification according to the carbon plane orientation is particularly useful in connection with dielectric measurements where increased contributions to the polarization occur when dipole groups are attached to the rotating chains. It is not necessarily true, however, that this type of rigid chain rotation or oscillation produces an increased mechanical compliance. In fact the large mechanical resonance dispersions and increased compliances re-

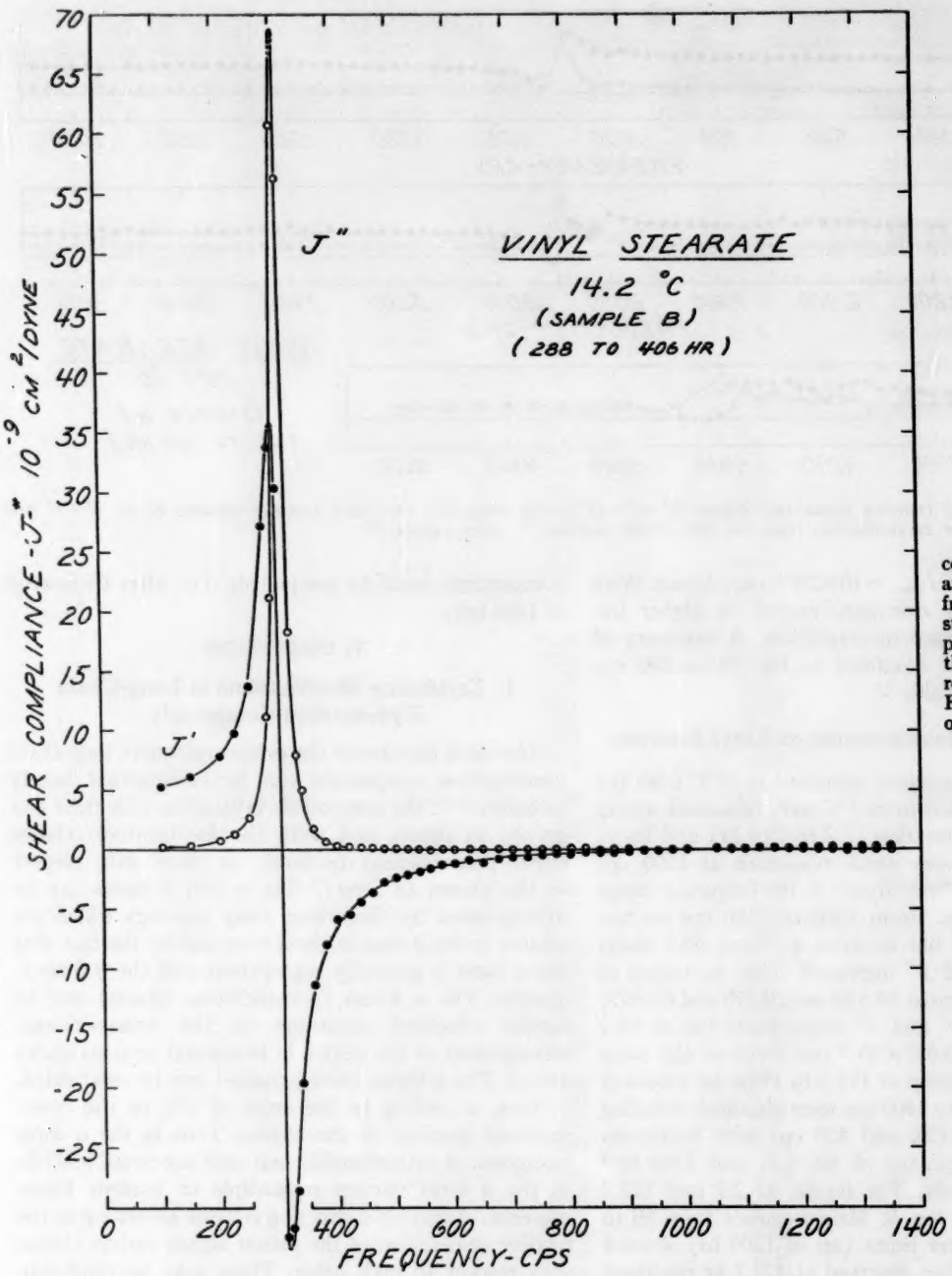

FIG. 5. Variation of complex shear compliance ($J^* = J' - iJ''$) with frequency for the vinyl stearate of Fig. 4 (sample B) at 14.2°C. Note that the scale is greatly reduced compared to Fig. 4. Solid points, J'; open points, J''.

ported here are observed for vinyl and ethyl stearate in the stable or β form while specific heat,[17] dielectric constant,[9] and nuclear magnetic resonance[18] measurements indicate that rotation takes place chiefly in the α forms of these types of esters.

Various modifications of structure have been reported for ethyl esters in both the perpendicular (α) and tilted (β) forms. Ethyl behenate, for example has two α and two β forms according to the density and dielectric constant measurements of Buckingham[9]; the liquid solidifies into an α_1 form at 47°C and then undergoes an irreversible transition into α_2 at 45°C. In both α forms the long spacing is 33.9 A. At 43°C an irreversible transition into a β_1 form occurred and at 30°C a reversible transition into a β_2 form was observed. Both β forms gave a long spacing of 30.1 A. As the temperature was subsequently raised and lowered around 30°C, however, the change in slope of the density *vs* tempera-

[17] Garner, Van Bibber, and King, J. Chem. Soc. **1931**, 1533.
[18] E. R. Andrews, J. Chem. Phys. **18**, 607 (1950).

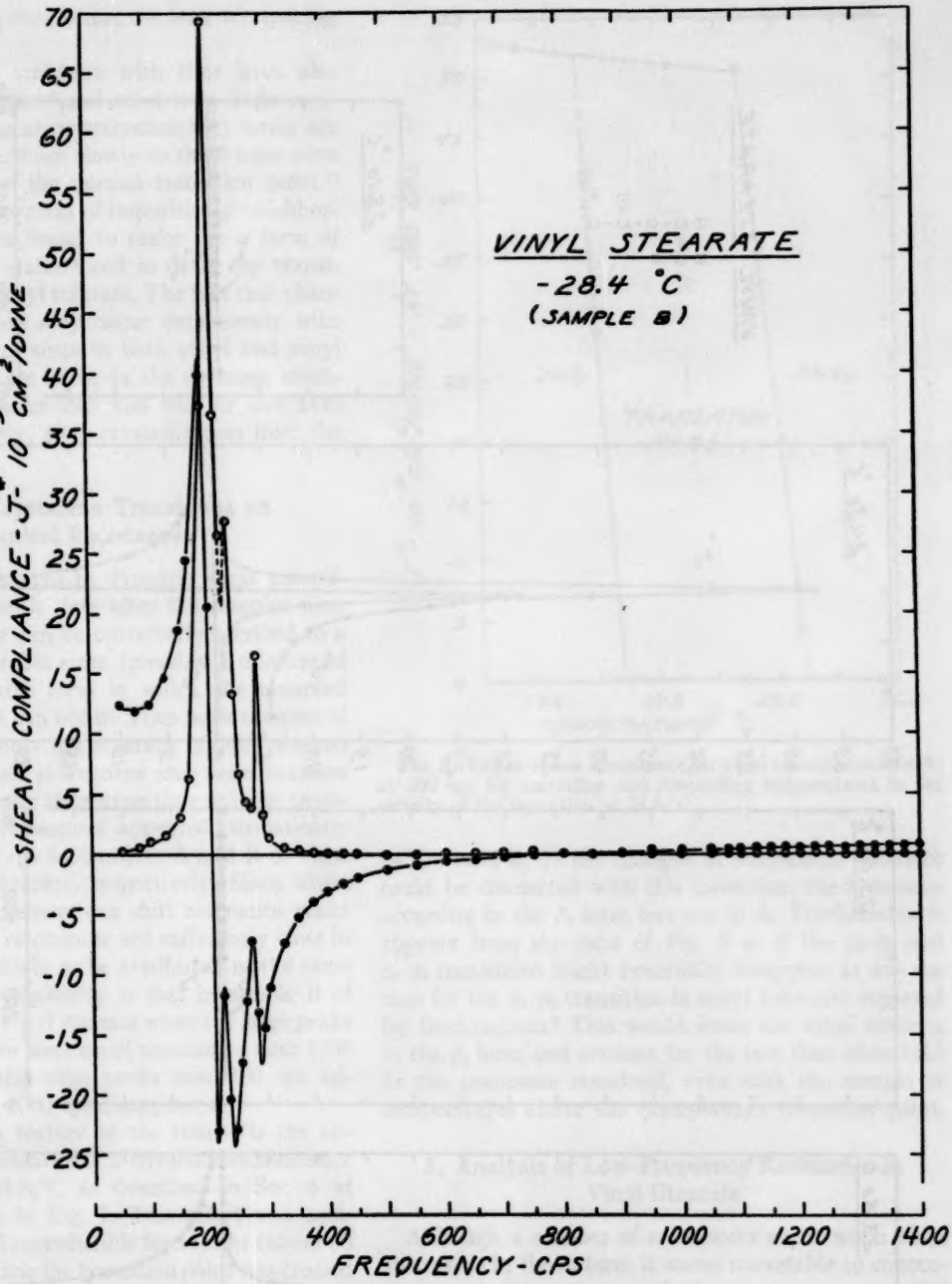

FIG. 6. Variation of complex shear compliance ($J^* = J' - iJ''$) with frequency for the vinyl stearate (sample B) at −28.4°C. Same scale as Fig. 5. Solid points, J'; open points, J''.

ture curve at 30°C became less pronounced, until it was finally very slight. This behavior of ethyl behenate is similar to that observed for vinyl stearate in the present investigation (see Fig. 3) where density measurements indicate four β forms. The temperature density coefficient for the β_1 and β_4 forms remains unchanged but after each heating cycle the β_2–β_3 transition becomes less pronounced. Unfortunately no x-ray measurements have been reported for vinyl stearate although Malkin[19] has reported both long and short spacings for ethyl stearate in a β form which indicate a monoclinic structure of the type shown in Fig. 10. Powder diffraction patterns of vinyl stearate cooled from the melt were obtained at six temperatures between 30 and 22°C and at 0°C in the present work, but no changes were observed by this method.[20] Thus it appears that the crystalline transitions occurring in vinyl stearate between 24 and 30°C are monoclinic to monoclinic, or

[19] T. Malkin, *Progress in the Chemistry of Fats* (Academic Press Inc., New York, 1952), Vol. 1, Chap. 1.

[20] The x-ray diffraction patterns were obtained through the courtesy of K. Vedam and R. Pepinsky.

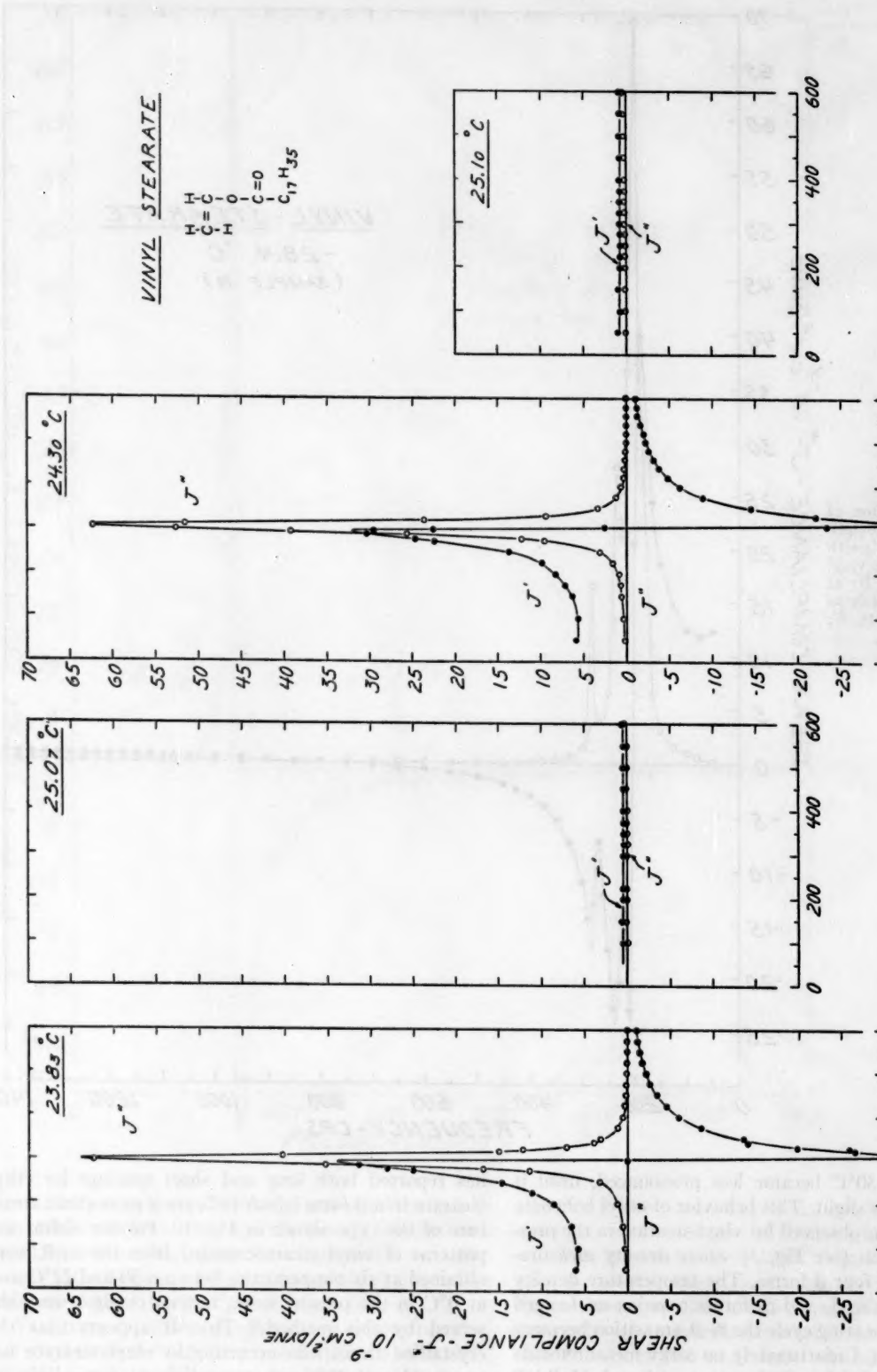

FIG. 7. Variation of complex shear compliance ($J^* = J' - iJ''$) with frequency for vinyl stearate (sample B) below and above the transition point at 24.8°C; same scale as Fig. 5. Solid points, J'; open points, J''.

monoclinic to triclinic, etc., where the long (c) spacing is unchanged.

Changes in crystal structure with time have also been noted for ethyl esters[6] and other long chain compounds; the α (hexagonal or orthorhombic) forms are often metastable and change slowly to the β form even at temperatures above the normal transition point.[13] The presence of a few percent of impurities of neighboring homologs has been found to make the α form of normal hydrocarbons stable[21] and to delay the transition to the β form[7] in ethyl stearate. The fact that changes in crystal structure may occur very slowly with time is of interest here since in both ethyl and vinyl stearate marked changes occur in the dynamic mechanical properties between 29.5 and 69.2 hr and 1415 to 1462 hr, respectively, after crystallization from the melt.

2. Effect of Crystalline Transitions on Mechanical Resonances

The remarkable changes in dynamic shear compliance which occured with time after the samples were formed from the melt can be tentatively ascribed to a change from a metastable state (possibly a mixture of two forms) to a stable form in which the observed mechanical resonance can occur. Thus both samples of vinyl stearate and the ethyl stearate initially showed only a few very small resonances and none between 50 and 600 cps. However after some time at room temperature tremendous resonances appeared permanently at 360, 305, and 275 cps for samples A and B of vinyl stearate and ethyl stearate, respectively. Since slight differences in static pressure can shift resonance peaks considerably[3,5] these resonances are sufficiently close in frequency and magnitude to be attributed to the same mechanism. Another similarity is that in sample B of vinyl stearate and in ethyl stearate when the large peaks were not present there were small resonances near 1000 cps, but whenever the large peaks near 300 cps appeared the ones near 1000 cps disappeared.

The most striking feature of the results is the appearance and disappearance of a tremendous resonance below and above 24.8$_5$°C as described in Sec. 4 of Part IV and shown in Fig. 7. This effect was completely reversible and reproducible for 1415 hr (about 58 days) during which time the transition point was crossed repeatedly and always with the same result: below 24.8$_5$°C a large resonance was present near 300 cps (along with many others at higher frequencies); above 24.8$_5$°C this resonance (and the others) disappeared. During this time the level of the compliance values above the transition (with no resonance) were steadily increasing, e.g., J' increased from 0.30×10^{-9} cm²/dyne at 120 hr to 0.65×10^{-9} cm²/dyne at 1412 hr. Since the density-temperature curves for vinyl stearate indicate a β_3 to β_4 transition occurring between 25 and

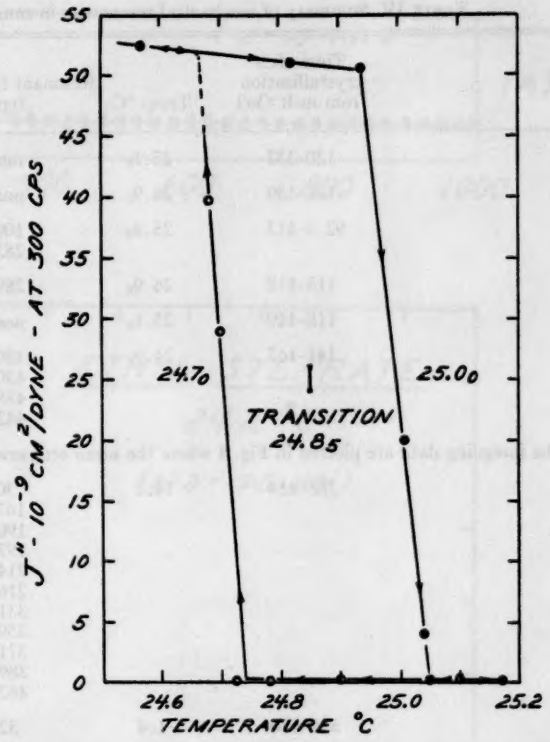

FIG. 8. Values of loss compliance for vinyl stearate (sample B) at 300 cps for ascending and descending temperatures in the vicinity of the transition at 24.8$_5$°C.

24°C (see Fig. 3) the changes in mechanical behavior could be connected with this transition; the resonance occurring in the β_4 form but not in β_3. Furthermore it appears from the data of Fig. 3 as if the β_2–β_3 and β_3–β_4 transitions might eventually disappear as was the case for the β_1–β_2 transition in ethyl behenate reported by Buckingham.[9] This would leave the vinyl stearate in the β_4 form and account for the fact that after 1415 hr the resonance remained, even with the sample at temperatures above the (temporary) transition point.

3. Analysis of Low-Frequency Resonance in Vinyl Stearate

Although a number of resonances occur when vinyl stearate is in the β_4 form it seems reasonable to concentrate attention at first on the large resonance near 300 cps. If some explanation can be found for its occurrence an understanding of the other resonances should be possible. Resonance dispersions of this kind have been fitted by assuming a generalized stress-strain relationship of the form[4,5]

$$s=k_0a+k_1(da/dt)+k_2(d^2a/dt^2) \qquad (1)$$

where s is the stress, a the strain, and k_0, k_1, and k_2 are constants. Then for a sinusoidal stress of circular frequency ω it can be established that the components

[21] A. E. Smith, J. Chem. Phys. 21, 2229 (1953).

TABLE IV. Summary of mechanical resonances in sample B of vinyl stearate at various times and temperatures.

Time after crystallization from melt (hr)	Temp °C	Resonant frequencies (cps)	Loss compliance maxima, J_{max}'' 10^{-9} cm²/dyne	Range (cps)
120–137	25.1_6	none	...	100–600
137–139	24.9_3	none	...	600–1000
92.5–113	25.4_0	1005	0.70	1000–2800
		2830	0.25	
113–118	24.9_0	2895	0.55	2800–3400
118–119	25.1_0	none	...	3400–4000
141–167	24.9_3	4200	0.20	4000–5000
		4300	0.25	
		4380	0.30	
		4425	0.30	
The foregoing data are plotted in Fig. 4 where the mean temperature is given as 25.1°C				
288–454	14.2	300	65–66	100–5000
		1675	1.3	
		1900	0.50	
		1975	8.	
		2145	0.20	
		2160	0.25	
		3310	0.20	
		3590	0.30	
		3710	0.15	
		3890	0.20	
		4620	0.30	
599–620	−1.4	320	45	100–1400
	−1.9	1685	0.30	1400–2800
		1910	0.45	
		1975	∽16	
		2190	0.10	
		2240	0.10	
759–816	−28.4	200	70.	50–2800
		230	28.	
		285	∽18.	
		1590	1.0	
		1735	0.35	
		1870	∽2.5	
		2590	0.20	
		2635	0.3	
		2770	0.3	
1095–1104	24.9	970	∽1.0	100–1400
1170–1176	14.0	310	∽67	100–1400
1245–1247	23.8_8	300	65–67	50–600
1275–1277	25.0_7	none	...	50–600
1290–1293	24.3_0	305	64–66	50–600
1412–1415	25.1_0	none	...	50–600
1462–1464	25.1_0	305	65–67	50–600
1606–1609	25.3_2	305	65–67	50–600
1773–1775	25.4_0	305	65–66	50–600

of complex shear compliance are

$$J' = J_a' + (1/k_0)\{(1-\omega^2/\omega_r^2)/[(1-\omega^2/\omega_r^2)^2+\omega^2\tau^2]\}, \quad (2)$$

$$J'' = J_a'' + (1/k_0)\{\omega\tau/[(1-\omega^2/\omega_r^2)^2+\omega^2\tau^2]\}, \quad (3)$$

where $\tau = k_1/k_0$, $\omega_r = (k_0/k_2)^{\frac{1}{2}}$, and J_a' and J_a'' take into account possible background compliances. Figure 11 illustrates the exactness with which the experimental data for vinyl stearate can be fitted by these expressions. Values of the constants of Eq. (1) selected to give the fit demonstrated in Fig. 11 are listed in Table VII.

Another interesting feature of the results is the appearance of a triplet resonance at low temperatures in

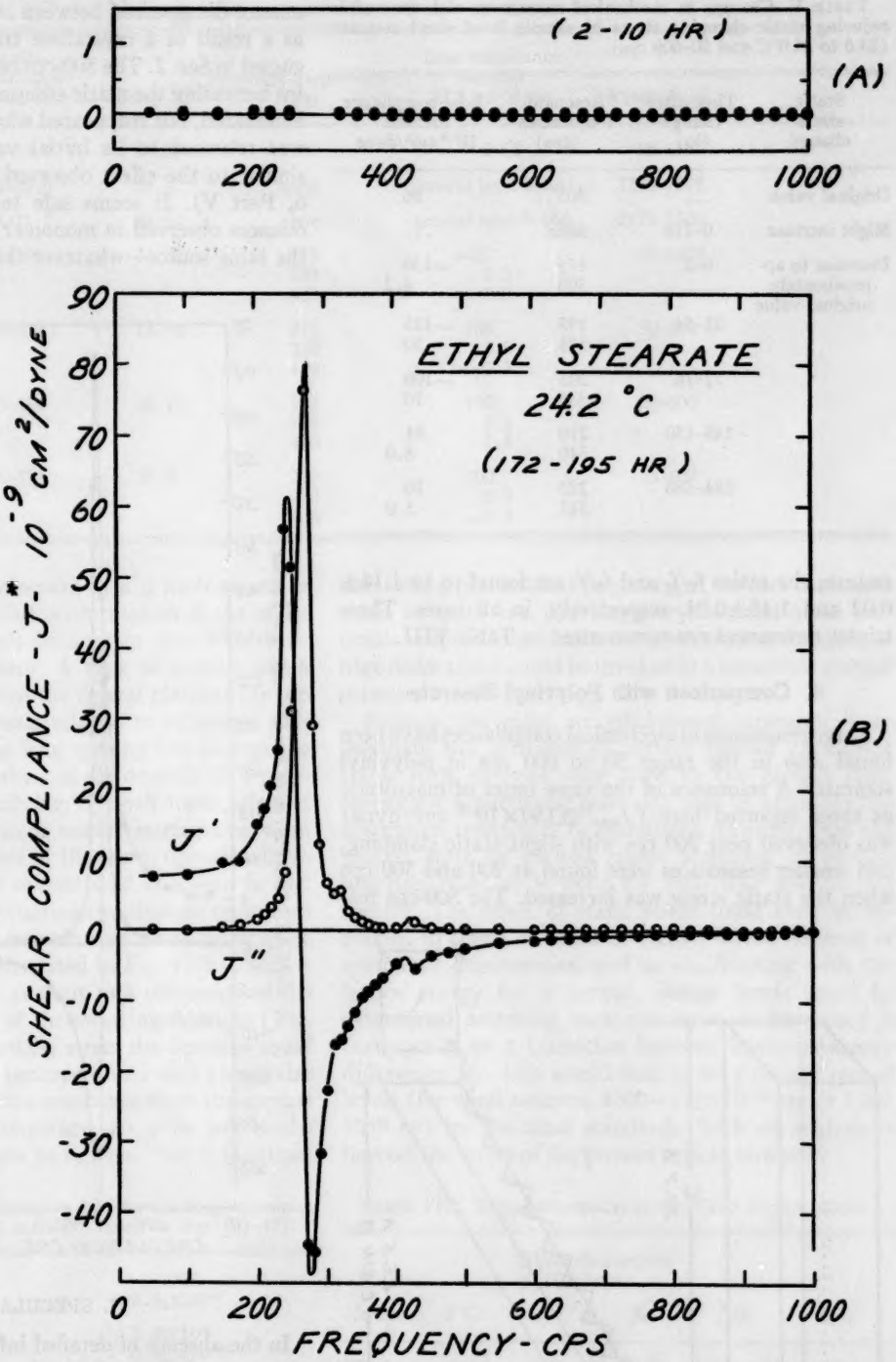

FIG. 9. Variation of complex shear compliance ($J^* = J' - iJ''$) with frequency for ethyl stearate at different times after crystallization from the melt: (A) 2.2 to 10.8 hr; (B) 172 to 195 hr. Scale in (B) reduced to one-half that of Fig. 5 and scale in (A) ten times that of (B). Solid points, J'; open points, J''.

vinyl stearate and at room temperature in ethyl stearate. Two subsidiary resonances appear on the high-frequency side of the main resonance at temperatures of 13.5°C and below in sample A of vinyl stearate; a similar triplet appears at −28.3°C in sample B. The associated resonances decrease in magnitude with increasing frequency and are smallest for ethyl stearate. The locations of the triplet resonances vary somewhat with temperature, from sample A to sample B of vinyl stearate, and from vinyl to ethyl stearate. The subsidiary frequencies in all cases however appear to be in a fixed ratio to the principal (largest) resonances. Thus if the resonances are denoted as occurring at frequencies f_1, f_2, f_3 where f_1 is the frequency of the principal res-

TABLE V. Changes in mechanical resonances with time after reducing static clamping stress in sample B of vinyl stearate (23.6 to 24.0°C and 50–600 cps).

Static stress change	Time after change (hr)	Resonant frequencies (cps)	Loss compliance maxima 10^{-9} cm²/dyne
Original value	...	305	66
Slight increase	0–219	none	...
Decrease to approximately original value	0–2	175	~150
		300	4.2
	51–54	195	~125
		325	10
	72–76	205	~100
		335	10
	148–150	210	81
		340	8.0
	384–386	225	70
		345	5.0

onance, the ratios f_2/f_1 and f_3/f_1 are found to be 1.14± 0.02 and 1.48±0.04, respectively, in all cases. These triplet resonances are summarized in Table VIII.

4. Comparison with Polyvinyl Stearate

Large resonances in mechanical compliances have been found also in the range 50 to 600 cps in polyvinyl stearate.[3] A resonance of the same order of magnitude as those reported here ($J_{max}'' \cong 150 \times 10^{-9}$ cm²/dyne) was observed near 200 cps with slight static clamping, and smaller resonances were found at 200 and 500 cps when the static stress was increased. The 500-cps resonance disappeared between 30.5 and 36.4°C, probably as a result of a crystalline transition of the type discussed in Sec. 2. The 500-cps resonance was also reduced by increasing the static compression; in one case it was eliminated, but reappeared when the static compression was returned to its initial value. This is, of course, similar to the effect observed for vinyl stearate (Sec. 6, Part V). It seems safe to conclude that the resonances observed in monomer and polymer arise from the same source—whatever that may be.

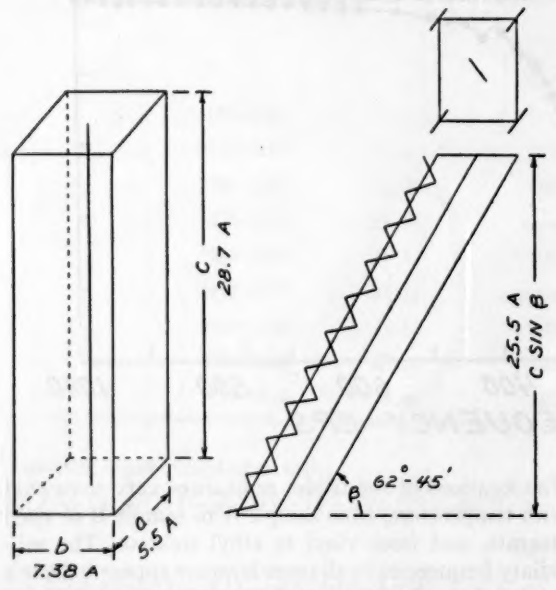

FIG. 10. Possible unit cell for a β form of ethyl stearate based on long and short spacings obtained from x-rays as reported by Malkin.[19]

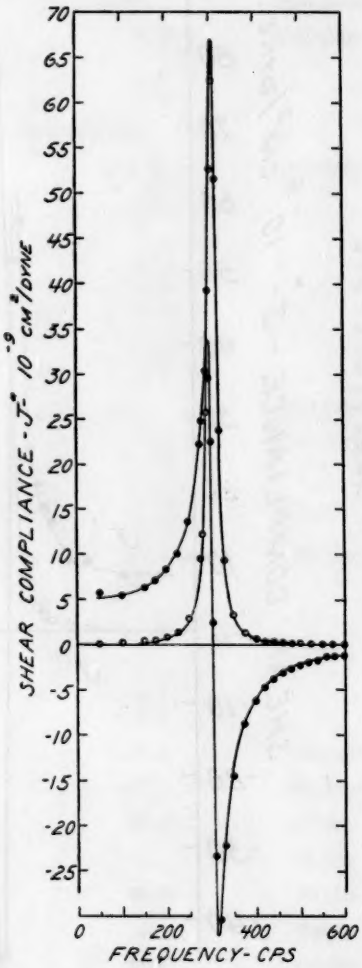

FIG. 11. Comparison of calculated values of compliance based on Eqs. (2)–(3) (solid lines) for the large resonance in sample B of vinyl stearate and experimental results at 24.3°C. Solid points, measured values of J'; open points, measured values of J''. The calculated curves are based on the empirical constants listed in Table VII.

VI. SPECULATION

In the absence of detailed information on the crystal structures of the various β forms of vinyl stearate it is impossible to draw any firm conclusions as to the exact mechanism responsible for the resonances occuring in the β_4 form. Enough general information about the structure of ethyl esters is available, however, to permit some speculation which might prove useful in planning future experiments or eliminating certain classes of phenomena. As has already been mentioned the fact

TABLE VI. Summary of mechanical resonances in ethyl stearate.

Time after crystallization from melt (hr)	Temp °C	Resonant frequencies (cps)	Loss compliance maxima 10^{-9} cm²/dyne	Range (cps)
2.3–10.8	24.2_9	1100	0.52	50–1190
26.8–29.5	24.5_8	none	general level 0.030	1200–2175
69.3–71.7	24.3_5	none	general level 0.060	2175–2560
172–196	24.2_0	275	~80	50–1400
		320	5.5	
		420	1.0	
314–318	24.0_0	275	106	50–600
		320	5.5	
		420	~2.5	
483–486	24.1_0	275	100	50–600
		325	5.5	
		430	2.5	
575–576	26.8	275	100	50–600
		325	6.0	
		430	~3.0	

that the large resonance occurs in a β form seems to preclude a direct connection with rotation of the molecule about its chain axis because in this form such rotation is virtually absent. A type of motion which might occur is a rotation of the crystal plane at the top of a small crystalline domain relative to its base in such a way as to maintain the long spacing but change the direction of tilt (orientation) of the domain. In a polycrystalline material consisting of small units oriented at random there must occur many interfaces between the units where the angles of tilt are in opposite directions leaving a diamond shaped void as shown in Fig. 12(a). Either of the neighboring two-domain complexes could then swing around into the void (if swinging space were available) as demonstrated in Fig. 12(b). Such a domain inversion would amount to a precession of the individual tilted chains of the swinging domains [Fig. 12(c)]. Under an alternating stress the domains could swing back and forth or perhaps rotate with an angular frequency ω_D giving rise to a resonance when the applied stress is at the same frequency. As with any model there are many objections to this one, but it is attractive since a precessional frequency of the sort envisaged could be quite low. For single crystals and other materials without long chains the precession or rotation of edge dislocations could be invoked in a somewhat similar manner.

Perhaps the most straightforward approach is to postulate the existence of certain excited crystalline states with energies very close to the ground state energy for a particular unit cell, and to attribute the absorption resonances to transitions occuring from the ground state to excited states according to certain selection rules as is done for molecular and atomic spectra. The effect of static stress could then be explained in terms of shifts in excited levels, removal of symmetry degeneracies, and so on. Starting with the lattice energy for a crystal, energy levels could be determined assuming each resonance at frequency f_r corresponds to a transition between levels of energy differences hf_r. This would lead to very closely spaced levels (for vinyl stearate, $h300 = 2.0\times10^{-24}$ erg or 1.2×10^{-12} ev) by the usual standards. Such an analysis is beyond the scope of the present article, however.

TABLE VII. Analysis of dispersion data for the large resonance in vinyl stearate (sample B) at 24.3°C based on Eqs. (2)–(3).

Resonant frequency f_r (cps)		305
Retardation time τ (sec)		$3.5_0\times10^{-4}$
Modulus k_0 (dyne/cm²)		2.2×10^{10}
$1/k_0$ (cm²/dyne)		0.45×10^{-10}
First derivative constant, k_1 (dyne-sec/cm²)		$7.7_7\times10^{5}$
Second derivative constant, k_2 (dyne-sec²/cm²)		6.0×10^{9}
Background comp. (cm²/dyne)	J_0'	0.45×10^{-9}
	J_0''	0

TABLE VIII. Triplet resonances in vinyl and ethyl stearate.

Sample	T°C	Triplet frequencies (±3 cps) f_1	f_2	f_3	f_2/f_1	f_3/f_1
Vinyl stearate A	13.5	420	475	615	1.13±.02	1.46±.02
	−1.3	350	405	510	1.16±.02	1.46±.02
	−27.8	300	340	435	1.13±.02	1.45±.03
Vinyl stearate B	−28.3	200	230	285	1.15±.03	1.43±.03
Ethyl stearate	24.0	275	320	420	1.16±.03	1.52±.03

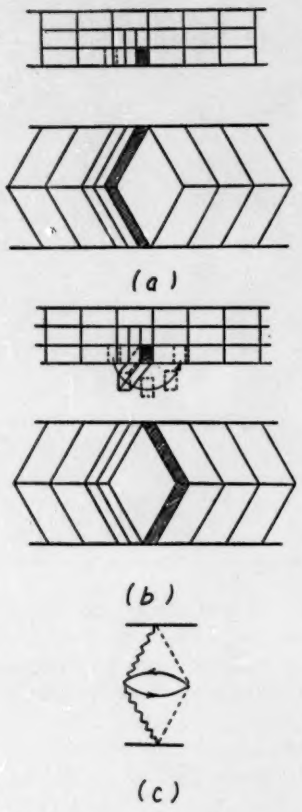

FIG. 12. Diagram illustrating possible precession of crystalline domains in the tilted (β) form of vinyl stearate.

VII. CONCLUSIONS

Complex shear compliance measurements on vinyl and ethyl stearate yield results depending critically on the particular crystalline modification in which these materials exist at the time of measurement. When first cooled from the melt the materials are in a metastable form and only a few very small resonance dispersions are noted in the range 50 to 5000 cps. At later times numerous large resonances appear; the largest is in the vicinity of 300 cps for both vinyl and ethyl stearate.

While the vinyl stearate is in a metastable state (for approximately 60 days) a reversible transition takes place at $24.8_5 \pm 0.1_5$°C such that above this temperature there is no resonance in the region from 50 to 600 cps, but below the transition the large resonance near 300 cps always appears. A transition between 24 and 25°C is also indicated by a break in the slope of density-temperature curves obtained for vinyl stearate. The appearance and disappearance of the huge resonance at 300 cps is tentatively ascribed to a transition occuring in the vinyl stearate while in its β form with the molecules tilted with respect to the planes formed by the terminal groups. X-ray powder diffraction photographs show no changes in the long spacing (between planes) at temperatures from 30 to 0°C so the transition must involve changes in cross-sectional packing of the chains or a change from a monoclinic to triclinic unit cell rather than any change in the angle of the tilt.

At lower temperatures the large resonance in vinyl stearate splits into a triplet; although the principal resonance frequency f_1 varies somewhat with temperature and for different samples, the ratios of the subsidiary triplet frequencies to f_1 is always constant.

The details of the crystalline modification occurring between 24 and 25°C in vinyl stearate are not as yet sufficiently clear to define a specific mechanism for the resonance phenomena, but the results prove conclusively that the dispersions are intimately connected with the crystalline state of the material. Future measurements are planned on other long chain hydrocarbons where transitions of a known character occur.

In the meantime one can speculate that a kind of mechanical spectroscopy eventually may be evolved yielding information on the actual crystalline state of solids in much the same way that electromagnetic spectra aid in determinations of molecular and atomic structure.

VIII. ACKNOWLEDGMENTS

Martin G. Broadhurst and Anthony J. Bur assisted in cooling curve and density determinations. Calculations were performed by Mrs. Ronald C. Althouse and Mrs. Thomas J. Zielinski who also assisted in some of the dynamic mechanical measurements.

Atomic Polarization. I. Vibrational Polarization of Gases*†

KARL H. ILLINGER‡ AND CHARLES P. SMYTH

Frick Chemical Laboratory, Princeton University, Princeton, New Jersey

(Received August 10, 1959)

A derivation is given for the vibrational polarization and the vibrational polarizability of a molecule in several degrees of approximation. From the expressions derived, the vibrational polarization is calculated for a large number of molecules. A discussion, within the framework of the present derivation, is given of the atomic polarization, and a detailed comparison with previous theories is made.

I. INTRODUCTION

THE so-called atomic polarization of a molecule may be defined by the frequency limits of the polarization terms at higher frequencies, the electronic polarization, and those at lower frequencies, the rotational or orientation polarization. For the isolated molecule, in the absence of external perturbing forces other than the electric field, the atomic polarization terms may be calculated exclusively from the transition probabilities and frequencies of all the possible transitions between vibrational states of the molecule. In keeping with the nomenclature of the other polarization types, which are named according to the type of transition to which they can be related, this contribution to the total polarization will be termed the vibrational polarization. In the presence of intermolecular forces, perturbation of the energy levels of the isolated molecule leads to the alteration of the transition frequencies and transition probabilities. Under conditions of strong interaction, absorption bands and related contributions to the polarization may result from an absorbing system, composed of more than one molecule, in which the component molecules are in strong mutual interaction. Consequently, the atomic polarization of a molecule may include both the vibrational polarization and polarization terms related to mechanisms of vibrational energy absorption depending upon strong intermolecular interactions.

The present work is concerned with the derivation of the vibrational polarization and the vibrational polarizability. An attempt at a rigorous derivation, with the sequence of degrees of approximation defined in the development, permits a closer examination of the validity of approximations inherent in previous treatments, which may all be deduced from the general expressions developed here. Furthermore, the data on vibrational intensities that have become available in the literature in recent years make numerical calculations possible for a large number of molecules.

* This research has been supported in part by the Office of Naval Research. Reproduction, translation, publication, use or disposal, in whole or in part, by or for the United States Government is permitted.

† This paper represents a part of the work to be submitted by Mr. Karl H. Illinger to the Graduate School of Princeton University in partial fulfillment of the requirements for the degree of Doctor of Philosophy.

‡ General Electric Fellow in Chemistry, 1958–1959.

II. THEORY

Quantum-mechanical perturbation theory leads to the following expression for the polarizability of a molecule in a quantum state n, randomly oriented in space in the presence of a time-dependent external electric field of frequency ν[1]:

$$(n \mid a \mid n) = \frac{2}{3h} \sum_{n'(n' \neq n)} \frac{\mid (n \mid p \mid n') \mid^2 \nu(n'; n)}{\nu^2(n', n) - \nu^2} \qquad (1)$$

where

$$\mid (n \mid p \mid n') \mid^2 = \sum_g \mid (n \mid p_g \mid n') \mid^2, \quad g = x, y, z,$$

and

$$(n \mid p_g \mid n') = \int \psi_n^* p_g \psi_{n'} d\tau$$

defines an axial component of the dipole moment matrix element associated with the transition $n \rightarrow n'$, between the states n and n', whose wave functions are denoted by ψ_n and $\psi_{n'}$, respectively. In Eq. (1), $\nu(n'; n)$ is the frequency corresponding to the transition $n \rightarrow n'$, p_g is the vector dipole moment component of the molecule along the g axis, and h is the Planck constant. In the general case, where the states n and n' are degenerate, consisting of sets of sublevels, $b = b_n$, and $b' = b_{n'}$, respectively, the total matrix element is given by

$$\mid (n \mid p \mid n') \mid^2 = \sum_{b,b'} \mid (n \mid M \mid n') \mid^2, \qquad (2)$$

where the summation is made over all the individual degenerate states b and b'.

On combining Eqs. (1) and (2), one obtains in the limit of the frequency of the external field approaching zero

$$\lim_{\nu \to 0} (n \mid a \mid n) = (n \mid \alpha \mid n)$$

$$= \frac{2}{3h} \sum_{n'(n' \neq n)} \frac{\sum_{b,b'} \mid (n \mid M \mid n') \mid^2}{\nu(n'; n)}. \qquad (3)$$

It is seen from this equation that the distortion polarizability, $(n \mid \alpha \mid n)$, of a molecule depends on two

[1] Eyring, Walter, and Kimball, *Quantum Chemistry* (John Wiley & Sons, Inc., New York, 1944), p. 121.

independent sets of terms which are highly specific for a given molecule: (a) the characteristic transition frequencies, $\nu(n';\ n)$, and (b) the matrix elements, $|\ (n\ |\ M\ |\ n')\ |^2$ associated with the transitions $n \rightarrow n'$, which determine the intensity of absorption at the frequency $\nu(n';\ n)$. If it is assumed that the dispersion of $(n\ |\ a\ |\ n)$ in terms of $|\ (n\ |\ M\ |\ n')\ |^2$ and $\nu(n';\ n)$ is given with sufficient accuracy in Eq. (1), which carries with it all the approximations made in first-order perturbation theory,[2] it remains to develop these two molecular quantities in terms of approximations which may be used to derive them from experimentally realizable quantities. The terms $\nu(n';\ n)$ can be measured directly by experiment, and consequently no further assumptions inhere in their use in Eqs. (1) and (3). On the other hand, the terms $|\ (n\ |\ M\ |\ n')\ |^2$ are not directly measurable and certain approximations must be made to permit their formulation by way of observable quantities, namely the intensities of absorption bands due to the transitions $n \leftrightarrow n'$.

The summation in Eqs. (1) and (3) is over all states $n'(n' \neq n)$ to which transitions occur from the fixed state n. If only transitions characterized by a specific change in quantum numbers designating the two states n and n' are included in the sum, the polarizability related to an individual transition $n \rightarrow n'$, with a fixed value of the quantum numbers necessary to specify state n, is given by

$$(n\ |\ \alpha\ |\ n') = \frac{2}{3h}\frac{\sum_{b,b'}|\ (n\ |\ M\ |\ n')\ |^2}{\nu(n';\ n)}. \quad (4)$$

In the foregoing, the designation n alone has appeared in the equations to specify the quantum state n. In the case that a quantum state n has associated with it a set of quantum states designated by a separate inner quantum number i, each of the matrix elements, $|\ (n\ |\ M\ |\ n')\ |^2$, is composed of the summation over all allowed values of i associated with n:

$$|\ (n\ |\ M\ |\ n')\ |^2 = \sum_i\{\sum_{a,a'}|\ (i, n\ |\ M\ |\ i', n')\ |^2\}, \quad (5)$$

where the summation over a, a' corresponds to the sum over all individual degenerate sublevels of a state i. Transitions characterized by a matrix element $|\ (i, n\ |\ M\ |\ i', n')\ |^2$ in the sum in Eq. (5) correspond to a change in quantum numbers: $(i,\ n) \leftrightarrow (i',\ n')$, subject to selection rules governing the transition, and result in an absorption frequency $\nu(i',\ n';\ i,\ n)$. Consequently, Eq. (4) is rewritten in terms of Eq. (5) as

$$(n\ |\ \alpha\ |\ n') = \sum_i (i, n\ |\ \alpha\ |\ i', n')$$

$$= \frac{2}{3h}\sum_i \frac{\sum_{b,b'}\sum_{a,a'}|\ (i, n\ |\ M\ |\ i', n')\ |^2}{\nu(i', n';\ i,\ n)}. \quad (6a)$$

At this point, it is convenient to differentiate between transitions in which the absolute energy of the molecule is increased by absorption of energy from the external electric field, and those in which the absolute energy of the molecule is decreased by emission of energy by the molecule. If the energy of the quantum state $(i',\ n')$ is greater than that of the state $(i,\ n)$, $(i,\ n\ |\ \alpha\ |\ i',\ n')$ denotes a positive contribution to the polarizability associated with the transition $(i,\ n) \rightarrow (i',\ n')$, having the absorption frequency $\nu(i',\ n';\ i,\ n)$. If the energy of state $(i',\ n')$ is less than that of state $(i,\ n)$, $(i,\ n\ |\ \alpha\ |\ i',\ n')$ will denote a negative contribution to the polarizability associated with the transition $(i,\ n) \rightarrow (i',\ n')$, having the emission frequency $\nu(i,\ n;\ i',\ n')$. The matrix elements for the transitions between state $(i,\ n)$ and $(i',\ n')$ are equal for the absorption and the emission transition; the absorption and the emission frequency are equal and opposite in sign. These conditions allow one to write

$$(n\ |\ \alpha\ |\ n') = \sum_i (i, n\ |\ \alpha\ |\ i', n') = -(n'\ |\ \alpha\ |\ n). \quad (6b)$$

Consider now N molecules, where N is the Avogadro number, distributed in thermal equilibrium at a given temperature T, over the states n and i, such that

$$\sum_n\{\sum_i N_{i,n}\} = \sum_n N_n = N. \quad (7)$$

Equation (7) expresses the assumption that the summation over all the energy states $(i,\ n)$ accounts for all the N molecules, implying that if there are energy states, m, of which the set of states n, is a subset, only the state of the particular value of m being considered is assumed to be populated. In particular, if the states n refer to the vibrational states of the molecule, the states i referring then to its rotational states, only a single electronic state, $m=0$, i.e., the ground electronic state, is assumed to be populated.

The polarization of the N_n molecules occupying the state n and the $N_{n'}$ molecules occupying the state n', related to the transition $n \leftrightarrow n'$, including the entire subset of transitions $(i,\ n) \leftrightarrow (i',\ n')$ summed over all i and i' is then given by

$$P(n;\ n') = \sum_i\{(i, n\ |\ P\ |\ i', n') + (i', n'\ |\ P\ |\ i, n)\}$$

$$= (4\pi/3)\sum_i\{N_{i,n} - N_{i',n'})\,(i, n\ |\ \alpha\ |\ i', n')\}. \quad (8)$$

For all transitions $n \leftrightarrow n'$, involving all combinations of states for which the change in quantum numbers is identical, $P(n;\ n')$ is summed over all n giving the polarization of the N molecules related to this transition as

$$P(\Delta n = \text{const.}) = (8\pi/9h)$$

$$\cdot\sum_n\left\{\sum_i \frac{(N_{i,n} - N_{i',n'})\sum_{b,b'}\sum_{a,a'}|\ (i, n\ |\ M\ |\ i', n')\ |^2}{\nu(i', n';\ i,\ n)}\right\}. \quad (9)$$

[2] See, for example, reference 1, Chap. 7.

Equations (6) and (9) will now be applied to develop expressions for the polarizability and the polarization related to vibrational transitions. In this case, the inner quantum number i in the previous notation corresponds to the rotational quantum number J, and the quantum states n correspond to vibrational states characterized by the set of vibrational quantum numbers: $v_1, v_2, v_3 \cdots v_k$. The dipole moment matrix element, $|(J, n \mid M \mid J', n')|^2$, for the transition characterized by the change in quantum numbers: $(J, n) \leftrightarrow (J', n') \equiv (J, v_1, v_2 \cdots v_k) \leftrightarrow (J', v_1', v_2' \cdots v_k')$, is related to the absolute line intensity, $A(J, n; J', n')$, for the transition between two of the degenerate vibrational sublevels: $b = b_n$ and $b' = b_{n'}$, and summed over all the individual degenerate rotational sublevels: $a = a_J$ and $a' = a_{J'}$, which are subsets of these vibrational levels, by the equation,[3]

$$g_J A(J, n; J', n') = (8\pi^3/3hc)(\mathfrak{N}_{J,n} - \mathfrak{N}_{J',n'})\nu(J', n'; J, n) \sum_{a,a'} |(J, n \mid M \mid J', n')|^2, \quad (10)$$

where $\mathfrak{N}_{J,n}$ and $\mathfrak{N}_{J',n'}$ are the number of molecules/cm^3 in the states defined by the set of vibrational quantum numbers n and n' and the rotational quantum numbers J and J', respectively. $\nu(J', n'; J, n)$ is the absorption frequency corresponding to a single line in the vibration-rotation band, c is the velocity of light, and g_J is the degeneracy of the lower rotational state, consisting of g_J rotational sublevels.

The summation of the line intensity terms in Eq. (10) over all the individual degenerate vibrational sublevels b_n yields, upon solving for the associated total vibrational matrix element summed over all possible combinations of the levels of the upper state with those of the lower state,[4]

$$\sum_{b,b'} \sum_{a,a'} |(J, n \mid M \mid J', n')|^2 = \frac{3hc}{8\pi^3} \frac{g_n g_J A(J, n; J', n')}{(\mathfrak{N}_{J,n} - \mathfrak{N}_{J',n'})\nu(J', n'; J, n)}, \quad (11)$$

where g_n is the degeneracy of the lower vibrational state, n, which consists of g_n vibrational sublevels.

Equations (9) and (6a) can now be combined with the value of the total vibrational matrix element obtained from Eq. (11) to give the polarization and the polarizability, respectively, related to the infrared active vibration-rotation band characterized by the vibrational transitions, $\Delta v_1 = j_1$, $\Delta v_2 = j_2 \cdots \Delta v_k = j_k$, as,

$$P(\Delta v_k = j_k) = \frac{c}{3\pi^2} \sum_n \left\{ \sum_J \frac{(N_{J,n} - N_{J',n'}) g_n g_J A(J, n; J', n')}{(\mathfrak{N}_{J,n} - \mathfrak{N}_{J',n'})\nu^2(J', n'; J, n)} \right\}, \quad (12)$$

and

$$(n \mid \alpha \mid n') = \frac{c}{4\pi^3} \sum_J \frac{g_n g_J A(J, n; J', n')}{(\mathfrak{N}_{J,n} - \mathfrak{N}_{J',n'})\nu^2(J', n'; J, n)}. \quad (13)$$

Equation (12) permits the exact evaluation of the polarization related to all the vibrational transitions associated with $\Delta v_k = j_k$, if the experimental quantities $g_n g_J A(J, n; J', n')$ and $\nu(J', n'; J, n)$ for each of the lines in the vibration-rotation band, and the molar volume, V_m, are known. If, in addition, the combined partition function for vibration and rotation, θ_{RV}, is accurately known, the polarizability can be exactly determined from Eq. (13). This is possible through substitution for the populations, $N_{J,n}$ and $N_{J',n'}$, and the populations per cm^3, $\mathfrak{N}_{J,n}$ and $\mathfrak{N}_{J',n'}$, in terms of the Maxwell-Boltzmann distribution of molecules among the energy levels:

$$N_{J,n} = (N/\theta_{RV}) \exp[-E(J, n)/kT], \quad (14)$$

and

$$\mathfrak{N}_{J,n} = (\mathfrak{N}/\theta_{RV}) \exp[-E(J, n)/kT], \quad (15)$$

where $E(J, n)$ is the energy of a molecule in the state (J, n). Equations (12) and (13) may then be written

$$P(\Delta v_k = j_k) = \frac{V_m c}{3\pi^2} \sum_n \left\{ \sum_J \frac{g_n g_J A(J, n; J', n')}{\nu^2(J', n'; J, n)} \right\}, \quad (16)$$

and

$$(n \mid \alpha \mid n') = (\theta_{RV} c/4\pi^2 \mathfrak{N}) \cdot \sum_J \frac{[1 - \exp(-u(J', n'; J, n))]^{-1} g_n g_J A(J, n; J', n')}{\exp[-E(J, n)/kT]\nu^2(J', n'; J, n)}, \quad (17)$$

where $u(J', n'; J, n)$ is defined by the relation

$$u(J', n'; J, n) = (hc/kT)\nu(J', n'; J, n).$$

These considerations show that the evaluation of $P(\Delta v_k = j_k)$ and $(n \mid \alpha \mid n')$ from individual line intensities and line frequencies according to Eqs. (16) and (17) is limited in exactness only by the exactness of Eqs. (1) and (10), and, in the case of the polarizability, further by the exactness of the partition function. It is important to note that the explicit form of

[3] B. L. Crawford, Jr., and H. L. Dinsmore, J. Chem. Phys. 18, 983, 1682 (1950).

[4] Compare with the Einstein coefficient of absorption for transitions between degenerate states, G. Herzberg, *Spectra of Diatomic Molecules* (D. Van Nostrand Company, Inc., Princeton, New Jersey, 1950), second edition, p. 21.

the vibrational matrix elements need not be known if this type of experimental data is available. Unfortunately, only a very few investigations providing the experimental quantities requisite for the use of Eqs. (16) and (17), even for restricted values of the j_k's, exist at this time. The experimental conditions of most intensity determinations result in the measurement of the integrated intensity of the pressure-broadened band, in which all rotational fine structure has been erased. Furthermore, due to the approximate coincidence of the set of frequencies, $\nu(n';\ n)$ over all values of n, the overlapping of intensity terms, $A(n;\ n')$, results in an experimental integrated band intensity in the vicinity of $\nu(n';\ n)$, the frequency at the center of the vibration-rotation band, given by the expression:

$$A_{\text{exp}}=A(\Delta v_k=j_k)=\sum_n g_n A(n;\ n')$$
$$=\sum_n\{\sum_J g_n g_J A(J, n;\ J', n')\}. \quad (18)$$

Equation (11) may now be used for the evaluation of any two terms, $g_n g_J A(J, n;\ J', n')$ and $g_{n''}g_{J''}A(J'',\ n'';\ J''',\ n''')$, where the latter term refers to a transition occurring between the lower state $(J'',\ n'')$ and the upper state $(J''',\ n''')$, consisting of the $g_{n''}g_{J''}$ substates: $c=a_{J''}$, $d=b_{n''}$, and the $g_{n'''}g_{J'''}$ substates, $c'=a_{J'''}$, $d'=b_{n'''}$, respectively. The ratio of these terms is given by

$$\frac{g_n g_J A(J, n;\ J', n')}{g_{n''}g_{J''}A(J'', n'';\ J''', n''')}=\frac{(\mathfrak{N}_{J,n}-\mathfrak{N}_{J',n'})\nu(J', n';\ J, n)\sum_{b,b'}\sum_{a,a'}|(J, n\,|\,M\,|\,J', n')|^2}{(\mathfrak{N}_{J'',n''}-\mathfrak{N}_{J''',n'''})\nu(J''', n''';\ J'', n'')\sum_{d,d'}\sum_{c,c'}|(J'', n''\,|\,M\,|\,J''', n''')|^2}. \quad (19)$$

Substitution for $g_n g_J A(J, n;\ J', n')$ in Eq. (18) supplies the relationship between the experimental total band intensity, $A(\Delta v_k=j_k)$, and the individual line intensity terms. If the combined equation is solved for $g_{n''}g_{J''}A(J'', n'';\ J''', n''')$, and the expression resulting from this step is substituted into Eq. (19), the individual line intensity terms can be evaluated as

$$g_n g_J A(J, n;\ J', n')$$
$$=A(\Delta v_k=j_k)\frac{F(J, v_k, j_k)}{\sum_n\{\sum_J F(J, v_k, j_k)\}}, \quad (20)$$

where

$$F(J, v_k, j_k)$$
$$=(\mathfrak{N}_{J,n}-\mathfrak{N}_{J',n'})\nu(J', n';\ J, n)\sum_{b,b'}\sum_{a,a'}|(J, n|M|J', n')|^2.$$

Since an expression for the individual line intensities has been obtained in Eq. (20), the associated polarization summed over all J and n, derived in Eq. (12) can now be expressed in terms of experimental quantities as

$$P(\Delta v_k=j_k)=\frac{cA(\Delta v_k=j_k)}{3\pi^2\sum_n\{\sum_J F(J, v_k, j_k)\}}$$
$$\cdot\sum_n\left\{\sum_J\frac{(N_{J,n}-N_{J',n'})\sum_{b,b'}\sum_{a,a'}|(J, n\,|\,M\,|\,J', n')|^2}{\nu(J', n';\ J, n)}\right\}. \quad (21)$$

Substitution of Eq. (20) into Eq. (13) allows the evaluation of the polarizability as

$$(n\,|\,\alpha\,|\,n')=\frac{cA(\Delta v_k=j_k)}{4\pi^3\sum_n\{\sum_J F(J, v_k, j_k)\}}$$
$$\cdot\sum_J\frac{\sum_{b,b'}\sum_{a,a'}|(J, n\,|\,M\,|\,J', n')|^2}{\nu(J', n';\ J, n)}. \quad (22)$$

It must be noted that Eqs. (21) and (22) have the same degree of exactness as Eqs. (12) and (13), if the experimental criterion expressed in Eq. (18) is satisfied. The continuation of the development of these equations, however, necessitates the evaluation of various sums over the rotational and vibrational quantum numbers, which is feasible only by approximate methods.

The summation of $F(J, v_k, j_k)$ over J which appears in Eqs. (21) and (22) may now be evaluated by the use of the expression for the integrated band intensity, $A(n;\ n')$, of a vibration-rotation band[5]

$$A(n;\ n')=\sum_J g_J A(J, n;\ J', n')$$
$$=(8\pi^3/3hc)(\mathfrak{N}_n-\mathfrak{N}_{n'})\nu(n';\ n)\,|\,(n\,|\,M\,|\,n')\,|^2, \quad (23)$$

where $\mathfrak{N}_n$ and $\mathfrak{N}_{n'}$ are the number of molecules per cm^3 in the vibrational states defined by the set of vibrational quantum numbers n and n', respectively, and $\nu(n';\ n)$ is the band center absorption frequency of the transition $n\leftrightarrow n'$.

Equation (23) is an approximation which must be examined by comparison with expressions for $A(n;\ n')$, which have been derived by means of an exact summation of the component intensities of the vibration-rotation band. If the interaction between vibration and rotation is neglected, and the assumption is made that the ratio $(2B_0/\nu(n';\ n))$, where B_0 is the rotational constant of the molecule, is negligible with respect to unity, the equations developed by exact summation, for the specific cases of diatomic molecules,[3,6,7] of parallel bands of linear polyatomic molecules,[3] of perpendicular bands of triatomic molecules,[8] and of spherical top

[5] Wilson, Decius, and Cross, *Molecular Vibrations* (McGraw-Hill Book Company, Inc., New York, 1955), p. 164.
[6] R. Herman and R. F. Wallis, J. Chem. Phys. **23**, 637 (1955).
[7] Hanson, Nielsen, Shaffer, and Waggoner, J. Chem. Phys. **27**, 40 (1957).
[8] D. F. Eggers, Jr. and B. L. Crawford, Jr., J. Chem. Phys. **19**, 1554 (1951).

molecules,[9] all reduce to Eq. (23). Since this approximation is accurate to a maximum error in $A(n;n')$ lying within the experimental error of intensity measurements of pressure-broadened bands, Eq. (23) will be used in the present derivation.

The summation of the intensity terms $A(n;n')$ over all the individual degenerate vibrational sublevels b, b', yields

$$g_n A(n;n') = \sum_J g_n g_J A(J,n;J',n')$$

$$= (8\pi^3/3hc)(\mathfrak{N}_n - \mathfrak{N}_{n'})\nu(n';n)\sum_{b,b'} |(n \mid M \mid n')|^2. \quad (24)$$

From Eqs. (11) and (24), and the definition of $F(J,v_k,j_k)$ in Eq. (20), it is evident that

$$G(v_k,j_k) = \sum_J F(J,v_k,j_k) = \frac{3hc}{8\pi^3}\sum_J g_n g_J A(J,n;J',n')$$

$$= (\mathfrak{N}_n - \mathfrak{N}_{n'})\nu(n';n)\sum_{b,b'} |(n \mid M \mid n')|^2. \quad (25)$$

In terms of the approximation for the band intensities, Eq. (23), the polarization and the polarizability are now given by the following relations, obtained by the combination of Eqs. (21) and (22), respectively, with Eq. (25),

$$P(\Delta v_k = j_k) = \frac{cA(\Delta v_k = j_k)}{3\pi^2 \sum_n G(v_k,j_k)}$$

$$\cdot \sum_n \left\{ \sum_J \frac{(N_{J,n} - N_{J',n'}) \sum_{b,b'} \sum_{a,a'} |(J,n \mid M \mid J',n')|^2}{\nu(J',n';J,n)} \right\}, \quad (26)$$

and

$$(n \mid \alpha \mid n') = \frac{cA(\Delta v_k = j_k)}{4\pi^3 \sum_n G(v_k,j_k)}$$

$$\cdot \sum_J \frac{\sum_{b,b'} \sum_{a,a'} |(J,n \mid M \mid J',n')|^2}{\nu(J',n';J,n)}. \quad (27)$$

Now to evaluate the sums over J in Eqs. (26) and (27), the matrix elements associated with the transitions $(J,n) \leftrightarrow (J',n')$ may be expressed in terms of the vibrational matrix elements corresponding to the set of these transitions summed over all J by the relation[5]

$$\sum_{a,a'} |(J,n \mid M \mid J',n')|^2$$

$$= \sum_{FgG'} (\Phi_{Fg})_{J,J'}^* (\Phi_{Fg'})_{J,J'} (n \mid M_g \mid n')^* (n \mid M_{g'} \mid n'), \quad (28)$$

where the terms $(\Phi_{Fg})_{J,J'}$ are the direction cosine matrix elements between the space-fixed axes, F, and the internally fixed axes, g. By neglecting the rotational quantization of the molecular energy levels and assuming that the vibrational and rotational energies are separable, one may write for the average value of the line frequency terms in the summation over J,

$$\nu(J',n';J,n)_{Av} = \nu(n',n) + \nu(J',J)_{Av} = \nu(n';n), \quad (29)$$

since $\nu(J';J)$ assumes positive and negative values in this summation. It can be shown[5] that, contingent upon the same assumption, the direction cosine matrix elements can be replaced by their nonquantized average value

$$[(\Phi_{Fg})_{J,J'}^* (\Phi_{Fg'})_{J,J'}]_{Av} = \langle \Phi_{Fg}^* \Phi_{Fg'} \rangle = \delta_{gg'} \tfrac{1}{3}. \quad (30)$$

Substitution of this result in Eq. (28), and use of the evaluated matrix element, together with the approximation of Eq. (29), in Eqs. (26) and (27), finally yields

$$P(\Delta v_k = j_k) = \frac{cA(\Delta v_k = j_k)}{3\pi^2 \sum_n G(v_k,j_k)}$$

$$\cdot \sum_n \frac{(N_n - N_{n'}) \sum_{b,b'} |(n \mid M \mid n')|^2}{\nu(n';n)}, \quad (31)$$

and

$$(n \mid \alpha \mid n') = \frac{cA(\Delta v_k = j_k)}{4\pi^3 \sum_n G(v_k,j_k)} \frac{\sum_{b,b'} |(n \mid M \mid n')|^2}{\nu(n';n)}. \quad (32)$$

Since the underlying assumptions which have been used for the evaluation of the sums over J in Eqs. (26) and (27), are exactly those which lead to the band intensity relation, Eq. (24), any further refinement would not be warranted in the absence of a general form of an equation for the intensity more exact than Eq. (23).

Returning to Eq. (31), for the polarization related to the transition $\Delta v_k = j_k$, one obtains the total polarization related to the infrared active vibrational transitions, $\Delta v = j_k$, by summation of the terms $P(\Delta v_k = j_k)$ over all k, with the result

$$P(\Delta v = j_k) = \sum_k P(\Delta v_k = j_k). \quad (33)$$

Consequently, the total vibrational polarization due to all possible vibrational transitions, $\Delta v_k = j_k$, for all values of k and j_k, can be evaluated from the relation

$$P(\Delta v) = \sum_{j_k} P(\Delta v = j_k) = \sum_{j_k} \{ \sum_k P(\Delta v_k = j_k) \}. \quad (34)$$

Similarly, the total vibrational polarizability of the molecule in its vibrational state n is then given according to Eq. (3) by summing $(n \mid \alpha \mid n')$ over all states n' as

$$(n \mid \alpha \mid n) = \sum_{n'(n' \neq n)} (n \mid \alpha \mid n'). \quad (35)$$

[9] P. N. Schatz and D. F. Hornig, J. Chem. Phys. **21**, 1516 (1953).

In order to calculate the summations over n in Eqs. (31)–(35), the matrix elements $|(n \mid M \mid n')|^2$ must now be expressed as an explicit function of the summation variable, v_k. In the foregoing development, the assumption of the noninteraction of vibration and rotation, as in the rigid rotor model, has been incorporated through the line intensity relation,[10] Eq. (10), and through Eqs. (23) and (29). The evaluation of the vibrational matrix elements may now be carried out in the anharmonic oscillator and the harmonic oscillator approximation.

General Limiting Case of the Anharmonic Oscillator Approximation

Before proceeding with this treatment, a limiting case of Eqs. (31) and (32) in which the evaluation of the polarization and the polarizability terms is independent of the form of the vibrational matrix element, will be discussed. If the Maxwell-Boltzmann law relations for $(N_n-N_{n'})$ and $(\mathfrak{N}_n-\mathfrak{N}_{n'})$ are substituted into Eqs. (31) and (32), it can be shown[11] that one obtains in the limit: $\exp(-u(n';0))\ll 1$, where n' is any upper state of the molecule, the limiting equations,

$$P(\Delta v_k=j_k)=\frac{V_m c}{3\pi^2}\frac{A(\Delta v_k=j_k)}{\nu^2(n';0)} \tag{36}$$

and

$$(0 \mid \alpha \mid n')=\frac{c}{4\pi^3\mathfrak{N}}\frac{A(\Delta v_k=j_k)}{\nu^2(n';0)}. \tag{37}$$

Equations (36) and (37) apply to all types of transitions $0\rightarrow n'$, irrespective of the form of the vibrational matrix element. In particular, they hold equally for transitions in which more than one vibrational quantum number changes, *viz.*, summation vibrations. Difference vibrations are not consistent with this limit since the upper states are considered unpopulated.

Anharmonic Oscillator—Rigid Rotor Approximation

Explicit formulas for the vibrational matrix elements of the form $|(v_k \mid M \mid v_k+j_k)|^2$ have been given by several authors.[3,12,13] If the general expression[13] derived from a Morse-type anharmonic oscillator model assuming a linear dipole moment function with internuclear distance is used, $|(v_k \mid M \mid v_k+j_k)|^2$ can be written, contingent upon the assumption $(2v_k+j_k)x_k\ll 1$, as

$$|(v_k \mid M \mid v_k+j_k)|^2 = |(0 \mid M \mid j_k)|^2(v_k+j_k)\,!\,(j_k!)^{-1}(1+j_k v_k x_k), \tag{38}$$

where x_k is the anharmonicity constant defined according to the convention for diatomic molecules, and therefore corresponding to $[x_k/\nu(v_k+j_k;v_k)]$ for polyatomic molecules.[14]

If the value of $|(v_k \mid M \mid v_k+j_k)|^2$ from Eq. (38) is now substituted into Eqs. (31) and (32) respectively, the polarization and the polarizability functions for the anharmonic oscillator-rigid rotor model, related to transitions where only one vibrational quantum number, v_k, changes its value, are derivable as

$$P(\Delta v_k=j_k)=\frac{cA(\Delta v_k=j_k)}{3\pi^2\sum_{v_k=0}^{\infty}\{I(v_k,j_k)\sum_{b,b'}H(v_k,j_k,x_k)\}} \cdot\sum_{v_k=0}^{\infty}\frac{[N(v_k)-N(v_k+j_k)]\sum_{b,b'}H(v_k,j_k,x_k)}{\nu(v_k+j_k;v_k)}, \tag{39}$$

and

$$(v_k \mid \alpha \mid v_k+j_k)=\frac{cA(\Delta v_k=j_k)}{4\pi^3\sum_{v_k=0}^{\infty}\{I(v_k;j_k)\sum_{b,b'}H(v_k,j_k,x_k)\}} \cdot\frac{\sum_{b,b'}H(v_k,j_k,x_k)}{\nu(v_k+j_k;v_k)}, \tag{40}$$

where

$$H(v_k,j_k,x_k)=(v_k+j_k)\,!\,(v_k!)^{-1}(j_k!)^{-1}(1+j_k v_k x_k),$$

$$I(v_k,j_k)=[\mathfrak{N}(v_k)-\mathfrak{N}(v_k+j_k)]\nu(v_k+j_k;v_k).$$

Further, the sum over the individual degenerate sublevels, b and b', can be written in terms of the degeneracies of the lower and upper vibrational states, $g(v_k)$ and $g(v_k+j_k)$, respectively. Since the total number of possible combinations between the $g(v_k+j_k)$ sublevels, b', and the $g(v_k)$ sublevels, b, is given by the product: $g(v_k)g(v_k+j_k)$, one may write

$$\sum_{b,b'}H(v_k,j_k,x_k)=g(v_k)g(v_k+j_k)H(v_k,j_k,x_k). \tag{41}$$

Equation (39) allows the calculation of the polarization term from the experimental quantities $\nu(v_k+j_k;v_k)$, $A(\Delta v_k=j_k)$, x_k, and V_m, with the degeneracies known from theory. With the additional exact knowledge of the vibrational partition function, θ_v, the polarizability term given by Eq. (40) may be calculated to the same order of exactness. The approximation introduced in the development of Eqs. (39) and (40) from Eqs. (31) and (32) is the evaluation of the vibrational matrix elements as given in Eq. (38). When transitions are considered in which more than one vibrational quantum number changes, i.e., combination bands, the matrix element must be evaluated from the defining Eqs. (1) and (2), since Eq. (38) does not apply in this case.

[10] See references 6 and 7 for the inclusion of vibration-rotation interaction in the theory of line intensities.

[11] K. H. Illinger, Thesis, Princeton University, 1959.

[12] H. S. Heaps and G. Herzberg, Z. Physik **133**, 48 (1952).

[13] R. C. Herman and K. E. Shuler, J. Chem. Phys. **21**, 373 (1953); **22**, 954 (1954).

[14] See, for example, G. Herzberg, *Infrared and Raman Spectra of Polyatomic Molecules* (D. Van Nostrand Company, Inc., Princeton, New Jersey, 1945), p. 205.

The vibrational partition function, θ_V, is defined by

$$\theta_V=\prod_{k,l}\{\sum_{v_k=0}^{\infty} g(v_k)\exp[-E(v_k)/kT]\cdot\sum_{v_l=0}^{\infty} g(v_l)\exp[-E(v_l)/kT]\}, \quad (42)$$

where the product extends over all the k infrared active vibrational modes with associated vibrational energies $E(v_k)$ and level degeneracies $g(v_k)$, and all the l Raman active, infrared inactive modes with associated vibrational energies $E(v_l)$ and level degeneracies $g(v_l)$. The terms $E(v_k)$ and $E(v_l)$, and, therefore, θ_V take into account the anharmonicity of the vibrational modes, in keeping with the present approximation.

Harmonic Oscillator—Rigid Rotor Approximation

The foregoing approximation reduces to the approximation below if the general functions for the anharmonic oscillator are given their special values for the harmonic oscillator

$$j_k=1 \text{ only, due to the selection rule: } \Delta v_k=j_k=1, \quad (43a)$$

$$\nu(v_k+j_k; v_k)=\nu(v_k+1; v_k)=\omega_k, \quad (43b)$$

where ω_k is the harmonic frequency of the kth normal mode of vibration, and consequently,

$$x_k=0 \quad (43c)$$

$$E(v_k)=\omega_k v_k; \quad E(v_l)=\omega_l v_l, \quad \text{and therefore} \quad (43d)$$

$$\exp(-E(v_k)/kT)=\exp(-u_k v_k),$$

$$\exp(-E(v_l)/kT)=\exp(-u_l v_l); \quad (43e)$$

since: $u(v_k+j_k; v_k)=u_k$, and $u(v_l+j_l; v_l)=u_l$

$$\theta_V^{\text{harm}}=\prod_{k,l}\{(1-e^{-u_k})^{-g_k}(1-e^{-u_l})^{-g_l}\}, \quad (43f)$$

where the terms g_k and g_l are the degeneracies of the kth and lth normal modes, respectively, and where the product is formed over all infrared active fundamentals, k, and all Raman active, infrared inactive fundamentals, l.

$$H(v_k, j_k, x_k)=H(v_k, 1, 0)=v_k+1. \quad (43g)$$

Substituting the terms evaluated in the Eqs., (43), into Eqs. (39) and (40), respectively, one obtains the harmonic oscillator-rigid rotor polarization and polarizability functions

$$P(\Delta v_k=1)=(V_m c/3\pi^2)(A_k/\omega_k^2), \quad (44)$$

and

$$(v_k\,|\,\alpha\,|\,v_k+1)=(c/4\pi^3)(A_k/\omega_k^2)[\sum_{b,b'}(v_k+1)/S(u_k, g_k)] \quad (45)$$

where

$$S(u_k, g_k)=\sum_{v_k=0}^{\infty}\{[\mathfrak{N}(v_k)-\mathfrak{N}(v_k+1)]g(v_k)g(v_k+1)\cdot(v_k+1)\} \quad (46)$$

and where A_k is the integrated absolute band intensity of the kth normal mode of vibration.

In the approximation neglecting anharmonicity effects which may lead to a splitting of the degeneracy, the degeneracy of the vibrational level v_k can be written in terms of the vibrational quantum number v_k as[15]

(a) for $g_k=1$, $g(v_k)=1$, for all v_k, (47a)

(b) for $g_k=2$, $g(v_k)=(v_k+1)$, (47b)

(c) for $g_k=3$, $g(v_k)=(1/2)(v_k+1)(v_k+2)$, (47c)

where g_k is the degeneracy of the kth normal mode of vibration.

These relations allow substitution into Eq. (46) to yield summands which, together with the use of the Maxwell-Boltzmann law relations, become explicit functions of the summation variable, v_k, and consequently permit complete evaluation of the sums for degenerate modes.

Each of the terms $P(\Delta v_k=1)$ given in Eq. (44) corresponds to a polarization term of the N molecules related to the vibrational transitions, $v_k\leftrightarrow v_k+1$, which may be described by an associated normal coordinate Q_k, and, uniquely in the case of nondegenerate vibrations, by a specific vibrational distortion of the molecular geometry. In the case of degenerate vibrations, the choice of possible normal mode representations is nonunique. The polarizability term corresponding to the transition $v_k\rightarrow v_k+1$, which may be defined in this case of a fundamental transition as the normal mode polarizability of the kth normal mode of vibration, is given by Eq. (45).

By using Eq. (45) to evaluate the normal mode polarizability for the transition $v_k=0\rightarrow v_{k'}=1$, $(0\,|\,\alpha\,|\,1)_k$, and dividing this expression into Eq. (45), one may write the simple relation

$$(v_k\,|\,\alpha\,|\,v_k+1)=(0\,|\,\alpha\,|\,1)_k[\sum_{b,b'}(v_k+1)/g_k], \quad (48)$$

where

$$(0\,|\,\alpha\,|\,1)_k=(c/4\pi^3)(A_k/\omega_k^2)[g_k/S(u_k, g_k)], \quad (49)$$

and where the equality for $v_k=1$, $g(v_k)=g_k$ has been employed. The summation $S(u_k, g_k)$ is evaluated by use of the relevant equation, (47a), (47b), or (47c).

The total vibrational polarizability for a molecule in the ground state is then given in the harmonic oscillator approximation by summation of the normal mode polarizabilities, $(0\,|\,\alpha\,|\,1)_k$, over all k normal

[15] Reference 14, p. 80.

modes of vibration. In general, the total vibrational polarizability for a molecule in the vibrational state n characterized by the set of vibrational quantum numbers: $(v_1, v_2 \cdots v_k)$ is given in the harmonic oscillator approximation by

$$(n \mid \alpha \mid n) = (v_1, v_2, \cdots v_k \mid \alpha \mid v_1, v_2, \cdots v_k) = \sum_k \{(v_k \mid \alpha \mid v_k+1) + (v_k \mid \alpha \mid v_k-1)\}. \quad (50)$$

On returning to Eq. (44) for the polarization related to the kth vibrational mode, one obtains the total vibrational polarization in the harmonic oscillator approximation, by summation of the terms $P(\Delta v_k=1)$ over all k, with the result

$$P(\Delta v=1) = \sum_k P(\Delta v_k=1) = (V_m c/3\pi^2) \sum_k (A_k/\omega_k^2). \quad (51)$$

The Eq. (51), given here for $P(\Delta v=1)$, is identical with an equation given without derivation by LeFèvre and Rao[16] and derived from the Kramers-Kronig relation by Whiffen,[17] if the frequency terms are consistently defined as the harmonic frequencies, ω_k, of the k normal modes of vibration, as given in Eq. (51).[18] The alternative definition of the frequency terms in the equation given in references 16 to 18 as the band center frequencies, $\nu(n'; 0)$, identifies them with Eq. (36) derived above. In reference 17, the equation is derived by applying the relationship between the real and the imaginary part of the dielectric constant of the system of N molecules directly to the integrated band intensity, $A(\Delta v_k=j_k)$ or A_k, leading to a relation limited to the approximations inherent alternatively in Eqs. (36) or (51). It can be shown[11] that if the Kramers-Kronig relation is applied rigorously to the individual transitions $(J, n) \leftrightarrow (J', n')$, an expression identical with Eq. (12) given above can be obtained, which can subsequently be carried through the series of approximations developed here.

Relation to Dipole Moment Derivatives

On the basis of approximating the total dipole moment of a molecule as a linear function of the harmonic oscillator normal coordinate Q_k, the following relation between the matrix element $|(v_k \mid M \mid v_k+1)|^2$ and the first derivative of the dipole moment with respect to the normal coordinate, evaluated at the equilibrium value of Q_k, can be established,[19,20]

$$|(v_k \mid M \mid v_k+1)|^2 = (h/8\pi^2\omega_k)(\partial\mu/\partial Q_k)_0^2 (v_k+1). \quad (52)$$

It is useful to have available an equation for the polarization and the polarizability involving this derivative. This can be accomplished with the aid of Eqs. (6a) and (8) in the approximation of a nonquantized summation over rotational states, and Eq. (52) to yield in the harmonic oscillator-rigid rotor approximation,

$$(0 \mid \alpha \mid 1)_k = (1/12\pi^2)(g_k/\omega_k^2)(\partial\mu/\partial Q_k)_0^2 \quad (53)$$

and

$$P(\Delta v_k=1) = (1/9\pi)[S'(u_k, g_k)/\omega_k^2](\partial\mu/\partial Q_k)_0^2, \quad (54)$$

where

$$S'(u_k, g_k) = \sum_{v_k=0}^{\infty} \{[N(v_k) - N(v_k+1)] g(v_k) g(v_k+1) \cdot (v_k+1)\}.$$

The equations for the polarization terms related to stretching and bending vibrations, respectively, derived by way of the classical theory of dispersion by Coop and Sutton,[21,22] can be derived from the general equation for the vibrational polarization in the harmonic oscillator approximation, Eq. (54), when the following further approximations are made. When it is assumed that the population of the kth vibrational ground state is equal to the total number of molecules, such that the term $\exp(-u_k)$ vanishes, Eq. (54) reduces to the special case,

$$P(0; 1)_k = (N/9h)(g_k/\omega_k^2)(\partial\mu/\partial Q_k)_0^2. \quad (55)$$

Then, by rewriting the frequency of the kth independent harmonic oscillator, to which Eq. (55) pertains, in terms of its force constant, a_k, by use of the relation

$$\omega_k^2 = a_k(4\pi^2 m_k)^{-1},$$

where m_k is the reduced mass of the harmonic oscillator, it is possible to express Eq. (55) in the form

$$P(0; 1)_k = (4\pi N/9)(g_k m_k/a_k)(\partial\mu/\partial Q_k)_0^2. \quad (56)$$

In the case of the stretching vibration of an independent oscillator composed of two nuclei, the normal coordinate Q_k can be transformed into the internal coordinate r_k, the internuclear distance, through the relation $Q_k = (m_k)^{\frac{1}{2}} r_k$, and Eq. (56) transforms into

$$P(0; 1)_k = (4\pi N/9)(g_k/a_k)(\partial\mu/\partial r_k)_0^2. \quad (57)$$

Equation (57) reduces to the first equation of Coop and Sutton if g_k is set equal to unity. This leads to the interesting conclusion that, in addition to the assumption that only the ground state is populated, the equation of Coop and Sutton is restricted to singly degenerate vibrational modes. Since the model implicit in classical dispersion theory does not directly take ac-

[16] R. J. W. LeFèvre and D. A. A. S. N. Rao, Australian J. Chem. **8**, 39 (1955).
[17] D. H. Whiffen, Trans. Faraday Soc. **54**, 327 (1958).
[18] See also, Herranz, Biarge, and Morcillo, Anal. real. soc. espan. fís. quím. **54B**, 623 (1958).
[19] Reference 5, p. 165, and Appendix III.
[20] B. Crawford, Jr., J. Chem. Phys. **29**, 1042 (1958).
[21] I. E. Coop and L. E. Sutton, J. Chem. Soc. **1938**, 1269.
[22] It should be noted that the equation given independently by Coop and Sutton for stretching vibrations is also implicit in the treatment of the vibrational susceptibility given by J. H. Van Vleck, Phys. Rev. **30**, 31 (1927).

count of the possibility of multiple degeneracies of energy levels, a situation very commonly encountered in vibrational states of molecules, this result is clearly foreshadowed.

In the case of a bending vibration of an independent harmonic oscillator composed of the vibrating system *A-B-A* at an equilibrium angle $(\pi-\phi_k)$, the normal coordinate associated with the bending motion of this symmetrical system is given by $Q_k=(m_k)^{\frac{1}{2}}\phi_k$. This relation is consistent with the following definition of the potential energy term associated with this bending motion,

$$V_k=\tfrac{1}{2}\lambda_k Q_k^2=\tfrac{1}{2}(a_k/m_k)Q_k^2=\tfrac{1}{2}a_k\phi_k^2,$$

where $\lambda_k=4\pi^2\omega_k$, and a_k is now the bending force constant. By transforming Eq. (56) in terms of the internal coordinate ϕ_k in this manner, one finds that

$$P(0;1)_k=(4\pi N/9)(g_k/a_k)(\partial\mu/\partial\phi_k)_0^2, \quad (58)$$

and $(\partial\mu/\partial\phi_k)_0^2$ is readily evaluated by differentiation of the component of the dipole moment along the symmetry axis in the plane *ABA*, $2(\mu_{AB})_0\sin(\phi_k/2)$, where $(\mu_{AB})_0$ is the equilibrium dipole moment of the group $A-B$ along the bond axis, yielding finally

$$P(0;1)_k=(4\pi N/9)(g_k/a_k)(\mu_{AB})_0^2\cos^2(\phi_k/2). \quad (59)$$

For a linear system *A-B-A*, such that $\phi_k=0$, as in the special case treated in the second equation of Coop and Sutton, $\cos^2(\phi_k/2)=1$, and the equation simplifies to

$$P(0;1)_k=(4\pi N/9)(g_k/a_k)(\mu_{AB})_0^2. \quad (60)$$

Equation (60) reduces to the second equation of Coop and Sutton, for a one-dimensional oscillator, with the same restriction as previously, namely a vibrational mode degeneracy of unity. The formal exclusion of vibrational modes with multiple degeneracies is a restriction of the applicability of the equations of Coop and Sutton. Although the vibrational degeneracy could be taken into account by explicitly counting the contributions of each degenerate sublevel of the first excited vibrational state in the one-dimensional oscillator model of Coop and Sutton, this counting procedure is defined unambiguously only in Eqs. (57) and (60). Moreover, the further ambiguity in describing a vibrational distortion in terms of one or more one- or two-dimensional oscillators, which arises in their method, is removed only when the degeneracy g_k is explicitly accounted for in the equations. It is clear from the preceding derivation leading to Eq. (60), involving $(\mu_{AB})_0$, that it is the bond moment related to the dipole moment derivative, $(\partial\mu/\partial Q_k)_0$, rather than the static bond moment, which must be employed in an equation relating the vibrational polarization term to the bond moment. The general dissimilarity between these two types of bond moment makes it imperative to use that which is consistent with the derivation.

In the equations derived thus far, the definition of the absolute intensity of a transition $(J,n)\leftrightarrow(J',n')$, $A(J,n;J',n')$,due to Wilson and Wells,[23] consistent with the relation to the dipole moment matrix element given by Eq. (11), has been used. In their definition, the integration of the experimental quantities over the frequency range comprised by the absorption band, is given by the relation

$$A=(1/pL)\int_{\text{band}}[I_0(\nu)/I(\nu)]d\nu=\int_{\text{band}}A(\nu)d\nu, \quad (61)$$

where p is the partial pressure of the absorbing gas, L is the path length in the absorption cell, $I_0(\nu)$ is the incident intensity, $I(\nu)$ is the transmitted intensity, and ν is the frequency.

Recently, the following alternative definition of this integration procedure has been suggested by Crawford,[20]

$$\Gamma=(1/pL)\int_{\text{band}}\ln[I_0(\nu)/I(\nu)]d\ln\nu$$
$$=\int_{\text{band}}[A(\nu)/\nu]d\nu. \quad (62)$$

Since this definition has been used by a number of investigators in the calculation of absolute infrared intensities from the experimental variables $I_0(\nu)$, $I(\nu)$, and ν, it is of interest to derive equations for the vibrational polarization and polarizability functions in the various approximations in its terms. The absolute intensity, $\Gamma(J,n;J',n')$, of a transition $(J,n)\leftrightarrow(J',n')$ in terms of the dipole moment matrix element is given, in the present notation, by[20]

$$\Gamma(J,n;J',n')=(J,n\mid\Gamma\mid J',n')+(J',n'\mid\Gamma\mid J,n)$$
$$=(8\pi^3/3hc)(\mathfrak{N}_{J,n}-\mathfrak{N}_{J',n'})\sum_{b,b'}\sum_{a,a'}|(J,n\mid M\mid J',n')|^2, \quad (63)$$

where $(J,n\mid\Gamma\mid J',n')$ and $(J',n'\mid\Gamma\mid J,n)$ are the absorption and the emission intensities, respectively.

It can be shown[11] by a derivation completely analogous to that given above that the definitions of Eqs. (62) and (63) lead to relations for the vibrational polarization and polarizability functions, the most important of which [cf. Eqs. (13), (16), (39), (18), (45), and (51)] are listed below.

$$(n\mid\alpha\mid n')=(c/4\pi^3)\sum_J\frac{\Gamma(J,n;J',n')}{(\mathfrak{N}_{J,n}-\mathfrak{N}_{J',n'})\nu(J',n';J,n)}, \quad (13')$$

and

$$P(\Delta v_k=j_k)=(V_m c/3\pi^2)\sum_n\left\{\sum_J\frac{\Gamma(J,n;J',n')}{\nu(J',n';J,n)}\right\}, \quad (16')$$

[23] E. B. Wilson, Jr., and H. A. Wells, J. Chem. Phys. **14**, 578 (1946).

where $\Gamma(J, n; J', n')$ is the experimental line intensity.

$$P(\Delta v_k=j_k)=\frac{c\Gamma(\Delta v_k=j_k)}{3\pi^2\sum_{v_k=0}^{\infty}\{[N(v_k)-N(v_k+j_k)]\sum_{b,b'}H(v_k, j_k, x_k)\}}\sum_{v_k=0}^{\infty}\frac{[N(v_k)-N(v_k+j_k)]\sum_{b,b'}H(v_k, j_k, x_k)}{\nu(v_k+j_k; v_k)}, \quad (39')$$

where:

$$\Gamma(\Delta v_k=j_k)=\sum_n\{\sum_J\Gamma(J, n; J', n')\} \quad (18')$$

is the experimental integrated absolute band intensity in the vicinity of $\nu(n', n)$.

$$(v_k \mid \alpha \mid v_k+1)$$

$$=(c/4\pi^3)(\Gamma_k/\omega_k)[\sum_{b,b'}(v_k+1)/S(u_k, g_k)], \quad (45')$$

and

$$P(\Delta v=1)=(V_m c/3\pi^2)\sum_k(\Gamma_k/\omega_k), \quad (51')$$

where Γ_k is the integrated absolute band intensity of the kth normal mode of vibration.

III. CALCULATIONS AND DISCUSSION

The vibrational polarization for the molecule in the gas phase at a pressure of 1 atmos, and a temperature of 300°K has been calculated for the molecules for which absolute intensities have been determined for all the infrared active vibrational fundamentals. In Table I are given the polarizations related to the transitions, $\Delta v_k=1$, 2, and 3, calculated from Eq. (16) for the three molecules for which absolute line intensities are available at this time.

In the calculation of $P(\Delta v_k=j_k)$ from Eq. (39), the following approximation of the frequency of an anharmonic fundamental vibration of a diatomic molecule has been used;[24]

$$\nu(v_k+1; v_k)=\omega_k-2\omega_k x_k-2\omega_k v_k x_k, \quad (64)$$

where the symbols have the meanings previously given to them. From Eq. (64) one may deduce the following expression for the frequency terms $\nu(v_k+j_k; v_k)$ required in Eq. (39),

$$\nu(v_k+j_k; v_k)=\sum_{v_k=v_k}^{v_k+j_k-1}\nu(v_k+1; v_k)=j_k(\omega_k-2\omega_k x_k)$$

$$-2\omega_k x_k\sum_{v_k=v_k}^{v_k+j_k-1}v_k. \quad (65)$$

If the terms ω_k, x_k, and $A(\Delta v_k=j_k)$, are known for a given vibrational transition of a diatomic molecule, Eq. (65) may be used to calculate the polarization in the anharmonic oscillator approximation from Eq. (39) by direct evaluation of the converging sums over v_k. In Table II the results of this calculation are given for a series of diatomic molecules.

Table III lists the results of the calculation of the total vibrational polarization in the approximation neglecting all except the first terms in the summations in Eq. (31), according to Eq. (36), summing over all the k normal modes. This approximation corresponds to a treatment taking into account the anharmonicity of the vibrations, but limiting the total vibrational polarization to the contributions associated with fundamental vibrational transitions.

In Table IV are given the results of the calculation in the strict harmonic oscillator approximation, according to Eq. (51), for a number of diatomic molecules.

In all the calculations the molar volume has been taken as the molar volume of an ideal gas at a pressure of 1 atmos and a temperature of 300°K.

A comparison of the results for $P(0;1)$ and $P(\Delta v=1)$ for HF, HCl, and DCl given in Table I and II, re-

TABLE I. Vibrational polarization for individual transitions for the gas at $p=1$ atm, $T=300$°K, calculated from Eq. (16).

	$P(0;1)$ (cm³)	$P(0;2)$ (cm³)	$P(0;3)$ (cm³)	Source of intensity value (references)[a]
HF	0.0167	...	...	(1)
HCl	0.0128	$6.97\cdot10^{-5}$	$2.27\cdot10^{-7}$	(2), (3)
DCl	0.0121	$4.44\cdot10^{-5}$	$9.29\cdot10^{-8}$	(3)

[a] References in parentheses are at end of article.

[24] Reference 4, p. 95.

TABLE II. Vibrational polarization for the transitions $\Delta v_k=1$ and $\Delta v_k=2$ in the anharmonic oscillator approximation, for the gas at $p=1$ atm, $T=300$°K, calculated from Eq. (39).[a]

	$P(\Delta v_k=1)$ (cm³)	$P(\Delta v_k=2)$ (cm³)	ω_k (cm⁻¹)	$x_k\cdot10^3$	Source of intensity value (references)[d]
HF	0.0167	...	4138.52	2.176	(1)
HCl	0.0130	0.000074	2989.74	1.741	(3)
DCl	0.0127	0.000052	2144.77[b]	1.255[b]	(3)
			2141.20[b]	1.260[b]	
HBr	0.0070	0.00002	2649.67	1.706	(4)
BrCl	0.0184	<0.00011	442.5[c]	0.339[c]	(5)
ICl	0.152	<0.00023	384.18	0.381	(5)
NO	0.015	0.00012	1904.03	0.7447	(4)
CO	0.043	0.000075	2170.21	0.6203	(6)

[a] Values of ω_k and x_k were taken from reference 4, p. 502 ff., except when noted.

[b] Taken from reference (31); first line refers to DCl^{35}, second to DCl^{37}.

[c] Taken from reference (5).

[d] References in parentheses are at end of article.

TABLE III. Total vibrational polarization in the general limiting case of the anharmonic oscillator approximation for the gas at $p=1$ atm, $T=300°K$, calculated from Eq. (36) summing over all k normal modes of vibration.

	$P(\Delta v=1)$ (cm³)	Source of intensity value (references)[a]
HF	0.0167	(1)
HCl	0.0130	(2)
DCl	0.0127	(3)
HBr	0.0070	(4)
BrCl	0.018	(5)
ICl	0.15	(5)
NO	0.015	(4)
CO	0.043	(6)
CO_2	0.85	(7), (8)
OCS	1.01	(9), (10)
N_2O	0.48	8
HCN	0.35	(11)
DCN	0.18	(11)
ClCN	0.13	(12)
BrCN	0.10	(12)
SO_2	0.84	(13)
C_2H_2	1.28	(14)
C_2D_2	0.92	(14)
C_2HD	0.95	(14)
C_2N_2	1.13	(15), (16)
NH_3	0.59	(17)
NF_3	1.94	(18)
PH_3	0.22	(17)
BF_3	2.19	(19)
H_2CO	0.17	(20)
CH_4	0.11	(21), (22)
CF_4	2.89	(32)
SiF_4	4.82	9
CH_3F	0.36	(23)
CD_3F	0.39	(23)
CHF_3	2.63	(33)
CH_3Cl	0.20	(24)
CD_3Cl	0.18	(24)
CH_2Br	0.16	(24)
CD_2Br	0.15	(24)
CH_3I	0.13	(24)
CD_3I	0.11	(24)
CH_3CN	0.070	(25)
CD_3CN	0.12	(12)
C_2H_4	0.33	(26)
cis-$C_2H_2D_2$	0.37	(26)
trans-$C_2H_2D_2$	0.32	(26)
C_2D_4	0.30	(26)
SF_6	5.07	9
C_2H_6	0.12	(27)
C_2D_6	0.13	(27)
C_2F_6	3.03	(28), (29)
C_6H_6	0.73	(30)
C_6H_5D	0.78	(30)
p-$C_6H_4D_2$	0.74	(30)

[a] References in parentheses are at end of article.

spectively, shows that the values of $P(\Delta v=1)$ obtained from Eq. (39) by using $A(0;1)$ from the direct summation of line intensities, and the band center frequency, $\nu(1;0)$, are in good agreement with the value for $P(0;1)$ calculated from Eq. (16) by the use of individual line intensities, $A(J,0;J',1)$, and line frequencies, $\nu(J',1;J,0)$. This finding supports the degree of accuracy assigned to the assumption pertaining to Eq. (23), the averaging procedure over all rotational states in general, as used again in the derivation, and the validity of the anharmonic oscillator approximation. All the molecules in Table II except BrCl and ICl fall into the category for which the approximation given by Eq. (36) is applicable with good accuracy. In the general case, where the upper states may have appreciable populations, Eq. (39) must be used instead. However, if the anharmonicity constant, x_k, is small compared to unity, the approximation for $P(\Delta v_k=1)$ given by Eq. (36) yields values in good agreement with those calculated from Eq. (39). This may be seen by comparison of the values for $P(\Delta v_k=1)$ for BrCl and ICl in Tables II and III. The values for $P(\Delta v=1)$ calculated in the strict harmonic oscillator approximation, according to Eq. (51), and given in Table IV, differ significantly from those calculated from Eq. (36), due to the difference between the band center frequency and the harmonic frequency. As may be seen by comparison of identical molecules in Tables III and IV, this difference in $P(\Delta v=1)$ diminishes with decreasing values of the anharmonicity constant.

It may be concluded that owing to the rather rapid convergence of the summations over v_k in Eq. (39), even in the case where excited states are populated with a considerable number of molecules, $P(\Delta v_k=1)$ is given to good approximation by the general limiting case of the anharmonic oscillator function, Eq. (36). The effect of decreasing frequencies of vibration, associated with a higher population of excited states and a consequent decrease in the accuracy of this approximation, and that of decreasing values of the anharmonicity constants, leading to an increase in this accuracy, are fortunately concomitant. As a consequence, Eq. (36) is a good approximation even for low-frequency transitions.

The assumption that the general limiting case of the anharmonic oscillator function, Eq. (36), summed over

TABLE IV. Vibrational polarization in the harmonic oscillator approximation for the gas at $p=1$ atm, $T=300°K$, calculated from Eq. (51).

	$P(\Delta v=1)$ (cm³)	Source of intensity value (references)[a]
HF	0.0153	(1)
HCl	0.0121	(2)
DCl	0.0121	(3)
HBr	0.0065	(4)
BrCl	0.018	(5)
ICl	0.15	(5)
NO	0.014	(4)
CO	0.042	(6)

[a] References in parentheses are at end of article.

all the k normal modes, or the harmonic oscillator function, Eq. (51), for $P(\Delta v=1)$, represents the strongly predominant contribution to the vibrational polarization of a molecule, is contingent upon the negligibility of the polarization contributions of overtone and combination bands. For diatomic molecules, theoretical considerations are substantiated by all experimentally investigated cases in predicting that the intensity values in the sequence: $A(0;\ 1)$, $A(0;\ 2)$, $\cdots A(0;\ j_k)$, decrease rapidly with increasing j_k.[25,26] This decrease in $A(0;\ j_k)$ or $A(\Delta v_k=j_k)$, and the accompanying increase in $\nu(j_k;\ 0)$ with increasing j_k, lead to a rapid decrease of $P(0;\ j_k)$ or $P(\Delta v_k=j_k)$ with j_k. The calculated values for the overtone contributions for diatomic molecules given in Tables I and II, compared to $P(\Delta v_k=1)$ for the same molecule, corroborate this generalization. Consequently, for a diatomic molecule $P(\Delta v=1)$ is a very good approximation for the total vibrational polarization.

In polyatomic molecules, overtone and combination vibrations may exhibit intensities very much larger than those expected from the considerations that hold for diatomic molecules, where no interaction can occur between vibrational levels of the same electronic state of the molecule. In the polyatomic molecule, interactions between energy levels of nearly equal energy, belonging to different vibrations but of the same symmetry species, may exist within the same electronic state of the molecule.[27] When this type of interaction, which leads to a perturbation of the original energy levels, occurs between a fundamental mode and an overtone or combination mode, the latter greatly increases in its intensity, which may become of the same order of magnitude as that of the fundamental interacting with it in Fermi resonance. In this event, $P(\Delta v=1)$ for the molecule, calculated from the integrated intensities $A(\Delta v_k=1)$, may be markedly lower than the true vibrational polarization. A correction may be made in the harmonic oscillator approximation by equating the intensity of the fundamental involved in the Fermi resonance to the experimental sum of intensities of the fundamental and the interacting vibration, "forbidden" in this approximation, and recalculating $P(\Delta v=1)$ on this basis. It has been shown in reference 20 that, in the harmonic oscillator approximation, the integrated intensity Γ_k is invariant under conditions of a resonance between two upper states involved in a vibrational transition. As a consequence, the correction necessary under these conditions for A_k is already satisfied in the case of Γ_k.

In so far as $P(\Delta v=1)$ is an accurate value for the true total vibrational polarization for a given molecule, and if, under these conditions, there exist no further mechanisms by which the molecule can absorb vibrational energy from an external electric field, $P(\Delta v=1)$ represents the atomic polarization of the molecule. At constant temperature, changes in pressure and especially transition to a condensed state may cause a marked alteration in the intermolecular forces and strongly modify the vibrational polarization of the molecule. Consequently, it is not in general justifiable to assume that the value for the vibrational polarization calculated for the molecule under the conditions of pressure and temperature specified here can be considered to apply under conditions where the intermolecular forces are appreciably different.

[25] Reference 14, p. 265.
[26] B. F. Gray and H. O. Pritchard, J. Mol. Spectroscopy **2**, 137 (1958).
[27] Reference 14, p. 215.

ACKNOWLEDGMENTS

The writers wish to express their indebtedness to Professor Donald F. Hornig for his kindness in reading and discussing this manuscript.

REFERENCES FOR TABLES I–IV

(1) G. A. Kuipers, J. Mol. Spectroscopy **2**, 75 (1958).
(2) Benedict, Herman, Moore, and Silverman, Can. J. Phys. **34**, 850 (1956).
(3) Benedict, Herman, Moore, and Silverman, J. Chem. Phys. **26**, 1671 (1957).
(4) S. S. Penner and D. Weber, J. Chem. Phys. **21**, 649 (1953).
(5) W. F. V. Brooks and B. Crawford, Jr., J. Chem. Phys. **23**, 363 (1955).
(6) S. S. Penner and D. Weber, J. Chem. Phys. **19**, 807, 974 (1951).
(7) L. C. Kaplan and D. F. Eggers, J. Chem. Phys. **25**, 876 (1956).
(8) Weber, Holm, and Penner, J. Chem. Phys. **20**, 1820 (1952).
(9) E. W. Wingfield and J. W. Straley, J. Chem. Phys. **22**, 1949 (1954).
(10) McKean, Callomon, and Thompson, J. Chem. Phys. **20**, 520 (1952).
(11) G. E. Hyde and D. F. Hornig, J. Chem. Phys. **20**, 647 (1952).
(12) R. W. Hendricks, Thesis, Brown University, 1956.
(13) J. E. Mayhood, Can. J. Phys. **35**, 954 (1957).
(14) Eggers, Hisatsune, and Van Alten, J. Phys. Chem. **59**, 1124 (1955).
(15) J. W. Schultz and D. F. Eggers, J. Mol. Spectroscopy **2**, 113 (1958).
(16) T. Miyazawa, J. Chem. Phys. **29**, 421 (1958).
(17) D. C. McKean and P. N. Schatz, J. Chem. Phys. **24**, 317 (1956).
(18) P. N. Schatz and I. W. Levin, J. Chem. Phys. **29**, 475 (1958).
(19) D. C. McKean, J. Chem. Phys. **24**, 1002 (1956).
(20) I. C. Hisatsune and D. F. Eggers, J. Chem. Phys. **23**, 487 (1955).
(21) Welsh, Pashler, and Dunn, J. Chem. Phys. **19**, 340 (1951).
(22) H. L. Welsh and P. J. Sandiford, J. Chem. Phys. **20**, 1646 (1952).
(23) G. D. Barnett, Thesis, University of Washington, 1957.
(24) Dickson, Mills, and Crawford, J. Chem. Phys. **27**, 445 (1957).
(25) A. V. Golton, Thesis, Oxford University, 1954.
(26) Golike, Mills, Person, and Crawford, J. Chem. Phys. **25**, 1267 (1956).
(27) Nyquist, Mills, Person, and Crawford, J. Chem. Phys. **26**, 552 (1957).
(28) Williams, Person, and Crawford, J. Chem. Phys. **23**, 179 (1955).
(29) Mills, Person, Scherer, and Crawford, J. Chem. Phys. **28**, 851 (1958).
(30) H. Spedding and D. H. Whiffen, Proc. Roy. Soc. (London) **A238**, 245 (1956).
(31) B. H. Van Horne and C. D. Hause, J. Chem. Phys. **25**, 56 (1956).
(32) B. Schurin, J. Chem. Phys. **30**, 1 (1959).
(33) Morcillo, Herranz and Biarge, Spectrochim. Acta **1959**, 110 (1959).

Thermodynamic Properties of Sulfuryl Fluoride from 12°K to Its Boiling Point. Entropy from Molecular and Spectroscopic Data

F. J. BOCKHOFF,* R. V. PETRELLA, AND E. L. PACE

Morley Chemical Laboratory, Western Reserve University, Cleveland, Ohio

(Received August 6, 1959)

The heat capacity of sulfuryl fluoride has been measured from 12 to 218°K. A lambda transition was observed at 65.7°K. The heat of fusion at the triple-point temperature, 137.34°K, was 1074 cal/mole. The heat of vaporization at the normal boiling point, 217.78°K, was 4596 cal/mole. The vapor pressure data are closely represented by the equation

$$\log_{10}P_{mm}=7.8323-1071.235/T-0.01391\log_{10}T.$$

The liquid density from 182 to 204°K is closely represented by the equation

$$d=2.576-0.004044T.$$

The entropy of sulfuryl fluoride gas has been calculated from the calorimetric data and the third law of thermodynamics to be 62.66 eu/mole at 217.78°K. The calculated spectroscopic entropy was 63.24 eu/mole. The discrepancy, 0.58 eu/mole is attributed to randomness in the solid at 0°K.

EIGHT of the nine expected vibrational fundamentals for sulfuryl fluoride have been assigned from a study of the infrared spectrum,[1] and six of these have been confirmed by an analysis of the Raman spectrum.[2] The one remaining fundamental, attributed to a symmetric SF_2 bending, was estimated through an interaction of excited vibrational states in the microwave region[3] to be 388 ± 15 cm^{-1}, although neither the fundamental nor any of its expected overtones or combinations was observed in the infrared or Raman spectra. Since the SF_2 bending frequency is the lowest of the nine fundamentals for SO_2F_2, its contribution to calculated thermodynamic functions is the largest, and an independent experimental confirmation is desirable.

It was the purpose of this research to provide calorimetric measurements whose precision[4] would allow the doubtful frequency to be determined within an error limit of ±20 cm^{-1}. However, a third-law entropy comparison is complicated by the strong possibility of randomness at absolute zero, due to the nearly equal sizes of the fluorine and oxygen atoms and the nearly tetrahedral symmetry[3] of the sulfuryl fluoride molecule.

SAMPLE PREPARATION AND PURITY

Approximately one-half mole of sulfuryl fluoride was prepared by the reaction of sulfur dioxide with argentic fluoride,[5] and was purified by fractional distillation at atmospheric pressure. Remaining traces of sulfur dioxide and possible silicon tetrafluoride were removed by washing in neutral potassium permanganate solution. Analysis of the mass spectrum and infrared spectrum of the purified sample indicated the possibility of a very small amount of carbon dioxide as a remaining impurity.

The purity and triple-point temperature of the sulfuryl fluoride, prepared in the above manner, were determined in an adiabatic calorimeter previously described by Pace *et al.*[6] The entire quantity, 53.951 g, of sample was transferred to the calorimeter by direct weighing, and equilibrium temperatures were determined for various fractions of sample melted. Temperatures were measured with a platinum resistance thermometer having an ice-point resistance of 25.5 ohms and calibrated by the National Bureau of Standards. The ice-point temperature is taken as 273.16°K.

The data are presented in Table I. Analysis of the data by usual methods[7] yielded a triple-point temperature of 137.34 ± 0.05°K for pure sulfuryl fluoride, which is slightly higher than the value of 136.5°K reported by Yost and Russell.[8] The calculated mole fraction of impurity of the calorimetric sample was 0.0029.

LIQUID DENSITIES

Liquid densities at various temperatures were required for subsequent calorimetric calculations.

A specially designed density bulb, having a volume of 8.3 cc, was calibrated at various reference marks on its capillary neck by weighing contained volumes of mercury at known temperatures. In making density determinations, 15.683 g of sulfuryl fluoride were condensed into the bulb at 195°K. A bath of dry ice and acetone surrounding the bulb was subsequently cooled by successive additions of liquid nitrogen, and volume

* Department of Chemistry and Chemical Engineering, Fenn College, Cleveland, Ohio.

[1] W. D. Perkins and M. K. Wilson, J. Chem. Phys. **20**, 1791 (1952).

[2] P. Bender and J. M. Wood, Jr., J. Chem. Phys. **23**, 1316 (1955).

[3] Lide, Mann, and Fristrom, J. Chem. Phys. **26**, 734 (1957).

[4] L. Pierce and E. L. Pace, J. Chem. Phys. **22**, 1271 (1954).

[5] H. J. Emeléus and J. F. Wood, J. Chem. Soc. **60**, 2183 (1948).

[6] Pace, Pierce, and Dennis, Rev. Sci. Instr. **26**, 20 (1955).

[7] F. D. Rossini, *Chemical Thermodynamics* (John Wiley & Sons, Inc., New York, 1950), p. 456.

[8] D. M. Yost and H. Russell, Jr., *Systematic Inorganic Chemistry* (Prentice-Hall, Inc., Englewood Cliffs, New Jersey, 1944), p. 307.

TABLE I. Equilibrium temperatures of fusion of sulfuryl fluoride (53.9506 g; 0°C=273.16°K.

Equilibrium temperature T (°K)	Fraction melted r	$1/r$
135.40	0.0123	81.3
136.81	0.182	5.49
137.01	0.336	2.98
137.12	0.522	1.91
137.22	0.709	1.41
137.43±0.05		0 (extrapolated)

readings were taken at equilibrium. After cooling the bath and sample to 182°K, the system was allowed to warm very slowly, with continuous stirring, to 204°K, and additional readings were taken at intervals. Temperatures were measured with a toluene thermometer whose calibration was found to be accurate within 0.1°K at the carbon dioxide fixed point (194.7°K). A slight correction was made for expansion of the glass bulb. The correction for vapor weight of sulfuryl fluoride was negligible.

The variation of d, the liquid density of sulfuryl fluoride, in g/cc, with T, the absolute temperature in °K, from 182 to 204°K, as determined by the method of least squares, is closely represented by the equation

$$d=2.567-0.004044T. \quad (1)$$

Twenty points were observed with a mean absolute deviation of 0.001 g/cc from the values calculated from Eq. (1).

HEAT CAPACITY MEASUREMENTS

The adiabatic calorimeter used for these measurements has been previously described.[6]

The measured heat capacities, taking one calorie as 4.1840 joules, are listed in Table II and plotted in Fig. 1. Under reversible conditions, the saturated heat capacity at constant temperature can be expressed as

$$C_s=dH/dT-VdP/dT, \quad (2)$$

where V and H refer to the molar volume and molar enthalpy of the condensed phase and P is the saturation vapor pressure. The total energy, E_x, of the calorimeter contents is given by

$$E_x=n'xE'+n'(1-x)E, \quad (3)$$

where n' is the number of moles of sample, x is the mole fraction of sample in the vapor phase, and E and E' are the molar internal energies of the condensed phase and the vapor phase, respectively. It can be readily shown that

$$n'x=(V_c-n'V)/V'-V), \quad (4)$$

where V_c is the total volume of the calorimeter, and V' is the molar volume of the vapor phase. Substituting Eq. (4) in Eq. (3), and noting that $H=E+PV$ and $(H'-H)/(V'-V)=TdP/dT$, one obtains

$$E_x=n'H+(V_c-n'V)TdP/dT-V_cP. \quad (5)$$

The total energy of the calorimeter and contents E_t is given by

$$E_t=E_c+n'H+(V_c-n'V)TdP/dT-V_cP, \quad (6)$$

where E_c is the energy of the empty calorimeter. By defining G, the gross heat capacity, as dE_t/dT and G_0, the heat capacity of the empty calorimeter, as dE_c/dT, one can differentiate Eq. (6) with respect to T and

TABLE II. Molar heat capacity of sulfuryl fluoride (mol wt: 102.066; 0.52859 mole; 0°C=273.16°K; 1 cal=4.1840 abs joules).

Temp °K	C_s, cal/°K/mole	Series	Temp °K	C_s, cal/°K/mole	Series
12.29	1.880	11	80.36	11.94	5
12.91	2.050	10	80.71	11.99[a]	20
15.12	2.723	11	81.25	12.02	7
15.75	2.916	10	81.33	12.01	4
18.96	3.850	11	84.50	12.27	6
19.81	4.177	10	85.06	12.29	5
23.49	5.108	11	86.13	12.37[a]	20
24.67	5.468	10	86.42	12.40	4
28.45	6.418	11	86.76	12.45	7
29.68	6.708	10	90.20	12.67	5
33.28	7.287	11	91.28	12.77[a]	20
34.99	7.824	10	92.31	12.85	7
38.47	8.425	11	95.14	13.07	5
38.79	8.529	10	96.76	13.23[a]	20
42.86	9.073	10	97.92	13.33	7
43.74	9.155	11	100.13	13.52	5
48.37	9.747	10	103.27	13.86	7
49.17	9.902	11	105.49	14.10	5
53.76	10.67	6	108.70	14.52	7
54.16	10.71	4	110.89	14.79	5
57.84	11.12	8	114.16	15.25	7
58.29	11.19	8	116.07	15.55	5
58.73	11.24	8	121.01	16.36	5
59.17	11.28	8	124.45	17.02	7
59.61	11.36	8	125.98	17.31	5
60.04	11.41	8	128.35	17.99	7
61.31	11.64	8	131.10	19.25	7
61.72	11.72	8	137.34	fusion	
62.13	11.82	8	142.34	25.83	18
62.53	11.89	8	143.13	25.81	16
62.62	11.88	9	147.28	25.80	16
62.93	11.96	8	149.80	25.79	19
63.27	12.03	9	152.54	25.73	16
63.33	12.10	8	155.76	25.72	19
63.73	12.14	8	158.11	25.67	16
63.90	12.30	9	164.02	25.57	16
64.12	12.31	8	167.54	25.46	19
64.51	12.46	8	169.89	25.40	16
64.53	12.48	9	173.39	25.34	19
65.02	12.75	8	175.74	25.25	16
65.15	12.82	9	177.08	25.21	17
65.7	lambda transition		181.56	25.12	16
			182.85	25.07	17
65.77	12.55	9	188.57	24.97	17
66.39	11.20	9	194.24	24.92	17
67.65	11.15	9	199.91	24.84	17
68.28	11.14	9	205.42	24.90	17
70.92	11.29	4	209.58	24.92	17
74.46	11.52	6	217.78	vaporization (1 atmos)	
76.16	11.64	4			
79.51	11.88	6			

[a] 0.52765 mole.

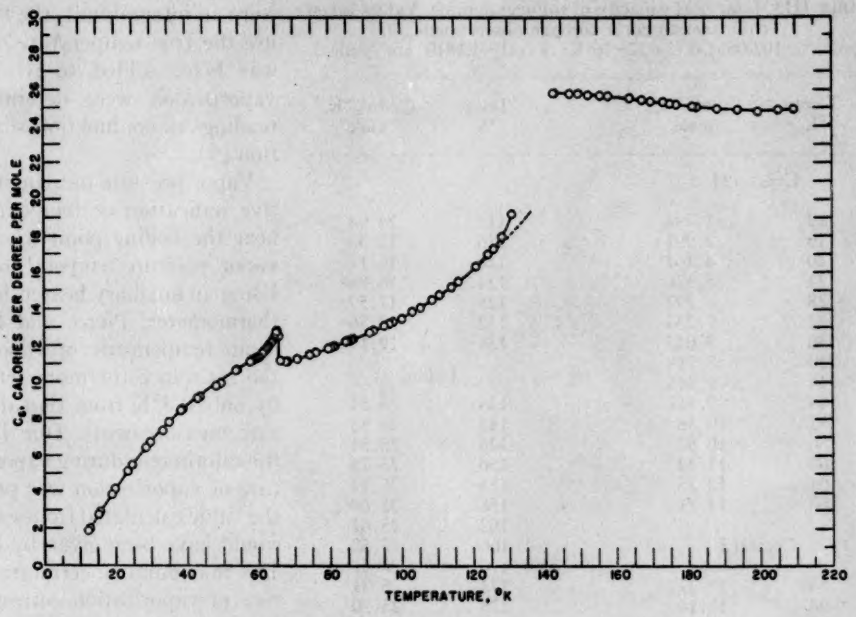

FIG. 1. The molar heat capacity of sulfuryl fluoride.

substitute Eq. (2) into the resultant expression to yield

$$C_s = M/n\{G - G_0 - T(d/dT)[(V_c - nv)(dP/dT)]\}, \quad (7)$$

where M is the molecular weight of the sample, n is the number of grams of sample, and v is the specific volume of the condensed phase. Equation (7) was used for the calculation of experimental saturated heat capacities. Specific volumes were calculated from Eq. (1) and dP/dT values were calculated from Eq. (9).

A 0.52859 gram-mole sample was used for all runs except Series 20. Due to loss of a portion of the sample on removal from the calorimeter, a final weight check on the sample could not be made. However, an indirect check was made by observing four separate heat capacities in the 80° to 97°K range (Series 20) with a sample mass of 0.52765 gram-mole. The mean deviation from the smooth heat capacity curve for the four check points was 0.06%. A comparison of this mean deviation (0.06%) with that of other C_s values from 80–97°K (0.08%) affords an excellent check on sample weight.

The mean deviation of the experimental points of Table II from a smooth curve is 0.09% above 50°K and 0.7% below 50°K.

Values of the saturated molar heat capacity taken from the smooth curve through the experimental points are presented in Table III. Due to extensive premelting, smooth values from 124°K to fusion (137.34°K) were taken from the dotted extrapolation of Fig. 1.

HEAT OF TRANSITION AND TRANSITION TEMPERATURE

Careful heat capacity measurements, taken over small temperature intervals in the range from 58 to 69°K, indicated a sharp peak in the heat capacity curve which appeared to extrapolate to an infinite value of C_s at 65.7°K. The heat capacity measurements gave no indication of a latent heat of transition. Based on the apparent absence of a latent heat of transition and the shape of the heat capacity curve,[9] the anomalous peak at 65.7°K was attributed to a lambda transition, which culminates on warming at 65.7°K.

Although the latent heat of the lambda transition was zero, an estimation of the heat involved in the transition, over a temperature range, was made by determining the area between the actual heat capacity curve and a curve interpolated between two smooth portions of the over-all heat capacity curve. The two curves shown are in Fig. 2. The approximate heat of the lambda transition ΔH_λ in the range from 38 to 72°K was graphically determined by the relation

$$\Delta H_\lambda = \int_{38°K}^{72°K} (C_s - C_i)\,dT, \quad (8)$$

where C_i was taken from the interpolated curve of Fig. 2. The calculated value for ΔH_λ was 14.5 cal/mole.

HEAT OF FUSION

Data for the heat of fusion are listed in Table IV. Heat of fusion measurements were made by starting at a temperature below fusion and adding sufficient heat to raise the temperature of the calorimeter above that of fusion. A sensible heat correction was then made for temperature rise of the calorimeter and contents. A premelting correction was also required for one of the determinations.

[9] H. N. V. Temperly, *Changes of State* (Cleaver-Hume Press, Ltd., London, 1956), pp. 232–240.

TABLE III. Molar heat capacity of sulfuryl fluoride. Values taken from smooth curve through observations (mol wt: 102.066; 0°C=273.16°K; 1 cal=4.1840 abs joules).

Temp °K	C_s, cal/°K/mole	Temp °K	C_s, cal/°K/mole
Crystal II			
12	1.794	112	14.94
16	2.991	116	15.53
20	4.161	120	16.17
24	5.176	124	16.86[a]
28	6.297	128	17.59[a]
32	7.233	132	18.36[a]
36	8.043	136	19.18[a]
40	8.719	Liquid	
44	9.318		
48	9.867	138	25.84
52	10.38	142	25.83
56	10.87	146	25.81
60	11.42	150	25.78
64	12.25	154	25.74
65	12.71	158	25.68
		162	25.61
Crystal I		166	25.52
		170	25.41
66	11.27	174	25.31
68	11.14	178	25.20
72	11.35	182	25.10
76	11.63	186	25.01
80	11.92	190	24.94
84	11.22	194	24.90
88	12.52	198	24.86
92	12.83	202	24.87
96	13.15	206	24.88
100	13.52	210	24.91
104	13.94	214	24.96
108	14.41	216	24.98

[a] Extrapolated.

VAPOR PRESSURE

Vapor pressure measurements for sulfuryl fluoride were obtained using a Gaertner precision cathetometer as a comparison instrument in conjunction with a standard meter bar. The data were fitted by the equation

$$\log_{10}P_{mm}=7.8323-1071.235/T-0.01391\log_{10}T, \quad (9)$$

which was derived by the method of least squares. The observed and calculated pressures are listed in Table V. The usual gravity, meniscus, and temperature corrections were applied. The average absolute difference between observed and calculated vapor pressures was 0.38 mm. The last column of Table V gives the pressure observed in this research minus the pressure calculated from the equation given by Yost and Russell.[8] Agreement is better at pressures above 200 mm than below and is excellent at 760 mm.

The normal boiling point, calculated from Eq. (9), is 217.78±0.01°K.

HEAT OF VAPORIZATION

Heat of vaporization measurements were made using the same heater as for all other calorimetric measurements. Since the resistance thermometer and heater were an integral unit, the thermometer could not measure the true temperature of the calorimeter while heat was being added to it. Thus, temperatures during vaporization were determined from vapor pressure readings in conjunction with the vapor pressure equation (9).

Vapor pressure measurements provided a very sensitive indication of temperature variation, particularly near the boiling point where dP/dT, the slope of the vapor pressure-temperature curve, was 39.5 mm/°K. Using an auxiliary heater, independent of the resistance thermometer, Pierce and Pace[4] have shown that the mean temperature of vaporization, as determined by the resistance thermometer, differed in the worst case by only 0.3°K from that determined from vapor pressure measurements. Due to thermal gradients within the calorimeter during vaporization, the actual temperature of vaporization was probably somewhere between the value calculated from vapor pressure and that which would have been given by the resistance thermometer. The maximum uncertainty of 0.3°K in the temperature of vaporization corresponds to an uncertainty of only four calories in the molar heat of vaporization.

The method of maintaining constant pressure during vaporization and the method of calculating heat of

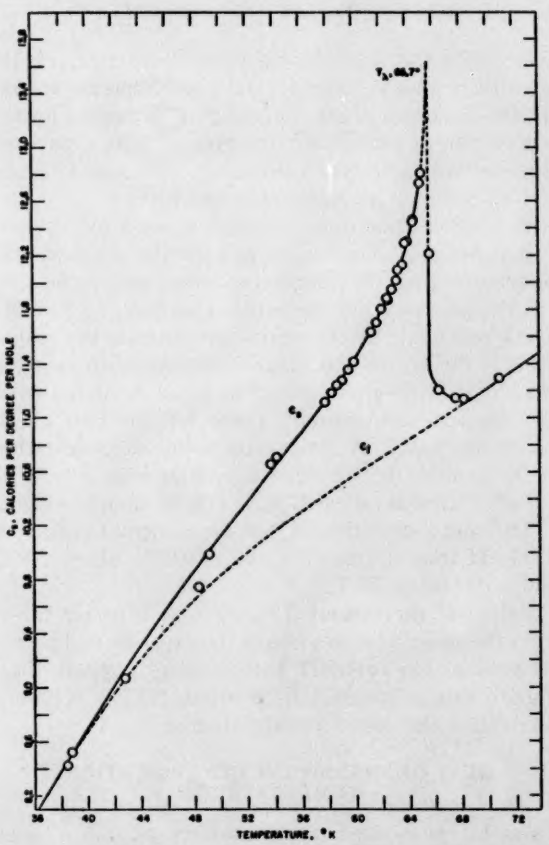

FIG. 2. The molar heat capacity of sulfuryl fluoride in the region of the lambda transition.

TABLE IV. Heat of fusion of sulfuryl fluoride (mol wt: 102.066; 0.52859 mole; triple point: 137.34±0.05 °K 0°C=273.16°K; 1 cal=4.1840 abs joules).

Temp interval °K	Corr heat input cal/mole	Sensible heat corr, cal/mole	Premelt corr cal/mole	Heat of fusion cal/mole
123.93–141.04	1752.34	−676.68	...	1075.7
124.12–141.62	1768.15	−696.15	...	1072.0
133.36–140.74	1373.21	−311.93	12.56	1073.8
		Av=1074±2		

vaporization have been described.[4,10] Corrections were made for heat leak to the surroundings and for temperature rise of the system (sensible heat correction). Pierce and Pace[4] have shown that a correction for superheating of the liquid due to hydrostatic head is negligible. In addition, calculations showed that no correction was necessary for pressure drop between the calorimeter and the manometer tap.

Table VI summarizes the data. The mean temperatures of vaporization were both close enough to the normal boiling point to obviate a correction in heat of vaporization to the normal boiling point.

ENTROPY FROM CALORIMETRIC DATA

The calculations of the entropy for the liquid and the gas at the normal boiling point are summarized in Table VII.

The gas imperfection correction ΔS_i assuming a Berthelot gas, is given by[11]

$$\Delta S_i=(27/32)(RT_c/P_cT). \qquad (10)$$

By solving the Berthelot equation of state for T_c/P_c, substituting in (10), and rearranging in terms of the

TABLE V. Vapor pressure of sulfuryl fluoride (normal boiling point=217.78±0.01°K; 0°C=273.16°K).

Temp. °K	P_{obs} int. mm Hg	P_{calc}[a] int. mm Hg	$P_{obs}-P_{calc}$ This research	$P_{obs}-P_{calc}$ Yost & Russell
164.603	19.43	19.66	−0.23	+2.89
171.846	37.29	36.94	+0.35	+4.30
179.022	66.11	65.64	+0.45	+4.83
186.361	112.95	112.92	+0.03	+4.06
192.727	174.32	174.80	−0.48	+2.40
198.416	251.46	252.01	−0.55	+0.56
205.209	379.82	380.15	−0.37	−1.27
209.556	487.80	487.69	+0.11	−1.66
212.892	586.72	586.33	+0.39	−1.12
215.887	687.61	688.41	−0.80	−1.36
218.080	771.67	772.09	+0.42	+0.56

[a] $\log_{10}P_{mm}=7.8323-1071.235/T-0.01391\log_{10}T$.

[10] Scott, Meyers, Rands, Brickwedde, and Bekkedahl, J. Research Natl. Bur. Standards 35, 39 (1945).

[11] I. M. Klotz, *Chemical Thermodynamics* (Prentice-Hall, Inc., Englewood Cliffs, New Jersey, 1950), p. 161.

TABLE VI. Molar heat of vaporization of sulfuryl fluoride (mol wt 102.066; normal boiling point: 217.78±0.01 °K 0°C=273.16°K; 1 cal=4.1840 abs joules).

Series	I	II
Mean temp of vaporization, °K	217.78	217.76
Moles vaporized	0.02603	0.03232
Total energy cal/mole	4647.2	4666.4
Heat leak correction, cal/mole	−34.6	−59.1
Sensible heat correction, cal/mole	−1.6	+7.2
Corr energy, cal/mole	4611.0	4614.5
Heat of vaporization cal/mole	4594.4	4598.0
Av, cal/mole	4596±2	

compressibility factor at the boiling point z_b we find

$$\Delta S_i=[12R(1-z_b)]/(6-T_b/T_c), \qquad (11)$$

where T_b is the normal boiling temperature. It is interesting to note that regardless of the method used for estimating the critical temperature T_c the error in ΔS_i will be small due to the form of the denominator of Eq. (11). Assuming that, for most compounds,[12] T_b/T_c is equal to 0.62, and taking R as 1.987 cal deg^{-1} mole^{-1}, one obtains

$$\Delta S_i=4.24(1-z_b), \qquad (12)$$

where ΔS_i is given in eu/mole. The molar vapor volume at the boiling point, used in determining z_b, was calculated from the Clapeyron equation.

TABLE VII. Molar entropy of sulfuryl fluoride (mol wt: 102.066; 0°C=273.16°K; 1 cal=4.1840 abs joules).

0–13.00°K, Debye extrapolation, (θ=94.2, 6 degrees of freedom)	0.759±0.04
13.00–65.70°K, $\int C_s(dT/T)$ (graphical)	10.908±0.06
65.70–137.34°K, $\int C_s(dT/T)$ (graphical)	10.143±0.01
Fusion, 1074/137.34	7.820±0.01
Entropy of liquid at solid-liquid-vapor triple point	29.630±0.12
137.34–217.78°K, $\int C_s(dT/T)$ (graphical)	11.683±0.00
Entropy of liquid at normal boiling point	41.313±0.12
Vaporization, 4596/217.78	21.104±0.01
Gas imperfection correction	0.247±0.02
Entropy of ideal gas at 217.78°K and one atmosphere pressure	62.66 ±0.15

[12] S. Glasstone, *Thermodynamics for Chemists* (D. Van Nostrand Company, Inc., New York, 1947), p. 502.

TABLE VIII. Molar entropy of sulfuryl fluoride in the ideal gas state from molecular and spectroscopic data (1 atmos; 217.78°K).

$S_t°$, eu	38.219
$S_r°$, eu	22.991
$S_v°$, eu	2.030
Total, eu	63.24
Calorimetric entropy, eu	62.66
Residual entropy, eu	0.58

ENTROPY FROM MOLECULAR AND SPECTROSCOPIC DATA

Translational and rotational entropy contributions $S_t°$ and $S_r°$, in entropy units, were calculated from relations given by Wagman *et al.*[13]:

$$S_t°=6.8635\log M-2.3141+11.4391\log T, \quad (13)$$

$$S_r°=2.2878\ (\log I_A I_B I_C\cdot 10^{117})-4.5757\log s-0.0332+6.8635\log T, \quad (14)$$

where M, the molecular weight, was taken as 102.066; T, the absolute temperature, was taken as 217.78°K; and s, the symmetry number, was taken as two. Values for I_A, I_B, and I_C, the moments of inertia, have been previously determined.[3]

The fundamentals used for the calculation of vibrational entropy contribution, with the exception of $\nu_4(A_1)$, the symmetric SF_2 bendng frequency, were taken from the infrared data of Perkins and Wilson[1] and the Raman data of Bender and Wood.[2] The $\nu_4(A_1)$ fundamental was taken, according to the microwave data of Lide *et al.*,[3] as 388 cm^{-1}. The fundamental frequencies used in the calculation of the vibrational entropy were:

$\nu_4(A_1)=388$ cm^{-1} $\quad \nu_2(A_1)=848$ cm^{-1}

$\nu_5(A_2)=388$ cm^{-1} $\quad \nu_3(B_2)=883$ cm^{-1}

$\nu_9(B_2)=539$ cm^{-1} $\quad \nu_1(A_1)=1269$ cm^{-1}.

$\nu_8(A_1)=544$ cm^{-1} $\quad \nu_6(B_1)=1502$ cm^{-1}.

$\nu_7(B_1)=553$ cm^{-1}

The entropy calculations are summarized in Table VIII.

DISCUSSION

The observed discrepancy of 0.58 eu per mole between the calorimetric entropy and the spectroscopic entropy is attributed to residual entropy at absolute zero, rather than to an incorrect assignment of the $\nu_4(A_1)$ fundamental. To provide good agreement between the calorimetric and spectroscopic entropies, the frequency of the $\nu_4(A_1)$ fundamental would have to be greater than 1000 cm^{-1}, which is extremely unlikely. On the other hand, randomness at absolute zero seems plausible due to the near symmetry[3] of the sulfuryl fluoride molecule. If the molecule were considered entirely symmetrical, the residual entropy should be R ln 6, or 3.56 eu per mole. The much lower observed value of 0.58 eu per mole implies a high degree of crystalline order based on six energy-equivalent positions for the molecule. Considering the slight asymmetry of the molecule and the partial crystalline ordering which occurs at the lambda transition, it appears that the number of equivalent molecular positions is nearer to two.

The results of the present work are insufficient in themselves to confirm the frequency of the symmetric SF_2 bending fundamental, $\nu_4(A_1)$, and the residual entropy value of 0.58 eu per mole is based on a ν_4 frequency of 388 cm^{-1}. Further gaseous heat capacity data would provide a confirmation of the ν_4 fundamental and allow the residual entropy to be determined more exactly.

[13] Wagman, Kilpatrick, Taylor, Pitzer, and Rossini, J. Research Natl. Bur. Standards **34**, 143 (1945).

Thermodynamic Properties of Trifluoromethanethiol from 12°K to Its Boiling Point. Entropy from Molecular and Spectroscopic Data

R. E. Dininny* and E. L. Pace

Morley Chemical Laboratory, Western Reserve University, Cleveland, Ohio

(Received August 17, 1959)

The heat capacity of trifluoromethanethiol has been measured from 12° to 227°K. The heat of fusion at the triple point temperature, 116.04°K, was 1177 cal mole^{-1}. The heat of vaporization at the normal boiling point, 235.16°K, was 4798 cal mole^{-1}. The vapor pressure has been measured, and the data are represented by the equation $\log_{10}p_{mm}=(-1352.568/T)-2.686918\log_{10}T+15.00409$. The entropy of trifluoromethanethiol gas calculated from the calorimetric data was 69.45±0.17 eu at 235.16°K. The result calculated from spectroscopic data and structural parameters for the molecule was 70.19 eu. The discrepancy of 0.74±0.17 eu has been attributed to a potential barrier of 1540±260 cal mole^{-1} restricting the internal rotation of the trifluoromethyl group.

INTRODUCTION

THIS paper presents the results of a calorimetric investigation directed towards determining the possible existence and magnitude of a potential barrier to internal rotation in the trifluoromethanethiol molecule. Since there is no reason to expect any residual entropy at absolute zero, one should be able to resolve any discrepancy between the calorimetric and spectroscopic entropy in terms of a barrier to the internal rotation of the trifluoromethyl group about the C—S bond.

CALORIMETRIC SAMPLE

The sample of trifluoromethanethiol was obtained from Dr. M. I. Bro of the Experimental Station of E. I. du Pont de Nemours and Company of Wilmington, Delaware. It was prepared by the method described by Muetterties[1] in which *bis* (trifluoromethylthio) mercury, $(CF_3S)_2Hg$, synthesized by the reaction of mercuric fluoride and carbon disulfide, is treated with anhydrous hydrochloric acid in dioxane.

The sample of trifluoromethanethiol, CF_3SH, was purified by distillation through a low temperature fractionating column by a procedure similar to that described by Booth and Bozarth.[2] There were indications that the compound was not stable particularly when it was condensed in a steel cylinder for weighing. As a result, the sample was introduced into the calorimeter directly from a Pyrex vacuum system without weighing.

All the calorimetric measurements were made on a single sample. A second triple point study carried out two weeks after the start of the measurements indicated that the purity of the sample had not changed. Upon removal of the sample from the calorimeter, it was evident that there had been some chemical change. The sample introduced into the calorimeter was a clear and colorless liquid, whereas the sample which was removed exhibited some opaqueness and an orange coloration when condensed in a glass trap. It also was apparent that some of the sample was left as an involatile residue in the calorimeter since the heat capacity of the empty calorimeter had increased by about 0.3%. In order to allow approximately for this loss, the preceding increase in heat capacity was converted to an equivalent amount in grams of the sample. This amount was then added to the amount of sample withdrawn from the calorimeter to give a total of 0.4678 mole for the calorimetric sample.

HEAT CAPACITY MEASUREMENTS

A description of the apparatus used in this investigation has been given.[3,4] The temperatures were measured with a platinum resistance thermometer having an ice point resistance of 25.5 ohms. The thermometer was calibrated by the National Bureau of Standards. The temperatures are reported on the basis of an ice point temperature of 273.16°K. One calorie has been taken equal to 4.1840 absolute joules.

The molar heat capacities as experimentally measured are listed in Table I and are shown graphically in Fig. 1. The heat capacities at rounded temperatures are listed in Table II.

The saturated heat capacities were determined from

$$C_s=(M/n)[(G-G_0)-T(d/dT)(V-nv)(dP/dT)], \quad (1)$$

where G is the heat capacity of the calorimeter when it contains n grams of sample; G_0, the heat capacity of the empty calorimeter; V, the volume of the calorimeter in cc; v, the specific volume of the sample; M, the molecular weight; P, the vapor pressure; and T, the absolute temperature. The liquid densities, in g cc^{-1}, were determined experimentally and are given by the expression

$$d=1.961-0.00239T \quad (2)$$

in the temperature range 150 to 230°K.

* Now at the Department of Chemistry, Union College, Schenectady, New York.

[1] E. L. Muetterties, U. S. Patent 2,729,663.

[2] H. S. Booth and A. R. Bozarth, Ind. Eng. Chem. 29, 470 (1937).

[3] Pace, Sasmor, and Heric, J. Am. Chem. Soc. 74, 4413 (1951).

[4] Pace, Pierce, and Dennis, Rev. Sci. Instr. 26, 20 (1955).

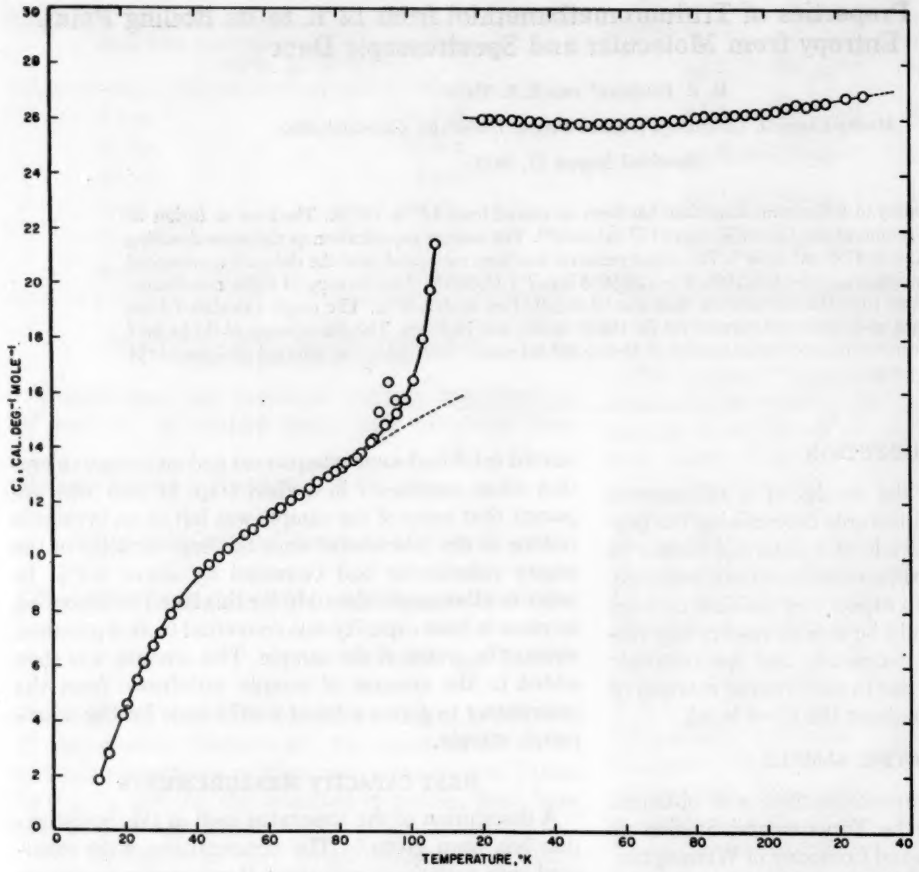

FIG. 1. Molar heat capacity of trifluoromethanethiol.

The heat capacity measurements show a precision of ±0.3% from 12°–50°K and ±0.1% from 50°–230°K.

Some scattering of the experimental heat capacities was observed in the premelting region around 95°K when a heater voltage of 10 v was used. The scattering was not observed when a heater voltage of 6 v was used in the same region. Therefore, it is believed that the scattered points which were observed represent non-equilibrium heat capacities resulting from a too rapid rate of heating.

HEAT OF FUSION

The heat of fusion was determined in the following manner. The calorimeter was brought to a temperature below the region in which premelting occurred. The calorimeter was then heated for a sufficient length of time to melt the entire sample and raise the temperature into the liquid range of the sample. The energy required to heat the solid and liquid phases was then subtracted from the energy input to yield the heat of fusion. The $\int GdT$ correction prior to fusion was obtained by using the extrapolated heat capacity curve shown as the dotted line in Fig. 1. The results of the heat of fusion measurements are listed in Table III.

The triple point temperature was determined from the melting curve. Successive increments of the sample were melted over a period of about eight hours. The equilibrium temperature for each increment was recorded. From these data, the triple point temperature of pure trifluoromethanethiol was found to be 116.04°K and the mole fraction of impurity in the sample was 0.013 by the procedure described by Rossini.[5] The equilibrium temperatures for various fractions melted are found in Table IV.

VAPOR PRESSURE

The vapor pressure was measured with a Gaertner high precision cathetometer used in conjunction with a standard meter bar. Gravity, meniscus, scale, and temperature corrections were applied to the data. The data are represented by the equation,

$$\log_{10} p_{mm} = (-1352.568/T) - 2.686918 \log_{10} T + 15.00409, \quad (3)$$

derived by the method of least squares. The least squares treatment of the data was carried out for a four constant equation but one of the constants was zero. The experimental vapor pressures as well as those calculated from Eq. (3) are found in Table V. The normal

[5] F. D. Rossini, *Chemical Thermodynamics* (John Wiley & Sons, Inc., New York, 1950), pp. 454–58.

boiling point of trifluoromethanethiol as calculated from Eq. (3) is 235.16°K.

HEAT OF VAPORIZATION

The heat of vaporization was carried out in a manner described by Scott.[6] The liquid was vaporized into one of two traps immersed in liquid nitrogen until constant pressure was attained. Rough adjustment of the takeoff rate was achieved by manipulation of a stopcock. Fine adjustment was made by means of a decade resistance box in series with the heater. When constant conditions were attained, the first trap was closed and the second opened simultaneously for collection of the vaporization sample for a known interval of time. Pressure readings were taken throughout the interval.

TABLE I. Molar heat capacity of trifluoromethanethiol. 0°C = 273.16°K; 1 cal = 4.1840 abs joules; mol wt = 102.08; sample = 0.4678 mole.

T°K	C_s cal deg^{-1} mole^{-1}	Series	T°K	C_s cal deg^{-1} mole^{-1}	Series
12.53	1.869	4	107.39	21.47	3
15.39	2.839	4	116.04	melting point	
19.20	4.237	4			
20.36	4.645	5	120.80	26.02	17
23.33	5.521	4	121.09	26.04	3
25.27	6.136	5	122.75	26.03	10
27.77	6.784	4	124.65	26.08	8
29.83	7.237	5	125.79	26.00	17
32.85	7.893	4	129.17	25.97	8
35.08	8.382	5	131.13	25.92	17
40.72	9.444	5	134.06	25.91	8
43.59	9.733	4	136.82	25.88	17
46.35	10.05	5	142.43	25.89	17
48.84	10.33	4	144.16	25.82	19
53.51	10.83	6	147.99	25.84	17
55.76	11.04	7	150.27	25.78	19
58.67	11.34	6	153.49	25.84	17
61.42	11.61	7	156.47	25.83	19
63.65	11.83	6	158.92	25.83	17
66.61	12.11	7	162.59	25.87	19
68.79	12.30	6	164.30	25.90	17
71.80	12.54	7	165.03	25.89	18
73.96	12.76	6	168.64	25.89	19
77.06	12.98	7	171.05	25.92	18
79.06	13.16	6	174.62	25.98	19
80.37	13.20	10	177.02	25.97	18
80.81	13.28	8	178.05	26.07	19
82.01	13.46	7	182.90	26.12	18
84.10	13.56	6	186.05	26.20	19
85.16	13.65	10	188.74	26.11	18
86.25	13.81	8	191.50	26.17	19
86.73	13.87	7	194.50	26.19	19
89.08	14.25	6	197.28	26.21	19
89.71	14.35	10	200.20	26.23	18
90.02	14.25	13	202.99	26.32	19
91.33	15.33	8	205.86	26.40	18
93.02	14.85	13	208.67	26.50	19
93.95	16.40	10	211.47	26.44	18
96.11	15.76	8	214.29	26.54	19
96.36	15.28	13	217.02	26.57	18
98.59	15.79	10	222.55	26.77	18
100.98	16.48	8	227.35	26.84	18
103.58	17.99	10	235.16	normal boiling point	
105.77	19.78	8			

[6] Scott, Meyers, Rands, Brickwedde, and Bekkedahl, J. Research Natl. Bur. Standards 35, 39 (1945).

TABLE II. Molar heat capacity of trifluoromethanethiol at rounded temperatures. Values taken from a smooth curve through the experimental data. 0°C = 273.16°K; 1 cal = 4.1840 abs joules; mol wt = 102.08; sample = 0.4678 mole.

T°K	C_s cal deg^{-1} mole^{-1}	T°K	C_s cal deg^{-1} mole^{-1}
15	2.691	130	26.00
20	4.516	135	25.93
25	6.048	140	25.89
30	7.317	145	25.84
35	8.348	150	25.85
40	9.192	155	25.85
45	9.887	160	25.89
50	10.48	165	25.91
55	10.99	170	25.94
60	11.48	175	26.01
65	11.96	180	26.08
70	12.41	185	26.14
75	12.84	190	26.18
80	13.26	195	26.23
85	13.65	200	26.28
90	14.22	205	26.36
95	14.91	210	26.46
100	15.71[a]	215	26.60
105	16.56[a]	220	26.71
110	17.50[a]	225	26.84
115	18.56[a]	230	26.96
		235	27.03
liquid		vapor	
120	26.08		
125	26.05		

[a] Extrapolated values.

When an auxiliary heater immersed in the sample was found to be inoperative, the temperature of the vaporization was established from the vapor pressure which was observed continuously during the vaporization. The operating characteristics of the calorimeter during vaporizations are well known.[7] Superheating of the liquid of the order of 0.1° exists during vaporizations at the rates which were used. In the case of the heat of vaporization of nitrogen trifluoride, simultaneous observation of the temperature of the calorimeter with a resistance thermometer located in the reentrant well of the calorimeter and as determined from the pressure of the vaporization was possible. The difference in the worst case was 0.3°. Also, one can perform a calculation of the pressure drop in the line leading from the calorimeter to the manometer and show that the temperature difference corresponding to the pressure drop is negligible (less than 0.01°). Therefore, the procedure which has been used here to determine the temperature of the vaporization introduces an uncertainty of between 0.1° and 0.3° in the temperature of the vaporization.

During the vaproization process, n moles of vapor leave the calorimeter increasing the dead space by nv where v is the molar volume of the liquid. This dead space is filled with nV moles of vapor where V is the molar volume of the vapor. The correct number of moles vaporized then is $n(1+v/V)$.

[7] L. Pierce and E. L. Pace, J. Chem. Phys. 23, 551 (1955).

TABLE III. Molar heat of fusion of trifluoromethanethiol at the triple point temperature of 116.04°K. 0°C=273.16°K; 1 cal=4.1840 abs joules; mol wt=102.08; sample=0.4678 mole.

Temp. interval °K	Energy input cal mole^{-1}	$\int GdT$ cal mole^{-1}	ΔH_f cal mole^{-1}
95.45–119.76	2090	913	1177
93.34–118.36	2094	917	1177

Heat leak and $\int GdT$ corrections were applied to the energy input.

The heat of vaporization is given by

$$\Delta H_v=(Q_{corr}/n)(1+v/V)^{-1}. \quad (4)$$

Since $v \ll V$, (4) may be written

$$\Delta H_v=(Q_{corr}/n)(1-v/V). \quad (5)$$

The heat of vaporization was measured at 236.50°K. This value was corrected to the normal boiling point, 235.16°K, by means of the relation,

$$d(\Delta H)/dT \approx C_{p(vapor)}-C_{p(liquid)}=\Delta C_p, \quad (6)$$

ΔC_p was estimated to be 10 cal mole^{-1} by using the heat capacity of the gas determined theoretically and the observed heat capacity of the liquid. A summary of the heat of vaporization measurements is presented in Table VI.

ENTROPY FROM CALORIMETRIC DATA

The results of the calculations of the calorimetric entropy are listed in Table VII. The gas imperfection was calculated from the Berthelot equation using the critical temperature of 373°K and critical pressure of 44.2 atmos estimated by the methods of Lydersen[8] and Riedel,[9] respectively.

The total estimated uncertainty of 0.17 eu can be broken down in the following manner: sample weight, 0.05 eu; heat capacity data, 0.06 eu; heat of fusion, 0.01 eu; heat of vaporization, 0.04 eu; and gas imperfection, 0.01 eu.

TABLE IV. Equilibrium temperatures for various fractions melted.

Temperature °K	Fraction melted
114.62	0.212
115.19	0.390
115.44	0.567
115.59	0.745
115.68	0.923
116.04	1.000 (extrapolated)

[8] A. L. Lydersen, "Estimation of critical properties of organic compounds," Coll. Eng., Univ. Wisconsin, Eng. Exptl. Station Rept. 3, Madison, Wisconsin (April, 1955).
[9] L. Riedel, Z. Elektrochem. **53**, 222 (1949).

TABLE V. Vapor pressure of trifluoromethanethiol (0°C=273.16°K).

Temperature °K	P_{obs} int mm Hg	P_{calc}[a] int mm Hg	$P_{obs}-P_{calc}$
167.75	9.20	9.19	0.01
175.32	18.17	18.21	−0.04
183.01	34.29	34.22	0.07
190.48	59.94	59.92	0.02
197.82	99.28	99.30	−0.02
205.05	157.15	157.01	0.14
211.93	235.38	235.37	0.01
218.52	337.64	337.61	0.03
224.09	449.19	449.61	−0.42
230.49	611.12	613.27	−2.15
236.03	792.51	789.97	2.54

[a] $\log_{10}P_{mm}=(-1352.568/T)-2.686918\log_{10}T+15.00409$.

SPECTROSCOPIC ENTROPY

The value assumed for the molar gas constant R in the calculations of the spectroscopic entropy was 1.9877 cal deg^{-1} mole^{-1}.[10] The translational contribution to the entropy was calculated from the relation,

$$S_T=R[\tfrac{5}{2}\ln T-\ln P+\tfrac{3}{2}\ln M-1.164], \quad (7)$$

with $T=235.16$°K, $P=1$ atmos, and $M=102.08$.

No electron diffraction or microwave data are available for trifluoromethanethiol, so it was necessary to assume reasonable values for the bond angles and bond distances in order to calculate the principal moments of inertia. The following bond angles and bond distances were used in the calculations: ∠F—C—S, 110°; ∠C—S—H, 100°; ∠F—C—F, 110°; S—H distance, 1.35 A; C—F distance, 1.36 A; and C—S distance, 1.83 A. These parameters were taken from the molecules CF_3Cl[11] and CH_3SH.[12] The atomic masses were: F, 3.155×10^{-23} g; C, 1.994×10^{-23} g; S, 5.323×10^{-23} g; and H, 0.1674×10^{-23} g. From these data, the product, $I_AI_BI_C$, of the principal moments of inertia was found to be 10.97×10^{-114} (in cgs units).

TABLE VI. Molar heat of vaporization of trifluoromethanethiol at the normal boiling point of 235.16°K. 0°C=273.16°K; 1 cal=4.1840 abs joules; mol wt=102.08.

Moles vaporized	0.04477	0.03525
Mean temperature of vaporization, °K	236.50	236.49
Corr energy input, cal mole^{-1}	4838	4829
$\int GdT$, cal mole^{-1}	−56	−31
Heat leak, cal mole^{-1}	4	−15
ΔH_v, cal mole^{-1} at 236.50°K	4786	4783
ΔH_v, cal mole^{-1} at 235.16°K	4799	4796

[10] J. W. M. DuMond and E. R. Cohen, Revs. Modern Phys. **25**, 691 (1953).
[11] H. W. Thompson and R. B. Temple, J. Chem. Soc. **1948**, 1422.
[12] Russell, Osborne, and Yost, J. Am. Chem. Soc. **64**, 165 (1942).

The contribution to the entropy due to external rotation was calculated according to

$$S_{R_e}=R[\tfrac{3}{2}\ln T+\tfrac{1}{2}\ln I_A I_B I_C-\ln\sigma+134.678]. \quad (8)$$

The symmetry number σ is unity for the CF_3SH molecule.

Further calculations were made to determine how sensitive the rotational entropy was to the value assumed for the C—S—H angle. The change in entropy resulting in an increase of the C—S—H angle from 90° to 110° is only 0.03 eu.

The entropy contribution due to internal rotation was calculated according to

$$S_{R_i}=R[-0.775+\tfrac{1}{2}\ln T+\tfrac{1}{2}\ln I_{\text{Red}}\times 10^{40}-\ln n] \quad (9)$$

where $n=3$. The reduced moment of inertia is 2.821×10^{-40} g cm^2.

The fundamentals of the molecule assigned from an analysis of the infrared spectrum were[13] ν_1-1136 cm^{-1}; ν_2-1179, 1167 cm^{-1}; ν_3-463 cm^{-1}; ν_4-521, 521 cm^{-1}; ν_5-763 cm^{-1}; ν_6-342, 342 cm^{-1}; ν_7-2618 cm^{-1}; ν_8- torsional mode; and ν_9-540 cm^{-1}.

TABLE VII. Calorimetric entropy of trifluoromethanethiol at the normal boiling point of 236.16°K and at 1 atmos pressure.

Process	eu/mole
0–12.53°K, Debye extrapolation, 18 deg of freedom, $\theta=142.6$	0.63
12.53–116.04°K, graphical integration	19.68±0.06
Fusion, 1177/116.04	10.14±0.02
Entropy of the liquid at the solid, liquid, vapor triple point	30.45±0.08
116.04–235.16°K, graphical integration	18.45±0.04
Vaporization, 4798/235.16	20.40±0.04
Gas imperfection, Berthelot equation, ($T_c=373$°K; $P_c=44.2$ atmos).	0.15±0.01
Entropy of the ideal gas at 235.16°K, 1 atmos pressure	69.45±0.17

TABLE VIII. Molar entropy of trifluoromethanethiol at 235.16°K and 1-atmos pressure from spectroscopic and molecular data.

Contribution	eu/mole
S (translational)	38.613
S (external rotational)	25.488
S (internal rotational)	2.734
S (vibrational)	3.357
Entropy of the ideal gas at 235.16°K and 1-atmos pressure	70.192

The resulting spectroscopic entropy is shown in Table VIII.

Comparison of this result with the calorimetric entropy shows a discrepancy of 0.74 eu. There is no reason to expect any randomness in the crystal, so the difference may be attributed to a potential barrier hindering the internal rotation of the trifluoromethyl group. Using Pitzer's tables,[14] the potential barrier was found to be 1540 cal mole^{-1} as compared with 1460 cal mole^{-1} for the molecule CH_3SH.[12] The uncertainty of ±0.17 eu in the calorimetric entropy results in an uncertainty in the magnitude of the barrier of ±260 cal mole^{-1}.

ACKNOWLEDGMENT

We are indebted to Dr. M. I. Bro of the Experimental Station of E. I. du Pont de Nemours and Company of Wilmington, Delaware, for the sample of trifluoromethanethiol used in this research.

The work described in this paper has received the support of the U. S. Atomic Energy Commission under contract AT (30-1)-824.

[13] R. E. Dininny and E. L. Pace, J. Chem. Phys. **31**, 1630 (1959).

[14] K. S. Pitzer, J. Chem. Phys. **5**, 469 (1937).

Interaction of Hydrogen with Tungsten*

T. W. HICKMOTT

General Electric Research Laboratory, Schenectady, New York

(Received September 15, 1959)

Measurements have been made under ultra-high vacuum conditions of the rates and isotherms for the adsorption of hydrogen on tungsten, the rate of desorption of hydrogen from tungsten, and the rate of formation of atomic hydrogen by an incandescent tungsten filament. When hydrogen chemisorbs on tungsten at 77°, the sticking probability is 0.1 and two distinct states of binding, α and β, may be isolated at adsorption pressures as low as 2.5×10^{-9} mm. Analysis of desorption kinetics of the most tightly bound state, β, shows that hydrogen chemisorbs as atoms since evaporation is second order in adsorbed hydrogen. For $n_\beta < 30\times10^{12}$ molecules/cm², $v_M=(5\times10^{-3})n^2\exp(-31\,000/RT)$molecules/cm²-sec. At higher coverages, a decrease in heat of desorption is observed which is due to surface heterogeneity. At equilibrium, the amount adsorbed in the β state obeys a Temkin isotherm between 273° and 373°K; evaporation of hydrogen in the β state occurs down to temperatures as low as 77°K. Isosteric heats agree with heats derived from desorption measurements. The α state, populated before the β state is saturated at 77°K, is proportional to hydrogen pressure and probably consists of molecular hydrogen on top of the primary atomically chemisorbed layer. The rate of evaporation of atomic hydrogen when the filament temperature is raised above 1100°K is $v_A=(2.2\times10^{13})n\exp(-67\,000/RT)$molecules/cm²-sec. For pressures below 10^{-7} mm and filament temperatures above 1475°K, the fraction of molecules striking the filament surface that is dissociated is constant and at least 0.05. Values of surface coverage and the rate of formation of atomic hydrogen as a function of filament temperature and hydrogen pressure are derived from experimental data.

I. INTRODUCTION

An essential preliminary to understanding such simple catalytic reactions as hydrogen-deuterium exchange, or ortho-para hydrogen conversion on tungsten is knowledge of the kinetic processes at the surface. Rates of chemisorption, rates of surface diffusion, and rates of evaporation of hydrogen from tungsten, as well as characterization of the states of binding are all needed.[1] Adsorption studies on tungsten filaments[2] and evaporated films[3-5] have provided a great deal of information on the stability and properties of chemisorbed hydrogen.[6] Measurements of kinetic processes include studies of surface diffusion[7] and the rate of formation of atomic hydrogen,[8,9] but attempts to apply ultra-high vacuum techniques to determine rates of adsorption[10,11] have been vitiated by spurious effects caused by operation of the ionization gauge used to measure pressures below 10^{-5} mm.[12] Atomic hydrogen, produced by the tungsten electron source of a conventional ionization gauge, reacts with glass to produce carbon monoxide, water vapor, and methane that contaminate the tungsten surface. It also adsorbs strongly on the glass walls introducing significant errors in quantitative measurements of hydrogen pressures. The present work reports measurements, made under ultra-high vacuum conditions, of the rate of chemisorption of hydrogen on tungsten, rates of evaporation of molecular and atomic hydrogen, and isotherms for the adsorption of hydrogen on tungsten using a modified ionization gauge that minimizes difficulties encountered in previous work.

EXPERIMENTAL METHODS

Vacuum Techniques

The vacuum system used[12] consisted of a $2\frac{1}{4}$ in. o.d. Pyrex bulb containing the tungsten adsorption sample, a Bayard-Alpert[13] ionization gauge, and an omegatron ion-resonance mass spectrometer,[14] separated from the pumps by a magnetically operated ground glass valve. The adsorbate was a 0.010 in. tungsten filament, 16 cm long, mounted on 0.150 in. Mo leads. Analysis of the tungsten, obtained from the Kulite Co., showed 0.003% C. After a very light electrolytic etch in 1*N* NaOH, the filament was aged by heating in vacuum of 10^{-9} mm at 2750°K for six hours and for 15 min at 3000°K.[15] The ionization gauge was modified by substituting a lanthanum boride-coated tantalum filament for one of the tungsten gauge filaments that served as an electron source. The low work function of this emitter[16] enabled the gauge to operate at a temperature

* Presented in part at the American Physical Society Meeting, Cambridge, Massachusetts, April, 1959.

[1] G. Ehrlich, J. Chem. Phys. **31**, 1111 (1959).

[2] J. K. Roberts, Proc. Roy. Soc. (London) **A152**, 445 (1935). See also, A. R. Miller, *The Adsorption of Gases on Solids* (Cambridge University Press, Cambridge, England, 1949).

[3] O. Beeck, Advances in Catalysis **2**, 151 (1950).

[4] B. M. W. Trapnell, Proc. Roy. Soc. (London) **A206**, 39 (1951).

[5] J. C. P. Mignolet, Rec. trav. chim. **74**, 685, 701 (1955).

[6] D. D. Eley, Advances in Catalysis **1**, 157 (1949).

[7] Gomer, Wortman, and Lundy, J. Chem. Phys. **26**, 1147 (1957).

[8] G. Bryce, Proc. Cambridge Phil. Soc. **32**, 648 (1936); J. K. Roberts and G. Bryce, *ibid.* **32**, 653 (1936).

[9] D. Brennan and P. C. Fletcher, Proc. Roy. Soc. (London) **A250**, 389 (1959).

[10] T. W. Hickmott and G. Ehrlich, J. Phys. Chem. Solids **5**, 47 (1958).

[11] J. Eisinger, J. Chem. Phys. **29**, 1154 (1958).

[12] T. W. Hickmott, J. Appl. Phys. **31**, 128 (1960); Bull. Am. Phys. Soc. Ser. II **3**, 259 (1958).

[13] D. Alpert, J. Appl. Phys. **24**, 860 (1953).

[14] Sommer, Thomas, and Hipple, Phys. Rev. **82**, 697 (1951).

[15] G. Ehrlich, J. Phys. Chem. **60**, 1388 (1956).

[16] J. M. Lafferty, J. Appl. Phys. **22**, 299 (1951).

(<1100°K) such that molecular hydrogen was not appreciably dissociated to form atomic hydrogen. This minimized excessive pumping of hydrogen by the gauge, and reduced production of contaminant species by interaction of atomic hydrogen with glass to negligible proportions. Electron currents less than 5×10^{-5} amp were used for nearly all pressure measurements; operation of the gauge at higher electron currents gave unreliable pumping speeds as well as producing excessive amounts of contaminant unless the sample bulb was immersed in liquid nitrogen. The ionization gauge constant of 4.4 (mm Hg)$^{-1}$ for hydrogen was obtained by calibration against a McLeod gauge with a gauge constant of 2.8×10^{-7}. The omegatron was used only to make qualitative observations of adsorption and to ascertain that the experimental results were characteristic of the interaction of hydrogen with tungsten. Analyzed reagent grade hydrogen was obtained in liter flasks from the Air Reduction Co. and used as received. The sample bulb of volume 285 cc could be thermostatted as desired; corrections for pressure differences due to the ionization gauge and adsorption sample being at different temperatures have been made when necessary.[17] Standard procedures for producing and measuring ultra-high vacua were used.[10,13,15] Residual gas pressures of $\sim1\times10^{-10}$ mm with ionization gauge and omegatron operating were obtained before hydrogen was admitted to the vacuum system.

Three different kinds of experiment will be reported; measurements of the kinetics of desorption of hydrogen from tungsten, measurements of isotherms and the kinetics of adsorption, and measurements of the rate of formation of atomic hydrogen. Experimental methods of working with high vacuum are common to all three; the experimental procedures and interpretation peculiar to each type of measurement will be discussed separately.

Rate of Formation of Atomic Hydrogen

The pressure, p_c mm, in a vacuum system of volume V cc at temperature T_c is determined at any instant by the difference in the rate of supply of molecules to the system and their rate of removal,[12]

$$(V/kT_c)(dp_c/dt)=F_M+F_F-F_W-\alpha F_H \text{ molecules/sec.} \quad (1)$$

F_M, the flow of molecular hydrogen into the system from the reservoir, is constant in any series of measurements. The flow of hydrogen out of the system is

$$F_W=(S_W/kT_c)(p_c-p_u)\cong(S_W/kT_c)p_c \text{ molecules/sec,} \quad (2)$$

where S_W is the effective pumping speed due to gauge, walls and port, p_u is the pressure on the low-pressure side of the ground glass valve and $p_c\gg p_u$. F_F gives the effect of the filament on molecular flow; for a saturated filament or one maintained at a constant temperature, $F_F=0$; αF_H is the rate of removal of molecular hydrogen from the system after dissociation on a hot filament and subsequent adsorption on the glass walls; F_H, the rate of dissociation of molecular hydrogen, depends on filament temperature and hydrogen pressure while α, the fraction of atomic hydrogen adsorbed by the glass, is primarily a function of the amount of atomic hydrogen previously adsorbed by the glass,[12] and the glass surface temperature.

The accuracy of measurements of the rate of formation of atomic hydrogen depends on complete removal from the vapor phase of all the free radicals formed. Langmuir,[18] in his early work on the properties and formation of atomic hydrogen by an incandescent filament, used liquid air-cooled glass to trap the atoms, but obtained erratic results due to marked fatigue effects in the efficiency of trapping of atomic hydrogen by glass. Other attempts to use liquid nitrogen-cooled glass as a trap have also proved unsatisfactory,[19] but all these measurements were made at hydrogen pressures of 10^{-3} mm and greater; if one works instead in a constant flow system at hydrogen flows of less than $\sim8\times10^{12}$ molecules/sec, glass surfaces baked at 250°C and cooled in liquid nitrogen give reproducible and efficient surfaces for the trapping of atomic hydrogen.

After the sample bulb has been baked at 250°C, it is immersed in liquid nitrogen and the tungsten filament is cleaned by flashing briefly to 2200°K. A flow of hydrogen, F_M, is established with the filament saturated and S_W is evaluated from the rate of increase of pressure on closing the port. The steady-state pressure in the cell, p_0, is determined by F_M and S_W. The filament is then raised to some temperature, T, ($1100°<T<1500°$K) and held constant. The pressure in the cell drops rapidly to a new value, p_a, and remains constant for about 30 sec before it begins to rise. The value of α corresponding to the minimum pressure, p_a, is α_0 and is assumed to be unity in order to calculate

$$F_H(T,p_a)=S_W(p_0-p_a)/kT_c \text{ (molecules/sec).} \quad (3)$$

By varying F_M, one obtains F_H as a function of pressure for different values of filament temperature. If the glass has not been baked before each run or if $F_M\gtrsim800\times10^{10}$ molecules/sec the pressure drop (p_0-p_a) on increasing the filament temperature will be too small and a low rate of formation of atomic hydrogen will be observed.

Filament temperatures above 1000°K were determined from the tables of Jones and Langmuir.[20] Cooling of the filament by the leads meant that the measured rate of formation of atomic hydrogen, F_H, was less than

[17] S. Dushman, *Vacuum Techniques* (John Wiley & Sons, Inc., New York, 1949), p. 65.

[18] I. Langmuir, J. Am. Chem. Soc. **34**, 1310 (1912); **37**, 417 (1915); **38**, 1145 (1916).

[19] N. S. Zaitsev, J. Phys. Chem. U.S.S.R. **14**, 644 (1940).

[20] H. A. Jones and I. Langmuir, Gen. Elec. Rev. **30**, 310, 354, 408 (1927).

if the whole filament were at the temperature of the center of the filament, T_m. To correct for lead cooling the area of the filament, a_e, corresponding to $0.95T_m < T < T_m$ was determined by standard methods.[21] At $T=0.95\ T_m$, the rate of production of atomic hydrogen is $\frac{1}{3}$ to $\frac{1}{4}$ that due to the central portion of the filament being at T_m. $F_H' = F_H/a_e$ (molecules/cm²-sec) is then the rate of formation of atomic hydrogen per unit area.

Isotherms and the Kinetics of Adsorption

Flash filament techniques for studying the kinetics of chemisorption have been presented in detail and will only be summarized here.[10,15,22] Determination of rates of adsorption and rates of desorption of hydrogen on tungsten depend on the measurement of F_F in Eq. (1). If the filament temperature is kept below 1050°K, $F_H=0$ and the rate of change of n, the concentration in molecules/cm² of hydrogen on tungsten is given by

$$F_F/a_f = (dn/dt) = \mu_2 p_c s - E \text{ molecules/cm}^2\text{-sec}. \quad (4)$$

a_f is the geometric area of the filament, $\mu_2\, p_c$ is the impingment rate per cm² of molecular hydrogen on the filament, s is the sticking probability, the probability that a molecule striking the filament is chemisorbed, and E is the rate at which molecular hydrogen evaporates from the surface. The actual surface area is unknown so the geometric area, $a_f=1.27$ cm², has been used. This is smaller than the true area by some unknown roughness factor. The two limiting cases, $\mu_2 p_c s \gg E$ and $\mu_2 p_c s \ll E$ correspond to conditions for determining rates of adsorption and desorption, respectively, while isotherms have been measured under equilibrium conditions; $dn/dt=0$, $\mu_2 p_c s = E$.

$$\mu_2\, p_c s \gg E$$

F_F, the rate of removal of hydrogen from the system by the cold filament, can be measured from the pressure drop while the filament is chemisorbing under constant flow conditions, just as $\alpha\ F_H$ is measured, and

$$s = F_F/\mu_2 p_a a_f = S_W(p_0 - p_a)/\mu_2 p_a a_f k T_c. \quad (5)$$

Alternatively, after the filament has adsorbed gas for some arbitrary time interval it may be heated quickly (flashed) to 1100°K to evaporate the adsorbed gas. From the resultant pressure increase and known system volume, the number of molecules adsorbed in time t is determined, $n = V\Delta p/a_f k T_c$ and

$$s = (1/\mu_2 p_c)\,(dn/dt), \quad (6)$$

where p_c is the cell pressure just before flashing at time t. The flash filament method has the advantage of not depending on the measured value of S_W; S_W need only be kept small enough that pumping from the system is negligible during the time to flash the filament (<0.2 sec). Both methods of measuring the sticking probability have been used with results in good agreement, though the flash filament method is more accurate.

If the filament is heated above 1100°K during flashing, a pressure *decrease* due to production of atomic hydrogen and its adsorption on the glass should be observed. Observations of a pressure increase on flashing the filament[10,11] from 1100° to 2200°K only occur if contamination produced by the ionization gauge is present in large enough amounts that the pressure increase caused by evaporation of contaminant species is larger than the pressure decrease due to pumping of hydrogen by gauge filament and the hot adsorption sample. To eliminate the production of atomic hydrogen during flash filament measurements a timer circuit has been used that cuts off the heating current after desorption of hydrogen is complete and before the filament temperature reaches 1100°K. Production of contamination by the gauge has limited measurements of the kinetics of adsorption to adsorption temperatures of 77°K and 194°K. At these temperatures, an electron current of 5×10^{-4} amp could be used since the cold glass trapped contaminant molecules. In measuring adsorption isotherms at higher temperatures, electron currents of 5×10^{-6} amp were used. The total amount adsorbed could be determined accurately, as could pressures of $1-150\times10^{-7}$ mm, which were used for isotherm measurements. However, pressures below $\sim1\times10^{-7}$ mm could not be measured accurately with such low electron currents. The upper pressure limit in determining isotherms was reached when the pressure increase on flashing the filament was smaller than the ambient cell pressure just before flashing.

$$E \gg \mu_2\, p_c s$$

The isothermal rate of evaporation of hydrogen from a tungsten filament may be expressed[10] as

$$-dn/dt = E = k_x n^x = n^x \nu_x \exp(-\Delta H_x/RT)$$
$$\text{molecules/cm}^2\text{-sec} \quad (T=\text{const}). \quad (7)$$

The order of the reaction is indicated by x, ν_x is the pre-exponential factor which is assumed independent of T to a first approximation and ΔH_x is the activation energy for the desorption process. If $1/T$ can be represented during a flash by $1/T = a_0 + b_0 t$, a condition that can be adjusted experimentally, and if $\Delta H_x \neq \Delta H_x(n)$, Eq. (7) can be integrated[10] to give

$$x=1,\ \ln(n_0/n) = [\nu_x R/(-\Delta H_x b_0)]\epsilon \exp(\Delta H_x/RT) \quad (8)$$
$$x=2,\ [(n_0-n)/nn_0]$$

where

$$\epsilon = \{1 - \exp[(\Delta H_x/R)(T^{-1} - T_0^{-1})]\}.$$

[21] Langmuir, MacLane, and Blodgett, Phys. Rev. **35**, 478 (1930).

[22] J. A. Becker and C. D. Hartman, J. Phys. Chem. **57**, 153 (1953).

T_0 is the temperature at which evaporation is just detected, and n_0 is the surface concentration of molecular hydrogen just before flashing the filament. Calculated from experimental data, ϵ has a negligible effect on the kinetics of desorption of hydrogen from tungsten.

To show that the assumptions on which Eq. (8) is derived are valid (i.e., that $E \gg \mu_z p_c s$), one needs to show that desorption of hydrogen depends on the rate at which the filament is heated and that the concentration term in Eq. (8), at a given temperature, is linear in the time to reach that temperature,

$$x=2, \quad \frac{d[(n_0-n)/nn_0]_{T=\text{const}}}{d(-1/b_0)} = (\nu_x R\epsilon/\Delta H_x)\exp(-\Delta H_x/RT) \quad (9)$$

$$x=1, \quad \frac{d[\ln(n_0/n)]_{T=\text{const}}}{d(-1/b_0)}.$$

If Eq. (8) is valid a plot of $1/\epsilon \ln n_0/n$ or $(n_0-n)/n\epsilon$ against $1/T$ determines the order of the desorption reaction as well as the heat of desorption, ΔH_x.

The kinetics of desorption have been obtained with an ac bridge, which uses the change in resistance as the filament is heated with a constant direct current to provide a signal proportional to filament temperature.[10] Temperature calibration differs from that used in measuring the rate of formation of atomic hydrogen. Desorption of adsorbed hydrogen as molecular hydrogen occurs below 1000°K. The filament temperature is initially uniform and equal to the temperature of the thermostatting bath. Since the temperature interval from 300° to 1100°K is traversed rapidly (<1.2 sec), cooling due to leads is negligible and the whole filament may be considered "ideal," at a uniform temperature throughout the time during which desorption occurs. Knowing R_0, the filament resistance at the adsorption temperature, the resistance, R, corresponding to any other temperature may be calculated,[23] and a temperature scale determined in terms of measured resistance changes on flashing the filament. Unfortunately, selection of R_0 during a flash has some uncertainty since an instrumental transient, whose magnitude depends on the heating current, occurs which shifts the zero point. This initial point has been determined by substituting in the bridge circuit a heavy wire-wound resistance of the same magnitude as the filament resistance, but one which does not heat appreciably when the flashing current is turned on.

EXPERIMENTAL RESULTS AND DISCUSSION

Rate of Desorption of Hydrogen from Tungsten

One of the important problems in adsorption is establishing whether a chemisorbed diatomic molecule is bound to the substrate in molecular form or dissociated and adsorbed as atoms. To explain his observations of the production of atomic hydrogen by an incandescent filament, Langmuir[18] suggested that hydrogen was chemisorbed as adatoms. This view received support from Roberts'[2] calorimetric measurements of the heat of adsorption of hydrogen by tungsten wires and also indirectly by comparison of total amounts of different gases adsorbed by tungsten films.[24,25] However, a direct determination that chemisorbed hydrogen is bound as atoms has not been reported. Although measurements of the kinetics of evaporation provide the most direct method of determining this and the heats of binding, only the desorption of nitrogen from tungsten has been examined in detail.[10,15] For nitrogen, the kinetics of evaporation closely approximate those that would be expected for an ideal two-dimensional gas in which collision of two adatoms with an energy greater than the heat of evaporation is the limiting step in desorption. Leypunsky[26] has studied the evaporation of hydrogen from metals by depositing atomic hydrogen on evaporated films of aluminum, copper, nickel and iron at 77°K and measuring the rate of evolution of molecular hydrogen on warming the film.

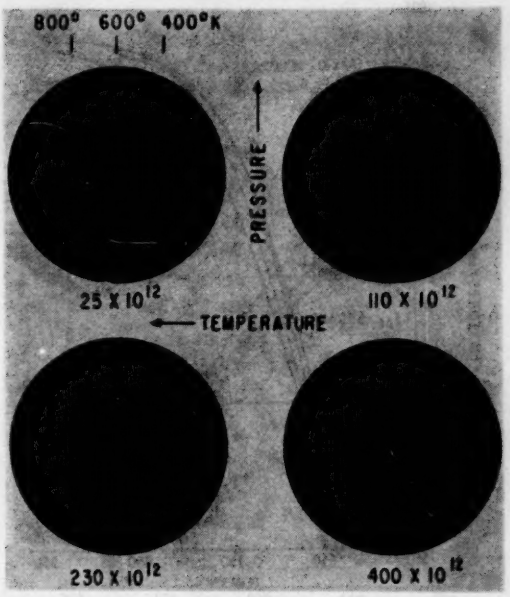

FIG. 1. Desorption of hydrogen from tungsten initially at 300°K. Temperature scale identical in each picture.

Pressure-temperature curves for the evolution of hydrogen from a tungsten filament, at four different initial coverages, after desorption at 300°K are shown in Fig. 1. Evaporation of chemisorbed hydrogen begins at successively lower temperatures as the initial cover-

[23] O. E. Forsythe and E. M. Watson, J. Opt. Soc. Am. **24**, 114 (1934).

[24] Beeck, Smith, and Wheeler, Proc. Roy. Soc. (London) **A177**, 62 (1940).

[25] E. K. Rideal and B. M. W. Trapnell, Proc. Roy. Soc. (London) **A205**, 409 (1951).

[26] O. I. Leypunsky, Acta. Physicochim. U.S.S.R. **5**, 271 (1936).

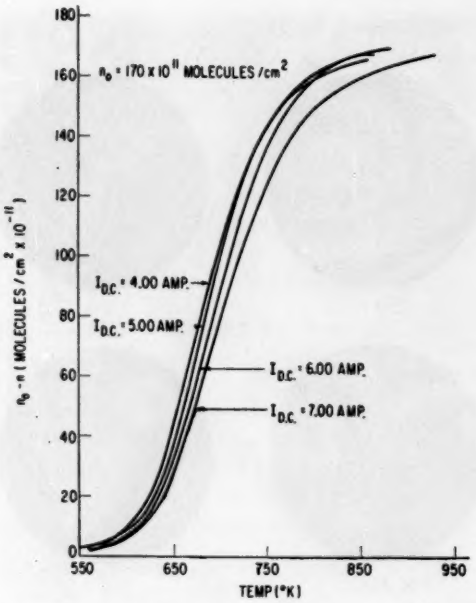

FIG. 2. Effect of rate of heating of filament on desorption of hydrogen from tungsten. Adsorption temperature, 300°K.

age increases; saturation evaporation occurs at the temperature of adsorption, and the total amount adsorbed depends on the hydrogen pressure just before flashing. Analysis of these curves according to Eq. (8) requires that $E \gg \mu_2 p_c s$, that $1/T = a_0 + b_0 t$, and that ΔH_x, the heat of evaporation, does not depend on the surface concentration of adsorbed hydrogen. To establish that $E \gg \mu_2 p_c s$, Fig. 2 shows the number of molecules/cm^2, $(n_0 - n)$, desorbed up to temperature T for different rates of heating of the filament, but for identical initial concentrations of adsorbed hydrogen. The slower the filament is heated (smaller heating current), the larger the amount of gas evaporated at lower temperatures. No correction has been made for pumping of hydrogen from the system during the flash although a decrease of the total peak height at lower heating rates shows that such an effect is operative. In spite of such pumping through the exit port, lower rates of heating result in larger values of $(n_0 - n)$ for a given value of T. Figure 3(a) shows that $1/T$ is linear in time over the temperature region in which evaporation occurs. By

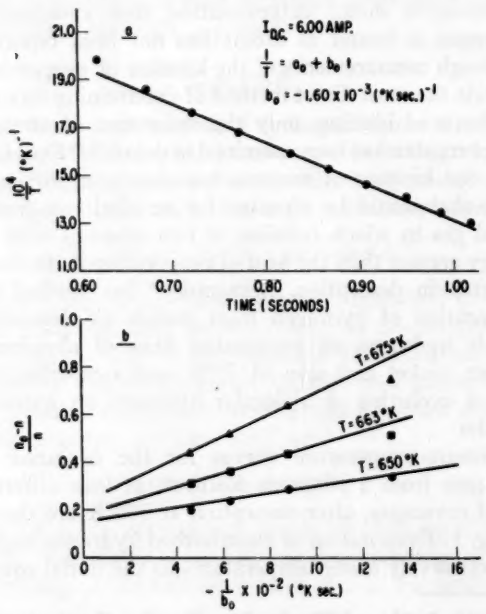

FIG. 3. (a) Reciprocal filament temperature, $1/T$, *vs* time during flashing with constant direct current. (b) Dependence of the integrated expression for second-order desorption kinetics on rate of heating of filament, at constant temperature.

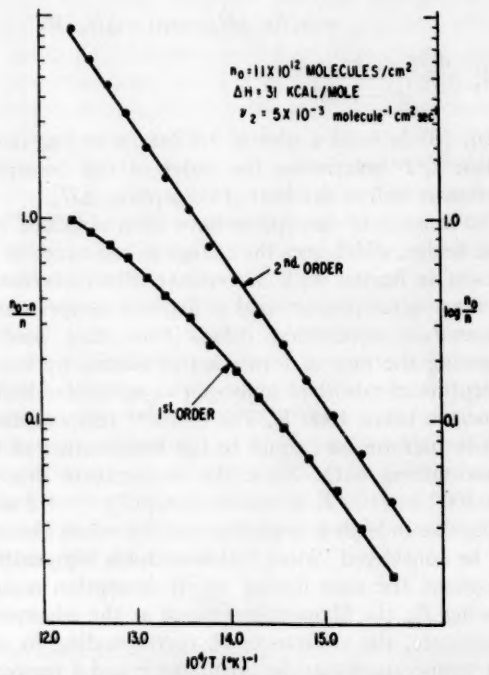

FIG. 4. Analysis of pressure-temperature curves for hydrogen on tungsten according to first-order and second-order kinetics.

varying the constant filament heating current for desorption, I_{de} (amp), it is found that $(-b_0) = [9.0 \times 10^{-5} + 4.2 \times 10^{-5} I_{de}^2]$ (deg K-sec)$^{-1}$.

Figure 4 compares first and second order desorption plots for hydrogen from tungsten at low coverage. The correction term in Eq. (8), ϵ, which depends on the heat of desorption and the temperature at which desorption just begins, is negligible and is not included. From the excellent fit to a second order equation over the whole temperature range, we conclude that hydrogen is chemisorbed as atoms rather than as molecules at low coverages. The limiting step in evaporation, second order in adsorbed hydrogen, involves collision of two adatoms with an energy greater than 31 kcal/mole and the subsequent evaporation of the molecule formed. That the competing reaction, adsorption, is not import-

ant is shown in Fig. 3(b) where $(n_0-n)/n$ is plotted against $(-1/b_0)$ at constant temperature and for constant initial concentration of adsorbed hydrogen molecules. The linearity of this indicates adsorption is negligible, in agreement with Eq. (9).

In deriving Eq. (8), ΔH_s, the heat of desorption, has been assumed to be independent of the surface concentration of hydrogen. Measurements of the heat of adsorption of hydrogen on tungsten wires[2] and tungsten films[3] have shown a marked decrease in the heat of adsorption with increasing coverage. Figure 5 shows the evaporation of hydrogen from tungsten for different initial coverages, analyzed as a second order reaction. At low initial coverages ($n_0<30\times10^{12}$ molecules/cm^2)

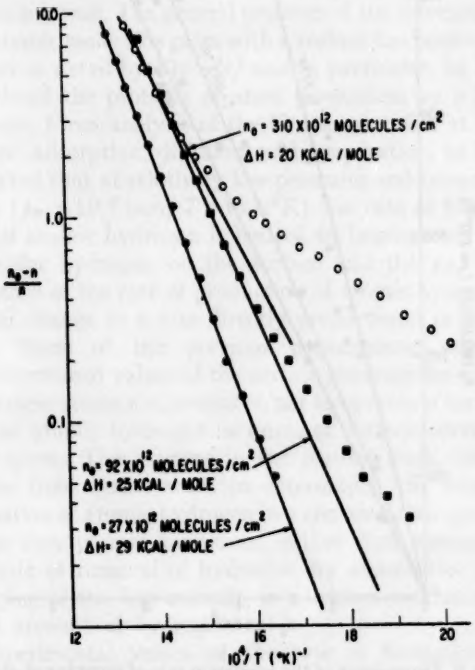

FIG. 5. Desorption of hydrogen from tungsten at different initial coverages, analyzed as a second-order reaction.

the heat of desorption is constant, and second order kinetics are accurately observed. At higher coverages marked deviations from Eq. (8) occur although for these coverages a heat of desorption which decreases with increasing coverage can be obtained for the most tightly bound hydrogen. Figure 6 shows that, at coverages close to saturation, the evolution of chemisorbed hydrogen is independent of the rate of heating of the filament except for pumping of hydrogen from the system which reduces the peak heights at low heating rates; the assumptions on which Eq. (8) is derived are not valid. This is in marked contrast to the desorption of nitrogen from tungsten where adsorption also occurs as atoms, but the heat of evaporation is constant up to the highest coverages.[10] For initial hydrogen coverages, $n_0<30\times10^{12}$ molecules/cm^2, the heat of desorption is

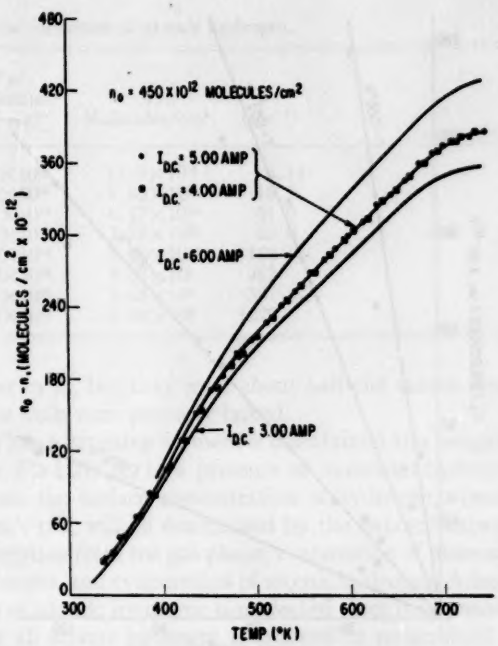

FIG. 6. Effect of rate of heating of filament on desorption of hydrogen from tungsten, at high coverages. Filament saturated at $p_2=5.2\times10^{-8}$ mm, $T=300$°K.

constant, as shown in Table I and ν_2, the pre-exponential factor for evaporation of hydrogen from tungsten, may be calculated from Eq. (8). Molecular hydrogen chemisorbs as atoms at low concentrations, and the rate of desorption is $dn/dt=-k_2n^2=-(5\times10^{-3})n^2\exp(-31\,000/RT)$ molecules/cm^2-sec. With a simple model of an ideal two-dimensional gas, the pre-exponential factor for evaporation is given by $\sigma[\pi kT/m]^{\frac{1}{2}}$, where σ is a hard sphere collision diameter, m is the mass of the hydrogen atom, and k is Boltzmann's constant. For $T=600$°K and $\sigma=1$ A, $\nu_2=4\times10^{-3}$, in excellent agreement with the experimental values. Thus, at low coverages, hydrogen chemisorbed on tungsten closely approximates an ideal two-dimensional gas for filament temperatures above 600°K.

Rate of Formation of Atomic Hydrogen

Langmuir, who first studied the formation and properties of atomic hydrogen produced by the interac-

TABLE I. Kinetics of desorption of hydrogen from tungsten at low surface coverages.

n_0 (molecules/cm^2)	ν_2 (molecules^{-1} cm^3 sec^{-1})	ΔH_2 (kcal/mole)
8.5×10^{12}	7.8×10^{-3}	31.2
11×10^{12}	4.9×10^{-3}	31.2
12×10^{12}	2.5×10^{-3}	30.6
14×10^{12}	6.2×10^{-3}	31.6
15×10^{12}	4.3×10^{-3}	30.8
18×10^{12}	10.3×10^{-3}	32.6
21×10^{12}	3.3×10^{-3}	31.0

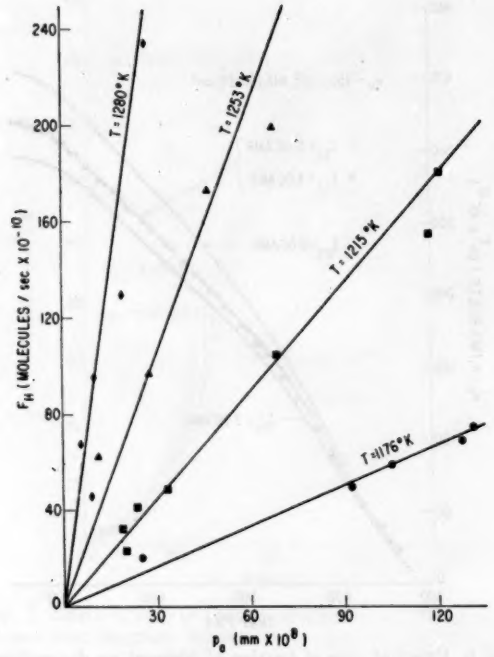

FIG. 7. Dependence of the maximum rate of pumping of atomic hydrogen, by glass at 77°K, on hydrogen pressure, at different tungsten filament temperatures.

tion of molecular hydrogen with an incandescent filament,[18] recognized that fatigue effects in the adsorption of atomic hydrogen by glass made his measured rates too low, but concluded that production of atomic hydrogen occurred from a dilute surface film. Supporting this view was the observation that electron emission from tungsten was unaffected by a hydrogen atmosphere. Bryce and Roberts,[8] using MoO_3 to trap the atomic hydrogen, found that Langmuir's measured rates of dissociation were too low by a factor of about 200, and determined that the rate of formation of atomic hydrogen was proportional to $p_{H_2}^{\frac{1}{2}}$ in the pressure range from 3×10^{-3} to 4×10^{-2} mm. Two mechanisms for the formation of atomic hydrogen were in accord with their measurements. One mechanism involved a nearly complete adsorbed film while the other

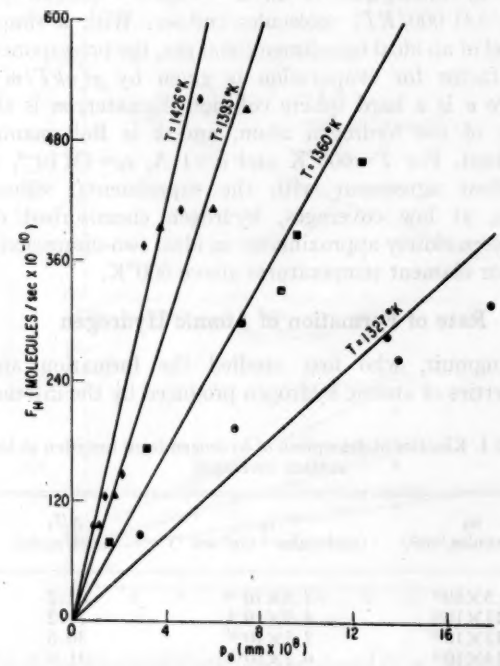

FIG. 8. Dependence of the maximum rate of pumping of atomic hydrogen, by glass at 77°K, on hydrogen pressure, at different tungsten filament temperatures.

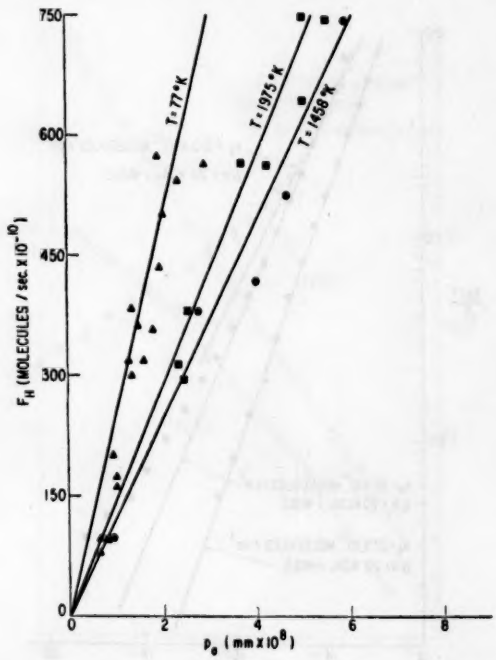

FIG. 9. Dependence of the maximum rate of pumping of atomic hydrogen, by glass at 77°K, on hydrogen pressure, at different tungsten filament temperatures.

assumed that evaporation of atomic hydrogen occurred from a dilute surface film. Bosworth's[27] measurements of the contact potential of hydrogen chemisorbed on tungsten caused them to favor the first mechanism with a surface coverage, $\theta\sim0.6-0.7$. More recent contact potential measurements[5] have discredited Bosworth's results and Brennan and Fletcher,[9] in reexamining the problem, have concluded that atomic hydrogen evaporates from a dilute surface layer. In extending the hydrogen pressure below 10^{-6} mm, they have observed a transition from a rate proportional to $p_{H_2}^{\frac{1}{2}}$ to one directly proportional to p_{H_2}. For 1×10^{-6} mm$<p_{H_2}<1\times10^{-2}$ mm, the rate of formation of atoms is $v_A=18\times10^{24}p_{mm}^{\frac{1}{2}}\exp(-52\ 600/RT)$ atoms/cm²-sec;

[27] R. C. L. Bosworth, Proc. Cambridge Phil. Soc. 33, 394 (1937).

TABLE II. Calculation of the rate constant for the formation of atomic hydrogen.

Temp (°K)	F_H (Molecules/sec)	p_a (mm)	F_H' (Molecules/cm²-sec)	n Molecules/cm²	k_A (sec⁻¹)
1176	51×10^{10}	90×10^{-6}	73×10^{10}	11.9×10^{10}	6.14
1215	135×10^{10}	90×10^{-6}	180×10^{10}	9.65×10^{10}	18.7
1253	210×10^{10}	60×10^{-6}	271×10^{10}	6.47×10^{10}	41.9
1280	139×10^{10}	15×10^{-6}	173×10^{10}	2.75×10^{10}	63.0
1327	217×10^{10}	10×10^{-6}	269×10^{10}	1.70×10^{10}	158
1360	212×10^{10}	5.0×10^{-6}	250×10^{10}	9.36×10^{9}	267
1393	294×10^{10}	4.0×10^{-6}	337×10^{10}	5.65×10^{9}	597
1426	311×10^{10}	3.0×10^{-6}	350×10^{10}	2.86×10^{9}	1220

the lower values found by earlier workers[8,19,28] are attributed to contamination of the tungsten filament by stopcock grease. The general problem of the interaction of diatomic molecular gases with a surface has been considered in detail by Ehrlich,[1] and in particular, he has considered the problem of atom production by a hot filament. From analysis of the kinetic processes at the surface, adsorption, diffusion, and evaporation, he has predicted that at relatively low pressures and temperatures ($p_{H_2}\sim10^{-6}$ mm, $T>1600°K$) the rate of formation of atomic hydrogen is limited by impingement of molecular hydrogen on the surface and the $p_{H_2}^{\frac{1}{2}}$ dependence of the rate of production of atomic hydrogen should change to a rate directly proportional to pressure. None of the previous experimental studies has determined values of the surface coverage for varying temperatures and pressures, nor have rates of formation of atomic hydrogen in terms of surface coverage been given. This is done in the present work, which differs from earlier work in determining the rate of formation of atomic hydrogen in a constant flow system under steady state conditions, rather than measuring the rate of removal of hydrogen, by atomization and trapping of the free radicals, in a system containing a fixed amount of hydrogen.

Experimental values of the rate of formation of atomic hydrogen for different values of temperature and pressure are shown in Figs. 7, 8, and 9. F_H, the pumping speed of the filament producing atomic hydrogen, evaluated from Eq. (3), is directly proportional to p_a, the minimum steady state pressure reached when the filament temperature is established and the glass bulb is cooled in liquid nitrogen. p_a has been corrected for thermal transpiration between gauge and filament.[17] Recombination of atomic hydrogen from the gas phase by glass at 77°K occurs at very low surface coverages of adsorbed hydrogen atoms.[12] Only $\sim1\times10^{12}$ atoms/cm² of glass bulb could be deposited before recombination became detectable; about half as much atomic hydrogen could be deposited on glass at room temperature before recombination was significant. If the glass sample bulb were not baked before every measurement, values of F_H were obtained that were linear in p_a, but they were about half the values found if the bulb were properly baked.

When a tungsten filament is maintained at a temperature $T>1100°K$, in a pressure of molecular hydrogen, p_c mm, the surface concentration of hydrogen, n(molecules/cm²), will be determined by the balance between adsorption from the gas phase, evaporation of molecular hydrogen, and evaporation of atomic hydrogen. Adsorption of atomic hydrogen is neglected since it is assumed that all atomic hydrogen is trapped or recombined by the walls. Evaporation of hydrogen atoms is proportional to the surface concentration while evaporation of molecular hydrogen is proportional to n^2,

$$dn/dt=\mu_2 p_c s-k_A n-k_2 n^2 \text{ molecules/cm}^2\text{-sec}, \quad (10)$$

where the rate of atomization is $k_A=\nu_A\exp(-\Delta H_A/RT)$ and $k_2=\nu_2\exp(-\Delta H_2/RT)$ may be determined from desorption kinetics. The rate of adsorption, $\mu_2 p_c s$, depends on filament temperature and gas temperature. To evaluate s, the fraction of molecules striking the surface that are adsorbed, one determines F_H for temperatures at which the impingment of molecular hydrogen limits the rate of formation of atomic hydrogen. When F_H is corrected for cooling by the leads, F_H' is the rate of formation of atomic hydrogen per unit area, $F_H'=F_H/a_e$, and $s=(1/\mu_2 a_e)dF_H/dp_a$. Figure 9 shows that $s=0.05$ for $T=1460°K$ and for $T=1975°K$. Thus, s is constant over a 500° temperature range in which atomic hydrogen formation is limited by impingment of molecular hydrogen on the incandescent tungsten filament. Evaluation of s for adsorption at 77°K, from Fig. 9, gives $s=(1/\mu_2 a_f)dF_H/dp_a=0.07$. Although the value for s derived in a later section from flash filament measurements, $s=0.1$, is somewhat higher than the value derived from measurements of pressure decrease due to pumping by the filament, there is no significant change in s over a temperature range from 77° to 2000°K. The fraction of the hydrogen molecules striking the surface that are chemisorbed by a filament at 77°K is nearly the same as the fraction of hydrogen molecules striking an incandescent filament that are dissociated, when the filament is hot enough that molecular impingment limits the formation of atomic hydrogen. F_H is derived from Eq. (3) under the assumption that α_0, the fraction of atomic hydrogen produced

[28] T. Ivanoiskaya and I. Mochan, J. Phys. Chem. U.S.S.R. **22**, 439 (1948).

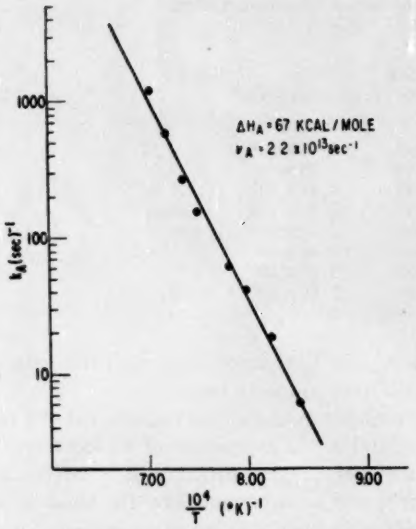

FIG. 10. Temperature dependence of the rate constant for the formation of atomic hydrogen by an incandescent tungsten filament.

by the filament that is trapped by the glass, is unity. Determination of s for an incandescent filament shows that the very lowest α_0 could be is 0.05. The exact value of α_0 is unknown, but the internal consistency of the experimental data and the excellent agreement with other work makes it improbable that the value differs significantly from unity.

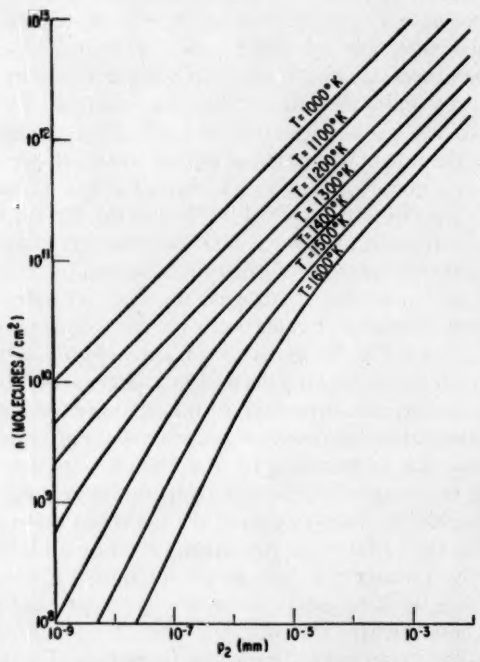

FIG. 11. Dependence of the surface concentration of hydrogen chemisorbed on tungsten on filament temperature and hydrogen pressure. Gas temperature, 298°K.

F_H is obtained under steady state conditions, $dn/dt=0$. By correcting for the temperature distribution along the filament,

$$F_H' = k_A n \quad \text{(molecules/cm}^2\text{-sec)} \tag{11}$$

and

$$n=[(\mu_2 p_c s - F_H')/k_2]^{\frac{1}{2}} \quad \text{molecules/cm}^2, \tag{12}$$

where

$$k_2=\nu_2 \exp(-\Delta H_2/RT)=(5\times10^{-3}) \exp(-31\,000/RT)$$

is derived from experimental measurements of desorption kinetics. Knowing n, one can solve for k_A in Eq. (11). Table II shows the calculation of n and k_A from the smoothed data for different filament tempera-

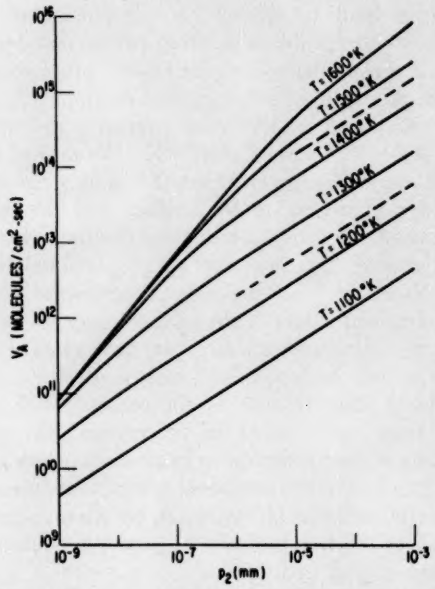

FIG. 12. Dependence of the rate of formation of atomic hydrogen on tungsten filament temperature and hydrogen pressure. Gas temperature, 298°K.

tures using $s=0.05$. Figure 10 shows that $\Delta H_A=67$ kcal/mole and $k_A=(2.2\times10^{13}) \exp(-67\,000/RT)$ sec^{-1}. From Eq. 10 the general steady state expression for n is obtained,

$$n=[-k_A+(k_A^2+4\mu_2 p_c s)^{\frac{1}{2}}]/k_2 \quad \text{molecules/cm}^2. \tag{13}$$

Figure 11 plots n for different values of p_c and T using $s=0.05$ and experimental values of k_A and k_2, while Fig. 12 shows the rate of formation of atomic hydrogen as a function of pressure and filament temperature. The dotted lines in Fig. 12 show the values of Brennan and Fletcher[9] for 1200°K and 1400°K. Agreement is within a factor of two, which is very good in view of the large temperature dependence of the reaction and the comparison of measurements made at pressures of 10^{-8} mm to results obtained at $10^{-4}-10^{-2}$ mm.

Combining data on rates of evaporation of molecular and atomic hydrogen from tungsten, a reasonable picture of evaporation processes at low coverage emerges.[1] For $n<30\times10^{12}$ molecules/cm^2 and T greater than 600°K hydrogen adatoms are freely mobile over the surface,[7] approximating an ideal two dimensional gas; desorption of molecular hydrogen involves the collision of two atoms with an energy greater than 31 kcal/mole. As the filament temperature is raised to 1100°K, the surface concentration drops, adatoms have to diffuse further over the surface before recombining, and the probablity of evaporation of hydrogen atoms increases correspondingly. Equality of the two rates occurs at higher pressures for higher temperatures as shown in Fig. 13 in which the ratio of v_M, the rate of molecular evaporation, to v_A, the rate of evaporation of atomic hydrogen, is plotted for different temperatures and pressures of molecular hydrogen. Here, likewise, a change from a dependence on $p_{H_2}^{\frac{1}{2}}$ to a linear pressure dependence is observed when $v_M/v_A\sim0.1$, reflecting the dependence of n and v_A on pressure; evaporation of atomic hydrogen only occurs from a dilute surface film. Consistent values of the tungsten-hydrogen bond energy are obtained from the two rate measurements. For $\Delta H_A=67$ kcal/mole and $\Delta H_2=31$ kcal/mole, the value of the heat of dissociation of molecular hydrogen, D, is $D=2\Delta H_A-\Delta H_2=103$ kcal/mole, in excellent agreement with accepted values.[29]

From considerations of detailed balancing, Ehrlich has shown[1] that K_p, the equilibrium constant for the

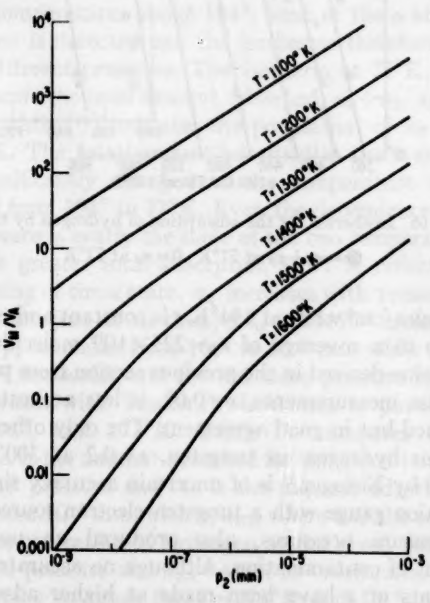

FIG. 13. Dependence of the ratio of the rate of evaporation of chemisorbed hydrogen as molecules to the rate of evaporation of chemisorbed hydrogen as atoms on filament temperature and hydrogen pressure. Gas temperature, 298°K.

[29] A. B. Gaydon, *Dissociation Energies* (Chapman and Hall, Ltd., London, England, 1953), p. 225.

TABLE III. Calculation of equilibrium constants from kinetic data.

Temp (°K)	K_p(atm)	K_p'(atm)	η_A
1200	3.87×10^{-14}	3.04×10^{-14}	0.20
1300	1.22×10^{-12}	5.08×10^{-13}	0.14
1400	2.42×10^{-11}	1.16×10^{-11}	0.16
1500	3.08×10^{-10}	1.49×10^{-10}	0.16
1600	2.94×10^{-9}	1.49×10^{-9}	0.16

dissociation of hydrogen in terms of partial pressures of atomic and molecular hydrogen, $K_p=p_1^2/p_2$, can be expressed as

$$K_p=(\nu_A^2/\nu_2)(\pi m_1kT)^{\frac{1}{2}}(\eta_2/\eta_A)\exp(-D/RT), \quad (14)$$

where the activation energy for adsorption has been placed equal to zero, m_1 is the mass of the hydrogen atom, η_2 is the equilibrium molecular sticking probability and η_A is the equilibrium sticking probability for atomic hydrogen. Table III shows accepted values of K_p[30] and values of the equilibrium constant calculated from experimental data, K_p', assuming $\eta_2/\eta_A^2=1$. No experimental values for η_2 or η_A have been reported though by analogy with the adsorption of cesium on tungsten, a value of $\eta_A=1$ might be expected. If a value of $\eta_2=s=0.05$ is used, derived from experimental data, values of η_A that are needed to bring K_p and K_p' into agreement are given in the last column of Table III. Experimental uncertainties in evaluating F_H and departure from equilibrium conditions mean that the numerical values of η_A are of no great significance. They suggest, however, that η_A may be less than unity and independent of temperature, just as s is found to be independent of temperature between 1475° and 2000°K.

Isotherms and the Kinetics of Adsorption

From changes in the work function when hydrogen is absorbed on tungsten, Mignolet[5] has deduced that two distinct states of binding exist. The primary chemisorbed layer increases the work function of tungsten, but at pressures of $\sim10^{-3}$ mm and higher and temperatures below 200°K he observed a decrease of work function as the metal saturated, which he attributed to adsorption of molecular hydrogen on top of the primary chemisorbed layer. Similar phenomena have been observed in the field emission microscope,[7,31] but no quantitative measurements of the population of this weaker state of binding have been reported. Figure 14 shows the desorption of hydrogen from tungsten when adsorption has been carried out with both gas and filament at 77°K. The pressure in the system is plotted against the time after the filament is flashed for different initial coverages, the heating current being cut off by a timer before the filament temperature goes over 1100°K and atomic hydrogen is produced. Two distinct states

[30] D. R. Stull and G. C. Sinke, *Thermodynamic Properties of the Elements* (American Chemical Society, Washington, 1956), p. 104.
[31] E. W. Müller, Ergeb. exakt. Naturw. **27**, 290 (1953).

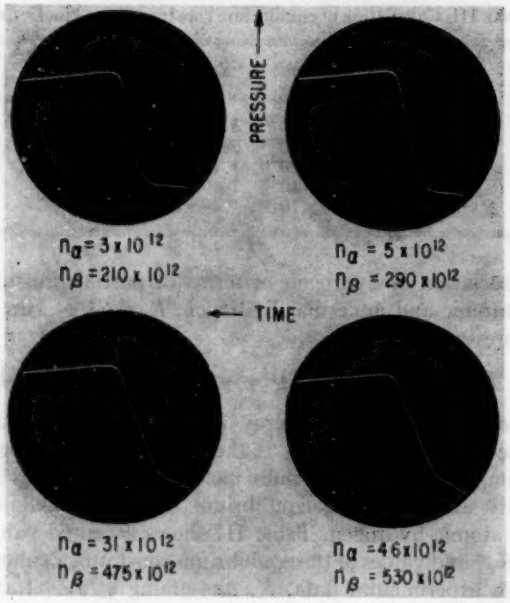
PRESSURE
TIME
$n_\alpha = 3 \times 10^{12}$
$n_\beta = 210 \times 10^{12}$
$n_\alpha = 5 \times 10^{12}$
$n_\beta = 290 \times 10^{12}$
$n_\alpha = 31 \times 10^{12}$
$n_\beta = 475 \times 10^{12}$
$n_\alpha = 46 \times 10^{12}$
$n_\beta = 530 \times 10^{12}$

FIG. 14. Desorption of hydrogen from tungsten after adsorption at 77°K. Note two states of binding. Oscilloscope sweep, 0.1 sec/cm.

of binding, α and β can be distinguished. Figure 15 shows the change in each state with time of adsorption as well as the rate of change of impingment of molecular hydrogen. The low temperature state of binding evaporates as molecular hydrogen, and is not due to contamination as the second, high temperature state of

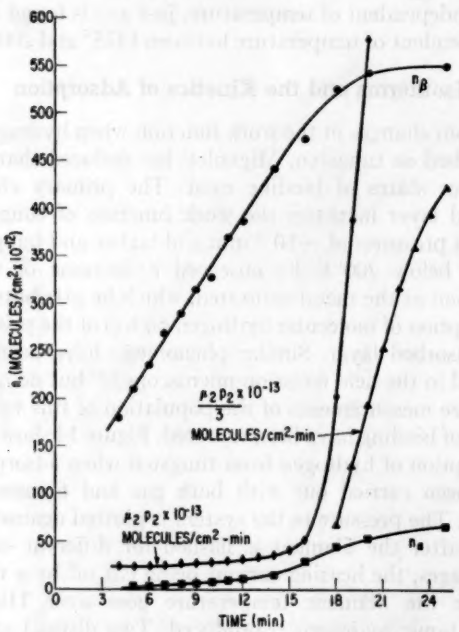

FIG. 15. Adsorption of hydrogen on tungsten at 77°K. n_α, n_β = number of molecules/cm² adsorbed in state α and β respectively. $\mu_2 p_2$ = number of molecules striking unit filament area per minute.

binding previously[10–12] reported was. The rate of formation of the α state is similar to that observed for the α state of CO on tungsten[32]; a small amount is observed while n_β is still increasing but the greatest increase in n_α occurs when occupation of the β state is nearly complete and the pressure in the system rises. Both α and β states are observed at an adsorption temperature of 87°K (liquid argon) but at 194°K none of the α state can be observed for pressures up to 2×10^{-5} mm though Mignolet's[5] work indicates some of the α state may be present at $p_{H_2} \cong 10^{-2}$ mm and 200°K. The sticking probability for molecular hydrogen on tungsten at 77°K, evaluated from Fig. 15, is $s = 0.1$ for $n_\beta < 275 \times 10^{12}$

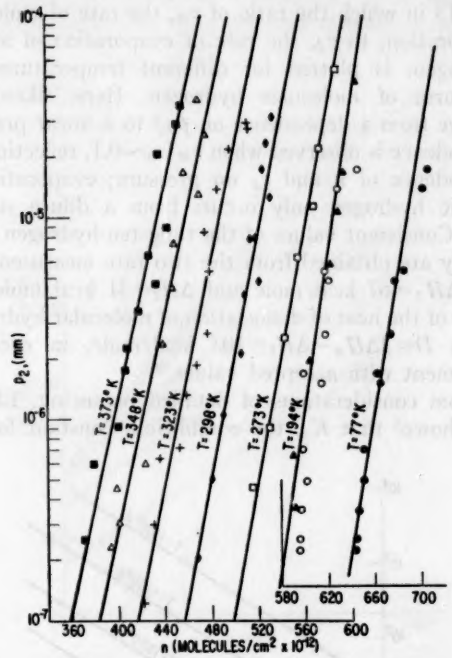

FIG. 16. Isotherms for the adsorption of hydrogen by tungsten.
● = $n_\alpha + n_\beta$ at 77°K; 0 = n_β at 77°K.

molecules/cm² while at 194°K s is constant and equal to 0.1 up to a coverage of $n_\beta = 225 \times 10^{12}$ molecules/cm.² The value derived in the previous section from pressure decrease measurements, $s = 0.07$, is less accurately determined but in good agreement. The only other value of s for hydrogen on tungsten, $s = 0.2$ at 300°K, reported by Eisinger,[11] is of uncertain accuracy since the ionization gauge with a tungsten electron source, used to measure pressures, also produced an unknown amount of contamination. Although no accurate measurements of s have been made at higher adsorption temperatures because of difficulties in measuring the very low adsorption pressures, it appears that s at 300°K is also about 0.08–0.1.

[32] T. W. Hickmott and G. Ehrlich, J. Chem. Phys. 24, 1263 (1956).

Trapnell[4] has determined isotherms for the adsorption of hydrogen on evaporated tungsten films for temperatures from 77°K to 273°K and pressures from 10^{-7} to 10^{-2} mm. Saturation occurred around 5×10^{-3} mm, with an isosteric heat of adsorption dropping to ~2 kcal/mole at $\theta=1$, the coverage at 10^{-4} mm and 77°K. However, this is the temperature range in which two states of binding may be present; the low heats are characteristic of the evaporation of the α state rather than of the β state of adsorbed hydrogen. Isotherms above 273°K can give isosteric heats for the β state of hydrogen.

Examination of the pressure-temperature curves in Fig. 1 shows that, at saturation, evaporation of hydrogen from tungsten begins as soon as the filament temperature is increased above the adsorption temperature.[10] Figure 16 shows isotherms for the chemisorption of hydrogen on tungsten at temperatures between 273° and 373°K, as well as for 77° and 194°K, plotted as a Temkin isotherm, n against log p_{H_2}. Within experimental error, which is estimated at about ±3%, the isotherms are reversible; equilibrium is established within seconds and identical coverages are obtained if equilibrium is approached from either higher or lower pressures. Values of the saturation coverage are particularly sensitive to small amounts of contamination that block sites for adsorption. Flashing the filament briefly to 2000°K before every measurement, with the ground glass port open, and use of a low electron current (5×10^{-6} amp) were essential in obtaining reproducible results.

For temperatures above 194°, none of the α state of hydrogen is detected and the isotherms therefore give n_β at different pressures. The isotherm at 77°K, however, shows the total amount adsorbed, $n_\alpha+n_\beta$, against $\log p_{H_2}$, while [0] indicates the population of n_β alone at 77°K. The total amount adsorbed in the β state is not significantly changed as the temperature is decreased from 194° to 77°K. Even the dependence of n_β on pressure is nearly the same at the two temperatures, and the greater total adsorption at 77°K reflects the populating of the α state. n_α increases with pressure at equilibrium just as n_β does; $\Delta n_\alpha\approx21\times10^{12}$ molecules/cm² as p_2 increases from 10^{-7} to 10^{-5} mm while $\Delta n_\beta\approx31\times10^{12}$ molecules/cm² for the same pressure change. Comparison with Trapnell's[4] isotherms is possible at 77°, 194°, and 273°K. Table IV compares A/A_0, where A is the amount adsorbed for the given temperature and pressure and A_0 is the amount adsorbed at 273°K and 10^{-7} mm, with n/n_{273}, where n is the equilibrium concentration of hydrogen at the given temperature and pressure and $n_{273}=488\times10^{12}$ molecules/cm² is the surface coverage for $T=273$°K and 10^{-7} mm. In general the values agree well at 10^{-7} mm. However, n/n_{273} at 10^{-5} mm is nearly equal to A/A_0 at 10^{-2} mm; the slope of n/n_{273} against log$p$ is much greater than the slope of A/A_0 against log$p$. Two possible explanations for the discrepancy are failure to reach equilibrium during the measurements on highly porous evaporated films or a possibility that the method of preparation of the tungsten films introduced an unknown amount of contamination which blocked some of the adsorption sites.[10] When hydrogen is adsorbed on evaporated tungsten films, a very rapid uptake of gas is followed by a slow uptake that may take several hours to equilibrate and has been attributed to adsorption of hydrogen into the metal structure.[3] Work with filaments shows that adsorption is reversible and that equilibrium of gas and metal is rapidly established. The large surface area of evaporated tungsten films may require a longer time to reach equilibrium with the gas phase than was allowed in Trapnell's experiments. Alternatively, examination of pressure changes when tungsten films are prepared as Trapnell's were, has shown that they are deposited with a significant amount of contamination. Both difficulties, establishment of equilibrium or surface contamination, are avoided by working with filaments of small area that can be easily cleaned before every measurement.

TABLE IV. Comparison of isotherms with data of Trapnell.[a]

	A/A_0			n/n_{273}		
p(mm)	0°C	−78°C	−183°C	0°C	−78°C	−183°C
10^{-7}	1.00	1.14	1.31	1.00	1.18	1.29
10^{-6}	1.03	1.16	1.32	1.09	1.23	1.35
10^{-5}	1.07	1.19	1.34	1.15	1.28	1.41
10^{-4}	1.10	1.23	1.36	1.22	1.32	1.47
10^{-3}	1.14	1.25	1.37			
10^{-2}	1.17	1.28	1.39			

[a] See reference 4.

To test obedience to the Temkin[33,34,35] isotherm, the surface coverage, n, must be proportional to $\log p_{H_2}$ and the resultant slope must be proportional to temperature. Both criteria are obeyed by the experimental data between 0° and 100°C; the isotherms may be expressed as

$$n=n_i+c\log p=352\times10^{12}+\{(101\times10^{15})/[T(°K)]\}+c\log p \text{ molecules/cm}^2. \quad (15)$$

The intercept of Eq. (15), n_i, is inversely proportional to temperature. Although it is not certain that adherence to the Temkin isotherm is of fundamental significance since the adsorption data can also be plotted as Freundlich isotherms,[4] it provides a convenient means of extrapolating the measurements to low coverages in order to obtain isosteric heats as a function of surface coverage. Figure 17 plots ΔH_s, the heat of adsorption derived from the Clausius-Clapeyron equation, as a function of n, the number of molecules of hydrogen/

[33] M. I. Temkin, J. Phys. Chem. U.S.S.R. **15**, 296 (1941).
[34] Brunauer, Love, and Keenan, J. Am. Chem. Soc. **64**, 751 (1942).
[35] B. M. W. Trapnell, *Chemisorption* (Butterworths Scientific Publications, Ltd., London, 1955), p. 124.

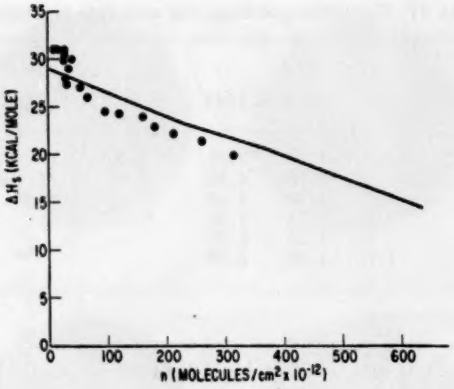

FIG. 17. The heat of adsorption of hydrogen on tungsten at different coverages. Solid line, isosteric heats. Solid points, desorption heats.

cm². In general, the variation of heat is linear in coverage. The value of ΔH_s at 20×10^{12} molecules/cm² involve extrapolations over a pressure range of ~14 decades. In spite of this, $\Delta H_s=28$ kcal/mole at low coverages, is in excellent agreement with $\Delta H_2=31$ kcal/mole found from desorption measurements at low coverages. Experimental values of desorption heats are also shown in Fig. 17. For $n>30\times10^{12}$ molecules/cm², the requirements on the use of Eq. (8) to analyze desorption data are not accurately obeyed; the heat is determined as in Fig. 5 at these coverages. The agreement between isosteric and desorption heats is excellent although the former involve extreme extrapolation of the experimental isotherms while the latter do not satisfy the requirements of Eq. 8. The value of ΔH_s, 15 kcal/mole at $n=600\times10^{12}$ molecules/cm², agrees with heats derived from calorimetric measurements of Roberts[2] and Beeck[3] and with isotherms of Trapnell,[4] while the total coverages of hydrogen are in good agreement with Roberts'[2] values and correspond to roughly one hydrogen atom per surface tungsten atom. The value of heat at low coverage, $\Delta H_2=31$ kcal/mole, is lower than the 45 kcal/mole found by Beeck and the 38 kcal/mole reported by Roberts. Gomer[7] has reported a heat of evaporation of 64 kcal/mole at low coverages, but this is incompatible with his observation that evaporation is complete in a few seconds at 600°K. This difference may simply reflect differences in the distribution of binding sites over the surface, comparable to differences found for the heats of binding of nitrogen on different samples of tungsten.[10] Values as disparate as 59 kcal/mole and 83 kcal/mole have been found for heats of desorption of nitrogen from 0.010 in. filaments off the same spool of wire, Beeck[3] reported a heat of adsorption of 95 kcal/mole for nitrogen on tungsten films, and Kisliuk[36] has reported values of 115 kcal/mole and 92 kcal/mole for isosteric and calorimetric measurements, respectively. A decrease in heat at coverages, $n>30\times10^{12}$ molecules/cm², shows that the surface is energetically heterogeneous.

Two principal mechanisms have been proposed for the H_2-D_2 exchange reaction and the ortho-para hydrogen conversion on tungsten. The Bonhoeffer-Farkas[6,37] mechanism requires that reaction take place between atoms chemisorbed on the surface, while the Rideal[38] mechanism postulates that a hydrogen molecule in a second layer, bound by van der Waals forces, can exchange hydrogen with adatoms in the primary chemisorbed film. The present work indicates that both mechanisms may be operative.[7,39] The Bonhoeffer-Farkas mechanism was originally questioned because Roberts' work appeared to indicate that chemisorbed hydrogen did not evaporate below 400°K, yet reaction occurred at 77°K. The isotherms in Fig. 17 show that evaporation of hydrogen from the primary chemisorbed layer occurs from 373°K down to 77°K provided the surface is saturated at the pressure of hydrogen used. The Bonhoeffer-Farkas mechanism would be operative over the entire temperature range but would be most important above 200°K. However, at temperatures below 200°K, a second state of binding is present whose population increases with increased hydrogen pressure, and both mechanisms for reaction may be operative. Detailed examination of the reaction would be necessary to assess the relative importance of each mechanism in this temperature range.

SUMMARY

When hydrogen chemisorbs on tungsten at 77°K, two distinct states of binding may be isolated at adsorption pressures as low as 2.5×10^{-9} mm. The most tightly bound state, β, is adsorbed as atoms with a sticking probability of 0.1 at 77°K; analysis of desorption kinetics at very low coverages ($n_\beta<30\times10^{12}$ molecules/cm²) shows evaporation is second order in the concentration of adsorbed hydrogen. At temperatures above 600°K, adatoms are freely mobile over the surface, approximating an ideal two dimensional gas, and the rate of evaporation of molecular hydrogen is $v_M=(5\times10^{-3})n^2\exp(-31\,000/RT)$ molecules/cm²-sec. As the surface coverage increases above $n_\beta=30\times10^{12}$ molecules/cm² a decrease in the heat of adsorption is observed which is due to heterogeneity of the surface. Evaporation of molecular hydrogen occurs at successively lower temperatures until, at saturation, evaporation occurs at the adsorption temperature. At equilibrium, the amount adsorbed in the β state obeys a Temkin isotherm, $n=n_i+c\log p_{H_2}$ over a temperature range of 273° to 373°K. For $n=600\times10^{12}$ molecules/cm², an isosteric heat of 15 kcal/mole is found. For $T=77$°K and 194°K, n_β is also proportional to the logarithm

[36] P. Kisliuk, J. Chem. Phys. **30**, 174 (1959); Bull. Am. Phys. Soc. Ser. II, **4**, 328 (1959).

[37] K. F. Bonhoeffer and A. Farkas, Z. physik. Chem. (Leipzig) **B12**, 231 (1931).

[38] E. K. Rideal, Proc. Cambridge Phil. Soc. **35**, 130 (1939).

[39] Couper, Eley, Hulatt, and Rossington, Bull. soc. chim. Belges **67**, 343 (1958).

of the pressure but the total amount adsorbed in the β state does not increase with a decrease in temperature. The increase in total amount adsorbed at 77°K is due to population of the α state which, at equilibrium at 77°K, amounts to 8–10% of the total adsorbed hydrogen, for equilibrium pressures between 10^{-7} and 10^{-6} mm. The α state begins to be populated before the β state is saturated and is proportional to hydrogen pressure. It probably consists of molecular hydrogen bound on top of the primary atomically chemisorbed layer.[5] If the filament temperature is raised above 1100°K, atomic hydrogen is formed from molecular hydrogen. The rate of evaporation of atomic hydrogen is $v_A = (2.2\times10^{13})\ n\ \exp(-67\ 000/RT)$ molecules/cm²-sec. For pressures below 10^{-7} mm and filament temperatures above 1475°K, the fraction of molecules striking the surface that is dissociated by the filament, s, is constant and at least 0.05. By using $s=0.05$ and the experimental value of the rate of evaporation of molecular hydrogen, n has been calculated as a function of temperature and pressure, and values of v_A are calculated in good agreement with values of Brennan and Fletcher.[9] Calculation from kinetic measurements of the equilibrium constant for the dissociation of hydrogen indicates that the sticking probability for atomic hydrogen on tungsten above 1200°K may be less than unity and nearly independent of temperature.

ACKNOWLEDGMENT

It is a pleasure to acknowledge many helpful discussions with Dr. Gert Ehrlich, throughout the course of this work.

Structure of Isobutylene*†

L. S. BARTELL AND R. A. BONHAM‡
Department of Chemistry, Iowa State University, Ames, Iowa

(Received September 11, 1959)

The molecular structure of gaseous isobutylene has been investigated by the sector-microphotometer method of electron diffraction. The major internuclear distances found, in terms of center of gravity parameters, r_g, were C—H (methyl) = 1.113±0.003 A (assumes ethylenic hydrogens have ethylene values), C=C = 1.331±0.003 A, C—C = 1.505±0.003 A, and $(C\cdots C)_{Me}$ = 2.498±0.005 A. Angles were C—C—H (methyl) = 110.4° and Me—C—Me~112°. Amplitudes of vibration were determined.

INTRODUCTION

IT has been observed in many investigations[1] that a C—C single bond adjacent to a triple bond in an unconjugated molecule is substantially shorter than the normal single bond. Until recently, however, there was doubt as to whether a carbon-carbon single bond adjacent to a double bond exhibited an analogous shortening. Recent studies of propylene and isobutylene by McHugh and Schomaker using the electron diffraction "visual" method,[2] and of propylene by Lide and Mann using microwave spectroscopy,[3] have indicated that the C—C bond in these compounds is, after all, appreciably shorter than the distance customarily associated with saturated compounds. These studies did not agree closely with each other in the C=C distance, however. Moreover, spectroscopic and diffraction results for the C=C bond even in ethylene itself were in disagreement. It seemed appropriate as an aid in the resolution of structural uncertainties in this important class of compounds to reinvestigate the structure of several olefins by the sector-microphotometer method of electron diffraction. The results for ethylene were published recently,[4] and confirmed the earlier diffraction results.

An additional structural feature of interest in isobutylene is the smallness of the Me—C—Me angle indicated for it, and for the similar molecule tetramethylethylene in an early electron diffraction study by Pauling and Brockway.[5] The reported angle of 111.5°,[5] little greater than the tetrahedral angle, was consistent with Pauling's theoretical conceptions of the time, but smaller than the angle popularly associated with olefinic sp^2 hybrid bonds today.

According to the present results, the smallness of the angle and shortness of the C—C bond are real but several lines of evidence suggest that the factors responsible may be different from those previously proposed.

PROCEDURE

A sample of cp isobutylene was used as obtained from the Matheson Company. Electron diffraction patterns were taken with an r^3 sector and treated as previously described.[6,7] The index of resolution was 0.93 for patterns recorded at the 10-cm camera distance and 0.77 for those recorded at 25-cm camera distance.

A procedure described fully elsewhere[8] was used for processing and analyzing data with the IBM 650 computer. Included in the analysis were corrections for specimen delocalization,[9] non-nuclear scattering, and Fourier integral termination errors. The asymmetry of vibrations of bonded pairs of atoms was taken into consideration in locating the centers of gravity of the internuclear distribution peaks. Corrections for the failure of the Born Approximation were applied to the amplitudes of vibration using the phase shifts of Hoerni and Ibers.[10] The value of b used in the radial distribution damping function was 0.00211.

Final parameters were deduced by fitting the experimental radial distribution function with Gaussian peaks by the method of steepest ascents.[8] Root-mean-square deviations between experimental and calculated curves were 0.44% and 0.93% of the maximum value of the principal C—C peak in the intervals 0.9A to 1.675A and 2.0A to 2.8A respectively. Internuclear distances reported in Table I are center of gravity parameters, r_g.[11] Standard errors were calculated as described else-

* Presented at the Fedorov Session on Crystallography, Leningrad, U.S.S.R., May 26, 1959.

† This research was supported by a grant from the Petroleum Research Fund administered by the American Chemical Society. Grateful acknowledgment is hereby made to the donors of said fund.

‡ Present address: Chemistry Department, Indiana University, Bloomington, Indiana.

[1] Pauling, Springall, and Palmer, J. Am. Chem. Soc. **61**, 927 (1939).

[2] J. P. McHugh and V. Schomaker, *A Report for the Year 1954–55 for the Division of Chemistry and Chemical Engineering*, California Institute of Technology.

[3] D. R. Lide, Jr., and D. E. Mann, J. Chem. Phys. **27**, 868 (1957).

[4] L. S. Bartell and R. A. Bonham, J. Chem. Phys. **27**, 1414 (1957); **31**, 400 (1959).

[5] L. Pauling and L. O. Brockway, J. Am. Chem. Soc. **59**, 1223 (1937).

[6] L. O. Brockway and L. S. Bartell, Rev. Sci. Instr. **25**, 569 (1954).

[7] L. S. Bartell and L. O. Brockway, J. Appl. Phys. **24**, 656 (1953).

[8] R. A. Bonham and L. S. Bartell, J. Chem. Phys. **31**, 702 (1959).

[9] L. S. Bartell, J. Appl. Phys., **32**, 252 (1960).

[10] J. A. Ibers and J. A. Hoerni, Acta Cryst. **7**, 405 (1954).

[11] The term r_g corresponds to the term $r_g(0)$ of L. S. Bartell, J. Chem. Phys. **23**, 1219 (1955).

where.[8,12] Standard errors quoted for bond angles correspond solely to the uncertainties in the r_g values from which they were calculated and not to possible interpretational uncertainties arising from the operational definition of the angle.

RESULTS

The experimental intensity function is compared in Fig. 1 with the intensity function calculated for the final model. The experimental radial distribution curve is shown in Fig. 2. The principal skeletal parameters of the molecule, deduced assuming C_{2v} symmetry, are listed in Table I. The resolving power of electron diffraction is insufficient to distinguish between the two ethylenic hydrogens and the six methyl hydrogens. In the analysis, it was assumed that the ethylenic hydrogen parameters were the same as in ethylene,[4] and the parameters of the principal hydrogen atoms, the methyl hydrogens, were determined accordingly.

TABLE I. Isobutylene parameters derived from radial distribution function and associated standard errors. Distances are in angstrom units.

	r_g	$\sigma_r(r)$[a]	$\sigma_{Tot}(r)$	l[b]	$\sigma_{Tot}(l)$
C—H_{Me}[c]	1.113	0.0019	0.003	0.079	0.004
C=C	1.331	0.0014	0.003	0.048	0.003
C—C	1.505	0.0010	0.003	0.059	0.003
C···H_{Me}[c]	2.161	0.010	0.011	0.101	0.009
(C···C)$_M$	2.498	0.002	0.005	0.078	0.004

∠Me—C—Me≃112° ∠C—C—H_{Me}[c]=110.4°±0.8°

[a] Effect of random intensity errors.
[b] Root-mean-square amplitudes of vibration.
[c] Assumes ethylenic H atoms have ethylene parameters.

The root-mean-square amplitudes of vibration, l, are of plausible magnitude. The C—H result agrees excellently with the value of 0.078 A calculated from force constant data by Kuchitsu[13] for *n*-butane. The C=C and C—C experimental amplitudes are appreciably greater than the values 0.042 A and 0.050 A calculated for ethylene and *n*-butane respectively.[13,14] Since there is no readily apparent reason for abnormally high carbon-carbon amplitudes in isobutylene, it is not unreasonable to regard the experimental amplitudes with suspicion. The amplitude of the nonbonded C···C composite peak is exactly the same as that observed in the *n*-hydrocarbons butane through heptane.[12,15]

The C—H and C=C bond lengths agree very closely with values found for related molecules listed in Table II, except for propylene as determined by microwave spectroscopy by Lide and Mann. For the latter determination, the abnormally long C=C bond may be associated with the somewhat doubtful hydrogen positions assumed in the analysis. The C—C bond in isobutylene is distinctly shorter than the bonds in *n*-alkanes, but in agreement with other values for single bonds adjacent to just one double bond.

The accuracy of the determination of the Me—C—Me angle was limited by the unfavorable geometry of the molecule. The three nonbonded C···C distances, which determine the angle, appear to be identical to within experimental error if the bending amplitudes are considered to be normal. The possibility cannot be excluded from diffraction data alone, however, that the bending amplitudes are smaller than usual, and the nonbonded distances are several hundredths of an angstrom unit different from one another. A change in the Me—C—Me angle of 2° has the same effect on the intensity function as a change of 0.005 A in the amplitude of the C···C vibrations. Equal C···C distances correspond to a Me—C—Me angle of 112.2°. It is probable that the actual angle does not differ from this value by more than 3° or 4°.

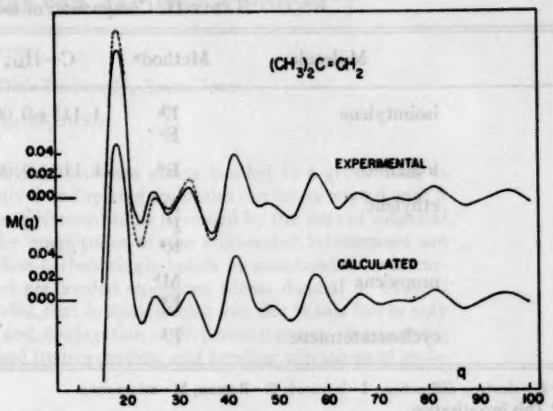

FIG. 1. Reduced intensity curves for isobutylene. The solid lines represent the total scattering function, $M(q)$, and the dashed line represents the nuclear scattering function, $M_c(q)$. The calculated curve has been multiplied by the experimental index of resolution.

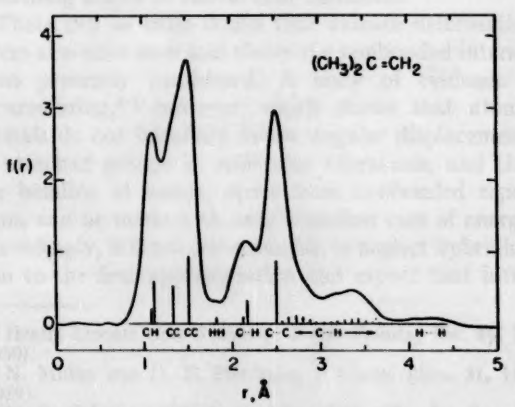

FIG. 2. Experimental radial distribution function for isobutylene.

[12] R. A. Bonham and L. S. Bartell, J. Am. Chem. Soc. **81**, 3491 (1959).
[13] K. Kuchitsu, Bull. Chem. Soc. Japan **32**, 748 (1959).
[14] K. Kuchitsu (private communication).
[15] Bonham, Bartell, and Kohl, J. Am. Chem. Soc. **81**, 4765 (1959).

TABLE II. Comparison of isobutylene with other molecules

Molecule	Method[a]	C—H_{Me}	C=C	C—C	∠C—C—C
isobutylene	E[b]	1.113±0.003	1.331±0.003	1.505±0.003	112°
	E[c]	...	1.33	1.50	113°
n-alkanes	E[d]	1.114±0.005	...	1.533±0.002	112.4°
ethylene	E[e]	...	1.333±0.002	...	...
	I[f]		1.337±0.003		
	R[g]		1.339±0.002		
propylene	M[h]	...	1.353	1.488	...
	E[c]		1.33	1.49	
cyclooctatetraene	E[i]	...	1.334±0.003	1.462±0.003	...

[a] E=electron diffraction; I=infrared; R=Raman; M=microwave.
[b] This investigation.
[c] Reference 2.
[d] Reference 15, average of *n*-butane, *n*-pentane, *n*-hexane, and *n*-heptane.
[e] Reference 4.
[f] H. C. Allen and E. K. Plyler, J. Am. Chem. Soc. **80**, 2673 (1958).
[g] J. M. Dowling and B. P. Stoicheff, Can. J. Phys. **37**, 703 (1959).
[h] Reference 3.
[i] Bastiansen, Hedberg, and Hedberg, J. Chem. Phys. **27**, 1311 (1957).

The C—C—H angle agrees to within experimental error with the analogous angle in the *n*-hydrocarbons butane through heptane.[15] The diffraction data were examined for possible information on the configuration and amplitude of libration of the methyl groups. Unlike the recently reported case of trimethylphosphine in which the disposition of the methyl groups was clearly indicated,[16] the present data were too insensitive for a definitive analysis. It seems likely, however, that the methyl configurations are staggered entirely analogously to those in trimethylphosphine or propane, if for the sake of a reference model, the double bond is envisioned as a pair of tetrahedral, bent bonds.

Particularly interesting among the results of the structure determination are the shortness of the trigonal C—C single bonds as compared with tetrahedral bonds, and the smallness of the Me—C—Me angle. It is apparent that the trend in each case is in a direction, which could be explained by effects of nonbonded intramolecular repulsions as well as effects of hybridization and hyperconjugation. To what extent these concepts, and intramolecular van der Waals forces in particular, are capable of correlating structural information is discussed in the following paper.

[16] L. S. Bartell and L. O. Brockway, J. Chem. Phys. **32**, 512 (1960).

ACKNOWLEDGMENTS

We are greatly indebted to Professor L. O. Brockway and the University of Michigan for making available the electron diffraction apparatus for this investigation. We also wish to thank Mr. D. Kohl for assistance in computations. The programming and executing of electronic digital computations were greatly facilitated by a grant from the National Science Foundation.

On the Effects of Intramolecular van der Waals Forces*†

L. S. BARTELL

Department of Chemistry, Iowa State University, Ames, Iowa

(Received October 15, 1959)

Evidence for the existence of strong nonbonded repulsions between atoms bonded to a given atom is cited. It is observed that bond angles in ethylene derivatives and related molecules can be correlated with a simple "hard sphere" model in which atomic positions are presumed to be governed by the sizes of spherical atoms packed around a given atom. Estimations of the magnitudes of the nonbonded interactions are presented. These indicate that the shortening of carbon-carbon single bonds in unsaturated hydrocarbons may be principally attributable to the relaxation of nonbonded repulsions across digonal or trigonal bonds as compared with tetrahedral bonds. It is suggested that intramolecular van der Waals forces may be even more important than effects of hybridization and conjugation or hyperconjugation in governing bond angles, bond distances, energies of isomerization and hydrogenation, and bending vibrations of molecules.

INTRODUCTION

THE important thermochemical effects of the attractive dispersion force components of intramolecular van der Waals forces have recently been pointed out by Pitzer *et al.*[1] The effects of repulsive intramolecular interactions have been explored in only the most rudimentary way, however. With the observation that several structural features of isobutylene, described in the preceding paper,[2] could be explained directly by effects of intramolecular van der Waals forces rather than the more specialized forces usually invoked, an examination of the structural and thermochemical consequences of intramolecular van der Waals forces was initiated. No accurate treatments are yet available for the description of such forces, but plausible functions could be constructed from the results of various published studies. Some of the more important implications of calculations based on these preliminary functions are presented below.

DISCUSSION

Structural Correlations

A striking structural feature of isobutylene is the apparent equilateral triangle formed by the three outer carbon atoms. This occurence suggests a simple steric model in which bond angles are considered to be governed principally by the sizes of atoms bonded to a given atom. In isobutylene, then, for simplicity, the difference between the methyl and ethylenic carbons is ignored and the C atom is assigned a radius, 1.25 A, which is just one-half of the nonbonded C···C distance. In order to extend the model to substituted ethylenes a set of atomic "radii" was determined by the following procedure. Radii of atoms X were taken as half the X···X distance in the compounds $H_2C=CX_2$, where X is C, H, F, or Cl. For comparison, some analogous carbonyl compounds were examined in which the oxygen radius was assigned with the above disregard for differences between =X and −X-, by taking half the O···O distance in formic acid. A radius for N was determined from urea. The radii for the atoms H, C, N, O, F, and Cl were 0.92 A, 1.25 A, 1.14 A, 1.13 A, 1.08 A, and 1.44 A, respectively, with an uncertainty of perhaps 0.01 A. The success of this extremely crude model is quite astonishing. In the molecules listed in Table I the 3 atoms bonded to the central carbon atom just touch each other, to within the apparent experimental error, or, in the case of molecules like $C_2(CN)_4$ with short bonds, overlap evenly. No relevant molecules with the above atoms for which reliable data were available were deliberately omitted from Table I. Acetone was not included because of irregularities in the various determinations published. An exhaustive search of the literature was not made.

It seems significant that the radii listed above are within about two hundredths of an angstrom unit of of the analogous radii that would be appropriate for describing angles in substituted methanes.

There can be little doubt that valence deformation forces also exist over and above the nonbonded interactions presently considered. A body of evidence is accumulating,[3-5] however, which shows that atomic orbitals do not faithfully follow angular displacements of attached groups in molecular vibrations, and that the bending of bonds, apart from nonbonded repulsions, can be made with only a modest cost of energy. Accordingly, it is not unreasonable to neglect hybridization to the first approximation and expect that intra-

* Presented in part at the Fedorov Session on Crystallography, Leningrad, U.S.S.R., May 26, 1959.

† This research supported by a grant from the Petroleum Research Fund administered by the American Chemical Society. Grateful acknowledgment is hereby made to the donors of said fund.

[1] W. E. Donath and K. S. Pitzer, J. Am. Chem. Soc. **78**, 4562 (1956); K. S. Pitzer, J. Chem. Phys. **23**, 1735 (1955); K. S. Pitzer and E. Catalano, J. Am. Chem. Soc. **78**, 4844 (1956); D. E. Petersen and K. S. Pitzer, J. Phys. Chem. **61**, 1252 (1957).

[2] L. S. Bartell and R. A. Bonham, J. Chem. Phys. **32**, 824 (1960).

[3] Heath, Linnett, and Wheatley, Trans. Faraday Soc. **46**, 137 (1950).

[4] N. Muller and D. E. Pritchard, J. Chem. Phys. **31**, 1471 (1959).

[5] N. V. Cohan and C. A. Coulson, Trans. Faraday Soc. **52**, 1163 (1956); L. Burnelle and C. A. Coulson, *ibid.* **53**, 403 (1957).

TABLE I. Substituted ethylenes and carbonyl derivatives with bond angles compatible with the hard sphere model.

$H_2CC(CH_3)_2$[a]	H_2CCH_2[b]	H_2CCF_2[c]	H_2CCCl_2[d]
H_2CCHCH_3[e]	F_2CCF_2[e]	Cl_2CCCl_2[d]	$(CN)_2CC(CN)_2$[f]
H_2CCHCl[e]	*cis*-1,2 $C_2H_2Cl_2$[d]	*tr*-1,2 $C_2H_2Cl_2$[d]	C_3H_4[g]
$HCOOH$[e]	Cl_2CO[e]	F_2CO[e]	$HCFO$[e,h]
CH_3CHO[h,i]	CH_3CFO[e]	CH_3CClO[e]	$(NH_2)_2CO$[e]
NH_2CHO[e]	$HOCO_2^-$[e]		

[a] See reference 2.
[b] L. S. Bartell and R. A. Bonham, J. Chem. Phys. **27**, 1414 (1957); **31**, 400 (1959).
[c] L. E. Sutton, *Tables of Interatomic Distances and Configuration in Molecules and Ions* (The Chemical Society, London, 1958).
[d] R. L. Livingston (private communication).
[e] J. P. McHugh and V. Schomaker, *A Report for the Year 1954–1955 for the Division of Chemistry and Chemical Engineering*, California Institute of Technology; D. R. Lide, Jr., and D. E. Mann, J. Chem. Phys. **27**, 868 (1957).
[f] D. A. Bekoe and K. N. Trueblood, Abstracts of Milwaukee Meeting of American Crystallographic Association (1958).
[g] Bastiansen, Hedberg, and Hedberg, J. Chem. Phys. **27**, 1311 (1957).
[h] R. Stratton and A. Nielsen, Abstracts of Honolulu Meeting of American Physical Society, 1959.
[i] Kilb, Lin, and Wilson, J. Chem. Phys. **26**, 1695 (1957).

molecular repulsions will play a prominent role in the determination of bond angles.

If the above "hard sphere" model has any virtue, a "soft sphere" model, employing London dispersion forces and nonbonded repulsive forces would presumably be even better. Unfortunately, no accurate potential functions are available for nonbonded interactions. It is possible, nevertheless, as is discussed in the Appendix, to devise plausible functions for investigating structural and thermochemical consequences of such interactions. For the purpose of the present comparisons this was done only for CC, CH, and HH interactions.

A preliminary examination of the soft sphere model makes it look as promising as the hard sphere model in correlating bond angles. A factor which renders the soft sphere model, for the present, little more fruitful in treating angles than the hard sphere model is as follows. It is the difference between large terms rather than the general magnitude of the terms that governs bond angles, according to the model, and these differences are not yet accurately predictable from theory. An empirical adjusting of parameters has been postponed, pending consideration of other effects discussed in the following.

The most important generalization to be drawn about nonbonded repulsions between atoms bonded to a given carbon atom is not so much the difference between various atoms as the similarity. This similarity has obscured the effects of intramolecular interactions. The near invariance of bond angles and bond distances in a series of substituted ethylenes, or in a series of substituted methanes suggests this approximate balance of terms. Thermochemical evidence seems to point to the same conclusion, at least for CC, CH, and HH interactions. Pitzer and Catalano[1] have shown that isomerization energies of paraffin hydrocarbons can be attributed principally to London dispersion contributions, (along with somewhat less important zero-point energy effects) in which nonbonded repulsions between atoms bonded to the same atom are ignored altogether. That these negative results are due to cancellations among large potentials (~ 3 kcal/mole per pair) rather than to repulsions which are negligible in the first place[6] is demonstrated by the informative analyses of vibrational spectra by Simanouti[7] and by Linnett and Heath.[8] These analyses indicate that repulsions between atoms bonded to a given central atom are entirely comparable to those anticipated for normal van der Waals repulsions.[9]

More amenable to treatment than effects depending upon differences between kinds of interactions are those depending upon differences in numbers of interactions due to changes in coordination number. For example, the C—C bond in isobutylene may be expected to be shorter than the C—C bond in isobutane or neopentane because there are three strong nonbonded repulsions acting on methyl carbons in the latter compounds compared with only two in the former. Similarly the C—H bond in ethylene or benzene should be shorter

[6] It has generally been assumed, as was put by L. Pauling, *The Nature of the Chemical Bond* (Cornell University Press, Ithaca, New York, 1939), p. 193, that atoms are "whittled down" on the side of covalent bonds, and accordingly do not exhibit strong repulsions of the kind invoked in the present paper. It is reasonable to expect some "whittling" but the present evidence indicates that the "whittling" is much more gently contoured than has usually been assumed.

[7] T. Simanouti, J. Chem. Phys. **17**, 245, 734, 848 (1949).

[8] J. W. Linnett and D. F. Heath, J. Chem. Phys. **19**, 801 (1951); Trans. Faraday Soc. **44**, 873, 878, 884 (1948); **45**, 264 (1949).

[9] It may be noted that the spectroscopic repulsive constants are somewhat irregular and that the values for H···H interactions are very low. R. S. Mulliken, however, cites evidence [R. S. Mulliken, J. Am. Chem. Soc. **72**, 4493 (1950); **77**, 887 (1955)] that H···H interactions are of the same magnitude as the others studied in the present investigation. It is doubtless due in large measure to this significant repulsion of H atoms, ignored by Linnett and Heath, that the C—Cl bond in CH_3Cl is prevented from being more than 0.1 A shorter than in CCl_4, as predicted by Linnett and Heath. That the bond in CH_3Cl is actually 0.015 A longer than in CCl_4 [Bartell and Brockway, J. Chem. Phys. **23**, 1860 (1955)] is probably due to appreciable differences between the C—Cl bonds themselves, rather than to a greater repulsion by H than Cl.

than that in, say, *n*-hexane. If Simanouti's force constants[7] for bond stretching are used with the potential functions in the Appendix, it is calculated that the C—C bond shortening in isobutylene due to relaxation of nonbonded interactions should be about 0.03_0 A. The C—H bond, according to the present crude potential functions, is more variable. In ethylene the magnitudes of repulsions are similar to those in methane, but less than those in longer *n*-alkanes by an amount corresponding to a shift in bond length of 0.02 A.

It is difficult to make reliable comparisons of experimental bond lengths both because of experimental uncertainties in most of the data reported and because of differences in operational definitions of bond lengths in different structural investigations. It is interesting, however, that the C—C bond length found for isobutylene in the present research is just 0.028 A shorter than that found for the *n*-alkanes butane through heptane in an earlier electron diffraction investigation using the same scheme of analysis.[10] The C—H bond lengths reported most often for ethylene[11–13] and benzene[14,15] are about 1.084 A, whereas those for saturated hydrocarbons range from 1.090 A to 1.120 A. It is not clear at present how real the scatter is, owing partly to the complicating effects on structural analyses of the large amplitudes of vibration of hydrogen atoms. Nevertheless, the experimental magnitudes of effects are sufficiently similar to the calculated effects of intramolecular van der Waals forces to lend support to the present hypotheses.

If the present model is extended to the C—C bonds in 1,3-butadiene and methyl acetylene, in which the repulsions are relaxed still further, shortenings of about 0.06 A are indicated. The experimental shortenings for the two molecules are 0.05 A[16,10] and 0.07 A,[17,10] respectively. The model predicts that the C=C bond in allene should be shorter than that in ethylene by nearly 0.03 A. This, again, is in agreement with experiment.[18] The present model appears to offer a basis for explaining all of the major trends of bond lengths with coordination number summarized in Fig. 2 of a recent paper by Costain and Stoicheff[19] and in the equations of Bernstein for nonaromatic molecules.[19]

Another example of intramolecular repulsions is the well-known difference in energy of about 0.8 kcal/mole between *trans* and *gauche* rotational isomers of *n*-butane.[20] According to the present potential functions the principal contribution to the energy difference results from H···H interactions, as it can be seen that extensive cancellations occur in the C···H and C···C terms, each of which is appreciably smaller than the largest H···H term. Consequently, the experimental energy difference is not a sensitive test of the C···H and C···C potential functions. It is encouraging to find, as will be described elsewhere, that the present H···H function leads to a result within a few hundred calories per mole of the experimental difference.

The approximate equality of C···C, C···H, and H···H repulsions for atoms bonded to the same carbon atom no longer applies for atoms bonded to adjacent carbon atoms. This differentiation has been proposed[21] to be one of the important factors contributing to the difference between the 1.544 A bond in diamond[22] and the 1.533 A bond in *n*-alkanes.[10]

Additional evidence for intramolecular nonbonded repulsions of the magnitude invoked here is provided by the structure and heat of formation of cyclobutane.[23] The carbon atoms diagonally across the ring approach each other unusually closely. The long 1.57 A C—C bond and 3.4 kcal/CH_2 mole excess energy of the molecule over that expected on the basis of valence deformation and torsional contributions, were correlated by Dunitz and Schomaker[23] in terms of the C···C repulsions. If the present model is used to compare cyclobutane (assuming 1.57 A C—C bonds and tetrahedral HCH angles) with a hypothetical C—CH_2—C unit with tetrahedral angles and 1.533 A C—C bonds,[10] it is found that the C···C interaction is about 5.4 kcal/CH_2 mole greater for cyclobutane. The energy to stretch the C—C bond to 1.57 A, not including contributions of nonbonded repulsions, would come to an additional 3.7 kcal if the force constant were 4×10^5 dynes/cm (here it must be taken into account that, in the absence of nonbonded repulsions, the equilibrium distance would be less than 1.533 A). These large destabilizing contributions are, however, compensated by a considerable extent according to the present model, by a 5.6 kcal relaxation of C···H interactions. The net destabilization energy, would then amount to about 3.5 kcal/CH_2 mole. It would be even somewhat less if the HCH angle were allowed to increase from 109.5° and relieve H···H repulsions subsequent to the above relief of C···H repulsions, in agreement with the experimental observation[23] that the HCH angle in cyclobutane is approximately 114°. Thus the calculations based on the present model are pleasingly (and prob-

[10] Bonham, Bartell, and Kohl, J. Am. Chem. Soc. **81**, 4765 (1959).
[11] L. S. Bartell and R. A. Bonham, J. Chem. Phys. **27**, 1414 (1957); **31**, 400 (1959).
[12] J. M. Dowling and B. P. Stoicheff, Can. J. Phys. **37**, 703 (1959).
[13] H. C. Allen and E. K. Plyler, J. Am. Chem. Soc. **80**, 2673 (1958).
[14] A. Langseth and B. P. Stoicheff, Can. J. Phys. **34**, 350 (1956).
[15] Almenningen, Bastiansen, and Fernhold, Norske Videnskaps-Akad. Skrifter NR3 (1958).
[16] Almenningen, Bastiansen, and Traetteberg, Acta Chem. Scand. **12**, 1221 (1958).
[17] L. Thomas, E. Sherrand, and J. Sheridan, Trans. Faraday Soc. **51**, 619 (1955).
[18] B. P. Stoicheff, Can. J. Phys. **33**, 811 (1955).
[19] C. C. Costain and B. P. Stoicheff, J. Chem. Phys. **30**, 777 (1959); H. J. Bernstein, J. Phys. Chem. **63**, 565 (1959).
[20] K. S. Pitzer, J. Chem. Phys. **8**, 711 (1940).
[21] L. S. Bartell, J. Am. Chem. Soc. **81**, 3497 (1959).
[22] K. L. Lonsdale, Phil. Trans. Roy. Soc. (London) **A240**, 1219 (1947).
[23] J. D. Dunitz and V. Schomaker, J. Chem. Phys. **20**, 1703 (1952).

ably somewhat fortuitously) in agreement with the thermochemical results, and suggest the need for inclusion of terms omitted in previous calculations of strain energies.

Some Implications of the Model

According to the present model, the C—C bond length "shortening" in isobutylene and other unsaturated compounds, previously ascribed to hyperconjugation and change in hybridization, can be largely accounted for in a straightforward manner by relaxation of nonbonded repulsions. It is relevant to inquire, then, whether the thermochemical evidence for hyperconjugation can also be attributed to nonbonded interactions. Here it is disappointing to observe that the energy differences to be accounted for are not as simple as the differences in bond lengths. The quasi-hyperconjugation energy depends upon the difference between equal numbers of terms, (over two dozen) each of which is comparable to the net energy effect, whereas the bond length difference depends principally upon one readily accessible term. A rough computation with the present model gave an approximately correct result for the energy but depended beyond the present limits of confidence upon the exact shape of the potential functions. It is possible, at present, only to say that the thermochemical results are of a magnitude easily accounted for by nonbonded repulsions. It will be interesting to see if simple potential functions will be forthcoming which are capable of correlating quantitatively bond angles and spectroscopic results as well as thermochemical results.

Several authors, and notably Dewar,[24] have recently cited evidence that hyperconjugation, and conjugation in nonaromatic molecules, are unimportant in the ground state of molecules, conclusions which are consistent with the present model. Dewar and Schmeising showed that there is no remaining need to invoke conjugative or hyperconjugative delocalization of appreciable magnitude if distinctions are made between trigonal and tetrahedral σ bonds. Dewar and Schmeising attributed all of the differences to hybridization effects, and used empirical structural and thermochemical data to fashion a consistent model. It is fair to remark, however, that nothing is really known about the state of hybridization of the σ electrons (nor is there even a universally accepted definition of hybridization),[25] and that the model of nonbonded repulsions can be substituted in part or in total with little change in effective result.[26]

Among the deficiencies of the present simple model is its inability to explain more than about 10% of the barrier to rotation about the C—C bond in ethane. This demonstrates compellingly that the model is limited in its representation of intramolecular nonbonded interactions. Nevertheless, it is attractive in its extreme simplicity and seems to capture enough truth to justify further investigation.

CONCLUSIONS

Nonbonded interactions in molecules appear to play a much more important role than is often recognized. Evidence is presented which suggests that such interactions may be even more important than effects of hybridization and conjugation or hyperconjugation in governing bond angles, bond distances, energies of isomerization and hydrogenation, and bending vibrations of molecules.

APPENDIX

The following potential functions were devised somewhat arbitrarily for the purposes of the present comparisons. For coefficients of the London r^{-6} dispersion energy terms the values of Pitzer and Catalano[1] were adopted for C···C, C···H, and H···H interactions.

For the repulsive C···C contribution, the Lennard-Jones r^{-12} form was assumed. The coefficient of the repulsive term was chosen to make the position of the minimum in the potential function occur at 3.5 A. Ingold *et al.*[27] have used the value 3.2 A for the minimum while more recently Kitaigorodskii[28] has used 3.6 A.

---

[24] M. J. S. Dewar and H. N. Schmeising, Tetrahedron **5**, 166 (1959). For theoretical evidence see R. S. Berry, J. Chem. Phys. **26**, 1660 (1957); **30**, 936 (1959). See also N. Muller and D. E. Pritchard, J. Am. Chem. Soc. **80**, 483 (1958).

[25] Hybridization is often, without fundamental justification, inferred from bond angles, it being assumed that bonds are not bent. In the present comparison between isobutylene and, say, *n*-butane, there is no difference between the experimental C—C—C angles in the two molecules and accordingly, by the foregoing criterion, no difference in hybridization.

[26] It is possible with the present model to deduce theoretically rough values of terms which Dewar and Schmeising evaluated empirically. The term of Dewar and Schmeising which was found to obviate the necessity of assuming conjugative interactions, was $[(E_{CC}'-E_{CC})-(E_{CH}'-E_{CH})]$ where the E_{ij} represent bond energies, the primed terms corresponding to trigonal bonds and the unprimed terms corresponding to tetrahedral bonds. The variation of bond energies with "hybridization" was determined from curves of bond energy *versus* length along with experimental differences between trigonal and tetrahedral bond lengths.

According to the present model the potential energy of a bond, taking into account only the force constant, k, and the largest nonbonded repulsions of approximate form Ar_{ij}^{-12}, is $V\sim\frac{1}{2}k(r-r_0)^2+Ar_{ij}^{-12}$. If the bond changes because of changes in A, since $\partial r_{ij}/\partial r\sim 0.8$, it follows that the change in bond length, Δr, with bond energy, ΔV, will be $\Delta r\sim 0.8\times 12\Delta V/r_{ij}k$. If $r_{ij}\sim 2.5\times 10^{-8}$ cm and $k\sim 4\times 10^5$ dynes/cm, the formula yields a bond energy change of about 150 kcal/mole per angstrom unit change in bond length. Dewar and Schmeising found 250 kcal and 150 kcal per angstrom for C—C and C—H respectively. G. Glockler [J. Chem. Phys. **21**, 1291 (1953); J. Phys. Chem. **61**, 31 (1957)] reported analogous values of 140–190 kcal and 140 kcal per angstrom, respectively. All of the empirical values cited are subject to appreciable error due to several crude values of bond distances assumed in the calculations, but agree well in magnitude with the result of the present model.

[27] Dostrovsky, Hughes, and Ingold, J. Chem. Soc. **1946**, 173.

[28] A. I. Kitaigorodskii, Fedorov Session on Crystallography, Leningrad, U.S.S.R., May 25, 1959. It should be pointed out that neither Ingold's nor Kitaigorodskii's functions were precisely 6–12 potentials.

The present function yields constants agreeing with Simanouti's spectroscopic constants to within the apparently rather wide limits of uncertainty of the latter.

For H···H interactions the repulsive term of the Lennard-Jones potential appeared too extreme in its dependence upon r to correlate rotational isomerization energies of hydrocarbons and intermolecular forces in crystals with second virial coefficients of gaseous H_2. Accordingly, a Buckingham (exp-6) potential was constructed to fit Mulliken's estimation[9] of H···H repulsive forces at small r ($\partial V/\partial r$ was fitted at 1.36 A), and Chang's analytic expression[29] for de Boer's calculations[30] of interactions of H_2 molecules at distances of 2.6 A and beyond. The resulting potential had a milder dependence on r and appeared more or less compatible with all quantities discussed in the foregoing.

The geometric mean of the C···C and H···H repulsive functions was tentatively adopted for the C···H repulsive potential function.

The over-all potential functions used, in cgs units, were:

$$V_{CC}(r)=20.8\times10^{-105}r^{-12}-22.6\times10^{-60}r^{-6}$$

$$V_{HH}(r)=4.58\times10^{-10}[\exp-(r/0.245\times10^{-8})]-3.42\times10^{-60}r^{-6}$$

$$V_{CH}(r)=8.68\times10^{-60}\{358[\exp-(r/0.490\times10^{-8})]-1\}r^{-6}.$$

[29] Wang Chang, Doctoral Dissertation, University of Michigan (1944).

[30] J. de Boer, Physica 9, 363 (1942).

Electron Diffraction Study of Monomethyl- and Dimethylphosphine*

L. S. BARTELL†

Institute for Atomic Research, Iowa State University, Ames, Iowa, and Department of Chemistry, University of Michigan, Ann Arbor, Michigan

(Received October 22, 1959)

The structural parameters of gaseous monomethyl- and dimethylphosphine were determined by the sector-microphotometer method of electron diffraction. Center of gravity bond distances and standard errors for the two molecules were, respectively: $r_{CP}=1.858\pm0.003$ A and 1.853 ± 0.003 A; $r_{CH}=1.094\pm0.008$ A and 1.097 ± 0.007 A; $r_{PH}=1.423\pm0.007$ A and 1.445 ± 0.02 A. The angles P—C—H were $109.6\pm1°$ and $109.8\pm0.7°$. In dimethylphosphine the angle C—P—C was $99.2\pm0.6°$. The methyl groups were found to be in staggered conformations. The distances and root-mean-square amplitudes of vibration agreed well with the values determined in recent studies of phosphine and trimethylphosphine.

INTRODUCTION

THE series of molecules PH_3, PH_2CH_3, $PH(CH_3)_2$, and $P(CH_3)_3$ plays a prominent role in theories of coordination complexes. The stabilities of complexes of the phosphines have been correlated with such properties of the free phosphine molecules as dipole moments, bond angles and hybridization, steric factors and other properties which, in turn, have been related to the assumed structure of the molecules.[1-4] An investigation of the structures of the molecules has never been made, however. A program was undertaken, accordingly, to study the series by the sector-microphotometer method of electron diffraction. The results for PH_3[5] and $P(CH_3)_3$[6] have already been reported and compared with spectroscopic studies[7,8] of the molecules. The structure determinations for PH_2CH_3 and $PH(CH_3)_2$ are presented in the following.

PROCEDURE

Samples of monomethyl- and dimethylphosphine were generously provided by Professor R. W. Parry of the University of Michigan. Electron diffraction patterns were recorded on Kodak medium lantern slides with an apparatus described earlier,[9] using 40-kv electrons and an r^3 sector. Experimental procedures followed those previously published.[10] Indices of resolution, $R=M_{expt}(s)/M_{theor}(s)$, of 0.88 and 0.92 were obobtained with monomethylphosphine for the 10-cm and 25-cm camera data, respectively. Corresponding indices of 0.79 and 0.83 were obtained with dimethylphosphine. The deviations from unity resulted principally from a uniform delocalization of the specimen throughout the camera chamber, and corrections were made for the effect.[11] Corrections ranged from 0 to 0.002 A.

The data were processed by a procedure closely resembling several described previously.[12,13] The Gaussian damping function used in the radial distribution integrand had a value of 0.1 at $s=31$. Included in the analysis were corrections for non-nuclear scattering and the failure of the Born approximation. For the latter correction the phase shifts calculated by Ibers and Hoerni[14] were used. The shifts suggested by Bartell and Brockway[12,15] are too small at small s. Fourier integral termination errors were corrected with the aid of an analytic approximation discussed elsewhere.[6]

Final parameters were deduced by fitting the experimental radial distribution function, $f(r)$, with Gaussian peaks by the method of steepest ascents.[16] The regions from 0.90 to 1.55 A, 1.70 to 2.00 A, and 2.15 to 2.80 A were fitted independently, and the results showed that the areas of the various regions were consistent. This is reflected in the least squares output of the index of resolution (adjusted to the 10-cm data) which, for the three regions was 0.878, 0.876, and 0.875 for monomethylphosphine and 0.801, 0.788, and 0.787 for dimethylphosphine. Root-mean-square deviations between experimental and calculated $f(r)$ curves decreased with r, approximately as $0.022r^{-1}$ and $0.030r^{-1}$

* Work performed in part in the Ames Laboratory of the U. S. Atomic Energy Commission.

† Institute for Atomic Research, Iowa State University, Ames, Iowa. The author wishes to express his appreciation to E. I. du Pont de Nemours and Company for a summer faculty fellowship during which the diffraction patterns were obtained.

[1] H. C. Brown, Rec. Chem. Progr. (Kresge-Hooker Sci. Lib.) **14**, 83 (1953).

[2] A. B. Burg, Rec. Chem. Progr. (Kresge-Hooker Sci. Lib.) **15**, 159 (1954).

[3] R. W. Parry and R. N. Keller, Chapter 3 in *The Chemistry of the Coordination Compounds* (Reinhold Publishing Corporation, New York, 1956), pp. 123–129.

[4] R. W. Parry and G. Kodama (to be published).

[5] L. S. Bartell and R. C. Hirst, J. Chem. Phys. **31**, 449 (1959).

[6] L. S. Bartell and L. O Brockway, J. Chem. Phys. **32**, 512 (1960).

[7] C. C. Loomis and M. W. P. Strandberg, Phys. Rev. **81**, 798 (1951); H. H. Nielsen, J. Chem. Phys. **20**, 759 (1952); V. M. McConaghie and H. H. Nielsen, *ibid.* **21**, 1836 (1953); M. H. Sirvetz and R. E. Weston, Jr., *ibid.* **21**, 898 (1953).

[8] D. R. Lide, Jr., and D. E. Mann, J. Chem. Phys. **29**, 914 (1958).

[9] L. O. Brockway and L. S. Bartell, Rev. Sci. Instr. **25**, 569 (1954).

[10] L. S. Bartell and L. O. Brockway, J. Appl. Phys. **24**, 656 (1953).

[11] L. S. Bartell, J. Appl. Phys. **32**, 252 (1960).

[12] Bartell, Brockway, and Schwendeman, J. Chem. Phys. **23**, 1854 (1955).

[13] I. L. Karle and J. Karle, J. Chem. Phys. **17**, 1052 (1949).

[14] J. A. Ibers and J. A. Hoerni, Acta Cryst. **7**, 405 (1954).

[15] L. S. Bartell and L. O. Brockway, Nature **171**, 978 (1953).

[16] R. A. Bonham and L. S. Bartell, J. Chem. Phys. **31**, 702 (1959).

for the monomethyl and dimethyl compounds respectively. The magnitude of the deviations corresponded to about 0.5% of the value of the main PC peak. Thus, the contribution of random intensity errors to the uncertainty in the PC distances is apparently only 0.001 A, as was found also in the case of trimethylphosphine.[6]

Standard errors were calculated as described elsewhere.[16,17] They include all known sources of error except those associated with the imperfectly understood uncertainities in the approximations of electron scattering theory. Standard errors quoted for bond angles correspond solely to uncertainties in the "center of gravity" r_g values[18] from which the angles were calculated and not to possible interpretational uncertainties associated with the operational definition of the angle. In the case of the P—C—H angles, account was taken of the effect of the uncertainty in the C···H_p peaks which could not be resolved from the stronger P···H_c peaks.

DISCUSSION OF RESULTS

Experimental and theoretical intensity functions are compared in Fig. 1. Experimental radial distribution

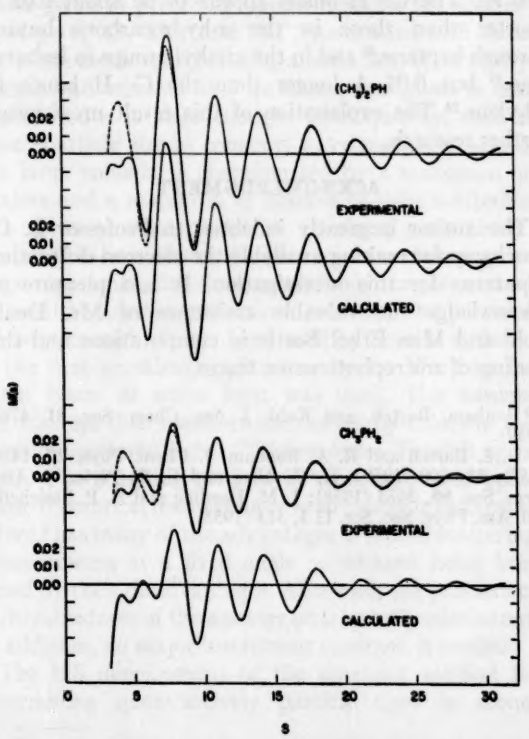

FIG. 1. Reduced intensity curves for monomethyl- and dimethylphosphine. The solid lines represent the total scattering function, $M(s)=(I_M/I_B)-1$ and the dashed lines represent the nuclear scattering functions, $M_c(s)$. The calculated curves have been multiplied by the experimental index of resolution.

[17] R. A. Bonham and L. S. Bartell, J. Am. Chem. Soc. **81**, 3491 (1959).

[18] The term r_g corresponds to $r_g(0)$ of L. S. Bartell, J. Chem. Phys. **23**, 1219 (1955).

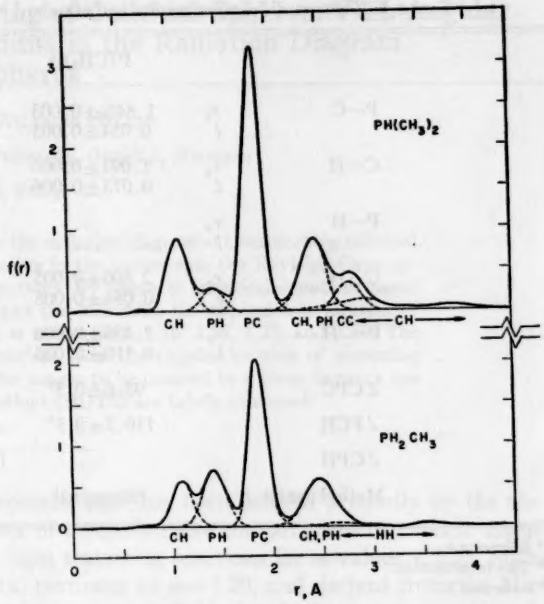

FIG. 2. Experimental radial distribution functions for monomethyl- and dimethylphosphine.

functions are shown in Fig. 2. For dimethylphosphine the data clearly indicate that the methyl groups are in staggered conformations, with a barrier to rotation about the P—C bond probably in excess of 1 kcal/mole. A much more accurate value of 2.6±0.5 kcal/mole was reported for the analogous barrier in trimethylphosphine by Lide and Mann[8] according to a microwave investigation. In the case of monomethylphosphine the data at all stages of refinement persistently exhibited H···H interactions indicative of a staggered conformation for the methyl groups. The interactions were not much stronger than the noise level of the data, however, so no quantitative assessment of the rotational barrier could be made.

The structural parameters determined in this investigation are listed in Table I with the parameters found in parallel electron diffraction investigations of phosphine[5] and trimethylphosphine.[6] The root-mean-square amplitudes of vibration appear to be of reasonable magnitudes. The distances and angles agree well among the molecules, with no more than the expected number of results differing from corresponding ones by amounts in excess of the standard errors.

A trend that appears significant is the decrease in the P—C bond length as the number of methyl groups increases. Although the total standard errors are about two parts per thousand, the random uncertainty appropriate in the comparison of the P—C bonds is only about one part per thousand. The shift between monomethyl- and trimethylphosphine is substantially larger than this, being about six parts per thousand. Recently, in another paper, the author[19] proposed ten-

[19] L. S. Bartell, J. Chem. Phys. **32**, 827 (1960).

TABLE I. Electron diffraction results and standard errors. Distances r_g and amplitudes l are in Angstrom units.

		$P(CH_3)_3$[a]	$PH(CH_3)_2$[b]	PH_2CH_3[b]	PH_3[c]
P—C	r_g	1.846$_5$±0.003	1.853±0.003	1.858±0.003	...
	l	0.054±0.003	0.053±0.003	0.055±0.003	...
C—H	r_g	1.091±0.006	1.097±0.007	1.094±0.008	...
	l	0.073±0.006	0.080±0.007	0.082±0.008	...
P—H	r_g	...	1.445±0.02	1.423±0.007	1.437±0.004
	l	...	0.070±0.02	0.077±0.008	0.085±0.008
C···C	r_g	2.800±0.005	2.821±0.010	...	...
	l	0.084±0.005	0.088±0.008	...	...
P···H	r_g	2.455±0.006	2.452±0.008	2.452±0.014	...
	l	0.110±0.006	0.114±0.007	0.124±0.010	...
∠CPC		98.6±0.3°	99.2±0.6°	...	...
∠PCH		110.7±0.5°	109.8±0.7°	109.6±1°	...
∠CPH		...	(96.5° assumed)	(96.5° assumed)	...
Methyl config.		Staggered	Staggered	Staggered	...

[a] Reference 6.
[b] This investigation.
[c] Reference 5.

tative potential energy functions to describe C···C, C···H and H···H intramolecular van der Waals interactions in hydrocarbon molecules. It is interesting, although of uncertain significance, that the forces derived from these functions imply both the direction and general magnitude of the trend observed in the phosphines. The trend in P—C bonds is opposite to that reported for Si—C bonds in an electron diffraction study of mono-, di-, and trimethylsilanes,[20] but in good agreement with recent, more precise microwave studies of mono-[21] and dimethylsilane.[22]

None of the other parameters show significant trends over the series. It may be noted that the P—H bond length, determined here in terms of r_g, is 0.01 A to 0.02 A higher than the spectroscopic r_0 values found for various isotopic species of phosphine in infrared and microwave studies.[7] This is apparently attributable to the operational difference between the parameters r_g and r_0[5]. The C—H bonds appear to be about 0.02 A shorter than those in the *n*-hydrocarbons butane through heptane,[23] and in the methyl groups in isobutylene,[19] but 0.01 A longer than the C—H bonds in ethylene.[24] The explanation of this result must await further research.

ACKNOWLEDGMENT

The author is greatly indebted to Professor L. O. Brockway for making available the electron diffraction apparatus for this investigation. It is a pleasure to acknowledge the valuable assistance of Mr. Denis Kohl and Miss Ethel Bortle in computations and the reading of microphotometer traces.

[20] A. C. Bond and L. O. Brockway, J. Am. Chem. Soc. **76**, 3312 (1954).
[21] R. W. Kilb and L. Pierce, J. Chem. Phys. **27**, 108 (1957).
[22] L. Pierce, J. Chem. Phys. **31**, 547 (1959).
[23] Bonham, Bartell, and Kohl, J. Am. Chem. Soc. **81**, 4765 (1959).
[24] L. S. Bartell and R. A. Bonham, J. Chem. Phys. **27**, 1414 (1957); **31**, 400 (1959); H. C. Allen and E. K. Plyler, J. Am. Chem. Soc. **80**, 2673 (1958); J. M. Dowling and B. P. Stoicheff, Bull. Am. Phys. Soc. Ser. II **3**, 313 (1958).

Theoretical Investigations on the Light Scattering of Colloidal Spheres. VIII. Angular Location of Intensity Maxima and Minima in the Radiation Diagram of Colloidal Spheres

MASAYUKI NAKAGAKI† AND WILFRIED HELLER

Department of Chemistry, Wayne State University, Detroit 2, Michigan

(Received July 23, 1959)

The angular position of scattering maxima and minima in the radiation diagram of nonabsorbing colloidal spheres is calculated for $(m-1)\to 0$ and for $m=1.20$, by using in the former case the Rayleigh-Gans approximation and in the latter the exact Mie scattering functions. By means of empirical equations based upon the discrepancies between the Rayleigh-Gans data and the Mie data, the approximate location of scattering maxima and minima is calculated also for the m values 1.05, 1.10, 1.15, 1.25, and 1.30. The expected precision and accuracy of particle size determinations from the angular location of scattering maxima and minima is discussed and the minimum angular ranges to be covered in a given instance are defined. A few pertinent features of the related La Mer method (HOTS) are briefly discussed.

INTRODUCTION

A CHARACTERISTIC feature of light scattering observed at a given angle γ is the periodic alternation of intensity maxima and minima as α increases.[1] The rate at which these maxima and minima vary with α, at a given m, depends on γ. This is apparent from results given in preceding publications on the scattering at $\gamma=0$,[2] 45,[3] 135,[3] and 180°.[1] Associated with these two phenomena is a periodic alternation of intensity maxima and mimima as γ increases, at a given m and α, provided α is large enough. Consequently, each α value (particle size at constant wavelength), provided it is large enough, is characterized by a maximum or maxima and a minimum or minima of light scattering at a given γ value or set of γ values, respectively. Scanning of the radiation diagram over a certain angular range represents, therefore, a relatively simple method for particle size determinations provided the particles are large enough. It has been used by several authors. In the first practical application, by La Mer,[4] an incident beam of white light was used. The minima and maxima then manifest themselves by colors in the laterally scattered light ("higher order Tyndall spectra"). The scanning method in monochromatic light, whose theoretical features have been briefly investigated before,[5] has many of the advantages of lateral scattering measurements at a fixed angle γ, without being burdened by their disadvantages. Above all, the problem of multivaluedness of the answers on α is easily eliminated. In addition, no major instrument constant is needed.

The full development of the scanning method for determining quantitatively particle sizes in monochromatic light has been delayed primarily by the absence of comprehensive computations of explicit angular light scattering functions for m values <1.33. Such data, pertinent to $m=1.20$, and derived from the Mie theory are now available for the four angles mentioned, and, in addition, for 90°.[6] These data, in conjunction with those which are easily derived for the limiting case of $(m-1)\to 0$, allow one now to ascertain the essential theoretical features of this method. To do this is the principal purpose of the present paper.

I. LIMITING CASE OF $(m-1)\to 0$

The true angular location of the minima and maxima of i^1 can be calculated without difficulty from the R–G–D equation[1] for the limiting case of $(m-1)\to 0$. This equation yields

$$S_\gamma\alpha_n = \tan(S_\gamma\alpha_n) \tag{1}$$

and

$$\sin(S_\gamma\alpha_n') = 0, \tag{2}$$

respectively. Here

$$\alpha = 2\pi r_s/\lambda, \tag{3}$$

$$S_\gamma = 2\cos(\gamma/2), \tag{4}$$

r_s is the radius of the particles, λ is the wavelength in the medium, n is any integer number, and α_n and α_n' represent the α values at which a minimum or maximum, respectively, of i, of order n, occurs at the particular γ value considered.

The α_n and α_n' values can be calculated even more simply[3] (see also reference 5) from the equations

$$\alpha_n = (n+\tfrac{1}{2})\pi/S_\gamma \tag{5}$$

and

$$\alpha_n' = n\pi/S_\gamma. \tag{6}$$

The results obtained with the latter equations are plotted in Fig. 1. It shows that successive orders (1–10)

* This work was supported by the Office of Naval Research.

† Visiting professor; permanent address: Faculty of Living Science, Osaka City University, Osaka, Japan.

[1] For the definition of the symbols used here see Heller, Nakagaki, and Wallach, J. Chem. Phys. **30**, 444 (1958).

[2] M. Nakagaki and W. Heller, J. Chem. Phys. **30**, 783 (1959).

[3] W. Heller and M. Nakagaki, J. Chem. Phys. **31**, 1188 (1959).

[4] See, e.g., D. Sinclair and V. K. La Mer, Chem. Revs. **44**, 245 (1949).

[5] W. B. Dandliker, J. Am. Chem. Soc. **72**, 5110 (1950).

[6] See a subsequent paper by Pangonis, Heller, and Economou (to be submitted for publication in J. Chem. Phys.)

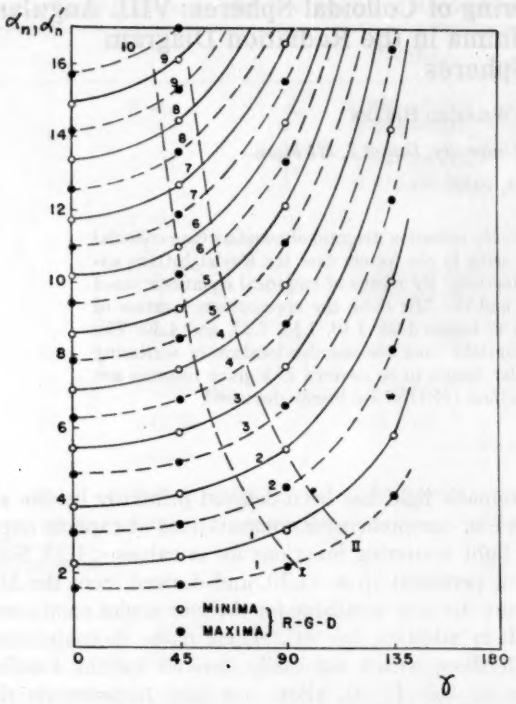

FIG. 1. The variation of α_n and α_n' with the angle γ if $m \rightarrow 1.0$. Here α_n and α_n' are the α values at which the scattered intensity reaches a minimum and maximum, respectively, of order n; incident beam unpolarized. Full curves represent α_n; dashed curves, α_n'; dotted curves I and II: see text; inscribed numbers (1–10), order n.

of maxima (dashed curves) and minima (full curves) originate at $\gamma=0°$ and move, with increasing α, toward larger γ values. The rate of this forward movement decreases continuously with increasing γ. Thus, both the first minimum and maximum are extremely sensitive to a change in particle size at γ values $<45°$, but are very insensitive to it once they have moved to a γ value $>135°$. An interesting detail is that the sensitivity to changes in particle size (α) decreases, at any γ, with an increase in the order of the maximum and minimum.

Experimentally, one determines the relative scattered intensity, I/I_0, where I is the intensity of light scattered by the unit volume of a dispersed system of a given concentration, per unit solid angle, and I_0 is the intensity of the incident beam. This quantity is proportional to i, so that the experimentally determined intensity maxima and minima coincide with those of i both with respect to the associated γ and α values. Numerical values for the angular location of these intensity maxima and minima are given in Table I for a series of selected α values.

The angular position of the maxima and minima may vary slightly with concentration unless one operates with highly dilute systems. For unusually exacting work, one may therefore wish to consider the maxima and minima of (I/I_0c) extrapolated to infinite dilution (c is the concentration of the scattering material). These maxima and minima also are identical in angular position with those of i if α is constant. They differ slightly, at constant γ, as a function of α, since I/I_0c is proportional to (i/α^3). In general, however, the difference is too small to be of practical consequence (see end of Sec. IV).

Figure 1 allows a rapid count of the number of maxima and minima expected between $\gamma=0°$ and $\gamma=180°$ at any α value. At $\alpha=16$, for example, the highest α value considered, the number of maxima and minima has already increased to 10 and 9, respectively. It is apparent from the data that it is sufficient to scan the radiation diagram between $\gamma=0°$ (backward direction) and γ_i in order to obtain a single-valued answer on α (particle size). The value of γ_i is defined here by the intersection of the main curves in Fig. 1 with curve I. The angular range between γ_i and $\gamma=0$ contains one maximum or one minimum. The accuracy of the result will be increased by enlarging the range to γ_i' defined by the intersections with curve II. This range contains both one maximum and one minimum. Not only their individual angular location but also their angular separation can then be used for particle size determinations. Both ranges decrease with increasing α. Thus, the range bordered by curve II decreases from (0–112°) at $\alpha=3$ to (0–53°) at $\alpha=15$. Finally, it is apparent that the minimum α value to which the scanning method can be applied at $(m-1)\rightarrow 0$ is 1.6 corresponding to a particle diameter of about 210 mμ if $\lambda_0=5460.73$ A, and the medium is water at 20°C.

II. CASE OF $m=1.20$ AND THE POTENTIALITIES OF THE SCANNING METHOD

By means of the data computed in this laboratory from the Mie theory for the scattering at $\gamma=0$, 45, 90, 135, and 180° if $m=1.20$, it is possible to give complete information for this particular case which, in practice, corresponds closely to that of polystyrene lattices. The α_n and α_n' values at these angles were obtained by numerical interpolation of the i_γ (α) curves. Their uncertainty is very small since the $\Delta\alpha$ intervals of the computed i values were throughout 0.2. In order to facilitate interpolations for other angles, the α_n and α_n' values, pertinent to incident unpolarized light, are plotted in Fig. 2 and 3, respectively, as a function of $(1/S_\gamma)$ (fully drawn curves). In this type of plot straight lines are obtained as long as α_n and α_n' are sufficiently small. At larger α_n (α_n') values, the lines degenerate into curves. From these data, Table II and Fig. 4 are derived which give for $m=1.20$ information corresponding to that furnished, for $(m-1)\rightarrow 0$, by Table I and by the curves I and II of Fig. 1, respectively.

The R–G–D values, dotted in Figs. 2 and 3, give throughout rigorously straight lines as required by Eqs. (5) and (6). These data differ substantially from the Mie data. The absolute differences are smallest for

TABLE I. The γ values, in degrees, at which intensity maxima and minima, of order n, occur if $m \rightarrow 1.0$. Unpolarized light; minima bracketted; R—G—D theory.

α \ n	1	2	3	4	5	6	7
1	...	...	...	...	...		
2	75 (−)	...	...	...	...		
3	112 (80)	...	...	...	...		
4	133 (108)	79 (30)	...	...	...		
5	145 (125)	101 (79)	42 (−)	...	...		
6	148 (136)	115 (100)	79 (48)	...	...		
7	153 (141)	125 (111)	94 (77)	53 (−)	...		
8	157 (145)	133 (120)	104 (93)	77 (56)	22 (−)		
10	162 (152)	143 (134)	122 (112)	102 (91)	77 (60)	40 (−)	...
12	165 (157)	149 (142)	133 (125)	116 (107)	97 (88)	78 (63)	48 (21)

TABLE II. The γ values, in degrees, at which intensity maxima and minima, of order n, occur if $m = 1.20$. Minima bracketted; Mie theory; unpolarized light.

α \ n	1	2	3	4	5	6
1	...	...	...	...	...	...
2	90 (25)	...	...	...	...	...
3	123 (99)	45 (−)	...	...	...	...
4	138 (121)	90 (70)	0 (−)	...	...	...
5	>145 (133)	113 (95)	72 (45)	...	...	...
6	>145 (141)	125 (111)	94 (77)	54 (20)	...	...
7	>145 (>145)	133 (121)	108 (94)	79 (62)	37 (12)	...
8	>145 (>145)	140 (129)	118 (106)	94 (80)	64 (50)	21 (8)

α \ n	1	2	3	4	5	6	7	8	9	10
10	>135 (>135)	>135 (>135)	131 (122)	113 (>90)	>90 (82)	70 (59)	46 (30)	13 (0)	...	...
12	>135 (>135)	>135 (>135)	>135 (132)	125 (>90)	>90 (>90)	>90 (85)	73 (66)	52 (44)	29 (15)	8 (−)

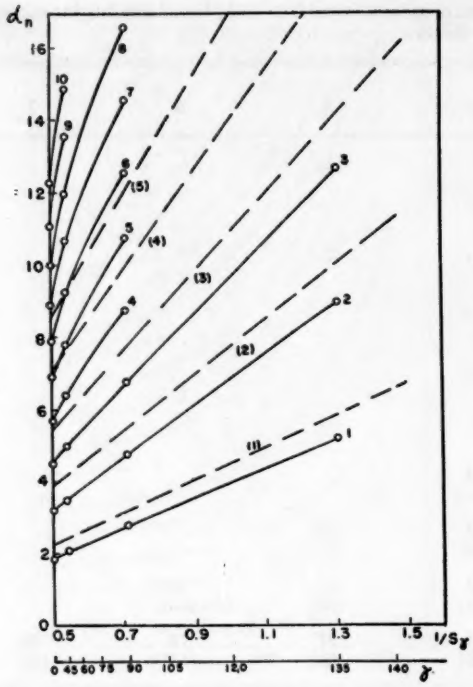

FIG. 2. The variation of α_n with $1/S_\gamma$ if $m=1.20$; unpolarized incident light. Full curves represent Mie data; dashed curves, R—G—D data.

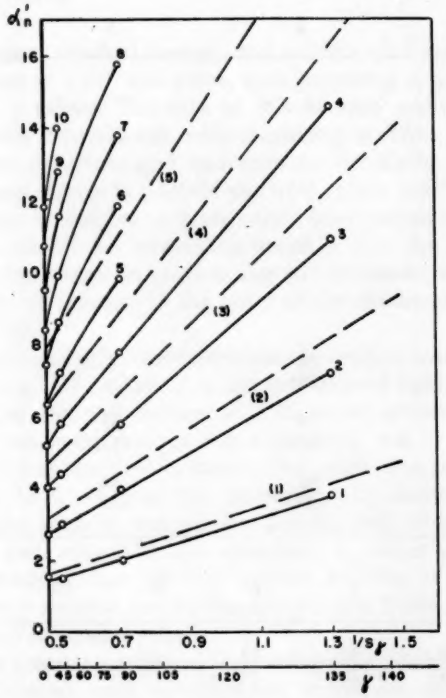

FIG. 3. The variation of α_n' with $1/S_\gamma$ if $m=1.20$; unpolarized incident light. Full curves represent Mie data; dashed curves, R—G—D data.

the first order maximum and minimum as they originate at $\gamma=0°$. The first minimum actually originates at $\alpha=1.9$ while the R—G—D value is $\alpha=2.25$.[7] The absolute differences increase with the forward movement of the maxima and minima toward larger α values and they increase also with their order. The percent differences, however, are almost independent of n (see next section). At $\alpha=15$, the radiation diagram contains already 12 maxima and 12 minima, three more of each than expected from the R—G—D equation. Even at an m value as small as 1.05, both absolute and percent differences, although much smaller, are quite significant. From data given in the next section, it follows that a particle weight derived from the R—G—D data is 13.1%, 45.4%, and 70.6% too large if $m=1.05$, 1.20, and 1.30, respectively.

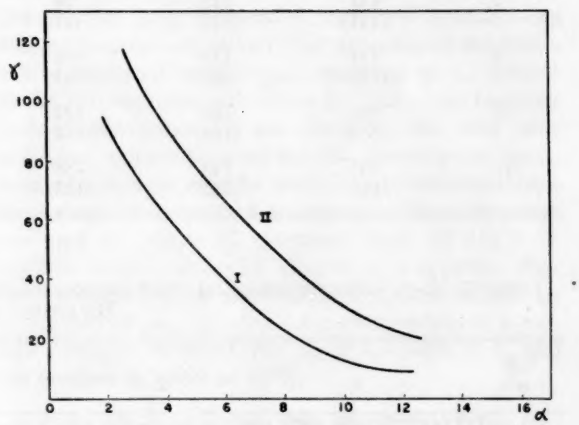

FIG. 4. Definition of the angular range to be covered for single-valued answers on particle size if $m=1.20$. Vertical distance between curve I (II) and abscissa defines angular range to be covered at given α value in order to pass through one maximum (one maximum and one minimum).

III. PRELIMINARY GENERALIZATION OF THE RESULTS

The preceding results allow one to describe the salient features of the radiation diagram fully at any α value for both $m=1.20$ and $m\to1.0$. In order to obtain rigorously correct results with the scanning method at any other m value, the variation of the angular maxima and minima with m should be known. It will be possible to evaluate this variation very accurately once the tedious and time-consuming computations of angular scattering functions for other m values have been completed which are being carried out at present by W. J. Pangonis. At present, it is possible to approximate the $\alpha_n(m)$ and $\alpha_n'(m)$ function to probably a satisfactory degree by using the percent differences between the available Mie data and the R—G—D data as the basis.

[7] This shows, incidentally, that the lower limiting α value above which the scanning method can be used, decreases with increasing m but without altering the accessible fraction of the colloidal range considerably.

The first finding important for this purpose is that the percent deviation of the R—G—D values of α_n and of α_n', from the Mie values (Δ_{R-G-D} and Δ_{R-G-D}', respectively) is, at any m, from 1.05–1.30, largely independent of n, with the doubtful exception of $n=1$. This follows for α_n and 90° scattering[6] from Table III. The fluctuations about an average Δ_{R-G-D} at a given m, are due in part to the slightly oscillatory character of the Mie data (too small to be apparent in graphs; see Fig. 5) and in part to uncertainties in the numerical interpolation of the exact position of minima between the pertinent $\Delta\alpha$ intervals of 0.2. Table IV shows that Δ_{R-G-D} and Δ_{R-G-D}' are largely independent of n at 45 and 135° also if $n>1$. At angles $\gamma<45°$, however, this independence ceases.

TABLE III. Percent deviation Δ of the R—G—D α_n values from the Mie α_n values at $\gamma=90$; m varied.[a] Here $\alpha_n=\alpha$ value at which a minimum of order n is expected. (The R—G—D values are throughout larger than the Mie values.)

n \ m	1.05	1.20	1.30
1	2.6	13.6	22.6
2	5.0	14.6	19.6
3	4.1	13.2	20.3
4	3.7	13.1	18.5
5	4.3	12.0	16.3
6	4.3	14.3	18.0
7	3.8	13.7	16.9
8	4.7	13.6	16.4
Δ_{Av}	4.1±1.3	13.3±1.3	19.5±3.2

[a] These data are calculated for linearly polarized light vibrating perpendicular to the plane of observation. Those for unpolarized light are nearly the same (see footnote 8 and column four in Table IVA).

The second finding of importance is that there exists a relatively simple Δ_{R-G-D} (m) function at a given α. This can easily be shown for $\gamma=90°$. Results to be described later yield the following pertinent data at $m=1.00$, 1.05, 1.20, and 1.30, respectively: $\alpha_1=3.18$, 3.0, 2.8, and 2.6; $\Delta\alpha_n=2.22$, 2.12, 1.96, and 1.90.[8] The graphical representation of the individual data in Fig. 5 yields the following equations:

$$\alpha_n=1.1+2.22n \quad (m\to 1.00) \quad (R-G-D) \quad (7)$$

$$\alpha_n=1.0+2.12n \quad (m=1.05) \quad (Mie) \quad (7a)$$

$$\alpha_n=0.9+1.96n \quad (m=1.20) \quad (Mie) \quad (7b)$$

$$\alpha_n=0.8+1.90n \quad (m=1.30) \quad (Mie). \quad (7c)$$

From this one obtains

$$\Delta_{R-G-D}=[(A'+B'n)/(A+Bn)]-1, \quad (8)$$

where A and B represent the intercept and the slope,

[8] The data given apply to incident polarized light vibrating perpendicular to the plane of observation. If the direction of vibration is in the plane of observation, $\alpha_1=3.18$, 3.8, 3.4, 3.2 and $\Delta\alpha_n=2.22$, 2.14, 1.86, and 1.72, respectively. The data for incident unpolarized light are paractically the same as the former.

TABLE IV. Percent deviations, Δ and Δ', of the R—G—D—α_n values and α_n' values from the Mie data at $m=1.20$; γ is varied; unpolarized light. ($\alpha_n'=\alpha$ value at which a maximum of order n is expected.)

	A:Δ			
n \ γ	0°	45°	90°	135°
1	12.5	16.7	14.3	15.7
2	24.5	19.4	14.0	12.2
3	21.1	18.0	13.2	12.6
4	23.5	19.1	13.2	
5	24.5	19.1	12.4	
6	21.4	18.3	14.3	
7	32.0	18.9	13.7	
8	33.3	20.3	13.6	
	B:Δ'			
n \ γ	0°	45°	90°	135°
1	5	13	11	8
2	16	13	11	14
3	18	16	15	13
4	21	17	14	13
5	25	18	13	
6	27	19	13	
7	31	20	13	
8	32	17	13	

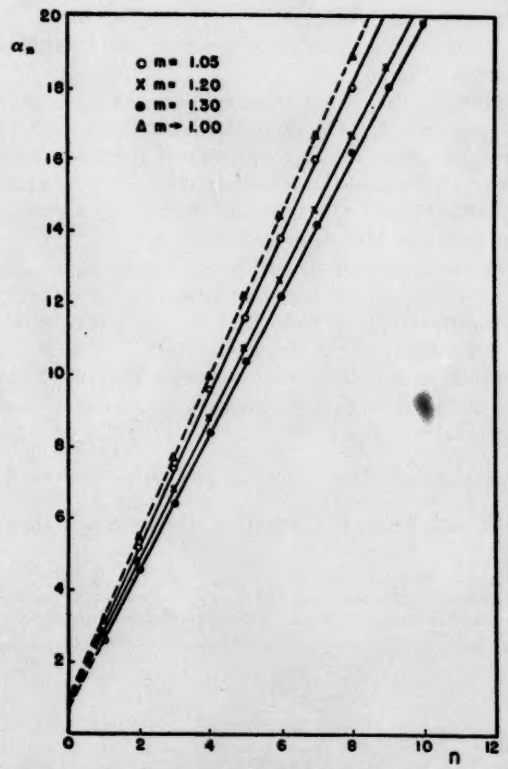

FIG. 5. Variation, at 90°, of the α value at which an intensity minimum, α_n, occurs with its order n; incident light is polarized, vibrating perpendicular to the plane of observation (data apply also very closely to incident natural light). Full curves represent Mie data; dashed curve, R—G—D data.

TABLE V. Average percent deviation of the R—G—D α_n values from the Mie values at various γ and m values; unpolarized light. [Data in italics calculated from Eq. (10).]

m \ γ	0	45	90	135
1.05	*15*	*9*	4.1	*3*
1.10	*19*	*12*	7.1	*6*
1.15	*22*	*16*	10.2	*9*
1.20	25.8	19.0	13.5	12.4
1.25	*29*	*22*	16.25	*15*
1.30	*32*	*25*	19.5	*18*

respectively, of the (nearly) straight lines obtained from the Mie data, and A' and B' are the corresponding R−G−D quantities. The resulting Δ_{R-G-D} (m) function shows that Δ_{R-G-D} increases monotonically with m at a slowly decreasing rate. Alternately, Δ_{R-G-D} (m) can be calculated from the average deviations given in the last row of Table III. These alternate data are satisfied by the equation, valid for $\gamma=90°$,

$$\Delta_{R-G-D}=-0.60+0.61m;\ (n>1). \qquad (9)$$

The respective straight line intersects this curve at $m>1.05$ and again at $m\sim1.20$. The Δ_{R-G-D} (m) values obtained by the two procedures differ at the most by 10% within the m range 1.05−1.25. Equation (9) and a corresponding equation for the deviation of the R−G−D maxima, Δ_{R-G-D}', was therefore used for the sake of simplicity.

Table V gives, in the third column, the Δ_{R-G-D} (m) values for $\gamma=90°$. On the other hand, the fourth row gives the mean Δ_{R-G-D} (γ) values for $m=1.20$, as obtained from Table IV A by neglecting $n=1$. The latter show that the R−G−D values deviate, at a given m, more from the Mie data the smaller γ.

The assumption shall now be made that Δ_{R-G-D} (m) is independent of γ. This assumption cannot be correct quantitatively. It is likely that Δ_{R-G-D} varies with m less if $\gamma>90°$ and more if $\gamma<90°$. Nevertheless, it is an acceptable first approximation pending the collection of more data from the Mie equations. On this basis, the general equation

$$\Delta_{R-G-D}(m,\gamma)=\Delta_{R-G-D}(\gamma)_{m=1.20}+0.61m-0.736 \qquad (10)$$

is obtained. From this equation, the data in italics in Table V have been calculated for $\Delta\alpha_n$. Similarly, Table VI gives the corresponding results for $\Delta\alpha_n'$. By means of these data, an "error contour chart" is constructed in Fig. 6. The length of the radius vector indicates the percent deviation of the α_n' values obtained from the R−G−D equation, excluding γ values >135°. Tables V and VI and Fig. 6 therefore should allow one to obtain the approximate true values of α_n' by applying the proper corrections to the easily calculated R−G−D data [Eq. (6)].[9] The corrected data, in turn, should allow one to obtain a practically useful estimate of particle size from the angular location of intensity maxima or minima at any m between 1.0 and 1.3.

Equations (7)–(7c) pertain strictly only to the minima of i and of the experimental quantity (I/I_0). The coefficients for the corresponding equations for (I/I_0c) are, however, practically the same at all n values. The same was found to be true for the maxima

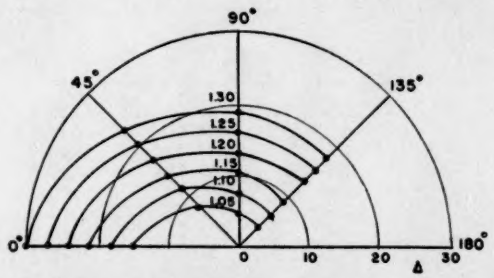

FIG. 6. Error contour chart for intensity maxima calculated from R—G—D equation. Length of radius vector represents per cent deviation Δ from Mie data; parameter, m.

equations for (I/I_0c) provided that $n\geqslant3$. Equation (10) and the results in Table V apply therefore to all three quantities. The results in Table VI and Fig. 6, however, apply to (I/I_0c) only with the restriction on n stated. The reason for the practical identity of the α_n and α_n' values of (I/I_0c) with those of i and (I/I_0) is that the rate of change of i near the maxima and minima is so large throughout that introduction of the factor (I/α^3) has practically no significant effect upon the location of the maxima and minima as a function of α. The differences in $\Delta\alpha_n$ and $\Delta\alpha_n'$—which determine the coefficients in the equations used—are evidently still smaller.

TABLE VI. Average percent deviation of the R—G—D α_n' values from the Mie values at various γ and m values; unpolarized light (data in italics calculated from approximating equation).

m \ γ	0	45	90	135
1.05	*15*	*8*	4.8	*4*
1.10	*18*	*11*	7.6	*6*
1.15	*21*	*14*	10.4	*9*
1.20	24	17	13.1	13
1.25	*27*	*20*	16.0	*15*
1.30	*30*	*23*	18.8	*17*

IV. THEORETICAL PRECISION AND ACCURACY OF THE SCANNING METHOD IN MONOCHROMATIC LIGHT

Information on the potential precision and accuracy of particle size determinations based upon the scanning method, may be derived from the Mie data pertinent

[9] It is noteworthy that the corrections necessary on deriving a particle weight rather than a particle diameter from the angular location of α are roughly 3 times larger than indicated by the chart in Fig. 6. Thus, in the most favorable case covered by the chart, the error in particle weight, on omitting the correction to the R—G—D equation, would be 9–10%, if the maximum occurs at 135° and if $m=1.05$.

to $m=1.20$, considering intensity maxima, which for obvious experimental reasons will generally be preferred to the minima. Since the maximum of the second order progresses from 45° to 90° as α increases from 3 to 4 (see Table II), the average precision, per degree, is here 0.02α. Thus, a change in particle diameter by about 25 A (assuming the use of 5461 A as the wavelength of the incident beam), should be measurable if the solid angle used is sufficiently small. The maximum of the fifth order progresses from 37° to 64° as α increases from 7 to 8 corresponding to an average displacement by 1° as the particle diameter changes by about 50 A. Theoretically, the absolute precision of the scanning method is therefore remarkably high, particularly at low orders and at angles $\gamma<90°$. It decreases with increasing order and, particularly, with increasing γ. However, the percent precision is relatively little affected by the order. Thus, in the examples given, the percent uncertainty in particle diameter is 0.4–0.7 in the first instance and 0.4–0.6 in the second. Such a high precision presupposes that the intensity maximum can be located with an uncertainty not in excess of ± 0.5 degree. This appears possible if the systems are sufficiently monodisperse. Otherwise, the maxima are bound to be too broad and shallow. The accuracy of the scanning method is, of course, distinctly smaller. It depends decisively on the primary $\Delta\alpha$ spacings used for the interpolation of the theoretical α_n and α_n' values. As these spacings have been 0.2 throughout, the uncertainty inherent in the absolute particle diameter can be estimated as being approximately ± 100 A.

The following practically important features of the scanning method have become apparent on the basis of the results discussed: (1) In order to obtain single-valued answers on particle size, it is not necessary to scan the entire radiation diagram. A properly selected angular range, which is smaller the larger α is, is sufficient. (2) The maxima and minima located nearest to $\gamma=0$ are most sensitive to changes in particle size. The proper angular range to be selected is, therefore, that of small angles of γ.[10] The method is, of course, applicable only above a certain particle size specified above.[11]

[10] On using the alternate definition of the scattering angle which originated with x-ray scattering, in which $\theta=(180°-\gamma)$ is the reference, the method proposed here would represent that of "large angle" scattering.

The fact that the scanning method is most sensitive to changes in particle size at low γ values, shows that its potential application for the determination of size distribution curves in heterodisperse systems should concentrate on this angular range (cf. a subsequent publication concerned with this problem).

[11] It is useful to draw attention to a potential pitfall which exists on searching for a minimum or minima within a narrow angular range centered at 90°. Spheres which are small compared to the wavelength of light used exhibit an intensity minimum at 90° in accordance with the well-known radiation diagram of Rayleigh spheres. This is a stationary minimum, independent of α and therefore independent of particle size and wave length as long as α is sufficiently small. If, therefore, an intensity minimum is observed at or near 90°, it may be advisable to check the wavelength dependence of its angular location. The possibility of confusion is, however, rather remote. No such problem exists, of course, for determinations of intensity maxima.

V. SCANNING METHOD IN WHITE LIGHT

Since the angular position of an intensity minimum or maximum is, at a given m, completely defined by α, it will, at a given particle diameter, vary with the vacuum wavelength λ_0. On using polychromatic light, one will therefore observe colors in the laterally scattered light, which vary with γ. This was observed first on sulfur sols by Ray,[12] but La Mer and collaborators were the first to study this phenomenon extensively.

They designated these colors as "higher order Tyndall spectra" (HOTS),[13] and used them for particle size measurements. The determination of the α values at which maxima or minima in light intensity are observed is then replaced by the determination of the α values at which an arbitrarily selected color "band" is observed. In La Mer's work "red bands" were selected. As already pointed out by van de Hulst,[14] there is no simple relation between the angular location of maxima or minima on the one hand and the angular location of specific bands on the other: a red band may be the result of an intensity maximum in the red or of an intensity minimum in the green. It is worthwhile adding to this observation that bands of a given general color, e.g., red bands, are bound to differ in hue and that only very specific ones will be practically monochromatic. The angular position of such "monochromatic bands" can be determined rather easily theoretically since they are bound to be located at that angle γ, where for a particular diameter D and m the (I/I_0) maxima in the red coincide with the minima in the green.

La Mer's work has shown that HOTS can be used as a useful and simple means for determining particle sizes in systems which contain sufficiently large particles of uniform size. La Mer's comparison with the results by sedimentation analysis[13] shows that sizes thus determined cannot be far off from the true sizes and the HOTS method is therefore undoubtedly satisfactory for many purposes. In precision and accuracy, it cannot be expected to be equivalent to the monochromatic method. Since a color band extends over a finite, although possibly quite small range of γ values, the precision is bound to be smaller than in monochromatic light. More important, however, is the problem of accuracy. The m value changes with wavelength. The true angular spectrum can, therefore, be calculated only by superimposing two, or preferably three, monochromatic radiation diagrams calculated for the m values pertinent to the respective two or three wavelengths. The considerable labor involved has thus far not been carried out. La Mer used a compromise procedure by calculating, for sulfur sols, the radiation diagram for 6290 A ($m=1.4274$) and 5240 A ($m=$

[12] B. Ray, Proc. Indian Assoc. Cultivation Sci. **7**, 1 (1921).

[13] See reference 4 and particularly I. Johnson and V. K. La Mer, J. Am. Chem. Soc. **69**, 1184 (1947).

[14] H. C. van de Hulst, *Light Scattering by Small Particles* (John Wiley & Sons, Inc., New York, 1957).

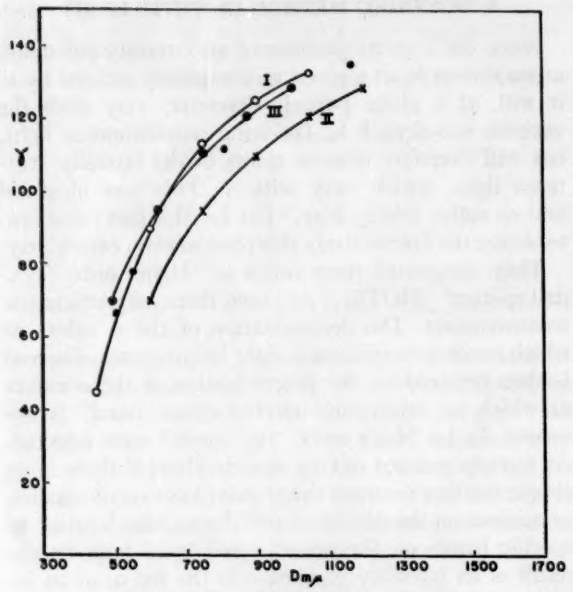

FIG. 7. Determination of monochromatic bands in HOTS I. Angular variation of second-order maximum of i with particle diameter D if $\lambda_0=6290$ A. II. Same for second-order minimum; $\lambda_0=6290$ A. III. Same as II except that $\lambda_0=5240$ A. Full circles: Exptl. results by La Mer and Plesner[16] (RED II).

1.4602) using in both cases the intermediate m value of 1.44 considered in the tabulation of scattering functions of Lowan.[15] It is, of course, possible to eliminate the uncertainties resulting from the dispersion effect—whose degree of importance still remains to be evaluated quantitatively—by using HOTS not as an absolute method, but as a method calibrated for a particular system. Thus, La Mer applied HOTS recently to particle size determinations on polystyrene latices subsequent to their standardization against electronmicroscopic data.[16] Since complete data for $m=1.20$ are available, and since polystyrene closely approximates this condition in the visible, it is of interest to compare La Mer's empirical results with those expected from theory. Curve I in Fig. 7 represents the angular variation of the second order i maximum with the particle diameter D, if $\lambda_0=6290$ A. Curve II gives corresponding information for the second-order i minimum. Both curves are derived from the data given in Table II. Curve III gives the variation of the second-order i minimum with D if $\lambda_0=5240$ A. No dispersion corrections are applied. The intersection of curves II and III defines the most monochromatic Red II. La Mer's results for Red II are indicated by the solid circles. In absence of experimental errors and on taking into account the effect of dispersion, the experimental data should be contained within the area bordered by curves II and III. While the shape of the curve that one could draw through the experimental points agrees very satisfactorily with that expected from theory, the experimental diameters are found to be throughout somewhat larger. The systematic character of this deviation and its direction suggest that the major part of the quantitative disagreement may be due to the omission of the dispersion corrections although they are far less consequential here than in the case of sulfur. Considering $[(\mu_{5240A}/\mu_{6290A})-1]$, where μ is the refractive index, the respective values are 6.96×10^{-3} and 23.0×10^{-3}, respectively.

[15] Tables of scattering functions for spherical particles; National Bureau of Standards, 1948.

[16] V. K. La Mer and I. W. Plesner, J. Polymer Sci. **24**, 147 (1957).

Experimental Study of the Shape of the *F*-Band Absorption in KCl

JOHN D. KONITZER AND JORDAN J. MARKHAM

Zenith Radio Corporation, Chicago 39, Illinois

(Received August 24, 1959)

The optical absorption due to *F* centers in KCl at temperatures between 4°K and 377°K has been measured. The authors believe they have eliminated the *K* band, and obtained the absorption due to transitions from the ground to the first excited state. The method of preparing "pure" *F* centers is discussed. The half-width, the point of maximum absorption, and the zeroth, first, and second moments have been measured in the above temperature range. The data establish Smakula's formula on a firm experimental basis for this center. The half-width in ev is given by the relation $0.163\,[\coth(71.0/\theta)]^{\frac{1}{2}}$, while the point of maximum absorption is at $2.340-0.027\coth(71.0/\theta)$, where θ is the absolute temperature. An equation has been found from which one may calculate the *F* band absorption. The shape of the band is temperature independent and is approximated by the low temperature form predicted by Pekar. The data on the whole support a generalized theory. The authors believe that the *F* band shape is due to the interaction of the *F* electron with localized modes whose average ground state frequency is 2.96×10^{12} sec^{-1}.

I. INTRODUCTION

THE general aspects of the absorption-emission spectra of atoms and molecules are understood. This knowledge is based on detailed studies of the simpler atoms and the simpler molecules. Solid state spectroscopy has not yet developed to the stage where even the simplest aspects are understood or can be formulated in a quantitative manner. In recent years, a great deal of effort has been given to the theory of the shape of bands in polar solids, but relatively little effort has been given to the experimental aspects of the problem.

With this in mind, we have selected one of the best-known solid state traps—the *F* center in KCl—and have studied some of its properties in considerable detail. We have limited our work to the shape of the absorption band associated with this center.[1] Several previous studies have been made. The first, due to Mollwo,[2] characterizes the problem in a general way. The second, due to Russell and Klick,[3] is a detailed analysis of the shape using the configurational coordinate model.[4] Hesketh and Schneider[5] have also measured the shape of the absorption band in KCl at 113° and 290°K. Quite recently Doyle[6] has calculated some interesting parameters related to the *F* band at 300°K, which will be described later in the text.

Unfortunately, the data of Russell and Klick do not agree with other published values (Fig. 1), and the authors do not believe that complete reliance can be placed on them. The reason for the difference between the data of Russell and Klick and that presented here is not known. It may be due to slight light leaks. Optical bleaching of the *F* band causes it to widen as subsidiary bands are produced.[7]

In view of the difference between Mollwo's results and the values reported by Russell and Klick, new data are presented here. It will be analyzed in terms of a recent synthesis[8] of the theories due to Pekar, Huang and Rhys, O'Rourke, Lax, and Meyer. Some of the concepts can be presented in an alternate form which requires a great deal less mathematical background. Therefore, the reader is also referred to the recent review of Klick and Schulman.[4] For the theory of references 4 and 8 to apply, we must assume that the *F* center has two bound states. During optical absorption, transitions occur between the ground and the excited state. This fact is firmly established as a result of the work done by the Göttingen School many years ago.[9]

Before embarking on this study, we wish to state some of the questions to be answered. The reader is referred to Seitz's general review of the field for the required background.[10] The terms which will be used are defined as follows:

ϵ—energy of an absorbed photon;
$\alpha(\epsilon)$—absorption constant at ϵ;
α_m—maximum value of α;
ϵ_m—photon energy at α_m;
ϵ_r—photon energy at half-height on the red side of ϵ_m;
ϵ_v—photon energy at half-height on the violet side of ϵ_m;
a_s—Smakula's constant (to be defined);
ω—average angular frequency of the phonons which influence the *F* center, when in the ground state;
θ—absolute temperature;

[1] A preliminary report of this study has been made. J. J. Markham and J. D. Konitzer, J. Chem. Phys. **29**, 673 (1958). Several corrections of this reference are made in the present paper.
[2] E. Mollwo, Z. Physik **85**, 56 (1933).
[3] G. A. Russell and C. C. Klick, Phys. Rev. **101**, 1473 (1956.)
[4] C. C. Klick and J. H. Schulman, Solid State Phys. **5**, 97 (1957).
[5] R. V. Hesketh and E. E. Schneider, Phys. Rev. **95**, 837 (1954).
[6] W. T. Doyle, Phys. Rev. **111**, 1072 (1958).
[7] J. D. Konitzer and J. J. Markham, Phys. Rev. **107**, 685 (1957).
[8] J. J. Markham, Revs. Modern Phys. **31**, 956 (1959).
[9] N. F. Mott and R. W. Gurney, *Electronic Processes in Ionic Crystals* (Oxford University Press, New York, 1948), Chap. IV.
[10] F. Seitz, Revs. Modern Phys. **26**, 7 (1954).

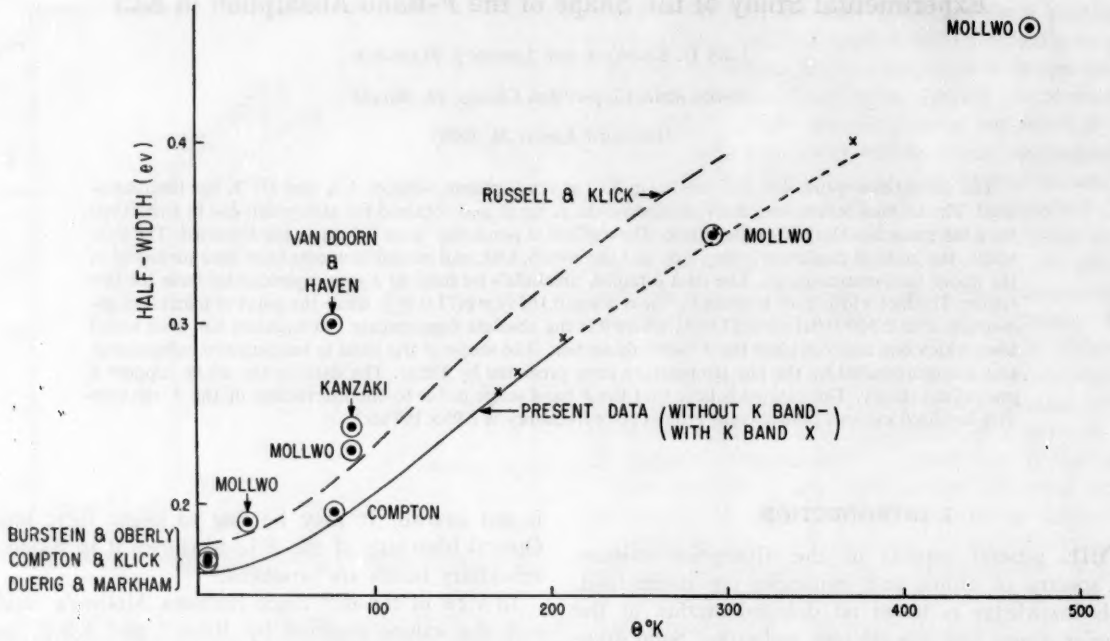

FIG. 1. The half-width of the F band in KCl *vs* temperature; a comparison of previously reported data with that presented in this paper. Burstein and Oberly, Compton and Klick, and van Doorn and Haven, reference 26; Compton (private communication); Kanzaki, reference 27; Mollwo, reference 2; Russell and Klick, reference 3; and Duerig and Markham, reference 11.

$H=\epsilon_v-\epsilon_r$, the half-width;

$M_n=\int\epsilon^n\alpha(\epsilon)d\epsilon$, the nth moment;

$\bar{\epsilon}=M_1/M_0$; and

$$m^2=1/M_0\int(\epsilon-\bar{\epsilon})^2\alpha(\epsilon)d\epsilon=(M_2/M_0)-(\bar{\epsilon})^2.$$

The questions are:

(A) Is the F center unique? It has been suggested that various types of centers exist, depending on the environment of the negative-ion vacancies which trap the electron. A comparison of data taken at various laboratories indicates that the centers produced by additive coloration have a larger H value than those produced by x irradiation.[11] This is supported by studies in KBr.[11] Many years ago, Gyulai additively colored KBr with potassium and sodium.[12] He found that the centers made from both metals were identical to first order. The absorption band associated with the centers formed from potassium was approximately 10% wider, however. Thus, the uniqueness of the F center has not been established, and on occasion, various types of centers have been postulated.

(B) Is the F center stable in the dark at a given temperature? The F center broadens on bleaching with light at 300°K. However, the problem of the dark stability has not been previously resolved.[13]

(C) May one replace $\bar{\epsilon}$ by ϵ_m; m by a constant times H; and M_0 by a constant times $\alpha_m H$? The theory is in terms of $\bar{\epsilon}$, m and M_0. The terms $\epsilon_m H$ and the product $\alpha_m H$ are the easily obtainable quantities and have been employed in the past.

(D) The temperature variation of M_0 and $\alpha_m H$ is of particular interest. If the relation

$$M_0=a_s\alpha_m H, \tag{1}$$

holds, where a_s (Smakula's constant) is temperature independent, we have an experimental proof of Smakula's famous equation. To the authors' knowledge an experimental verification of this equation has not been given.

(E) Is ϵ_v temperature independent? Mollwo's measurements indicate it is. The theory has not developed to the point where it can explain this phenomenon. The simplicity of the fact, if true, requires an explanation.

(F) Is the absorption shape temperature independent? Theory suggests that an absorption center has a Pekarian shape at very low temperature and is Gaussian at high temperatures (Reference 8, Sec. 9). A difference in the shape has been reported between 113° and 290°K.[5]

[11] Reference 10, see also W. H. Duerig and J. J. Markham, Phys. Rev. **88**, 1043 (1952); and Mador, Markham, and Platt, Phys. Rev. **91**, 1277 (1953).

[12] Z. Gyulai, Z. Physik **37**, 889 (1926).

[13] Botden, van Doorn, and Haven, Philips Research Repts. **9**, 469 (1954); C. Z. van Doorn, *ibid.* **13**, 296 (1958).

(G) What is the thermal dependence of m or H and of $\bar{\epsilon}$ or ϵ_m? Theories for their dependencies exist and a detailed comparison should produce information regarding absorption centers and the vibrations of the ions around the center.

II. APPARATUS

(1) Optical Cell

Absorption measurements were made between 1.0 ev and 3.5 ev against air as a blank with a Beckman spectrophotometer (DU) using the full sensitivity of the photomultiplier. During the course of this investigation, checks of the photometer system indicated that the calibration was within the limits specified by the manufacturer. The order in which the points were taken did not affect the absorption curve. Measurements of the crystal were made in Hersh's Pyrex double Dewar[14] which he modified so that it can be used at almost any temperature above 2.5°K.[15] The changes are shown in Fig. 2. Except for the brass rod, everything below the stainless steel container was made of copper. The brass rod acted as a thermal resistance between the heater and the liquid coolant (He or N_2). Power was applied to the heater to maintain the crystal at any temperature above that of the refrigerant. The total emf from three thermocouples in series was fed into a controller (Wheelco). This allowed a very small temperature change to be amplified and gave a stable crystal temperature. In this cell, of 200 ml capacity, nitrogen lasts four hours at 120°K but only one hour near 290°K. With this arrangement the crystal would reach 79°K and remain constant within 15 min after the nitrogen addition. When the refrigerant was liquid helium, the lowest temperature obtained was 13°K. The helium lasted about 50 min at this temperature but only 20 min at 30°K. The latter time was still sufficient to take a complete optical absorption measurement. The unmodified cell can be used between 4.5° and 2.5°K.

The nitrogen boiling point was lowered to 64°K by passing helium gas cooled to 78°K through the nitrogen.

Temperatures were measured by a copper-constantan thermocouple which was soldered directly to the bottom of the crystal holder. The thermocouples used were calibrated at boiling nitrogen, boiling oxygen, and boiling helium temperatures, against a constantan-copper thermocouple obtained from Professor J. Aston of Pennsylvania State University.

At 14°K the temperature varied 1°K during the measurement; at 21°K the variation was 0.7°K; while at 29°K the temperature changed only 0.1°K.

This arrangement permits measurements from about 10° to 300°K with an accuracy of 0.1 to 0.5°K. Our measurements were made on systems at equilibrium so that the crystal temperature equals the thermocouple temperature. With no refrigerant in the container, the cell can also be used above 300°K. The highest value employed in these experiments was 377°K.[16]

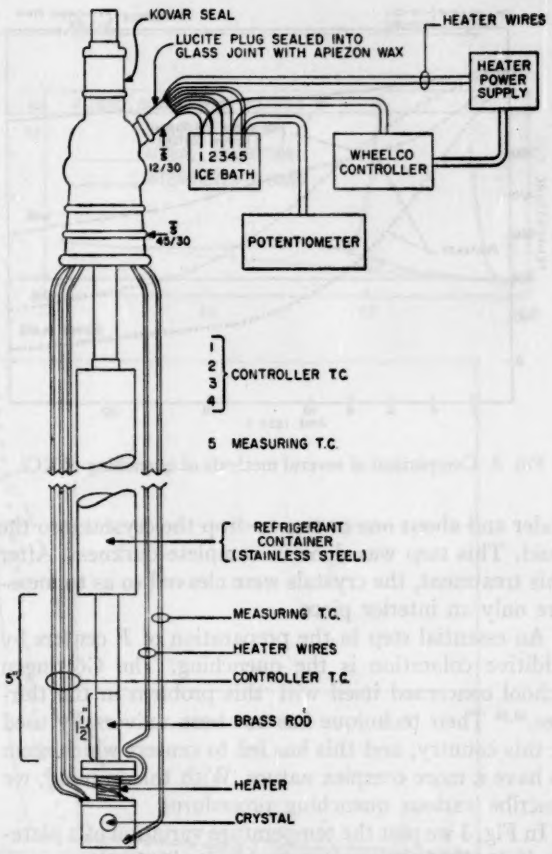

FIG. 2. The inner pot of the experimental glass Dewar showing the modifications.

(2) Sample Preparation

The F centers were made by additive coloration, and by exposure to 140 Kvp x-rays. The crystals were obtained from the Harshaw Chemical Company. The additive coloration was made in the equipment developed by Noble.[17] The samples were additively colored with potassium or sodium in an evacuated stainless steel cylinder. The crystal was maintained at 750°C (app) (26° below its melting point) for periods of three to four hours. The potassium was approximately at 310°C, or such that the absorption of a 1-mm thick crystal was about 1.0 absorption unit ($\log_{10} I(\text{air})/I$) at liquid nitrogen temperature. This corresponds to a concentration of 4×10^{18} (app) based on Smakula's equation with $f=0.81$. After coloration, the cylinder was opened and the glowing crystal was removed and dropped into oil. It takes about 30 sec to open the cyl-

[14] H. N. Hersh, Phys. Rev. **105**, 1158 (1957).
[15] R. W. Ure, Jr., Rev. Sci. Instr. **28**, 836 (1957).
[16] The only limiting factor is the melting point of the solder joining the sensing parts of the thermocouple. Absorption measurements have been made on KI at 520°K.
[17] G. A. Noble, J. Chem. Phys. **31**, 931 (1959).

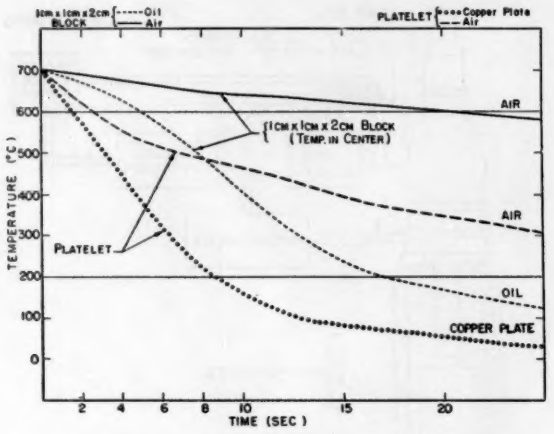

FIG. 3. Comparison of several methods of quenching of KCl.

inder and about one or two to drop the crystal into the fluid. This step was done in complete darkness. After this treatment, the crystals were cleaved so as to measure only an interior piece.

An essential step in the preparation of F centers by additive coloration is the quenching. The Göttingen School concerned itself with this problem in the thirties.[18,19] Their technique has not been universally used in this country, and this has led to centers which seem to have a more complex nature. With this in mind, we describe various quenching procedures.

In Fig. 3 we plot the temperature variation of a platelet (0.1×1×1 cm app) and a block (1×1×2 cm app) as a function of time. The temperature was measured by means of a chromel-alumel thermocouple. The thermocouple was wrapped around the platelet in one case and embedded in the middle of the block in the other. We believe that the curves on the block represent the temperature of the interior, but that the temperature of the exterior drops much faster than the graph indicates. For instance, in an air-quench, the exterior of a block drops from 650° to 400°C in $\frac{1}{4}$ sec and to 200°C in 2.5 sec. Quenches using H_2O or CCl_4 are much faster; however, the crystals are usually cracked or shattered; hence, unusuable for optical work.

In addition to quenching the block in oil, the technique used in Göttingen was explored. The blocks were densely colored and allowed to cool slowly. These blocks were not strained, and could be readily cleaved into platelets. The platelets were reheated to about 600°C for a few minutes, and were then quenched on a copper plate in complete darkness. We believe that the reheating to 600°C (the value used in Göttingen) is most important. This point has not been studied in detail, however. Quenching from lower temperatures probably does not completely remove the secondary centers which form along with the F if the block is cooled slowly.

The name "Göttingen technique" refers to the second process, while the first is an "oil quench."

A block of densely colored KCl was obtained from Professor H. Pick of Stuttgart. It was cleaved, heated and quenched on a copper plate before measurements were taken. "Pick" refers to these samples. Harshaw crystals were x-irradiated at room (X-RT) and liquid nitrogen (X-LNT) temperatures. A coloration of KCl was made using sodium (KCl:Na), in which the Göttingen technique was used. Another sample was colored with potassium in pyrex. Again, the Göttingen technique was employed.

The crystals were cleaved and handled under a red light from a Kodak wratten safelight filter, series No. 2, which transmits no light to the violet of 640 mμ; otherwise, the crystals were kept completely in the dark at room temperature.

III. DATA

(1) General Shape of the Absorption Band

Figure 4 shows what might be called typical F-absorption spectra at several temperatures. The "absorption" here includes the reflection from the crystal surfaces. An adjustment has to be made so that there is no discontinuity at the point where the transition between the red and ultraviolet photocells of the Beckman occurs; hence, the zero on the y axis is arbitrary. This explains why the transmission in the long-wave region is better than that given by Fresnel's reflection equation. In the analysis of the curve we assume that the "base line" increases in going from the red to the ultraviolet, due to the scattering from the surfaces. This conclusion is supported by measurements on surfaces of various degrees of roughness. On occasion one has gases which are either adsorbed on the surface or react with it. This also changes the "base line."

Figure 5 represents what the authors believe is the absorption of the "pure" F band. These curves were obtained by subtracting the "base line"—a straight line from the red side to the lowest point on the violet side of the F band—and the K band. (See small diagram in Fig. 4.) We do not believe that the "K center" is identical to the F. (See figure in reference 7.) The theory is based on the transition between two levels, and the effect of the third level (or another center) must be eliminated.[20] If other levels exist, they will not affect the results of this paper.

The method used to eliminate the K band is somewhat arbitrary. There is, therefore, an uncertainty in the ultraviolet which will not affect M_0, H, ϵ_m, or $\bar{\epsilon}$ at low temperatures,[21] though it will influence m. Since

[18] E. Mollwo, Nach. Ges. Wiss. Göttingen II, 1932, 254.

[19] G. Glaser and W. Lehfledt, Nach. Ges. Wiss. Göttingen II, 1936, 91.

[20] We do not agree with the procedure used by Doyle (reference 6), who simply takes the net integrated area.

[21] Mador, Markham, and Platt of reference 11, used a different method to obtain H. The procedure employed here can be used on KBr. It gives a slightly *smaller* value of H than previously reported.

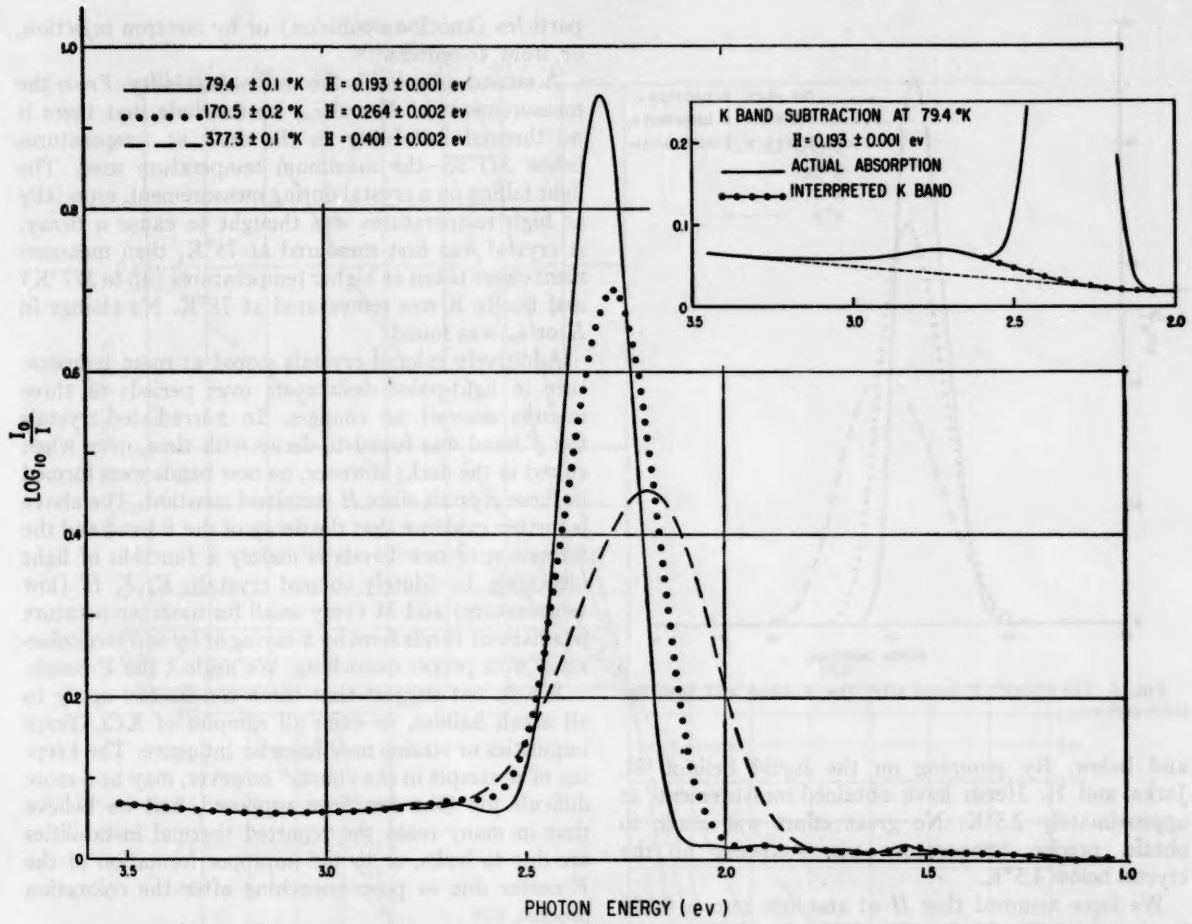
79.4 ± 0.1 °K H = 0.193 ± 0.001 ev
170.5 ± 0.2 °K H = 0.264 ± 0.002 ev
377.3 ± 0.1 °K H = 0.401 ± 0.002 ev
K BAND SUBTRACTION AT 79.4 °K
H = 0.193 ± 0.001 ev
ACTUAL ABSORPTION
INTERPRETED K BAND
LOG10 I0/I
PHOTON ENERGY (ev)

FIG. 4. The data as obtained from the spectrophotometer, and the method of obtaining the base line and the elimination of the *K* band (see text).

the *K* band elimination becomes increasingly difficult above 170°K, the burden of the analysis rests on data taken below this temperature. Here the *K* band affects *H* by less than 1%.

In disagreement with reference 5, we note the red side can be approximated by one Gaussian curve, and the violet by another. Figure 6 has been made to illustrate this point. A Gaussian curve gives a single straight line through ϵ_m on this type of plot. Notice that the curves for $\epsilon<\epsilon_m$ and for $\epsilon>\epsilon_m$ join smoothly at ϵ_m, though not as two straight lines. Since these curves join smoothly, as shown in the enlarged view, the *F* band cannot be described completely by two separate Gaussian curves. The fact that the slopes for the violet and red sides are different, shows that the *F* band is nonsymmetrical. We may extend these curves to a relative absorption value of 0.01 with essentially the same results. The slight deviation we ascribe to inaccuracies due to the low value of the absorption in the tails of the band. A similar conclusion is not possible for our unpublished data on the *F* center of NaCl.

The difference between the "pure" and the "impure" *F* band can be detected by measuring *H* at low temperature. This paper only concerns itself with the pure *F* band as far as it can be determined. In some cases a very small A band was observed at 2.07 ev at 78°K, approximately that found by Petroff.[22] It was so slight, however, that one can ignore it. The presence of the *A*, *B*, and *K* bands suggests the possibility that there may be other bands underlying the *F* band. On the basis of one or two points it is possible to "imagine" a faint band at about 2.42 ev (at 78°K). Resolution of any of these bands will involve an extreme amount of care.

(2) Effects of Sample on *H* Value—Preparation and History

In this subsection we want to answer our first question of the Introduction, A. The data is given in Table I which includes all reliable values of *H*. Since quenching is an art and hardly a science, an element of judgment has been used in preparing the table. Included in this table are values of *H* at boiling helium temperatures

[22] S. Petroff, Z. Physik **127**, 443 (1950).

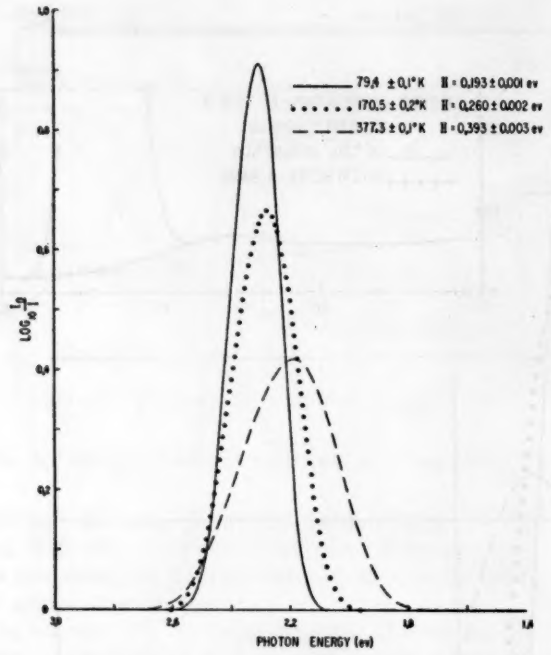

FIG. 5. The "pure" F band after the K band and base line subtractions.

and below. By pumping on the liquid helium, R. Jarka and H. Hersh have obtained measurements at approximately 2.5°K. No great effort was made to obtain precise temperature measurements of the crystal below 4.5°K.

We have assumed that H at absolute zero is 0.163 by the use of Fig. 1, where the K band was subtracted.

We conclude that the F centers prepared by various techniques are essentially identical and that the variation from crystal to crystal though measurable is very small. If a particular sample is measured many times, its value of H will be within the limits specified in Table II. There is, however, a larger variation in H due to the history of the sample. This conclusion is based on work done on the F center in KBr.[11] Since the measurement was limited to one sample, we ascribe no importance to the larger values obtained with Pick's sample or when the additive coloring was done with Na. The conclusion here is that a unique F center is formed by all methods of coloration.[23] This agrees with a previous study, provided one assumes that the additively colored previously used had been inadvertently bleached during the handling—a strong possibility. We believe that the variations reported from time to time are due to light leaks, and that it is impossible to detect any changes in the F center environment by means of optical absorption measurements. We have made no measurements on F centers formed by ionizing heavy particles (knock-on collision) or by electron injection, or from U centers.

A second question is the thermal stability. From the measurements of H and ϵ_m, we conclude that there is no thermal instability in the dark at temperatures below 377°K—the maximum temperature used. The light falling on a crystal during measurement, especially at high temperatures was thought to cause a decay. A crystal was first measured at 78°K, then measurements were taken at higher temperatures (up to 377°K) and finally it was remeasured at 78°K. No change in H or ϵ_m was found.

Additively colored crystals stored at room temperature in light-proof desiccators over periods of three months showed no changes. In x-irradiated crystals the F band was found to decay with time, even when stored in the dark; however, no new bands were formed in these crystals since H remained constant. The above is further evidence that the decay of the F band and the formation of new bands is mainly a function of light bleaching. In dilutely colored crystals, K, F, F' (low temperature) and M (very small for room temperature irradiation) bands form by x-raying or by additive coloration with proper quenching. We neglect the V bands.

We do not suggest that these conclusions apply to all alkali halides, or even all samples of KCl. Trace impurities or strains may have an influence. The keeping of a sample in the "dark," however, may be a more difficult job than has been supposed, and we believe that in many cases the reported thermal instabilities are due to leaks, or to the improper formation of the F center due to poor quenching after the coloration process.

TABLE I.

Method of coloration	Number of measurements	Average H at 78°K in ev with K band
X-raying at 78°K	2	0.193
X-raying at 300°K	7	0.195
Additive coloration with K (with both types of quenching)	13	0.195
Additive coloration with Na (Göttingen quench)	1	0.199
Additive coloration with K in glass (Göttingen quench)	1	0.195
Pick's sample (Göttingen quench)	1	0.197
Weighted average		0.195
Average value with K band subtracted		0.194
Average H at 4.5°K with K band	10	0.165
Average H at approx. 205°K (x-irradiated and measured at 2.5°K) with K band	2	0.164

[23] Identical conclusions may have been made previously in the literature. Until now this conclusion was not, however, based on reliable experimental evidence.

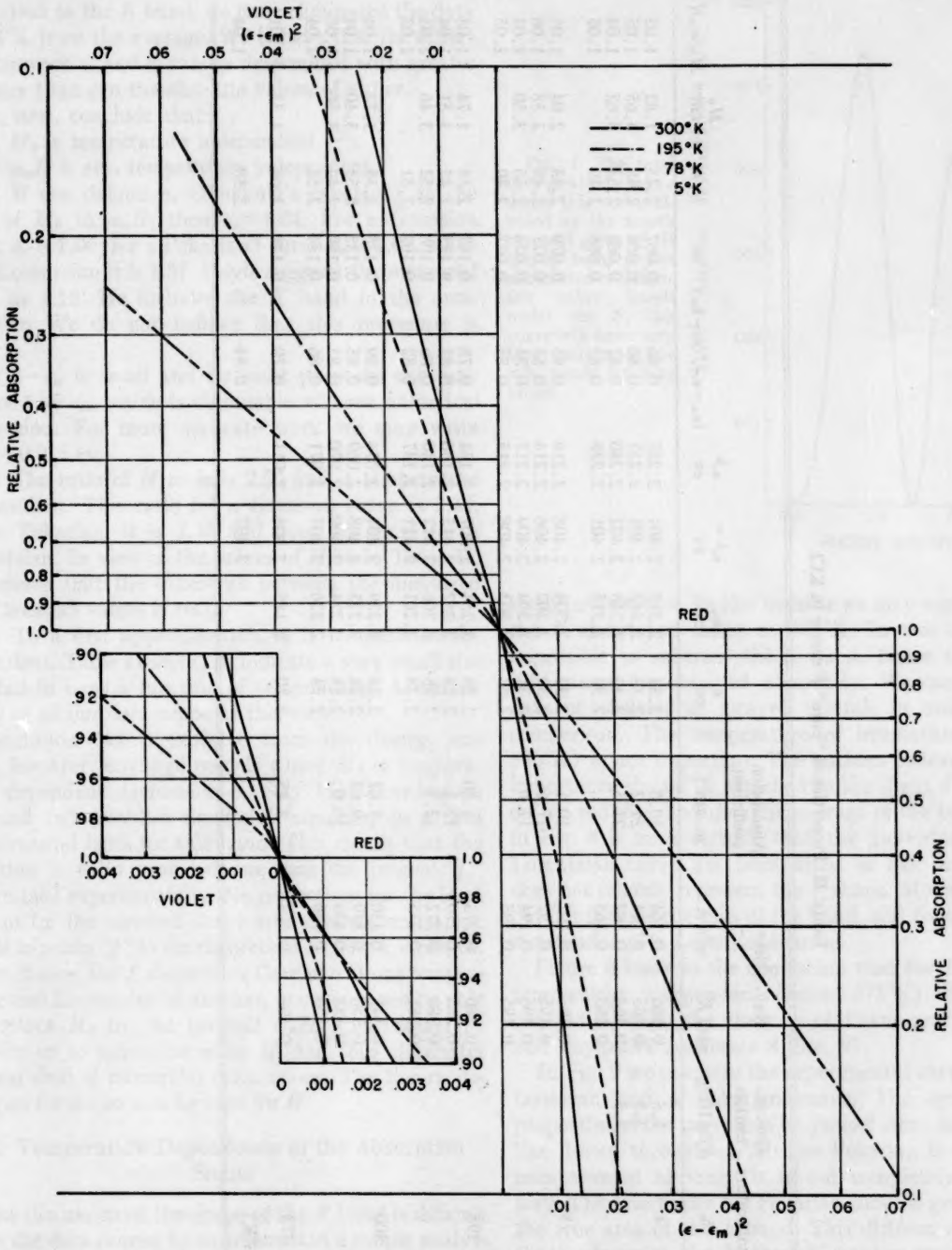

FIG. 6. Comparison of the symmetry of the two sides of the *F* band (see text).

(3) Moments of Distribution

The theory is given in terms of the moments, M_0, M_1, and m. For analytic curves various relations between these quantities exist. Since an analytic description of the *F* shape has not been given, we are forced to use numerical integration. Our procedure is illustrated in Fig. 7. If the band resulted from an overlapping of several absorption centers, the effect would show up in Fig. 7, since the shape of this curve depends critically on the absorption of the edges of the band. A composite structure, when the *F* is bleached, shows up as large bulges on the ultraviolet side. Table II shows the data at five temperatures for two additively colored crystals and for one x-rayed crystal to illustrate the reproduci-

TABLE II. Properties of "pure" F center in KCl.

Sample preparation	Temperature °K	Concentration $Nf\times10^{-1}{}_k$	Half-width[a] with K	Half-width[a] w/o K	Absorption coefficient α_m cm^{-1}	$\bar{\epsilon}$ ev	ϵ_m ev	$\epsilon_v{}^{b,c}$ ev	$\epsilon_r{}^b$ ev	$(\epsilon_m-\epsilon_r)/(\epsilon_v-\epsilon_m)$	m	H/m	M_0 ev cm^{-1}	$M_0/\alpha_m H$
X-rayed RT	4.5	1.8	0.166	0.164	10.6	2.33	2.313	2.401	2.237	0.86	0.067	2.45	1.82	1.05
Additive I		3.5	0.165	0.164	21.2	2.32	2.313	2.401	2.237	0.86	0.066	2.48	3.65	1.05
Additive II		3.5	0.164	0.162	21.5	2.32	2.313	2.402	2.240	0.82	0.064	2.53	3.62	1.04
average			0.165	0.163		2.32	2.313	2.401	2.238	0.85	0.066	2.49		1.05
X-rayed RT	78		0.193	0.192	10.1	2.32	2.304	2.408	2.216	0.85	0.079	2.43	2.04	1.05
Additive I			0.195	0.192	17.6	2.32	2.302	2.406	2.214	0.85	0.077	2.49	3.58	1.06
Additive II			0.196	0.194	17.6	2.31	2.304	2.409	2.215	0.85	0.076	2.55	3.50	1.03
average			0.195	0.193		2.32	2.303	2.408	2.215	0.85	0.077	2.49		1.05
X-rayed RT	195		0.280	0.273	6.20	2.28	2.254	2.407	2.134	0.78	0.107	2.55	1.74	1.03
Additive I			0.283	0.279	12.1	2.28	2.262	2.415	2.136	0.82	0.113	2.47	3.51	1.04
Additive II			0.280	0.272	12.3	2.28	2.266	2.412	2.140	0.86	0.108	2.52	3.46	1.03
average			0.281	0.275		2.28	2.261	2.411	2.137	0.82	0.109	2.51		1.03
X-rayed RT	300		0.347	0.330	5.02	2.24	2.229	2.404	2.074	0.89	0.128	2.58	1.72	1.04
Additive I			0.350	0.339	9.63	2.24	2.225	2.408	2.069	0.85	0.135	2.51	3.40	1.04
Additive II			0.353	0.339	10.0	2.24	2.224	2.409	2.070	0.83	0.139	2.44	3.56	1.05
average			0.350	0.336		2.24	2.226	2.407	2.071	0.86	0.134	2.51		1.04
X-rayed RT	373		0.402	0.393	3.45	2.20	2.185	2.404	2.011	0.79	0.146	2.69	1.37	1.01
Overall average (excluding 373°K)								2.407		0.84		2.50		1.04

[a] Values are within ±0.002.
[b] Values are wethin ±0.003.
[c] Without K btnd.

bility. Due to the K band, we have eliminated the data at 373°K from the average. We believe that the difference between ϵ_v and ϵ_r can be determined with greater accuracy than can the absolute values of either.

We, now, conclude that:

(a) M_0 is temperature independent.

(b) $\alpha_m H$ is also temperature independent.

(c) If one defines a_s (Smakula's constant) as the ratio of M_0 to $\alpha_m H$, then $a_s = 1.04$. For a Gaussian curve, a_s is 1.06; for a Pekarian[24] curve a_s is 1.07, while for a Lorentzian it is 1.57. Doyle suggests the measured value as 1.19. He includes the K band in the area, however. We do not believe that this procedure is correct.

(d) $\bar{\epsilon} - \epsilon_m$ is small and for most purposes one may replace $\bar{\epsilon}$ by ϵ_m, which is obtainable without numerical integration. For more accurate work we may write $\bar{\epsilon} = \epsilon_m + 0.015$ ev.

(e) The ratio of H to m is 2.50 and is temperature independent. This ratio for a Gaussian curve is 2.35. For a Pekarian, it is 2.36 and does not exist for a Lorentzian. In view of the values of H/m in Table II, we believe that the difference between the measured and Gaussian values is real.

(f) To a first approximation, ϵ_v is temperature independent. Table II seems to indicate a very small rise and fall in ϵ_v as a function of temperature. A further study of all our data supports this view.

Conclusion (a) is expected from the theory; one may, however, envisage models where M_0 is temperarure dependent (reference 8, Sec. 17). Conclusions (a) and (b) establish Smakula's equation on a firm experimental basis for this band. This means that the equation is valid provided one uses the proper "f," determined experimentally. No corrections for the local field or for the assumed shape are required, unless one wants to relate "f" to the theoretical oscillator strength. If per chance, the F shape were Gaussian at one temperature and Lorentzian at another, one would not be able to replace M_0 by the product $\alpha_m H$. Conclusion (e) permits us to substitute m by H, and thus eliminates a great deal of numerical calculations. The theory developed for m can now be used for H.

(4) Temperature Dependence of the Absorption Shape

The discussion of the shape of the F band is difficult since the data cannot be represented in a simple analytical fashion. Theory suggests (reference 8, Sec. 9) that it is Pekarian at low, and Gaussian, at high temperatures. With this purpose in mind, Fig. 8 was constructed. In it the true F absorption is divided by α_m and the photon energy is divided by H. Then by shifting the origin of the x axis we superimposed the points ϵ_v/H and ϵ_r/H for every temperature. Figure 8 indicates that the shape at 5°K is identical with that at room temperature. In like manner we may superimpose the F absorption taken at 373°K. In this case it is impossible to subtract the K band, hence the violet side cannot be obtained accurately. We can use the data of additive or x-rayed crystals in making this comparison. The temperature of irradiation (78 or 300°K) is not important. The authors believe that no importance should be attached to the slight differences on the red side, and that the average of the two curves in Fig. 8 is more reliable than the individual one. A Lorentzian curve has been fitted in like manner. It does not reliably represent the F shape. Mollwo's[2] data did not include the tails of the band, and thus gave the appearance of a Lorentzian curve.

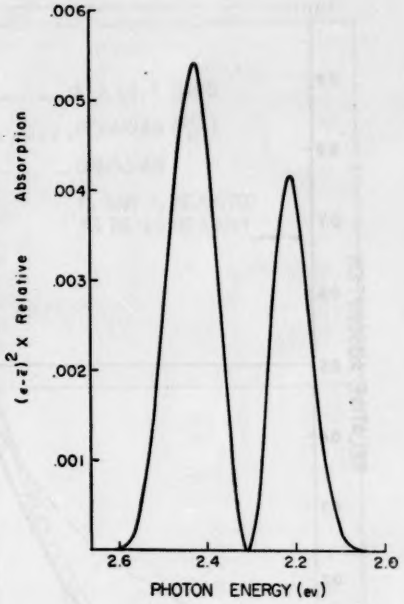

FIG. 7. The total integrated area under this curve divided by the zeroth moment gives m^2. If the K band is not subtracted or if there are other bands under the F, this curve will have very long tails and one side would be very broad.

Figure 8 leads to the conclusion that the F shape is temperature independent (below 373°K). This is in contradiction to the theories of Pekar and of Kubo and Toyozawa (reference 8, Sec. 9).

In Fig. 9 we compare the experimental curves with a Gaussian and a Pekarian curve. The symmetrical properties of the curve can be judged from the vertical line drawn through ϵ_m/H. The Pekarian is a definite improvement although it is not completely satisfactory. The area under the Pekarian curve is greater than the true area of the F band. This difference accounts for the decrease of a_s in the measured curve relative to the Gaussian or Pekarian. To further compare the measured absorption, we note that in Table II, $(\epsilon_m - \epsilon_r)/(\epsilon_v - \epsilon_m)$ is 0.84. This should be compared to a value of 0.9 obtained for a Pekarian shape (reference 8, Fig. 10). Although Pekar's analytic expression does not completely describe the data, we shall nevertheless refer to the shape by this name.

A single Gaussian is not a satisfactory representation. We may, however, obtain a simple analytical expression

[24] A Pekarian curve is defined in reference 8, Sec. 9.

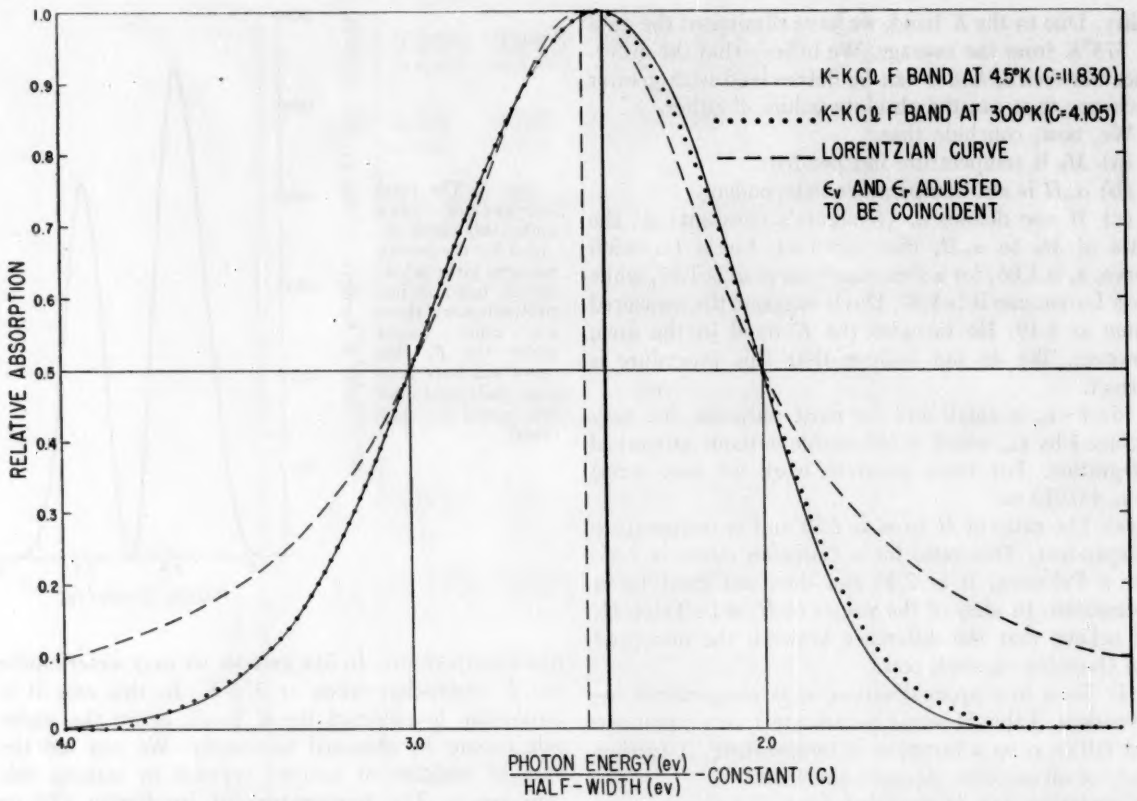

FIG. 8. Comparison of the shape of the F band at two temperatures with a Lorentzian curve. The scale is arbitrarily adjusted so that the half-widths occur at the same points. The vertical line corresponds to the peak and illustrates the nonsymmetry of the F band.

for α by using two Gaussian curves, one for $\epsilon > \epsilon_m$, and another for $\epsilon < \epsilon_m$. This is the double Gaussian. We now obtain the following experimental representation of the F band:

$$\alpha(\epsilon) = \alpha_m \exp\{-a_v^2(\epsilon-\epsilon_m)^2\} \text{ for } \epsilon > \epsilon_m$$
$$= \alpha_m \exp\{-a_r^2(\epsilon-\epsilon_m)^2\} \text{ for } \epsilon < \epsilon_m, \quad (2)$$

where

$$a_v = (1.84/H)[ln2]^{\frac{1}{2}} = (1.53/H), \quad (2a)$$

and

$$a_r = (2.19/H)[\ln 2]^{\frac{1}{2}} = (1.82/H). \quad (2b)$$

Analytical expressions for ϵ_m and H will be given in the next section. α_m can be calculated from the concentration by means of Smakula's equation. Eq. (2) is a good "experimental equation" which breaks down only at ϵ_m (Fig. 6). The equation is a better description of the curve on the violet side than on the red. While Eq. (2) can be improved by the addition of more adjustable parameters, the authors believe that it is more reliable than a limited number of absorption measurements. We stress that the equation applies only to the "pure" F center absorption in KCl (the K band is subtracted).

Before leaving this section, we should like to consider the accuracy of the data. We note that H is determined from the points where $\alpha/\alpha_m \geq \frac{1}{2}$ and a change in the base line will not have a major effect. m is determined by the tails of the F absorption (Fig. 7). In general, bands underneath the F will distort the tails and have a major influence on this "area." Measurements have been made on crystals which were poorly quenched. In this case, there is little relation between H and m (Table III). Column 13 of Table II, however, indicates that the ratio of H to m is constant, and approximately the expected theoretical value. This, we believe, is a very good indication that the procedure used here is valid. This includes our method of getting the data and its treatment. A critical step in this whole experiment is the preparation of the crystal. This was to be expected from previous measurements on the properties of the F center.[18,19] Our procedure of preparation is identical with that of Becker and Pick,[25] hence one suspects that our centers will give pure F luminescence.

IV. ANALYSES

(1) H vs θ

In Fig. 1 we compare various reported values of H.[26] Differences of the order of 0.005 ev are to be ex-

[25] K. Becker and H. Pick, Nach. Ges. Wiss. Göttingen II, 1956, 167.

[26] C. Z. van Doorn and Y. Haven, Philips Research Repts. **11**, 479 (1956); W. D. Compton and C. C. Klick, Phys. Rev. **110**, 349 (1958); E. Burstein and J. J. Oberly, "Low Temperature Physics," Natl. Bur. Standard Circ. No. 519, 285 (1952).

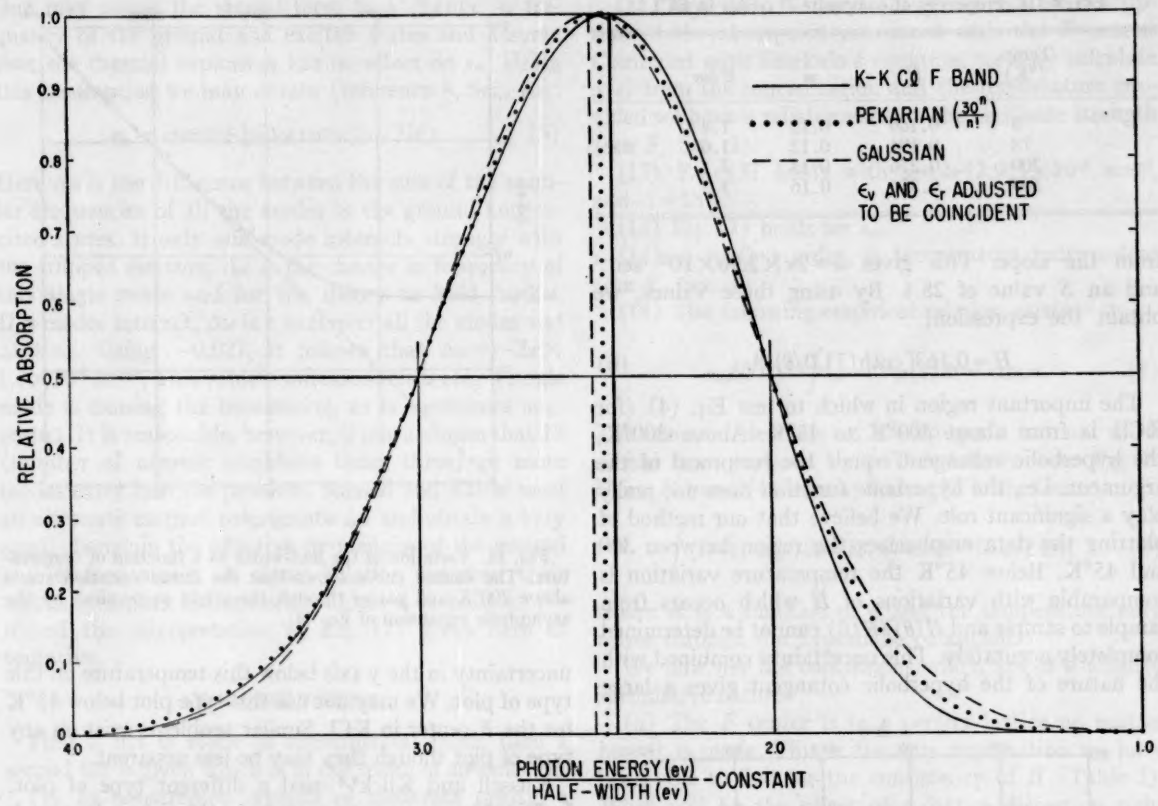

FIG. 9. Comparison of the shape of the *F* band with the Gaussian and the Pekarian shape.

pected, depending on the method used to obtain the "base line." Differences of the same order will occur depending on the history and purity of the sample. The H determined by the same method on two samples colored by the identical process vary by 0.002 to 0.004 ev. These two corrections do not account for the discrepancy shown between our data and the study of Mollwo, of Russell and Klick, and of Kanzaki.[27] Van Doorn and Haven report only one significant figure. Kanzaki reports his values to three significant figures.

The simplest theory (reference 4, and reference 8, Sec. 10) gives the following relation:

$$m^2=\hbar^2\omega^2 S\coth[(\hbar\omega/2k\theta)] \qquad (3)$$

where S is the Huang Rhys factor, ω is the effective phonon angular frequency (ground state), and θ is the absolute temperature; while $\hbar$ and k have their usual meaning. In view of the measurements given in Table II we replace m by $H/2.50$ and write;

$$H^2(\theta)=H^2(0)\coth(\hbar\omega/2k\theta), \qquad (4)$$

where

$$H(0)=2.50\hbar\omega S^{\frac{1}{2}}. \qquad (5)$$

We obtain $H(0)\approx H(4°\text{K})$ directly from Fig. 1; hence, there is only one unknown ω. The data should answer two questions: (a) Does relation (4) hold and; (b) What is ω? To answer these questions we plot $\coth^{-1}[H^2(\theta)/H^2(0)]$ against $1/\theta$. The result is given in Fig. 10. At some temperatures a great many values have been taken, and the average of H is known. At others, only one value has been measured. The vertical lines, therefore, represent our best judgment as to the uncertainties. The uncertainty increases as θ approaches zero, since $H^2(\theta)/H^2(0)$ approaches unity. Because of the uncertainty in H due to the history of the crystal, one may not extend this curve to temperatures below 45°K.

We conclude from Fig. 10 that Eq. (4) truly represents the temperature variation of H, and we find no measurable deviation from this equation. One may show that if two frequencies are important for the broadening, or if a temperature independent term should be added to (4), that it could be detected on the plot shown in Fig. 10 (reference 8, Sec. 11). We hence conclude that no effects such as proposed by Meyer[28] exists. Further, only modes of a single frequency affect the *F* center. From this data we are unable to decide on the number of modes. The frequency, however, is measured

[27] Kanzaki, Phys. Rev. **110**, 1063 (1958). He suggests that his data agree with that reported in reference 7. Our comparison of the published values does not support his conclusion.

[28] H. J. G. Meyer, Physica **20**, 1016 (1954).

TABLE III. Properties of composite F center in KCl.

Temp. (°K)	H	m	H/m
5	0.169	0.12	1.4
78	0.194	0.12	1.6
200	0.276	0.13	2.1
300	0.356	0.16	2.2

from the slope. This gives $\omega=2\pi\times2.96\times10^{12}$ sec^{-1} and an S value of 28.4. By using these values, we obtain the expression;

$$H=0.163[\coth(71.0/\theta)]^{\frac{1}{2}}. \quad (6)$$

The important region in which to test Eq. (4) (for KCl) is from about 300°K to 45°K. Above 300°K, the hyperbolic cotangent equals the reciprocal of the argument, i.e., the hyperbolic function does not really play a significant role. We believe that our method of plotting the data emphasizes the region between 300 and 45°K. Below 45°K the temperature variation is comparable with variations of H which occurs from sample to sample and $H(\theta)/H(0)$ cannot be determined completely accurately. This uncertainty combined with the nature of the hyperbolic cotangent gives a large uncertainty in the y axis below this temperature on this type of plot. We may not use this type plot below 45°K for the F center in KCl. Similar problems exist on any type of plot though they may be less apparent.

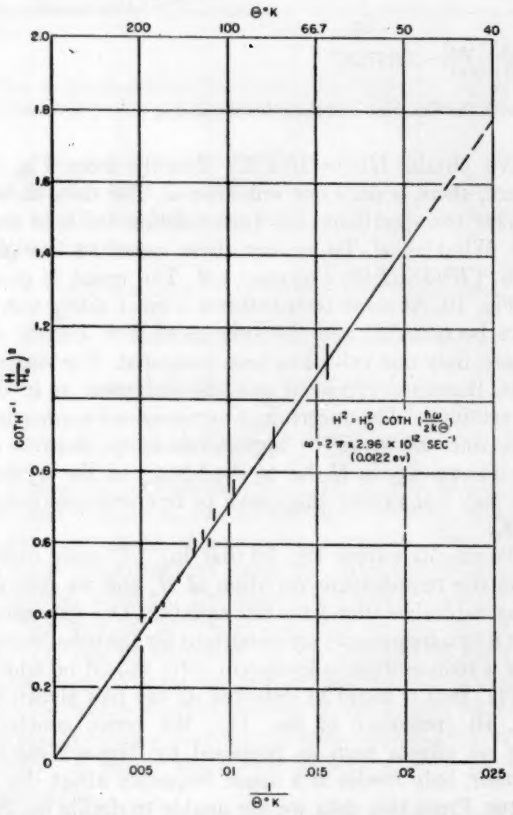

FIG. 10. Hyperbolic cotangent plot of the measured values of the half-width vs the reciprocal of the temperature. From this graph the frequency of the local modes is determined.

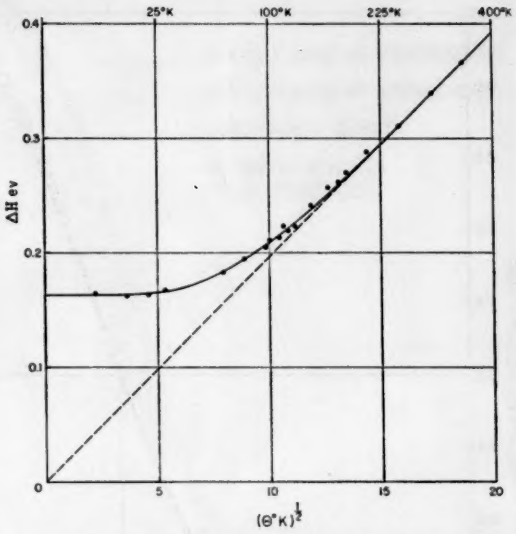

FIG. 11. Variation of the half-width as a function of temperature. The dashed curve shows that the linear variation starts above 200°K and passes through the origin as required by the asymptotic expansion of Eq. (4).

Russell and Klick[3,4] used a different type of plot. In Fig. 11 we present our data in this form since such plots have appeared several places. Note that the data gives a straight line only at high temperature (above 200°K), and it is difficult to judge whether the departure from a straight line is given correctly by Eq. (4).

(2) ϵ_m vs θ

From Fig. 12, the following expression has been obtained for the peak absorption in ev:

$$\epsilon_m=2.340-0.027\coth(71.0/\theta). \quad (7)$$

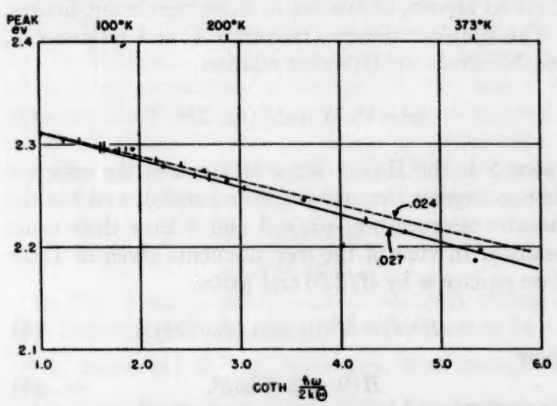

FIG. 12. Variation of the peak wavelength of the F band as a function of temperature. From the slope of this curve the empirical constants of Eq. (7) are derived.

One may relate the second term to a change in frequency of the ground and excited states and assume that the thermal expansion has no effect on ϵ_m. Using this assumption we may obtain (reference 8, Sec. 10):

$$\epsilon_m = \text{const} + \tfrac{1}{2}\hbar\Delta\omega \coth(\hbar\omega/2k\theta). \quad (8)$$

Here $\Delta\omega$ is the difference between the sum of the angular frequencies of all the modes in the ground and excited states. If only one mode interacts strongly with the trapped electron, $\Delta\omega$ is the change in frequency of this single mode and for the theory to hold $\Delta\omega \ll \omega$. If n modes interact, $\Delta\omega$ is a sum over all the modes and $\Delta\omega \ll n\omega$. Using -0.027, it follows that $\Delta\omega = -2\pi \times 1.3 \times 10^{13}$ sec^{-1}. This value is unreasonable if only a single mode is causing the broadening, as is sometimes suggested. It is reasonable, however, if one assumes that 18 (number of nearest nieghbors times three) or more modes enter into the problem. Russell and Klick[3] used an alternate method to estimate $\Delta\omega$ and obtain a very small change in the effective frequencies of the ground and excited states. A direct relation between their results and ours is impossible unless n is known. We regard the interpretation of Eq. (7) given here as tentative.

V. CONCLUSIONS

First a list is made of experimental facts, then a second list is given which is in the realm of speculation.

(1) In nonstrained crystals of moderate purity, a unique F center is formed. The absorption shape is independent of the way it is produced. Slight variations occur because of the past history of the sample[29] (see A, Sec. I).

(2) The F centers produced by additive coloration are completely stable in the dark at room temperatures and below (see B, Sec. I).

(3) Aging in the dark does not produce coagulation bands (M, R, N, etc) or colloids (see B, Sec. I).

(4) Our measured absorption concerns processes which involve only two bound states; otherwise, we would not have obtained such a simple H to m relation.

(5) $m = cH$, where c is independent of θ ($c = 0.40$).

(6) $\bar{\epsilon}$ approximately equals ϵ_m ($\bar{\epsilon} = \epsilon_m + 0.015$ in ev).

(7) M_0 is temperature independent.

(8) $\alpha_m H$ is porportional to M_0; this establishes Smakula's equation experimentally ($a_s = 1.04$) (see D, Sec. I).

(9) The shape below 373°K is independent of the temperature.

(10) The shape is nonsymmetrical but can be approximated very well by two Gaussians.

(11) Eqs. (2), (4), and (7) give a reliable description of the absorption associated with the F center. Combined with Smakula's equation, we may calculate $\alpha(\epsilon)$ from the concentration and the temperature provided we have a reliable value of the oscillator strength (see F, Sec. I).

(12) Eq. (3) holds with $\omega = 2\pi(2.96) \times 10^{12}$ sec^{-1}, and $S = 28.4$.

(13) Eq. (7) holds for ϵ_m.

(14) ϵ_v to first order, is temperature independent (see E, Sec. I).

(15) The following empirical relation exists:

$$(\alpha_m H^{n+1})^{-1} \int (\epsilon - \bar{\epsilon})^n \alpha(\epsilon) d\epsilon = \text{const}. \quad (8)$$

The constant depends on the integer n but not on θ. ϵ_m has been replaced by $\bar{\epsilon}$. This follows from Fig. 8. Using (1) and (4) we may write (8) in the form:

$$\int (\epsilon - \bar{\epsilon})^n \alpha(\epsilon) d\epsilon = K(n) \coth^{n/2}(\hbar\omega/2k\theta), \quad (9)$$

where K is a function of n and the temperature only arises through the hyperbolic cotangent.

We now list the conclusions which are of a slightly speculative nature:

(a) The F center is in a perfect lattice no matter how it is made. This is the only explanation we have been able to find for the consistency of H (Table I). What will be the effect of a lattice distortion right around the F center? If we are dealing with local modes, ω is in the forbidden gap and the frequencies of these modes will not be greatly affected by a distortion. The way the ions are displaced, and the wave function in the excited state will, however, be affected. This means a change in S, which would have been detected[30] (for a complete definition of S, and an analysis of the problem, see the Appendix).

(b) The F center is mainly influenced by local modes which are more than one in number. We arrive at this because of the values of ω and $\Delta\omega$.

(c) We believe that Pekar's explanation of the shape of the F band at low temperatures is correct (reference 8, Sec. 9).[31] Higher order terms must be added to explain the shapes at high temperatures. This conclusion is somewhat weak because it fails to explain why the shape is temperature independent. It seems, however, to be the only appropriate one in view of the theory and data.

(d) The thermal shift in the peak position is explained in terms of a frequency change (reference 8, Sec. 10), i.e., -0.027 of Eq. (7) is really an effect due

[29] We have not studied centers made by radiation which could directly knock ions out of their lattice sites, those made from U centers, nor those made by electron injection. We believe these F centers will be identical with those described here. This is only an assumption which should be checked. Compton's value (see Fig. 1) was obtained on crystals colored by 50 kv x-rays and 2 Mev electrons. The value of H remained the same. This supports our conclusions.

[30] There are several experiments which can most readily be explained in terms of centers which are close together. We do not question these experiments or their interpretations, but point out an essential difficulty which at present has not been resolved.

[31] Pekar assumes that $\Delta\omega = 0$; this is only approximately true as can be seen from Eq. (7). The positions of the emission data also suggest this (reference 8, Secs. 9 and 10).

to a frequency change between the ground and excited states. This means that ϵ_m is not simply a function of the interionic distances as has been suggested in the past. The thermal change of ϵ_m between 4° to 300°K is about a third of that obtained in going from one alkali halide to another.[32]

(e) Sources for the creation of negative-ion vacancies exist, and play a role in x-rayed, and in additively colored crystals. While the F center is in a nearly perfect environment [(a) in the foregoing], it is slightly influenced by the sample's past history and purity. We could not explain these deviations if the center formation only involved the perfect lattice.

The difference between (a) and (e) is the proximity of the vacancy source. It must be at least four or five lattice sites away. This means that vacancies make quite a few jumps during F center formation (even at 4°K) which is most difficult to understand.

We believe that the major conclusions, the first set (1 to 15) are on firm ground about which there can be little question. The authors are well aware that some experimental data exist that do not agree with the second list (a) to (e). This list, however, seems to be the only possible one at this stage of the development of our knowledge.

ACKNOWLEDGMENT

We would like to thank Dr. H. N. Hersh and Dr. G. A. Noble for the use of their equipment and many helpful suggestions, Dr. W. D. Compton for measurements of H at liquid nitrogen temperature, R. Jarka for the use of his data at helium temperature, and Professor H. Pick for additively colored crystals. We also acknowledge some very helpful discussions with Professor F. Seitz and Professor R. Hilsch.

VI. APPENDIX

Here an argument is presented to indicate why we believe that a distortion of the lattice will influence $H(0)$ but not ω. Most probably the modes which influence the F centers are the local ones which cluster about negative-ion vacancies. In a linear chain one may show that these modes are in the forbidden gap.[33] The concept of a "forbidden gap" can not be applied to the actual modes of an alkali halide without modifications. Nevertheless, we expect that the frequency of the local modes is confined to a small region between the optical and acoustical branches. Hence, the presence of a point imperfection near an F center will not greatly influence ω of Eq. (3).

The authors believe, however, that S will be sensitive to nearby point imperfections. To show this, we require the development of reference 8. S, of our Eq. (3), has the form:

$$S=(2\hbar\omega^3)^{-1}\sum_j \epsilon_j^2, \tag{10}$$

where we are using an effective frequency. If the q_j's are the coordinates associated with the local modes, then;

$$\epsilon_j=\int(\partial V/\partial q_j)(\phi_\mu^2-\phi_g^2)d\tau. \tag{11}$$

Here V is the potential in which the trapped electron finds itself; the q_j's have the dimension of length (mass)$^{\frac{1}{2}}$, while ϕ_μ and ϕ_g are the upper and ground state wave functions. To obtain Eq. (11) Feynman's theory has been used.

$(\partial V/\partial q_j)$ acts like a generalized force and may for some region in space have a r^{-2} dependence. The authors believe that $(\partial V/\partial q_j)$ and ϕ_g will not be very sensitive to a nearby imperfection, although the relation between the q's and the ionic displacements may be slightly affected. ϕ_u spreads over five lattice sites and will be greatly influenced by imperfections surrounding the negative-ion vacancies. We, therefore, believe that an imperfection close to an F center will lead to changes in ϵ_j of at least several percent. In view of Eq. (10), this means a change in $H(0)$ of several percent as well. Table I indicates that one would require a series of measurements to be certain of the value of H to 2% but that such accuracies are possible.

Actually, we would expect ϕ_u to change appreciably if there were a point imperfection within three to five lattice distances. H will vary more than 2 or 3% and our measurements would readily detect the change. It is important to remember that the excited wave function is involved in $H(0)$. Of course, if only a small fraction of the negative-ion vacancies are near imperfections, our technique of measurement will not detect them.

Note added in proof.—An analysis of the data of Fig. 10 by the method of least squares would not fit the curve as drawn unless each point were individually weighted. This graph was therefore drawn subjectively and is the "best" line in the authors' opinion.

---

[32] Ivey's relation [H. T. Ivey, Phys. Rev. **72**, 341 (1947)] holds very well for the F center in LiF, NaF, KF, NaCl, KCl, KBr, and KI when ϵ_m is measured at 4°K, and the standard interionic distances are used; F. Seitz, *Modern Theory of Solids* (McGraw-Hill Book Company, New York, 1940), p. 52.

[33] Mazur, Montroll, and Potts, J. Wash. Acad. Sci. **46**, 2 (1956).

Theory of the Heat of Transport of Electrolytic Solutions*

EUGENE HELFAND,† *Bell Telephone Laboratories, Incorporated, Murray Hill, New Jersey*

AND

JOHN G. KIRKWOOD,‡ *Sterling Chemistry Laboratory, Yale University, New Haven, Connecticut*

(Received September 2, 1959)

The limiting concentration dependence of the heat of transport of an ionic component of a dilute solution of electrolyte is determined. The theory is based on recasting the Bearman-Kirkwood statistical mechanical expression for the heat current into a form linear in the particle diffusion currents and identifying the coefficients with the heat of transport. Ion-ion interactions are treated exactly to order $c^{\frac{1}{2}}$ by using a nonequilibrium correlation function determined from the Debye-Hückel radial distribution function by Brownian particle theory. A hydrodynamical model is employed for the analysis of the effect of ion-solvent interactions. Indications are that the latter contributions are often, but not always, negligible. There is accord between the theory and experimental data.

I. INTRODUCTION

SEEBECK'S measurements of the thermoelectric potential in a metallic circuit were the first recorded systematic observations on an irreversible heat-matter cross effect. Since that time (1824), other manifestations of these effects, such as thermal diffusion, the Soret stationary state, and the Dufour effect, have been the object of extensive research. Agar has reviewed the field, emphasizing the behavior of electrolytic solutions.[1]

In describing the afore-mentioned processes one may use, equivalently, the heat of transport, the transported entropy, the thermal diffusion ratio, the Soret coefficient, or any of a number of quantities which are all related. The heat of transport was first introduced by Eastman in his quasi-thermodynamic studies of thermal diffusion. The utility of this quantity in a systematic formulation of irreversible thermodynamics from the point of view of the linear laws and reciprocal relations is brought out in the monograph of DeGroot.[2]

Recent years have witnessed several important developments in the field of heat-matter cross effects. On the experimental side Agar and co-workers have developed three independent means of measuring the heat of transport of electrolytes in the range of applicability of limiting laws. Further details of these techniques are discussed in Sec. 9.

Of more direct relevance to the present work is Bearman, Kirkwood, and Fixman's calculation of the heat of transport of a nonelectrolyte in solution.[3] Their formulation is based on more comprehensive principles of statistical mechanics than earlier lattice theories [the lattice theories[4,5] amount to a neglect of the difference between singlet and pair space velocities (cf. Sec. 2) and an approximation to the remaining terms], and serves as a basis for the extension to electrolytic solutions.

Although Bearman, Kirkwood, and Fixman adopt a semiphenomenological approach in their paper, the same results may be obtained by application of Brownian motion theory, and it is the latter scheme which we shall employ. There are two new difficulties which arise. The first is that the Fokker-Planck-Chandresekhar equations, from which a statistical theory of the phenomenological coefficients can be derived,[6] is an equation applicable when there are mostly small momentum changes in a force relaxation time,[7] and is therefore not obviously suited for systems containing ionic components. This problem has recently been examined and it is found that the obstacle can be surmounted by treating the short range and the long range forces separately.[8] The former give rise to the usual dissipative terms with friction constants which are autocorrelation functions of the short range part of the forces only. Poisson's equation provides a means of handling the long range Coulomb forces. In this way one obtains equations equivalent to those employed by Debye, Hückel, Onsager, and Falkenhagen in their formulations of the limiting laws for conduction, diffusion, and viscosity.

A second predicament is that the ion-solvent interaction effects cannot be treated solely by means of the method outlined in the previous paragraph. Thus, in the theory of conduction and diffusion one must introduce an electrophoretic drag. So, too, in the theory of the heat of transport it will be found that the ion-solvent effects require special attention. This problem has not been completely solved, but the analysis in

* Based in part on a dissertation submitted by Eugene Helfand in partial fulfillment of the requirements for the degree of Doctor of Philosophy at Yale University.

† National Science Foundation Predoctoral Fellow, 1955–1958.

‡ Posthumously.

[1] J. N. Agar, Revs. Pure Appl. Chem. **8**, 1 (1958).

[2] S. R. DeGroot, *Thermodynamics of Irreversible Processes* (North-Holland Publishing Company, Amsterdam, 1952).

[3] (a) Bearman, Kirkwood, and Fixman, *Advances in Chemical Physics* (Interscience Publishers, Inc., New York, 1958), Vol. I, p. 1.

[3] (b) R. J. Bearman and J. G. Kirkwood, J. Chem. Phys. **28**, 136 (1958).

[4] K. Wirtz, Ann. Physik **36**, 295 (1939).

[5] K. G. Denbigh, Trans. Faraday Soc. **48**, 1 (1952).

[6] J. G. Kirkwood, J. Chem. Phys. **14**, 180 (1946).

[7] Reference 6; and John Ross, J. Chem. Phys. **24**, 375 (1956).

[8] E. Helfand, dissertation, Yale University (1958).

Sec. 6 indicates that contributions are small for many salts of interest.

After a brief review of the pertinent principles of the statistical mechanics of irreversible processes and of the phenomenological theory of heat-matter cross terms, we shall present the details of the calculation of the heat of transport of strong electrolytes. As with many other properties of ionic species, a $c^{\frac{1}{2}}$ (c is concentration) limiting behavior in dilute solutions is found. It is this limiting slope which will be specifically calculated.

2. STATISTICAL EXPRESSIONS FOR IRREVERSIBLE FLOWS

Ensemble theory may be profitably applied to systems either in or out of thermodynamic equilibrium. Explicit calculations divide into two parts. The first is the formulation of expressions for the desired properties as tractable functionals of low order distribution functions and the molecular properties. The second is the determination of the required distribution functions. The former task has been performed with about equal success for equilibrium and steady-state systems and this section presents aspects of this previous work which are relevant to the heat of transport calculation. Details may be found in another reference.[3b]

The system under consideration is composed of ν ionic species, in numbers $N_1, \cdots, N_\nu$, and N_0 solvent molecules. Each ion is envisioned as a hard sphere charge so that its microscopic state is specified by three dimensional position and momentum vectors. The solvent molecules will be viewed as point dipoles so that two additional degrees of freedom are relevant. These are specified by a directional vector, for example $\mathbf{e}_\mu$, a unit vector in the direction of the dipole $\boldsymbol{\mu}$, and the conjugate angular momenta (which will not enter into the calculation).

In the treatment of electrolytes in solution, certain phenomena can be taken into account by considering the solvent as a dielectric continuum. The hypothesis is that the effect of preferential orientation of solvent in the neighborhood of an ion can be emulated by introducing a dielectric constant into the mutual interaction potentials, $V_{\alpha\beta}$. This is done after the statistical formulas have been integrated down to pair space.

Statistically mechanically, the properties of the system are described by generic distribution functions, $f_{\alpha\beta}^{(2)}$, in the space of pairs. For α and β ionic $f_{\alpha\beta}^{(2)}(\mathbf{r}_1, \mathbf{r}_2, \mathbf{p}_1, \mathbf{p}_2)d^3\mathbf{r}_1 d^3\mathbf{r}_2 d^3\mathbf{p}_1 d^3\mathbf{p}_2$ is the probability of simultaneously finding a particle of type α within $d^3\mathbf{r}_1$, $d^3\mathbf{p}_1$ of the state $\mathbf{r}_1$, $\mathbf{p}_1$ and one of type β within $d^3\mathbf{r}_2$, $d^3\mathbf{p}_2$ of $\mathbf{r}_2$, $\mathbf{p}_2$. No time dependence is indicated since consideration will be limited to stationary states. The distribution functions $f_{\alpha 0}^{(2)}(\mathbf{r}_1, \mathbf{r}_2, \mathbf{e}_{\mu 2}, \mathbf{p}_1, \mathbf{p}_2)$ and $f_{00}^{(2)}(\mathbf{r}_1, \mathbf{e}_{\mu 1}, \mathbf{r}_2, \mathbf{e}_{\mu 2}, \mathbf{p}_1, \mathbf{p}_2)$ contain dependency on the orientation of the solvent.

An integration of $f_{\alpha\beta}^{(2)}$ over $\mathbf{r}_2$, $\mathbf{p}_2$, that is over the possible states of β, yields the singlet space generic distribution function $f_\alpha^{(1)}$.

If $f_{\alpha\beta}^{(2)}$ is integrated over momenta $\mathbf{p}_1$ and $\mathbf{p}_2$, the pair space concentration, $c_{\alpha\beta}^{(2)}$, results. A further integration over position of β yields the ordinary particle concentration, c_α. For $\alpha=0$ (solvent) an integration over orientations, $\mathbf{e}_{\mu 1}$, is required to obtain $c_0(\mathbf{r}_1)$, but in the absence of external fields $c_0(\mathbf{r}_1)=4\pi c_0(\mathbf{r}_1, \mathbf{e}_{\mu 1})$.

For the description of pair space concentration, it is convenient to introduce a correlation function, $g_{\alpha\beta}^{(2)}$, by means of the equation $c_{\alpha\beta}^{(2)}=c_\alpha c_\beta g_{\alpha\beta}^{(2)}$.

The particle diffusion currents, $\mathbf{j}_\alpha$, which have magnitude equal to the average number of particles of type α crossing unit normal area per unit time, are related to the average velocities, and are given by

$$\mathbf{j}_\alpha = c_\alpha(\mathbf{u}_\alpha - \mathbf{u}) = \int (1/m_\alpha)(\mathbf{p}_1 - m_\alpha \mathbf{u}) f_\alpha^{(1)} d^3\mathbf{p}_1. \quad (2.1)$$

The mass average velocity, $\mathbf{u}$, is

$$\mathbf{u} = \sum_{\alpha=0}^{\nu} m_\alpha c_\alpha \mathbf{u}_\alpha \Big/ \sum_{\alpha=0}^{\nu} m_\alpha c_\alpha. \quad (2.2)$$

Similarly, a pair space particle diffusion current may be defined by

$$\mathbf{j}_{\alpha\beta,1}^{(2)} = c_{\alpha\beta}^{(2)}(\mathbf{u}_{\alpha\beta,1}^{(2)} - \mathbf{u})$$

$$= \iint (1/m_\alpha)(\mathbf{p}_1 - m_\alpha \mathbf{u}) f_{\alpha\beta}^{(2)} d^3\mathbf{p}_1 d^3\mathbf{p}_2. \quad (2.3)$$

Physically, the pair space velocity $\mathbf{u}_{\alpha\beta,1}^{(2)}$ is the average velocity of particles of type α at $\mathbf{r}_1$ (with orientation $\mathbf{e}_{\mu 1}$ if solvent) when a particle of type β is at $\mathbf{r}_2$ (with $\mathbf{e}_{\mu 2}$). The subscript 1 of $\mathbf{j}_{\alpha\beta,1}^{(2)}$ and $\mathbf{u}_{\alpha\beta,1}^{(2)}$ indicates that the vector is in the space of the particle at $\mathbf{r}_1$.

The heat current density, $\mathbf{q}$, by definition is the total energy flow (relative to the mass average velocity) less the diffusive flow of energy and work. This latter part which is subtracted off for convenience of the thermodynamic theory is

$$\sum \mathbf{j}_\alpha(\bar{E}_\alpha + p\bar{v}_\alpha) = \sum \mathbf{j}_\alpha \bar{H}_\alpha,$$

where $\bar{E}_\alpha$, $\bar{v}_\alpha$, and $\bar{H}_\alpha$ are, respectively, the partial molecular energy, volume, and enthalpy, and p is the pressure.

Irving and Kirkwood[9] derived a statistical expression for the heat current density of a pure fluid by comparing the equation of energy transport obtained from macroscopic considerations with that gotten from the Liouville equation. Bearman and Kirkwood[3b] have generalized this result to mixtures. The form of the

[9] J. H. Irving and J. G. Kirkwood, J. Chem. Phys. **18**, 817 (1950).

heat current density appropriate to the present problem is

$$\mathbf{q}=\mathbf{q}_K+\mathbf{q}_V-\sum_{\alpha=0}^{\nu}\mathbf{j}_\alpha\bar{H}_\alpha, \tag{2.4}$$

$$\mathbf{q}_K=\sum_{\alpha=0}^{\nu}\int(1/2m_\alpha^2)(\mathbf{p}_1-m_\alpha\mathbf{u})^2(\mathbf{p}_1-m_\alpha\mathbf{u}) \times f_\alpha^{(1)}(\mathbf{r}_1,\mathbf{p}_1)d^3\mathbf{p}_1, \tag{2.5}$$

$$\mathbf{q}_V=(\mathbf{q}_V)_{\text{ion-ion}}+(\mathbf{q}_V)_{\text{ion-solv}}+(\mathbf{q}_V)_{\text{solv-solv}}, \tag{2.6}$$

$$(\mathbf{q}_V)_{\text{ion-ion}}=\tfrac{1}{2}\sum_{\alpha=1}^{\nu}\sum_{\beta=1}^{\nu}\int[V_{\alpha\beta}(r)\mathbf{1}-\mathbf{r}\nabla_r V_{\alpha\beta}(r)] \cdot\mathbf{j}_{\alpha\beta,1}^{(2)}(\mathbf{r}_1,\mathbf{r}_2)d^3\mathbf{r}, \tag{2.7}$$

$$(\mathbf{q}_V)_{\text{ion-solv}}=\tfrac{1}{2}\sum_{\alpha=1}^{\nu}\iint[V_{\alpha 0}(\mathbf{r},\mathbf{e}_\mu)\mathbf{1}-\mathbf{r}\nabla_r V_{\alpha 0}(\mathbf{r},\mathbf{e}_\mu)] \cdot[\mathbf{j}_{\alpha 0,1}^{(2)}(\mathbf{r}_1,\mathbf{r}_2,\mathbf{e}_\mu)+\mathbf{j}_{0\alpha,1}^{(2)}(\mathbf{r}_1,\mathbf{r}_2,\mathbf{e}_\mu)]d^3\mathbf{r}d^2\mathbf{e}_\mu, \tag{2.8}$$

$$(\mathbf{q}_V)_{\text{solv-solv}} =\tfrac{1}{2}\iiint[V_{00}(\mathbf{r},\mathbf{e}_{\mu 1},\mathbf{e}_{\mu 2})\mathbf{1}-\mathbf{r}\nabla_r V_{\alpha 0}(\mathbf{r},\mathbf{e}_{\mu 1},\mathbf{e}_{\mu 2})] \cdot\mathbf{j}_{00,1}^{(2)}(\mathbf{r}_1,\mathbf{r}_2,\mathbf{e}_{\mu 1},\mathbf{e}_{\mu 2})d^3\mathbf{r}d^2\mathbf{e}_{\mu 1}d^2\mathbf{e}_{\mu 2}, \tag{2.9}$$

where these equations are to be applied with the dielectric continuum approximation.

The vector $\mathbf{q}_K$ is the mean kinetic energy current density. The flow $\mathbf{q}_V$ arises directly from the mutual interactions. Each of its integrals has two parts. The term containing the potentials $V_{\alpha\beta}$ represents the mean flow of potential energy crossing unit surface with the particles. The portion with the forces, $\nabla_r V_{\alpha\beta}$, arises from work done by particles on one side of a unit surface on those located on the other side. This results in a flow of work, or, equivalently, energy, across this surface.

3. PHENOMENOLOGY OF HEAT OF TRANSPORT

The heat of transport§ of component α, Q_α^*, may be operationally defined in two seemingly different ways. This duality is a consequence of the Onsager reciprocal relations.

The first definition refers to a system in mechanical equilibrium ($\nabla p+\sum c_\alpha\mathbf{X}_\alpha=0$, where $\mathbf{X}_\alpha$ is the external force on a particle of type α) and in a Soret stationary state (all particle diffusion currents equal to zero). Under such conditions the gradients of total chemical potential are related to the temperature gradient by the proportionality

$$\nabla_T\tilde{\mu}_\alpha=-Q_\alpha^*\nabla\ln T. \tag{3.1}$$

§ Our Q_α^* is not DeGroot's Q_α^* (reference 2). It is similar to his Q_α^{**} except that ours is on a per mole, rather than a per gram, basis, and is not defined relative to a reference component.

The total chemical potential, $\tilde{\mu}_\alpha$, is equal to a chemical part plus the potential of any external force. The symbol ∇_T indicates that the gradient does not include that part due to the functional dependence of $\tilde{\mu}_\alpha$ on T, so that

$$\nabla_T\tilde{\mu}_\alpha=\nabla\tilde{\mu}_\alpha-(\partial\mu_\alpha/\partial T)_{p,\tau}\nabla T, =\nabla\tilde{\mu}_\alpha+T\bar{S}_\alpha\nabla\ln T. \tag{3.2}$$

The Gibbs-Duhem equation for a system in mechanical equilibrium is

$$\sum c_\alpha\nabla_T\tilde{\mu}_\alpha=0, \tag{3.3}$$

which may be combined with Eq. (3.1) to yield the relation

$$\sum c_\alpha Q_\alpha^*=0. \tag{3.4}$$

The above definition, or its extension to systems with diffusion, serves as the basis for most experimental determinations of the heat of transport. It may also be employed in a theoretical development. Work is being done at present on this aspect of the problem, but the tack adopted in this paper revolves about an alternative picture of the heat of transport.

In a system in which no temperature gradients exist the heat flow is given by

$$\mathbf{q}=\sum Q_\alpha^*\mathbf{j}_\alpha. \tag{3.5}$$

Since the particle diffusion currents are not linearly independent [cf. Eqs. (2.1) and (2.2)], the further condition

$$\sum c_\alpha Q_\alpha^*=0 \tag{3.6}$$

is required to complete the unique specification of the heats of transport.

Comparison of Eqs. (3.5) and (2.4)–(2.9) indicates that if the latter equations can be cast into a form linear in the singlet space particle diffusion currents, then the coefficients will be statistical expressions for the heats of transport providing they are chosen to satisfy the restraint of Eq. (3.6).

4. KINETIC ENERGY CURRENT

A very simple estimate of the kinetic energy current may be obtained by assuming that the singlet space distribution function is locally Maxwellian; i.e.,

$$f_\alpha^{(1)}(\mathbf{r}_1,\mathbf{p}_1)=[c_1(\mathbf{r}_1)/(2\pi m_\alpha kT)^{\frac{3}{2}}] \cdot\exp[-(\mathbf{p}_1-m_\alpha\mathbf{u}_\alpha)^2/2m_\alpha kT]. \tag{4.1}$$

In this case, one finds that to terms linear in diffusion currents

$$\mathbf{q}_K=\tfrac{5}{2}kT\sum_\alpha\mathbf{j}_\alpha, \tag{4.2}$$

A somewhat more sophisticated derivation of this result[3] may be based on the Fokker-Planck-Chan-

dresekhar equation adapted for ionic species. The right-hand side of Eq. (4.2) is the initial term in a series expansion in the reciprocal of the friction constants.

In condensed systems, kinetic terms of totally dissipative processes are very small. The contribution of Eq. (4.2) to the heat flow is exactly balanced by the ideal gas part of the enthalpy, which, according to Eq. (2.4), must be subtracted off.

5. FLOW $(\mathbf{q}_V)_{\text{ion-ion}}$

The problem of obtaining an expression for $\mathbf{q}_V$ which is linear in the singlet space particle diffusion currents is seen to be equivalent to the problem of writing $\mathbf{j}_{\alpha\beta,1}^{(2)}$ as a linear form in the $\mathbf{j}_\alpha$'s. The latter desideratum was already encountered in the development of the theories of diffusion, conduction, and viscosity.

According to the Brownian motion theory, for α and β both ionic components of an isothermal system, one has (cf. Appendix 1)

$$\mathbf{j}_{\alpha\beta,1}^{(2)}=c_{\alpha\beta}^{(2,0)}\left[(\mathbf{u}_\alpha-\mathbf{u})+D_\alpha^0\nabla_r(g_{\alpha\beta}^{(2,1)}(\mathbf{r})/g_{\alpha\beta}^{(2,0)}(r))\right.$$
$$\left.+(z_\alpha eD_\alpha^0/kT)\nabla_r\phi_\beta^{(2,1)}(-\mathbf{r})\right], \quad (5.1)$$

which is correct to terms linear in nonequilibrium quantities. D_α^0 is the self-diffusion coefficient of ion α in an infinitely dilute solution, while $z_\alpha e$ is its charge. The vector separation $\mathbf{r}$ is equal to $\mathbf{r}_2-\mathbf{r}_1$.

In this equation, the correlation function, $g_{\alpha\beta}^{(2)}$, has been considered as being equal to its equilibrium value (the radial distribution function) plus a nonequilibrium part; i.e.,

$$g_{\alpha\beta}^{(2)}(\mathbf{r})=g_{\alpha\beta}^{(2,0)}(r)+g_{\alpha\beta}^{(2,1)}(\mathbf{r}). \quad (5.2)$$

The electrical potential at a point located at $-\mathbf{r}$ from an ion of type β at $\mathbf{r}_2$ has similarly been split into an equilibrium and nonequilibrium part,

$$\phi_\beta^{(2)}(-\mathbf{r})=\phi_\beta^{(2,0)}(r)+\phi_\beta^{(2,1)}(-\mathbf{r}). \quad (5.3)$$

Both $\phi_\beta^{(2)}$ and $\phi_\beta^{(2,0)}$ satisfy a Poisson's equation so that the difference satisfies the relation

$$\nabla_r^2\phi_\beta^{(2,1)}(-\mathbf{r})=-(4\pi e/\epsilon)\sum_{\gamma=1}^{\nu}z_\gamma c_\gamma g_{\beta\gamma}^{(2,1)}(-\mathbf{r}), \quad (5.4)$$

where ϵ is the dielectric constant.

Equation (5.1) for the pair space particle diffusion currents may be obtained[8] from the Fokker-Planck-Chandresekhar equations in singlet and pair space. It has been derived previously by an *ad hoc* extension to molecular species of the theory of the motion of a Brownian particle.[10] The equivalence of the form of Eq. (5.1) with the previous results is demonstrated in Appendix 1.

By reversing the roles of α and β in $\mathbf{j}_{\alpha\beta,1}^{(2)}$ and replacing $\mathbf{r}$ by $-\mathbf{r}$ an expression for $\mathbf{j}_{\alpha\beta,2}^{(2)}$ is obtained.

Equations for the unknown function $g_{\alpha\beta}^{(2,1)}/g_{\alpha\beta}^{(2,0)}$ are derived by combining Eq. (5.1) with the pair space equation of continuity, which for a stationary state may be written

$$\nabla_{r_1}\cdot\mathbf{j}_{\alpha\beta,1}^{(2)}+\nabla_{r2}\cdot\mathbf{j}_{\alpha\beta,2}^{(2)}=0. \quad (5.5)$$

In the resulting expressions, some terms may be neglected since they lead to higher c^1 order contributions to the transport properties. These terms are recognized by their order in the ionic charge.[10] The final set of ν^2 coupled equations is

$$(D_\alpha^0+D_\beta^0)\nabla_r^2[g_{\alpha\beta}^{(2,1)}(\mathbf{r})/g_{\alpha\beta}^{(2,0)}(r)]$$
$$-(4\pi e^2/\epsilon kT)\sum_{\gamma=1}^{\nu}z_\gamma c_\gamma\{D_\alpha^0 z_\alpha[g_{\beta\gamma}^{(2,1)}(-\mathbf{r})/g_{\beta\gamma}^{(2,0)}(r)]$$
$$+D_\beta^0 z_\beta[g_{\alpha\gamma}^{(2,1)}(\mathbf{r})/g_{\alpha\gamma}^{(2,0)}(r)]\}$$
$$=(\mathbf{u}_\beta-\mathbf{u}_\alpha)\cdot\nabla_r\ln g_{\alpha\beta}^{(2,0)}, \quad \alpha,\beta=1,\cdots,\nu. \quad (5.6)$$

A solution may be sought in a spherical harmonic series. There obviously is no azimuthal dependence. It appears from Eq. (5.6) and the boundary conditions, which we shall subsequently state, that only the $\cos\theta$ term is nonvanishing. Thus, let us assume that

$$(D_\alpha^0+D_\beta^0)[g_{\alpha\beta}^{(2,1)}(\mathbf{r})/g_{\alpha\beta}^{(2,0)}(r)]=\psi_{\alpha\beta}(r)\mathbf{e}_r\cdot\mathbf{e}_z, \quad (5.7)$$

where the positive z axis is taken in the direction of $\mathbf{q}$ (we restrict considerations to unidirectional macroscopic flow). The insertion of the constant $D_\alpha^0+D_\beta^0$ and the spherically symmetric $g_{\alpha\beta}^{(2,0)}(r)$ is convenient and innocuous.

Rewriting Eq. (5.6) in terms of $\psi_{\alpha\beta}$, one has

$$(d^2\psi_{\alpha\beta}/dr^2)+(2/r)(d\psi_{\alpha\beta}/dr)-(2/r^2)\psi_{\alpha\beta}$$
$$-(4\pi e^2/\epsilon kT)\sum_{\gamma=1}^{\nu}z_\gamma c_\gamma[z_\beta(D_\beta^0/D_\alpha^0+D_\gamma^0)\psi_{\alpha\gamma}$$
$$-z_\alpha(D_\alpha^0/D_\beta^0+D_\gamma^0)\psi_{\beta\gamma}]$$
$$=\mathbf{e}_z\cdot(\mathbf{u}_\beta-\mathbf{u}_\alpha)(z_\alpha z_\beta e^2/\epsilon kT)e^{-\kappa r}(1+\kappa r)/r^2, \quad (5.8)$$

where also the Debye-Hückel radial distribution function

$$g_{\alpha\beta}^{(2,0)}=\exp[-(z_\alpha z_\beta e^2/\epsilon kT)(e^{-\kappa r}/r)] \quad (5.9)$$
$$\kappa^2=(4\pi e^2/\epsilon kT)\sum_{\gamma=1}^{\nu}c_\gamma z_\gamma^2,$$

[N.B., $\kappa=0(c^{\frac{1}{2}})$] has been inserted.

[10] H. S. Harned and B. B. Owen, *The Physical Chemistry of Electrolytic Solutions* (Reinhold Publishing Corporation, New York, 1958), Chap. 2.

The correlation function in both equilibrium and nonequilibrium systems approaches unity at large interparticle distances. One boundary condition which the perturbation part must satisfy, therefore, is

$$\lim_{r\to\infty}\psi_{\alpha\beta}(r)=0. \tag{5.10}$$

The second boundary conditions in problems such as this is often based on a hydrodynamic requirement.[11] A somewhat simpler condition, which will serve to determine the lowest order terms in κ depends on the requirement that the perturbation part of the correlation function not blow up as the concentration of electrolyte becomes small. This boundary condition is applied by setting equal to zero terms in $\psi_{\alpha\beta}$ which go as $1/\kappa$ for $\kappa\to 0$; mathematically,

$$\lim_{\kappa\to 0}\psi_{\alpha\beta}<\infty. \tag{5.11}$$

Before considering a solution let us note that Poisson's equation, (5.4), indicates that the form of the perturbation to the local potential is

$$\phi_\alpha^{(2,1)}(\mathbf{r})=-(4\pi e/\epsilon)\sum_{\gamma=1}^{\nu}c_\gamma z_\gamma[\chi_{\alpha\gamma}(r)/(D_\alpha^0+D_\gamma^0)]\mathbf{e}_r\cdot\mathbf{e}_z, \tag{5.12}$$

which leads to the equation

$$(d^2\chi_{\alpha\gamma}/dr^2)+(2/r)(d\chi_{\alpha\gamma}/dr)-(2/r^2)\chi_{\alpha\gamma}=g_{\alpha\gamma}^{(2,0)}\psi_{\alpha\gamma}. \tag{5.13}$$

The boundary conditions on $\chi_{\alpha\gamma}$ are identical with those imposed on $\psi_{\alpha\gamma}$ for similar reasons.

In Appendix 2, Eqs. (5.8) and (5.13) are solved to the desired degree of accuracy to obtain expressions for the ψ's and χ's of ionic species as linear functions of the singlet space velocities. Insertion of these results renders the pair space velocity in the form,

$$\mathbf{j}_{\alpha\beta,1}^{(2)}=c_{\alpha\beta}^{(2,0)}(\mathbf{u}_\alpha-\mathbf{u})+\frac{D_\alpha^0}{D_\alpha^0+D_\beta^0}\mathbf{e}_z\cdot\left[\frac{\psi_{\alpha\beta}}{r}\mathbf{1}+\left(\frac{d\psi_{\alpha\beta}}{dr}-\frac{\psi_{\alpha\beta}}{r}\right)\mathbf{e}_r\mathbf{e}_r\right]+\frac{4\pi z_\alpha e^2 D_\alpha^0}{\epsilon kT}\sum_{\gamma=1}^{\nu}\frac{c_\gamma z_\gamma}{D_\beta^0+D_\gamma^0}\mathbf{e}_z\cdot\left[\frac{\chi_{\beta\gamma}}{r}\mathbf{1}+\left(\frac{d\chi_{\beta\gamma}}{dr}-\frac{\chi_{\beta\gamma}}{r}\right)\mathbf{e}_r\mathbf{e}_r\right], \tag{5.14}$$

which is linear in singlet space velocities.

Appendix 3 demonstrates that this leads to a heat current density

$$(\mathbf{q}_V)_{\text{ion-ion}}=\sum_{\alpha=1}^{\nu}\left[\sum_{\beta=1}^{\nu}c_\beta h_{\alpha\beta}+0(\kappa^2)\right]\mathbf{j}_\alpha, \tag{5.15}$$

$$h_{\alpha\beta}=\tfrac{1}{2}\int_a^\infty(V_{\alpha\beta}-\tfrac{1}{3}rV_{\alpha\beta}')g_{\alpha\beta}^{(2,0)}4\pi r^2dr, \tag{5.16}$$

where a is the ion radius (which enters only as κ^2a^2 and higher order terms). The term with the h integrals comes from the first term on the right-hand side of Eq. (5.14). It is quasi thermodynamic in the sense that it involves averages over the equilibrium ensemble. The $\mathbf{r}$ dependent parts of the pair space velocity contribute only terms of order κ^2 to the heat of transport.

6. FLOW $(\mathbf{q}_V)_{\text{ion-solv}}$

A detailed knowledge of the equilibrium ion-solvent correlations would be required for a Brownian motion treatment paralleling that of the previous section. Lacking the ability to perform this more rigorous treatment, we shall attempt to obtain as much information as possible from a simplified model.

We seek $\mathbf{j}_{\alpha 0,1}^{(2)}(\mathbf{r}_{12},\mathbf{e}_\mu)$ and $\mathbf{j}_{\alpha 0,2}^{(2)}(\mathbf{r}_{12},\mathbf{e}_\mu)$. Let us first assume that the fixing of a solvent molecule in the neighborhood of an ion instead of averaging over this solvent's position does not significantly affect the ions velocity so that

$$\mathbf{j}_{\alpha 0,1}^{(2)}=c_{\alpha 0}^{(2)}(\mathbf{r}_{12},\mathbf{e}_\mu)[\mathbf{u}_\alpha-\mathbf{u}]. \tag{6.1}$$

This approximation is in keeping with a continuum picture of the solvent.

To determine the pair space velocity of a solvent molecule near an ion we adopt the hydrodynamical model used by Debye and Hückel to calculate the electrophoretic force.[12] The solvent is viewed as a uniform continuum of viscosity η (orientation dependencies are thus smoothed). The ions are charged spheres of radius b_α, which may include a solvation shell. To lowest order in electrolyte concentration $\mathbf{u}_{\alpha 0,2}^{(2)}$ may be equated to $\mathbf{u}_{\alpha 0,1}^{(2)}+\mathbf{v}_\alpha$, where $\mathbf{v}_\alpha(r)$ is the relative average velocity of a volume element located at $\mathbf{r}$ with respect to ion α.

The velocity $\mathbf{v}_\alpha$ may be found as a solution of the Navier-Stokes equation,

$$\eta\nabla\times\nabla\times\mathbf{v}_\alpha=-\nabla p+\mathbf{K}_\alpha. \tag{6.2}$$

The exact nature of the local pressure, $p(\mathbf{r})$, need not concern us. The average volume force on the element is given in terms of two particle average forces[13] by

$$\mathbf{K}_\alpha(\mathbf{r})=\sum_{\gamma=0}^{\nu}c_\gamma g_{\alpha\gamma}^{(2,0)}\mathbf{F}_{\alpha\gamma,2}^{(2)}. \tag{6.3}$$

In the bulk of the solution $\mathbf{K}_\alpha$ vanishes so that

$$\sum_{\gamma=0}^{\nu}c_\gamma\mathbf{F}_\gamma^{(1)}=0. \tag{6.4}$$

On assuming the solvent is uniform and approximating the pair space forces by their singlet space values, we have

$$\mathbf{K}_\alpha=\sum_{\gamma=1}^{\nu}c_\gamma(g_{\alpha\gamma}^{(2,0)}-1)\mathbf{F}_\gamma^{(1)}. \tag{6.5}$$

[11] Reference 3(a); reference 10, p. 156.

[12] P. Debye and E. Hückel, Phys. Z. 24, 305 (1923).

[13] Reference 3(a), Eq. (IV.4).

The singlet forces may be written, to lowest order in κ, as the negative of the ion-solvent friction constant times the relative singlet velocity of ion and solvent. Thus,

$$K_\alpha = -\sum_{\gamma=1}^{\nu} c_\gamma \zeta_\gamma^0 (g_{\alpha\gamma}^{(2,0)} - 1)(\mathbf{u}_\gamma - \mathbf{u}_0), \qquad (6.6)$$

$$\zeta_\gamma^0 = kT/D_\gamma^0,$$

into which the linearized Debye-Hückel radial distribution function may be inserted.

The Navier-Stokes equation is to be solved together with the pair space equation of continuity, which, for a uniform fluid in a stationary state, is

$$\nabla \cdot \mathbf{v}_\alpha = 0. \qquad (6.7)$$

The first boundary condition is the asymptotic one

$$\lim_{r\to\infty} \mathbf{v}_\alpha = \mathbf{u}_0 - \mathbf{u}_\alpha. \qquad (6.8)$$

The other boundary condition has its origin in the requirement that the viscous fluid will not slip at the ion sphere, so that

$$\mathbf{v}(b_\alpha \mathbf{e}_r) = 0.$$

Solution of these equations[12] and a transformation from $\mathbf{r}$ to $-\mathbf{r}$ yields, when $e^{-\kappa r}$ is expanded as $1-\kappa r$,‖

$$\mathbf{j}_{0\alpha,1}^{(2)} = c_{\alpha 0}^{(2)} \Big\{ (\mathbf{u}_\alpha - \mathbf{u}) + \mathbf{e}_z \cdot \Big[(\mathbf{u}_0 - \mathbf{u}_\alpha) + \frac{4\pi z_\alpha e^2}{6\pi\eta\kappa\epsilon kT} \sum_{\gamma=1}^{\nu} c_\gamma z_\gamma \zeta_\gamma^0 (\mathbf{u}_0 - \mathbf{u}_\gamma) \Big\{ \mathbf{e}_r \cos\theta \Big(1 - \frac{3b_\alpha}{2r} + \frac{b_\alpha^3}{2r^3} \Big) - \mathbf{e}_\theta \sin\theta \Big(1 - \frac{3b_\alpha}{4r} - \frac{b_\alpha^3}{4r^3} \Big) \Big\} \Big] \Big\}. \qquad (6.9)$$

The product of inserting the pair space particle diffusion currents (6.1) and (6.9) into $(\mathbf{q}_V)_{\text{ion-solv}}$ is

$$(\mathbf{q}_V)_{\text{ion-solv}} = 2\sum_{\alpha=1}^{\nu} c_0 h_{\alpha 0} \mathbf{j}_\alpha + \sum_{\alpha=1}^{\nu} (c_\alpha \mathbf{j}_0 - c_0 \mathbf{j}_\alpha)[A_\alpha + \kappa(z_\alpha \zeta_\alpha^0 / 6\pi\eta)\tilde{A}], \qquad (6.10)$$

$$h_{\alpha 0} = \tfrac{1}{2} \iint [V_{\alpha 0} - (r/3)(\partial/\partial r) V_{\alpha 0}] g_{\alpha 0}^{(2,0)} d^3\mathbf{r} d^2\mathbf{e}_\mu, \qquad (6.11)$$

$$A_\alpha = \tfrac{1}{2} \iint \{ [V_{\alpha 0} - (r/3)(\partial/\partial r) V_{\alpha 0}] \cdot [1 - (3b_\alpha/2r) + (b_\alpha^3/2r^3)] + \tfrac{1}{2} V_{\alpha 0} [(b_\alpha/r) - (b_\alpha^3/r^3)] \} g_{\alpha 0}^{(2,0)} d^3\mathbf{r} d^2\mathbf{e}_\mu, \qquad (6.12)$$

$$\kappa^2 \tilde{A} = (4\pi e^2/\epsilon kT) \sum_{\gamma=1}^{\nu} c_\gamma z_\gamma A_\gamma. \qquad (6.13)$$

‖ Equation (6.10) is obtained from either Eq. (6.9) or its precursor with $e^{-\kappa r}$ not expanded. The difference enters as terms of higher order in κ.

This result possesses certain unsatisfactory features which we discuss below, but let us look at its qualitative implications. If details of the ion and solvent structure are ignored then the interaction potential depends only on the square of the ion's charge. In a solution where all the ions are of the same valence type, if the sizes of the ions are the same then the A integrals are the same and by electroneutrality $\tilde{A}$ vanishes. Therefore, to lowest order, $\tilde{A}$ may be considered as linear in differences of ion size, or, in the spirit of Stokes' Law, linear in the differences of mobility. After completing the theory and comparing with the data, we will be in a position to discuss this term further.

Equation (6.10) has the weakness that major contributions to the integrand come from the region close to the ion. In this portion of space several of the approximations involved in the derivation, such as the neglect of differences between singlet and pair forces and the use of the linearized Debye-Hückel distribution, are questionable. (In contrast, the electrophoretic drag problem leads to integrals with major contributions at distance $1/\kappa$.) The result is probably an overestimate of the ion-solvent contribution since one expects less κ dependence in the radial distribution function at close distances (compare with the theory of ion pairing where no κ dependence is assumed up close).

7. FURTHER SOLVENT CONTRIBUTIONS TO HEAT FLOW

The solvent-solvent interactions lead, to the desired order, to a term

$$(q_V)_{\text{solv-solv}} = c_0 h_{00} \mathbf{j}_0, \qquad (7.1)$$

$$h_{00} = \tfrac{1}{2} \iiint [V_{00} - (r/3)(\partial/\partial r) V_{00}'] g_{00}^{(2,0)} d^3\mathbf{r} d^2\mathbf{e}_{\mu 1} d^2\mathbf{e}_{\mu 2}. \qquad (7.2)$$

If we had attempted a completely molecular treatment of the solvent, we would have had to consider terms like those arising from solvent oriented by an ion interacting with other solvent and ions, but these are the effects which the introduction of the dielectric constant covers.

8. HEAT OF TRANSPORT

The results of Secs. 4 to 7 may be united to yield as an expression for the heat current,

$$\mathbf{q} = \sum_{\alpha=0}^{\nu} Q_\alpha^* \mathbf{j}_\alpha, \qquad (8.1)$$

$$Q_\alpha^* = (5/2)kT - \bar{H}_\alpha + \sum_{\beta=1}^{\nu} c_\beta h_{\alpha\beta} + 2c_0 h_{\alpha 0} - c_0 A_\alpha - (c_0 z_\alpha kT/6\pi\eta D_\alpha^0)\tilde{A}\kappa + 0(\kappa^2) \quad \alpha = 1, \cdots, \nu, \qquad (8.2)$$

$$Q_0^* = (5/2)kT - H_0 + c_0 h_{00} + \sum_{\alpha=1}^{\nu} c_\alpha A_\alpha.$$

The heats of transport have been properly identified if Eq. (3.6) is satisfied. Inserting (8.2) and (8.3) reveals

$$\sum_{\alpha=0}^{\nu} c_\alpha Q_\alpha^* = \tfrac{5}{2}kT\sum_{\alpha=0}^{\nu} c_\alpha + \sum_{\alpha,\beta=0}^{\nu} c_\alpha c_\beta h_{\alpha\beta} - \sum_{\alpha=0}^{\nu} c_\alpha \bar{H}_\alpha = 0, \quad (8.4)$$

by using a well-known equilibrium result.[14]

For ionic components $h_{\alpha\beta}$ may be evaluated with the coulomb potential and the linearized Debye-Hückel radial distribution function. Part of $c_\beta h_{\alpha\beta}$ diverges when integration is performed over an infinite volume, but upon summing over β these divergencies vanish by electroneutrality. The remaining part is, to order κ,

$$\sum_{\beta=1}^{\nu} c_\beta h_{\alpha\beta} = -2z_\alpha^2 e^2\kappa/3\epsilon. \quad (8.5)$$

The integrals $h_{\alpha 0}$ and A_α may be written as their infinite dilution value plus a concentration dependent part. The order of the latter part depends upon how much κ dependence is put into $g_{\alpha 0}^{(2,0)}$. This problem is similar to that which arises in the calculation of chemical potential[15] and polarization energy.[16] If we allow the potential of mean force to contain the interaction of solvent and ion atmosphere, we would be taking certain terms into account twice. When properly treated the first concentration dependence of the integrals is $0(\kappa^2)$.

The limiting law for the heat of transport of an ionic species is

$$Q_\alpha^* = Q_\alpha^{*0} + \mathcal{S}(Q_\alpha^*)\kappa, \quad (8.6)$$

$$\mathcal{S}(Q_\alpha^*) = -\mathcal{S}(\bar{H}_\alpha) - (2z_\alpha^2 e^2/3\epsilon) - (c_0 z_\alpha kT\tilde{A}/6\pi\eta D_\alpha^0), \quad (8.7)$$

where $\mathcal{S}(\bar{H}_\alpha)$ is the limiting slope for partial molecular heat content *vs* κ:

$$\mathcal{S}(\bar{H}_\alpha) = -\frac{3z_\alpha^2 e^2}{4\epsilon}\left(1 + T\frac{\partial \ln\epsilon}{\partial T} + \frac{T}{3}\frac{\partial \ln\eta}{\partial T}\right). \quad (8.8)$$

Individual ion heats of transport are experimentally unobtainable. The heat of transport of neutral salts, defined by

$$Q_\pm^* = \nu_+ Q_+^* + \nu_- Q_-^*$$

may be measured (the ν's are standard notation for number of ions in the neutral "molecule"). The slope of the limiting law is

$$\mathcal{S}(Q_\pm^*) = -\mathcal{S}(\bar{H}_\pm) - (2e^2/3\epsilon)\sum \nu_\alpha z_\alpha^2 - (c_0 kT\tilde{A}/6\pi\eta)\sum(\nu_\alpha z_\alpha/D_\alpha^0). \quad (8.9)$$

The summation in the last term goes as a difference in mobility (recall that $\tilde{A}$ has the same behavior). This further decreases the importance of ion-solvent interaction contributions.

Although neither the single ion entropy $\bar{S}_\alpha$ nor heat of transport Q_α^* is measurable separately, the combination

$$\bar{\bar{S}} = \bar{S}_\alpha + (Q_\alpha^*/T), \quad (8.10)$$

called the transport entropy, is. We find for the slope of the limiting law for

$$\bar{\bar{S}}_\alpha + k\ln m_\alpha,$$

$$\mathcal{S}(\bar{\bar{S}}_\alpha) = -(z_\alpha^2 e^2/6\epsilon T) - (c_0 z_\alpha k\tilde{A}/6\pi\eta D_\alpha^0). \quad (8.11)$$

The ion-solvent term is much more important here than in Eq. (8.9), both because of the lack of the summation factor, and because the ion-ion term is smaller.

A last point to be noted is that from Eq. (8.3), or more simply from Eq. (3.6), it is seen that the heat of transport of the solvent is of order κ^2.

9. COMPARISON WITH EXPERIMENTS

Results of measurements on the heat of transport of electrolytes in the range of applicability of the limiting laws are scant. The most informative data are those obtained by Agar and Turner[17] using a conductimetric method. Aqueous solutions of NaCl, NaBr, KCl, KBr, and KI were studied at 25°C and at four concentrations in the range from 0.0025 to 0.02 molar. A value at 0.05 m is available by extrapolation of the thermogravitational results of Alexander.[18] In Columns 5, 4, and 7 of Table I the coefficients of the best least squares quadratic fits to a plot of Q^* (in kcal/mole) *vs* $m^{\frac{1}{2}}$ is presented. A quadratic was chosen because in this concentration range good fits to other electrolytic properties can be obtained by considering only terms to order m. Included also are interval allowances for each value. These are determined by multiplying the square root of the residual mean square by 2.92, the appropriate factor for 90% confidence limits with a mean square error based on two degrees of freedom.

To test the hypothesis that all 1:1 electrolytes have a common slope (except for a small ion-solvent term), the calculation was redone with the constraint that all the curves have the same $m^{\frac{1}{2}}$ coefficient. The coefficients found in this way are reported in Columns 6 and 8, and in Column 3 of $Q_{1:1}^*$. The best common slope is -2.58 ± 0.89. Allowances are calculated with a factor of 1.76 to produce estimates of 90% confidence based on fourteen degrees of freedom. Comparison of the residual mean square for this constrained fit, which is

[14] Terrill L. Hill, *Statistical Mechanics* (McGraw-Hill Book Company, Inc., New York, 1956), Eqs. (30.10) and (30.20).
[15] J. G. Kirkwood, Chem. Revs. **19**, 275 (1936).
[16] A. B. Lidiard, Phys. Rev. **112**, 54 (1958).
[17] J. N. Agar and J. C. R. Turner (to be published); J. C. R. Turner, dissertation, University of Cambridge (1955); J. N. Agar, in *The Structure of Electrolytic Solutions*, edited by W. J. Hamer (John Wiley and Sons, Inc., New York, 1959).
[18] K. F. Alexander, Z. physik. Chem. (Leipzig) **203**, 212 (1954). The extrapolation to 25°C and correction for a 5% error in analysis were performed by Dr. J. N. Agar, whom we thank for supplying these results.

TABLE I. Theoretical predictions and least squares quadratic fit to the data.

1	2	3	4	5	6	7	8
Property	Limiting slope (coefficient of $m^{\frac{1}{2}}$)			Value at infinite dilution		Coefficient of m	
	theoretical ion-ion term	quasitheoretical ion-solvent term	experimental	individual	common slope	individual	common slope
Q_{NaCl}^* (kcal/mole)	−2.57	0.18	−4.11±5.39	1.10±0.31	1.01±0.06	5.99±19.13	0.65±3.37
Q_{KCl}^*	−2.57	0.001	−2.68±2.49	1.05±0.14	1.04±0.06	2.60±8.84	2.28±3.37
Q_{NaBr}^*	−2.57	0.20	−2.32±4.88	0.76±0.28	0.77±0.06	0.77±17.30	1.71±3.37
Q_{KBr}^*	−2.57	0.004	−1.63±1.49	0.72±0.09	0.77±0.06	0.35±5.29	3.69±3.37
Q_{KI}^*	−2.57	0.002	−2.18±0.98	0.14±0.06	0.20±0.06	2.33±3.48	3.72±3.37
Q_{LiI}^*	−2.57	...	−2.58±0.89	...	...	...	...
Q_{TlClO}^*	−2.57	0.01	...	...	...	...	...
$Q_{CdSO_4}^*$	−20.53	1.6	...	...	...	...	...
$\bar{S}_{Tl^+}$ (eu/mole)	−.777	−0.33	...	...	...	...	...
$\bar{S}_{Cd^{++}}$	−6.22	12.9[a]	6.7[a]	...	...	...	...

[a] Basis for ion-solvent term calculation.

7.74×10^{-4}, with the average of the mean squares of the unconstrained fits, which is 8.74×10^{-4}, leads one to conclude that the hypothesis of a common limiting slope is statistically tenable.

Considering only the ion-ion term the theory predicts a limiting concentration dependence of 2.57 $m^{\frac{1}{2}}$. Agreement with the individual and common experimental slopes is acceptable. In view of the error margin room for an ion-solvent term exists.

Less complete analysis can be made of the initial and final thermoelectric power experiments of Agar and Breck[19] on $TlClO_4$. These measurements, performed at six concentrations in the range 0.05 and 0.256m, are difficult to interpret because of the higher molarity and the large scatter. The heat of transport and the transported entropy of Tl^+ are shown in Figs. 1 and 2 with the visual curves drawn so as to come in at the values predicted by the ion-ion terms of Eqs. (8.9) and (8.11). Further clarification of these data would be useful.

Breck and Agar[20] have applied the same method to a study of the 2:2 salt $CdSO_4$. The heat of transport and the transported entropy of Cd^{++} are plotted in Figs. 3 and 4. On the abscissa, the point where $\kappa^2e^2/\epsilon kT=1$ is indicated. This is one of the dimensionless expansion parameters of the Debye-Hückel theory (the other is κa). All the concentrations are greater than this value so that any attempt to fit the curve with a quadratic is unsound. Nevertheless, the data are quite smooth and good visual curves can be drawn.

The ion-ion term of Eq. (8.11) for the $m^{\frac{1}{2}}$ coefficient of

$$\bar{S}_{Cd^{++}}+R\ln m_{Cd^{++}}\ \text{(in eu/mole)}$$

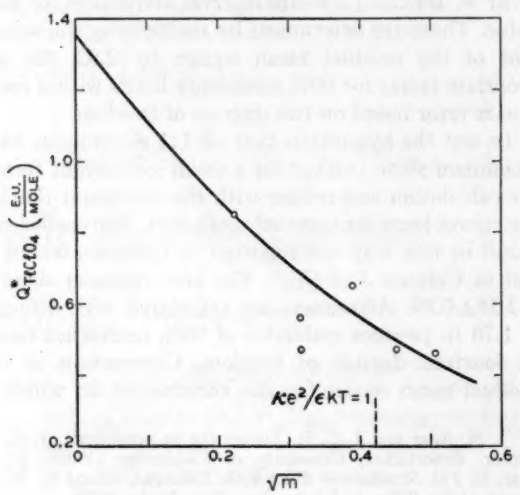

FIG. 1

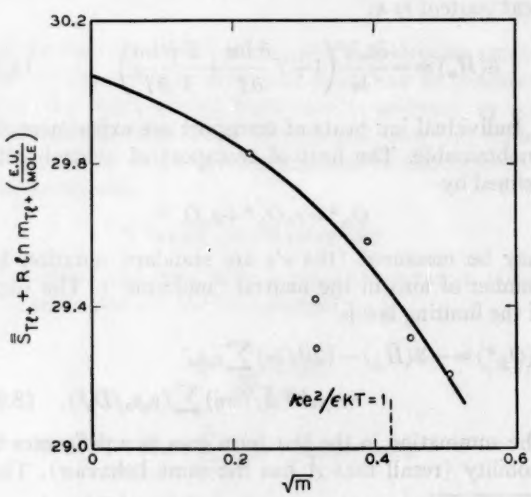

FIG. 2

[19] J. N. Agar and W. G. Breck, Trans. Faraday Soc. 53, 167 (1957).

[20] W. G. Breck and J. N. Agar, Trans. Faraday Soc. 53, 175 (1957).

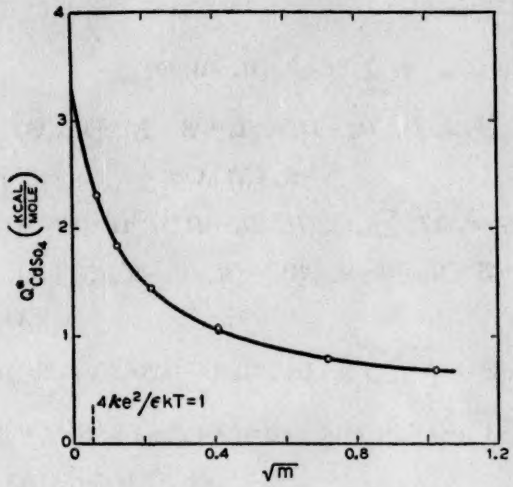

FIG. 3

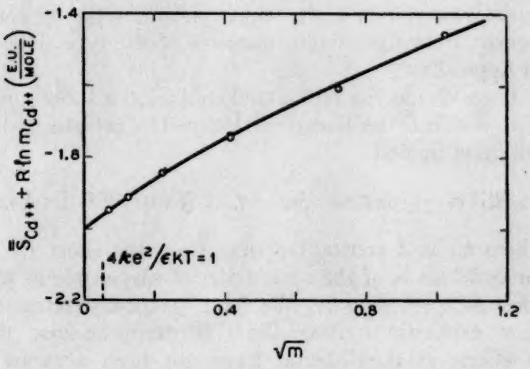

FIG. 4

is -6.22 while the slope read off the curve is $+6.7$. A value of $\bar{A}_{CdSo_4}$ of 81 is required to explain this difference. When this $\bar{A}$ is used in the heat of transport equation, the ion-solvent term is 1.6 compared with an ion-ion contribution of -20.53.

If as an approximation, we postulate that for a simple salt with ions of equal valence $\bar{A}$ is proportional to the magnitude of the charge and to the difference between the self-diffusion constants of the cation and the anion, then from the $CdSO_4$ value of $\bar{A}$ one obtains the estimates of the ion-solvent contributions to the limiting slope given in Column 3 of Table I. As noted earlier, the solvent effect is much less important for the heat of transport of the salt than for the ion transported entropy.

10. ACKNOWLEDGMENT

The authors would like to express their appreciation to Dr. Martin B. Wilk and Miss Marilyn J. Huyett for performing the statistical analysis of the experimental data.

APPENDIX 1

Equation (5.1) for the pair space diffusion current is given in a somewhat different form in standard references on the theory of electrolytes.[21] One finds (in our notation)

$$\mathbf{u}_{\alpha\beta,1}^{(2)}=\mathbf{u}-(D_\alpha^0/kT)[kT\nabla_{r_1}\ln c_\beta g_{\alpha\beta}^{(2)}(\mathbf{r}) + z_\alpha e\nabla_{r_1}\phi_\beta^{(2)}(-\mathbf{r})+z_\alpha e\nabla_{r_1}\phi_\alpha^{(2)}(0)-\mathbf{X}_\alpha]. \quad \text{(A1.1)}$$

The equivalence follows after one notes that as $r\to\infty$, this equation becomes

$$\mathbf{u}_\alpha=\mathbf{u}-(D_\alpha^0/kT)[kT\nabla_{r_1}\ln c_\beta+z_\alpha e\nabla_{r_1}\phi_\alpha^{(2)}(0)-\mathbf{X}_\alpha], \quad \text{(A1.2)}$$

while at equilibrium it is

$$\mathbf{u}=\mathbf{u}-(D_\alpha^0/kT)[kT\nabla_{r_1}\ln g_{\alpha\beta}^{(2,0)}(r) + z_\alpha e\nabla_{r_1}\phi_\beta^{(2,0)}(r)]. \quad \text{(A1.3)}$$

The latter is one of the basic assumptions behind the Debye-Hückel theory.

The last point involved in establishing the correspondence is that since Eq. (A1.1) is already linear in nonequilibrium quantities, multiplication by $c_{\alpha\beta}^{(2)}$ or $c_{\alpha\beta}^{(2,0)}$ is equivalent.

APPENDIX 2

The set of Eqs. (5.8) may be written as the one matrix equation

$$L\Psi-\kappa^2\mathfrak{A}\Psi=\Lambda\, e^{-\kappa r}(1+\kappa r)/r^2, \quad \text{(A2.1)}$$

where we define the differential operator

$$L=(d^2/dr^2)+(2/r)(d/dr)-(2/r^2). \quad \text{(A2.2)}$$

The unknown functions have been arranged into a $1\times\nu^2$ column matrix, Ψ, which is partitioned into ν equisized parts. The β element of the α partition is $\psi_{\alpha\beta}$. Similarly, Λ is the column matrix such that

$$(\Lambda)_{\alpha\beta}=(z_\alpha z_\beta e^2/\epsilon kT)(\mathbf{u}_\beta-\mathbf{u}_\alpha)\cdot\mathbf{e}_z. \quad \text{(A2.3)}$$

$\mathfrak{A}$ is a $\nu^2\times\nu^2$ matrix partitioned into ν^2 square parts such that the β,λ element of the α,γ partition is

$$\kappa^2(\mathfrak{A})_{\alpha\gamma\beta\lambda}=(4\pi e^2/\epsilon kT)c_\gamma z_\gamma[\delta_{\alpha\lambda}z_\beta D_\beta^0/(D_\alpha^0+D_\gamma^0) - \delta_{\beta\lambda}z_\alpha D_\alpha^0/(D_\beta^0+D_\gamma^0)]. \quad \text{(A2.4)}$$

Define $\mathfrak{B}$ by the equation $\mathfrak{A}=\mathfrak{B}^2$. The unit matrix is $\mathfrak{I}$.

[21] Reference 10, Eqs. (2-3-1) and (2-5-3).

Ψ and $\mathbf{A}$ may be regarded as vectors of vector elements, while $\mathfrak{A}$ is a matrix of matrix elements.

The solution of Eq. (A2.1) which satisfies the boundary conditions (5.10) and (5.11) is

$$\mathbf{\Gamma}=\kappa^{-1}(\mathfrak{B}^2-\mathfrak{J})^{-1}[\exp(-\kappa\mathfrak{B}r)(\mathfrak{J}+\kappa\mathfrak{B}r)/r^2 -\mathfrak{J}\exp(-\kappa r)(1+\kappa r)/r^2]\mathbf{A}. \quad \text{(A2.5)}$$

We may now consider the equation for the χ functions which determine the perturbation to the local electrical potential. It can be shown that the approximation of replacing $g_{\alpha\beta}^{(2,0)}$ on the right-hand side of Eq. (5.13) by its asymptotic value, unity, is equivalent to approximations which have already been introduced in deriving Eq. (5.8); i.e., terms which yield higher than c^1 contributions to the transport properties are not retained. Therefore, we may write, in matrix form,

$$L\mathbf{X}=\Psi, \quad \text{(A.26)}$$

which has as the solution satisfying boundary conditions (5.10) and (5.11).

$$\mathbf{X}=\kappa^{-4}(\mathfrak{B}^2-\mathfrak{J})^{-1}\{-\mathfrak{B}^{-2}[1/r^2-\exp(-\kappa\mathfrak{B}r)(\mathfrak{J}+\mathfrak{B}r)/r^2 +\mathfrak{J}[1/r^2-\exp(-\kappa r)(1+\kappa r)/r^2]\}\mathbf{A}. \quad \text{(A2.7)}$$

$\mathfrak{B}$ is singular, but this causes no difficulty since the first term inside the brace is a symbolic representation of the series expansion.

APPENDIX 3

The purpose of this appendix is to derive Eq. (5.15) for the ion-ion potential flow using the results of the previous section. The insertion of Eq. (5.14) into Eq. (2.7) yields

$$(\mathbf{q}_V)_{\text{ion-ion}}=\mathbf{e}_z\sum_{\alpha,\beta=1}^{\nu}\{c_\alpha c_\beta h_{\alpha\beta}(\mathbf{u}_\alpha-\mathbf{u})\cdot\mathbf{e}_z +c_\alpha c_\beta(D_\alpha^0/D_\alpha^0+D_\beta^0)\kappa^{-2}\mathbf{\Omega}^{\alpha\beta}(\mathfrak{B}^2-\mathfrak{J})^{-1}[\mathfrak{K}_{\alpha\beta}(\mathfrak{B}) -\mathfrak{K}_{\alpha\beta}(\mathfrak{J})]\mathbf{A} +(4\pi e^2/\epsilon kT)\sum c_\gamma z_\gamma z_\alpha(D_\alpha^0/D_\beta^0+D_\gamma^0)\kappa^{-4}\mathbf{\Omega}^{\beta\gamma}(\mathfrak{B}^2-\mathfrak{J})^{-1} \cdot(-\mathfrak{B}^{-2}[\mathfrak{K}_{\alpha\beta}(0)-\mathfrak{K}_{\alpha\beta}(\mathfrak{B})]-[\mathfrak{K}_{\alpha\beta}(0)-\mathfrak{K}_{\alpha\beta}(\mathfrak{J})])\mathbf{A}\}, \quad \text{(A3.1)}$$

$$\mathfrak{K}_{\alpha\beta}(\mathfrak{B})=\int_a^\infty\{[(V_{\alpha\beta}-\tfrac{1}{3}rV_{\alpha\beta}')\exp(-\kappa\mathfrak{B}r)(\mathfrak{J}+\kappa\mathfrak{B}r)/r^3] -[(V_{\alpha\beta}-rV_{\alpha\beta}')\exp(-\kappa\mathfrak{B}r)(\mathfrak{J}+\kappa\mathfrak{B}r+\tfrac{1}{3}\kappa^2\mathfrak{B}^2r^2)/r^3]\} \times g_{\alpha\beta}^{(2,0)}4\pi r^2dr, \quad \text{(A3.2)}$$

and $h_{\alpha\beta}$ is defined in Eq. (5.16). It is convenient to introduce a row matrix $\mathbf{\Omega}^{\alpha\beta}$ with γ elements of the λ partition equal to $\delta_{\alpha\gamma}\delta_{\beta\gamma}$ which picks out the $\alpha\beta$ component from the column matrices of the type defined in Appendix 2.

If we divide $V_{\alpha\beta}$ into a coulombic and a short range part and use the linearized Debye-Hückel radial distribution we find

$$\mathfrak{K}_{\alpha\beta}(\mathfrak{B})=-[(8\pi z_\alpha z_\beta e^2/3\epsilon a)+t_{\alpha\beta}][\mathfrak{J}+0(\kappa^2\mathfrak{B}^2)], \quad \text{(A3.3)}$$

where $t_{\alpha\beta}$ is a constant arising from the short range forces which is of the same order of magnitude as the constant preceding it. We have purposely refrained from explicitly writing the $\kappa^2\mathfrak{B}^2$ term because the functions in the integral have not been accurately obtained to this order of magnitude.

To finally arrive at Eq. (5.15) one need only substitute and note that $\Lambda=0(\mathbf{j}_\alpha\cdot\mathbf{e}_z/c_\alpha)$.

Semiempirical Calculation on the Electronic Structure of the Nitrogen-Containing Heterocyclic Molecules. IV. Electronic Structure of Pyridine

TOSINOBU ANNO*

Chemical Laboratory, General Education Department, Kyushu University, Ootsubo-machi, Fukuoka, Japan

(Received September 25, 1959)

The semiempirical theory on the electronic structure of the nitrogen heterocycles, proposed in Part I of this series, is applied to pyridine. Only the singlet levels are considered in this paper, deferring the discussions on the triplet levels to a later publication. Doubly excited as well as singly excited configurations are taken into CI calculation. The hybridization parameter λ of the nitrogen nonbonding AO determined so that the calculated value of the lowest singlet-singlet $n-\pi$ transition energy agrees with the experimental value is $+0.5439$ which corresponds to 22% s character of the nitrogen nonbonding AO. By assuming this value of λ, the lower singlet levels of this molecule are calculated and compared with experiment. The calculation shows that a hidden $n-\pi$ transition ($^1A_2-^1A_1$ transition) exists in the neighborhood of the strong 4.8-ev band which is assigned to a $\pi-\pi$ transition.

1. INTRODUCTION

THE electronic structure of the pyridine molecule has been investigated by many theoreticians as well as experimentalists. The analysis of the near ultraviolet absorption spectrum of pyridine vapor was undertaken by Henri and Angenot[1] and later by Sponer and Stücklen.[2] In the latter work the transition concerned was assumed to be of $\pi-\pi$ type. Kasha[3] suggested that the long-wavelength side of the near ultraviolet absorption system of this molecule was due to an excitation of a nonbonding electron of nitrogen ($n-\pi$ transition). This suggestion is supported by the fact that the long-wavelength edge of this system disappears as the polar solvent is used.[4] In a later publication,[5] concerning the near ultraviolet vapor absorption spectra of the three isomeric picolines which have nearly the same electronic structure as pyridine as far as the π and the nonbonding electrons of the nitrogen atom are concerned, Rush and Sponer described a conclusive evidence for two electronic transitions in these molecules in the vicinities of 35 500 and 38 500 cm^{-1}. They assigned the former to an $n-\pi$ transition while the latter was assigned to a $\pi-\pi$ transition. Moreover, these authors described that the latter $\pi-\pi$ system may be overlapped by another transition, probably an $n-\pi$ transition, in β-picoline. Stephenson[6] measured the near-ultraviolet absorption spectra of various substituted pyridines in iso-octane and ethyl alcohol solutions. The vacuum ultraviolet spectrum of pyridine was studied by Pickett, Corning, Wieder, Semenow, and Buckley[7] down to 65 000 cm^{-1}.

Theoretical works on the electronic structure of pyridine have also been performed by many authors. Among these works only those which have bearing on the singlet levels will be referred to. Since the explorative work by Wheland and Pauling,[8] naive LCAO MO calculation based on the one-electron approximation has been performed by various authors[9] and many of physical and chemical properties of this substance, such as electronic spectrum, dipole moment, bond length, and chemical reactivity with various reagents, are interpreted. On the other hand semiempirical molecular-orbital methods with explicit considerations of electronic interactions have been appeared in recent years[10–12] and the calculations on the electronic structure and spectrum of pyridine have been performed.[10,13,14] In all of these works only the π electrons are considered explicitly.

A theoretical discussion of $n-\pi$ transition of pyridine was given by Orgel,[15] but no quantitative calculation of the transition energy was given. A simple semiempirical scheme where the one-electron LCAO MO formalism is complemented with theoretically computed electronic repulsion integrals was proposed for both the $\pi-\pi$ and the $n-\pi$ transition energies by

* Temporary address: Mathematical Institute, 10 Parks Road, Oxford, England.

[1] V. Henri and P. Angenot, Compt. rend. **200**, 1032 (1935); **201**, 895 (1935); J. chim. phys. **33**, 641 (1936).

[2] H. Sponer, Revs. Modern Phys. **16**, 224 (1944); H. Sponer and H. Stücklen, J. Chem. Phys. **14**, 101 (1946).

[3] M. Kasha, Phys. Rev. **76**, 161 (1949); Discussions Faraday Soc. **9**, 14 (1950).

[4] F. Halverson and R. C. Hirt, J. Chem. Phys. **19**, 711 (1951); H. P. Stephenson, J. Chem. Phys. **22**, 1077 (1954); Andon, Cox, and Herington, Trans. Faraday Soc. **50**, 918 (1954).

[5] J. H. Rush and H. Sponer, J. Chem. Phys. **20**, 1847 (1952).

[6] H. P. Stephenson, J. Chem. Phys. **22**, 1077 (1954).

[7] Pickett, Corning, Wieder, Semenow, and Buckley, J. Am. Chem. Soc. **75**, 1618 (1953).

[8] G. W. Wheland and L. Pauling, J. Am. Chem. Soc. **57**, 2086 (1935).

[9] H. C. Longuet-Higgins and C. A. Coulson, Trans. Faraday Soc. **43**, 87 (1947); P.-O. Löwdin, J. Chem. Phys. **19**, 123 (1951); Orgel, Cottrell, Dick, and Sutton, Trans. Faraday Soc. **47**, 113 (1951); D. W. Davies, *ibid.* **51**, 449 (1955); Anno, Ito, Shimada, Sadô, and Mizushima, Bull. Chem. Soc. Japan **30**, 638 (1957).

[10] R. Pariser and R. G. Parr, J. Chem. Phys. **21**, 466, 767 (1953).

[11] J. A. Pople, Trans. Faraday Soc. **49**, 1375 (1953).

[12] L. Goodman and H. Shull, J. Chem. Phys. **22**, 1138 (1954); **23**, 33 (1955).

[13] R. McWeeny and T. E. Peacock, Proc. Phys. Soc. (London) **A70**, 41 (1957), R. McWeeny, *ibid.* **A70**, 593 (1957).

[14] K. Nishimoto and N. Mataga, Z. physik. Chem. (Frankfurt) **12**, 335 (1957); N. Mataga and K. Nishimoto, *ibid.* **13**, 140 (1957).

[15] L. E. Orgel, J. Chem. Soc. **1955**, 121.

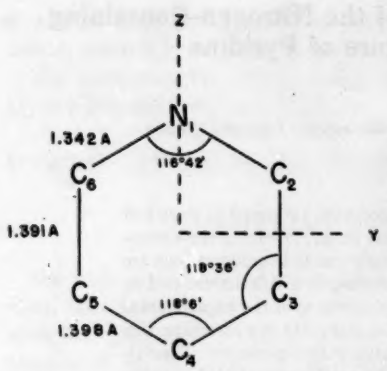

FIG. 1. The structure of and the numbering of ring atoms in the pyridine molecule.

Goodman and Shull[12] and was used, with the additional simplification of incorporating the electron repulsion integrals into β^{spec}, related to the theoretical nearest neighbor-AO exchange integral, β^*, by Goodman and Harrell[16] for the calculation of $n-\pi$ transition energies of various nitrogen heterocyclics.

In the present paper results of calculation on the $n-\pi$ and $\pi-\pi$ transitions of pyridine by using the semiempirical theory proposed in Part I[17] of this series will be given. Only the singlet levels will be considered in this paper. In addition to obtain the theoretical energy levels of the pyridine molecule, the purpose of the present work is to see if the conclusion that the nitrogen nonbonding AO may be considered to have much lower s character than usually assumed, reached in the case of pyrazine,[18] also applies to pyridine.

2. METHOD OF CALCULATION

The calculation is based on the semiempirical ASP-LCAO-MO-CI method proposed in Part I[17] of this series. The structural model assumed is given in Fig. 1.[19] The molecule is planar in the ground electronic state and belongs to the point group C_{2v}. Figure 1 also shows the numbering of the ring atoms and the designation of the coordinate axes upon which the definitions of symmetry species given in Table I are based.

Coulomb repulsion integrals over AO's were obtained in the same manner as described in Part I.[17] The hybridization parameter λ of the nitrogen nonbonding AO, which is defined by Eq. (39) in Part I, will be described in a later section. The form of π MO's is the same as used for pyrazine[17,18,20] [see Eq. (53) of reference 17] except that in the present case the fourth atom is not nitrogen but carbon. The nonbonding MO was taken to be the "nonbonding AO" of the nitrogen atom. The values of core integrals β_{CC} and β_{CN} assumed were the same as in the previous papers.[17,18,20] The core integrals α's were determined in the manner analogous to that used in a previous paper,[17] neglecting the penetration integrals. An orbital configuration having four singly occupied orbitals gives two singlet functions and there is some arbitrariness in constructing these two functions. The forms used for these two functions and the notations describing all the singlet functions are those of Murrell and McEwen.[21] In CI calculation, the procedures adopted were as follows unless otherwise stated: the doubly excited as well as singly excited configurations were considered; however, some amounts of labor to solve secular equations of higher degrees were avoided in the same manner as in a previous paper.[18]

TABLE I. Symmetry species for the point group C_{2v}.

	I	$C_2(z)$	$\sigma_v(xz)$	$\sigma_v'(yz)$
A_1	1	1	1	1
A_2	1	1	−1	−1
B_1	1	−1	1	−1
B_2	1	−1	−1	1

TABLE II. The lower singlet configurations of species A_1 and their interactions with the ground configuration.

Configuration x	Energy $E(x)$	$(x \mid x_0)$[a]	$(x \mid x_0)^2/\{E(x)-E(x_0)\}$
x_0	0.0000	...	...
x_2^4	6.2312	0.0003	0.000 000
x_1^3	6.7598	−1.3330	0.262 861
x_0^3	8.5234	−1.0679	0.133 797
x_1^5	9.4657	−0.8174	0.070 585

[a] $(x \mid x_0)=\int x\mathbf{H}x_0 d\tau$, where $\mathbf{H}$ is the total Hamiltonian of the eight-electron system and the integration should be extended to the space coordinates of the eight electrons.

3. HYBRIDIZATION PARAMETER OF NITROGEN NONBONDING AO

As is mentioned in Sec. 1, one of the purposes of the present work is to see whether the calculated $n-\pi$ transition energy, which agrees with experiment, is obtained for pyridine by assuming the λ value obtained from the pyrazine spectrum. From the preliminary calculation by assuming $\lambda=0.339$, which was determined from the pyrazine spectrum in Part II[18] of this series, the lowest $n-\pi$ ($^1B_1-^1A_1$) transition energy is obtained to be 3.21 ev which is somewhat lower than the experimental value of 4.31 ev. This fact may suggest that the value of λ of the nitrogen nonbonding AO of the pyridine molecule is somewhat different from that of the pyrazine molecule. Therefore, we have determined the hybridization parameter λ of the nitrogen orbital so as to bring the calculated $n-\pi$ ($^1B_1-^1A_1$) transition energy into agreement with the experimental value.

[16] L. Goodman and R. W. Harrell, J. Chem. Phys. **30**, 1131 (1959).
[17] T. Anno, J. Chem. Phys. **29**, 1161 (1958).
[18] T. Anno and A. Sadô, J. Chem. Phys. **29**, 1170 (1958).
[19] C. H. Townes and A. L. Schawlow, *Microwave Spectroscopy* (McGraw-Hill Book Company, Inc., New York, 1955), p. 112.
[20] T. Anno and A. Sado, J. Chem. Phys. **32**, 619 (1960), Part III of this series.
[21] J. N. Murrell and K. L. McEwen, J. Chem. Phys. **25**, 1143 (1956).

TABLE III. The lower singlet configurations of species A_1 and their interactions with x_2^4 and with x_1^3.

Configuration x	Energy $E(x)$ (ev)	$(x \mid x_2^4)$[a] (ev)	$(x \mid x_2^4)^2/\{E(x)-E(x_2^4)\}$ (ev)	$(x \mid x_1^3)$[a] (ev)	$(x \mid x_1^3)^2/\{E(x)-E(x_1^3)\}$ (ev)
x_0	0.0000	0.0003	0.000 000	−1.3330	−0.262 861
x_2^4	6.2312	...	...	0.9766	1.804 289
x_1^3	6.7598	0.9766	1.804 280	...	...
x_0^3	8.5234	0.0651	0.001 848	0.8790	0.438 104
x_1^5	9.4657	0.0651	0.001 310	−0.4544	0.076 307
x_{22}^{33}	10.0977	−0.0113	0.000 033	−0.0113	0.000 038
$x_{21}^{43}(1)$	10.7810	0.6665	0.097 635	−0.0001	0.000 000
x_{11}^{33}	11.1276	0.0000	0.000 000	−1.3330	0.406 815
x_0^5	11.9486	0.6339	0.070 281	−0.6537	0.082 355
$x_{21}^{43}(2)$	13.3458	1.1544	0.187 311	−0.0002	0.000 000
x_{11}^{44}	13.8675	0.0113	0.000 016	0.0113	0.000 017
$x_{20}^{43}(2)$	14.1280	1.6339	0.338 065	0.7930	0.085 346
x_{22}^{35}	14.3596	1.2741	0.199 711	0.3476	0.015 898
$x_{20}^{43}(1)$	14.5126	1.4349	0.248 622	0.9494	0.116 262
x_{10}^{33}	15.0323	0.0000	0.000 000	1.8592	0.417 845
$x_{21}^{45}(2)$	15.0703	−0.0011	0.000 000	−0.7930	0.075 669
$x_{21}^{45}(1)$	15.4549	0.8181	0.072 561	−0.9494	0.103 663
x_{22}^{55}	15.9224	−0.0226	0.000 052	0.0000	0.000 000
x_{11}^{55}	15.9746	0.0000	0.000 000	0.5261	0.030 036
x_{00}^{33}	16.2379	0.0000	0.000 000	−0.1189	0.001 491
$x_{20}^{45}(2)$	16.3246	0.5772	0.033 007	0.0000	0.000 000
$x_{10}^{35}(2)$	16.5710	0.0000	0.000 000	0.5772	0.033 957

[a] See footnote a in Table II.

In order to get the value of hybridization parameter λ, configurational energies and interaction matrix elements are calculated, leaving λ as a parameter. If the coefficients of mixing of different configurations, which are taken into the secular equation, into a wave function representing a state and the energy depression due to the second-order perturbation are carried over from the preliminary calculation assuming λ=0.339, expressions for the lowest $n-\pi^*$ ($^1B_1-^1A_1$) transition energy can be obtained in terms of λ. From the condition that this expression reproduces the experimental value of 4.31 ev, an algebraic equation of fourth degree in λ is obtained.† This equation has two real roots as well as two imaginary ones. Two real roots thus obtained are λ=+0.5439 and −0.6168, of which the latter is discarded from the reasons described in a previous paper.[18] Therefore we take λ=+0.5439. This corresponds to 22% s character of nitrogen nonbonding AO and would suggest that the s character of nitrogen nonbonding AO is somewhat larger in pyridine than in pyrazine. The author, however, does not necessarily insist that this difference is real since the calculations are based upon many approximations. The important point is the fact that the derived value of s character is much smaller than the value usually assumed not only in the case of pyrazine but also in the case of pyridine.

† If the orthogonal relation of the bond-forming orbital of the nitrogen atom holds in the nitrogen heterocyclic molecules, the electron configuration of the nitrogen atom depends on λ. Therefore, the one-center integral $(\pi_N\pi_N \mid \pi_N\pi_N)$ would depend upon λ, if the procedure adopted in (26) of Part I[17] is followed. If we take this λ dependence of $(\pi_N\pi_N \mid \pi_N\pi_N)$ into account, the degree of this equation becomes six, as in the case of Part II.[18] In the present paper, this λ dependence is neglected and $(\pi_N\pi_N \mid \pi_N\pi_N)$ is taken simply to be 12.8333 ev contrary to the case of Part II.

4. FINAL CALCULATION

Now that the "best" value of λ to bring the calculated lowest $n-\pi^*$ transition energy into agreement with experiment is obtained we proceed to the calculation of various energy levels assuming this value of λ. The procedures adopted will be described in this section.

Species A_1

In Table II the energies of lower singlet configurations of species A_1 and their interactions with the ground configurations are given. The depression of the ground state by CI is calculated by selecting the more important configurations as described in a previous section.

The lower excited states of $^1A_1$ species are undoubtedly derived from x_2^4 and x_1^3 by CI. Table III

TABLE IV. The singly and doubly excited singlet configurations of species A_2 and their interactions with x_n^4.

Configuration x	Energy $E(x)$ (ev)	$(x \mid x_n^4)$[a] (ev)	$(x \mid x_n^4)^2/\{E(x)-E(x_n^4)\}$ (ev)
x_n^4	7.7777	...	...
x_{n2}^{23}	9.5988	0.0080	0.000 035
x_{n2}^{44}	12.9671	0.8200	0.129 571
$x_{n2}^{36}(2)$	13.6130	0.7090	0.086 144
$x_{n1}^{43}(1)$	13.9407	2.4115	0.943 587
$x_{n2}^{36}(1)$	14.8110	−0.9009	0.115 396
$x_{n1}^{43}(2)$	14.8843	3.1777	1.420 901
$x_{n0}^{43}(1)$	15.4274	1.9602	0.502 292
$x_{n0}^{43}(2)$	15.9664	1.8233	0.405 976
x_{n2}^{56}	17.3241	0.0160	0.000 026
$x_{n1}^{45}(2)$	17.5867	0.8974	0.082 100
$x_{n0}^{45}(2)$	19.0690	1.1012	0.107 396
$x_{n1}^{45}(1)$	19.4929	2.2443	0.429 944
$x_{n0}^{45}(1)$	21.0292	0.9073	0.062 120

[a] See footnote a in Table II.

TABLE V. The lower singlet configurations of species B_1 and their interactions with x_n^3

Configuration x	Energy $E(x)$ (ev)	$(x \mid x_n^3)$[a] (ev)	$(x \mid x_n^3)^2/\{E(x)-E(x_n^3)\}$ (ev)
x_n^3	6.3715	...	...
x_n^5	10.4085	−1.9453	0.937 377
$x_{n2}^{34}(1)$	10.9895	0.5473	0.064 863
x_{n1}^{23}	11.9353	3.3041	1.962 162
$x_{n2}^{34}(2)$	12.6107	0.9284	0.138 147
x_{n0}^{23}	13.7145	1.6619	0.376 129
$x_{n2}^{54}(2)$	15.4419	−0.7930	0.069 330
$x_{n1}^{25}(2)$	15.9988	2.4503	0.623 640
$x_{n2}^{54}(1)$	16.3211	−0.9494	0.090 593

[a] See footnote a in Table II.

shows the lower singlet configurations of this species and their interactions with x_2^4 and with x_1^3. Because of the strong interaction between x_2^4 and x_1^3 (small energy difference and large interaction matrix element) we must include in the secular equation all the configurations which interact strongly either with x_2^4 or with x_1^3 or with both. Table III shows that we would have to solve the secular equation of the eleventh degree if we considered the doubly excited configurations even if we followed the criteria of selecting more important configurations adopted in the calculation of pyrazine spectrum.[18] In this case, therefore, only the singly excited as well as the ground configurations are taken into the secular equation, neglecting all the doubly excited configurations.

Species A_2

Table IV shows the configurational energies of all the singly and doubly excited configurations of species $^1A_2$ together with their interaction with x_n^4 which has the lowest energy among them. In this case a configuration lying more than 10 ev above the lowest but interacting fairly strongly with it exists [$x_{n1}^{45}(1)$ given in Table IV]. Therefore, all the singly and doubly excited configurations are considered for the calculation of species $^1A_2$ although three configurations which have $(x \mid x_n^4)^2/\{E(x)-E(x_n^4)\}$ ranging between 0.10∼0.13 ev are not taken into the secular equation and are taken into account only by the second-order perturbation theory as those which have $(x \mid x_n^4)^2/\{E(x)-E(x_n^4)\}<0.10$ ev.

TABLE VI. The lower singlet configurations of species B_2 and their interactions with x_2^3.

Configuration x	Energy $E(x)$ (ev)	$(x \mid x_2^3)$[a] (ev)	$(x \mid x_2^3)^2/\{E(x)-E(x_2^3)\}$ (ev)
x_2^3	5.1647	...	...
x_1^4	7.0496	−1.0644	0.601 065
x_2^5	8.3180	−0.5196	0.085 619
x_0^4	9.2606	0.0113	0.000 031
x_{22}^{34}	9.9448	0.0462	0.000 446
x_{21}^{23}	10.3192	0.8363	0.135 687
x_{12}^{44}	11.8297	−0.0080	0.000 009
x_{11}^{43}	12.2041	0.0080	0.000 009
$x_{21}^{25}(2)$	14.2954	1.5519	0.263 769
x_{22}^{54}	14.3261	1.3427	0.196 787
x_{20}^{23}	14.3433	−0.9340	0.095 042
$x_{21}^{25}(1)$	14.8736	−1.1570	0.137 879

[a] See footnote a in Table II.

Species B_1

In Table V the lower singlet configurations of species B_1 and their interactions with x_n^3, the lowest one among them, are given. Although the configuration $x_{n2}^{34}(2)$ gives the second-order energy perturbation slightly larger than 0.1 ev to x_n^3 it was neglected in the secular equation to avoid solution of a sixth-degree secular equation and was considered only by the second-order perturbation theory.

TABLE VII. The calculated and observed lower energy levels of pyridine (singlets only).

Symmetry	Type of transition from the ground state	Energy above the ground state (ev) Calc	Obs
A_1	...	0.00	0.00
B_1	$n-\pi$	(4.31)	4.31[a]
B_2	$\pi-\pi$	4.32	4.75[a]
A_2	$n-\pi$	5.04	(4.52)[b]
A_1	$\pi-\pi$	5.81	6.41[c]
A_1	$\pi-\pi$	7.58	7.23[c]
B_2	$\pi-\pi$	7.69	
B_1	$n-\pi$	8.69	...

[a] See reference 5.
[b] Estimated from β-picoline spectrum (reference 5).
[c] See reference 7.

Species B_2

Table VI for species $^1B_2$ is similar to Table V for species $^1B_1$. As in the previous case of species B_1 solving a sixth-degree secular equation was avoided by considering x_{21}^{23} only through the second-order perturbation theory.

5. DISCUSSIONS

In Table VII the theoretical energy levels calculated as described above are compared with experimental values. It is now established, through the works of Sponer *et al.*,[2,5] Kasha,[3] Halverson and Hirt,[4] Stephenson,[6] and Herington *et al.*,[4] that the pyridine molecule has the lowest $^1B_1$ and $^1B_2$ states at 4.31 and 4.75 ev above the ground state, respectively. The transitions to two states from the ground state are of an $n-\pi$ and $\pi-\pi$ types, respectively. Since the former transition energy is used to determine the value of λ, the hybridization parameter of the nitrogen nonbonding AO, the corresponding calculated value is enclosed in parentheses. The calculated energy of the lowest $^1B_2$ state is found to be 4.32 ev which is slightly lower than the experimental value of 4.75 ev. Such a slight disagreement also exists in the case of the lowest $\pi-\pi$ ($^1B_{3u}$, $^3B_{3u}-{}^1A_g$) transition energies of pyrazine[18,20] and is due probably to the slightly inadequate values of β_{CC}

or β_{CN} or both. This point will be discussed at some length in the subsequent publications on the benzene and the 1, 3, 5-triazine molecules.

Rush and Sponer[5] suggested tentatively that two electronic transitions exist in the region between 36 000–38 000 cm^{-1} of the spectrum of β-picoline. They assigned 37 380 cm^{-1} (4.63-ev) band to the 0, 0 band of the first $\pi-\pi$ transition which constitutes the counterpart of the 4.75-ev band of pyridine. On the other hand, the band at 36 475 cm^{-1} (4.52 ev) in the β-picoline spectrum was assigned with some reservation to the 0, 0 band of $^1A''\leftarrow{}^1A'$ $(n-\pi)$ transition which goes over to $^1A_2\leftarrow{}^1A_1$ in pyridine. The corresponding calculated value for pyridine is 5.04 ev. Therefore, it seems to be probable that the suggestion proposed by Rush and Sponer is correct and further experimental verification of this suggestion is awaited with interest.

The vacuum ultraviolet absorption spectrum of pyridine was studied by Pickett *et al.*[7] Their absorption curve shows absorption maxima at 6.41 and 7.23 ev. The calculated value of 5.81 ev ($^1A_1-{}^1A_1$) corresponds probably to the former. The theoretical value corresponding to the latter maximum is either 7.58 ev ($^1A_1-{}^1A_1$) or 7.69 ev ($^1B_2-{}^1A_1$). It may also probable that two electronic transitions are contained in the 7.23-ev band although we cannot say with confidence because of the lack of the experimental data.

6. ACKNOWLEDGMENTS

The author wishes to thank Professor S. Imanishi and Dr. Y. Kanda for their encouragement throughout this work. He is also indebted to Mr. A. Sadô for helpful discussions and to Miss J. Mukainaka for her assistance in the calculation.

THE JOURNAL OF CHEMICAL PHYSICS VOLUME 32, NUMBER 3 MARCH, 1960

Proton Relaxation Times in Protein Complexes of Paramagnetic Ions*†

ARNOLD WISHNIA‡

Department of Chemistry, Yale University, New Haven, Connecticut

(Received September 21, 1959)

Proton longitudinal relaxation times in dilute solutions of Fe^{3+}, iron conalbumin (FeCon), and ferrihemoglobin (Hb^+), have been measured at 40 and 60 Mc. The static magnetic moment is 5.9 Bohr magnetons for all three species; the ratios of $1/NT_1$ for Fe^{3+}, Fe Con, and Hb^+ are 1:0.72:0.026. For the proteins the relevant correlation time τ_c in Solomon's expression for the dipolar contribution to T_1 is the electron spin relaxation time τ_S of the paramagnetic ion, which for Fe Con is 3×10^{-11} sec. τ_S may contribute to τ_c in other complexes of Fe^{3+} and Cr^{3+}. A simple model for Hb^+ shows the heme Fe to be 4 A from the surface of the protein.

I. INTRODUCTION

IN 1948, Bloembergen, Purcell, and Pound[1] developed a general theory, based on random motions with a correlation time τ_c, for the effect of magnetic dipole-dipole interactions on proton longitudinal and transverse relaxation times, T_1 and T_2.

Subsequently, Solomon[2] reconsidered systems of like and unlike spins and derived the currently accepted expression for the effect of pure dipolar interaction.

To explain the inadequacy of the dipolar mechanism in HF, Solomon and Bloembergen[3] proposed a scalar interaction of spins, $A\mathbf{I}\cdot\mathbf{S}$, for which a theory was developed. Bloembergen then suggested,[4] and low-field studies confirmed,[5] a spin-exchange interaction in Mn^{2+} solutions, where T_1/T_2 is far from unity.

The complete equation for T_1, then, is

$$1/NT_1=\tfrac{4}{5}[S(S+1)g^2\beta^2\gamma_I{}^2p/r^6]\{[\tau_c/1+(\omega_I-\omega_S)^2\tau_c{}^2]+[3\tau_c/(1+\omega_I{}^2\tau_c{}^2)]+[6\tau_c/1+(\omega_I+\omega_S)^2\tau_c{}^2]\}+\tfrac{2}{3}S(S+1)(A/\hbar)^2p\{[\tau_c/1+(\omega_I-\omega_S)^2\tau_c{}^2]\}. \quad (1)$$

However, (1) may be considerably simplified. In the present instance τ_c is the order of 10^{-11} sec, $\omega_I\tau_c\ll1$, $\omega_I\ll\omega_S$. In addition, it has been amply demonstrated[6–8]

---

* Contribution No. 1584, Sterling Chemistry Laboratory, Yale University.

† This work was supported in part from funds under Office of Naval Research Contract No. NONR 609 (24).

‡ Present address: Department of Biochemistry, Dartmouth Medical School, Hanover, New Hampshire.

[1] Bloembergen, Purcell, and Pound, Phys. Rev. **73**, 679 (1948).
[2] I. Solomon, Phys. Rev. **99**, 559 (1955).
[3] I. Solomon and N. Bloembergen, J. Chem. Phys. **25**, 261 (1956).
[4] N. Bloembergen, J. Chem. Phys. **27**, 572 (1957).
[5] R. S. Codrington and N. Bloembergen, J. Chem. Phys. **29**, 600 (1958).
[6] J. King and N. Davidson, J. Chem. Phys. **29**, 787 (1958).
[7] Bernheim, Brown, Gutowsky, and Woessner, J. Chem. Phys. **30**, 950 (1959).
[8] L. O. Morgan and A. W. Nolle, J. Chem. Phys. **31**, 365 (1959).

TABLE I. Molar paramagnetic susceptibilities.[a]

	$\chi\times10^6$ cgsu	$\chi\times10^6$ cgsu[b]	μ Bohr magnetons
$K_3Fe(CN)_6$	2180[c]	2200	...
HbCN	2610[d]	2600	2.50
HbOH	8340[d]	8400	4.48
Hb^+	14 040[d]	14 200	5.83
Fe Con	...	14 600	5.92

[a] The data are corrected for the diamagnetism of the bulk protein.
[b] This work.
[c] Reference 17.
[d] Reference 15.

for Mn^{2+}, and therefore *a fortiori* for Fe^{3+}, that the scalar term in T_1 may be neglected. In the megacycle region for proton resonance frequencies, $(\omega_I/2\pi)$, (1) becomes

$$1/NT_1=\tfrac{4}{3}\cdot S(S+1)g^2\beta^2\gamma_I^2(p/r^6)\cdot\{3\tau_c+[7\tau_c/(1+\omega_S^2\tau_c^2)]\}. \quad (2)$$

Here N is the molar concentration of paramagnetic ions, Np the fraction of protons associated with ions, g the electron g factor, β the Bohr magneton, γ_I the proton gyromagnetic ratio, r the ion-proton distance; τ_c in (1) is the electron spin relaxation time τ_S, the mean lifetime of a hydrate-proton τ_h, or their sum $1/\tau_c=1/\tau_S+1/\tau_h$.

The theory for the correlation time τ_c has undergone similar development. The original authors[1] assumed that in solutions of paramagnetic ions the relevant random motion was the translational diffusion of water molecules; using $r^2/12D$ as the correlation time, they concluded that

$$1/T_1=2\pi\gamma^2\mu^2{}_{eff}/5aD. \quad (3)$$

Experimental work was reported in terms of an inverse first-power dependence on a, the distance of closest approach of proton and ion, or, after converting aD into viscosity, in terms of "effective dipole moment."[1,9,10]

Broersma[11] assumed that the tumbling motions of the hydrated ion could be effective in relaxation; in his formulation the rotational term, $m_2a_2^2/D_{rot}b_2^6$, is, for representative systems, an order of magnitude greater than the translational term, $4\pi n/(D_1+D_2)(a_1+a_2)$ (m_2 is the number of water molecules in the hydrate, n the number of free water molecules per cc.; the a's are the radii and b_2 is the ion-proton distance.) Consequently, recent work[4-8] has interpreted τ_c as the rotational correlation time for the hydrated ion.

[9] R. L. Conger and P. W. Selwood, J. Chem. Phys. **20**, 383 (1952).
[10] Morgan, Nolle, Hull, and Murphy, J. Chem. Phys. **25**, 206 (1956).
[11] S. Broersma, J. Chem. Phys. **24**, 659 (1956).

It has been suggested that in certain cases the electron spin relaxation time τ_S would serve as an effective correlation time for the dipolar proton relaxation.[1,12]

Morgan and Nolle[8] have attributed the behavior of Ni^{2+}, Co^{2+}, and Nd^{3+} to this phenomenon. For Cu^{2+}, Fe^{3+}, and Cr^{3+}, τ_S is probably of the same order of magnitude as the rotational correlation time.[6]

Well-defined protein complexes of Fe^{3+} and Cu^{2+} (e.g., hemoglobin, iron conalbumin, copper conalbumin) exist, for which $\tau_S\ll\tau_c$. A study of these complexes should clarify the role of τ_S in the solutions of the hydrated ions themselves.

In addition, recent reports[13,14] of the depth of Fe in hemoglobin have relied on the translational mechanism of relaxation. If use is made of Eq. (3), with its dependence on a low power of the ion-proton distance, a gross overestimation of the distance of Fe from the protein surface results. With the more satisfactory theory now available, and an understanding of the role of τ_S, a more reliable value may be obtained.

II. EXPERIMENTAL

A. Preparations

The inorganic solutions were prepared from reagent grade chemicals by weight. $Fe(NH_4)(SO_4)_2\cdot12H_2O$ was dissolved in $0.1N$ $HClO_4$.

Ferrihemoglobin (Hb^+) was prepared from a crystalline paste of oxyhemoglobin‡ by air oxidation at pH 4.9 in acetate buffer at room temperature.[15] The solution was dialyzed against water, filtered, and deionized by passage through a mixed-bed ion exchange column. Ferrihemoglobin cyanide (HbCN) and hydroxide (HbOH) were prepared from this stock solution by careful addition of dilute NaCN or KOH. The pH for Hb^+ and HbCN was 6.8; for HbOH, 10.2. Hb^+, HbCN, and HbOH were characterized by their spectra. The static suceptibilities, especially for HbOH, also demonstrate the stability of the preparations.

TABLE II. Proton T_1 relaxation times.[a]

	$(1/NT_1)\times10^{-4}$ sec^{-1}mole^{-1} 60Mc, 28.8°C	$(1/NT_1)\times10^{-4}$ sec^{-1}mole^{-1} 40Mc, 25.8°C
Fe^{3+}	0.931	0.973
Fe Con	0.672[b]	0.716[b]
Hb^+	0.0275, 0.0238[c]	
HbCN	0.00368	
H_2O	3.73 sec	3.45 sec

[a] Corrected for solvent contribution.
[b] Corrected for contribution of conalbumin.
[c] Second value assumes HbCN contributes only for protein.

[12] A. I. Rivkind, Doklady Akad. Nauk S.S.S.R. **102**, 1107 (1955).
[13] N. Davidson and R. Gold, Biochim. et Biophys. Acta **26**, 370 (1957).
[14] Bovey, Matsumiya, and Lumry, Abstracts, Am. Chem. Soc. 135th meeting, April, 1959, p. 17c.
‡ Generously supplied by Professor J. H. Wang.
[15] Coryell, Stitt, and Pauling, J. Am. Chem. Soc. **59**, 633 (1937).

Conalbumin and iron conalbumin were prepared according to Warner and Weber[16] and deionized.

Solutions for static suceptibility measurements were deoxygenated by bubbling nitrogen. Samples for relaxation time determinations were degassed by several cycles of freezing, pumping, and thawing on a 0.1 μ Hg vacuum line and sealed off; these showed no concentration changes on subsequent analysis.

B. Measurements

Static magnetic susceptibilities were determined by the Guoy method,[17] using an air-water calibration, a water-water inhomogeneity correction, and $K_3Fe(CN)_6$ as a check. The magnet was a 4-in. Varian model V 4004. The results are given in Table I.

Proton relaxation times were determined on an a Varian V 4300 B high-resolution NMR spectrometer at the two frequencies available at Yale, 40 and 60 Mc. The method was adiabatic rapid-reversal fast passage,[18,19] the technique not unlike King and Davidson's.[6] The null point was estimated visually on the oscilloscope and the spacing determined on the Sanborn recorder. At least ten observations were made on each sample, at different sweep rates and field positions. The reproducibility was always better than 5% and often approached 1%.

Some determinations on a few samples were made at a steady-state saturation, using the equation

$$\exp(-t_2/T_1)=\tfrac{1}{2}[1+\exp(-T/T_1)].$$

The results agreed with those for a single passage starting from equilibrium, where $T_1=t_2/\ln 2$. Concentrations were arranged to give experimental T_1's between 0.5 and 3.7 sec.

The results, calculated per mole of iron, are given in Table II and Fig. 1. The differences between 40 and 60 Mc may or may not be significant; they are slightly smaller than the change in η/T.

III. DISCUSSION

The value of NT_1 for Fe^{3+} in Table II is consistent with the data of Morgan *et al.*[10] for Fe^{3+} and Codrington and Bloembergen[5] for Mn^{2+}. Other investigations of Fe^{3+} [1,3] and Mn^{2+} [6,8] suggest a value larger by a factor of 1.5. Systematic error seems to be a property of the various techniques;[7,8] the weight of evidence may favor the larger relaxation times, but we are not in a position to resolve the discrepancy. It has been assumed that at least the relative values reported here are not affected.

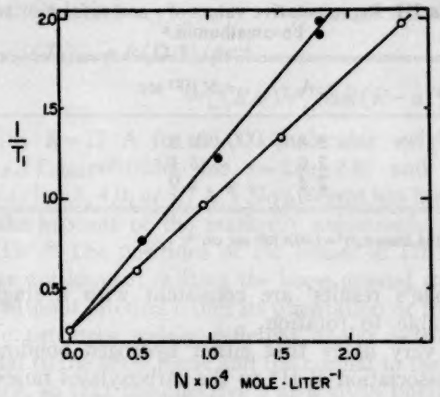

FIG. 1. Proton relaxation times at 60 Mc. Ordinate, $1/T_1$, sec^{-1}; abscissa, N, the concentration of Fe, $\times 10^4$ mole-$liter^{-1}$. Fe conalbumin, open circles; Fe^{3+}, filled circles.

Conalbumin binds two ferric ions per molecule of 76 600 molecular weight.[20] The complex contains one HCO_3^- for each Fe^{3+}.[20] From the spectra and the number of protons dissociated by the reaction at different *p*H Warner and Weber concluded that each Fe^{3+} was also coordinated to three phenolate moieties of the tyrosine residues in the protein.[20] This relationship was confirmed by the author[21] from the spectrophotometric titrations of conalbumin and Fe-conalbumin. The remaining two ligands are presumably water molecules. It is therefore not surprising that the Fe^{3+} retains a moment of 5.9 Bohr magnetons in the complex.

The phenols which coordinate to the Fe^{3+} titrate normally in the absence of iron, with a reasonable value for the intrinsic pK and the electrostatic interaction factor[21]; the phenolic hydroxyl groups are within 1 A of the solvent.[22] It was concluded that the Fe^{3+} is on the surface of the protein, and was in fact the basis for choosing conalbumin as a model compound. The great efficiency of Fe-conalbumin in relaxing proton spins, 0.72 that for Fe^{3+} itself, strongly supports this conclusion.

This efficiency is itself a problem: there are only five protons in the first coordination sphere, and regions further out are shielded in part by the protein. An explanation will be advanced after the following examination.

The data of King and Davidson[6] for Mn^{2+} and its complexes are remarkable. For Mn^{2+}, Mn-nitrilotriacetate $[Mn(NTA)^{1-}]$, Mn-ethylene-diaminetetraacetate $[Mn(EDTA)^{2-}]$, with six, two, and no water molecules, respectively, in the coordination sphere, NT_1 runs as 1.57, 2.35, and 3.05. This would be a striking confirmation of the translational first-power dependence of Eq. (3), which we have discarded, not without a certain act of faith, were it not that Morgan

[16] R. C. Warner and I. Weber, J. Biol. Chem. **191**, 173 (1951).
[17] See L. Michaelis in *Physical Methods of Organic Chemistry*, edited by A. Weissberger (Interscience Publishers, Inc., New York, 1949), second edition, p. 1885 ff., or P. W. Selwood, *ibid.*, p. 2451 ff.
[18] L. E. Drain, Proc. Phys. Soc. (London) **A62**, 301 (1949).
[19] Chiarotti, Christiani, Giullotto, and Lanzi, Nuovo cimento **12**, 519 (1954).
[20] R. C. Warner and I. Weber, J. Am. Chem. Soc. **75**, 5094 (1953).
[21] A. Wishnia (Ph.D.thesis, New York University, 1957).
[22] C. Tanford, J. Am. Chem. Soc. **79**, 5340 (1957).

TABLE III. Representative values of r and τ_c for Fe^{3+} and Fe-conalbumin.[a]

r, A	$\tau_c \times 10^{11}$ sec
2.8	4.8
2.6	3.1
2.4	1.9

[a] Computed from $\tau_c/r^6 = 1.00 \times 10^{35}$ sec cm^{-6}.

and Nolle's results[8] are consistent with a single τ_c attributable to rotation.

It is very likely that either hydrogen bonding or actual association of H^+ to the carboxylates raises the effective proton population of the coordination sphere to 4 for $Mn(EDTA)^{2-}$ and 7 for $Mn(NTA)^{1-}$, and that the longer τ_c for the larger complexes does the rest. If chemical exchange of relaxed protons is important in spreading the effect of paramagnetic ions to the whole solution, then, since the mean lifetime of protons on $Mn(H_2O)_6^{2+}$ is 10^3 times the rotational correlation time,[7] and the mean lifetime of a proton on a carboxylate must almost by definition be much less, the probability of finding a proton on a carboxylate need be only about as large as 10^{-3} to give the proper effect.

Rotation and electron spin relaxation, which affect the protons of the first hydration shell, combine as

$$(1/\tau_c)_{exp} = (1/\tau_c)_{rot} + 1/\tau_S. \qquad (2a)$$

The translational contribution to T_1 arises from more distant protons. This correlation time is therefore not to be averaged in, even though τ_c and $r^2/12D$ (for small r) are both of the order of 10^{-11} sec. Rather, the mechanism contributes an additive term to $1/T_1$.

Using Broersma's formulation,[11] and distances appropriate to Fe^{3+}, the rotational and translational contributions are in the ratio 8:1. If $\pi n/aD$, with $a = 4$ A (see the following), and $D = 10^{-5}$ cm^2 sec^{-1}, is compared with the value of $3p\,\tau_c r^{-6}$ computed from Eq. (2), using the experimental data and constants for Fe^{3+}, it is seen that the translational term is not more than $\frac{1}{7}$ the total. The translation effect has been neglected in the subsequent computations.

At the present time only the product $\tau_c r^{-6}$ has been determined for Fe^{3+}.§ τ_c is extremely sensitive to changes in r. Representative values are given in Table III. The upper limit is 2.8 A, since it depends on using the van der Waals radius of oxygen 1.4 A which is excessive in pure water and presumably more so in the strong field of Fe^{3+}. King and Davidson[6] seem to have used 2.44 A for the larger Mn^{2+} hydrate.

§ Undue weight should not be given to conclusions drawn from the small differences in NT_1 at 40 and 60 Mc (Table II). However, the frequency dependence in Eq. (2) gives values of τ_c of 3.0 and 2.5×10^{-11} sec for Fe^{3+} and Fe=conalbumin, respectively.

For Fe^{3+}, $\tau_S \geq 1.35 \times 10^{-10}$ sec.|| From Eq. (2a), the most likely value of τ_{rot} is 4.0×10^{-11} sec, and τ_S contributes 23% of τ_{exp}, with 14 and 36% as possible limits.

In the case of Fe-conalbumin, translational contributions must be smaller than for Fe^{3+}, owing to partial shielding of the solvent by the protein, and may be neglected. The experimental correlation time is thus necessarily the electron spin relaxation time τ_S. If one invokes association of H^+ to the phenolates, to give an $\frac{8}{12}$ effectiveness *vs* Fe^{3+}, then $\tau_c^{Fe} = \tau_S^{con}$. If the probability factor p is kept at $\frac{5}{12}$ that of Fe^{3+}, τ_S^{con} is correspondingly larger.

It should be possible to establish the relationships by extending this study to lower frequencies, and by investigating the temperature dependence of T_1 in the manner of Gutowsky and co-workers.[7]

There is some evidence that the relevant τ_c for Cr^{3+} is the electron spin relaxation time. The data of Morgan *et al.*[10] for various Cr^{3+} complexes are summarized in Table IV. Except for the hydrate, and possibly the oxalate, there are no rapidly exchangeable protons in the coordination spheres. If the H_2O of the next shell is required to rotate with the ions, the rotational correlation times become prohibitively long; accordingly, a tumbling τ_c seems unlikely. Nevertheless, calculation of r using Eq. (2) gives reasonable numbers for the Cr—H distances, if it is assumed that the H_2O dipole orientation changes with the sign of the ion. For example, the F—H separation in CrF_6^{3-} is between 1.5 and 2.0 A depending on the angle chosen for Cr—F—H. Relaxation of protons by flipping the electron spins deprives the coordination sphere of its unique role (if τ_S is the shortest correlation time the protons are treated as stationary), but the sixth-power dependence on r is preserved, and the nearest neighbors still dominate. The fact that $Cr(NH_3)_6^{3+}$ is $\frac{1}{12}$ as effective as $Cr(H_2O)_6^{3+}$ may be used to justify the assumption, implicit in the foregoing discussion, that, at the present state of approximation, the contribution of protons in more distant shells may be neglected in calculating r.

TABLE IV. Cr—H distances in Cr^{3+} complex solutions.[a]

Complex	$NT_1 \times 10^4$ sec mole	r, A[b]	
$Cr(H_2O)_6^{3+}$	1.40	[2.80]	[2.60]
CrF_6^{3-}	7.4	3.70	3.43
$Cr(NH_3)_6^{3+}$	16.8	4.24	3.93
$Cr(C_2O_4)_3^{3-}$	17.0	4.24	3.94
$Cr(CN)_6^{3-}$	20.5	4.38	4.07
$Cr(en)_3^{3+}$	20.0	4.36	4.05

[a] NT_1 from reference 10.

[b] Computed from $(r_1/r_2)^6 = T_1^1/T_1^2$ using the bracketed values of r_i for $Cr(H_2O)_6^{+3}$. There are presumably more water molecules in the first hydration layer of the larger ions than the smaller, but using $(r_1/r_2)^4$ would exaggerate these differences for ions of these dimensions; positive and negative ions would have to be treated separately.

|| J. King (Ph.D. thesis, California Institute of Technology, 1958). This was brought to the attention of the author by the referee.

Ferrihemoglobin

To calculate the depth of Fe^{3+} in Hb^+ one must assume a value for τ_S and a model for the protein molecule. The value τ_S will be taken as equal to that for conalbumin; if τ_S is shorter because of the interaction of the ferric ions on the same molecule, the actual value of the Fe—H will be still smaller than the estimates obtained.

It is assumed that the protein is a sphere of radius R centered on the origin. The independent Fe is located on the Z axis at a distance a from the origin; the distance D to a point on the protein surface is then $D=(R^2+a^2-2aR\cos\theta)^{\frac{1}{2}}$. We average D^{-6} over the sphere and find

$$\langle D^{-6}\rangle=\frac{\int_0^{\pi}\int_0^{2\pi}[R^2\sin\theta d\phi d\theta/(R^2+a^2-2aR\cos\theta)^3]}{\int_0^{\pi}\int_0^{2\pi}R^2\sin\theta d\phi d\theta}$$

$$=(1/8aR)\{[1/(R-a)^4]-[1/(R+a)^4]\} \quad (4)$$

$[1/(R+a)^4$ may be neglected].

It is further assumed that the surface density of protons on the sphere is the same for Hb^+ as for $Fe(H_2O)_6^{3+}$: $P=p(R/r)^2$. On this basis there are about 600 water molecules in the hydration shell of Hb^+, about 20% of the weight of the protein.

The ratio of T_1 for Fe^{3+} and Hb^+ may be computed from the relation

$$(T_1)_{Fe}/(T_1)_{Hb}=P\langle D^{-6}\rangle/pr^{-6}$$

$$=[(R/r)^2r^6/8aR(R-a)^4]. \quad (5)$$

With $R=27$ A for 66 000 molecular weight, and $(T_1)_{Fe}/T_1)_{Hb}=0.0256$, for $r=2.8$, 2.6, and 2.4 A, $(R-a)$ is 4.3, 4.0, or 3.7 A.¶ No attempt has been made to take account of the markedly anisotropic g factor for Hb^+.[23] The positions of the hemes in Hb^+ are of course not known; shifting the heme around the molecule without altering either its orientation or the depth of Fe produces widely different angles between the normal to the heme plane and the normal to the protein surface, so that the effective g at a given point on the protein may not be determined. $1/T_1$ presumably averages g^2 as well as $1/r^6$.

However, since g^2 changes by only a factor of 9, 4 A is in error by no more than a factor of 1.7. A better estimate will require a determination of τ_S.

ACKNOWLEDGMENTS

The author wishes to acknowledge his stimulating discussions with Professor N. Bloembergen and Professor Martin Saunders, and especially the helpful encouragement of Professor John G. Kirkwood.

¶ The use of 0.0256 assumes that the residual electron spin in HbCN contributes nothing to the relaxation. If the value 0.0295, corrected only for solvent, is used, the estimates are decreased by exactly 0.1 A.

[23] J. E. Bennett and D. J. E. Ingram, Nature 177, 275 (1956).

Electron Attachment in $C_8F_{16}O$

J. VON HOENE AND W. M. HICKAM

Technology Department, Westinghouse Research Laboratories, Beulah Road, Churchill Borough, Pittsburgh 35, Pennsylvania

(Received September 23, 1959)

The negative ion spectrum of $C_8F_{16}O$[6] at low electron energies has been obtained using the mass spectrometer. The most intense peaks are identified as $C_8F_{16}O^-$, $C_7F_{14}^-$, $C_6F_9O^-$, $C_4F_8O^-$, $C_4F_7O^-$, $C_3F_6O^-$, and CF_3O^- ions. Formation of the CF_3O^- ion requires a rearrangement process. Appearance potentials and attachment energy ranges of the most intense peaks are given. Positive and negative ion fragmentation of the molecule is discussed relative to the components of the mixture, perfluoro-2-butyltetrahydrofuran and perfluoro-2-propyltetrahydropyran and its separation.

I. INTRODUCTION

THE high thermal stability, resistance to chemical reaction, and high electric strength of certain of the perfluorocarbons have led to interest in such compounds in the electrical industry.[1–4] It is generally believed that the high electric strength of such gases relative to nitrogen arises from their ability to attach electrons.[5] A study of electron impact in a completely fluorinated cyclic ether[6] having the empirical formula, $C_8F_{16}O$, was made. The material, prepared by an electrolytic process,[7,8] is an odorless, colorless liquid having a vapor pressure of 3 cm at room temperature. It is nonexplosive and nonflammable and can be heated to 600°C without evidence of decomposition. It is believed to consist of a mixture of five- and six-membered ring compounds. The oxygen atom is contained in the ring and the fluorinated side chain is believed to be in the second position.[9] In Fig. 1 is shown the proposed structure for the two components, i.e., perfluoro-2-butyltetrahydrofuran and perfluoro-2-propyltetrahydropyran. In the present investigation, the negative and positive ion spectra of the components of the mixture have also been obtained.

II. EXPERIMENTAL

Separation of the mixture was carried out on the gas chromatograph using activated alumina. The chromatographic record shows two major peaks, which are interpreted as major fractions plus evidence of two others. The two major fractions are designated as component I and II in the order of their appearance and represent at least 95% of the mixture. One of the minor fractions showed great similarity to component II mass spectrometrically. The minor fractions are believed to be represented by the empirical formula $C_8F_{16}O$. Relative amounts of the two major fractions determined from the areas of the peaks placed the concentration at 35 mole % component I and 65 mole % component II. By using these cuts as calibrations, the mass spectrometer analysis of the mixture was 40 mole % component I, and 60 mole % component II. Both positive and negative ion mass spectra of the two cuts reveal large differences which suggest that component I is the six-membered ring compound and component II is the five-membered ring compound. Evidence for this tentative identification will be discussed later.

The positive ion spectra were obtained using the 21-103C Consolidated mass spectrometer with 70 ev electrons. The mass spectrometer utilized in the negative ion measurements was a 90° sector type instrument of conventional ion source design. Electron currents of less than 3 μa were used to minimize space charge effects which influence such measurements. The entire ion source was operated from batteries. Operating pressures of the mass spectrometer were well within the range for which linearity of positive ion current *vs* pressure was observed.

III. RESULTS AND DISCUSSION

In taking the measurements, a mixture of SF_6 and the $C_8F_{16}O$ component being studied was introduced. The SF_6^- ion curve is used as an internal standard for establishing the appearance potential and attachment energy range. The appearance potential is determined by the vanishing current as compared to that of SF_6^-, which is considered zero.[5,10] The attachment energy range for the formation of SF_6^- is considered zero, and the difference in the widths of the two curves is taken as the attachment energy range of the ion being measured. In the case of ions formed with excess energy, the range may represent a minimum value. It is realized that the energy resolution would not permit the separation of two or more capture peaks occurring with small energy separation.

[1] J. H. Simon, Ind. Eng. Chem. **39**, 238 (1947).
[2] A. V. Grosse, G. H. Cady, Ind. Eng. Chem. **39**, 367 (1947).
[3] L. Berberich *et al.*, Elec. Eng. **74**, 788 (1955).
[4] P. Narbut and A. Maslin, Am. Inst. Elec. Engrs. Conf. Paper No. 59–415, Winter General Meeting, New York (February, 1959).
[5] W. M. Hickam and D. Berg, J. Chem. Phys. **29**, No. 3, 517 (1958).
[6] FC–75, Minnesota Mining and Manufacturing Company.
[7] Minnesota Mining and Manufacturing Company, British No. 718318 (November 10, 1954).
[8] L. J. Halls, Minnesota Mining and Manufacturing Company, private communication.
[9] FC–75, Technical Data, Fluorochem. Div., Chem. Prod. Group, Minnesota Mining and Manufacturing Company (1957).
[10] W. M. Hickam and R. E. Fox, J. Chem. Phys. **25**, 642 (1956).

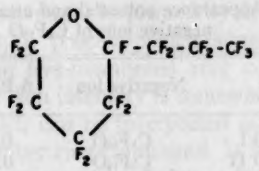

Perfluoro-2-propyltetrahydropyran (mol. wt. 416)

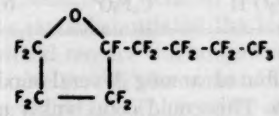

Perfluoro-2-butyltetrahydrofuran (mol. wt. 416)

FIG. 1. Proposed structures for the six ($C_8F_{16}O$[I]) and five ($C_8F_{16}O$[II]) member ring components of $C_8F_{16}O$.

In obtaining the appearance potentials for all the negative ions of $C_8F_{16}O$ using SF_6^- as an internal standard, one cannot check the electron energy distribution in the electron beam under similar electric and magnetic field conditions because of the large mass difference. In order to establish that the distribution was not influenced by these factors, the electron energy distribution was obtained from the derivative of the electron cutoff curve.[10] The retarding curve on the electron beam, i_e, its derivative, $N(V)$, and the SF_6^- curve obtained are shown in Fig. 2. All curves were normalized to the same peak height for ease of comparison. Similar data for the $C_8F_{16}O^-$ component I are shown in Fig. 3. Data for component II closely resemble that for component I. These results show that the same distribution curve was obtained when focused for mass 416 ($C_8F_{10}O^-$) as

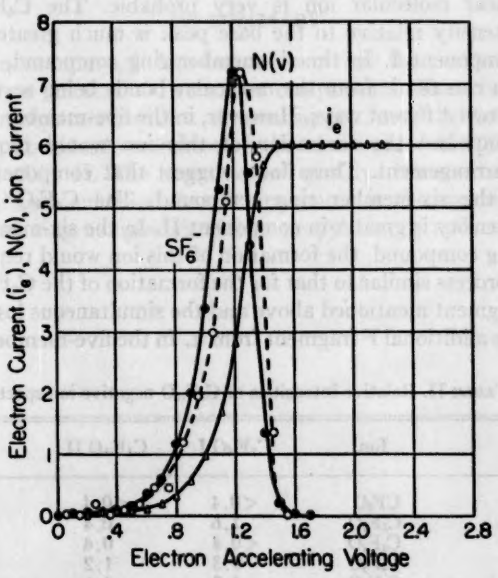

FIG. 2. Comparison of the SF_6^- curve to the electron energy distribution utilized. The two curves have been adjusted to the same height. The high energy side of the $N(v)$ curve is to the left.

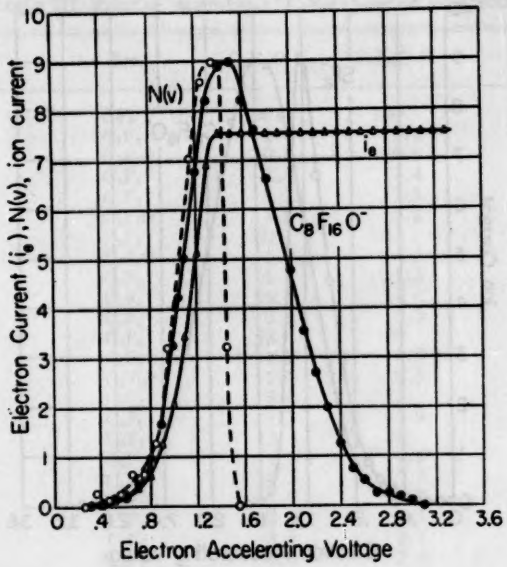

FIG. 3. Comparison of the $C_8F_{16}O$[I] curve to the electron energy distribution utilized. The two curves have been adjusted to the same height. The high energy side of the $N(v)$ curve is to the left.

for mass 146 (SF_6^-), indicating that these instrumental changes did not alter the electron distribution.

Figure 4 shows the SF_6^- curve along with the $C_8F_{16}O^-$ curve. Comparison of the two curves indicates that the appearance potential of $C_8F_{16}O^-$ is possibly 0.1–0.2 v higher than SF_6^- and that the attachment energy range as measured by the difference in the widths of the two curves is about 1.2 ev. In Fig. 5 is shown similar

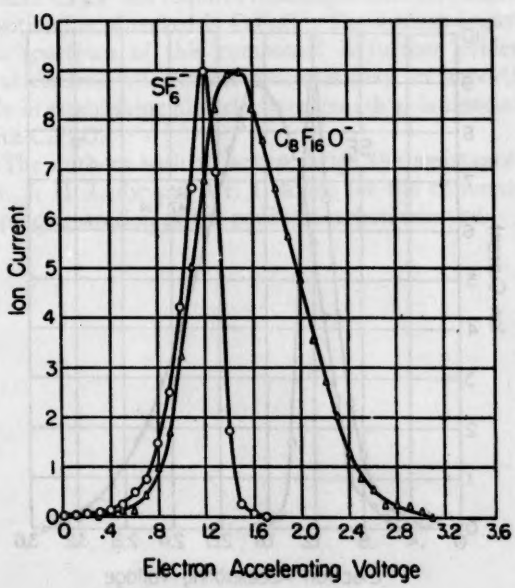

FIG. 4. Comparison of the SF_6^- curve from SF_6 and the $C_8F_{16}O^-$ curve from $C_8F_{16}O$[I] after adjustment to the same height.

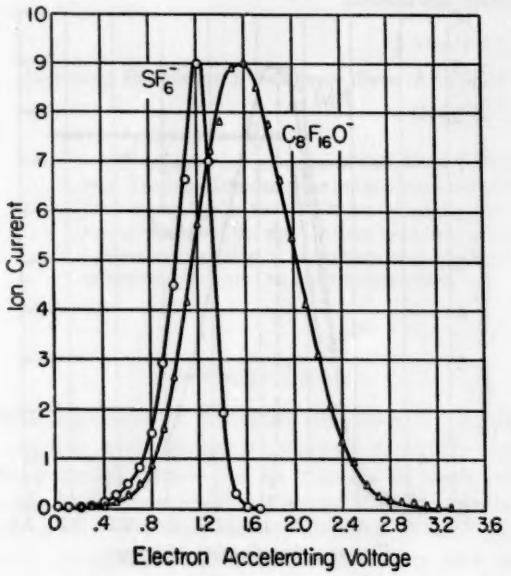

FIG. 5. Comparison of the SF_6^- curve from SF_6 and the $C_8F_{16}O^-$ curve from $C_8F_{16}O$[II] after adjustment to the same height.

data obtained from component II. The appearance potential and attachment energy range for these two components are approximately equal. The magnitude of the $C_8F_{16}O^-$ peak observed in the mixture is comparable to that of SF_6^- when a 50–50 mixture is used.

The large attachment energy range requires that the electron be able to impart considerable energy to the molecule. Possibly, the explanation for such a large cross section is associated with the formation of $C_8F_{16}O^-$ ion in an excited state in such a manner that the energy

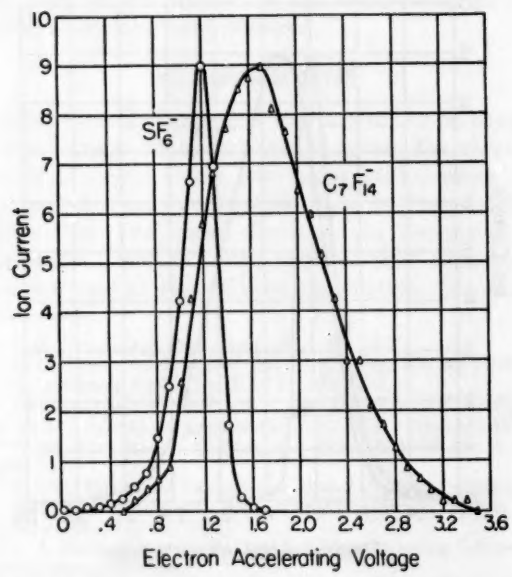

FIG. 6. Comparison of the SF_6^- curve from SF_6 and the $C_7F_{14}^-$ curve from $C_8F_{16}O$[I] after adjustment to the same height.

TABLE I. Appearance potential and attachment energy range for negative ions of $C_8F_{16}O$ I and II.

Gas	Negative ion	A.P. (ev)	Range (ev)
$C_8F_{16}O$ I	$C_8F_{16}O$	0.2	1.3
$C_8F_{16}O$ II	$C_8F_{16}O$	0.2	1.2
$C_8F_{16}O$ I	C_7F_{14}	0.4	1.5
$C_8F_{16}O$ II	C_7F_{14}	0.4	0.8
$C_8F_{16}O$ I	C_8F_9O	0.8	1.9
$C_8F_{16}O$ II	C_8F_9O	0.7	1.7

is distributed among several modes of vibration and rotation. This could conceivably allow the ion to exist in an excited state for a long time before the energy could be concentrated in a mode, which would result in either the ejection of an electron or a dissociative process. Possibly, the life time of the $C_8F_{16}O^-$ ion might be associated with the opening of the ring.

In Fig. 6 is shown the curve obtained for the $C_7F_{14}^-$ ion of $C_8F_{16}O$ I. The appearance potential is some 0.4 ev and the attachment energy range 1.5. A summary of the average appearance potential and attachment energy ranges relative to SF_6 for three of the major ions is shown in Table I.

The relative intensities of the most abundant negative ions of the two components are shown in Table II. In addition to these, $C_3F_7O^-$, $C_5F_9^-$, $C_4F_9O^-$, $C_6F_{11}^-$, $C_6F_{11}O^-$, $C_6F_{12}^-$, $C_7F_{12}^-$, $C_7F_{13}^-$, $C_7F_{14}O^-$, and $C_8F_{16}^-$ ions were detected at a low intensity in the mixture. The inability to observe these ions in the separated components is believed due to the limited sample size available rather than their absence in the spectrum. The large $C_7F_{14}^-$ ion indicates that removal of a CF_2O fragment and the resulting opening of the ring to form a linear molecular ion is very probable. The $C_4F_8O^-$ intensity relative to the base peak is much greater in component I. In the six-member ring compound, this ion can result from the molecular bonds being severed in two different ways. However, in the five-member ring compound the formation of this ion would require rearrangement. These facts suggest that component I is the six-member ring compound. The $C_4F_7O^-$ ion intensity is greater in component II. In the six-member ring compound, the formation of this ion would require a process similar to that for the formation of the $C_4F_8O^-$ fragment mentioned above and the simultaneous loss of one additional F fragment from it. In the five-membered

TABLE II. Relative intensities of $C_8F_{16}O$ negative ion spectra.

Ion	$C_8F_{16}O$ I	$C_8F_{16}O$ II
CF_2O	<0.4	<0.4
C_3F_6O	1.6	0.4
C_4F_7O	<0.4	0.4
C_4F_8O	9.3	1.2
C_8F_9O	4.7	4.1
C_7F_{14}	24	7
$C_8F_{16}O$	100	100

ring compound, this ion could be formed by detachment of the butyl group, a process which suggests that component II is the five-membered ring compound. Similarly, the $C_8F_9O^-$ ion intensity is somewhat greater in component I which can be interpreted as evidence that this is a six-member ring compound. It is interesting to note that a large number of the major negative ions contain the oxygen atom. The CF_3O^- ion was observed in both components. A detailed check of the isotopic peaks of this ion substantiated the identification. Its formation would require rearrangement.

The intensities relative to CF_3^+ for some of the positive ions are shown in Table III. The relative abundances of the CF_3 positive ion are approximately equal for both fractions. No parent molecular ion is observed. The heaviest positive ion fragment detected is $C_8F_{15}O^+$ (m/e 397). The intensity of $C_4F_7O^+$ ion of component II is about six times the same ion of component I. As in the formation of the $C_4F_7O^-$ ion, this ion represents the ring of the five-member ring compound, and it would require considerably more fragmentation to arise from the six-member ring compound. Similarly, the $C_8F_9O^+$ ion represents the ring of the six-member ring compound, and in component I it is seven times the intensity of the ion in component II. These facts along with those associated with the $C_4F_8O^-$ and $C_4F_7O^-$ ion intensity indicate that component I is the six-member ring compound, and component II the five-member ring compound. Major peaks in the positive ion spectrum do not contain the oxygen atom. In addition to the above differences in the positive ion spectra of both components, there are two peaks which are detected in $C_8F_{16}O$ II at *m/e* 66.7 and 145, which appear to have originated from metastable ions.

TABLE III. Relative intensities of $C_8F_{16}O$ positive ion spectra.

Ion	$C_8F_{16}O$ I	$C_8F_{16}O$ II
CF_3	100	100
C_2F_3	1.4	1.2
C_2F_3O	0.4	0.6
C_2F_3	2.5	2.4
C_3F_3	8.1	7.1
C_3F_3O	3.6	3.2
C_3F_4	60	43
C_3F_3O	1.7	1.6
C_3F_4	1.7	1.5
C_2F_5	16	14
C_4F_4	0.6	0.5
C_3F_5	35	26
C_4F_5	1.0	0.8
C_3F_5O	1.0	0.5
C_3F_6	5.6	11
C_4F_6	1.1	0.9
C_3F_7	13	30
C_4F_7	6.6	4.4
C_5F_7	0.3	0.2
C_4F_7O	1.0	5.7
C_4F_8	0.4	0.3
C_4F_9	3.4	2.7
C_5F_9	3.0	2.4
C_5F_9O	1.4	0.2
C_8F_{11}	0.9	0.5
$C_8F_{15}O$	0.8	0.7

IV. SUMMARY

In summary, it has been shown that the perfluorocarbon consists of two major components. These have been separated with a chromatograph, and their relative abundance calculated to be of the order of 40% I and 60% II. The negative and positive ion spectrum exhibited evidence that component I is the six-membered ring compound with a propyl chain, and component II is the five-membered ring with the butyl chain. A number of negative ions are found, the most abundant being $C_8F_{16}O^-$ at a level comparable to SF_6^- from SF_6. The $C_8F_{16}O^-$ ion in both the pyran and furan form exhibit an appearance potential of the order of 0.2 v and an attachment energy range of 1.2 ev relative to SF_6. The second most abundant negative ion is $C_7F_{14}^-$, which possibly results from the opening of the ring and the emission of a CF_2O fragment. The formation of CF_3O^- ion requires rearrangement. The heaviest positive ion observed is $C_8F_{15}O^+$. The intense negative ion spectrum of this compound is further evidence that electron attachment processes play an important role in establishing high electric strength as is associated with $C_8F_{16}O$.

The authors wish to acknowledge the assistance of Dr. J. H. Lady and Mr. I. Kesse for the chromatographic separation of the perfluorocarbon mixture.

Chemically Induced Vibrational Excitation: Hydroxyl Radical Emission in the 1–3 Micron Region Produced by the $H+O_3$ Atomic Flame*

DAVID GARVIN, *Frick Chemical Laboratory, Princeton University, Princeton, New Jersey*

AND

H. P. BROIDA AND H. J. KOSTKOWSKI, *National Bureau of Standards, Washington, D. C.*

(Received September 24, 1959)

A detailed investigation has been performed in the 1- to 3-μ wavelength region on the radiation emitted by the hydroxyl radical from a low-pressure flame of ozonized oxygen and atomized hydrogen. Wavelengths and photon intensities have been obtained for about 300 lines in the OH vibration-rotation bands $V-V-\Delta V$ where $\Delta V=3$, $V=9$ to 5, and for $\Delta V=2$, $V=9$ to 2. Relative photon band intensities have been determined from the overdetermined set of data by a method of successive approximations using an IBM 650 computer. Dipole moment parameters have been calculated using the above data and Morse oscillator transition probabilities.

Approximate rotational and vibrational Boltzmann distributions exist with an average rotational "temperature" of 560°K for the P branches, 460°K for the R and Q branches, and a vibrational "temperature" of 9250°K for the $\Delta V=2$ and 3 bands. The absence of radiation from levels $V>9$ confirms the nonthermal character of the excitation and its dependence on the energetics of the reaction $O_3+H\rightarrow OH+O_2$. Moreover, flux calculations based on the assumption that in this case collisional deactivation transition probabilities are proportional to the radiation probabilities show that there is an appreciable OH production in all levels $V\leqslant 9$ and the main flux of OH through any population level is via $\Delta V=1$ transitions. Possible causes for the large changes in line intensity with pressure and smaller but significant changes with flows or concentrations are discussed.

INTRODUCTION

THE character of the radiation produced in the low-pressure atomic flame that results on mixing H atoms with ozone has been ascribed to

$$H+O_3\rightarrow OH^*+O_2,$$

$$OH^*\rightarrow OH+h\nu,$$

and has been reported on previously.[1–4] This communication summarizes detailed studies of the hydroxyl radical bands emitted between 1 and 3 μ. Following an exposition of the experimental procedure and the results derived therefrom, the mode of production of the hydroxyls, and several subsequent physicochemical processes are discussed.

EXPERIMENTAL

The description and operation of the apparatus in which the radiation was produced was that used for the study of this flame in the photographic infrared region.[4] The spectroscopic technique differed appreciably. The flame, viewed end on as before, was reflected by a plane mirror onto a spherical mirror which focused the source onto the entrance slit of the monochrometer. This instrument was a modified Perkin-Elmer Model 99 double-pass spectrometer using 13-cycle modulation and the P-E Model 81 amplifier. The modifications, similar to those described by Lord and McCubben,[5] included the replacement of the prism and Littrow mirror by a 3×3 in. plane grating and the substitution of a dry ice–acetone-cooled lead sulfide detector for the thermocouple.

In this work both a 7500 line/in. and a 15 000 line/in. grating were used. Higher order spectra were removed by filters placed in front of the entrance slit. A Corning 2540 Filter was used for the region from 1.0 to 1.9 μ and a Baird Associates germanium filter at longer wavelengths.

The spectral slit widths varied from 3 to 10 cm^{-1} and were sufficiently large that the observed peak intensity of a single OH line should be proportional to its actual integrated intensity. Also the peak intensity observed for a number of unresolved OH lines should be proportional to the sum of the integrated intensities of the individual lines, at least within the experimental accuracy, if the maximum separation of the lines is less than 1 cm^{-1}. In most cases the last condition holds for the unresolved lambda doublets, hence only observed peak intensities for the two resolved spin doublet components of each rotational line are reported here.

Mercury, helium, and water vapor lines were superimposed on the flame spectrum in order to obtain the wavelength calibration of the spectrometer. Hydroxyl lines that lie in the nieghborhood of calibrating lines are probably accurate to within 2 A; the others are probably within 5 A of their true values.

The spectrometer was calibrated for relative intensity response against a tungsten strip lamp operated at a

* Supported by the U. S. Air Force under Contract No. AF-18(603)134 (with Princeton University) and No. CSO 680-56-30 (with the National Bureau of Standards). Air Force Office of Scientific Research Tech. Note 59-746.

[1] McKinley, Garvin, and Boudart, J. Chem. Phys. **23**, 784 (1955).

[2] T. M. Cawthon, Jr., and J. D. McKinley, Jr., J. Chem. Phys. **25**, 585 (1956).

[3] F. Kraus, Z. Naturforsch. **12A**, 479 (1957).

[4] David Garvin, J. Am. Chem. Soc. **81**, 3173 (1959).

[5] R. C. Lord and T. K. McCubben, J. Opt. Soc. Am. **45**, 441 (1955).

brightness temperature of about 1435°C (Int. 1948). This radiation was weakened to the intensity level of the OH lines by reflection from a piece of spectrally calibrated MgO. The alternative, the use of a lower brightness temperature was avoided because data on the emissivity of tungsten at such low temperatures were not available. The energy received by the spectrometer detector per unit wavelength interval was calculated from the blackbody radiation law, corrections being made for changes in the emissivity of W,[6] the reflectance of the MgO and the dispersion of the spectrometer with wavelength. In computing intensities of the OH lines allowance was made for the transmission of the quartz window on the source. The accuracy of the relative intensities of OH lines is estimated to be better than 20% except for the weakest lines. This estimate is based on these factors: (a) uncertainty in the relative emissivity of W=±5%; (b) uncertainty in brightness temperature and due to nonuniformity of the tungsten strip=±5%; and (c) reproducibility of the OH lines, which was ±2% for the strongest and ±10% for those $\frac{1}{10}$ as strong.

RESULTS

The spectral region from 1.05 to 3.2 μ was surveyed. About 300 lines (unresolved lambda doublets) assignable to OH vibration rotation bands were identified in the region from 1.076 to 2.360 μ. These comprised lines in the P, Q, and R branches of each of the following bands: $\Delta V=3$: 9–6, 8–5, 7–4, 6–3, 5–2; $\Delta V=2$: 9–7, 8–6, 7–5, 6–4, 5–3, 4–2, 3–1, and 2–0. In addition weak emission probably due to the 4–1 band appeared. No definite indications were found near 3 μ of any of the $\Delta V=1$ bands, but this was a region of low sensitivity for the instrument. No evidence was found of bands originating in the 10th vibrational level, i.e., 10–7 and 10–8, although these were expected on the basis of previous work.[3,4] A very small number of lines, all relatively weak, could not be assigned with certainty to OH; they remain unidentified.

The general appearance of the higher bands described earlier[4] apply to those found here, except that the R branches come to a head at larger values of K (the rotational quantum number) and the first few Q branch lines often appeared as unresolved spin doublets.

A. Wavelengths, Identifications, and Energy Levels

The wavelengths of OH lines, corrected to vacuum conditions, were determined from the spectrometer dispersion calibration and are reported in Table I along with their identifications. The wavelengths agree closely with those calculated from energy level data[7,8] for all bands originating in $v=6$. Because of some minor discrepancies among the energy levels for $v=7$, 8, and 9 which could be calculated from previous work,[2,3] these were recalculated from the data reported here. They are given in Table II.

B. Intensities

The relative photon intensities of the lines are also reported in Table I. These, as well as the rotational and vibrational level population estimates made from them (but not the derived dipole moment parameters) are dependent upon the experimental method used to produce and observe the radiation.

(*1*) *Experimental conditions.*—In the normal course of this work hydrogen atoms produced by a high-voltage electrode discharge in moist hydrogen were mixed with ozonized oxygen. The data in Table I are based on this. The effect on intensities of flow rates, reagent concentrations, and pressure is described in the following. Variations in intensity refer to the Q (1) lines of the bands.

(a) At constant total pressure and hydrogen flow either an increase in the ozone content of the ozonized oxygen stream or an increased flow rate of the latter increased the line intensities linearly without changing appreciably the relative intensity from band to band.

(b) At constant ozonized oxygen flow and total pressure, the variation of hydrogen flow through the electrode discharge increased the intensities markedly, a 50% flow increase causing threefold, fourfold, and fivefold changes in 4–2, 5–3, and 6–4 $Q(1)$ lines, respectively.

(c) A marked pressure effect was found. Intensities decrease with pressure increase, the change being more marked for higher overtone bands. This is shown in Fig. 1.

(d) Both a high-voltage electrode discharge and a microwave generator were used to produce hydrogen atoms in both moist and dry hydrogen. All of these gave about the same intensity for 4–2 $Q(1)$, but the 6–4 $Q(1)$ was, surprisingly, variable:

6–4 $Q(1)$ Intensity relative to 4–2 $Q(1)$

	Dry H_2	Moist H_2
High voltage	0.86	0.93
Microwave	1.01	0.50.

In addition use of both exciting sources in series on moist H, reduced the 4–2 Q line 18% without changing the 6–4 intensity.

(*2*) *Rotational analysis.*—The apparent rotational temperature of the hydroxyl radicals was determined

[6] J. C. DeVos, Physica **20**, 690 (1954).

[7] G. H. Dieke and H. M. Crosswhite, "The ultraviolet bands of OH: Fundamental data" ["Bumblebee Series" Report No. 87 (The Johns Hopkins University, Baltimore, Maryland, 1948)].

[8] R. C. Herman and G. A. Hornbeck, Astrophys. J. **118**, 214 (1953).

TABLE I. Wavelengths, intensities, and identifications for OH vibration-rotation lines emitted in the H—O_3 flame at 4.2 mm Hg. Wavelengths in A reduced to vacuum. Relative intensities: $I/\nu^4 = Nf$.

Vibrational Transition: 2-0			3-1		4-2		5-3		6-4		7-5		8-6		9-7		
Line Desig.	A°	Nf	A°	Nf	A°	Nf	A°	Nf	A°	Nf	A°	Nf	A°	Nf	A°	Nf	
R head	13907			a	15467		4-2	P(4)		f			7-5	P(6)	21008		f
$R_1(5)$			2-0	$P_1(4)$			16302	91	5-3	$P_1(5)$c	18292	70	19540	137	8-6	P(7)	a
$R_2(5)$	14018	ad					4-2	$P_2(5)$					.572	we	8-6	P(7)	a
$R_1(4)$	043	d	14739	74	3-1	$P_2(5)$					17282	146	330	90	591	253	8-6	P(7)	a
$R_2(4)$	059	d	759	w	3-1	$P_2(5)$					311	.96	352	d	616	200	8-6	P(7)	a
$R_1(3)$			2-0	$P_2(5)$	3-1	$P_1(5)$	16388	161			330	181	6-4	$P_1(6)$	640	324	8-6	P(7)	a
$R_2(3)$	102	d	2-0	$P_1(5)$	15569	115	413	111a	5-3	$P_2(6)$	18433	145	675	217	21155	22			
$R_1(2)$	132	d	14832	120	579	171		$R_2(3)$	5-3	$P_1(6)$	459	212	7-5	$P_2(7)$	174	126			
$R_2(2)$	161	48d	863	80	3-1	$P_2(6)$a					17427	144	505	129	749	255	228	130	e
$R_1(1)$	186	58d	2-0	$P_2(6)$	3-1	$P_1(6)$a	503	134			450	150	6-4	$P_1(7)$	770	286	246	142	
$R_2(1)$	224	25b	14931	66	15708	83	553	87	5-3	$P_2(7)$a	18587	111	838	149	8-6	$P_1(8)$			
Q (1)	343	82a	15059	235	832	308	691	316	655	365a	745	367	20005	d	505	492	c		
Q (2)		Q (1)	075	107	850	138	708	157	670	164a	765	d	030	d	539	261	c		
Q (3)	374	32	087	51	872	69	4-2	$P_2(8)$	699	179	797	97e	066	d	576	92			
Q (4)	400	25b	111	31	899	96a	4-2	$P_1(8)$	734	45	842	de		d	536	40			
Q (5)			143	40a			16806	bw	775	18					9-7	$P_2(2)$	c		
$P_2(2)$	467	37	186	81	975	120	840	120	812	130	915	291a	191	d	708	136	c		
$P_1(2)$	518	82	240	160	16034	87	905	271c	881	233	990	d	274	332	797	308			
$P_2(3)$	561	59	287	148	084	182	955	193	936	201	19069	d	342	365a	870	242			
$P_1(3)$	602	105	333	238	134	325	17018	341	18004	369	112	d	410	531	953	408			
$P_2(4)$	664	83	396	177	193	242c	077	257	069	253	192	d	497	618	22050	393			
$P_1(4)$	699	143a	433	313	235	378c	123	374	119	412	251	610	560	613	121	529			
$P_2(5)$	780	118a	508	186a	316	262c	208	309c	212	d	348	405	669	312	247	324			
$P_1(5)$	800	141a	542	303c	350	340c	247	445c	255	d	398	555	725	599	312	548			
$P_2(6)$	886	a	632	231a	444	285	358	245a	364	d	517	542a	856	398	459	300			
$P_1(6)$	908	81	663	295a	477	346	385	457a	401	ad	559	587a	905	541	517	439			
$P_2(7)$	15008	36	761	90	585	130	503	222a	528	ad	697	400a	21060	400a	691	267			
$P_1(7)$	025	47	783	119	616	174	530	219	560	ad	732	402	102	439a	757	315			
$P_2(8)$			4-2	Q (4)	732	163a	6-4	Q(1,2)	703	d	890	218	276	263	953	196			
$P_1(8)$	3-1	Q (5)	15918	76	755	129a	686	155a	729	d	922	257	315	328c	23000	271			
$P_2(9)$					888	42s	831	97	888	133	20097	d	9-7	Q(1)	223	134			
$P_1(9)$					5-3	$P_1(2)$	852	97	7-5	$P_2(2)$	126	d	9-7	Q(2)	265	173			
$P_2(10)$					17055	43	18010	40			20315	88	759	124f	515	81			
$P_1(10)$							031	74	19088	92ef	8-6	$P_2(3)$f			550	123	f		

Vibrational Transition: 5-2			6-3		7-4		8-5		9-6		SUPPLEMENTAL				
Line Desig.	A°	Nf	A°	Nf	A°	Nf	A°	Nf	A°	Nf	A°	Line Desig.	A°	Line Desig.	
R head	10701		11263	f	11976		12754		13672		11263	6-3 R head			
$R_1(2)$					12005	10.5	776				294				
$R_2(2)$					029	12.5a					12614	?			
$R_1(1)$	10749		11352	6.3c	058	e	802	15.7	715	20.8	13640	?			
$R_2(1)$			380				833	7.1	749	10.7	16272	5-3 R(6)	18292	7-5 R?	
Q (1)	10837	7.9	440	10.0	121	15.9	902	22.7	823	19.2	17172	6-4 R(8)	18330		
Q (2)											191	6-4 R(7)	18352		
Q (3)			471	e			936	6.9			19297	6-4 $P_2(11)$	18682	?	
Q (4)			488	e							318	6-4 $P_1(11)$	18842	?	
Q (5)											20576	7-5 $P_1(11)$			
$P_2(2)$			508	4.25	194	4.46	981	8.4b	2-0	R head	20801	7-5 $P_2(12)$			
$P_1(2)$	10927	4.4	540	6.6	228	9.5	13017	14.4	13948	21.3	20824	7-5 $P_1(12)$			
$P_2(3)$	951	3.9	566	7.1	254	7.9	051	14.0	981	25.1	21008	9-7 R(7)			
$P_1(2)$	975	6.9	592	9.5	287	12.9	082	22.5	2-0	$R_2(5)$	21028	9-7 $R_1(5)$	21357	?	
$P_2(4)$	11009	4.34	627	7.2	323	9.0	126	16.7			22027	8-6 $P_2(11)$	21373	?	
$P_1(4)$	11030	8.3	11650	10.5	12351	15.6	12154	26.8			22345	8-6 $P_1(12)$			
$P_2(5)$			692	6.3	397	10.1	209	23.8			22586	?			
$P_1(5)$	090	6.9 b	716	10.6	420	13.7	234	25.5			22625	8-6 $P_2(13)$			
$P_2(6)$	143	3.90	766	w	482	9.3	300	15.0	14258	17.8	22651	8-6 $P_1(13)$			
$P_1(6)$	154	5.9	788	9.3	499	10.4	324	21.8	283	25.8	23863	9-7 P (11)			
$P_2(7)$	213		846	3.96	571	7.4	401	13.1							
$P_1(7)$	227	4.9 w	863	6.4	586	8.0	420	17.9							
$P_2(8)$	6-3	R head					512	7.5							
$P_1(8)$	6-3	R head			674	be	527	11.7							
$P_2(9)$	6-3	$R_2(1)$					639	e							

[a] Overlapped by another line, intensity shown is the sum.
[b] Broad.
[c] Minor overlap.
[d] Water vapor absorption interference.
[e] Questionable wavelength.
[f] See supplemental list.

from the intensity distribution within each band. Plots of log (photon intensity/rotational line strength) *vs* upper state energy level were prepared, using the line strengths given by Benedict, Plyler, and Humphreys[9] as in earlier work. These plots, prepared separately for the P, Q, and R branches, were reasonably straight lines, although with appreciable scatter. Rotational "Temperatures" for the P branches, including both lambda components of each line, of 12 bands averaged 560±30°K with a range from 617 to 497°K. (One band, 9–6, with T_R=375 was omitted.) Where available, R and Q branch rotational temperatures were about 100°K less. The scatter in "temperatures" from band to band showed no definite progression with Δv or with upper state.

(3) *Vibrational analysis.*—In our earlier work the relative intensities of the vibrational bands were determined from the average of ratios of intensities of lines with the same rotational quantum number in pairs of bands. This method required the assumption that the rotational line strengths were independent of the extent of vibration excitation. In line with the analysis by Herman, Rothery, and Rubin[10] of the influence of rotation on the intensities of rotation-vibration lines, another technique has been employed. For a given pair of bands, the intensity ratios for P and R branch lines with the same K were plotted against $\pm K$, respectively, and the interpolated intensity ratio at K=0 was determined. Since the rotational correction is zero at this point (and increases with K), the interpolated value should approximate very well the true vibrational intensity ratio $N_v f_{v\Delta v}/N_{v'} f_{v'\Delta v'}$ (N_v is the population in the vth level and $f_{v,\Delta v}$ the transition probability for the transition $v \rightarrow v-\Delta v$). In addition, ratios of intensities of the $Q(1)$ lines were determined. These yield approximately the same quantity. (The ratio technique automatically corrects for the quasi-thermal rotational distribution without imposing an intermediate averaging process in the calculation.) Such ratios were determined for contiguous bands and for all pairs with the same upper state, and, where data appeared to be unreliable, for noncontiguous bands.

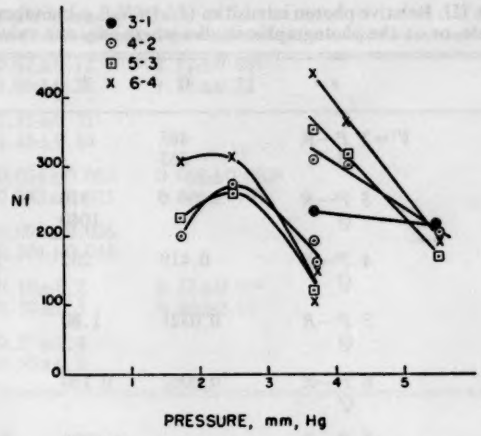

FIG. 1. Variation with pressure of relative photon intensities of hydroxyl emission bands.

This procedure overdetermines the relative intensities for the 13 bands observed (for the $P-R$ plots 21 ratios were determined). Formally the reduction of this overdetermined set is the same as that described by Worthing and Geffner[11] for determining the most probable values of the fundamental physical constants. Here the twelve simultaneous linear equations were solved for the relative band intensities by successive approximations (Gauss-Siedel and Gauss methods) using an IBM 650 computor. This machine technique was applied to the $P-R$ branch interpolations, and to the Q branch ratios (both based on the data in Table I). (The "best set" previously reported for the bands in the photographic region was prepared in this manner.) In all three cases both weighted and unweighted sets of ratios were treated, the weights being set (approximately) inversely proportional to scatter of the data. The weighted $P-R$ interpolation and photographic infrared region results, arbitrarily adjusted to the same scale by equating the value for the 5–2 band which appears in both sets, and the $Q(1)$ results are reported in Table III. The weighted $P-R$ results, based on a larger set of data, are considered the most reliable. Unweighted results agree with those shown within 15% in all and within 5% in half the cases.

Machine solutions of such problems are highly desirable. Twenty to eighty iterations of each set were required before the approximations gave results stable to three figures for each band intensity. When using the "Bell I Interpretive Code" one-half to one and one-half hours of IBM 650 machine time were required per

TABLE II. Energy levels (cm⁻¹, vac.) for OH in vibrational states 7, 8, and 9 based on measured P branch lines in the bands 7–4, 7–5, 8–5, 8–6, 9–6, and 9–7.

	v=7		v=8		v=9	
K	f_1	f_2	f_1	f_2	f_1	f_2
1	21 537	21 667	23 950	24 081	26 187	26 314
2	21 599	21 709	24 010	24 121	26 242	26 354
3	21 687	21 785	24 094	24 191	26 322	26 421
4	21 801	21 888	24 203	24 288	26 424	26 510
5	21 942	22 013	24 334	24 411	26 548	26 626
6	22 107	22 174	24 492	24 559	26 696	26 766
7	22 297	22 356	24 672	24 732	26 865	26 927
8	22 516	22 569		24 925	27 057	27 115
9	22 758	22 808			27 271	27 328

[9] Benedict, Plyler, and Humphreys, J. Chem. Phys. **21**, 398 (1953).

[10] Herman, Rothery, and Rubin, J. Mol. Spectroscopy **2**, 369 (1958).

[11] A. G. Worthing and J. Geffner, *Treatment of Experimental Data* (John Wiley & Sons, New York, 1943), p. 216 ff.

TABLE III. Relative photon intensities ($I/\nu^4 = N_v f_{v,\Delta v}$) of vibrational bands of OH. $P-R$: based on interpolated value for the rotationless state, or on the photographic studies where only one value is shown. Q: based on the $Q(1)$ line. All values are weighted results.

	$v=$	0	1	2	3	4	5	6	7
$V'=2$	$P-R$	465							
	Q	363							
3	$P-R$	69.9	970						
	Q		1040						
4	$P-R$	0.419	232	1210					
	Q			1360					
5	$P-R$	0.0321	1.80	309[a]	1330				
	Q			354	1460				
6	$P-R$	0.0067	0.150	810	482	1380			
	Q				444	1610			
7	$P-R$		0.0328	0.465	22.3	645	1570		
	Q					701	1620		
8	$P-R$			0.115	1.50	48.1	1,000[b]	2120	
	Q						1,000	...	
9	$P-R$			0.0195	0.157	1.63	72.0	1390	2090
	Q							846	2170
10	$P-R$				0.00176	0.0169			

[a] Tie point between photometric and photographic data.
[b] Arbitrary base value for both $P-R$ and Q sets.

problem. The slow (and erratic) convergence coupled with arithmetic errors makes hand solutions unreliable and unprofitable.

(4) *Dipole moment parameters.*—The method used to extract the dipole moment parameters of OH, using Morse oscillator transition probabilities and a series expansion of the dipole moment about the equilibrium position has been described elsewhere.[4] Values for the additional integrals needed here are given in Table IV and the dipole parameters in Table V.

(5) *Vibrational level population estimates.*—The + values for the dipole parameters of the $P-R$ set give transition moment integrals significantly different from zero. The − set of roots does not, a situation found earlier for the photographic region bands. Limited tests indicate that the Q set roots also give null transition moments. Accordingly the analysis of vibrational level populations was based upon the + roots of the $P-R$ set. This is summarized in Fig. 2 which also contains the result of applying these constants to the $\Delta v=5$ series of the laboratory work and to Meinel's night

TABLE IV. Transition moment integrals for the Morse Oscillator with a series dipole moment, $k=39.57$ (OH). (See reference 5 for additional values and definitions.)

			${}_1I_{vv'}$			
$v=$	3	4	5	6	7	8
$\Delta v=1$	−0.333	−0.333	−0.321	−0.303	−0.280	−0.252
			$(I_2-\ln k)$			
$\Delta v=1$				−0.569	−0.680	−0.808
			$(I_3-(\ln k)^2)$			
$\Delta v=1$	−1.91	−2.48	−3.02	−3.60	−4.30	−5.05
$\Delta v=2$	+4.67	+3.99	+3.26	+2.49	+1.66	
$\Delta v=3$	+8.81	+7.88	+7.20	+6.33		

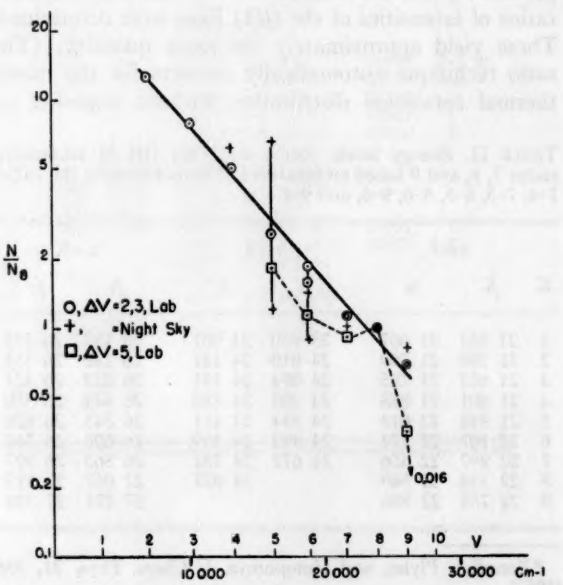

FIG. 2. Relative populations of hydroxyl radicals observed in the $H+O_3$ reaction at 4.2 mm Hg, based on dipole moment parameters determined from $\Delta v=2$ and 3 intensities.

TABLE V. Transition moment parameters for OH.

$(M_2/\beta M_1+3M_1\ln k/\beta^2 M_1)$[a]	$P-R$	+:	0.57±0.12	1.12±0.04[b]
		−:	3.06±0.22	1.23±0.22
	Q	+:	1.31±0.31	
		−:	2.25±0.45	
$(M_3/\beta^2 M_1)$	$P-R$	+:	0.034±0.013	0.068±0.003[b]
		−:	0.233±0.021	0.076±0.01
	Q	+:	0.094±0.026	
		−:	0.204±0.043	
$(M_2/\beta M_1)$[c]	$P-R$	+:	0.19±0.2	0.37±0.05[b]
		−:	0.50±0.3	0.40±0.14
	Q	+:	0.27±0.4	
		−:	0.50±0.6	

[a] $\ln k=3.68$, $\beta=2.32\times10^8$ cm^{-1}; all values in table are positive.
[b] Reference 5 (in which the symbols used here are defined).
[c] Derived from items above, propagated standard error shown.

sky observations.[12] This plot, interpreted in terms of a Boltzmann distribution, yields a vibrational "temperature" of 9250°K for the $\Delta v=2$ and $\Delta v=3$ bands.

DISCUSSION

The increased precision of the photometric data compared to the photographic results has removed some of the earlier ambiguities and also has justified the view that the behavior of this system is quite complex. Moderately concordant Boltzmann population distributions among rotational levels in different bands have been found, and the discrepancy between rotational analyses based on the two spin doublet components has disappeared. Molecular parameters derived from low Δv transitions do not invariably lead to transition probabilities equal to zero (within experimental error). This indicates, as may be expected, that the Morse oscillator model is more reliable for small than for large deviations from harmonic oscillator behavior. It is unfortunate, however, that the parameters needed for mapping the dipole moment variation with internuclear distance are highly unreliable—a situation due to the propagation of errors. It remains true, on the other hand, as shown by the signs and magnitudes of these parameters that higher order terms are appreciable and that the dipole moment is probably changing rapidly over the range of interest.

The vibrational population estimates confirm the nonthermal character of the excitation, and its dependence on the energetics of the $O_3+H\rightarrow OH+O_2$ reaction. The absence of radiation from level $v=10$ here, and the very low intensity level previously reported are the strongest indicators. The approximate Boltzmann distribution for levels with $v\leq9$ raises an interesting question concerning the levels in which the excited hydroxyls are produced.

It may be assumed that the system observed here is in a steady state; that the rate of disappearance of OH in any level is equal to its rate of formation. According to weak interaction (Landau-Teller) theories, transition probabilities for collisional deactivation are proportional to the radiation probabilities,[13] and hence a system in which collisional quenching is important[14] will behave in the same manner as one in which radiation loss is the main mode of deactivation. Thus the observed populations and transition probabilities may be used to determine the details of the steady state flux through any population level. When, for a given level, the rate of appearance of OH from higher states and the rate of its disappearance to all lower levels are calculated it becomes apparent that the main flux is via $\Delta v=1$ transitions. However, in all cases the flux into a state is less than the flux out. The difference is construed as the rate of production in that state. The fluxes based on Table I data and also the differences for the data taken in the pressure study are given in Table VI. (Magnitudes in the last three columns are only approximately comparable.) Thus, an appreciable rate of production of hydroxyls is indicated for all levels. The markedly higher rate for level 4 suggests the occurrence of the (adiabatic) process producing electronically excited oxygens:

$$H+O_3\rightarrow OH(v=4)+O_2(^1\Sigma_g^+).$$

Since the enthalpy of the reaction is 27 200 to 28 600 cm^{-1}, excitation of the oxygen (>13 195 cm^{-1}) leaves 14 100 to 15 400 cm^{-1} for hydroxyl excitation. This is sufficient for $v=4$ but not for $v=5$. The forbidden "atmospheric" bands of oxygen, originating in the $^1\Sigma_g^+$ state, were observed by Cawthon and McKinley[3] in very long exposures of this flame. The analysis here confirms that the emitter is produced in the primary reaction.

[12] A. B. Meinel, Astrophys. J. **111**, 555; **112**, 120 (1950).

[13] For applications to this type of system see Bazley, Montroll, Rubin, and Shuler, J. Chem. Phys. **28**, 700 (1958); and earlier papers in their series.

[14] Strong collisional quenching is suggested by the rate measurements: David Garvin and J. D. McKinley, Jr., J. Chem. Phys. **24**, 1256 (1956).

TABLE VI. Steady state analysis of excited OH production.

(Population numbers are on an arbitrary scale. First five columns refer to 4.2 mm data only.)

Population		Influx rate $\Sigma N_i f_{il}$	Efflux $N_l \Sigma f_{jl}$	Rate of production		
V_l	N_l	$i=1+l$	$j=0$ to $(l-1)$	4.2 mm	3.7 mm	5.5 mm
2	7760	480	469	−11	−34[a]	−51[a]
3	4860	431	480	+49	+58	+150
4	3100	250	430	180	149	149
5	1630	153	248	95	73	45
6	984	109	153	44	74	43
7	700	91.5	108	10.5		
8	626	50	91.5	41.5		
9	407	4	55.4	51.4		
10	40[a]		5[a]	5[a]		

[a] Estimates based on extrapolations.

This finding raises the question of the state of the oxygen molecule that is formed along with OH in levels higher than $v=4$. Adiabatic (spin) requirements permit vibrational excitation of ground state oxygen ($^3\Sigma_g^-$). In addition, production in the $^1\Delta_g$ level (7918 cm^{-1}) is allowed. Since transitions from either of the singlet states to the ground state are forbidden, the presence of metastable oxygen molecules in appreciable amounts in this system is indicated. They may be expected to enhance the rate of decomposition of ozone, and probably to react with hydrogen via

$$O_2+H_2 \rightarrow HO_2+H.$$

A few rough thermochemical calculations will serve to put the preceding discussion in perspective.† If the enthalpy of the primary reaction is taken as 77.1 kcal/mole and the mole fractions after reaction, as OH=0.028, O_2=0.937, H_2=0.035 (see reference 5), then the total gas mixture could be heated adiabatically at constant pressure from 300 to 600°K. This final temperature is slightly higher than the observed rotational temperatures, but does indicate nearly complete rotational, and, presumably, translational and PV equilibration. If initially both the OH and O_2 product molecules were fully excited under constant volume conditions, but the rest of the mixture was not, their temperature would be 6000–6500°K, appreciably lower than the observed steady-state population distribution of OH. If OH alone were excited, its initial temperature would be about 15 000°K. A similar estimate applies to the case where only the internal degrees of freedom of OH and O_2 are initially excited. These estimates do not allow for dissociation, the energy of reaction being too small to permit this. These comparisons alone emphasize the nonthermal nature of the radiation. They also suggest that the observed vibrational distribution represents a partial (and appreciable) relaxation from the initial distribution of energy. If the latter is given by the rate of production figures in Table VI, then the indication is that vibrational energy distributions relax more rapidly toward Boltzmann distributions than toward thermal equilibrium.

The changes in intensities produced by varying the experimental conditions are the results of changes in reagent flows, quenching, and hydrodynamics. The linear increase in line intensity with either ozone or ozonized oxygen flow may be attributed to more reaction acts per unit time, ozone being in short supply. The marked intensity increase with hydrogen flow rate is due, in the first instance, to constriction of the inner, ozone bearing, stream and hence the reaction zone to the volume viewed by the spectrograph. Increased H-atom flow also contributes to this constricting effect. [Although the stability of the experimental system indicated that there was always an excess of hydrogen atoms (all ozone being destroyed), there was no assurance that the spectrograph viewed all parts of the flame zone equally.]

Of more interest are the relative intensity changes from band to band. The larger increases in line intensities in bands with high upper states as the hydrogen mole fraction increases suggests a much lower quenching efficiency for H_2 than for O_2. However, it is difficult to account for the relative changes from band to band on this basis quantitatively. An alternate explanation is than an efficient secondary reaction occurs

$$OH+H_2 \rightarrow H_2O+H, \qquad \Delta H=-13 \text{ to } -17 \text{ kcal/mole},$$

$$E^*=14 \text{ kcal/mole}.$$

Hydroxyls with $v \geq 2$ have sufficient excitation to provide the activation energy,[15–17] hence the reaction may well be efficient. Since the lower levels have higher populations, this process coupled with reaction of this new H atom with ozone can repopulate the upper levels

† We are indebted to Professor D. F. Hornig for suggesting these comparisons.

[15] W. Frankenburger and H. Klinkhardt, Trans. Faraday Soc. 27, 431 (1931).
[16] G. von Elbe and B. Lewis, J. Am. Chem. Soc. 54, 552 (1932).
[17] A. B. Callear and J. C. Robb, Trans. Faraday Soc. 51, 649 (1955).

preferentially. The curious negative rates of formation in level $v=2$ may be a result of this.

The most obvious cause of the decreased intensities at higher pressures would be collisional quenching. However, these experiments were made at high hydrogen flows, which means, taken together with the constricting effect of the pressure increase, that more of the reaction zone was viewed at the higher pressure. Also, the quenching follows a typical low for the variation of intensity with pressure: $I=a/(1+bP)$ only for $v'=3$. For $v'=4$, $I=c/P$, and for $v'=5$, 6 and 7, $I=d/P^2$, where d depends on the vibrational level. This strong dependence on pressure is due to a decreased rate of production of hydroxyls in the upper levels at higher pressures (see Table VI). The cause of this is not clear. A decreased discharge efficiency at the higher pressure would expand the reaction zone, and also decrease the contribution of the secondary reaction to the repopulation of the upper levels. In addition, three-body reactions

$$H+O_2+O_2\rightarrow OH+O_2+O_2^*(^1\Sigma_g^+)$$

or the sequence

$$H+O_2\rightarrow OH^*+O_2, \qquad OH^*+O_2\rightarrow OH+O_2^*(^1\Sigma_g^+)$$

may be important. Any level of OH above $v=4$ can provide sufficient excitation for the latter. For this to be the favored quenching mode, it can be visualized only as a strong interaction comparable to that which occurs in a chemical reaction. At present a choice between these alternatives is not possible.

ACKNOWLEDGMENTS

The authors are indebted to Dr. K. E. Shuler and Dr. A. M. Bass for assistance and helpful discussions during the course of this work. One of us (D.G.) wishes to thank the National Bureau of Standards for extending a Visiting Fellowship during the summer of 1956 when the experiments were performed. Professor F. S. Acton and Mr. A. M. Jaffe carried out the machine computations. Extensive calculations were made by William B. Mather, C. William Jansing, and R. T. Skeel. To all of them we express our appreciation.

THE JOURNAL OF CHEMICAL PHYSICS VOLUME 32, NUMBER 3 MARCH, 1960

Unperturbed Chain Dimensions of Polymeric Chains*

C. A. J. HOEVE

Mellon Institute, Pittsburgh, Pennsylvania

(Received May 4, 1959)

Methods are given for the calculation of polymer chain dimensions unperturbed by excluded volume effects but dependent on restricted rotation around the chain bonds as a result of interactions between substituents on neighboring chain atoms. The matrix methods used by most previous investigators are valid only for cases where the rotations, or pairs of neighboring rotations, are noninteracting. The methods recently developed by Lifson to account for interactions between any two consecutive rotations in chains of the type $(CR_2)_i$ are extended to chains of the type $(CH_2—CR_2)_i$ and isotactic chains of the type $(CH_2—CHR)_i$.

As an illustration the chain dimensions of polyisobutylene are calculated by using parameters from x-ray data in the crystalline state and results from stress-temperature measurements on amorphous networks. Reasonable agreement is obtained with experimental data on dilute solutions of polyisobutylene.

INTRODUCTION

CURRENTLY much attention is being focused on the study of the dimensions of polymer chains in solution. In view of the increasing availability of relevant experimental results, the calculation of average dimensions from the detailed geometry of the chain has assumed considerable importance. It is well known that these dimensions are dependent on interactions of the segments with one another and on interactions of the segments with the solvent. Of paramount importance is the hindrance to rotation around each bond in the chain. Moreover, this hindrance to rotation about a given bond must depend in general on the angles of rotation for neighboring bonds. An adequate theory should take account of these interactions between rotations. Achievement of this end poses severe mathematical difficulties. It has consequently been customary to adopt, implicitly or explicitly, the simplifying assumption that bond rotations are mutually independent.

Not only are interactions between near neighboring bonds to be reckoned with; it is also necessary to take cognizance of longer range interactions,[1] which give rise to an excluded volume effect. However, if the sequence of the chain atoms between two interacting segments is long, this interaction can be treated as one between independent segments and is therefore analogous to a solvent effect. For a dilute solution in any given solvent it has been shown that by a proper choice of the temperature (the Θ point) the conformations of the chain are not perturbed by excluded volume effects.[1] This appears to be true also for concentrated solutions and for the polymer in bulk. Under these circumstances the chain dimensions are determined only by the potential energy associated with angles of rotation around neighboring bonds. In the following, all considerations will apply exclusively to unperturbed chains. It is the object of this paper to present methods for taking account of the interdependence of rotations in a general way and to illustrate application of these methods.

Volkenstein[2] has recently given an account of the calculation of chain dimensions using the powerful methods of matrix algebra, originally employed by Eyring.[3] These methods for chains in which the rotations are assumed to be mutually independent were extended[4,5] in the following way to chains of the types $(CH_2—CR_2—)_i$ and $(CH_2—CHR—)_i$ in which rotations are pairwise interdependent. The rotations around the bonds connecting the CH_2 groups with neighboring C atoms were assumed interdependent due to interactions between the bulky R groups, but the rotations around the bonds connecting the CR_2 or CHR groups with the neighboring CH_2 groups were assumed independent of each other. With these assumptions, essentially the same mathematical methods can be used as for independent rotations. Agreement with experiment was greatly improved by this device. However, it is to be expected that in many cases these assumptions are unrealistic. Very recently Lifson[6] showed how interactions between any two consecutive rotations in chains of the type $(CR_2)_i$ can be taken into account. In the following section these methods are applied to other types of chains.

METHODS

The methods developed here are based on those given by Volkenstein and Ptitsyn[2] and Lifson.[5,6] Since, however, minor differences exist, the principles of the procedure are briefly outlined.

An orthogonal coordinate system is attached to each bond of the chain, the Z axis pointing in the direction of

* Paper presented in part at the American Physical Society Meeting in April, 1959 at Cambridge, Massachusetts.

[1] P. J. Flory, *Principles of Polymer Chemistry* (Cornell University Press, Ithaca, New York, 1953), Chap. 14.

[2] M. V. Volkenstein, J. Polymer Sci. **29**, 441 (1958).

[3] H. Eyring, Phys. Rev. **39**, 746 (1932).

[4] O. B. Ptitsyn and I. A. Sharonov, Zhur. Tekh. Fiz. **27**, 2744 and 2762 (1957).

[5] S. Lifson, J. Chem. Phys. **29**, 80 (1958).

[6] S. Lifson, J. Chem. Phys. **30**, 964 (1959).

each bond. The Y axis is located in the plane of this bond and that of the preceding one and points in the direction which forms the smallest angle with the Z axis of the previous bond. The X axis forms a right-handed coordinate system with the Y and Z axis. For a given set of rotational angles, each bond vector is represented by a column vector $(00l)$ in its own coordinate system, where l is the bond length. If, however, all bond vectors are expressed in a common coordinate system, for example that corresponding to the first bond, the components of the resultant are easily found as the sum of the components of the bond vectors. The transformation $\mathbf{T}_i$ which transforms the $(i+1)$th coordinate system into that of the ith is a third order matrix and is given by

$$\mathbf{T}_i=\begin{pmatrix} -\cos\phi_i & -\alpha_i\sin\phi_i & \beta_i\sin\phi_i \\ \sin\phi_i & -\alpha_i\cos\phi_i & \beta_i\cos\phi_i \\ 0 & \beta_i & \alpha_i \end{pmatrix}, \qquad (1)$$

where $\alpha_i=\cos\theta_i$; $\beta_i=\sin\theta_i$; θ_i is 180° minus the bond angle; and ϕ_i is the angle of rotation, the *trans* conformation corresponding to $\phi_i=0$.

Although the treatment can easily be generalized to include unequal bond lengths, the bond length is here supposed to be equal for each bond. The vector representing the end-to-end distance is then given by

$$\mathbf{r}_0=(\mathbf{E}+\mathbf{T}_1+\mathbf{T}_1\mathbf{T}_2+\mathbf{T}_1\mathbf{T}_2\mathbf{T}_3+\cdots+\mathbf{T}_1\mathbf{T}_2\cdots\mathbf{T}_{n-1})\begin{pmatrix}0\\0\\l\end{pmatrix}, \qquad (2)$$

where n is the number of bonds in the chain. $\mathbf{E}$ is the unit matrix of order 3. The square of the end-to-end distance r_0^2 is given by $\mathbf{r}_0{}^T\mathbf{r}$, where $\mathbf{r}_0{}^T$ indicates the transpose of $\mathbf{r}_0$. This symbolism will be used throughout. Hence

$$r_0^2=l^2(001)(\mathbf{E}+\mathbf{T}_1{}^T+\mathbf{T}_2{}^T\mathbf{T}_1{}^T+\cdots+\mathbf{T}_{n-1}{}^T\cdots\mathbf{T}_1{}^T)\times(\mathbf{E}+\mathbf{T}_1+\mathbf{T}_1\mathbf{T}_2+\cdots+\mathbf{T}_1\cdots\mathbf{T}_{n-1})\begin{pmatrix}0\\0\\1\end{pmatrix}. \qquad (3)$$

In the evaluation of this product it is to be noted that all matrices are orthogonal and therefore $\mathbf{T}_i{}^{-1}=\mathbf{T}_i{}^T$. Furthermore, since only the elements of the third row and third column of the matrix products contribute to the resultant of the operations indicated in Eq. (3), all terms $\mathbf{T}_3{}^T\mathbf{T}_2{}^T\mathbf{T}_1{}^T$, etc. may be replaced by their transposes $\mathbf{T}_1\mathbf{T}_2\mathbf{T}_3$, etc. We shall be interested in the *mean* square end-to-end distance. Hence, it will be necessary to take averages of all matrix products. In the averaging of a matrix product each of its elements is to be averaged over the rotational angles ϕ, the appropriate statistical weights being applied. Incorporation of these considerations permits the average to be expressed as

$$\langle r_0^2\rangle=nl^2(001)[\mathbf{E}+2(\langle\mathfrak{J}_\nu\rangle+\langle\mathfrak{J}_\nu\mathfrak{J}_{\nu+1}\rangle+\langle\mathfrak{J}_\nu\mathfrak{J}_{\nu+1}\mathfrak{J}_{\nu+2}\rangle+\cdots)]\begin{pmatrix}0\\0\\1\end{pmatrix}, \qquad (4)$$

if n is large, where

$$\langle\mathfrak{J}_\nu\rangle=(n-1)^{-1}(\langle\mathbf{T}_1\rangle+\langle\mathbf{T}_2\rangle+\langle\mathbf{T}_3\rangle+\cdots+\langle\mathbf{T}_{n-1}\rangle),$$

$$\langle\mathfrak{J}_\nu\mathfrak{J}_{\nu+1}\rangle=(n-2)^{-1}(\langle\mathbf{T}_1\mathbf{T}_2\rangle+\langle\mathbf{T}_2\mathbf{T}_3\rangle+\cdots\langle\mathbf{T}_{n-2}\mathbf{T}_{n-1}\rangle),$$

etc. Equation (4) is expressed as an infinite series. This is permissible if the series converges, which is true in all cases of interest. This equation is completely general in that it is valid for all chains subject to interactions of any sort whatever.

In the simple case, where the rotations are independent of each other

$$\langle\mathbf{T}_i\mathbf{T}_{i+1}\rangle=\langle\mathbf{T}_i\rangle\langle\mathbf{T}_{i+1}\rangle,$$

$$\langle\mathbf{T}_i\mathbf{T}_{i+1}\mathbf{T}_{i+2}\rangle=\langle\mathbf{T}_i\rangle\langle\mathbf{T}_{i+1}\rangle\langle\mathbf{T}_{i+2}\rangle, \quad \text{etc.}$$

However, in general, depending on the chemical composition of the chain, not all bonds i, $i+1$, etc. are equivalent. If the repeating unit along the chain comprises j consecutive segments, then $\langle\mathbf{T}_i\rangle=\langle\mathbf{T}_{i+j}\rangle$ for all i. If, for example, the repeating unit consists of one bond in the chain $\langle\mathbf{T}_i\rangle=\langle\mathbf{T}\rangle$ for all i and Eq. (4) reduces to

$$\langle r_0^2\rangle=nl^2(001)[(\mathbf{E}+\langle\mathbf{T}\rangle)(\mathbf{E}-\langle\mathbf{T}\rangle)^{-1}]\begin{pmatrix}0\\0\\1\end{pmatrix}. \qquad (5)$$

Even when the rotations corresponding to $\mathbf{T}_i$, $\mathbf{T}_{i+1}$, $\cdots$, $\mathbf{T}_{i+k}$ are dependent on each other, but the rotation corresponding to $\mathbf{T}_{i+k+1}$ is independent of the former rotations, the same method can still be applied by grouping together the matrices which are interdependent, as has been shown by others.[4,5]

Recently Lifson[6] extended these methods to include interactions between *every* pair of consecutive rotations. This situation is more general in that a correlation exists between the probabilities of occurrence for the rotational states of any two chain bonds in the chain. The process of grouping matrices together cannot then be applied, and more elaborate methods are needed. Following Lifson,[6] for simplicity a chain of the type $(CR_2)_i$ is assumed, although as will be shown subsequently, the method can easily be extended to other cases. Consider that the rotational angle ϕ around each bond may assume m distinct values: $\phi^{(1)}, \phi^{(2)}, \cdots, \phi^{(m)}$. Although all chain bonds are equivalent, it is convenient to number them with the indices ν, $\nu+1$, etc. The partition function is given by

$$Z=\sum\exp[-\epsilon(\phi_1,\phi_2,\cdots,\phi_n)/kT], \qquad (6)$$

where ϵ is the potential energy expressed as a function of all rotational angles, k and T are, respectively, the

Boltzmann constant and the absolute temperature. The summation extends over all m values of each of the variables $\phi_1, \phi_2, \cdots, \phi_n$. Lifson[6] observed that the model assumed here is a one-dimensional Ising model[7] for nearest neighbor interactions and gave an elegant method for calculating $\langle f(\phi) \rangle$, the average of a function of any rotational angle. The result obtained by him is given by

$$\langle f(\phi) \rangle = \xi^* \mathbf{F} \xi, \tag{7}$$

where ξ^* and ξ are, respectively, the eigenrow and eigenvector belonging to the largest eigenvalue λ of the matrix

$$\mathbf{u} = \begin{pmatrix} u_{11} & \cdots & u_{1m} \\ \cdot & & \cdot \\ \cdot & & \cdot \\ \cdot & & \cdot \\ u_{m1} & \cdots & u_{mm} \end{pmatrix}$$

and

$$u_{ij} = \exp[-\{\epsilon(\phi_{\nu+1}^{(j)}) + \epsilon(\phi_\nu^{(i)}, \phi_{\nu+1}^{(j)})\}/kT].$$

$\mathbf{F}$ is a diagonal matrix of order m, defined as follows:

$$\mathbf{F} = \begin{pmatrix} f(\phi^{(1)}) & 0 & \cdots & 0 \\ 0 & f(\phi^{(2)}) & & \cdot \\ \cdot & & \cdot & \cdot \\ \cdot & & \cdot & \cdot \\ \cdot & & \cdot & \\ 0 & \cdots & \cdots & f(\phi^{(m)}) \end{pmatrix}.$$

Here ξ^* and ξ are considered to be mutually normalized, so that $\xi^*\xi = 1$.

Furthermore, the average of the product of two or more consecutive functions $f(\phi_\nu)$, $g(\phi_{\nu+1})$, $h(\phi_{\nu+2})$, etc. is given by[6]

$$\langle f(\phi_\nu) g(\phi_{\nu+1}) \rangle = \lambda^{-1} \xi^* \mathbf{FuG} \xi,$$

$$\langle f(\phi_\nu) g(\phi_{\nu+1}) h(\phi_{\nu+2}) \rangle = \lambda^{-2} \xi^* \mathbf{FuGuH} \xi, \quad \text{etc.} \tag{8}$$

The following treatment deviates slightly from that of Lifson,[6] but leads to an equivalent result.

Define for convenience a matrix $\mathbf{C}$ according to the following equation

$$\mathbf{C} = \mathbf{u}/\lambda.$$

In order to calculate the probability $a_j(\nu)$ that the rotational angle around bond ν is $\phi_\nu^{(j)}$, Eq. (7) is applied, where all diagonal elements of $\mathbf{F}$ are taken to be zero except the jth one which is taken to be unity. Probabilities for consecutive rotational angles are obtained in an analogous fashion. The result is as follows:

$$a_j(\nu) = \xi_j^* \xi_j, \qquad a_{jk}(\nu, \nu+1) = \xi_j^* c_{jk} \xi_k,$$

$$a_{jkl}(\nu, \nu+1, \nu+2) = \xi_j^* c_{jk} c_{kl} \xi_l, \quad \text{etc.} \tag{9}$$

[7] G. F. Newell and E. W. Montroll, Revs. Modern Phys. **25**, 353 (1953).

In order to calculate the averages of products of matrices, these probabilities have to be multiplied by the corresponding matrices followed by summation over all j, k, and l. For example,

$$\langle \mathbf{T}_\nu \mathbf{T}_{\nu+1} \mathbf{T}_{\nu+2} \rangle = \sum_j \sum_k \sum_l \xi_j^* c_{jk} c_{kl} \xi_l \mathbf{T}^{(j)} \mathbf{T}^{(k)} \mathbf{T}^{(l)}, \tag{10}$$

where $\mathbf{T}^{(j)}$, $\mathbf{T}^{(k)}$, and $\mathbf{T}^{(l)}$ are the matrices representing the rotations corresponding to $\phi^{(j)}$, $\phi^{(k)}$, and $\phi^{(l)}$. Other averages can be obtained similarly. These equations can be written in matrix language, if first the following matrices are defined:

$$\mathbf{X}^* = [\xi_1^* \mathbf{E}, \cdots \xi_m^* \mathbf{E}],$$

$$\mathbf{X} = \begin{pmatrix} \xi_1 \mathbf{E} \\ \cdot \\ \cdot \\ \cdot \\ \xi_m \mathbf{E} \end{pmatrix},$$

$$\mathbf{D} = \begin{pmatrix} \mathbf{T}^{(1)} & \mathbf{0} & \cdots & \mathbf{0} \\ \mathbf{0} & \mathbf{T}^{(2)} & & \cdot \\ \cdot & & \cdot & \cdot \\ \cdot & & \cdot & \cdot \\ \cdot & & \cdot & \\ \mathbf{0} & \cdots & \cdots & \mathbf{T}^{(m)} \end{pmatrix},$$

and

$$\mathbf{W} = \begin{pmatrix} u_{11}\mathbf{E} & \cdots & u_{1m}\mathbf{E} \\ \cdot & & \cdot \\ \cdot & & \cdot \\ \cdot & & \cdot \\ u_{m1}\mathbf{E} & \cdots & u_{mm}\mathbf{E} \end{pmatrix}.$$

The matrix $\mathbf{D}$ is a symbolical "diagonal" matrix, the "elements" being the m transformation matrices, corresponding to the m possible angles of rotation. $\mathbf{0}$ denotes the zero matrix of order 3. Let, furthermore, the following matrices be defined:

$$\mathbf{S} = \lambda^{-1}\mathbf{WD} \quad \text{and} \quad \mathbf{V} = \mathbf{X}^*\mathbf{D}.$$

According to the rules of matrix multiplication, we have then

$$\langle \mathbf{T}_\nu \rangle = \mathbf{VX}, \qquad \langle \mathbf{T}_\nu \mathbf{T}_{\nu+1} \rangle = \mathbf{VSX},$$

$$\langle \mathbf{T}_\nu \mathbf{T}_{\nu+1} \mathbf{T}_{\nu+2} \rangle = \mathbf{VS}^2\mathbf{X}, \quad \text{etc.} \tag{11}$$

The equation for $\langle r_0^2 \rangle$ can now be obtained by substitution of Eq. (11) into Eq. (4). We have then

$$\langle r_0^2 \rangle = nl^2(001)[\mathbf{E} + 2\mathbf{V}(\mathbf{E}_{3m} - \mathbf{S})^{-1}\mathbf{X}] \begin{pmatrix} 0 \\ 0 \\ 1 \end{pmatrix}, \tag{12}$$

where $\mathbf{E}_{3m}$ is a unit matrix of order $3m$, to be distinguished from the unit matrix $\mathbf{E}$ of order 3.

Equation (12) is somewhat different from the result of Lifson,[6] but appears to be equivalent.

Although only interactions between two consecutive rotations are assumed here, the method may readily be

extended to cases where interactions occur between any finite number of consecutive rotations. The procedure is analogous to that of Zimm and Bragg[8] in treating polypeptides.

If the repeating unit along the chain contains more than one bond, the treatment has to be modified. As an example, the method is now extended to chains of the type $(CR_2-CH_2)_i$ and isotactic chains of the type $(CHR-CH_2)_i$. In both chains the repeating unit comprises two chain bonds. Syndiotactic chains may be treated in a similar way, if it is borne in mind that the repeating unit comprises four chain bonds in that case. However, attention is focused here on the former types.

The partition function is again given by Z as defined by Eq. (6). On proceeding along the chain, consecutive bonds are not equivalent in this case, but all even numbered bonds are equivalent as well as all uneven ones. Let ν and $\nu+1$ denote, respectively, an even and an uneven numbered bond. Two matrices $\mathbf{u}'$ and $\mathbf{u}''$ corresponding to bonds ν and $\nu+1$ are now defined as follows:

$$u_{ij}'=\exp[-\{\epsilon(\phi_\nu^{(j)})+\epsilon(\phi_{\nu-1}^{(i)},\phi_\nu^{(j)})\}/kT],$$

and

$$u_{ij}''=\exp[-\{\epsilon(\phi_{\nu+1}^{(j)})+\epsilon(\phi_\nu^{(i)},\phi_{\nu+1}^{(j)})\}/kT].$$

As will become apparent in the following, it is useful to distinguish the functions of the angles of rotation around bonds ν and $\nu+1$. Let them be given by $f'(\phi_\nu)$ and $f''(\phi_{\nu+1})$, respectively. It is, furthermore, convenient to introduce the following diagonal matrices:

$$\mathbf{F}'=\begin{pmatrix} f'(\phi_\nu^{(1)}) & & & \\ & \cdot & & \\ & & \cdot & \\ & & & f'(\phi_\nu^{(m)}) \end{pmatrix}$$

and

$$\mathbf{F}''=\begin{pmatrix} f''(\phi_{\nu+1}^{(1)}) & & & \\ & \cdot & & \\ & & \cdot & \\ & & & f''(\phi_{\nu+1}^{(m)}) \end{pmatrix}.$$

The eigenvalues and eigenvectors of the matrix product $\mathbf{u}'\mathbf{u}''$ play a role analogous to that before. Let the largest eigenvalue of this product be λ and let the mutually normalized eigenrow and eigenvector again be denoted by ξ^* and ξ, respectively. We have then for the averages of products of the functions $f(\phi)$, beginning with bond ν,

$$\langle f_\nu'\rangle=\xi^*\mathbf{u}'\mathbf{F}'\mathbf{u}''\xi/\lambda, \qquad \langle f_\nu' f_{\nu+1}''\rangle=\xi^*\mathbf{u}'\mathbf{F}'\mathbf{u}''\mathbf{F}''\xi/\lambda,$$

$$\langle f_\nu' f_{\nu+1}'' f_{\nu+2}'\rangle=\xi^*\mathbf{u}'\mathbf{F}'\mathbf{u}''\mathbf{F}''\mathbf{u}'\mathbf{F}'\mathbf{u}''\xi/\lambda^2, \text{ etc.} \quad (13)$$

[8] B. H. Zimm and J. K. Bragg, J. Chem. Phys. 28, 1246 (1958).

For bonds beginning with bond $\nu+1$ we have

$$\langle f_{\nu+1}''\rangle=\xi^*\mathbf{F}''\xi, \qquad \langle f_{\nu+1}'' f_{\nu+2}'\rangle=\xi^*\mathbf{F}''\mathbf{u}'\mathbf{F}'\mathbf{u}''\xi/\lambda,$$

$$\langle f_{\nu+1}'' f_{\nu+2}' f_{\nu+3}''\rangle=\xi^*\mathbf{F}''\mathbf{u}'\mathbf{F}'\mathbf{u}''\mathbf{F}''\xi/\lambda, \text{ etc.} \quad (14)$$

The averages of the corresponding transformation matrices can be obtained straightforwardly, if, in analogy to the previous case, the following matrices are first defined:

$$\mathbf{X}^*=[\xi_1^*\mathbf{E}\cdots\xi_m^*\mathbf{E}],$$

$$\mathbf{X}=\begin{pmatrix} \xi_1\mathbf{E} \\ \cdot \\ \cdot \\ \cdot \\ \xi_m\mathbf{E} \end{pmatrix},$$

$$\mathbf{W}'=\begin{pmatrix} u_{11}'\mathbf{E} & \cdots & u_{1m}'\mathbf{E} \\ \cdot & & \cdot \\ \cdot & & \cdot \\ \cdot & & \cdot \\ u_{m1}'\mathbf{E} & \cdots & u_{mm}'\mathbf{E} \end{pmatrix},$$

$$\mathbf{W}''=\begin{pmatrix} u_{11}''\mathbf{E} & \cdots & u_{1m}''\mathbf{E} \\ \cdot & & \cdot \\ \cdot & & \cdot \\ \cdot & & \cdot \\ u_{m1}''\mathbf{E} & \cdots & u_{mm}''\mathbf{E} \end{pmatrix},$$

$$\mathbf{D}'=\begin{pmatrix} \mathbf{T}_\nu^{(1)} & & & \\ & \cdot & & \\ & & \cdot & \\ & & & \mathbf{T}_\nu^{(m)} \end{pmatrix},$$

and

$$\mathbf{D}''=\begin{pmatrix} \mathbf{T}_{\nu+1}^{(1)} & & & \\ & \cdot & & \\ & & \cdot & \\ & & & \mathbf{T}_{\nu+1}^{(m)} \end{pmatrix}.$$

Here $\mathbf{W}'$ and $\mathbf{W}''$ are square matrices of order $3m$. $\mathbf{D}'$ and $\mathbf{D}''$ are symbolical "diagonal" matrices the "elements" being the transformation matrices corresponding, respectively, to the angles of rotation $\phi_\nu^{(1)}, \phi_\nu^{(2)}, \cdots, \phi_\nu^{(m)}$ and $\phi_{\nu+1}^{(1)}, \phi_{\nu+1}^{(2)}, \cdots\phi_{\nu+1}^{(m)}$. In order to simplify the notation, the following matrices are defined:

$$\mathbf{R}=\lambda^{-1}\mathbf{W}'\mathbf{D}'\mathbf{W}''\mathbf{D}'' \quad \text{and} \quad \mathbf{Z}=\lambda^{-1}\mathbf{W}'\mathbf{D}'\mathbf{W}''.$$

It is then easy to show that

$$\langle\mathbf{T}_\nu\rangle=\mathbf{X}^*\mathbf{Z}\mathbf{X}, \qquad \langle\mathbf{T}_\nu\mathbf{T}_{\nu+1}\rangle=\mathbf{X}^*\mathbf{R}\mathbf{X},$$

$$\langle\mathbf{T}_\nu\mathbf{T}_{\nu+1}\mathbf{T}_{\nu+2}\rangle=\mathbf{X}^*\mathbf{R}\mathbf{Z}\mathbf{X}, \text{ etc.} \quad (15)$$

$$\langle\mathbf{T}_{\nu+1}\rangle=\mathbf{X}^*\mathbf{D}''\mathbf{X}, \qquad \langle\mathbf{T}_{\nu+1}\mathbf{T}_{\nu+2}\rangle=\mathbf{X}^*\mathbf{D}''\mathbf{Z}\mathbf{X},$$

$$\langle\mathbf{T}_{\nu+1}\mathbf{T}_{\nu+2}\mathbf{T}_{\nu+3}\rangle=\mathbf{X}^*\mathbf{D}''\mathbf{R}\mathbf{X}, \text{ etc.} \quad (15a)$$

Finally, on substituting Eqs. (15) and (15a) into Eq. (4) we have

$$\langle r_0^2\rangle = nl^2(001)[\mathbf{E}+\mathbf{X}^*\mathbf{Z}\mathbf{X}+\mathbf{X}^*(\mathbf{D}''+\mathbf{R}) \times(\mathbf{E}_{3m}-\mathbf{R})^{-1}(\mathbf{E}_{3m}+\mathbf{Z})\mathbf{X}]\begin{pmatrix}0\\0\\1\end{pmatrix}. \quad (16)$$

As an example, the method is applied below to the polyisobutylene chain.

CHAIN DIMENSIONS OF POLYISOBUTYLENE

From x-ray diffraction studies Liquori[9] has shown that the polyisobutylene chain crystallizes in a helical form with 16 chain bonds per 5 turns of the helix. Assuming that the length of each C—C bond is 1.54 A, that bond angles for all main chain bonds are identical, and that the angles of rotation about these bonds are likewise identical, the bond angle $(180-\theta)°$ is found to be 114° and the absolute value of the angle of rotation $\phi=82°$. Although the crystal may be constructed from both right- and left-handed helices corresponding to $\phi^{(1)}=+82°$ and $\phi^{(2)}=-82°$, a given chain must of course conform to one sense or the other throughout the crystal lattice. No such restrictions apply, however, in the amorphous state and both angles of rotation may readily occur in different portions of the same chain. Upon examination of models, it is found that large steric hindrances between CH_3 groups on alternate C atoms in the structure $—C(CH_3)_2—CH_2—C(CH_3)_2—$ disallow angles of rotation of different sign for the bonds connecting the CH_2 group with the two neighboring $C(CH_3)_2$ groups. However, the sign of the pair of rotational angles of these bonds and that of neighboring pairs may be different. In general a multiplicity of potential energy minima may exist. In the case of polyisobutylene, however, the severity of the steric hindrances is such as to virtually preclude rotational angles other than those close to +82° or −82°. Recent nuclear magnetic resonance measurements on polyisobutylene by Powles[10] are consistent with the concept that the interlocking of methyl groups in the crystalline and amorphous state is very similar. Therefore, for each pair only two combinations of angles have to be taken into account: $(+\phi, +\phi)$ and $(-\phi, -\phi)$. By assuming moreover that these combinations occur at random, independent of neighboring pairs, Ptitsyn and Sharonov[4] calculated values for $\langle r_0^2\rangle$ only slightly smaller than the values deduced from dilute solution measurements. In this procedure, however, no account is taken of possible energy differences between different conformations. Therefore, according to this treatment, the chain dimensions are independent of temperature.

Recent measurements[11] of the stress-temperature relationship for crosslinked polyisobutylene samples indicate that $\langle r_0^2\rangle$ decreases slightly with increase in temperature. A correlation evidently exists between successive pairs; either perpetuation of rotation in the same sense, or its reversal, must be favored. The effect of this correlation is considered in the following:

According to the assumptions made, only two matrices have to be taken into account: the matrices **A** and **B** obtained by substituting $+\phi$ and $-\phi$, respectively, for ϕ_k in Eq. (1),

$$\mathbf{A}=\begin{pmatrix}-\cos\phi & -\alpha\sin\phi & \beta\sin\phi\\ \sin\phi & -\alpha\cos\phi & \beta\cos\phi\\ 0 & \beta & \alpha\end{pmatrix}, \quad (17)$$

$$\mathbf{B}=\begin{pmatrix}-\cos\phi & \alpha\sin\phi & -\beta\sin\phi\\ -\sin\phi & -\alpha\cos\phi & \beta\cos\phi\\ 0 & \beta & \alpha\end{pmatrix}. \quad (18)$$

If the rotation sense of a pair were completely independent of that of its predecessor, then according to Eq. (4), after suitably arranging terms and summing,

$$\langle r_0^2\rangle = nl^2(001)(\mathbf{E}+\mathbf{P})(\mathbf{E}-\mathbf{Q})^{-1}(\mathbf{E}+\mathbf{P})\begin{pmatrix}0\\0\\1\end{pmatrix}, \quad (19)$$

$$\mathbf{P}=(\mathbf{A}+\mathbf{B})/2 \quad \text{and} \quad \mathbf{Q}=(\mathbf{A}^2+\mathbf{B}^2)/2.$$

This is the result obtained by Ptitsyn and Sharonov.[4] Consider next that a correlation exists between the consecutive pairs. The matrices $\mathbf{u}'$ and $\mathbf{u}''$ are then given by

$$\mathbf{u}'=\begin{pmatrix}1 & \delta\\ \delta & 1\end{pmatrix} \quad \text{and} \quad \mathbf{u}''=\begin{pmatrix}1 & 0\\ 0 & 1\end{pmatrix},$$

where $\delta=\exp(-\Delta F/kT)$. Here ΔF is the free energy difference between the sequences $(+\phi, +\phi, -\phi, -\phi)$ and $(+\phi, +\phi, +\phi, +\phi)$. The largest eigenvalue of the matrix product $\mathbf{u}'\mathbf{u}''$ is given by $\lambda=1+\delta$. The corresponding eigenrow and eigenvector in a mutually normalized form are given by

$$\xi^*=[\tfrac{1}{2} \quad \tfrac{1}{2}] \quad \text{and} \quad \xi=\begin{pmatrix}1\\1\end{pmatrix}.$$

[9] A. M. Liquori, Acta Cryst. **8**, 345 (1955).
[10] J. G. Powles, Proc. Phys. Soc. (London) **B69**, 281 (1956).
[11] To be published. In this connection see Flory, Hoeve, and Ciferri, J. Polymer Sci. **34**, 337 (1959).

The other matrices required for Eq. (16) are given as follows:

$$\mathbf{D}'=\mathbf{D}''=\begin{pmatrix}\mathbf{A} & \mathbf{0}\\ \mathbf{0} & \mathbf{B}\end{pmatrix},\qquad \mathbf{Z}=(1+\delta)^{-1}\begin{pmatrix}\mathbf{A} & \delta\mathbf{B}\\ \delta\mathbf{A} & \mathbf{B}\end{pmatrix},$$

$$\mathbf{R}=(1+\delta)^{-1}\begin{pmatrix}\mathbf{A}^2 & \delta\mathbf{B}^2\\ \delta\mathbf{A}^2 & \mathbf{B}^2\end{pmatrix},$$

$$\mathbf{X}^*=[\tfrac{1}{2}\mathbf{E}\quad \tfrac{1}{2}\mathbf{E}],\quad \text{and}\quad \mathbf{X}=\begin{pmatrix}\mathbf{E}\\ \mathbf{E}\end{pmatrix}.$$

On substitution in Eq. (16) we have

$$\langle r_0^2\rangle=nl^2(001)[\mathbf{E}+\tfrac{1}{2}(\mathbf{A}+\mathbf{B})+\tfrac{1}{2}(\mathbf{A}^2+\mathbf{A}\quad\mathbf{B}^2+\mathbf{B})$$
$$\times(\mathbf{E}_{3m}-\mathbf{R})^{-1}(\mathbf{E}_{3m}+\mathbf{Z})\mathbf{X}]\begin{pmatrix}0\\0\\1\end{pmatrix}. \quad (20)$$

If no correlation existed, i.e., if $\Delta F=0$, then δ would equal one, and the probabilities for the pair $(+\phi, +\phi)$ to be followed by the pairs $(+\phi, +\phi)$ and $(-\phi, -\phi)$ would be equal. In general these probabilities are equal, respectively, to c and $(1-c)$ where $c=(1+\delta)^{-1}$. Since the interaction between methyl groups on alternate C atoms is large and the correlation between the pairs appears to be weak, we may reasonably assume that the correlation is caused by a difference predominantly in energy $\Delta\epsilon$ between the aforementioned sequences. We have, therefore,

$$c=[1+\exp(-\Delta\epsilon/kT)]^{-1}. \quad (21)$$

According to recent stress-temperature studies[11] on polyisobutylene the value of $d(\ln\langle r_0^2\rangle/)d(\ln T)$ is approximately -0.06 at 47°C. Since the correlation is small, it is profitable to expand $\langle r_0^2\rangle$ in a Taylor series as follows:

$$\langle r_0^2\rangle=\langle r_0^2\rangle_{c=\frac{1}{2}}+(c-\tfrac{1}{2})(d\langle r_0^2\rangle/dc)_{c=\frac{1}{2}}+\cdots. \quad (22)$$

If c is close to 0.5, the higher terms in Eq. (22) can be neglected. On differentiating Eq. (20) and substituting the parameters obtained from the x-ray data, we find that

$$(1/nl^2)(d\langle r_0^2\rangle/dc)_{c=\frac{1}{2}}=25.1. \quad (23)$$

Furthermore, the value for $\langle r_0^2\rangle_{c=\frac{1}{2}}$ is needed. It can be obtained from Eq. (19) and is given by

$$\langle r_0^2\rangle_{c=\frac{1}{2}}=6.28nl^2. \quad (24)$$

With the aid of Eqs. (21)–(24) and the value $d(\ln\langle r_0^2\rangle)/d(\ln T)=-0.06$ it follows that at 47°C. $c=0.516$ and $\langle r_0^2\rangle/\langle r_{0f}^2\rangle=3.31$, where $\langle r_{0f}^2\rangle$ is the value for the mean square end-to-end distance assuming tetrahedral bond angles and free rotation. In fact $\langle r_{0f}^2\rangle=2nl^2$. The value of c corresponds to an energy difference $\Delta\epsilon=40$ cal/mole. For comparison the value found by Ptitsyn and Sharonov[4] without taking into account the correlation was $\langle r_0^2\rangle/\langle r_{0f}^2\rangle=3.14$.

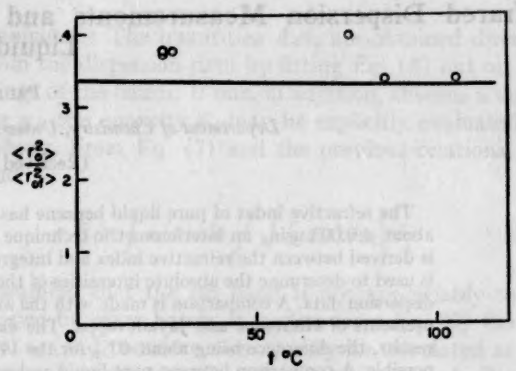

FIG. 1. Comparison between the calculated and measured values of $\langle r_0^2\rangle/\langle r_{0f}^2\rangle$. Circles denote the experimentally determined points. The line represents the calculated values.

In Fig. 1 the experimental data of Fox and Flory[12] obtained in several dilute solutions at the corresponding Θ points are compared with the calculated values represented by the straight line. Considering all experimental errors involved, it is seen that the agreement between calculated and measured values of $\langle r_0^2\rangle$ is satisfactory. Moreover, it is possible that some scattering of the experimental values, determined in different solvents, is due to influences of the solvent on the chain dimensions at the Θ point.

The foregoing interpretation affords a remarkably complete account of the conformations of the polyisobutylene chain as they exist in dilute solutions and in the amorphous undiluted state as well. This description is more detailed than that available for any other polymer.

ACKNOWLEDGMENTS

The author is much indebted to Dr. S. Lifson of the Weizmann Institute in Israel and Dr. P. J. Flory of Mellon Institute for clarifying discussions pertaining to this paper.

Support of the investigations, described in this paper, by the National Science Foundation is gratefully acknowledged.

[12] T. G. Fox and P. J. Flory, J. Am. Chem. Soc. 73, 1909 (1951).

Infrared Dispersion Measurements and Integrated Absorption Coefficients for Pure Liquid Benzene*

PAUL N. SCHATZ

Department of Chemistry, University of Virginia, Charlottesville, Virginia

(Received August 17, 1959)

The refractive index of pure liquid benzene has been measured in the 2-to 21-μ region to an accuracy of about ± 0.003 using an interferometric technique developed by Kagarise and Mayfield. A general relation is derived between the refractive index and integrated absorption coefficients of a pure liquid. The relation is used to determine the absolute intensities of the fundamental vibrations of pure liquid benzene from the dispersion data. A comparison is made with the same intensities determined in the direct absorption measurements of Hisatsune and Jayadevappa. The dispersion values appear to be higher than the absorption results, the difference being about 40% for the 14.8 μ fundamental where the most accurate comparison is possible. A comparison between pure liquid and gas intensities is also made.

A brief discussion is given of the advantages and limitations of the dispersion method in determining integrated intensities in liquids.

INTRODUCTION

VERY few absolute infrared intensity measurements have been made on pure liquids. This is due mainly to the difficulties involved in obtaining accurate path lengths for the very thin samples which must be used in absorption measurements. A quite thin sample is necessary even for a moderately intense band, and for strong bands, the cell length problem becomes very formidable indeed. On the other hand, Kagarise and Mayfield[1] have recently developed a simple method of making moderately accurate refractive index measurements on liquids in the 2- to 22-μ region. It is possible to calculate absolute absorption intensities for pure liquids from such dispersion measurements. Furthermore, the greater the intensity of the band, the more accurately its intensity can be calculated from the dispersion data. Consequently, dispersion and absorption measurements should complement each other since weak band intensities can presumably be measured accurately in absorption, and strong band intensities can be calculated accurately from dispersion data.

This paper presents the results of infrared dispersion measurements on pure liquid benzene between 2 and 21 μ. The data are of relatively low accuracy (± 0.003), and hence the calculated intensities have substantial uncertainties associated with them. Only the 14.8-μ band intensity is thought to be accurate to better than $\pm 10\%$. An interesting comparison is possible with the direct absorption intensity measurements on liquid benzene reported by Hisatsune and Jayadevappa.[2,3] It is also possible to test the Polo-Wilson equation[4] since the absolute intensities of the benzene fundamentals have been measured in the gas phase.[5]

THEORY

A very general relation between the integrated absorption coefficients and the index of refraction may be established in the following way. A complex dielectric constant is defined by the equation,

$$\epsilon = \epsilon_1 - i\epsilon_2. \tag{1}$$

It can easily be shown[6] that $\epsilon_1 = n^2(1-k^2)$, $\epsilon_2 = 2n^2k$, and $\alpha = 4\pi k n\nu/c$, where n is the index of refraction, k is the absorption index, and α is the absorption coefficient defined by Lambert's law ($I = I_0 e^{-\alpha l}$). The integrated absorption coefficient measured experimentally in a direct absorption measurement is given by

$$A_i = \int_{\text{band}} \alpha(\nu)\, d\nu, \tag{2}$$

where the integration is carried out over the ith absorption band. We now make use of the well-known relation[7]

$$\epsilon_1(\nu) - \epsilon_\infty = (2/\pi) \int_0^\infty [\epsilon_2(u)\, u\, du/(u^2 - \nu^2)] \tag{3}$$

where ϵ_∞ is the dielectric constant extrapolated from the visible ($\equiv n_v^2$). Let us confine our attention to a frequency (ν) in a region where there is no appreciable absorption ($k=0$). If we make use of the relations given previously, Eq. (3) becomes

$$n^2(\nu) - n_v^2 = (c/\pi^2) \int_0^\infty [n(u)\alpha(u)\, du/(u^2 - \nu^2)]. \tag{4}$$

We note that the quantity α is appreciable only in the

* Presented, in part, at the Symposium on Molecular Structure and Spectroscopy, The Ohio State University, Columbus, Ohio, June, 1959.

[1] R. E. Kagarise and J. W. Mayfield, J. Opt. Soc. Am. **48**, 430 (1958); Naval Research Laboratory Report 5088 (1958).

[2] I. C. Hisatsune and E. S. Jayadevappa, J. Chem. Phys. **30**, 848 (1959).

[3] Paper presented at the symposium on Molecular Structure and Spectroscopy, The Ohio State University, Columbus, Ohio, June, 1959; J. Chem. Phys. (to be published).

[4] S. R. Polo and M. K. Wilson, J. Chem. Phys. **23**, 2376 (1955).

[5] H. Spedding and D. H. Whiffen, Proc. Roy. Soc. (London) **A238**, 245 (1956).

[6] C. J. F. Böttcher, *Theory of Electric Polarisation* (Elsevier Publishing Company, Amsterdam, Netherlands, 1952), Chap. VIII.

[7] H. Frohlich, *Theory of Dielectrics* (Oxford University Press, New York, 1949), Chap. I.

immediate vicinity of the various absorption bands, and consequently, we may rewrite Eq. (4) as follows:

$$n^2(\nu)-n_\nu^2=(c/\pi^2)\sum_i\int_i[n\alpha_i du/(u^2-\nu^2)], \quad (5)$$

where the summation extends over all absorption bands below the visible, and $\int_i$ denotes an integration over the ith absorption band [$n(u)$ and $\alpha(u)$ have been abbreviated simply as n and α]. We observe that the factor $(u^2-\nu^2)^{-1}$ may be taken outside the integral and set equal to $(\nu_i^2-\nu^2)^{-1}$. This follows because ν has been chosen far from the resonance frequency (ν_i) and hence the remainder of the integrand is virtually a constant in the neighborhood of the singularity $u=\nu$. The singularity, therefore, makes essentially no contribution to the integral whose entire value then comes from the region $u=\nu_i$ where the function $(u^2-\nu^2)^{-1}$ varies only slowly. Equation (5) thus becomes

$$n^2(\nu)-n_\nu^2=(c/\pi^2)\sum_i(\nu_i^2-\nu^2)^{-1}\int_i n\alpha_i du. \quad (6)$$

If we define a mean refractive index $\bar{n}_i$ by the equation

$$\bar{n}_i=\int_i n\alpha_i du \Big/ \int_i \alpha_i du, \quad (7)$$

we finally obtain the result

$$n^2(\nu)-n_\nu^2=(c/\pi^2)\sum_i[\bar{n}_i A_i/(\nu_i^2-\nu^2)]. \quad (8)$$

This equation expresses the desired relation between the integrated absorption coefficients (A_i) and the index of refraction. The derivation has involved no assumptions whatever about the nature of the molecular interactions in the liquid. In the case of a gas, $\bar{n}_i\approx 1$, and Eq. (8) reduces to the familiar Kramers dispersion formula. For a liquid, $\bar{n}_i$ differs appreciably from 1, and Eq. (8) must be used. This was not done in a recent paper on the intensity of the antisymmetric stretching fundamental of liquid CS_2.[8] That result has now been corrected.[9,10]

To get a clearer picture of the significance of $\bar{n}_i$, we shall assume the following familiar functional form for ϵ[6]:

$$\epsilon-n_\nu^2=(c/\pi^2)\sum_j[A_j\bar{n}_j/(\nu_j^2-\nu^2+i\gamma_j\nu)]. \quad (9)$$

The summation extends over all absorption bands below the visible. γ_j is a damping constant characteristic of the transition, and it is generally small compared to ν_j. γ_j will then be approximately the band width at half maximum intensity.[11] (We note that the real part of Eq. (9) reduces to Eq. (8) at frequencies far from resonance.) The quantities $A_i\bar{n}_i$ are obtained directly from the dispersion data by fitting Eq. (8) out on the wings of the bands. If one, in addition, chooses a value for γ_i, the quantity $\bar{n}_i$ may be explicitly evaluated as follows. From Eq. (7) and the previous relations, we find

$$\bar{n}_i=\int_i \epsilon_2(\nu)\nu d\nu \Big/ \int_i [\epsilon_2(\nu)/n]\nu d\nu. \quad (10)$$

Assuming that the ith band is not appreciably overlapped by other bands, it is clear from Eq. (9) that ϵ_1 and ϵ_2 (and therefore also n) may be calculated at all frequencies through the ith absorption band. Consequently, the integrals in Eq. (10) can be calculated numerically and the value of $\bar{n}_i$ obtained. Actually, the numerator of Eq. (10), to a good approximation, is $(c/2\pi)A_i\bar{n}_i$, but, the denominator must be numerically integrated. In practice it seems best to calculate both integrals numerically since only a small amount of extra work is required to evaluate the numerator. A numerical check is then provided by the relation,

$$\int_i \epsilon_2\nu d\nu\approx(c/2\pi)A_i\bar{n}_i.$$

In the case of the 14.8-μ band of benzene, $\bar{n}_i$ was evaluated by the procedure just described in a few hours using a desk calculator. It will be suggested in the following that, to a good approximation, $\bar{n}_i=n_i'$ irrespective of the intensity of the ith band. n_i' is the index of refraction at the ith resonance frequency (ν_i) due to all absorptions except the ith one.

EXPERIMENTAL

The dispersion data were obtained using an interferometric technique which has been described in detail by Kagarise and Mayfield.[1] Briefly, one uses an interferometer constructed from a conventional infrared liquid cell through the use of polished germanium plates as windows. From the spacings of the interference fringes obtained with the empty cell, one can compute the cell thickness. The changes in spacings resulting when the cell is filled with liquid can then be related directly to the refractive index. The procedure is straightforward, but care most be exercised in indexing the fringes in the vicinity of absorption bands. By making runs using several different cell thicknesses, it is usually possible to arrive at unique indexings of all fringes.

Mallinckrodt analytical reagent grade (thiophene free) benzene was used in this work without further purification. The infrared spectrum gave no indication of the presence of impurities. The experimental results corrected to 20°C are shown in Table I. The temperature coefficient used was -0.00064 deg^{-1}.[12,13] A Perkin-

[8] P. N. Schatz, J. Chem. Phys. **29**, 959 (1958).
[9] E. E. Ferguson and R. E. Kagarise, J. Chem. Phys. **31**, 236 (1959).
[10] P. N. Schatz, J. Chem. Phys. **31**, 1146 (L) (1959).
[11] See, for example, Kauzmann, *Quantum Chemistry* (Academic Press, Inc., New York, 1957), p. 567.
[12] *International Critical Tables* **7**, 15.
[13] R. Mecke, Jr., and K. Rosswog, Z. Elektrochem. **60**, 47 (1956).

TABLE I. Refractive indices of liquid benzene at 20°C.

λ(μ)	$n^{20°}$	λ(μ)	$n^{20°}$	λ(μ)	$n^{20°}$
2.01	1.479	5.31	1.471	12.00	1.456
2.09	1.480	5.37	1.470	12.14	1.450
2.12	1.479	5.43	1.464	12.30	1.445
2.17	1.477	5.47	1.453	12.46	1.442
2.19	1.477	5.58	1.484	12.57	1.436
2.31	1.476	5.63	1.476	12.61	1.434
2.39	1.475	5.72	1.477	12.75	1.426
2.42	1.475	5.79	1.473	13.02	1.430
2.49	1.478	5.88	1.472	13.14	1.419
2.59	1.478	5.96	1.469	13.29	1.408
2.68	1.477	6.06	1.471	13.33	1.405
2.78	1.477	6.15	1.468	13.44	1.399
2.90	1.476	6.24	1.470	13.71	1.376
2.95	1.475	6.36	1.470	14.00	1.328[a]
3.02	1.475	6.45	1.464	14.20	1.272[a]
3.04	1.475	6.90	1.489	14.40	1.166[a]
3.09	1.474	6.99	1.481	14.56	1.014[a]
3.11	1.473	7.09	1.476	14.60	0.984[a]
3.13	1.472	7.25	1.481	14.70	1.120[a]
3.16	1.472	7.36	1.475	14.77	1.503[a]
3.18	1.469	7.50	1.473	14.80	1.752[a]
3.20	1.466	7.57	1.471	14.84	1.930[a]
3.33	1.498	7.64	1.474	14.90	2.012[a]
3.34	1.492	7.80	1.472	15.00	1.928[a]
3.36	1.489	7.94	1.468	15.06	1.868[a]
3.38	1.484	8.11	1.469	15.20	1.770[a]
3.41	1.484	8.28	1.466	15.40	1.691[a]
3.44	1.482	8.34	1.462	15.60	1.646[a]
3.46	1.479	8.38	1.457	16.00	1.598[a]
3.50	1.481	8.78	1.472	16.32	1.575
3.53	1.480	8.86	1.470	16.61	1.566
3.62	1.478	9.06	1.467	16.85	1.556
3.72	1.477	9.15	1.464	17.14	1.550
3.80	1.477	9.25	1.462	17.46	1.544
3.91	1.476	9.32	1.455	17.78	1.539
4.03	1.475	9.40	1.452	18.12	1.534
4.16	1.475	9.42	1.452	18.46	1.527
4.26	1.477	9.47	1.441	18.89	1.525
4.35	1.476	10.32	1.473	19.27	1.520
4.50	1.475	10.47	1.472	19.73	1.518
4.56	1.476	10.59	1.468	20.23	1.515
4.67	1.475	10.72	1.466	20.68	1.512
4.78	1.474	10.84	1.465		
4.90	1.473	10.99	1.461		
4.96	1.471	11.15	1.461		
5.02	1.468	11.29	1.457		
5.18	1.476	11.43	1.454		
5.24	1.473	11.57	1.449		

[a] Calculated points—see text.

Elmer Model 21 infrared spectrophotometer employing CaF_2, NaCl, and CsBr prisms was used. The refractive indices are generally believed to be accurate to about ±0.003. The accuracy in the 16- to 21-μ region is probably a little lower. The points given between 14.0 and 16.0 μ were *calculated* as explained in the following.

It was possible to check the results in the 2- to 5.8-μ region with the considerably more accurate data reported by Jaffe and Oppenheim.[14] The agreement was within ±0.002 at all points reported by them.

RESULTS AND DISCUSSION

To obtain the quantities $\bar{n}_i A_i$ for the various infrared bands from the data in Table I, it is necessary to know the electronic contribution to the refractive index (n_v^2). In this work, the following expression was used:

$$n_v^2 = 2.178 + [0.02409/(\lambda^2 - 0.01714)], \quad (11)$$

where λ is expressed in microns. This equation was taken from the *International Critical Tables*[12] with slight modification. Since the contribution to n^2 from the infrared bands is relatively small, it is essential that n_v^2 be known accurately. The expression given here fits the experimental points for the visible region listed in the *International Critical Tables*. In addition, it is in excellent agreement with the points listed by Jaffe and Oppenheim[14] between 1.36 and 1.96 μ (where the infrared bands still make an almost negligible and easily estimated contribution). Equation (8) may now be fit, and the resulting values of $\bar{n}_i A_i$ are listed in Table II.

In order to compute the A_i's, it is now necessary to know the values of the corresponding $\bar{n}_i$. We note from Eq. (9) that the ith band makes zero contribution to $\epsilon_1[=n^2(1-k^2)]$ at the resonance frequency (ν_i). It therefore follows that for a relatively weak band ($k \ll 1$), the refractive index at ν_i is just n_i', where n_i' is the refractive index at ν_i due to all absorptions except the ith one. Furthermore, the refractive index is antisymmetric about the point ν_i, being lower than n_i' on the high-frequency side and higher than n_i' on the low-frequency side. Since $\epsilon_2\nu$ is symmetric about ν_i, it seems reasonable to assume that $\bar{n}_i = n_i'$ for weak absorptions. (Clearly, this is rigorously true in the limit of zero intensity.) For intense absorption bands, the situation is not as simple; k may be quite appreciable compared to one, and the refractive index varies drastically through the band. It is by no means true that $n = n_i'$ at ν_i. For example, in the case of the 14.8-μ band of benzene, $n_i' = 1.482$ whereas $n(\nu_i) = 1.755$. Therefore, $\bar{n}_i$ was calculated for this band by a numerical evaluation of the integrals in Eq. (10) as described previously; γ_i was chosen to be 10.8 cm^{-1}, the bandwidth at half maximum intensity corrected for finite slit width.[15] The result of the calculation was $\bar{n}_i = 1.488$, whereas $n_i' = 1.482$. Thus even for this intense band, the assumption that $\bar{n}_i = n_i'$ is an excellent one. To check the sensitivity of the calculation to the various parameters involved, $\bar{n}_i$ was computed again, first doubling γ_i, and then doubling both γ_i and $A_i\bar{n}_i$. In each case, the value of $\bar{n}_i$ was within 1% of n_i'. It therefore seems quite possible that the assumption, $\bar{n}_i = n_i'$, will be a good approximation for any infrared band. The values of n obtained (for $\gamma = 10.8$ cm^{-1}) in the calculations are listed in Table I for the 14- to 16-μ region.

It has been observed that the 14.8-μ band has an appreciable asymmetry, the half-width computed from the high-frequency side being about 2.7 cm^{-1} greater than that computed from the low-frequency side.[15]

[14] J. H. Jaffe and U. Oppenheim, J. Opt. Soc. Am. **47**, 782 (1957).

[15] E. S. Jayadevappa, doctoral dissertation, Department of Chemistry, Kansas State University (1959).

TABLE II. Dispersion and absorption intensities for liquid benzene.

Band (μ)	$\bar{n}_i A_i$ (10^3 darks[a])	$\bar{n}_i$	A_i (dispersion) (10^3 darks[a])	A_i (absorption)[b] (10^3 darks[a])
3.29(E_{1u})	12.44	1.475	8.4 ±2.9	4.99±0.03[d]
6.76(E_{1u})	4.11	1.473	2.8 ±1.1[e]	2.24±0.03[e,d]
9.65(E_{1u})	2.62	1.467	1.8 ±0.7	1.15±0.01[e]
				1.19±0.08[f]
14.8(A_{2u})	20.91	1.488	14.1 ±1.2	9.54±0.14[e]
				10.6 ±0.8[f]
5.10	2.02	1.47	1.4 ±0.8	...
5.51	2.45	1.47	1.7 ±0.7	...
8.51	0.88	1.47	0.60±0.4	...
11.76	0.48	1.45	0.33±0.2	...
12.9	0.21	1.42	0.14±0.1	...

[a] cm^{-1}/millimoles per cm^3.
[b] Hisatsune and Jayadevappa, see references 2 and 3.
[c] Includes bands at 1394 and 1530 cm^{-1}.
[d] Wing correction not included.
[e] Wing correction included.
[f] Ramsay's method 1, see references 2 and 3.

Since the function $\epsilon_2\nu/n$ (which is directly proportional to α) had already been evaluated in calculating $\bar{n}_i$, it was a simple matter to determine whether this function predicts an asymmetry. The calculation indeed showed an asymmetry in the correct direction, the difference in half-widths being about 1.4 cm^{-1} as compared to the 2.7 cm^{-1} found experimentally. This asymmetry results from the way in which the refractive index varies through the band (see Table I).† This sort of effect should be expected generally for intense, narrow bands.

The final integrated absorption coefficients are listed in Table II along with the estimated errors. The $\bar{n}_i$ were computed from the relation, $\bar{n}_i = n_i'$, except for the 14.8-μ band where the calculated value was used. The errors in the A_i's are estimated by determining how much variation of each value is necessary to cause a clear discrepancy between the observed and calculated dispersion curves. We see that more accurate dispersion data are necessary if reasonably accurate intensities are to be obtained for any but the 14.8-μ band.

It should be noted that the accuracy with which a given intensity can be determined from dispersion data depends not only on the magnitude of the intensity but also on the frequency at which the band occurs. This may be seen very simply as follows. Suppose we wish to compute the contribution of the ith band to $[n^2(\nu)-n^2_\infty]$ at a frequency X sec^{-1} away from ν_i. According to Eq. (8), this contribution will be $(c/\pi^2)(\bar{n}_i A_i/\nu_i^2-\nu^2)$, where now $(\nu_i-\nu)=\pm X$. The contribution is therefore, $(c/\pi^2)[\bar{n}_i A_i/\pm X(2\nu_i \mp X)]$. It is clear that at a given frequency interval from a band, the contribution of the band gets larger as ν_i gets smaller. It follows, therefore, that a given band intensity can be determined with increasing accuracy as the wavelength at which the band occurs increases.

Hisatsune and Jayadevappa[2,3] have made direct absorption measurements of the intensities of the benzene fundamentals in the pure liquid using cells of known thickness. Their results are presented in the last column of Table II. A reasonably accurate comparison of the absorption and dispersion methods is possible only for the 14.8-μ band where it is seen that the dispersion intensity is about 40% higher than the absorption intensity. This discrepancy is rather disappointing since it is outside the estimated errors. In view of the difficulties involved in the direct absorption measurements, it would seem reasonable to expect that the dispersion result might be closer to the true intensity.‡ A comparison of the two methods for the 6.76- and 9.65-μ bands shows agreement within the wide limits of uncertainty in the dispersion intensities, although more accurate dispersion data are needed to permit a good comparison. For the 3.29-μ band, the difference in results lies somewhat outside the limits of error. However, it is possible that this discrepancy would be removed if a wing correction were applied to the absorption measurement. Again, more accurate dispersion data are necessary. We note that the dispersion results always seem to be higher than the absorption measurements.

It is interesting to extrapolate the square of the refractive index to infinite wavelength since it should then approach the static dielectric constant. The contribu-

†*Note added in proof.*—Professor A. D. Buckingham has pointed out to the author that if this explanation is correct, one should expect this band to become symmetrical if the benzene is diluted with an inert solvent since n will then be effectively constant. An examination of the data in reference 15 for several solvents very clearly reveals this expected behavior.

‡*Note added in proof.*—In the course of the calculation of $\bar{n}_i$, both n and k were calculated throughout the 14.8-μ band. It was therefore possible to immediately calculate the expected reflection spectrum of the band. When a comparison is made with experiment, excellent agreement is obtained using the dispersion intensity, but the agreement is poor if the absorption intensity is used. This would seem to provide strong support for the intensity obtained from the dispersion measurements. The details of this reflection work on benzene as well as similar work on several other liquids will be presented jointly with Professor David A. Dows in a future publication.

TABLE III. Tests of the Polo-Wilson equation for pure benzene.

band (μ)	A_1 (10^3 darks[a])	A_g[f] (10^3 darks[a])	A_1/A_g (exptl)	A_1/A_g (theoret.)
3.29 (E_{1u})	4.44[b,c]	6.01	0.74	1.31
6.76 (E_{1u})	1.91[b,c]	1.31	1.46	1.31
9.65 (E_{1u})	1.17[b,d]	0.88	1.33	1.31
14.8 (A_{2u})	14.1[e]	8.82	1.60	1.33

[a] cm^{-1}/millimoles per cm^2.
[b] Histasune and Jayadevappa, see references 2 and 3.
[c] Wing correction not included.
[d] Wing correction included.
[e] This paper.
[f] Spedding and Whiffen, see reference 5.

tion from the visible is clearly 2.178 [Eq. (11)]. From Eq. (8) it follows that the contribution of each infrared band is $(\tilde{n}_i A_i \lambda_i^2/c\pi^2)$. The sum of the contributions of all the infrared bands listed in Table II is 0.0620 so that $n_\infty^2 = 2.240$. On the other hand, $\epsilon_\infty = 2.283$.[13] There is thus a discrepancy of 0.043 between n_∞^2 and ϵ_∞. This indicates that there should be appreciable absorption between 14.8 μ and the radio frequency region. It is known[16] that there are absorption bands beyond 14.8 μ, but it is difficult to know whether these account for most of the discrepancy. We do note that the contribution of a band is directly proportional to the square of its wavelength, so that even relatively weak bands at very long wavelengths can make substantial contributions to n_∞^2.

The absolute intensities of the benzene fundamentals have been measured in the gas phase.[5] Polo and Wilson have shown[4] that both the Debye and Onsager equations predict the same relation between the intensity in a pure liquid (A_1) and the intensity for the corresponding gas (A_g), namely,

$$A_1/A_g = (n^2+2)^2/9n. \qquad (12)$$

Table III shows a comparison between Eq. (12) and the experimental results for benzene. In Table III, A_1 for the 14.8-μ band is the value calculated from the dispersion data, whereas the other A_1's are taken from Hisatsune and Jayadevappa.[2,3] For each band, the n of Eq. (12) was chosen as the corresponding $\tilde{n}_i$ given in Table II. None of the values of $\tilde{n}_i$ differs greatly from the value of n which one would obtain merely by extrapolating from the visible.

For the 6.76-, 9.65-, and 14.8-μ bands, the agreement is probably as good as one can expect in view of the simple model upon which Eq. (12) is based. The 3.29-μ band shows a striking deviation from Eq. (12). The comparison of gas and liquid intensities for pure benzene and the study of benzene intensities in various solvents have been discussed in detail elsewhere,[3,15] and no further discussion will be given here.

In one other case where an accurate comparison is possible between pure liquid and gas, namely the antisymmetric stretching fundamental of CS_2, the experimental ratio (A_1/A_g) is 1.30, and the theoretical ratio is 1.42. (See reference 8 as corrected by reference 10.)

CONCLUSIONS

It should be possible to obtain fairly accurate absolute infrared intensities for a variety of pure liquids by following the procedures outlined in this paper. The interferometric procedure is quite simple for determining refractive indices to an accuracy of about ± 0.003. However, this relatively low accuracy means that the intensities of weak bands cannot be obtained. The minimum intensity required for an accurate determination will depend on the location of the band, the situation becoming steadily more favorable with increasing wave length. Only liquids with relatively simple spectra or with isolated bands can be dealt with readily since it is very difficult to handle regions containing several overlapping bands. Dispersion data cannot be obtained in areas of strong absorption because the minimum cell thickness is limited by the need for well-defined interference fringes. Hence, intensities are obtained from the dispersion data on the wings of the bands. It is simpler to deal with nonpolar liquids because one does not have the added complication of strong absorption regions beyond the range of the measurements (22 μ). However, the method has been applied recently to some simple polar molecules by Kagarise.[17]

One of the obvious uses for liquid intensity data is the comparison they afford with the intensity of the same molecule in the gaseous state. Such comparisons yield information about intermolecular interactions and can be used to test various models which have been proposed to explain the changes in intensity accompanying condensation.[3,15] There are a number of molecules whose intensities have been studied in the vapor phase on which it should be feasible to make dispersion measurements in the liquid. We plan to carry out further studies on such molecules. It should also be possible to use the same experimental techniques to make dispersion measurements on solids provided one

[16] G. Herzberg, *Infrared and Raman Spectra of Polyatomic Molecules* (D. Van Nostrand Company, Inc., Princeton, New Jersey, 1945).

[17] R. E. Kagarise, Naval Research Laboratory Report 5277 (1959).

can grow a crystal between the germanium plates of the interferometer.

ACKNOWLEDGMENT

The author would like to acknowledge a very helpful discussion with Professor Robert H. Cole. Thanks are due to Dr. Hisatsune and Dr. Jayadevappa for making available a copy of their manuscript prior to publication. The author would also like to express his appreciation for a National Science Foundation grant which supported this work.

THE JOURNAL OF CHEMICAL PHYSICS VOLUME 32, NUMBER 3 MARCH, 1960

Infrared and Raman Spectra of Fluorinated Ethanes. XII. 1,1,2,2-Tetrafluoroethane*

PETER KLABOE AND J. RUD NIELSEN

Department of Physics, University of Oklahoma, Norman, Oklahoma

(Received September 2, 1959)

The infrared absorption spectra of gaseous CHF_2—CHF_2 at five temperatures between 30° and 170°C and of the crystalline solid at −170°C have been obtained with a Perkin-Elmer double-pass spectrometer equipped with CsBr, NaCl, and LiF prisms. The Raman spectrum of the liquid at 20°, −25°, and −80°C has been photographed with a 3-prism glass spectrograph of reciprocal linear dispersion 15 A/mm at 4358 A, and polarization measurements have been made. In the gaseous and liquid states the compound exists as a mixture of two rotational isomers of symmetries C_{2h} and C_2, respectively, the former (trans) being the more stable. In the crystalline state only the trans configuration is present. A value of 1160±100 cal/mole was found for the enthalpy difference ΔH^0 in the gas. In the liquid ΔH^0 is much smaller. With some uncertainties, the vibrational fundamentals have been assigned for each isomer.

INTRODUCTION

THE vibrational spectra of a number of halogenated ethanes having asymmetrical end groups have been studied with special reference to rotational isomerism,[1-5] but complete assignments of fundamental frequencies have been made only for CH_2Cl—CH_2Cl[6] and $CHCl_2$—$CHCl_2$.[7] In the present paper infrared and Raman spectral data are reported for CHF_2—CHF_2, the rotational isomerism exhibited by this compound in the gaseous and liquid states is studied, all vibrational fundamentals for the gauche form and all but the two lowest fundamentals for the trans form are assigned, and the spectra are interpreted in detail.

EXPERIMENTAL RESULTS

The sample (bp−16°C at 746 mm pressure) was prepared and purified in the laboratory of Henne at Ohio State University. The spectra indicate that the purity is high. The infrared absorption spectrum of the gas at room temperature was recorded with the aid of a Perkin-Elmer Model 112 spectrometer equipped with CsBr NaCl, and LiF prisms and 6- and 10-cm cells. To study the rotational isomerism, the infrared spectrum of the gas in an electrically heated 10-cm cell was obtained also at 70°, 110°, 140°, and 170°C. Moreover, the infrared spectrum of the crystalline solid at −170°C was recorded by means of a low-temperature cell somewhat similar to that described by Lord *et al.*[8] The Raman spectrum of the liquid in a sealed Raman tube at 20°, −25°, and −80°C, was photographed with an Applied Research Laboratories 3-prism glass spectrograph of reciprocal linear dispersion 15 A/mm at 4358 A. Polarization measurements were made by the method of Crawford and Horwitz.[9] The infrared spectra are shown in Figs. 1–6, and the wave numbers of the observed absorption maxima (or in some cases "shoulders") are listed in Table I. The Raman spectral data are presented in Table II.

INTERPRETATION

The large number of strong bands observed indicates that the compound exists as a mixture of rotational isomers. The fact that a number of strong bands present

* This work has been supported by the U. S. Atomic Energy Commission under Contract At-(40-1)-1074.

[1] S.-I. Mizushima, *Structure of Molecules and Internal Rotation* (Academic Press, Inc., New York, 1954).

[2] R. E. Kagarise and L. W. Daasch, J. Chem. Phys. **23**, 113, 130 (1955).

[3] R. E. Kagarise, J. Chem. Phys. **23**, 207 (1955); **24**, 300, 1264 (1956); **26**, 380 (1957); **29**, 680 (1958).

[4] T. Yoshino and H. J. Bernstein, Can. J. Chem. **35**, 339 (1957).

[5] J. K. Wilmshurst and H. J. Bernstein, Can. J. Chem. **35**, 734 (1957).

[6] J. Nakagawa and S.-I. Mizushima, J. Chem. Phys. **21**, 2195 (1953).

[7] Zietlow, Cleveland and Meister, J. Chem. Phys. **24**, 142 (1956).

[8] Lord, McDonald, and Miller, J. Opt. Soc. Am. **42**, 149 (1952).

[9] B. L. Crawford, Jr., and W. Horwitz, J. Chem. Phys. **15**, 882 (1947).

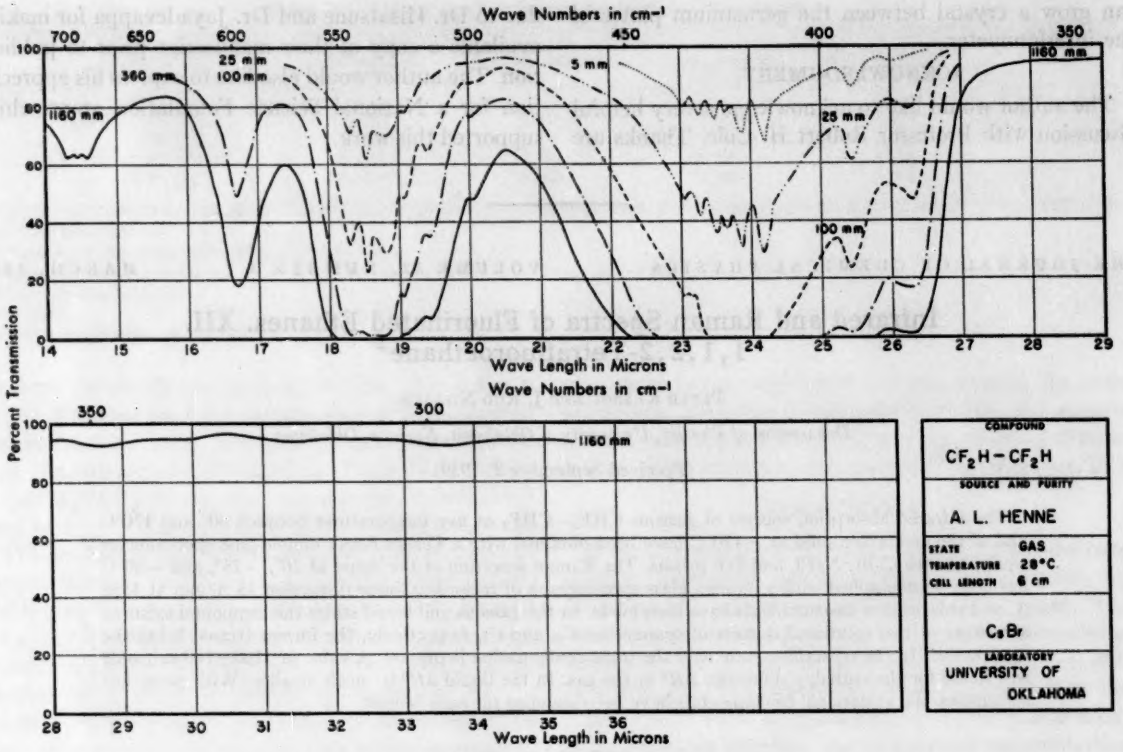

FIG. 1. Infrared absorption spectrum of gaseous CHF_2—CHF_2 (CsBr prism).

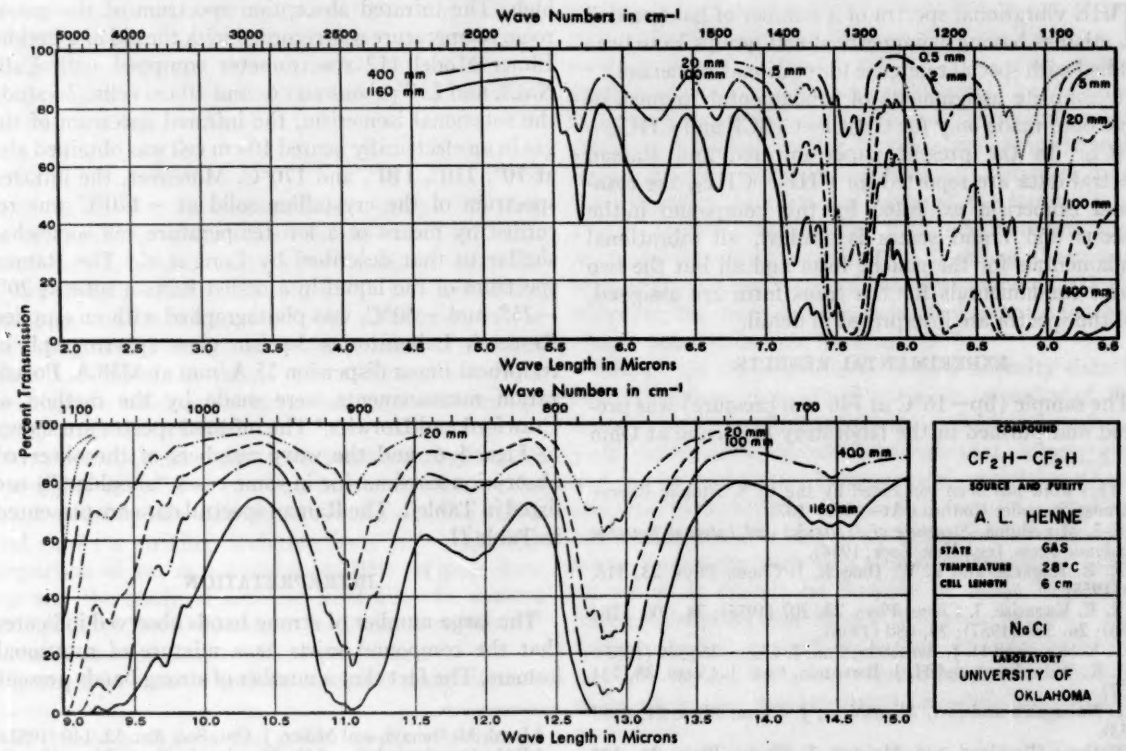

FIG. 2. Infrared absorption spectrum of gaseous CHF_2—CHF_2 (NaCl prism).

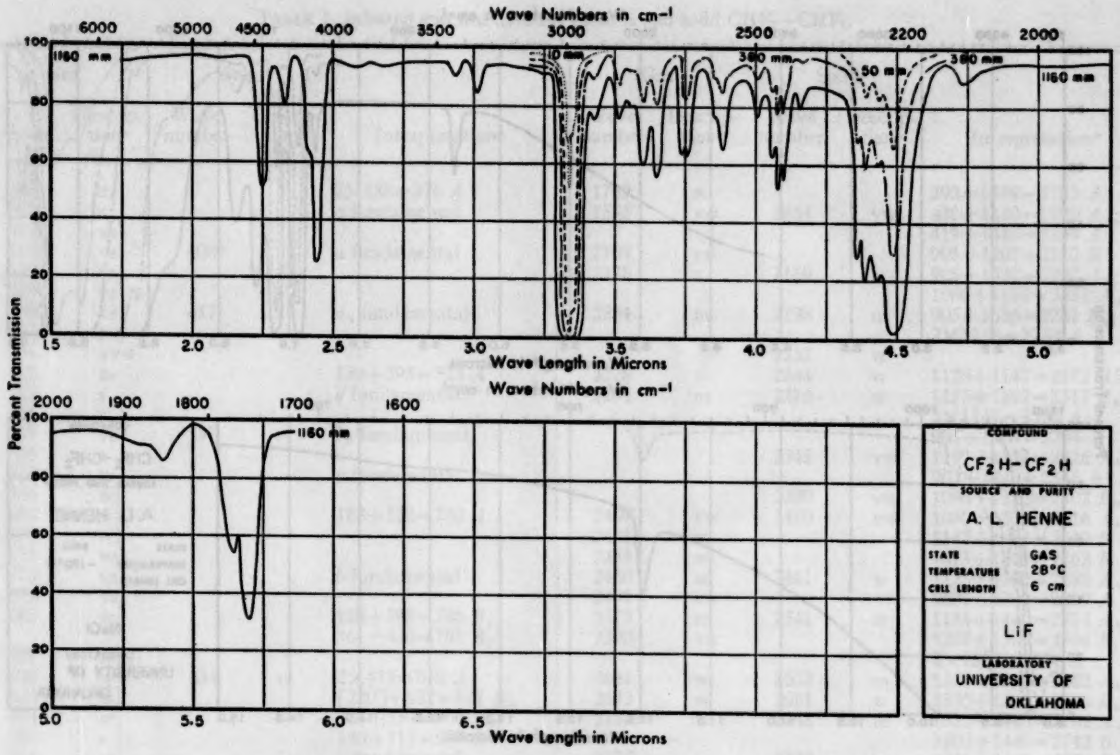

FIG. 3. Infrared absorption spectrum of gaseous CHF_2—CHF_2 (LiF prism).

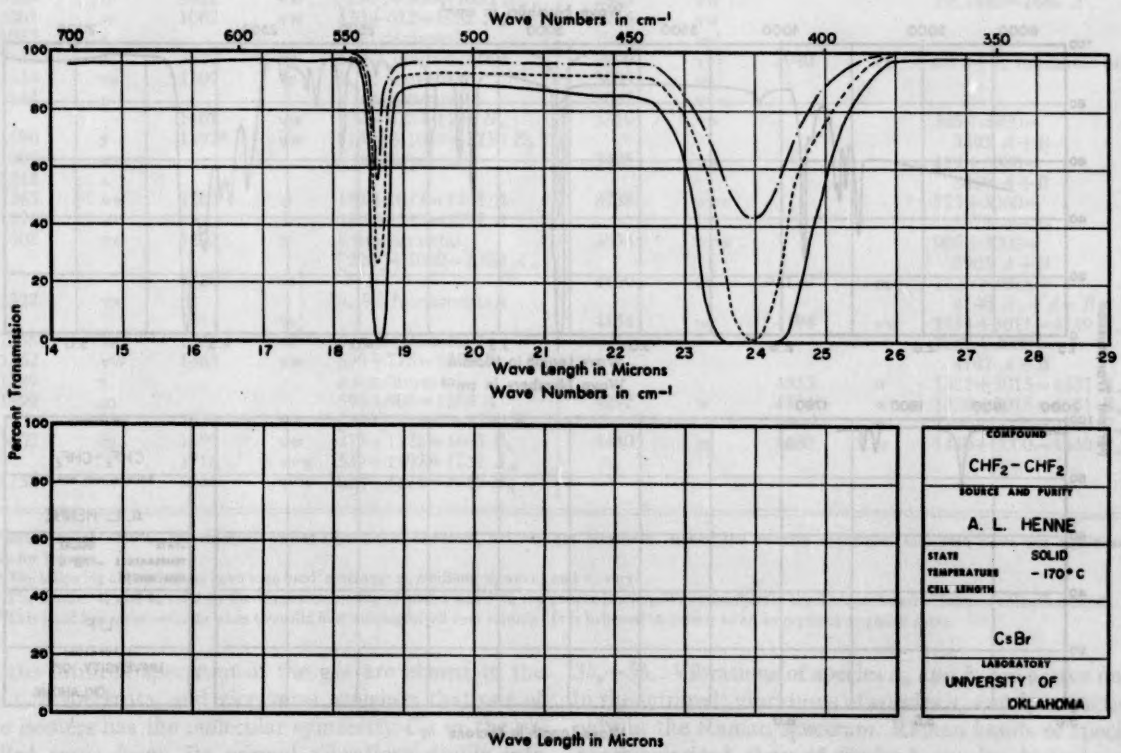

FIG. 4. Infrared absorption spectrum of solid CHF_2—CHF_2 at −170°C (CsBr prism).

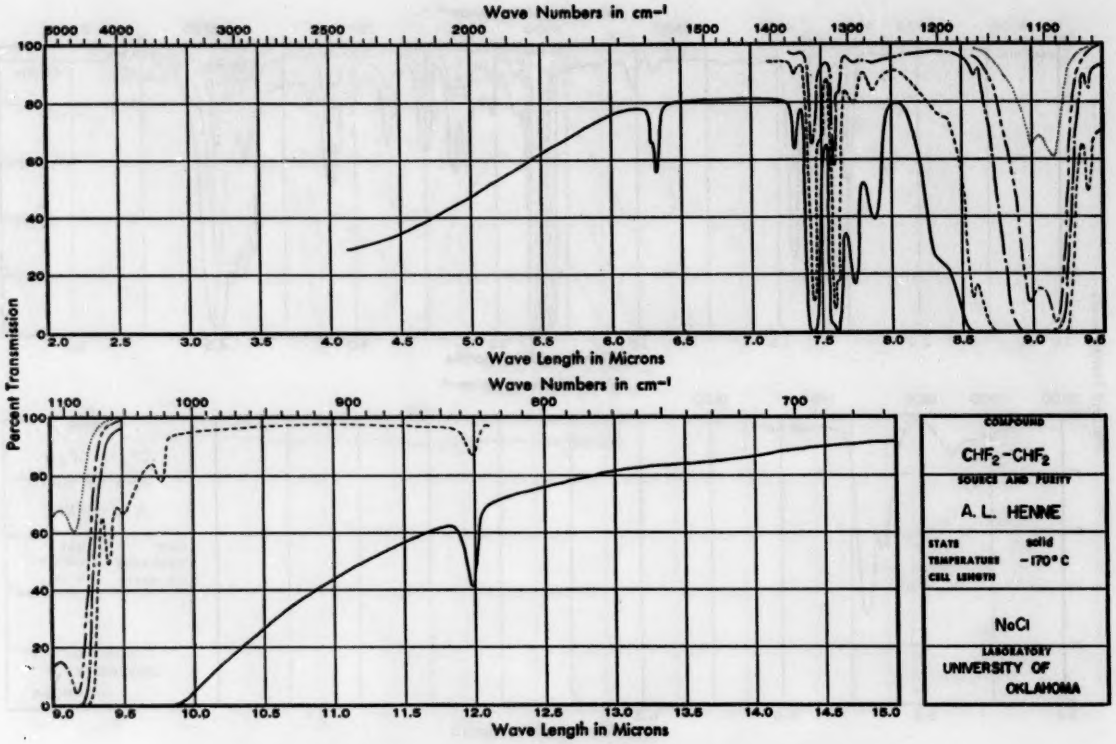

FIG. 5. Infrared absorption spectrum of solid CHF_2—CHF_2 at −170°C (NaCl prism).

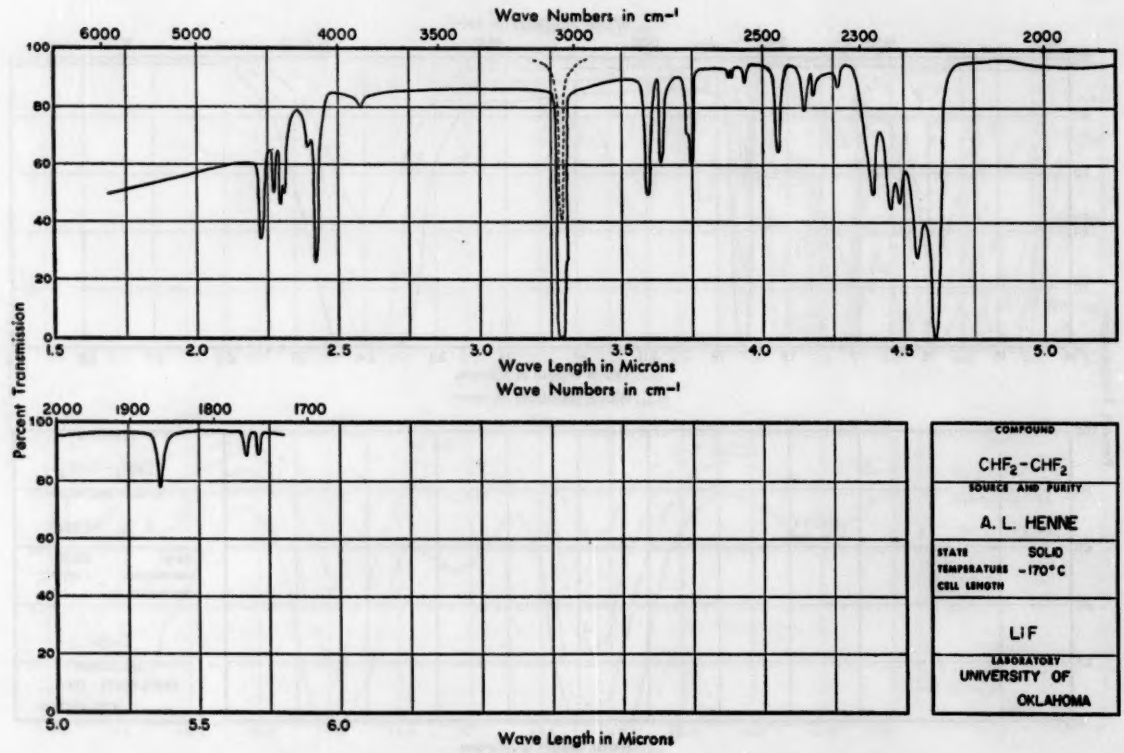

FIG. 6. Infrared absorption spectrum of solid CHF_2—CHF_2 at −170°C (LiF prism).

TABLE I. Infrared spectral data for gaseous and solid CHF_2—CHF_2.

Gas		Solid[a]		
Wave number	Description[b]	Wave number	Description[b]	Interpretation[c]
380	m			2×188=376 *A*
393	s			*a* fundamental
413	vs			
419	vs	408[d]		*a* fundamental
423	vs			
425	vs			
430	vs	417	s	a_u fundamental
434	s			
501	vvw			
515	m			130+393=523 *A*
522	s			*b* fundamental
531	s			
539	vs	537	s	b_u fundamental
546	s			
598	m			*a* fundamental
685	w			
692	w			188+522=710 *A*
698	w			
772	vs			
775	vs			*b* fundamental
779	vs			
785	m			188+598=786 *B*; 361+430=791 B_u
831	w			
840	w	834	m	2×419=838 *A*;
845	w			[220]+622=842 B_u
893	w			361+539=900 B_u;
905	s			130+775=905 *B*
911	w			*a* fundamental
918	vw			393+522=915 *B*
1013	vw			419+598=1017 *A*
1029	m	1021	vw	[130]+905=1035 A_u
1061	w	1062	vw	430+622=1052 A_u
1073	s			*b* fundamental
1125	s	1089	vs	a_u+*a* fundamentals
1134	vs	1109	vs	b_u fundamental
1147	s			*a* fundamental
		1161	vw	539+622=1161 B_u
1196	s	1192[d]	vw	[130]+1080=1210 B_u
1207	vs			*b* fundamental
1214	s			
1265	vw	1263	w	188+1073=1261 *A*
1276	w			130+1147=1277 *A*
1302	vs	1292	w	*b* fundamental; [220]+1080=1300 A_u
		1310	vs	
1322	vs			a_u+*b* fundamentals
		1314	vs	
1336	vs	1344	vs	b_u fundamental
1362	vw	1363	vw	598+775=1373 *B*
1389	s			*a* fundamental
1499	m			598+905=1503 *A*
		1579	vw	[220]+1360=1580 B_u
1603	m	1599	vw	478+1125=1603 B_u
		1716	vvw	539+1192=1731 A_u
1754	m	1751	vvw	622+1134=1756 B_u
1769	w			393+1389=1782 *A*
1855	vw	1864	vw	430+1440=1870 A_u; 419+1440=1859 *A*
2109	vw			905+1207=2112 *B*
2228	s	2169	s	905+1322=2227 A_u; 1080+1134=2214 A_u
2254	m	2198	m	905+1336=2241 B_u; 2×1125=2250 *A*
		2232	w	
2278	m	2244	w	1125+1147=2272 *A*?
2291	m	2276	w	1125+1192=2317 B_u; 2×1147=2294 *A*; 905+1389=2294 *A*
		2345	vw	1192+1134=2326 A_u; 905+1440=2345 *A*?
		2390	vw	1080+1322=2402 B_u
2407	vw	2410	vw	1080+1336=2416 A_u
2441	w			1147+1302=2449 *B*
2453	w			1073+1389=2462 *B*
2460	w	2461	w	1125+1360=2485 A_u
2491	vw			1207+1302=2509 *A*
2573	m	2541	w	1134+1440=2574 A_u
2590	vw			1207+1389=2596 *B*; 2×1302=2604 *A*
2664	w	2672	m	1322+1360=2682 A_u
2672	w	2681	w	1336+1360=2696 B_u
2739	w	2748	m	1322+1440=2762 A_u; 1302+1440=2742 *B*
2775	w	2780	m	1336+1440=2776 B_u; 2×1389=2778 *A*
2807	vw			1389+1440=2829 *A*
2845	vw			2×1440=2480 *A*
2916	vw			
2987	vs			
2996	vs	3040	vs	*a*+*b*+b_u fundamentals
3003	vs			
3067	vvw			
3319	vw			393+3000= 3393 *A*+*B*
3405	vw			419+3000= 3419 *A*+*B*
3738	vvw			775+3000= 3775 *A*+*B*
3834	vvw			905+3000= 3905 *A*+*B*
4100	m	4129	m	1125+3015= 4140 A_u+*A*+*B*
4134	w	4184	vw	1134+3015=4149 B_u; 1147+3000= 4147 *A*+*B*
		4333	w	1322+3015=4337 A_u
4297	w	4354	w	1336+3015=4351 B_u
		4390	w	1360+3000=4360 B_u
4440	m	4480	w	1440+3000=4440 B_u

[a] Solid film at −170°C. The thickness varied from record to record, but was not measured. Hence the relative intensities indicated have less significance than for the gas.

[b] The following abbreviations have been used: s, strong; m, medium; w, weak; and v, very.

[c] The species a_u and b_u refer to the trans isomer, the species *a* and *b* to the gauche isomers. Wave numbers in brackets are inferred from combination bands.

[d] This band was observed only when the solid film was deposited very rapidly. It is believed to belong to an amorphous or glassy state.

in the infrared spectrum of the gas are absent in the Raman spectrum, and vice versa, suggests that one of the isomers has the molecular symmetry C_{2h} or the so-called trans form. Its normal vibrations divide into symmetry species in the following manner: $6a_g+4a_u+3b_g+5b_u$. Vibrations of species a_u and b_u are active only in the infrared; vibrations of species a_g and b_g are active only in the Raman spectrum. Raman bands of species a_g are polarized, those of species b_g are depolarized.

It is also found, however, that a number of strong

TABLE II. Raman spectral data for liquid CHF_2—CHF_2.

Wave number	Description[a]	Exciting Hg lines[b]	Interpretation[c]
ca 130	vw	*e*	*a* fundamental
188	w	*e*	*b* fundamental
361	s, sh(0.4)	±*e*, *k*	a_g fundamental
413	m (0.8)	±*e*, *k*	*a* fundamental
478	m (dp)	*e*	b_g fundamental
522	m (dp)	*e*	*b* fundamental
578	vw	*e*	188+393=581 *B*
594	s, sh (0.2)	±*e*, *k*, *i*	*a* fundamental
622	vs, sh (0.2)	±*e*, *k*, *i*	a_g fundamental
772	m, d (0.8)	*e*, *k*	*b* fundamental
837	w	*e*	2×413=826 *A*; 2×*ca* 420=*ca* 840 A_g
901	s (0.3)	*e*, *k*, *i*	$a+a_g$ fundamentals
1080	w	*e*	b_g fundamental
1094	vs (0.3)	*e*, *k*	*a* fundamental
1147	s (0.6)	*e*, *k*	*a* fundamental
1192	m (dp)	*e*, *k*	$b+b_g$ fundamentals
1247	vw	*e*	130+1125=1255 *A*; 361+901=1262 A_g
1321	m (0.7)	*e*	*b* fundamental
1360	s (0.3)	*e*, *k*	$a+a_g$ fundamentals
1440	m, b (0.3)	*e*	$a+a_g$ fundamentals
3010–3025	vs (0.2)	*e*, *k*, *i*	$a+a_g+b$ fundamentals

[a] The following abbreviations have been used: s, strong; m, medium; w, weak; v, very; d, diffuse; sh, sharp; dp, depolarized; b, broad. The numbers in parentheses are measured depolarization ratios.

[b] The meanings of the Kohlrausch symbols are: *e* 4358 A, *k* 4047 A, *i* 4078 A; ± indicates that the Raman band has been observed both as a Stokes and an anti-Stokes shift.

[c] Fundamentals of species a_g and b_g refer to the trans isomer, those of species *a* and *b* to the gauche isomers.

infrared and Raman bands coincide. This indicates that the other rotational isomers consist of two enantiomorphic forms of symmetry C_2 obtained from the trans form by rotating one of the CHF_2 groups a certain angle (probably close to 120°) about the C—C bond in either direction. These two gauche forms will have identical vibrational frequencies, and their normal vibrations divide into 10 of species *a* and 8 of species *b*. All of them are active in both spectra. Raman bands of species *a* are polarized; those of species *b* are depolarized.

These conclusions are strongly supported by the fact that, with a few exceptions which will be discussed in the following, none of the infrared bands observed in the solid has counterparts in the Raman spectrum. This shows that, as in the case of 1,2-dichloroethane,[1] only the trans form is present in the crystal. The solid formed by slow condensation of the vapor at −170°C appears to be almost completely crystalline. However, when the solid film is formed very fast an appreciable fraction of the material appears to be in an amorphous or glassy state.

Assuming the internuclear distances C—C=1.54, C—F=1.37, C—H=1.093 A, and tetrahedral angles, one finds the following principal moments of inertia for the trans form: 169.4, 274.4, and 420.7×10^{-40} g cm^2. The axes of smallest and largest moments of inertia lie in the symmetry plane, the latter making an angle of 64°57′ with the C—C bond. Infrared bands of species a_u should, therefore, have type *B* contours in the spectrum of the gas, while bands of species b_u should have contours that are hybrids of types *A* and *C*. Extrapolations from Badger and Zumwalt's curves[10] give a *QQ* separation of 7 cm^{-1} for type *B* bands and *PR* separations of 15 and 18 cm^{-1} for *A* and *C* bands, respectively.

With the additional assumption that one end group is rotated 120° relative to the other, the principal moments of inertia of the gauche form are found to be 214.9, 315.4, and 338.4×10^{-40} g cm^2. The axis of intermediate moment of inertia coincides with the twofold symmetry axis. Thus, infrared bands of species *a* should have type *B* contours, while those of species *b* should have contours that are hybrids between types *A* and *C*. The *QQ* separation for type *B* bands should be 3 cm^{-1} and the *PR* separations for bands of types *A* and *C* should be 16 and 19 cm^{-1}, respectively.

On the basis of these criteria, it has been possible to make practically complete assignments of vibrational fundamentals for both trans and gauche isomers. For brevity, the isomer, or isomers, to which a frequency is ascribed will not be stated explicitly in what follows but will be implied by the species assignment, a_g, a_u, b_g, and b_u referring to the trans and *a* and *b* to the gauche isomer. The very strong band at 2996 cm^{-1}, and the prominent shoulders at 3003 and 2987 cm^{-1}, in the infrared spectrum of the gas must represent the b_u fundamental of the trans isomer and the *a* and *b* fundamentals of the gauche isomer associated with C—H stretching. In the Raman spectrum of the liquid the a_g fundamental of the trans isomer and the *a* and *b* fundamentals of the gauche overlap to form what appears to be a single broad band with maximum near 3015 cm^{-1}. In the infrared spectrum of the crystalline solid a very strong band is found at 3040 cm^{-1} which is interpreted as the b_u C—H stretching mode of the trans isomer.

In the region from 900 to 1500 cm^{-1} 9 fundamentals are expected for each isomer, their vibrations consisting of C—C stretching, C—F stretching, and C—H bending. The fact that fewer than the expected number of bands are found indicates that some of the observed frequencies are common to trans and gauche isomers. For this reason, and because some of the frequency shifts on going from gas to solid are quite large in this region, there is some uncertainty in the assignment of some of these fundamentals.

The broad, polarized Raman band at 1440 cm^{-1}, which has no observed counterpart in the infrared spectrum, is interpreted as overlapping a_g and *a* fundamentals, probably involving mainly C—H bending. The strong, diffuse but polarized, Raman band at 1360 cm^{-1}, to which there corresponds a strong infrared band at 1389 cm^{-1} in the gas but none in the solid, is also interpreted as overlapping a_g and *a* fundamentals. The motion is probably largely C—F stretching. The in-

[10] R. M. Badger and L. R. Zumwalt, J. Chem. Phys. 6, 711 (1938).

frared bands at 1336 and 1344 cm^{-1} in gas and solid, respectively, are assigned as a b_u fundamental. To the strong infrared band at 1322 cm^{-1} in the gas there appear to correspond a Raman band at 1321 cm^{-1} in the liquid and two infrared bands at 1314 and 1310 cm^{-1} in the crystalline solid. The intensity ratio of the latter two bands varies with the temperature at which crystallization takes place, indicating that they belong to different crystal forms. All of these bands are interpreted as an a_u and a b fundamentals. The rather low values of the observed depolarization ratio of the Raman band is assumed to be caused by experimental uncertainty. The very strong infrared band at 1302 cm^{-1} in the gas is interpreted as a b fundamental, in spite of the facts that no corresponding Raman band was observed and that a weak infrared band was found in the solid at 1292 cm^{-1}. The latter is believed either to be caused by a small amorphous or glassy component of the solid or to be a combination band.

The very strong infrared band at 1207 cm^{-1}, which is absent in the crystal, and the medium intensity Raman band at 1192 cm^{-1} are interpreted as a b fundamental, and the Raman band is also ascribed to an overlapping b_g fundamental. The strong infrared band at 1147 cm^{-1} in the gas and the strong and apparently polarized Raman band at the same wave number are assigned as an a fundamental.

The very intense infrared band at 1134 cm^{-1} in the gas is shifted to 1109 cm^{-1} in the solid and has no corresponding Raman band. It is interpreted as a b_u fundamental. Although it is not well separated from the band just mentioned, there appears to be a strong infrared band near 1125 cm^{-1} in the gas and at 1089 cm^{-1} in the crystal. A corresponding Raman band is observed at 1094 cm^{-1}. It is assumed that these arise from overlapping a_u and a fundamentals. The weak Raman band observed at 1080 cm^{-1} is assigned as a b_g fundamental, and the strong infrared band at 1073 cm^{-1} is interpreted as a b fundamental. The strong band at 905 cm^{-1} in the gas, which is not present in the crystal, and the strong, polarized band at 901 cm^{-1} in the Raman spectrum, are interpreted as overlapping a and a_g fundamentals. They probably involve largely C—C stretching.

The infrared band at 775 cm^{-1} in the gas is absent in the solid but a depolarized Raman band is found at 772 cm^{-1}. These evidently represent a b fundamental. The strong Raman bands at 622 and 594 cm^{-1} are both polarized. The former has no counterpart in the infrared spectrum, the latter corresponds to a medium intensity infrared band at 598 cm^{-1} found only in the spectrum of the gas. These bands must be interpreted as an a_g and an a fundamental, respectively. The infrared band at 539 cm^{-1} in the gas has definitely a PQR structure with PR separation 15 cm^{-1}. A corresponding band is found at 537 cm^{-1} in the spectrum of the solid but none is observed in the Raman spectrum, These bands are assigned as a b_u fundamental. The motions associated with the four last-mentioned fundamentals can probably best be described as deformations of the CF_2H groups.

Overlapping the b_u fundamental at 539 cm^{-1}, a rather strong infrared band of uncertain contour appears near 522 cm^{-1} in the spectrum of the gas, but no indication of such a band is observed in the solid. A medium intensity Raman band occurs at 522 cm^{-1}. These bands are assigned as a b fundamental. The depolarized Raman band at 478 cm^{-1}, which has no counterpart in the infrared spectrum, is assigned as a b_g fundamental.

In a wide region around 425 cm^{-1} the infrared absorption by the gas is extremely strong but very complex, indicating the presence of more than one fundamental. In the infrared spectrum of the solid there is a single strong band with maximum at 417 cm^{-1}. However, when the sample was solidified very rapidly, presumably forming a mixture of crystalline aggregate and glass, a second, weaker band was observed at 408 cm^{-1}. In the Raman spectrum a medium intensity, slightly polarized band is found at 413 cm^{-1}. The latter is interpreted as an a fundamental and the infrared band in the crystalline solid is assigned as an a_u fundamental. The wave numbers for these fundamentals in the gas cannot be given accurately but are assumed to be 419 and 430 cm^{-1}, respectively.

A strong infrared band is observed at 393 cm^{-1} in the gas but not in the solid. Although no corresponding Raman band was found, it is assigned as an a fundamental. The strong, polarized Raman band at 361 cm^{-1} has no infrared counterpart and is therefore assigned as an a_g fundamental. The weak Raman band at 188 cm^{-1} is interpreted as a b fundamental. The vibrations associated with the fundamentals mentioned having wave numbers 522 cm^{-1} or lower may be roughly characterized as rocking motions.

There remain the lowest a fundamental of the gauche isomer and the two lowest fundamentals of the trans isomer. The a fundamental, involving largely twisting, may be represented by a weak and somewhat uncertain Raman band at 130 cm^{-1}. The two fundamentals of the trans isomer, of species b_u (rocking) and a_u (twisting) lie outside the range of the CsBr prism and are inactive in the Raman spectrum. There is some evidence from combination bands that they lie near 220 and 130 cm^{-1}, respectively, but this is quite uncertain.

The assigned fundamentals are listed in Tables III and IV. The validity of these assignments may be tested by the sum rule derived by Mizushima *et al.*[11] For the gauche isomer $\Sigma\nu_i^2=33.02\times10^6$. By taking the uncertain values mentioned above for the two lowest fundamentals, one finds 32.74×10^6 for the corresponding sum for the trans isomer. The difference is less than 0.9%. The lower value found for the trans isomer may result from the fact that half of the fundamental vibrational frequencies for this isomer are obtained from the Raman spectrum of the liquid phase. The

[11] Mizushima, Shimanouchi, Nakagawa, and Miyake, J. Chem. Phys. **21**, 215 (1953).

TABLE III. Fundamental vibrational frequencies of trans $CHF_2—CHF_2$ (in cm^{-1}).[a]

Species	Infrared (gas)	Infrared (solid)	Raman (liquid)	Approximate motion
a_g			*ca.* 3015 vs	CH stretching
a_g			1440 m,b(0.3)	CH bending
a_g			1360 s(0.3)	CF stretching
a_g			901 s(0.3)	CC stretching
a_g			622 vs(0.2)	CHF_2 deformation
a_g			361 s(0.4)	Rocking
a_u	1322 s	1314(1310) vs		CH bending
a_u	1125 vs	1089 s		CF stretching
a_u	*ca* 430 s	417 vs		Rocking
a_u	[130][b]	[130][b]		Twisting
b_g			1192 m(dp)	CH bending
b_g			1080 w	CF stretching
b_g			478 m(dp)	Rocking
b_u	*ca* 3000 vs	3040 vs		CH stretching
b_u	1336 s	1344 s		CF stretching
b_u	1134 vs	1109 s		CH bending
b_u	539 s	537 s		CHF_2 deformation
b_u	[220][b]	[220][b]		Rocking

[a] See footnote b, Table I, and footnote a, Table II, for the explanation of the abbreviations used.
[b] Wave numbers in brackets are inferred from combination bands.

empirical sum rule of Bernstein and Pullin[12] is also quite well satisfied, the sums being $\Sigma\nu_i=19\,940$ for the gauche and $\Sigma\nu_i=19\,690$ for the trans isomer.

In terms of the assigned fundamentals, it has been possible to assign all the observed Raman bands and practically all of the infrared bands. However, because of the large dependence of many of the frequencies upon the state of aggregation, the correlation of several bands in the three spectra is very difficult, and their interpretations are therefore somewhat uncertain. Most, if not all, of the very weak bands that have been left uninterpreted can be explained as ternary combination bands. However, in view of the large number of fundamentals such interpretations are in most cases not unique and have therefore not been included in Table II.

ENTHALPY DIFFERENCE BETWEEN THE ROTATIONAL ISOMERS

As the $CHF_2—CHF_2$ gas was heated from 30° to 170°C the infrared bands assigned to the gauche isomer increased in intensity, while those assigned to the trans form became weaker, showing that the latter is the more stable. For the purpose of determining the enthalpy difference the peak extinctions of the following bands were measured at 30°, 70°, 110°, 140°, and 170°C: trans, 1134, 1322, and 539 cm^{-1}; gauche, 1207, 775, and 598 cm^{-1}; and the graphical method of Bernstein[13] was used. The following result was obtained:

$$\Delta H^0=1160\pm100 \text{ cal/mole}.$$

[12] H. J. Bernstein and A. D. A. Pullin, J. Chem. Phys. **21**, 2188 (1953).
[13] H. J. Bernstein, J. Chem. Phys. **18**, 897 (1950).

Because of the uncertainty in several of the fundamental vibrational frequencies, especially the two lowest frequencies for the trans isomer, the energy difference ΔE_0^0 was not calculated.

The three identical Raman exposures, at 25°, −25°, and −70°C, did not reveal any appreciable intensity variations with temperature, indicating that ΔH^0, is much smaller, probably less than 400 cal/mole, for the liquid state. This can be explained only in part by Onsager's theory of dielectrics,[14] according to which a spherical molecule of dipole moment μ and radius a loses the potential energy

$$E_r=(\epsilon-1)\mu^2/(2\epsilon+1)a^3,$$

when transferred from vacuum ($\epsilon=1$) to a medium of dielectric constant ϵ. By using the bond moments $\mu_{C-H}=0.4$, $\mu_{C-F}=1.45$ debyes,[15] one finds by simple vector addition the values 1.73 D for the gauche and 0 for the trans isomer. The dielectric constant of liquid $CHF_2—CHF_2$ is not known. However, since the formula is not very sensitive to changes in ϵ, it is probably a fairly good approximation to put $\epsilon\cong10$, which is the value given for 1,2-dichloroethane.[16] When taking $a=1.6$ A, one finds

$$E_p \text{ (gauche)}=320 \text{ cal/mole}, E_r \text{ (trans)}=0.$$

While this is of the right order of magnitude it is considerably smaller than the observed change in ΔH^0.

DISCUSSION

It is of interest to compare the results found here with those previously reported for $CHCl_2—CHCl_2$

TABLE IV. Fundamental vibrational frequencies of *gauche* $CHF_2—CHF_2$ (in cm^{-1})[a]

Species	Infrared (gas)	Raman (liquid)	Approximate motion
a	*ca* 3000 vs	*ca* 3015 vs,b	CH stretching
a	...	1440 m,b(0.3)	CH bending
a	1389 s	1360 s(0.3)	CF stretching
a	1147 s	1147 s(0.6)	CH bending
a	1125 s	1094 vs(0.3)	CF stretching
a	905 s	901 s(0.3)	CC stretching
a	598 m	594 s(0.2)	CHF_2 deformation
a	*ca* 419 vs	413 m(0.8)	Rocking
a	393 s	...	Rocking
a		*ca* 130 vw	Twisting
b	*ca* 3000 vs	*ca* 3015 vs,b	CH stretching
b	1322 s	1321 m(0.7)	CF stretching
b	1302 vs	...	CH bending
b	1207 vs	1192 m(dp)	CH bending
b	1073 s	...	CF stretching
b	775 vs	772 m,d(0.8)	CHF_2 deformation
b	522 m	522 m(dp)	Rocking
b	...	188 w	Rocking

[a] For abbreviations used, see footnote b, Table I, and footnote a, Table II.

[14] L. Onsager, J. Am. Chem. Soc. **58**, 1486 (1936).
[15] C. P. Smyth, *Dielectric Behavior and Structure* (McGraw-Hill Book Company, Inc., New York, 1955).
[16] P. Walden, Z. physik. Chem. **70**, 596 (1909).

and $CHBr_2$—$CHBr_2$. In the case of both of these compounds the gauche isomer is the more stable in the liquid state,[17] the enthalpy differences being 1100 and 910 cal/mole, respectively. $CHCl_2$—$CHCl_2$ crystallizes in the gauche form, while $CHBr_2$—$CHBr_2$ crystallizes as trans or gauche according to the experimental conditions.[17] For gaseous $CHCl_2$—$CHCl_2$ ΔH^0 is very small.[1,18] No information is available about gaseous $CHBr_2$—$CHBr_2$.

It is rather difficult to understand why CHF_2—CHF_2 behaves differently from the two other compounds. If, as claimed by Mizushima,[19] steric hindrance is the most important factor in determining the relative stability of the rotational isomers of halogenated ethanes, one would expect $CHCl_2$—$CHCl_2$ and $CHBr_2$—$CHBr_2$ to have a greater rather than a smaller probability of existing in the trans form than CHF_2—CHF_2. The stabilization of the trans form of this compound may be a result of intramolecular hydrogen bonding which should be nearly twice as strong in the trans as in the gauche form.

ACKNOWLEDGMENT

The writers are indebted to Professor Albert L. Henne and Dr. Leonard H. Beck of Ohio State University for providing the sample.

[17] R. E. Kagarise, J. Chem. Phys. **24**, 300 (1956).
[18] J. R. Thomas and W. D. Gwinn, J. Am. Chem. Soc. **71**, 2785 (1949).
[19] See reference 1, p. 68.

THE JOURNAL OF CHEMICAL PHYSICS VOLUME 32, NUMBER 3 MARCH, 1960

Electron-Population Analysis and the Dipole Moment of the LiH $^1\Sigma^+$ Excited State*

A. M. KARO

Lawrence Radiation Laboratory, University of California, Livermore, California

(Received September 28, 1959)

Detailed consideration is given to some properties of the first excited electronic state. Following the analysis proposed by Mulliken, SCF LCAO-MO coefficients are used to obtain qualitative information about the electron distribution. Comparison is made with earlier work with respect to the description of the excited state in terms of the interacting configurations. In addition to the excited-state dipole moment, the effective electric moment between the ground and excited states is also calculated. From this, the oscillator strength for the first allowed transition is computed as a function of the internuclear distance.

I. INTRODUCTION

In an early extensive treatment by Mulliken[1] of the low-lying electronic states of simple heteropolar diatomic molecules, the alkali metal hydrides were examined in detail because of interest in the unusual form of the $A\,^1\Sigma^+$ potential curves. In particular, attention was given to the excited $^1\Sigma^+$ state of LiH. The shape of the potential curve was accounted for, in the absence of good molecular wave functions, by an approximate perturbation treatment between the homopolar $Li(^2S)\cdot H$ state and the completely ionic Li^+H^- state. A subsequent analysis by Rosenbaum[2] showed that there should be sufficient interaction between these two configurations around 9 au to predict unequivocally dissociation to $Li(^2P)+H$. Both treatments emphasized the predominant Li^+H^- character of the excited molecular wave function at internuclear distances somewhat greater than the equilibrium separation.

Recent calculations have resulted in good wave functions for the first excited state over a range of internuclear distances from 2 to 8 au.[3] In terms of the curvature around the minimum, the position of the minimum, and the dissociation energy associated with the potential curve, it appears very likely that the wave functions obtained are quite adequate for describing the excited state. Other than describing the characteristics of the potential curve, however, only brief mention has been given in these recent papers to the excited state.

In the present paper the discussion is extended by describing the excited state with respect to the interacting configurations. Results of both the determinantal AO and MO calculations are examined. The first method is more directly related to the early papers in which just such interacting configurations were considered. The second method provides a different sort of insight into the nature of the excited state, by considering the charge distribution among the available configurations and the MO's. The dipole moment of the excited state is also evaluated, as well as the matrix element of the

* This work was performed under the auspices of the U. S. Atomic Energy Commission.
[1] R. S. Mulliken, Phys. Rev. **50**, 1028 (1936).
[2] E. J. Rosenbaum, J. Chem. Phys. **6**, 16 (1938).
[3] A. M. Karo and A. R. Olson, J. Chem. Phys. **30**, 1232 (1959)

TABLE I. Enumeration of configurations ϕ_r.

(a) Determinantal AO configurations.

ϕ_1: $(1/\sqrt{2})[s(\alpha)s(\beta)S(\alpha)h(\beta)-s(\alpha)s(\beta)S(\beta)h(\alpha)]$

ϕ_2: $(1/\sqrt{2})[s(\alpha)s(\beta)p_0(\alpha)h(\beta)-s(\alpha)s(\beta)p_0(\beta)h(\alpha)]$

ϕ_3: $s(\alpha)s(\beta)h(\alpha)h(\beta)$

ϕ_4: $s(\alpha)s(\beta)S(\alpha)S(\beta)$

ϕ_5: $(1/\sqrt{2})[s(\alpha)s(\beta)S(\alpha)p_0(\beta)-s(\alpha)s(\beta)S(\beta)p_0(\alpha)]$

ϕ_6: $s(\alpha)s(\beta)p_0(\alpha)p_0(\beta)$

(b) Determinantal MO configurations.

ϕ_1: $1\sigma(\alpha)1\sigma(\beta)2\sigma(\alpha)2\sigma(\beta)$

ϕ_2: $(1/\sqrt{2})[1\sigma(\alpha)1\sigma(\beta)3\sigma(\alpha)4\sigma(\beta)-1\sigma(\alpha)1\sigma(\beta)3\sigma(\beta)4\sigma(\alpha)]$

ϕ_3: $1\sigma(\alpha)1\sigma(\beta)3\sigma(\alpha)3\sigma(\beta)$

ϕ_4: $1\sigma(\alpha)1\sigma(\beta)4\sigma(\alpha)4\sigma(\beta)$

ϕ_5: $(1/\sqrt{2})[1\sigma(\alpha)1\sigma(\beta)2\sigma(\alpha)3\sigma(\beta)-1\sigma(\alpha)1\sigma(\beta)2\sigma(\beta)3\sigma(\alpha)]$

ϕ_6: $(1/\sqrt{2})[1\sigma(\alpha)1\sigma(\beta)2\sigma(\alpha)4\sigma(\beta)-1\sigma(\alpha)1\sigma(\beta)2\sigma(\beta)4\sigma(\alpha)]$

dipole moment operator between the ground and excited states.

II. ELECTRON-POPULATION ANALYSIS

Recent descriptions of electron populations in molecules have been largely based on the scheme proposed by Mulliken[4] for SCF LCAO-MO calculations. The popularity of this sort of analysis is, no doubt, in large part due to the resulting graphic illustrations of hybridization, charge localization within the molecule, and electron promotion by configuration interaction (CI). If the usefulness of this type of description can be demonstrated in small molecules, its popularity can be expected to increase as attention is turned to the rigorous calculation of larger systems and, in particular, to organic structures.

The electron populations of the ground states of LiH and HF were analyzed in detail in a preceding paper.[5] There, caution was emphasized because the bonding properties of the orbitals in HF were found to be very sensitive to the choice of Slater or Hartree-Fock basis functions. At the same time, however, a more promising indication was also noted in that the use of the better basis orbitals gave results in closer agreement with experiment.

The use of Hartree-Fock lithium functions in the present case permits somewhat more confidence in the population analysis. Because the lithium $2s$ and $2p$ orbitals can be adequately described by relatively few exponential functions, it is also probable that the picture presented will remain essentially unchanged for other recent LiH calculations[6] where the basis functions are orthonormal sets of exponential orbitals.

Definitions of the gross and total atomic populations and of the subtotal and total overlap populations have been given in earlier reports for single-determinant wave functions[4] and for multi-configuration wave functions.[5]

The enumeration of the determinantal AO and MO configurations ϕ_r is given in Table I. These configurations represent, as usual, completely normalized antisymmetric products (Slater determinants) of the given AO's or MO's (AP AO's or AP MO's). The $1s$, $2s$, and $2p$ AO's on lithium and the $1s$ AO on hydrogen are represented by s, S, p_0, and h, respectively. Overlap integrals between the AO's have been given previously.[3]

Table II lists the coefficients a_r for the expansion of several normalized molecular wave functions Ψ in terms of the ϕ_r. It is apparent that for Ψ's composed of AP AO configurations ϕ_2 is the limiting configuration at large values of r, in agreement with the analysis of Rosenbaum. For both the ground and the excited states the dominant configurations are ϕ_1, ϕ_2, and ϕ_3. A clearly defined analogous trend has not yet developed among the AP MO configurations, although one expects the limiting configuration to be ϕ_6. However, it is necessary to consider the changing character of the MO's with internuclear distance, as well as the weights of the configurations. Population analysis allows both factors to be taken into consideration.

A comparison of the excited-state functions in terms of the energy is made in Table III. The single-configuration wave functions exhibit correct general behavior. Marked improvement occurs in the two-term function because of s, p hydridization. Thus, in contrast with earlier predictions,[1,2] the strongest interaction is between the two nonpolar configurations, ϕ_1 and ϕ_2, the Li^+H^- state contributing relatively little over the range of r considered here.

The distribution of the electron population among the AO's is shown in Table IV, where the single determinant (SD) $\Psi=\phi_5$ is compared with the six-term Ψ (CI). The configuration ϕ_6 remains the lowest excited state between 2 and 8 au, although it should eventually transform to the atomic states, $Li(^2S)+H$, corresponding to the dissociated molecular ground state. From the usual MO correlation diagrams it is seen that the 3σ and 4σ MO's change, respectively, to the lithium $2s$ and $2p$ AO's, so that the configuration corresponding to the excited state of the molecule at large r is ϕ_6. It can also be seen that CI allows for the promotion of electrons from the $2s$ to the $2p$ AO, or, equivalently, from the 3σ to the 4σ MO [cf. Table V(a)].

The electron distribution among the configurations, given in Table V(b), indicates, also, that ϕ_5 is by far the most important configuration up to 5 or 6 au. As r increases, the shift of population is expected to be from

[4] R. S. Mulliken, J. Chem. Phys. **23**, 1833, 1841 (1955).
[5] A. M. Karo, J. Chem. Phys. **31**, 182 (1959).
[6] Miller, Friedman, Hurst, and Matsen, J. Chem. Phys. **27**, 1385 (1957); A. C. Hurley, *ibid.* **28**, 532 (1958).

TABLE II. Coefficients for the configuration terms for several excited-state molecular wave functions (a_i for values of r_0).

(a) Determinantal AO configurations.

Configuration	2.0	2.6	3.0	3.5	4.0	5.0	6.0	7.0	8.0
ϕ_1	0.84756	0.76801	0.72318	0.68026	0.64218	0.54606	0.37972	0.20649	0.09435
ϕ_2	0.85582	0.85753	0.84668	0.83063	0.82034	0.82698	0.87058	0.91662	0.95201
ϕ_3	0.19633	0.15036	0.13186	0.12286	0.12540	0.14819	0.17328	0.17386	0.14320
ϕ_4	0.11595	0.05633	0.02266	−0.00466	−0.01793	−0.02177	−0.01525	−0.00829	−0.00467
ϕ_5	0.10822	0.06577	0.04747	0.03283	0.02372	0.01421	0.00863	0.00517	0.00414
ϕ_6	−0.03599	−0.03550	−0.02299	−0.00874	0.00031	0.00581	0.00532	0.00116	−0.00037
ϕ_1	0.81738	0.76211	0.73040	0.69676	0.66095	0.55996	0.38717	0.20935	0.09562
ϕ_2	0.76609	0.79508	0.80716	0.81280	0.81455	0.82799	0.87180	0.91649	0.95164
ϕ_3	0.20242	0.16496	0.14478	0.13129	0.13010	0.14928	0.17341	0.17391	0.14323
ϕ_1	0.62141	0.62014	0.61376	0.59605	0.56289	0.44519	0.27192	0.13261	0.05841
ϕ_2	0.91994	0.92016	0.91715	0.91383	0.91579	0.94098	0.97818	0.99517	0.99914

(b) Determinantal MO configurations.

Configuration	2.0	2.6	3.0	3.5	4.0	5.0	6.0	7.0	8.0
ϕ_1	0.06578	0.07659	0.08776	0.10784	0.13904	0.23900	0.37947	0.47064	0.46516
ϕ_2	0.25441	0.26442	0.27276	0.28503	0.29667	0.30214	0.24784	0.13114	−0.01923
ϕ_3	0.17030	0.17952	0.18802	0.20096	0.21692	0.25002	0.27601	0.28501	0.28830
ϕ_4	−0.02067	−0.03298	−0.03795	−0.04744	−0.06208	−0.11402	−0.20535	−0.30829	−0.37998
ϕ_5	−0.94912	−0.94362	−0.93826	−0.92901	−0.91599	−0.87588	−0.80495	−0.71304	−0.62351
ϕ_6	0.01554	0.02185	0.02798	0.03793	0.05211	0.09437	0.16818	0.27677	0.40865

TABLE III. Excited-state energies (ry).[a]

	Determinantal AO configurations				Determinantal MO configurations	
r_0	(1-term Ψ: ϕ_2)	(2-term Ψ: ϕ_1, ϕ_2)	(3-term Ψ: ϕ_1, ϕ_2, ϕ_3)	(6-term Ψ)	(1-term Ψ: ϕ_5)	(6-term Ψ)
2.0	0.25530	0.33486	0.32598	0.30734	0.40253	0.30640
2.6	0.08384	0.16383	0.15747	0.15167	0.25545	0.15160
3.0	0.04219	0.11829	0.11295	0.11087	0.21879	0.11089
3.5	0.02572	0.09217	0.08727	0.08665	0.20051	0.08671
4.0	0.02882	0.08177	0.07652	0.07610	0.19789	0.07618
5.0	0.05523	0.08102	0.07323	0.07285	0.21539	0.07291
6.0	0.08712	0.09551	0.08500	0.08480	0.25222	0.08483
7.0	0.10578	0.10782	0.09785	0.09779	0.29579	0.09780
8.0	0.11869	0.11911	0.11263	0.11261	0.35595	0.11262

[a] Energies are relative to the separated, unexcited neutral atoms taken to be zero on the energy scale.

ϕ_5 to ϕ_6 and is just becoming strongly evident at 8 au. In any case, the limiting behavior of the excited state is by no means as well delineated in the SCF MO method as in the determinantal AO calculation. In addition, since both six-term wave functions are nearly equivalent in terms of the energy and dipole moment, the population analysis does not give a quantitatively true picture of the charge distribution at large r, although the qualitative trends are correct.

Subtotal and total overlap populations are given in Table VI. The effective overlap populations $n(i;\text{CI})$ for the MO's and the total overlap populations n are plotted in Fig. 1. With respect to the overlap populations, the chief effect of CI comes from electron promotion from the nonbonding 3σ MO to the strongly antibonding 4σ MO. Thus, the total overlap decreases markedly, although the energy around the minimum is lowered more than 0.1 ry.

Of considerable interest is the correlation observed here (and also seen previously[3]) between the shape of the total overlap curve as a function of internuclear distance and the calculated potential curve. This correlation has been emphasized by plotting the potential curve for the excited state in Fig. 1. Not only does the minimum of the potential curve correspond to the region of maximum overlap, but also the broad behavior of the minimum is reproduced in the dependence of the overlap on internuclear distance.

Table VII gives the overlap distribution among the MO's and the configurations. Values of $n(i)$ are based on total occupancy of the MO's $[N(i)=2]$, and the values for $n(i;\text{CI})$ are the actual or "effective" bond-

TABLE IV. Gross atomic populations, $N(p_k)$.

r_0		$N(1s)$	$N(2s)$	$N(2p)$	$N(H)$
2.0	SD	1.9936	0.6568	0.5767	0.7729
	CI	1.9936	0.6779	0.6085	0.7200
2.6	SD	1.9986	0.6948	0.5887	0.7179
	CI	1.9986	0.7105	0.6208	0.6701
3.0	SD	1.9994	0.7250	0.5924	0.6832
	CI	1.9994	0.7370	0.6245	0.6391
3.5	SD	1.9997	0.7584	0.5870	0.6549
	CI	1.9997	0.7664	0.6200	0.6139
4.0	SD	1.9998	0.7859	0.5717	0.6426
	CI	1.9998	0.7897	0.6065	0.6040
5.0	SD	2.0000	0.8299	0.5236	0.6465
	CI	2.0000	0.8150	0.5617	0.6233
6.0	SD	2.0000	0.8671	0.4615	0.6714
	CI	2.0000	0.7954	0.5053	0.6993
7.0	SD	2.0000	0.9022	0.3842	0.7136
	CI	2.0000	0.7335	0.4789	0.7876
8.0	SD	2.0000	0.9351	0.2980	0.7669
	CI	2.0000	0.6640	0.5257	0.8103

ing strengths of the MO's allowing for CI. As was found for the ground state, the bond in the excited state over the whole range of r considered is primarily due to the bonding 2σ electrons. In distributing the overlap population among the configurations, it was found, for the ground state, that ϕ_1 is the only bonding configuration. Here, ϕ_5 is the principal bonding configuration, with ϕ_1 contributing considerably at larger distances.

III. DIPOLE MOMENTS

From a näive viewpoint, the early prediction that the excited state is characterized at intermediate values of r by the Li^+H^- configuration leads to the expectation of a negative dipole moment. On the contrary, the moment at nearly every stage of approximation considered here turns out to be positive and large, out to 6 au. The decrease in the moment at larger distances represents only a relatively small contribution from the Li^+H^- configuration. This result is in agreement with the relatively low weight given to the Li^+H^- term in the total wave function.

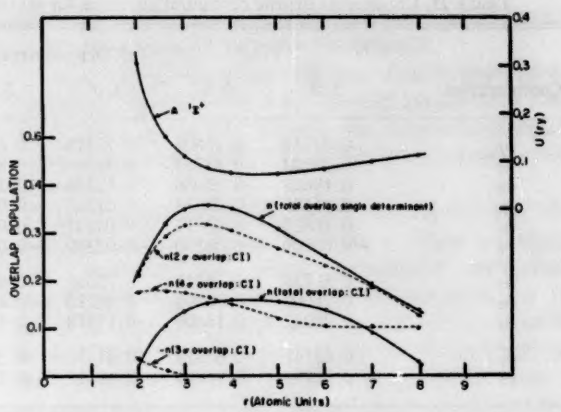

FIG. 1. Partial and total overlap populations for LiH, as a function of CI and internuclear distance.

Dipole moment integrals, not given previously, are listed in Table VIII. Table IX presents the compiled dipole moment results for the excited state functions that have been discussed. The best dipole moment values for both Σ states are plotted in Fig. 2 to emphasize the change in the moment during the transition. Although neither one of the nonpolar AO configurations, ϕ_1 and ϕ_2, considered separately, gives a positive moment from 2 to 8 au, the best linear combination results in a moment that compares well with the six-term Ψ. Results for the three-term Ψ indicate that the effect of including the Li^+H^- configuration is more noticeable at distances greater than 6 au.

The MO configuration ϕ_5 is a good approximation to the excited state at small values of r, and here the computed moment is in partial agreement with that calculated from the six-term Ψ. The transformation of ϕ_5

TABLE V. Total atomic populations.

(a) Electron distribution among the MO's

	2.0	2.6	3.0	3.5	4.0	5.0	6.0	7.0	8.0
1σ	2.0000	2.0000	2.0000	2.0000	2.0000	2.0000	2.0000	2.0000	2.0000
2σ	0.9097	0.9026	0.8965	0.8877	0.8804	0.8903	0.9642	1.0280	0.9885
3σ	1.0236	1.0248	1.0254	1.0251	1.0212	0.9835	0.8617	0.6881	0.5554
4σ	0.0667	0.0726	0.0781	0.0872	0.0984	0.1262	0.1740	0.2839	0.4561

(b) Electron distribution among the configurations, ϕ_r

	2.0	2.6	3.0	3.5	4.0	5.0	6.0	7.0	8.0
$N(\phi_1)$	0.0173	0.0235	0.0308	0.0465	0.0773	0.2285	0.5760	0.8860	0.8655
$N(\phi_2)$	0.2589	0.2797	0.2976	0.3250	0.3520	0.3652	0.2457	0.0688	0.0015
$N(\phi_3)$	0.1160	0.1289	0.1414	0.1615	0.1882	0.2500	0.3047	0.3249	0.3325
$N(\phi_4)$	0.0035	0.0043	0.0058	0.0090	0.0154	0.0520	0.1687	0.3802	0.5775
$N(\phi_5)$	3.6033	3.5617	3.5213	3.4522	3.3561	3.0687	2.5918	2.0337	1.5550
$N(\phi_6)$	0.0010	0.0019	0.0031	0.0058	0.0109	0.0356	0.1131	0.3064	0.6680

TABLE VI. Subtotal overlap populations, $n(p_k, q_l)$.

r_0		$n(1s, H)$	$n(2s, H)$	$n(2p, H)$	n(total overlap)
2.0	SD	−0.0692	0.0745	0.2112	0.2165
	CI	−0.0748	−0.0356	0.1285	0.0181
2.6	SD	−0.0220	0.1194	0.2202	0.3176
	CI	−0.0246	0.0114	0.1191	0.1059
3.0	SD	−0.0099	0.1292	0.2294	0.3487
	CI	−0.0112	0.0273	0.1206	0.1367
3.5	SD	−0.0036	0.1250	0.2373	0.3587
	CI	−0.0041	0.0340	0.1242	0.1541
4.0	SD	−0.0013	0.1118	0.2397	0.3502
	CI	−0.0015	0.0333	0.1271	0.1589
5.0	SD	−0.0002	0.0791	0.2287	0.3077
	CI	−0.0002	0.0291	0.1257	0.1546
6.0	SD	0.0000	0.0498	0.2015	0.2513
	CI	0.0000	0.0317	0.1071	0.1388
7.0	SD	0.0000	0.0273	0.1640	0.1913
	CI	0.0000	0.0299	0.0601	0.0900
8.0	SD	0.0000	0.0128	0.1227	0.1355
	CI	0.0000	0.0207	0.0089	0.0296

to neutral atomic states on dissociation can be associated with the decreasing value of the moment at 7 and 8 au.

The apparent dipole moment, based on the gross atomic charges, is also given in Table IX. Near the equilibrium distances, the results agree with the exact calculation. Elsewhere, there is only qualitative agreement. In general, it has been found that the sign of the apparent moment is correct but that not much confidence should be placed in the magnitude.

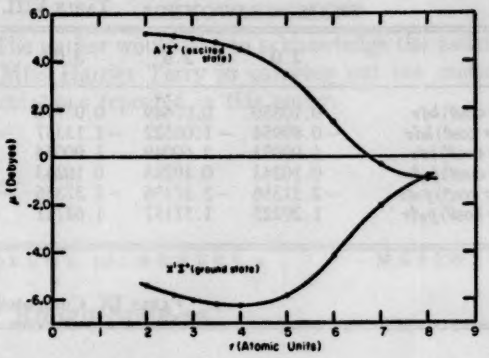

FIG. 2. Dipole moments for the ground and excited states of LiH, as a function of internuclear distance.

IV. DIPOLE STRENGTH OF THE $^1\Sigma^+ - {}^1\Sigma^+$ TRANSITION

Experimental values of the dipole moment have not yet been reported for either the ground or the excited state. A related experimental quantity is the dipole derivative at the equilibrium internuclear separation. A comparison between calculated and experimental values reported by Norris and Klemperer[7] showed reasonable agreement with respect to sign and order of magnitude.

Another possibility for comparison is the effective electric moment of the transition. The matrix element of the dipole moment between the two $^1\Sigma^+$ states,

$$R^{10} = e\int \Psi_1 \tau \Psi_0 d\tau,$$

can be easily computed theoretically and compared with the experimental integrated absorption coefficient

TABLE VII. Overlap populations.

(a) Overlap population distribution among the MO's

		2.0	2.6	3.0	3.5	4.0	5.0	6.0	7.0	8.0
$n(i)$:	1σ	0.0160	0.0035	0.0014	0.0006	0.0003	0.0001	0.0000	0.0000	0.0000
	2σ	0.4692	0.6509	0.7025	0.7135	0.6904	0.5980	0.4808	0.3612	0.2537
	3σ	−0.0683	−0.0228	−0.0080	0.0027	0.0094	0.0172	0.0218	0.0214	0.0174
	4σ	−5.2862	−4.9522	−4.4960	−3.7748	−3.0497	−1.9036	−1.1770	−0.7256	−0.4413
$n(i;$ CI):	1σ	0.0160	0.0035	0.0014	0.0006	0.0003	0.0001	0.0000	0.0000	0.0000
	2σ	0.2134	0.2938	0.3149	0.3167	0.3039	0.2662	0.2318	0.1857	0.1254
	3σ	−0.0349	−0.0117	−0.0041	0.0014	0.0048	0.0085	0.0094	0.0074	0.0048
	4σ	−0.1764	−0.1797	−0.1755	−0.1645	−0.1501	−0.1201	−0.1024	−0.1030	−0.1006

(b) Overlap population distribution among the configurations, ϕ_r

	2.0	2.6	3.0	3.5	4.0	5.0	6.0	7.0	8.0
$n(\phi_1)$	0.0021	0.0038	0.0054	0.0083	0.0134	0.0342	0.0692	0.0800	0.0549
$n(\phi_2)$	−0.1723	−0.1737	−0.1674	−0.1532	−0.1338	−0.0861	−0.0355	−0.0060	−0.0001
$n(\phi_3)$	−0.0015	−0.0006	−0.0002	0.0001	0.0005	0.0011	0.0017	0.0017	0.0014
$n(\phi_4)$	−0.0046	−0.0054	−0.0065	−0.0085	−0.0118	−0.0247	−0.0496	−0.0690	−0.0637
$n(\phi_5)$	0.1950	0.2828	0.3069	0.3096	0.2938	0.2360	0.1628	0.0973	0.0527
$n(\phi_6)$	−0.0006	−0.0010	−0.0015	−0.0022	−0.0032	−0.0058	−0.0098	−0.0139	−0.0156

[7] W. G. Norris and W. Klemperer, J. Chem. Phys. 28, 749 (1958).

TABLE VIII. Dipole moment integrals.

	2.0	2.6	3.0	3.5	4.0	5.0	6.0	7.0	8.0
$\int s(r\cos\theta)\,hd\tau$	0.10850	0.07649	0.05770	0.03913	0.02578	0.01056	0.00414	0.00158	0.00060
$\int S(r\cos\theta)\,hd\tau$	−0.89954	−1.06522	−1.13357	−1.17301	−1.16725	−1.05608	−0.87281	−0.67401	−0.49408
$\int h(r\cos\theta)\,hd\tau$	1.99973	2.60049	3.00044	3.49908	3.99695	4.99972	6.01831	6.99503	7.98666
$\int s(r\cos\theta)\,p_\sigma d\tau$	0.10243	0.10243	0.10243	0.10243	0.10243	0.10243	0.10243	0.10243	0.10243
$\int S(r\cos\theta)\,p_\sigma d\tau$	−2.37356	−2.37356	−2.37356	−2.37356	−2.37356	−2.37356	−2.37356	−2.37356	−2.37356
$\int h(r\cos\theta)\,p_\sigma d\tau$	1.29225	1.51157	1.63721	1.75962	1.83795	1.86279	1.74339	1.53258	1.28344

TABLE IX. Computed dipole moments (in debye units).

	Determinantal AO configurations			Determinantal MO configurations		Apparent moment, $r_0 Q(H)$	
r_0	(2-term Ψ)	(3-term Ψ)	(6-term Ψ)	(1-term Ψ)	(6-term Ψ)	SD	CI
2.0	5.071	5.359	5.139	5.535	5.133	1.154	1.423
2.6	5.077	5.126	4.999	5.922	5.001	1.863	2.179
3.0	5.049	4.981	4.907	6.198	4.909	2.415	2.751
3.5	4.953	4.783	4.758	6.542	4.761	3.068	3.433
4.0	4.742	4.491	4.496	6.850	4.500	3.632	4.025
5.0	3.817	3.418	3.436	7.290	3.441	4.490	4.786
6.0	2.147	1.392	1.397	7.447	1.403	5.009	4.583
7.0	0.857	−0.357	−0.360	7.266	−0.354	5.093	3.778
8.0	0.252	−0.908	−0.911	6.608	−0.906	4.738	3.857

TABLE X. Computed electric moments and oscillator strengths.

	2.0	2.6	3.0	3.5	4.0	5.0	6.0	7.0	8.0	∞
R^{10}	2.370	2.825	3.065	3.363	3.754	4.865	6.103	6.505	6.355	6.030
f^{10}	0.072	0.100	0.112	0.121	0.132	0.165	0.211	0.237	0.245	0.254

by means of the relation

$$\int k_\nu d\nu = (8\pi^3\nu_{10}/3hcN_0)\,|\,R^{10}\,|^2, \qquad (1)$$

where N_0 is the number of atoms per cm³ in the ground state. Experimental results may also be given in terms of the oscillator strength,

$$f^{10} = (8\pi^2 mc\nu_{10}/3he^2)\,|\,R^{10}\,|^2, \qquad (2)$$

where m and e are the mass and charge of the electron, respectively.

Table X gives values for the effective electric moment of the transition R^{10} (in units of 10^{-18} esu-cm) and for the oscillator strength f^{10} at each internuclear distance. There are several reasons why the intensity of this transition is expected to be relatively strong with f values between 0.1 and 1. In the first place, high-intensity transitions are usually associated with parallel transitions ($\Delta\Lambda=0$). The example here is closely related to a class of transitions that Mulliken has termed charge-transfer spectra.[8] Characterizing this type of transition is electron promotion from bonding to nonbonding or antibonding orbitals. In other words, some aspects of charge resonance appear in the transition, as can be seen from the change in sign of the dipole moment or, more qualitatively, from the change in the gross atomic populations.

The variation of the electric moment with internuclear distance over the range involved is assumed small in the quantum-mechanical formulation of the Franck-Condon principle.[9] Earlier work on H_2[10] showed the theory to be in disagreement with experiment and indicated that the r variation of the electric moment could not be disregarded. A large change of the moment with r, but in the opposite direction, occurs here also, although not so pronounced in the important region between 2.6 and 4.0 au.

Unfortunately, experimental values for the transition probabilities do not appear to be in the literature. It would be interesting to compare such results with the computed values of Table X in the event that dipole moments for the ground and excited states are not forth-

[8] R. S. Mulliken, J. Chem. Phys. 7, 20 (1939).

[9] G. H. Herzberg, *Spectra of Diatomic Molecules* (D. Van Nostrand Company, Inc., Princeton, New Jersey, 1950), p. 199.

[10] H. M. James and A. S. Coolidge, Phys. Rev. 55, 184 (1939).

coming in the near future. A reasonable check with respect to these off-diagonal elements of the dipole moment would give more confidence in the computed diagonal elements.

ACKNOWLEDGMENT

The author would like to acknowledge the assistance of Miss Harriet Terry in carrying out the numerical calculations reported in this paper.

THE JOURNAL OF CHEMICAL PHYSICS VOLUME 32, NUMBER 3 MARCH, 1960

Rotational Relaxation of Rough Spheres*

B. WIDOM

Department of Chemistry, Cornell University, Ithaca, New York

(Received October 1, 1959)

A theory of rotational relaxation of spherical top molecules in an inert gas is given, under the assumption that the molecules and atoms collide as rough spheres. Some general aspects of relaxation theory are first discussed and a theorem is presented which, under some circumstances, allows the problem to be greatly simplified. The rotational relaxation problem is then solved both for two- and three-dimensional systems. If I is the moment of inertia of the rotating molecule, m the reduced mass of the atom-molecule system, and a the sum of the atomic and molecular radii, and if $b=I/ma^2$, then the most important result of the three-dimensional theory is that $Z_{\text{eff}}=\frac{3}{8}(1+b)^2/b$, where Z_{eff} is the number of collisions suffered by each molecule in a time equal to the relaxation time. This is the analog of a result previously derived by Wang Chang and Uhlenbeck for self-relaxation in the pure molecular gas. Values of Z_{eff} are calculated for a variety of mixtures of spherical top molecules with inert gases.

1. INTRODUCTION

IN a dilute gas which is in thermal equilibrium at absolute temperature T, the distribution of the molecules among translational and internal states is uniquely determined by T and by the dynamical properties of the separated particles, quite independently of the details of the occasional intermolecular collisions which occur. But when the gas is not at thermal equilibrium then under a very wide range of circumstances it is precisely these rare intermolecular collisions which are primarily responsible for the ultimate establishment of the equilibrium distribution, and the time required for equilibrium to be approached depends on the details of the molecular interactions.

This picture is simplest when it is imagined that most of the gas consists of identical point particles (which will be called atoms) with no variable internal states, and that these particles have always an equilibrium velocity distribution characteristic of a single fixed temperature T; and that dilutely dispersed in this gas is another set of identical particles (which will be called molecules) that do have internal states that can be changed by collision, but which have stationary centers of mass. By having many more atoms than molecules, one may neglect molecule-molecule interactions and consider only atom-molecule collisions; and by having even the gas of atoms dilute, one may neglect triple and higher order collisions.

The particular case which will be treated here is that in which the molecules are rigid rotors, and what is sought is a detailed description of the time evolution of the distribution of molecules among rotational states, given an arbitrary initial distribution. The problem will be treated entirely classically, and solved first for a two-dimensional system, and then for a three-dimensional one.

In the two-dimensional problem the molecules are taken to be circles lying in the plane of the gas, the center of mass of each circle coinciding with its geometric center, but no other assumption being made about the distribution of mass within the circle. In the three-dimensional problem the molecules are taken to be spheres, the center of mass of each sphere coinciding with its geometric center, and the distribution of mass within the sphere such that the molecule is a spherical top (three equal principal moments of inertia). These two sets of requirements are strictly analogous, in that in both cases an axis about which the molecule can rotate is of necessity a principal axis passing through the mass and geometric center, and the moment of inertia about such an axis has only one possible value, I.

It is further specified that the spheres or circles are rough, and that their collisions with the atoms are impulsive; this is essentially the Bryan-Pidduck

* This research was supported by the U. S. Air Force through the Air Force Office of Scientific Research of the Air Research and Development Command under contract No. AF 18(603)-111.

model.[1] The condition of roughness is that the vector velocity difference between the atom and that point of the circle or sphere at which impact occurs, changes its sign upon collision, and this condition, when combined with the laws of impulsive motion,[2] completely determines the collision dynamics.

The reason for specifying a circular or spherical periphery for the molecule is that then every collision with an atom consists of only one impact, i.e., the phenomenon of impact multiplicity[3] (called "chattering" by Dahler[4]), which ordinarily introduces enormous complications, does not then occur. The additional restrictions on the nature of the rotating molecules are made to insure that their angular velocities and angular momenta are always parallel, with a single fixed constant of proportionality (the moment of inertia I), this being an obviously desirable simplification. The apparent restrictions that the atoms have no size and that the molecular centers of mass be stationary, are not really restrictions at all; for the more general case, one has merely to replace the atomic mass, to be called m, by the reduced mass of the atom-molecule system; and to replace the molecular radius, to be called a, by the sum of the atomic and molecular radii. Then the requirement that the atomic velocity distribution be always Maxwellian with a fixed T becomes a specification of the distribution of *relative* velocities of the atomic and molecular mass centers; and the requirement that the atoms be structureless point particles becomes the restriction that they shall be incapable of undergoing any change in state other than translational. The latter requirement is obviously fulfilled by inert gas atoms at temperatures where electronic excitation is rare.

In Sec. 2 the general theory of the relaxation problem is outlined, mostly in a language which is independent of the nature and number of the internal molecular states. It is shown how the time evolution of the distribution function is determined by the transition probability per unit time. The latter is a symmetrizable kernel the eigenvalues of which lead to the relaxation times of the process, and one of these is identified as *the* relaxation time τ. The usual convention is followed of introducing the related quantity $Z_{\text{eff}}=Z\tau$, where Z is the total number of collisions per unit time suffered by each molecule. Finally, a general theorem is stated which, under some circumstances, allows the eigenvalue problem, for the case in which the molecule has more than one degree of freedom, to be reduced to a much simpler problem, and it is pointed out that the theorem applies, in particular, to the three-dimensional rotor case.

In Sec. 3 the dynamics of the two-dimensional case are discussed, the transition probability is found, and the eigenvalue problem is solved. If I is the molecular moment of inertia, a the molecular radius, and m the atomic mass, and if one defines the parameter $b=I/ma^2$, then it is found that for this two-dimensional case,

$$Z_{\text{eff}}=\begin{cases}\frac{1}{2}(1+b), & \text{if } b>1\\ \frac{1}{4}(1+b)^2/b, & \text{if } b<1.\end{cases} \tag{1.1}$$

In Sec. 4, the dynamics of the three-dimensional case are discussed, the transition probability is found, and the eigenvalue problem is solved. It is found that

$$Z_{\text{eff}}=\tfrac{3}{8}(1+b)^2/b. \tag{1.2}$$

In both cases, then, Z_{eff} is independent of temperature and depends only on the ratio of I to ma^2, becoming large (collisions inefficient) when I is either much greater than or much less than ma^2, and having its minimum value (collisions most efficient) when I and ma^2 are exactly equal.

In Sec. 5, the theory is applied to concrete examples and values of Z_{eff} for rotational relaxation are predicted for mixtures of various spherical top molecules with inert gases.

2. OUTLINE OF THE THEORY

The general theory of the relaxation problem will be briefly outlined in this section. The conditions described in Sec. 1 will be assumed, except that the nature and number of the internal molecular states (the degrees of freedom which are approaching equilibrium) are at first left unspecified, and the atom-molecule interaction may be of any form just so long as it leads to the existence of a finite collision number Z.

By an internal state of the molecule will be meant any set of constant values of independent action variables, equal in number to the number of internal degrees of freedom. These are then the constant values that these dynamical variables have when the molecule executes its natural motions unperturbed by collision. When the molecule undergoes collision with an atom its state is in general changed, that is, its action variables take on a new set of values, these again remaining constant until the next collision.

When the molecule is the plane rotor described in Sec. 1 its state is uniquely determined by a single action variable, which may conveniently be taken to be the angular momentum L perpendicular to the plane of rotation, and having the range of values

$$-\infty<L<\infty, \tag{2.1}$$

positive and negative values corresponding to rotation in opposite directions. For the three-dimensional rotor

[1] S. Chapman and T. G. Cowling, *The Mathematical Theory of Non-Uniform Gases* (Cambridge University Press, Cambridge, England, 1939), pp. 199–205.
[2] E. T. Whittaker, *Analytical Dynamics* (Dover Publications, New York, 1944), fourth edition, pp. 50–51.
[3] B. Widom, J. Chem. Phys. **28**, 918 (1958).
[4] J. S. Dahler, J. Chem. Phys. **30**, 1447 (1959).

described in Sec. 1 three independent action variables are required to specify the state, and these may conveniently be chosen to be the magnitude of the angular momentum, the component of the angular momentum along an arbitrarily chosen axis fixed in space, and the component of the angular momentum along an arbitrarily chosen axis fixed in the body, denoted, respectively, by J, M, K, and having the range of values,

$$0 \leq J < \infty$$
$$-J \leq M \leq J$$
$$-J \leq K \leq J. \tag{2.2}$$

In the general case, the variables specifying the state of the molecule will be represented by the single symbol x (or y), and then dx (or dy) will be an element of volume in the space of states. An integral such as $\int \cdots dx$ written without indicated limits will imply integration over the entire space.

Let $k(x, y)dy$ be the probability per unit time that a molecule initially in state x will make a transition to states in the range y, $y+dy$; let $c(x, t)dx$ be the fraction of all the molecules which at time t have states in the range x, $x+dx$; let $f(x)dx$ be the fraction of all the molecules that would be found with states in the range x, $x+dx$ if the molecular system were in thermal equilibrium at the temperature of the atomic gas; and let Z be the total number of collisions per unit time suffered by each molecule. Then,

$$\int k(x, y)dy = Z \tag{2.3}$$

$$f(x)k(x, y) = f(y)k(y, x) \tag{2.4}$$

$$\partial c(x, t)/\partial t = \int k(y, x)c(y, t)dy - Zc(x, t). \tag{2.5}$$

Equation (2.3) is the condition that the transition probability be complete and Eq. (2.4) is the condition that it satisfy detailed balance. The object of the relaxation theory is the solution of Eq. (2.5) with an arbitrarily prescribed $c(x, 0)$.

If $S(x, y)$ is defined to be the kernel

$$S(x, y) = S(y, x) = [f(x)/f(y)]^{\frac{1}{2}}k(x, y), \tag{2.6}$$

the symmetry of which is a consequence of Eq. (2.4); and if $\phi_i(x)$ and $\lambda_i (i=0, 1, 2, \cdots)$ are its eigenfunctions and eigenvalues, so that

$$\int S(x, y)\phi_i(y)dy = \lambda_i \phi_i(x); \tag{2.7}$$

then the solution of Eq. (2.5) is

$$c(x, t) = [f(x)]^{\frac{1}{2}} \sum_{i=0}^{\infty} h_i \phi_i(x) \exp[-(Z-\lambda_i)t], \tag{2.8}$$

where

$$h_i = \int [f(x)]^{-\frac{1}{2}} c(x, 0)\phi_i(x)dx \Big/ \int \phi_i^2(x)dx.$$

Thus, the problem of finding $c(x, t)$ when $c(x, 0)$ is prescribed, is equivalent to the problem of finding the eigenfunctions and eigenvalues of the symmetrized kernel $S(x, y)$.

The eigenvalues may be numbered in such a way that

$$-\infty < \lambda_\infty < \cdots < \lambda_2 < \lambda_1 < \lambda_0 = Z, \tag{2.9}$$

where by λ_∞ is meant

$$\lambda_\infty = \lim_{N \to \infty} \lambda_N.$$

This limit must be finite, not $-\infty$, corresponding to the fact that in Eq. (2.8) every mode of decay to equilibrium is limited by a finite collision number Z and cannot, therefore, be infinitely fast. That no eigenvalue λ_i can exceed Z corresponds to the fact that in Eq. (2.8) no term may increase with time. That the upper limit Z is actually attained by one of the eigenvalues, λ_0, corresponds to the fact that one term in Eq. (2.8) must be independent of t, in order that

$$c(x, \infty) = f(x), \tag{2.10}$$

which is the equilibrium distribution. From Eqs. (2.8) and (2.10) it is seen that, with no attempt at normalization,

$$\phi_0(x) = \text{const}[f(x)]^{\frac{1}{2}}, \tag{2.11}$$

so that the largest eigenvalue λ_0 and the corresponding eigenfunction $\phi_0(x)$ are known from general principles regardless of the details of $S(x, y)$. That $[f(x)]^{\frac{1}{2}}$ is an eigenfunction of $S(x, y)$, with eigenvalue Z, is equivalent to the completeness condition of Eq. (2.3).

The transition probability $k(x, y)$ is proportional to Z, and therefore, so is $S(x, y)$ and therefore, so is each eigenvalue λ_i.

The relaxation times are $(Z-\lambda_i)^{-1} (i=1, 2, 3, \cdots)$. The largest of these determines the approach of $c(x, t)$ to $f(x)$ when the system is close to equilibrium, and is therefore identified as *the* relaxation time, τ. Thus,

$$\tau = (Z-\lambda_1)^{-1} \tag{2.12}$$

and since each λ_i is proportional to Z, the relaxation time is inversely porportional to Z. The usual conven-

tion will be followed of introducing Z_{eff},

$$Z_{eff}=Z\tau, \tag{2.13}$$

so that

$$Z_{eff}=(1-\lambda_1/Z)^{-1}. \tag{2.14}$$

Z_{eff} is the number of collisions suffered by each molecule in a time equal to the relaxation time, or, much less precisely, it is the number of collisions required to establish equilibrium. Since each λ_i is proportional to Z, it follows that Z_{eff} is independent of Z. The concentration of the atom gas enters the problem only through Z, so Z_{eff} is independent of this concentration, unlike τ, which is inversely proportional to it.

Under some circumstances, it is meaningful to describe the state of the system with a number of action variables which is less than the number of internal degrees of freedom of the molecule, and it is possible to have the preceding theory hold even with this contracted set of variables. The result is a less detailed description of the approach to equilibrium than would be obtained with a complete set of action variables, but characterized nevertheless by exactly the same set of relaxation times as in the more complete description.

This possibility arises when the variables previously symbolized by x (and, correspondingly, by y) may actually be separated into two groups, say x_1, x_2 (and, correspondingly, y_1, y_2), such that when the transition probability $k(x_1, x_2; y_1, y_2)$ is integrated over the full range of y_2 (a range which may very well depend on y_1) it leads to a function of x_1 and y_1 alone, independently of x_2. If this is the case, and if the resulting function of x_1, y_1 is called the contracted transition probability $k(x_1, y_1)$, then this hypothesis takes the form,

$$k(x_1, y_1)=\int k(x_1, x_2; y_1, y_2)dy_2. \tag{2.15}$$

Contracted distributions $c(x_1, t)$ and $f(x_1)$ may be defined in terms of the original uncontracted functions $c(x_1, x_2; t)$ and $f(x_1, x_2)$ by

$$c(x_1, t)=\int c(x_1, x_2; t)dx_2$$

$$f(x_1)=\int f(x_1, x_2)dx_2. \tag{2.16}$$

Furthermore, since the original uncontracted kernel $k(x_1, x_2; y_1, y_2)$ and uncontracted equilibrium distribution $f(x_1, x_2)$ satisfy detailed balance in the form of Eq. (2.4), it follows by integration over x_2 and y_2 that the contracted functions satisfy the identical condition; and therefore, also that the contracted kernel $S(x_1, y_1)$ defined by

$$S(x_1, y_1)=[f(x_1)/f(y_1)]^{\frac{1}{2}}k(x_1, y_1) \tag{2.17}$$

is symmetric. Finally, the eigenfunction $\phi_i(x_1, x_2)$ may also be contracted by the definition

$$\phi_i(x_1)=[f(x_1)]^{-\frac{1}{2}}\int[f(x_1, x_2)]^{\frac{1}{2}}\phi_i(x_1, x_2)dx_2 \tag{2.18}$$

and from Eqs. (2.6), (2.7), (2.15), and (2.17), it follows that this contracted ϕ_i is an eigenfunction of the contracted S, with the same eigenvalue λ_i that belongs to the uncontracted ϕ_i and S. Indeed, *the contracted quantities defined by Eqs.* (2.15)–(2.18) *satisfy all the relations of Eqs.* (2.3)–(2.14), *inclusive, that are satisfied by the uncontracted quantities, and do so with the same set of eigenvalues* λ_i.

The importance of this observation for the purposes of the present work lies in the fact that in the three-dimensional case treated in Sec. 4 the transition probability $k(J, M, K; J', M', K')$ satisfies the hypothesis of Eq. (2.15) with respect to integration over K' and M'; and therefore, by the above theorem, for purposes of finding τ and Z_{eff} it is sufficient to find and study the contracted transition probability

$$k(J, J')=\int_{-J'}^{J'}\int_{-J'}^{J'}k(J, M, K; J', M', K')dK'dM'. \tag{2.19}$$

That the right-hand side of Eq. (2.19) is independent of M and K, which is the crucial point, is a consequence of the following two obvious properties of the previously described model: (i) The internal component of angular momentum K is of no relevance in determining either the M' or the J' that result from any collision with initially prescribed M and J. (ii) Since the incidence of impinging atoms is completely isotropic, the probability per unit time of producing J' in some prescribed range depends only on the initial J but not on the initial M. Note that the content of these two statements is quite different; the first says that for producing a given M' and a given J', the initial K is irrelevant *in each collision*, whereas the second says that for producing a given J' the initial M is irrelevant *on the average*.

3. TWO-DIMENSIONAL MODEL

As explained in Sec. 2, the state of the rotating molecule may be defined by the value of the angular momentum L perpendicular to the plane of rotation, the range of L being

$$-\infty<L<\infty. \tag{3.1}$$

The equilibrium distribution function is then

$$f(L)=(2\pi IkT)^{-\frac{1}{2}}\exp(-L^2/2IkT), \quad (3.2)$$

where I is the moment of inertia of the molecule about its only axis of rotation, k is Boltzmann's constant, and T is the constant absolute temperature of the gas of atoms.

Let p_r be the radial component of the momentum of the atom at the instant of impact with the periphery of a rotating circle (molecule); it does not matter whether the inward or outward direction is chosen for $p_r>0$. Let p_t be the tangential component of the momentum of the atom at the instant of impact, and take it to be positive when it corresponds to the same (arbitrarily chosen) direction of rotation that is associated with positive values of L. Let a be the molecular radius and m the atomic mass. Then the condition of roughness, as defined in Sec. 1, when combined with the laws of impulsive motion, is equivalent to the following three conditions which, in turn, completely determine the collision dynamics:

$$p_r'=-p_r$$

$$L'+ap_t'=L+ap_t$$

$$L'^2/2I+(p_t'^2+p_r'^2)/2m=L^2/2I+(p_t^2+p_r^2)/2m. \quad (3.3)$$

Unprimed and primed quantities refer, respectively, to the instant before and the instant after impact. These three conditions specify that, (i) the radial component of the momentum of the atom is simply reflected upon impact, but its magnitude is left unchanged, (ii) the total angular momentum of the atom and of the rotating circle about the circle's axis of rotation is conserved in the collision, and (iii) the total kinetic energy of the atom and of the rotating circle is conserved in the collision.

The final state L' may be expressed in terms of the initial conditions by solving Eqs. (3.3):

$$(I+ma^2)L'=(I-ma^2)L+2Iap_t. \quad (3.4)$$

This is the same result as in the head-on collision of two particles, where ap_t and ma^2 are the momentum and mass of one particle, while L and I are the momentum and mass of the second. Equality of masses in the related problem is then analogous in the present problem to the condition $I=ma^2$. It will be seen later that this special case has certain unique features, which might then explain the peculiar relaxation behavior previously found for a string oscillator undergoing collisions with particles of mass identical to its own.[3]

To find the transition kernel it will be convenient to express Eq. (3.4) in another way. Let $q(L, L'; p_t)dL'$ be the probability that a molecule in state L will make a transition to states in the range L', $L'+dL'$ when it suffers a collision in which the tangential component of the momentum of the colliding atom at the instant of impact is initially p_t. Then, according to Eq. (3.4),

$$q(L, L'; p_t)=\delta\{L'-[(I-ma^2)/(I+ma^2)]L$$
$$-[2I/(I+ma^2)]ap_t\}. \quad (3.5)$$

The transition kernel is then found directly as

$$k(L, L')=\int_{-\infty}^{\infty}q(L, L'; p_t)z(p_t)dp_t, \quad (3.6)$$

where $z(p_t)dp_t$ is the number of collisions per unit time suffered by each molecule, in which p_t lies in the range p_t, p_t+dp_t. From kinetic theory,

$$z(p_t)=Z(2\pi mkT)^{-\frac{1}{2}}\exp(-p_t^2/2mkT), \quad (3.7)$$

where Z is the total number of collisions per unit time suffered by each molecule. An explicit formula for $k(L, L')$ follows easily from Eqs. (3.5)–(3.7). Furthermore, with the equilibrium distribution function given in Eq. (3.2), the symmetrized kernel $S(L, L')$ may then be readily constructed as shown in Eq. (2.6). It is to be recalled that solving the relaxation problem amounts to finding the eigenfunctions and eigenvalues of S.

The expression for $S(L, L')$ is somewhat cumbersome, but may be considerably simplified by the following change of notation. Let

$$b=I/ma^2 \quad (3.8)$$

and define new variables ξ and η to replace L and L':

$$2(2IkT)^{\frac{1}{2}}\xi=(b+b^{-1})^{\frac{1}{2}}L$$

$$2(2IkT)^{\frac{1}{2}}\eta=(b+b^{-1})^{\frac{1}{2}}L'. \quad (3.9)$$

Finally, replace $S(L, L')$ by the symmetric kernel $\sigma(\xi, \eta)$:

$$(b^{\frac{1}{2}}+b^{-\frac{1}{2}})Z\sigma(\xi, \eta)=(8\pi IkT)^{\frac{1}{2}}S(L, L'). \quad (3.10)$$

Then, if $S(L, L')$ is derived in the manner outlined above, the related kernel σ is found to be

$$\sigma(\xi, \eta)=\exp\{-(\xi^2+\eta^2)+2[(b^2-1)/(b^2+1)]\xi\eta\}. \quad (3.11)$$

Furthermore, if $\chi_i(\xi)$ and σ_i are the eigenfunctions and eigenvalues of $\sigma(\xi, \eta)$ with ξ, η in the range $-\infty$ to ∞, then these are related to the eigenfunctions $\phi_i(L)$ and

eigenvalues λ_i of $S(L, L')$ by

$$\phi_i(L)=\chi_i(\xi)$$

$$\lambda_i=[(1+b)/(1+b^2)^{\frac{1}{2}}\pi^{\frac{1}{2}}]Z\sigma_i. \quad (3.12)$$

It is shown in Appendix I that the eigenfunctions and eigenvalues of $\sigma(\xi, \eta)$, for the range $-\infty<\xi, \eta<\infty$, are

$$\chi_n(\xi)=\psi_n\{[8/(b+b^{-1})]^{\frac{1}{2}}\xi\}$$

$$\sigma_n=\pi^{\frac{1}{2}}[(1+b^2)^{\frac{1}{2}}/(1+b)][(b-1)/(b+1)]^n \quad (3.13)$$

with $n=0, 1, 2, \cdots$. Here, $\psi_n(x)$ is the parabolic cylinder function defined by

$$\psi_n(x)=\exp(x^2/4)(-d/dx)^n\exp(-x^2/2), \quad (3.14)$$

with no attempt made at normalization.

From Eqs. (3.12) and (3.13),

$$\lambda_n=[(b-1)/(b+1)]^nZ \quad (n=0, 1, 2, \cdots), \quad (3.15)$$

but these are not necessarily ordered in accordance with Eq. (2.9). It is seen that the largest eigenvalue is indeed Z, as required by Eq. (2.9), and the corresponding eigenfunction $\phi_0(L)$ is indeed a constant multiple of $[f(L)]^{\frac{1}{2}}$, as required by Eq. (2.11). The lower limit of the eigenvalues is finite and each eigenvalue is proportional to Z, these properties, too, being in accord with the general theory.

The next to the largest eigenvalue, called λ_1 in Sec. 2, corresponds to $n=1$ when $b>1$ but to $n=2$ when $b<1$. Then, from Eqs. (2.14) and (3.15),

$$Z_{eff}=\begin{cases}\frac{1}{2}(1+b) & \text{if } b>1\\ \frac{1}{4}(1+b)^2/b & \text{if } b<1.\end{cases} \quad (3.16)$$

Thus, Z_{eff} is independent of temperature and depends only on the ratio of I to ma^2; it takes its minimum value (unity, in this case) when I and ma^2 are exactly equal, and it is large when I is either much greater than or much less than ma^2. These properties of Z_{eff} will again be found in the three-dimensional model.

It is seen from Eq. (3.15) that in the special case $b=1$ the eigenvalues are infinitely degenerate. On recalling the previously noted analogy between this problem and that of the head-on collision of hard spheres, this infinite degeneracy is seen to be the probable explanation for the lack of a true relaxation time in the model of a string oscillator suffering impulsive collisions with particles of mass identical to its own. This is not certain, however, because the analogy between the two problems fails in two respects. First, the phenomenon of impact multiplicity appears in the earlier problem but not in the present one, and secondly, in the analog of Eq. (3.7) in the string-oscillator problem, an additional factor of $|p_i|$ appears on the right-hand side.

4. THREE-DIMENSIONAL MODEL

As explained in Sec. 2, the state of the rotating molecule may be defined by the three quantities $J=|\mathbf{J}|$, $M=\mathbf{J}\cdot\mathbf{u}$, $K=\mathbf{J}\cdot\mathbf{v}$, where $\mathbf{J}$ is the angular momentum of the rotating molecule, $\mathbf{u}$ is an arbitrary unit vector fixed in space, and $\mathbf{v}$ is an arbitrary unit vector fixed in the molecule. The range of the variables is

$$0\leq J<\infty$$

$$-J\leq M\leq J$$

$$-J\leq K\leq J. \quad (4.1)$$

The equilibrium distribution function is then

$$f(J, M, K)=\pi(2\pi IkT)^{-\frac{1}{2}}\exp(-J^2/2IkT), \quad (4.2)$$

independently of M and K. Here, I is the common value of the moment of inertia of the molecule about any axis through its center.

It was seen in Sec. 2 that for purposes of finding τ and Z_{eff}, it is sufficient to study the relaxation of the single dynamical variable J, and to work with the correspondingly contracted kernels and distribution functions. From Eqs. (2.16), (4.1), and (4.2), the contracted equilibrium distribution function is

$$f(J)=4\pi(2\pi IkT)^{-\frac{1}{2}}J^2\exp(-J^2/2IkT). \quad (4.3)$$

Let $\mathbf{p}$ be the momentum of the colliding atom, let $p=|\mathbf{p}|$, and let $\mathbf{r}$ be the vector from the center of the molecule to that point of its surface at which impact occurs. Let a again be the molecular radius (so that $|\mathbf{r}|=a$) and m the atomic mass. Then, the condition of roughness, as defined in Sec. 1, when combined with the laws of impulsive motion, completely determines the collision dynamics. In particular, it is found that

$$\mathbf{p}'\cdot\mathbf{r}=-\mathbf{p}\cdot\mathbf{r}$$

$$\mathbf{J}'+\mathbf{r}\times\mathbf{p}'=\mathbf{J}+\mathbf{r}\times\mathbf{p}$$

$$J'^2/2I+p'^2/2m=J^2/2I+p^2/2m. \quad (4.4)$$

As before, unprimed and primed quantities refer, respectively, to the instant before and the instant after impact. These three conditions are completely analogous to those for the two-dimensional problem in Eqs. (3.3): (i) Reflection of the radial component of $\mathbf{p}$, (ii) conservation of total angular momentum, and (iii)

conservation of total kinetic energy. These relations amount to five scalar conditions, and they are therefore not in themselves sufficient to determine the collision dynamics, since the problem involves six degrees of freedom. This differs from the two-dimensional case, where the three scalar conditions of Eqs. (3.3) were just enough to determine the dynamics since only three degrees of freedom were involved. Since the dynamics are, however, determined even in the present case, the condition of roughness and the laws of motion together must imply a sixth scalar conservation law in addition to those of Eqs. (4.4). In any event, the dynamics can be completely worked out, and the final angular momentum $\mathbf{J}'$ may be readily expressed in terms of the initial conditions[1]:

$$(I+ma^2)\mathbf{J}'=(I-ma^2)\mathbf{J}+2m\mathbf{r}\cdot\mathbf{J}\mathbf{r}+2I\mathbf{r}\times\mathbf{p}. \quad (4.5)$$

The relaxation problem will be worked out here only in its contracted form. The uncontracted transition kernel $k(J, M, K; J', M', K')$ is quoted for reference in Appendix II, but its derivation, being somewhat involved, is not reproduced. The contracted kernel will be found directly from the collision dynamics, rather than by integration of the uncontracted transition probability.

To find the contracted transition kernel $k(J, J')$ it will be convenient to express the relevant aspects of Eq. (4.5) in another way. Let $q(J, J'; \mathbf{r}, \mathbf{p})dJ'$ be the probability that a molecule in state J will make a transition to states in the range J', $J'+dJ'$ when it suffers a collision of prescribed $\mathbf{r}$ and $\mathbf{p}$. Then, according to Eq. (4.5),

$$q(J, J'; \mathbf{r}, \mathbf{p})=\delta\{J'-[1/(I+ma^2)][(I-ma^2)^2J^2 +4mI(\mathbf{r}\cdot\mathbf{J})^2+4I^2\,|\,\mathbf{r}\times\mathbf{p}\,|^2+4I(I-ma^2)\mathbf{J}\cdot\mathbf{r}\times\mathbf{p}]^{\frac{1}{2}}\}. \quad (4.6)$$

If now $z(\mathbf{r}, \mathbf{p})d\sigma d\tau$ is the number of collisions per unit time suffered by each molecule, in which $\mathbf{r}$ lies in the element of area $d\sigma$ on a sphere of radius a and $\mathbf{p}$ lies in the element of volume $d\tau$ in momentum space, then the transition kernel is found directly as

$$k(J, J')=\iint_{-\mathbf{p}\cdot\mathbf{r}>0} q(J, J'; \mathbf{r}, \mathbf{p})z(\mathbf{r}, \mathbf{p})d\sigma d\tau, \quad (4.7)$$

where the obviously necessary requirement[1] $-\mathbf{p}\cdot\mathbf{r}>0$ confines $\mathbf{r}$ to a hemisphere for any fixed $\mathbf{p}$ or confines $\mathbf{p}$ to a half-space for any fixed $\mathbf{r}$. From kinetic theory,

$$z(\mathbf{r}, \mathbf{p})=[Z/2a(2\pi amkT)^2](-\mathbf{p}\cdot\mathbf{r})\exp(-p^2/2mkT), \quad (4.8)$$

where Z is again the total number of collisions per unit time suffered by each molecule. Equations (4.6)–(4.8) determine $k(J, J')$, and it is worked out in detail in Appendix III. Furthermore, with the contracted equilibrium distribution function given in Eq. (4.3), the contracted symmetric kernel $S(J, J')$ may then be readily constructed as shown in Eq. (2.17). It is again to be recalled that solving the relaxation problem amounts to finding the eigenfunctions and eingenvalues of S.

The expression for $S(J, J')$ may be considerably simplified by changes of notation completely analogous to those in Eqs. (3.8)–(3.10). Again let

$$b=I/ma^2 \quad (4.9)$$

and define new variables ξ and η to replace J and J':

$$2(2IkT)^{\frac{1}{2}}\xi=(b+b^{-1})^{\frac{1}{2}}J$$
$$2(2IkT)^{\frac{1}{2}}\eta=(b+b^{-1})^{\frac{1}{2}}J'. \quad (4.10)$$

Finally, replace $S(J, J')$ by the symmetric kernel $\sigma(\xi, \eta)$:

$$(b^{\frac{1}{2}}+b^{-\frac{1}{2}})^2Z\sigma(\xi, \eta)=(2IkT)^{\frac{1}{2}}(b+b^{-1})^{\frac{1}{2}}S(J, J'). \quad (4.11)$$

Then, with $S(J, J')$ found in the manner outlined above, using the result of Appendix III, the resulting expression for the kernel σ is

$$\sigma(\xi, \eta)=\exp[-(\xi^2+\eta^2)]\int_0^{\min(\xi,\,\eta)}\exp(2l^2) \times I_0\{2[(b^2-1)/(b^2+1)](\xi^2-l^2)^{\frac{1}{2}}(\eta^2-l^2)^{\frac{1}{2}}\}dl, \quad (4.12)$$

where standard notation has been used for the Bessel function of imaginary argument,[5] and where "min (ξ, η)" means the smaller of the two numbers ξ and η. Furthermore, if $\chi_i(\xi)$ and σ_i are the eigenfunctions and eigenvalues of $\sigma(\xi, \eta)$ with ξ, η in the range 0 to ∞, then these are related to the eigenfunctions $\phi_i(J)$ and eigenvalues λ_i of $S(J, J')$ by

$$\phi_i(J)=\chi_i(\xi)$$
$$\lambda_i=2[(1+b)^2/(1+b^2)]Z\sigma_i. \quad (4.13)$$

It is shown in Appendix IV that the eigenfunctions and eigenvalues of $\sigma(\xi, \eta)$, for the range $0\leq\xi, \eta<\infty$, are

$$\chi_n(\xi)=\psi_{2n+1}\{[8/(b+b^{-1})]^{\frac{1}{2}}\xi\}$$
$$\sigma_n=[(1+b^2)/4(1+b)^2]\int_0^1(1-x)^{-\frac{1}{2}}[1-4bx/(1+b)^2]^n dx \quad (4.14)$$

[5] G. N. Watson, *Theory of Bessel Functions* (Cambridge University Press, Cambridge, England, 1944), second edition, p. 77.

TABLE I. Atomic and molecular radii, in units of 10^{-8} cm.

He	1.5	GeH_4	2.5	CF_4	2.6
Ne	1.6	SiH_4	2.5	SF_6	3.1
A	1.9	CH_4	2.1	CCl_4	3.3
Kr	2.0	CD_4	2.1	$SiBr_4$	3.6
Xe	2.3	$C(CH_3)_4$	3.5		

with $n=0, 1, 2, \cdots$. The parabolic cylinder functions $\psi_n(x)$ are defined in Eq. (3.14).

From Eqs. (4.13) and (4.14),

$$\lambda_n=\tfrac{1}{2}Z\int_0^1(1-x)^{-\frac{1}{2}}\{1-[4b/(1+b)^2]x\}^n dx, \tag{4.15}$$

and these are already ordered in accordance with Eq. (2.9). The special condition $b=1$ does not here lead to degeneracy, as it did in the two-dimensional problem. The largest eigenvalue λ_0 is indeed Z, as required by Eq. (2.9), and the corresponding eigenfunction $\phi_0(J)$ is indeed a constant multiple of $[f(J)]^{\frac{1}{2}}$, as required by Eq. (2.11). The lower limit of the eigenvalues is finite (zero, in this case) and each eigenvalue is proportional to Z, these properties, too, being in accord with the general theory.

The next to the largest eigenvalue λ_1 is easily calculated from Eq. (4.15), and then it follows from Eq. (2.14) that

$$Z_{eff}=\tfrac{3}{8}(1+b)^2/b. \tag{4.16}$$

As in the two-dimensional case, Z_{eff} is independent of temperature and depends only on the ratio of I to ma^2. It takes its minimum value ($\frac{3}{2}$, in this case) when I and ma^2 are exactly equal.

5. APPLICATIONS

The result contained in Eq. (4.16) is here applied to calculate values of Z_{eff} for rotational relaxation in a variety of mixtures, each consisting of a gas of spherical top molecules dilutely dispersed in a rare gas. As noted in Sec. 1, the mass m which appears in the definition $b=I/ma^2$ is to be identified with the reduced mass of the atom-molecule system, while the radius a is to be identified with the sum of the atomic and molecular radii. The remaining parameter I is to be taken literally as the molecular moment of inertia.

The radius assumed here for each of the molecules and atoms in question is given in Table I. The values of Z_{eff} which then follow from Eq. (4.16) for each atom-molecule pair are given to the nearest integer in Table II. Since the smallest possible value of Z_{eff} is $\frac{3}{2}$, when rounded off to the nearest integer the smallest possible value is 2.

The theory predicts that Z_{eff} is independent of temperature, i.e., that the corresponding relaxation time is inversely proportional to $T^{\frac{1}{2}}$ at fixed density or proportional to $T^{\frac{1}{2}}$ at fixed pressure.

When Z_{eff} is greater than about 10, it can probably be found from measurements of acoustic dispersion or absorption.[6] A practical difficulty which could arise is that when rotational relaxation is slow, translational relaxation of the molecules might also be slow, and these two phenomena might be difficult to resolve. Also, the present theory would then lose some of its quantitative significance since it was based on the assumption of instantaneous translational equilibration. On the other hand, if translational relaxation does accompany the rotational relaxation, the difference between the low- and high-frequency specific heats would be greater than if rotational relaxation occurred alone, and this would at least make the combined relaxation more easily apparent.

It is easy to show that the next to the slowest mode of rotational relaxation would probably not be experimentally resolvable from the slowest. Let

$$Z_{eff}'=(1-\lambda_2/Z)^{-1}, \tag{5.1}$$

by analogy with Eq. (2.14), so that Z_{eff}' is Z times the relaxation time of the next to the slowest mode, in the same way that Z_{eff} is Z times the relaxation time of the slowest. The eigenvalue λ_2 can be calculated explicitly from Eq. (4.15), and the resulting Z_{eff}' is then found to be related to Z_{eff} itself by

$$Z_{eff}'=5Z_{eff}^2/(10Z_{eff}-6). \tag{5.2}$$

On the other hand, it was seen before that $Z_{eff}\geq\frac{3}{2}$, so it follows from Eq. (5.2) that

$$\tfrac{1}{2}Z_{eff}<Z_{eff}'\leq\tfrac{5}{6}Z_{eff}. \tag{5.3}$$

Thus, the next to the longest relaxation time always lies between $\frac{1}{2}$ and $\frac{5}{6}$ of the longest, and the two are therefore almost surely unresolvable.

TABLE II. Z_{eff} for rotational relaxation of spherical top molecules in an inert gas, to the nearest integer.[a]

	He	Ne	A	Kr	Xe
GeH_4	**5**	**18**	**33**	**52**	**73**
SiH_4	**5**	**15**	**23**	**32**	**40**
CH_4	**6**	**15**	**22**	**27**	**33**
CD_4	**3**	**9**	**13**	**17**	**21**
$C(CH_3)_4$	**2**	**2**	**3**	**5**	**6**
CF_4	**2**	**2**	**3**	**4**	**6**
SF_6	**2**	**2**	**2**	**4**	**5**
CCl_4	**2**	**2**	**2**	**3**	**4**
$SiBr_4$	**4**	**2**	**2**	**2**	**2**

[a] For the six entries in bold face type, $b>1$; for the remaining entries, $b<1$.

[6] For a recent experimental determination of rotational Z_{eff}, and some references to earlier work, see Bauer, Kneser, and Sittig, J. Chem. Phys. **30**, 1119 (1959).

TABLE III. Z_{rot} for rotational self-relaxation of spherical top molecules, to the nearest integer.

GeH_4	63	CD_4	12	SF_6	7
SiH_4	28	$C(CH_3)_4$	7	CCl_4	6
CH_4	18	CF_4	6	$SiBr_4$	5

Self-relaxation in the pure molecular gases is not covered by the present theory since the explicit assumption was made that one of the collision partners (the atom) is itself incapable of undergoing a change in rotational state. However, the rotational relaxation time in a pure rough-sphere gas has been found by Wang Chang and Uhlenbeck,[7] and in the present notation their result is

$$Z_{rot}=\tfrac{3}{8}(1+2b)^2/b,$$

which becomes identical to Eq. (4.16) for small b. In the definition $b=I/ma^2$, the reduced mass m is now half the molecular mass, and the effective radius a is now twice the molecular radius. Values of Z_{rot} for self-relaxation are quoted in Table III. The radii in Table I were again assumed. It is to be noted that now the smallest possible value of Z_{rot} is 3, and that it occurs when $b=\frac{1}{2}$. Also, in a pure molecular gas b cannot exceed $\frac{1}{2}$.

APPENDIX I

It will be shown here that the eigenfunctions and eigenvalues of the kernel $\sigma(\xi, \eta)$ in Eq. (3.11), are given by Eq. (3.13). The range of the variables is $-\infty<\xi, \eta<\infty$.

The parabolic cylinder functions defined by Eq. (3.14) satisfy the well-known generating relation,

$$\exp(-s^2/2+sx-x^2/4)=\sum_{n=0}^{\infty}(1/n!)\psi_n(x)s^n. \quad \text{(A1.1)}$$

Let

$$x=[8/(b+b^{-1})]^{\frac{1}{2}}\xi$$

$$y=[8/(b+b^{-1})]^{\frac{1}{2}}\eta.$$

With $\sigma(\xi, \eta)$ given by Eq. (3.11), the integral

$$\int_{-\infty}^{\infty}\sigma(\xi, \eta)\exp(sy-y^2/4)d\eta \quad \text{(A1.2)}$$

may be explicitly evaluated in terms of x and s. If the resulting expression is then written as an infinite series by application of Eq. (A1.1), it is found that the integral (A1.2) is equal to

$$\pi^{\frac{1}{2}}[(1+b^2)^{\frac{1}{2}}/(1+b)]$$

$$\times\exp(s^2/2)\sum_{n=0}^{\infty}(1/n!)\psi_n(x)[(b-1)s/(b+1)]^n.$$

On the other hand, by direct application of Eq. (A1.1) to the integrand in (A1.2), it is seen that the integral may also be written as

$$\exp(s^2/2)\sum_{n=0}^{\infty}(1/n!)s^n\int_{-\infty}^{\infty}\sigma(\xi, \eta)\psi_n(y)d\eta.$$

By equating coefficients of equal powers of s in these two series, it is established that

$$\int_{-\infty}^{\infty}\sigma(\xi, \eta)\chi_n(\eta)d\eta=\sigma_n\chi_n(\xi),$$

where σ_n and $\chi_n(\xi)$ are as given in Eq. (3.13).

APPENDIX II

Here, the uncontracted kernel $k(J, M, K; J', M', K')$ for the three-dimensional problem will be quoted, but not derived. By continuing to use the abbreviation $b=I/ma^2$, and letting

$$A=JJ'(1+b)^2Z/2\pi^2bIkT$$

$$B=[(b-1)J^2-(b+1)J'^2]/4bIkT$$

$$C=(b-b^{-1})/8IkT,$$

the kernel may be written

$$k(J, M, K; J', M', K')$$

$$=Ae^B\int_{\mathfrak{R}}\frac{\exp[-C\Lambda^2+F(\Lambda)]I_0[F(\Lambda)]}{G_1^{\frac{1}{2}}(\Lambda)G_2^{\frac{1}{2}}(\Lambda)}d\Lambda$$

where the functions F, G_1, G_2 of the integration variable Λ, and the range of integration $\mathfrak{R}$, are defined as follows:

$$F(\Lambda)=[-\tfrac{1}{4}(J^2-J'^2)^2/\Lambda^2-\tfrac{1}{4}\Lambda^2+\tfrac{1}{2}(J^2+J'^2)]/4bIkT$$

$$G_1(\Lambda)=(\Lambda^2-\Lambda_1^2)(\Lambda_2^2-\Lambda^2)$$

$$G_2(\Lambda)=(\Lambda^2-\Lambda_3^2)(\Lambda_4^2-\Lambda^2),$$

the constants $\Lambda_i (i=1, 2, 3, 4)$ being the *positive* square roots of

$$\Lambda_1^2=[(J^2-K^2)^{\frac{1}{2}}-(J'^2-K'^2)^{\frac{1}{2}}]^2+(K-K')^2$$

$$\Lambda_2^2=[(J^2-K^2)^{\frac{1}{2}}+(J'^2-K'^2)^{\frac{1}{2}}]^2+(K-K')^2$$

$$\Lambda_3^2=[(J^2-M^2)^{\frac{1}{2}}-(J'^2-M'^2)^{\frac{1}{2}}]^2+(M-M')^2$$

$$\Lambda_4^2=[(J^2-M^2)^{\frac{1}{2}}+(J'^2-M'^2)^{\frac{1}{2}}]^2+(M-M')^2.$$

[7] C. S. Wang Chang and G. E. Uhlenbeck, Report CM-681, Project NOrd 7924, University of Michigan (1951). The author is grateful to Prof. J. S. Dahler for having informed him of this earlier result.

The range of integration $\mathfrak{R}$ is

$$\max(\Lambda_1, \Lambda_3) \leq \Lambda \leq \min(\Lambda_2, \Lambda_4).$$

This range may have no extent, i.e., the initial state J, M, K and the final state J', M', K' may be such that $\max(\Lambda_1, \Lambda_3) > \min(\Lambda_2, \Lambda_4)$. For such pairs of states,

$$k(J, M, K; J', M', K') \equiv 0.$$

With the equilibrium distribution function given by Eq. (4.2), it is seen that the transition probability quoted here satisfies detailed balance in the form of Eq. (2.4). It is also symmetric with respect to the external and internal components of angular momentum, M and K:

$$k(J, M, K; J', M', K') = k(J, K, M; J', K', M').$$

APPENDIX III

The contracted transition kernel $k(J, J')$ will here be derived from Eqs. (4.6), (4.7), and (4.8).

In Eq. (4.7), first fix $\mathbf{r}$ and integrate over $\mathbf{p}$. The $\mathbf{p}$ integration is performed by first writing

$$-\mathbf{p} = \alpha(\mathbf{r}/a) + \beta[(\mathbf{r}\times\mathbf{J})/|\,\mathbf{r}\times\mathbf{J}\,|] + \gamma[\mathbf{r}\times(\mathbf{r}\times\mathbf{J})/a\,|\,\mathbf{r}\times\mathbf{J}\,|]$$

so that α, β, γ are the variable components of $-\mathbf{p}$ in a rectangular coordinate system defined by $\mathbf{r}$ and $\mathbf{J}$. The range of $\mathbf{p}$ is the half-space $-\mathbf{p}\cdot\mathbf{r} > 0$, so the ranges of the integration variables α, β, γ are

$$0 \leq \alpha < \infty$$

$$-\infty < \beta < \infty$$

$$-\infty < \gamma < \infty.$$

The integrations over α and γ can then be carried out, with the result that

$$k(J, J') = Ae^{-B}\int \exp[mC(\mathbf{r}\cdot\mathbf{J})^2] \times \int_{\beta_1}^{\beta_2} \frac{\exp[C(I-ma^2)\,|\,\mathbf{r}\times\mathbf{J}\,|\,\beta]}{[(\beta-\beta_1)(\beta_2-\beta)]^{\frac{1}{2}}} d\beta d\sigma, \qquad (\mathbf{r}\cdot\mathbf{J})^2 < a^2J'^2$$

where

$$A = (I+ma^2)^2 J' Z / 16\pi^2 ma^4 I^2 kT$$

$$B = [(I+ma^2)^2 J'^2 - (I-ma^2)^2 J^2]/8ma^2 I^2 kT$$

$$C = (2ma^2 IkT)^{-1};$$

where now, as indicated, the integration over $\mathbf{r}$ is limited to that portion of the spherical surface for which $(\mathbf{r}\cdot\mathbf{J})^2 < a^2J'^2$; and where β is limited to the range $\beta_1 < \beta < \beta_2$, the quantities β_1 and β_2 being, respectively, the smaller and larger of the two numbers

$$-[(I-ma^2)/2Ia^2]\,|\,\mathbf{r}\times\mathbf{J}\,| \pm [(I+ma^2)/2Ia^2] \times [a^2J'^2 - (\mathbf{r}\cdot\mathbf{J})^2]^{\frac{1}{2}}.$$

The integral over β can now be evaluated[8] in terms of a Bessel function of imaginary argument and zero order, I_0.

It remains to carry out the integration over $\mathbf{r}$. Let

$$d\sigma = (a/J)\, d(\mathbf{r}\cdot\mathbf{J})\, d\phi,$$

where ϕ is an azimuthal angle of rotation about $\mathbf{J}$. Then, the integration over ϕ is trivial, and $k(J, J')$ is left expressed as a single integral, with $\mathbf{r}\cdot\mathbf{J}$ the integration variable. With the definitions of Eqs. (4.9) and (4.10), and the new integration variable $t = (b+b^{-1})^{\frac{1}{2}}\mathbf{r}\cdot\mathbf{J}/2a(2IkT)^{\frac{1}{2}}$, the final result is

$$k(J, J') = \frac{(b^{\frac{1}{2}}+b^{-\frac{1}{2}})^2}{(b+b^{-1})^{\frac{1}{2}}} \frac{Z}{(8IkT)^{\frac{1}{2}}} (\eta/\xi) \times \exp[-(\xi^2+\eta^2) + 2(\xi^2-\eta^2)/(b+b^{-1})]Q,$$

where Q is the integral

$$Q = \int_{-\min(\xi,\,\eta)}^{\min(\xi,\,\eta)} \exp(2t^2) I_0\left[2\frac{b^2-1}{b^2+1}(\xi^2-t^2)^{\frac{1}{2}}(\eta^2-t^2)^{\frac{1}{2}}\right] dt.$$

APPENDIX IV

It will be shown here that the eigenfunctions and eigenvalues of the kernel $\sigma(\xi, \eta)$ in Eq. (4.12), are given by Eq. (4.14). The range of the variables is $0 \leq \xi, \eta < \infty$.

The parabolic cylinder function $\psi_n(x)$ defined in Eq. (3.14) may be written as the product of $\exp(-x^2/4)$ with a Hermite polynomial in x of degree n. Thus,

$$\psi_{2n+1}(x) = \exp(-x^2/4)\, x \sum_{\mu=0}^{n} f_\mu x^{2\mu}, \qquad \text{(AIV.1)}$$

with the appropriate coefficients f_μ. Then, after applying Eq. (AIV.1), the integral

$$\int_0^\infty \sigma(\xi, \eta)\psi_{2n+1}\{[8/(b+b^{-1})]^{\frac{1}{2}}\eta\}\, d\eta \qquad \text{(AIV.2)}$$

may be evaluated in the following way: (i) The kernel is itself defined as an integral over t in Eq. (4.12), so

[8] Reference 5, p. 79, Eq. (9).

(AIV.2) is a double integral over t and η; make the change of variable

$$(\xi^2-t^2)^{\frac{1}{2}}=\tau_1$$

$$(\eta^2-t^2)^{\frac{1}{2}}=\tau_2,$$

so that

$$\int_0^\infty\int_0^{\min(\xi,\eta)}\cdots\eta dtd\eta=\int_0^\xi\int_0^\infty\cdots(\xi^2-\tau_1^2)^{-\frac{1}{2}}\tau_1\tau_2 d\tau_2 d\tau_1.$$

(ii) Apply the binomial theorem to the integral powers of $(\tau_2^2+\xi^2-\tau_1^2)$, which appear in the integrand, expressing them in terms of powers of τ_2^2 and of $(\xi^2-\tau_1^2)$. (iii) Carry out the integration over τ_2 by means of Hankel's formula (to which Kummer's first transformation has been applied).[9] (iv) Integrate over τ_1.

As the result of these operations, it is found that the integral (AIV.2) becomes

$$\exp(-x^2/4)x\sum_{\mu=0}^{n}g_\mu f_\mu x^{2\mu}, \qquad \text{(AIV.3)}$$

where $x=[8/(b+b^{-1})]^{\frac{1}{2}}\xi$, where the coefficients f_μ are the same as in Eq. (AIV.1), and where g_μ is itself a complicated double summation over indices ρ and ν:

$$g_\mu=\sum_{\rho=\mu}^{n}\sum_{\nu=0}^{\rho}\cdots. \qquad \text{(AIV.4)}$$

But only a factor $(\rho-\nu)!$ in the summand of Eq. (AIV.4) couples the two indices ρ and ν. The two sums may then be uncoupled by writing

$$(\rho-\nu)!=[\Gamma(\rho+\tfrac{3}{2})/\Gamma(\nu+\tfrac{1}{2})]\int_0^1 s^{\rho-\nu}(1-s)^{-\frac{1}{2}}ds$$

and then summing before integrating. Each summation can be performed separately, with the result that

$$g_\mu=\frac{1+b^2}{4(1+b)^2}\int_0^1(1-s)^{-\frac{1}{2}}\left[1-\frac{4bs}{(1+b)^2}\right]^n ds,$$

independently of μ. That g_μ is independent of μ is the crucial point, and it then follows that

$$\int_0^\infty\sigma(\xi,\eta)\chi_n(\eta)d\eta=\sigma_n\chi_n(\xi),$$

where $\chi_n(\xi)$ and σ_n are as given in Eq. (4.14).

[9] Reference 5, p. 394, Eq. (3).

Proton Magnetic Resonance Study of the Structure of Barium Chloride Dihydrate*

A. A. SILVIDI AND J. W. MCGRATH

Department of Physics, Kent State University, Kent, Ohio

(Received September 25, 1959)

The proton magnetic resonance absorption spectrum of barium chloride dihydrate has been obtained experimentally at room temperature using a Pound-Watkins spectrometer. The results indicate that there are four pairs of p–p directions in the crystal. The p–p distance and direction angles of these four pairs are: 1.58 A, $\alpha_0=90°$, $\beta_0=58°$, $\gamma_0=148°$; 1.58 A, $\alpha_0=90°$, $\beta_0=58°$, $\gamma_0=32°$; 1.59A, $\alpha_0=148°$, $\beta_0=58°$, $\gamma_0=90°$; 1.57 A, $\alpha_0=32°$, $\beta_0=58°$, $\gamma_0=90°$. The experimental error for the p–p distance is ± 0.02 A and for the direction angles it is $\pm 4°$. By using experimental data, x-ray analysis, and the concept of hydrogen bonding the positions of the hydrogen atoms were determined.

INTRODUCTION

THE determination of the crystal structure of barium chloride dihydrate by x-rays was first attempted by Naray-Szabo and Sasvari.[1] A difficulty in determining its complete structure was due to the fact that the barium atom contains so many electrons that it tended to obscure the chlorine and oxygen atoms. Jensen[2] was successful in completing the study. $BaCl_2 \cdot 2H_2O$ crystals are monoclinic with space group $C_{2h}^5(P2_1/n)$. There are four molecules per unit cell. The location of the hydrogen atoms of the water molecules could not be determined by x-ray studies. Jensen assumed that the water molecules link two Ba atoms at distances of about 2.85 A and also make two distinct contacts with Cl atoms. To locate the hydrogens in this crystal, a proton magnetic resonance study was made using the Pake[3] technique.

EXPERIMENT

The experimental equipment was the same as that described elsewhere[4,5] with the following new parameters: rf = 27.00 Mcps, $H_0 = 6341$ gauss, modulation amplitude = 0.75 gauss, sweep speed = 0.02021 gauss/sec.

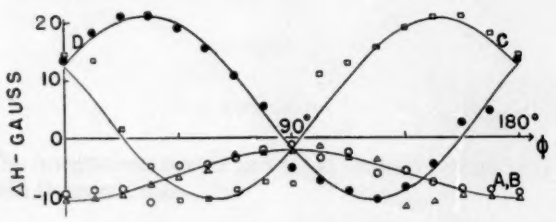

FIG. 1. Pake curves for barium chloride rotated about the c axis. The solid curves are a plot of Eq. (1). For curves A and B: $2\alpha=10.7$ g, $\phi_0=90°$ and $\delta=58.7°$. For curve C: $2\alpha=10.4$ g, $\phi_0=31.5°$ and $\delta=0°$; for curve D: $2\alpha=10.8$ g, $\phi_0=-31.7°$ and $\delta=0°$. The experimental points are represented as follows: Circles, curve A; triangles, curve B; squares, curve C; filled circles, curve D.

The crystals were grown in this laboratory and cut so that the largest crystals could be mounted in the rf coil. Two crystals were used; one was rotated about the a axis, the other about the c axis. The measurements were made at room temperature.

If the proton pairs exhibit only dipole-dipole interaction the line pair separation, ΔH in gauss, is related to the orientation of the crystal by the formula[3]

$$\Delta H = 2\alpha[3\cos^2(\phi+\phi_0)\cos^2\delta - 1], \qquad (1)$$

where $2\alpha = 3\mu/r^3$, μ is the proton magnetic moment, r is the proton-proton separation, ϕ is the angle between the external magnetic field H_0 and a reference axis attached to the crystal that is in the plane of crystal rotation, ϕ_0 is the angle between the projection of the $p-p$ line onto the plane of rotation and the reference axis in the crystal, and δ is the angle between the $p-p$ line and the plane of rotation. Measuring ΔH for several ϕ's allows one to compute r, ϕ_0, and δ.

RESULTS

Figure 1 shows the Pake curves for the c-axis case. The method of obtaining and analyzing these curves is described elsewhere.[3–5] There are a few experimental points which miss the theoretical curves quite badly. This may have been due to the fact that the derivative curves showed some evidence of saturation. To correct for this effect during the analysis of the absorption curves, an appropriately amplitude-varied standard curve[4,5] was used. In spite of this, for a few angles, the resolution of the absorption curve was not good. There are eight water molecules per unit cell of $BaCl_2 \cdot 2H_2O$ but Fig. 1 shows that there are four pairs of $p-p$ directions in the crystal. These will be labeled A, B, C, and D. The Pake curves for the a-axis case are not shown since they are very similar to those in Fig. 1. The differences between the curves of the a-axis case and the c-axis case will now be described. The curve in Fig. 1, which resulted from pair D, is now caused by

* Partially supported by the U. S. Air Force through the Air Force Office of Scientific Research under Contract AF 49(638)-168.

[1] St. v. Naray-Szabo and K. Sasvari, Z. Krist. **A97**, 235 (1937).
[2] A. Tovborg Jensen, Kgl. Danske Videnskab. Selskab. Mat.-fys. Medd. **22**, No. 3 (1945).
[3] G. E. Pake, J. Chem. Phys. **16**, 327 (1948).
[4] A. A. Silvidi and J. W. McGrath, J. Chem. Phys. **30**, 1028 (1959).
[5] McGrath, Silvidi, and Carroll, J. Chem. Phys. **31**, 1444 (1959).

TABLE I. Values of ϕ_0 and δ for the Pake curves.

Proton pairs	c axis		a axis	
	ϕ_0	δ	ϕ_0	δ
A	90°	58.8°	32.5°	0°
B	90	58.8	58.3	0
C	58.5	0	90	58.5
D	31.8	0	90	58.5

pair A (when rotating about the *a* axis). Similarly, the curve which resulted from pair C is now caused by pair B; the curve which resulted from pair A is now caused by pair C; and the curve which resulted from pair B is now caused by pair D. Fortunately, this interchange of Pake curves allowed us to use pairs C and D of the *c*-axis case and pairs A and B of the *a*-axis case for determining the $p-p$ distances and orientations. The curves from the remaining pairs, A and B from the *c*-axis and C and D from the *a*-axis, were not as accurate. Table I lists values of ϕ_0 and δ for all cases.

The data (minimum ΔH, ϕ_0, and δ) of the *c*-axis and *a*-axis cases yield values for $p-p$ separations and direction angles (measured with respect to the positive crystallographic axes) of the $p-p$ vectors that are given in Table II. The experimental error for the $p-p$ distances is ±0.02 A and for the direction angles it is ±4°.

DISCUSSION

Knowledge of the orientations of the $p-p$ vectors from the magnetic resonance experiment, the positions of the chlorine and oxygen atoms from the x-ray analysis and the normal H—O—H water angle allowed the location of the hydrogen atoms in the crystal.[4,5] Figures 2 and 3 are projections of the $BaCl_2 \cdot 2H_2O$ crystal structure with the hydrogen atoms in positions to satisfy the requirements.

Table III lists the calculated bond distances and the calculated direction angles of the $p-p$ vectors when they are placed as in Figs. 2 and 3. The agreement between the calculated and experimental orientations is very good. The H—O—H angle is larger than the accepted 108° value. It must be noted that the calculations were based on an assumption of straight hydrogen bonds. For some hydrates it has been noted that the hydrogen bonds are bent. For this crystal the hydrogen bonds could be bent inward to make the normal 108° H—O—H angle and the direction angles would not be changed so that this situation may exist.

TABLE II. Experimental results for barium chloride dihydrate.

		Proton pairs			
		A	B	C	D
p-p distances in A		1.58	1.58	1.59	1.57
Direction angles	α_0	90°	90°	148°	32°
	β_0	58	58	58	58
	γ_0	148	32	90	90

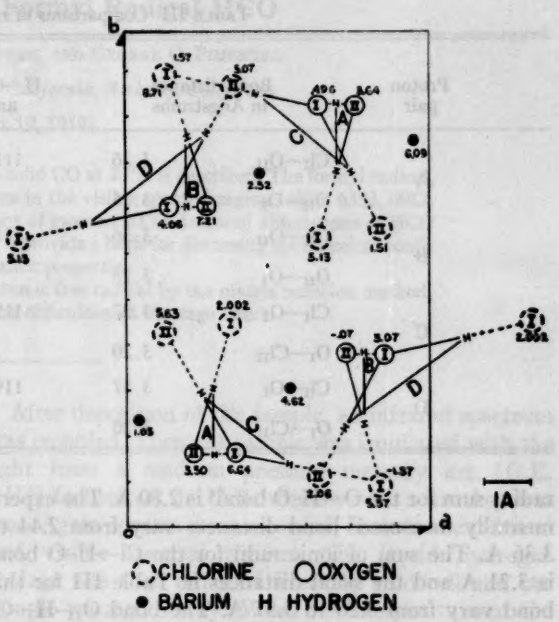

FIG. 2. Projection of the barium chloride structure in the *a*–*b* plane.

The hydrogens form bonds in two distinct ways:

$$Cl_I—H—O_I—H—Cl_{II} \text{ and } Cl_I—H—O_{II}—H—O_I.$$

The bond distance for the Cl—H–O bond is consistent with the sum of ionic radii. For example, the ionic

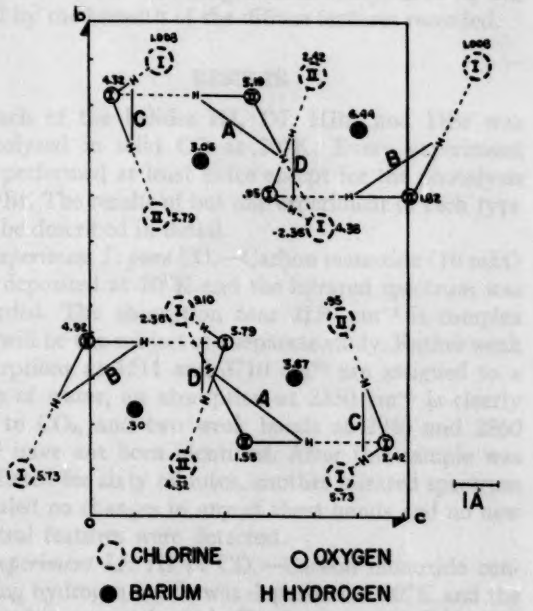

FIG. 3. Projection of the barium chloride structure in the *b*–*c* plane.

TABLE III. Comparisons of results for barium chloride dihydrate.

Proton pair	Bond distance in Angstroms		H—O—H angle	Direction angles	Calculated values	Experimental values from Table II
A	Cl_I-O_{II}	3.36	111°35′	α_0	89°49′	90°
				β_0	58°10′	58
	$O_{II}-O_I$	3.25		γ_0	148°8′	148
B	$Cl_I—O_{II}$	3.36	111°39′	α_0	90°12′	90
				β_0	58°12′	58°
	$O_{II}—O_I$	3.25		γ_0	31°56′	32°
C	$Cl_I—O_I$	3.57	119°40′	α_0	144°48′	148°
				β_0	54°45′	58°
	$O_I—Cl_{II}$	3.20		γ_0	89°26′	90°
D	$Cl_I—O_I$	3.57	119°44′	α_0	35°12′	32°
				β_0	54°45′	58°
	$O_I—Cl_{II}$	3.20		γ_0	90°34′	90°

radius sum for the O—H–O bond[6] is 2.80 A. The experimentally measured[7] bond distances vary from 2.44 to 3.36 A. The sum of ionic radii for the Cl—H–O bond is 3.21 A and the bond distances in Table III for this bond vary from 3.20 to 3.57 A. The bond O_{II}–H—O_I with a distance of 3.25 A, may seem a little large since the only other larger reported value of 3.36 A is given by Ernst.[8] However, it must be pointed out that O_I forms a peculiar complex in that there are three hydrogens surrounding it (see Figs. 2 and 3). This has been noted before.[5]

[6] L. Pauling, *Nature of the Chemical Bond* (Cornell University Press, Ithaca, New York, 1940), p. 346.
[7] Nakamoto, Margoshes, and Rundle, J. Am. Chem. Soc. **77**, 6480 (1955).
[8] T. Ernst, Z. physik. Chem. **B20**, 65 (1933).

CONCLUSION

This proton magnetic resonance study of barium chloride dihydrate shows that there are four proton-proton orientations in this crystal. The $p-p$ distances and direction angles are given in Table II.

The experimental data, together with the existing x-ray structure information and the hydrogen bond concept, indicate that the location of hydrogen atoms is that shown in Figs. 2 and 3.

Infrared Detection of the Formyl Radical HCO

GEORGE E. EWING, WARREN E. THOMPSON, AND GEORGE C. PIMENTEL
Department of Chemistry, University of California, Berkeley, California

(Received October 19, 1959)

The photolysis of HI, DI, HBr, and DBr suspended in solid CO at 20°K is described. The formyl radical, HCO or DCO, is produced, as shown by broad absorptions in the visible spectral region (6695, 6352, 6052, 5789, 5548, 5330, 5102 A) which correspond to absorptions of gaseous HCO. Infrared absorptions of HCO (at 1860 and 1091 cm^{-1}) and of DCO (at 1860 and 856 cm^{-1}) provide a basis for discussing the chemical bonding of this free radical, and for calculating its thermodynamic properties.

These experiments, the first infrared detection of a triatomic free radical by the matrix isolation method, depend upon reactivity of the matrix, possibly eliminating difficulties of the cage effect.

HERZBERG and Ramsay[1] have detected the formyl radical, HCO, by its absorption in the visible spectral region. These authors, who reviewed earlier, less definite identifications of HCO, deduced its structural parameters in the ground and excited states. More recently, Johns and Ramsay[2] have been able to fix one of the vibrational frequencies of the ground state, viz., the bending mode. Since this analysis is based on "hot" bands, the prospect of learning the other two vibrational frequencies in a similar fashion is not promising.

Formyl has not been detected previously in the infrared region. This statement seems almost unnecessary since, with the possible exception of NH_2[3], the only triatomic free radicals observed in the infrared region are reasonably stable (e.g., NO_2, ClO_2). A complete vibrational analysis for HCO would permit calculation of its thermodynamic properties, it would clarify further the structure (the arrangement HOC is not yet completely excluded[1]), and it would add to our knowledge of the chemical bonding in free radicals.

This paper presents the results of photolysis of HI, DI, HBr, and DBr, each in a solid carbon monoxide matrix. Thus these experiments differ from the usual inert matrix isolation methods: the matrix was deliberately selected to be a reactant.

EXPERIMENTAL

The hydrogen halide gas was mixed with carbon monoxide gas in a mole ratio between 400 and 600 (moles CO/moles hydrogen halide). Between 15 and 30 mM of this gas mixture were deposited over a period of six to ten hours onto a CsBr window held at 20°K. The optical path of the cold cell[4] was fitted with one KBr and one BaF_2 external window. The latter served as a photolysis window.

After deposition of the sample, an infrared spectrum was recorded. Then the sample was irradiated with the light from a medium pressure mercury arc (G.E. AH4) focused on the CsBr window with a fused quartz lens. Again spectra were recorded, both in the infrared and visible spectral regions. The liquid hydrogen coolant was then removed from the cold cell and the sample warmed slowly. When the temperature of the support window reached 45°K, liquid hydrogen was transferred into the cold cell to recool the sample to 20°K. This operation, called a "diffusion operation," permits diffusion and possibly reaction of the molecules isolated in the matrix.

Infrared spectra were recorded with a Perkin-Elmer Model 21 Spectrophotometer equipped with sodium chloride optics. Frequency accuracy is estimated to be ±30, ±20, and ±10 cm^{-1} at, respectively, 3000, 2000, and 1000 cm^{-1}. In the visible spectral region spectra were recorded with a Cary Model 14 Spectrophotometer. The wavelength uncertainty, ±10 A, was fixed by the breadth of the diffuse features recorded.

RESULTS

Each of the halides HI, DI, HBr, and DBr was photolyzed in solid CO at 20°K. Every experiment was performed at least twice except for the photolysis of DBr. The results of but one experiment of each type will be described in detail.

Experiment I: *pure* CO.—Carbon monoxide (16 mM) was deposited at 20°K and the infrared spectrum was recorded. The absorption near 2150 cm^{-1} is complex and will be the subject of a separate study. Rather weak absorptions at 1611 and 3710 cm^{-1} are assigned to a trace of water, an absorption at 2350 cm^{-1} is clearly due to CO_2, and two weak bands at 2940 and 2860 cm^{-1} have not been identified. After this sample was irradiated for sixty minutes, another infrared spectrum revealed no changes in any of these bands and no new spectral features were detected.

Experiment II: HI *in* CO.—Carbon monoxide containing hydrogen iodide was deposited at 20°K and the infrared spectrum shown in Fig. 1 was recorded (dashed curve). The frequencies and intensities of the observed

[1] G. Herzberg and D. A. Ramsay, Proc. Roy. Soc. (London) A233, 34 (1955).
[2] J. W. C. Johns and D. A. Ramsay, Paper E6, Symposium on Molecular Structure and Spectroscopy, The Ohio State University, Columbus, Ohio, June 15–19, 1959.
[3] R. C. Lord and C. H. Sederholm, Spectrochim. Acta (to be published).
[4] E. D. Becker and G. C. Pimentel, J. Chem. Phys. 25, 224 (1956).

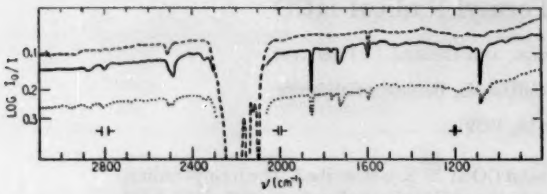

FIG. 1. Experiment II: Infrared spectrum of HI in solid CO. (M/R=440, T=20°K). Broken line: before photolysis; solid line: after 8 min photolysis; dotted line: after diffusion.

bands are listed in Table I together with the presumed identities of the absorbing species. The absorption of HI (near 2230 cm^{-1}) is obscured by the absorption of the matrix. The presence of HBr is revealed by the band at 2507 cm^{-1}; this impurity was detected in varying amounts in each of the several experiments involving HI. Other trace impurities are water and CO_2. A spectrum recorded from 7000 to 4000 A showed no bands, only heavy scattering which varied from an optical density of 1.0 to 1.7 over this wavelength region.

The sample was then irradiated for 8 min and the infrared spectrum shown in Fig. 1 (solid curve) was recorded. As shown in Table I, nine new features appeared. The band at 2350 cm^{-1} is assigned to CO_2, and the three bands at 2870, 2800, and 1730 cm^{-1} are assigned to formaldehyde. Since the last three bands are close in frequency and relative intensity to three of four bands observed in the spectrum of formaldehyde suspended in solid CO [2862 (0.01), 2791 (0.01), 1739 (0.10), and 1497 (0.01) cm^{-1}], there is little doubt in this assignment. The very weak band at 1760 cm^{-1} is assigned to glyoxal since the most intense infrared absorption of gaseous glyoxal is found at 1730 cm^{-1}.[5] The very weak band at 1121 cm^{-1} and the three prominent bands at 2493, 1860, and 1091 cm^{-1} could not be assigned to stable species.

In the visible region, a series of broad bands was recorded after photolysis. These are listed in the first column of Table II.

After this spectral study, a diffusion operation was performed. An infrared spectrum then showed the partial loss of the bands of monomeric water and of the impurity HBr—evidence that diffusion had occurred during this "diffusion operation." The bands assigned to formaldehyde and to CO_2 remained unchanged. In contrast, the three unassigned bands decreased in intensity by about a factor of two, behavior appropriate to a reactive species.

Experiment III: DI *in* CO.—Carbon monoxide containing deuterium iodide was deposited at 20°K and the infrared spectrum recorded. The frequencies and intensities of the observed bands are shown in Table III. The absorptions at 1411 and 1188 cm^{-1} are undoubtedly due to HDO and D_2O, respectively, and indicate the ratio of DI/(HI+DI) is in the range 0.80 to 0.90 (presuming complete equilibration between water and the deuterium iodide).

TABLE I. Experiment II: Photolysis of hydrogen iodide in solid CO (T=20°K) (intensities=logI_0/I).

ν(cm^{-1})	Before photolysis	After 8 min photolysis	After diffusion	Assignment
3710	0.01	0.02	0.01	H_2O
2507	0.03	0.04	0.02	HBr
2100–2250	∞	∞	∞	CO
1611	0.04	0.04	0.02	H_2O
2870	...	0.01	0.01	H_2CO
2800	...	0.02	0.02	H_2CO
2493	...	0.05	0.02	(?)
2350	...	0.02	0.01	CO_2
1860	...	0.10	0.05	HCO
1760	...	0.01	0.01	$(CHO)_2$
1730	...	0.05	0.05	H_2CO
1121	...	0.01	...	(?)
1091	...	0.10	0.05	HCO

[5] H. W. Thompson, Trans. Faraday Soc. **36**, 988 (1940).

TABLE II. Absorption spectra in region 7000–4000 A.

Expt. II		Band origins[1,a]	Upper vibrational state	Difference matrix−gas
		13 222.33 cm^{-1}	0, 6, 0	
		...	0, 7, 0	
6695 A	14 937 cm^{-1}	14 758.00	0, 8, 0	+175 cm^{-1}
6352	15 743	(15 516.8)	0, 9, 0	+226
6052	16 523	16 269.59	0, 10, 0	+253
5789	17 274	(17 016.4)	0, 11, 0	+258
5548	18 025	17 757.34	0, 12, 0	+268
5330	18 762	(18 492.5)	0, 13, 0	+269
5102	19 600	19 221.75	0, 14, 0	+378

[a] Parenthetical values are derived by quadratic interpolation.

The sample was photolyzed for one minute, and a second infrared spectrum was recorded. This procedure was then repeated twice with additional photolysis periods of one minute and twenty minutes. The progressive reduction in intensity of the band at 1589 cm^{-1} indicates the photolytic decomposition of DI. This loss of DI was accompanied by the growth of seven new spectral features, three of which appeared after the first photolysis. The band at 2350 cm^{-1} is again assigned to CO_2 and the band at 1770 cm^{-1} could be assigned to DBr from reaction with the CsBr window. Two of the bands observed in Experiment II were observed, 1860 and 1091 cm^{-1} as well as two distinct new bands, 1940 and 856 cm^{-1}, and one doubtful feature at 1100 cm^{-1}. A diffusion operation caused a reduction in intensity of all features except those of the matrix.

Experiment IV: HBr *in* CO.—This experiment was similar to Expt. II, but the results, given in Table IV, are simpler. Only two of the spectral features observed after photolysis in Expt. II were detected, those at 1860 and 1091 cm^{-1}. These bands disappeared with diffusion and a new band at 1124 cm^{-1} appeared (note that the

TABLE III. Experiment III: Photolysis of deuterium iodide in solid CO ($T=20°K$) (intensities $=\log I_0/I$).

ν(cm^{-1})	Before photolysis	After photolysis 1 min	2 min	22 min	After diffusion	Assignment
2747	0.03	[a]	[a]	0.03	0.00	D_2O
2100–2250	∞	∞	∞	∞	∞	CO
1589	0.09	0.09	0.07	0.05	0.01	DI
1411	0.02	[a]	[a]	0.02	0.005 ?	HDO
1188	0.06	[a]	[a]	0.04	0.03	D_2O
2350	...	[a]	[a]	0.03	0.005 ?	CO_2
1940	...	0.04	0.05	0.07	0.05	(?)
1860	...	0.03	0.06	0.05	0.01	DCO, HCO
1770	...	...	...	0.01	0.005 ?	DBr (?)
1100	...	...	...	0.005 ?	0.00	(?)
1091	...	...	...	0.02	0.005 ?	HCO
856	...	0.01	0.02	0.02	0.00	DCO

[a] Spectrum not recorded in this region.

region near 2493 cm^{-1} was obscured in this experiment by the intense absorption of HBr).

Experiment V: DBr *in* CO.—Table V shows the frequencies and intensities of the absorptions observed prior to photolysis. The relative intensities of the bands of HBr and DBr as well as those of the bands of HDO and D_2O indicate the sample contained 75±5% deuterium. Since the two estimates agree, equilibration between water and DBr has occurred (which was assumed in Expt. III).

Photolysis of this sample for 45 min caused only a slight decrease in the band at 2507 cm^{-1} (due to HBr) and no detectable change in the band at 1800 cm^{-1} (due to DBr). Perhaps the fact that the ultraviolet absorption coefficient of DBr is significantly less than that of HBr[6] accounts for the absence of photolysis of DBr.

This photolysis was accompanied by the growth of the two bands at 1860 and 1091 cm^{-1} observed in Expts. II to IV. In addition, a very weak feature near 1940 cm^{-1} duplicates the absorption at this frequency observed in Expt. III but not in II or IV.

DISCUSSION

Detection of Formyl Radicals

Experiment II gives strong evidence that the photolysis of HI in solid CO at 20°K produces the formyl radical HCO. Four of the seven absorption features detected in the visible spectral region correspond well to the *Q* band heads recorded by Herzberg and Ramsay[1] for gaseous HCO. The other three features correspond equally well to the interpolated odd vibrational states (which were observed in the gas phase only through diffuse *R* branches[1]). The matrix frequencies exceed those of the gas phase band heads by a few hundred wave numbers, as shown in the last column of Table II.* These differences are less than half as large as those reported by Norman and Porter[7] for the CS radical in a hydrocarbon glass. Robinson and McCarty summarize their evidence on the shifts observed in argon matrices for five species: HNO, −57 cm^{-1}; NH_2, +25 cm^{-1}; NO_2, +55–70 cm^{-1}; NH, −165 cm^{-1}; OH, −300 cm^{-1} (matrix frequency-gas frequency).[8] The matrix shifts observed here are not abnormal and the one-to-one correspondence of the matrix bands to those of gaseous formyl leaves no doubt that the matrix species is the same.

This detection of HCO is substantiated by the infrared spectral features produced during the photolyses of Expts. II–IV. Clearly the band at 1091 cm^{-1} is in an appropriate spectral region to be assigned to ν_3, the HCO bending mode (for example, compare the bending mode of HNO at 1110 cm^{-1}, as reported by Brown and Pimentel[9]). Furthermore, in Expt. III a new band was detected at 856 cm^{-1} which is readily assigned as the bending mode of DCO. These assignments are in convincing agreement with the values deduced by Johns and Ramsay,[2] 1083 cm^{-1} (HCO) and 847 cm^{-1} (DCO).

TABLE IV. Experiment IV: Photolysis of hydrogen bromide in solid CO ($T=20°K$).

ν(cm^{-1})	Before photolysis	After 35 min photolysis	After diffusion	Assignment
2507	0.35	0.34	0.30 (broad)	HBr
2350	0.01	0.02	0.02	CO_2
2100–2250	∞	∞	∞	CO
1611	0.04	0.02?	0.00	H_2O
1860	...	0.04	0.00	HCO
1124	...	...	0.02	(?)
1091	...	0.03	0.00	HCO

[6] Bates, Halford, and Anderson, J. Chem. Phys. **3**, 531 (1935).

* We have selected the correlation which gives the smallest matrix shifts.

[7] I. Norman and G. Porter, Proc. Roy. Soc. (London) **A230**, 399 (1955).

[8] G. W. Robinson and M. McCarty, Jr., J. Chem. Phys. **28**, 350 (1958).

[9] H. W. Brown and G. C. Pimentel, J. Chem. Phys. **29**, 883 (1958).

TABLE V. Experiment V: Photolysis of deuterium bromide in solid CO ($T=20°K$).

$\nu(cm^{-1})$	Before photolysis	After 45 min photolysis	Assignment
2747	0.02	0.02	D_2O
2507	0.21	0.19	HBr
2100–2250	∞	∞	CO
1800	0.38	0.38	DBr
1411	0.03	0.03	HDO
1188	0.04	0.03	D_2O
1940	...	0.005?	(?)
1860	...	0.02	HCO
1091	...	0.01	HCO

Without doubt, these infrared absorptions and the electronic transitions listed in Table II show that the formyl radical has been produced in the solid carbon monoxide matrix. This is the first firmly established infrared detection of a triatomic free radical by the matrix isolation method.

Vibrational Frequencies of the Formyl Radical

In addition to the bending mode, formyl has two stretching modes. One of these, the carbonyl stretching mode ν_2 is expected in the spectral region near 6 μ. A suitable band is listed in Tables I and IV, the band at 1860 cm^{-1}. This band is produced both from HI and HBr with approximately the same intensity relative to the HCO band at 1091 cm^{-1}. This band is also detected in Expts. III and IV, but with higher relative intensity. Thus we are led to assign this same band as ν_2 of DCO. The absence of a detectable deuterium isotope effect in ν_2 is in reasonable accord with the absorptions of HNO and DNO, for which this mode differs by 10 cm^{-1} or less.[9] Another convincing example is provided by the α excited state of HCN. Herzberg and Innes[10] find that the C—N stretching modes of the α states of HCN and DCN are the same, 1506 cm^{-1}, within their experimental uncertainty.

The assignment of ν_1 is less clear. In Expt. II there is a band at 2493 cm^{-1} which could be assigned to this C—H stretching mode, although this frequency is much lower than expected on the basis of comparison to stable molecules. In Expts. III and V a new band appears at 1940 cm^{-1} which could be assigned as the deuterated counterpart. However, there are strong objections to these assignments. Probably the most direct is the intensity of the band at 1940 cm^{-1} relative to those of the bands at 856 and 1860 cm^{-1} in Expt. III. The band at 1940 cm^{-1} seems to grow more rapidly during photolysis and disappear more slowly during diffusion than either of the other two bands, the discrepancies in behavior being apparently beyond the uncertainty in the photometry. Furthermore, it would be difficult to rationalize the absence of an isotope shift in the ν_2 band at 1860 cm^{-1} if ν_1 were at 1940 cm^{-1}. Though the assignment of the bands 2493 and 1940 cm^{-1} as ν_1 of HCO and DCO is not definitely ruled out, we regard it to be improbable. We presume that ν_1 for HCO is near 3000 cm^{-1} and it was not observed because of the characteristically low absorption coefficients of C—H stretching modes. The bands at 2493 and 1940 cm^{-1} remain unassigned.

TABLE VI. Structural parameters of the ground state of the gaseous formyl radical (after Herzberg and Ramsay[1]).

$r(C—H)=r(C—D)=1.08$ A (assumed)
$r(C=O)=1.20$ A
$\angle HCO=119°\,30'$
$\nu_3(HCO)=1083\ cm^{-1}$
$\nu_3(DCO)=847\ cm^{-1}$

TABLE VII. Normal coordinate analysis for the formyl radical.

	Calc.	Exptl.
$\nu_2(HCO)$	(1860 cm^{-1})	1860 cm^{-1}
$\nu_3(HCO)$	(1091 cm^{-1})	1091 cm^{-1}
$k(C=O)$	$13.89\cdot10^5$ dynes/cm	...
$k(HCO)$	$0.679\cdot10^{-11}$ dyne-cm	...
$\nu_2(DCO)$	1849 cm^{-1}	1860 cm^{-1}
$\nu_3(DCO)$	839 cm^{-1}	856 cm^{-1}

The assignments of ν_2 and ν_3 provide a basis for normal coordinate analysis. If ν_1 is indeed near 3000 cm^{-1}, it is a reasonable approximation to reduce the order of the G matrix in the usual way. The required structural parameters of the ground state of HCO have been given by Herzberg and Ramsay[1] and are shown in Table VI. Assuming these parameters are applicable to this species in the matrix, we can substitute the frequencies assigned to HCO into the secular determinant and determine

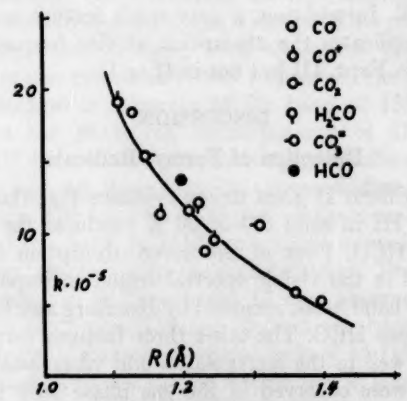

FIG. 2. Force constant *vs* bond length for C—O bonds. References: CO, CO^+: G. Herzberg, *Molecular Spectra and Molecular Structure* (D. Van Nostrand Company, Inc., Princeton, New Jersey, 1950); CO_2, CO_2^-: G. Herzberg, *Infrared and Raman Spectra of Polyatomic Molecules* (D. Van Nostrand Company, Inc., Princeton, New Jersey, 1945), and *Tables of Interatomic Distances and Configuration in Molecules and Ions* (The Chemical Society, London, 1958); H_2CO: E. Ebers and H. Nielson, J. Chem. Phys. 6, 311 (1938) and reference b, Table VIII.

[10] G. Herzberg and K. K. Innes, Can. J. Phys. 35, 842 (1957).

two force constants. These constants permit calculation of the corresponding frequencies of DCO. The results are shown in Table VII. Though the two frequencies assigned to HCO lead to two sets of force constants, only one set is acceptable. The second pair, $5.11 \cdot 10^{+5}$ dynes/cm and $1.85 \cdot 10^{-11}$ dyne-cm, give calculated frequencies for DCO of 1440 and 1105 cm^{-1}, in serious disagreement with experiment.

Bonding in the Formyl Radical

The carbon-oxygen bond length and stretching frequency of formyl can be compared to those of stable molecules. Layton, Kross, and Fassel[11] plotted C—O bond length *vs* frequency for about fifty compounds and deduced a correlating curve. This curve suggests that a bond length of 1.20 A corresponds to a C—O stretching frequency of 1800 cm^{-1}. The observed frequency 1860 cm^{-1} differs from this prediction by an amount within the scatter of the data defining the curve of Layton *et al.*

A more meaningful comparison is to be found in the bond length-force constant correlation. Figure 2 shows a plot based on well-known molecules. Again the datum point for HCO agrees reasonably well with the smooth curve based on the data for stable molecules. The carbon-oxygen bond of formyl is thus found to be a somewhat stronger bond than that of formaldehyde. This shows that the formyl radical has the expected structure

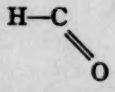

and not the unlikely but possible[1] alternate structure,

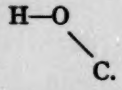

An interesting comparison is found in the force constants and structural parameters of HCO, H_2CO, and HNO. As seen in Table VIII, formyl resembles formaldehyde more nearly than does nitroxyl, though nitroxyl is isoelectronic with formaldehyde. Formyl retains the angular arrangement appropriate to sp^2 hybridization and the carbon-oxygen bond is slightly stronger than that of formaldehyde. Nitroxyl, on the other hand, has approximately the angle of sp^3 hybridization and the N—O bond is slightly weaker than a normal double bond (e.g., compare the N—O bond of nitrous acid, 1.20A).[12]

TABLE VIII. Structural parameters of molecules resembling the formyl radical.

	HNO	HCO	H_2CO
No. valence electrons	12	11	12
∠HXO	108°[a]	120°[1]	125° 48'[b]
r(X—O)	1.23 A	1.20 A	1.23 A
k(X=O)·10^{-5}	10.5[a]	13.9	12.3
k(HXO)·10^{+11}	0.67[a]	0.68	HCO 0.83 HCH 0.38

[a] F. W. Dalby, Can. J. Phys. **36**, 1336 (1958).
[b] Davidson, Stoicheff, and Bernstein, J. Chem. Phys. **22**, 289 (1954).

[11] Layton, Kross, and Fassel, J. Chem. Phys. **25**, 135 (1956).

TABLE IX. Thermodynamic properties of HCO (cal/deg-mole).

T °K	C_p°	$(H°-H_0°)/T$	$-(F°-H_0°)/T$	$S°$
273.16	8.18	7.99	43.60	51.59
298.16	8.26	8.01	44.30	52.31
300	8.27	8.01	44.35	52.36
400	8.70	8.13	46.67	54.79
500	9.18	8.29	48.50	56.79
600	9.66	8.48	50.02	58.50
700	10.11	8.68	51.35	60.03
800	10.52	8.88	52.52	61.40
900	10.89	9.09	53.58	62.66
1000	11.22	9.28	54.55	63.83
1100	11.50	9.47	55.44	64.91
1200	11.76	9.65	56.27	65.92
1300	11.98	9.82	57.05	66.87
1400	12.17	9.98	57.78	67.77
1500	12.34	10.13	58.48	68.62
2000	12.92	10.77	61.49	72.25
3000	13.43	11.58	66.02	77.61
4000	13.63	12.07	69.43	81.50
5000	13.73	12.40	72.16	84.55

The bonding of HCO has been discussed by Walsh[13] in terms of a bond angle correlation diagram and by Linnett[14] in somewhat greater detail. From the correlation diagram, the expected symmetry of the ground state is $^2A'$. However, the spectroscopic data of Herzberg and Ramsay[1] lead them to suggest that the lower state of the observed electronic transition is more probably $^2A''$. There remains the question of whether the electronic transition involves the ground state. We feel that the observation of this same transition with a sample at 20°K (in the present work) supports the belief that the lower state is indeed the ground state. Hence there seems to be a conflict in the two deductions concerning the symmetry of the ground state of HCO.

Thermodynamic Properties of the Formyl Radical

The vibrational frequencies and moments of inertia of HCO provide a basis for calculation of its thermodynamic properties.[15] The structural parameters given in Table VI give a product of the three moments of

[12] Jones, Badger, and Moore, J. Chem. Phys. **19**, 1599 (1951).
[13] A. D. Walsh, J. Chem. Soc. **1953**, 2288.
[14] J. W. Linnett, Can. J. Chem. **36**, 24 (1958).
[15] Ribaud has estimated thermodynamic properties for both HCO and HOC [G. Ribaud, Publ. sci. et tech. ministère air (France) No. **266**, 143 (1952)]. Presumably these values are based upon guesses of the structure and the vibrational frequencies. The frequencies are not specified. Apparently the vibrational contributions to the free energy and to the entropy were omitted, presumably unintentionally.

inertia equal to $4.73 \cdot 10^{-118}$ g^3—cm^6. Our calculations are based on the frequencies 3000, 1860, and 1083 cm^{-1} using the harmonic oscillator approximation. The first frequency is our guess of ν_1, 1860 cm^{-1} is taken from the present work, and 1083 cm^{-1} is the value of ν_3 deduced by Johns and Ramsay.[2] The results are collected in Table IX. The free energy function would be changed by +0.08 cal/deg mole at 1500°K if ν_1 were as low as 2490 cm^{-1} and the entropy by +0.21 eu at this same temperature. At 300°K, the changes would be negligible.

Reaction H+CO=HCO

The reaction of H atoms with carbon monoxide in the gas phase can be induced by mercury photosensitized decomposition of H_2.[16–19] The direct reaction of H atoms with CO was postulated although Farkas and Sachsse proposed a third body is necessary.[19] Of more direct relation to the present work are the experiments of Geib and Harteck.[20] These workers mixed hydrogen atoms (from a discharge tube) with carbon monoxide at 83°K. No reaction was detected (chemical methods were used). Since reaction is obtained under the photolytic matrix conditions, the result of Geib and Harteck could be attributed to an appreciable activation energy for the reaction of H atoms with CO or to destruction of HCO by H atoms to give H_2 and CO.

It may be added that the conditions under which HCO was prepared in the present work might be approximated in certain astrophysical phenomena. For example, H atoms could react with CO in the interstellar dust particles and in comets.[21]

[16] H. S. Taylor and A. L. Marshall, J. Phys. Chem. **29**, 1140 (1925).
[17] W. Frankenberger *et al.*, Z. Elektrochem. **36**, 757 (1930).
[18] M. Barak and H. S. Taylor, Trans. Faraday Soc. **28**, 569 (1932).
[19] L. Farkas and H. Sachsse, Z. physik. Chem. **B27**, 111 (1934).
[20] K. H. Geib and P. Harteck, Ber. **66B**, 1815–1825 (1933).
[21] G. Herzberg, Mem. soc. roy. sci. Liège **15**, 291 (1955).

CONCLUSIONS

The spectroscopic evidence provides a conclusive identification of the formyl radical in these matrix experiments. Since the matrix electronic absorptions are the same as those observed in the gas phase photolysis experiments,[1] this work shows that the absorption spectrum observed by Herzberg and Ramsay definitely involves the ground state. The infrared absorptions provide detailed information about the bonding in this free radical and a basis for calculation of its thermodynamic functions.

This work provides the first positive infrared identification of a triatomic free radical by use of the matrix isolation method (excepting, of course, NO_2). The technique differs in character from that used in earlier experiments in this laboratory; the matrix is selected because of its potential reactivity with the photolysis products rather than because of its inertness. This is similar to the experimental method used by Ingram and co-workers.[22] These workers produce free radicals by photolysis of H_2O_2 with the intent of inducing hydrogen abstraction from various matrices (using the electron spin resonance detection method). We feel the reactive matrix method constitutes an effective way of circumventing the inhibition of photolysis by the cage effect.

ACKNOWLEDGMENT

We would like to thank Dr. Bruce Mahan for many helpful discussions concerning this work. Grateful appreciation is expressed for research support by the American Petroleum Institute Research Project 54 and the United States Air Force through the AFOSR of the Air Research and Development Command, under Contract No. 49(638)-1.

[22] For a summary, see M. Fujimoto and D. J. E. Ingram, Trans. Faraday Soc. **54**, 1304 (1958).

THE JOURNAL OF CHEMICAL PHYSICS VOLUME 32, NUMBER 3 MARCH, 1960

Correlation of Rates of Intramolecular Tunneling Processes, with Application to Some Group V Compounds

R. STEPHEN BERRY

Department of Chemistry, The University of Michigan, Ann Arbor, Michigan

(Received October 19, 1959)

A method is presented whereby the WKB expression for tunneling frequencies permits correlation of these frequencies for members of homologous series of molecules. The necessary data required are the tunneling rate for one member of the series, and structural parameters and vibrational frequencies for all members of interest. The method is applied to ND_3, NF_3, PH_3, and AsH_3, using NH_3 as the molecule whose frequency is known. The method also is used to support the hypothesis that pseudorotation occurs in the trigonal bipyramids PF_5 and PCl_5.

I. INTRODUCTION

THE study of intramolecular tunneling motions has focused on the evaluation of two characteristic quantities: the energy level splittings or tunneling frequencies, on one hand, and the heights of energy barriers inhibiting internal motions, on the other. Barrier heights have been examined extensively[1] because they are sensitive parameters and easily understood whenever the shape of a barrier is well established. And in the class of molecules for which barriers are best known, the barrier shape is well represented by a cosine function.[2] In contrast, there are many systems which can exhibit intramolecular tunneling for which the barrier shape is not well established, and, in fact, for which tunneling may have been observed for but one or two members of a large series. When one is faced with such a situation, it is more useful to be able to estimate the tunneling frequency than to try to evaluate a barrier height. First, the tunneling frequency or energy-level splitting is often directly observable; second, the barrier height is meaningful only if the form of the potential-energy surface is known. With relatively exact data regarding the energy-level separations, one can try to investigate the shape of the potential in detail. Without such information, the barrier height itself gives very little information about the observable properties and dynamical behavior of a molecule. It therefore becomes useful to be able to estimate tunneling frequencies by some process which does not depend in any critical way on exact shapes or heights of potential barriers.

The ensuing discussion develops a method for estimating tunneling frequencies for members of a homologous series of compounds. The motivation for this treatment is twofold. First, hopefully, it will provide a semiquantitative method whose accuracy is sufficient to allow one to select the appropriate experimental technique for determining any desired tunneling frequency in the laboratory. It should enable one, for example, to choose between infrared, microwave, and radio-frequency spectroscopy as possible tools for determining a given tunneling rate. Second, the method is used to develop a possible interpretation of the observed behavior of PF_5 and PCl_5, an interpretation based on the hypothesis that internal tunneling occurs in these molecules.

In Sec. II, a general treatment is developed in which one obtains tunneling frequencies for any member of a homologous series if the appropriate frequency is known for a single member. The method, based on the Dennison-Uhlenbeck formulation of the WKB approach,[3] uses as its primary data the structural parameters and vibration frequencies of the various molecules under consideration. Section III is devoted to the application of the method to the pyramidal molecules ND_3, NF_3, PH_3, and AsH_3; NH_3 is taken as the molecule whose tunneling frequency is known. This application provides a basis from which one can assess the accuracy of the method and determine which of several possible approximations is most appropriate. Finally, Sec. IV contains a discussion of the possibility of internal motion in PF_5 and PCl_5, with an attempt to reconcile the available experimental results for these two molecules.

II. GENERAL FORMULATION

An expression for the tunneling frequency for an internal motion, like the inversion of ammonia, has been derived by Dennison and Uhlenbeck,[3] using the WKB method. They find that if the tunneling motion consists predominantly of one normal vibrational mode, and if ν = tunneling frequency, ν_0 = vibrational frequency, μ = reduced mass for tunneling coordinate, s = displacement along the tunneling coordinate, $s_0 = s$ at which $E = V(s)$, measured from the barrier maximum, $V(s)$ = potential energy, and ϵ = total energy, then

$$\nu = (\nu_0/\pi)e^I, \tag{1}$$

where

$$I = -(1/\hbar)\int_{-s_0}^{s_0}\{2\mu[V(s)-\epsilon]\}^{\frac{1}{2}}ds. \tag{2}$$

[1] For a review of recent results, see E. B. Wilson, Proc. Natl. Acad. Sci. U. S. 43, 816 (1957).

[2] D. R. Herschbach and J. D. Swalen, J. Chem. Phys. 29, 761 (1958).

[3] D. M. Dennison and G. E. Uhlenbeck, Phys. Rev. 41, 313 (1932).

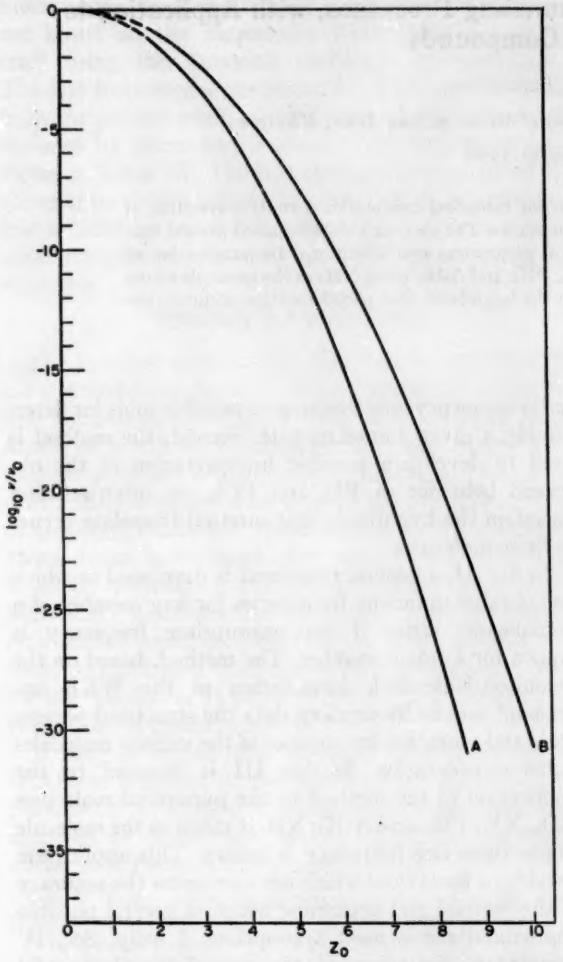

FIG. 1. Logarithmic curves of the ratio of the tunneling frequency ν to the principal vibrational frequency ν_0 along the tunneling coordinate, vs the reduced distance Z_0 (number of classical amplitudes for oscillator of frequency ν_0) from the potential minimum to the potential barrier maximum. Curve A represents the quadratic approximation, Curve B the cosine form.

The expression for I can be integrated for a variety of potentials V. With the barrier height $V(s=0)$ sufficiently high, so that two or more vibrational levels lie below the barrier, it is convenient for us to change the variable of integration. When V is high, the lowest vibrational state is approximately that of a harmonic oscillator with frequency $\omega_0=2\pi\nu_0$; we introduce the variable

$$Z=(\mu\omega_0/\hbar)^{\frac{1}{2}}r, \tag{3a}$$

where r is the displacement along the tunneling coordinate with the origin at a potential minimum. Then if R is the distance from the origin to the potential maximum, we let

$$Z_0=(\mu\omega_0/\hbar)^{\frac{1}{2}}R. \tag{3b}$$

The dimensionless variable Z has as its unit the classical amplitude of oscillation for an oscillator of frequency ω_0, in its lowest quantum state. Therefore at s_0, $Z=1$. The expression for I becomes

$$I=-2(2/\hbar\omega_0)^{\frac{1}{2}}\int_1^{Z_0}[V(Z)-\epsilon]^{\frac{1}{2}}dZ. \tag{4}$$

If we let $\epsilon=\frac{1}{2}\hbar\omega_0$, then

$$I=-2\int_1^{Z_0}[V(Z)/\epsilon-1]^{\frac{1}{2}}dZ, \tag{5}$$

which is a particularly useful form to use for the integration. For most reasonable potentials, V has a quadratic leading term, so that the tunneling frequency will vary roughly as

$$\nu\sim\exp-Z_0^2f(Z_0), \tag{6}$$

where $f(Z_0)$ is constant or slowly varying compared with Z_0^2. If V is formed from two intersecting parabolas, then the integrated expression gives, for the nth vibrational level,

$$I_q=-[Z_0(Z_0^2-2n-1)^{\frac{1}{2}}-(2n+1)\log Z_0+(Z_0^2-2n-1)^{\frac{1}{2}}]. \tag{7}$$

Alternatively, if V is represented as a cosine function,

$$V_{\cos}=\tfrac{1}{2}V_0[1-\cos(\pi Z/Z_0)], \tag{8}$$

then for a state of energy ϵ,

$$I_{\cos}=(16\sqrt{2}/\pi^3)Z_0^2[E(k)-(\epsilon/V_0)K(k)], \tag{9}$$

where $k=[(V_0-\epsilon)/V_0]^{\frac{1}{2}}$ and $E(k)$ and $K(k)$ are the complete elliptic integrals of the second and first kinds, respectively. Approximating ϵ as $\hbar\omega_0/2$ as we have done, with ω_0 the circular frequency for a harmonic oscillator

TABLE I. Data used for treatment of NH_3-like molecules.

Molecule	r_{X-Y} (A)	θ[a]	ν_2[b] (cm^{-1})	μ (amu)
NH_3	1.014[c]	25° 2'[c]	1055[c,d]	2.47[c]
ND_3	1.014[c]	25° 2'[c]	805[d]	4.20[c]
NF_3	1.371[e]	26° 3'[e]	505[f]	11.24
PH_3	1.42[g]	32° 45'[g]	992[h]	2.73
AsH_3	1.52[g]	33° 50'[g]	974[i]	2.88

[a] θ is the angle between the X—Y bond and the plane perpendicular to the molecular symmetry axis.
[b] Frequencies are observed values except for NH_3, ND_3, and AsH_3, where harmonic frequencies were used (see reference 11 and d, below).
[c] See reference 12.
[d] D. M. Dennison, Revs. Modern Phys. 12, 175 (1940).
[e] P. Kisliuk, J. Chem. Phys. 22, 86 (1954).
[f] Bailey, Hale, and Thompson, J. Chem. Phys. 5, 274 (1937).
[g] C. C. Loomis and M. W. P. Strandberg, Phys. Rev. 81, 798 (1951); L. S. Bartell and R. C. Hirst, J. Chem. Phys. 31, 449 (1959).
[h] V. M. McConaghie and H. H. Nielsen, J. Chem. Phys. 21, 1336 (1953).
[i] V. M. McConaghie and H. H. Nielsen, Phys. Rev. 75, 633 (1949).

TABLE II. Parameters, tunneling frequencies and times for NH_3-like molecules. Upper values are taken with Y_3 moving as a rigid triangle, lower values with the X—Y bond length held constant.

Molecule	Quadratic approximation Z_0	ν(sec^{-1})	τ(sec)	Cosine approximation Z_0	ν(sec^{-1})	τ(sec)
NH_3	2.88			3.42	2.3786×10^{10} (obs.)[a]	
ND_3	3.29	1.84×10^{9}	2.7×10^{-10}	3.91	1.43×10^{9} 1.6×10^{9} (obs.)[a] 1.25×10^{9} (calc.)[b]	3.5×10^{-10}
NF_3	5.96 5.98	0.031 0.023	16 .22	7.08 7.10	0.015 0.012	33 42
PH_3	5.26 5.38	156. 45.2	3.2×10^{-3} 1.1×10^{-2}	6.25 6.39	78.5 21.4	6.4×10^{-3} 2.3×10^{-2}
AsH_3	5.90 6.06	0.130 0.020	3.9 25	7.00 7.19	5.9×10^{-2} 1.5×10^{-3}	8.5 53

[a] See reference 4.
[b] See reference 4 or 8.

whose force constant is the same as that of V_{cos}, then Eq. (9) can be simplified by the substitution

$$\epsilon/V_0=\pi^2/4Z_0^2. \tag{10}$$

In both these cases, the tunneling frequency is indeed roughly dependent on $\exp(-AZ_0^2)$. This suggests that one might correlate tunneling frequencies for similar molecules by assuming any reasonable potential, providing (a) one knows the tunneling frequency for one molecule of the set, and (b) the tunneling coordinate is dominated by one normal mode, or at least by modes of comparable frequency. Then the quantity Z_0 becomes a parameter of correlation only, and depends on the potential form chosen; at the same time the form of Z_0 demands that for any two substances A and B, their Z_0 parameters be related by the condition that

$$Z_0(\mathrm{A})/Z_0(\mathrm{B})=(\mu_A\omega_{0A}/\mu_B\omega_{0B})^{\frac{1}{2}}(R_A/R_B). \tag{11}$$

The masses μ_A and μ_B, the frequencies ω_{0A} and ω_{0B}, and the distances R_A and R_B are determined in a great number of cases by the symmetry, the structural parameters, and the normal vibration frequencies. Consequently one can pick a likely analytical form for V, and reading values from a plot of $\log_{10}(\nu/\nu_0)$ *vs* Z_0, determine the approximate tunneling rate for any member of a homologous series, knowing previously the rate for one member only.

In Fig. 1 are plotted the curves of $\log_{10}(\nu/\nu_0)$ *vs* Z_0 for the cosine and parabolic potentials. The two curves are nearly parallel, and the similarity of results they give is demonstrated in Sec. III.

III. APPLICATION TO SOME XY_3 PYRAMIDAL MOLECULES

The tunneling process corresponding to the inversion of NH_3 and similar molecules provides a straightforward test of the method developed in Sec. II. Inversion splittings are well known for NH_3 and ND_3, but have not been observed spectroscopically for any heavier homologs.[4] The problem of inversion frequencies has been treated by several authors.[5–11] Of principal interest have been the barrier shape and height although there has been one method developed to correlate the NH_3, PH_3, and AsH_3 barriers and tunneling frequencies.[11] The most accurate potential for which both NH_3 and ND_3 tunneling frequencies are known is the one developed by Manning[8]; this, together with the observed results, will serve as a standard for our approximation method.

The tunneling frequencies of ND_3, NF_3, PH_3, and AsH_3 were calculated four ways; the two potentials were each tried with the assumptions that in XY_3, the XY bond lengths remain constant, or alternatively, that Y_3 moves as a rigid triangle. The tunneling coordinate of NH_3 almost certainly is dominated by one normal coordinate, the ν_2 vibration. This vibration in turn, expressed in valence force-field coordinates, consists principally of the S_2 angle-bending vibration[12]:

$$S_1/S_2=1/10.96,$$

based on the data contained in Table I. (This value is

[4] C. H. Townes and A. L. Schawlow, *Microwave Spectroscopy* (McGraw-Hill Book Company, Inc., New York, 1955).
[5] F. Hund, Z. Physik **43**, 805 (1927).
[6] P. M. Morse and E. C. G. Stueckelberg, Helv. Phys. Acta **4**, 337 (1931).
[7] N. Rosen and P. M. Morse, Phys. Rev. **42**, 210 (1932).
[8] M. F. Manning, J. Chem. Phys. **3**, 136 (1935).
[9] F. T. Wall and G. Glockler, J. Chem. Phys. **5**, 314 (1937).
[10] R. R. Newton and L. H. Thomas, J. Chem. Phys. **16**, 310 (1948).
[11] C. C. Costain and G. B. B. M. Sutherland, J. Phys. Chem. **56**, 321 (1952).
[12] G. Herzberg, *Infrared and Raman Spectra* (D. Van Nostrand Company, Inc., Princeton, New Jersey, 1945). See especially, pp. 154–157, 175–177.

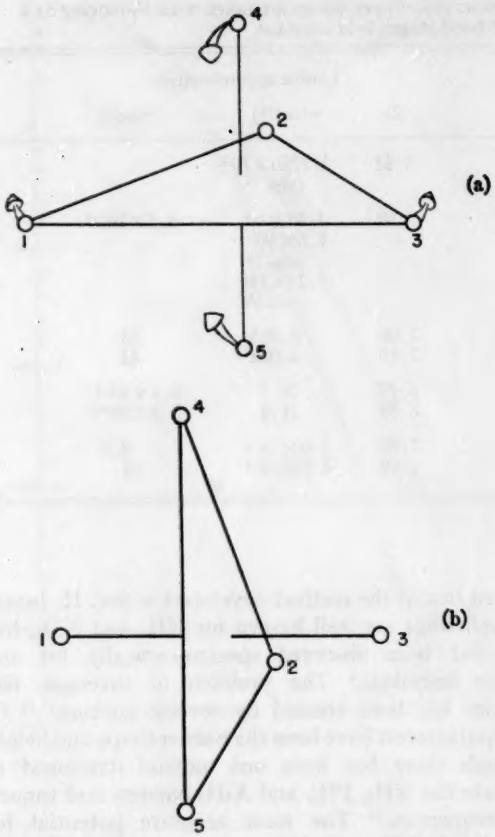

FIG. 2. Schematic representation of pseudorotation in the trigonal bipyramid.

not in exact agreement with that of reference 11; by using this value for S_1/S_2, the potential computed in the Costain-Sutherland treatment is about 100 cm^{-1} less than the value reported.) We therefore take the ν_2 vibration as the one to be substituted for ν_0 in Eq. (1) and (11); as Costain and Sutherland[11] point out, it is more appropriate to use the normal vibration frequency of the state in question than the observed infrared frequency. This has been done whenever normal frequencies were available. The effective masses have been taken as constants, with

$$\mu = 3m_x m_y/(m_x+3m_y).$$

The expression is almost unaffected by the angle-dependent contribution which would appear in a rigorous treatment. Structural parameters, effective masses, and vibration frequencies are given in Table I.

Table II gives the results obtained with the four sets of assumptions. Several points should be noted. First, the frequencies found for ND_3, with quadratic and cosine potentials of 1840 and 1430 mc, respectively, should be compared with the observed value of 1600 mc and with the value computed by Manning as 1250 mc. Second, the tunneling frequencies for PH_3 and AsH_3 are much closer to each other than the frequency of NH_3 to either. This seems quite reasonable in light of the similarities in bond lengths, angles, effective masses, and frequencies. It also is interesting that NF_3, with its rather flat structure, tunnels at a rate very close to AsH_3; in the former, the effective mass is the principal cause of the low frequency; in the latter, the actual distance which the hydrogens must move is the major source of the slow rate. Finally, the most important of all, we see that the various approximations all lead to the same order of magnitude in their predictions, so that one might have enough confidence in the method to estimate rates for the purpose of designing experiments.

IV. PENTAHALIDES OF PHOSPHORUS

The molecules PF_5 and PCl_5 have been the subject of a variety of studies which have suggested the possibility that they might exhibit internal motions. Both molecules are trigonal bipyramids so that, at any instant, the halogen atoms occupy two kinds of sites; three are assigned to equatorial positions, and the other two to polar positions. The F^{19}-resonance spectrum of PF_5 has been observed by Gutowsky, McCall, and Slichter.[13] They report only a single fluorine resonance peak (split into a doublet due to P−F coupling), so that either the five fluorines are equivalent to a measurement as slow as NMR, or the chemical shifts and P−F couplings are accidentally identical for fluorines at both kinds of sites. The latter possibility is rather unlikely, particularly in light of the data to be cited regarding PCl_5, so it will not be considered further.

The infrared spectrum of PF_5 has been observed by Gutowsky and Liehr,[14] who find an apparently normal spectrum for a trigonal bipyramid. This suggests that the fluorine atoms may exchange at a rate slow compared with the time necessary to establish sharp vibrational levels, and fast compared with the inverse line widths associated with nuclear resonance measurements. Hence any exchange process which the fluorines

TABLE III. Data used for treatment of PF_5 and PCl_5.

Molecule	r_{X-Y} of XY_2 (A)	r_{XY} of XY_2 (A)	ν_0 (cm^{-1})
PF_5	1.57[a]	1.57[a]	534[c] or ~180 (assumed)
PCl_5	2.04[b]	2.18[b]	335[d] or 100[d]

[a] L. O. Brockway and J. Y. Beach, J. Am. Chem. Soc. **60**, 1836 (1938).
[b] See reference 16.
[c] See reference 14.
[d] See reference 15.

[13] Gutowsky, McCall, and Slichter, J. Chem. Phys. **21**, 279 (1953).
[14] H. S. Gutowsky and A. D. Liehr, J. Chem. Phys. **20**, 1652 (1953).

TABLE IV. Parameters, tunneling frequencies and times for PF_5 and PCl_5. Upper values are derived using the high-frequency values of Table III, lower values using the lower frequencies.

Molecule	Quadratic approximation			Cosine approximation		
	Z_0	$\nu(\text{sec}^{-1})$	τ	Z_0	$\nu(\text{sec}^{-1})$	τ
PF_5	4.37	10^5 (assumed)		5.17	10^5 (assumed)	
PCl_5	6.41	2.4×10^{-5}	5.8 hr	7.59	9.6×10^{-4}	12.8 hr
		1.2×10^{-4}	41 sec		6×10^{-4}	1.4 min

undergo should occur at a frequency between about 10^{-8} and 10^{-2} sec.

Now we turn to the data regarding PCl_5. Infrared and Raman spectra have been taken and analyzed by Wilmshurst and Bernstein.[15] The structure is known from electron diffraction work of Rouault.[16] The possibility of internal exchange is suggested in the isotopic exchange studies of Downs and Johnson.[17,18] They report that three chlorines are capable of very rapid exchange, giving complete equilibration in 5 sec or less; the other two chlorine nuclei do exchange, but attain 90% of their equilibrium isotopic concentration only after 100 min. Presumably the two slowly exchanging chlorines are those occupying the polar positions, and the rate difference truly is due to a difference in reactivity of the two kinds of sites. By inference, then, it is likely that the two kinds of sites in PF_5 are also different chemically, so that instantaneous determination of electron density around the two positions would yield two different results. The reactivity of chlorines in PCl_5 thus lends credence to the hypothesis that some kind of exchange process establishes the F^{19} equivalence in PF_5 for NMR observations.

One particularly attractive possible mechanism for the exchange process in PF_5 and PCl_5 is a purely internal pseudorotation as indicated in Fig. 2. The motion leaves the molecule in a rotated and permuted form of its original state.[19] If the internal exchange or pseudorotation hypotheis is tenable, the disparity between the necessary PF_5 and PCl_5 exchange rates must be rationalized. For this we may use the method developed in Sec. II.

The data, including the vibration frequencies of possible importance, are collected in Table III. It would be desirable to be able to attribute the tunneling coordinate with a single normal mode, but unfortunately this cannot be done necessarily. In addition to the problem of finding normal coordinates for PF_5, whose spectrum is not entirely known, there seems to be some doubt about the assignments of the ν_6 and ν_7 e' vibrations. The tentative assignment of Gutowsky and Liehr[14] suggested that the PX_3 deformation is ν_6, at 534 cm^{-1} for PF_5. The normal coordinate analysis of Wilmshurst and Bernstein[15] gives ν_6 as the PX_2 polar bend in PCl_5 at 335 cm^{-1}, and ν_7 as the PX_3 deformation at 100 cm^{-1}. The assignments of Wilmshurst and Bernstein however, may be questioned because they found it necessary to call the 394-cm^{-1} band degenerate, assigning it to two vibrations of the same symmetry, the ν_1 and ν_2 a_1' modes. It is conceivable but surprising that such a combination shows no significant splitting. In any case, we can compute the data of interest using both the 534 and 335-cm^{-1} bands and the assumed frequency of 180 cm^{-1} for PF_5 with the observed 100-cm^{-1} PCl_5 band. These two combinations give results which are all relatively satisfactory for reconciling the tunneling rates.

We assume that the tunneling frequency of PF_5 is halfway between the limits set by its normal infrared spectrum and its single NMR peak; namely, we assume that $\nu(PF_5)\sim10^5$ sec^{-1}. Then with the assistance of Fig. 1, we compute the corresponding Z_0. To calculate the PCl_5 tunneling frequency, we need to know the distance traveled by the point representing the tunneling particle. We supposed that the halide moves along a straight line from one kind of position to the other, so that the P—X distance varies linearly with displacement. Then the average P−X distance along this coordinate is used to calculate Z_0 for PCl_5. Note that in contrast to the NH_3-like molecules, the moving nuclei in trigonal bipyramids all must travel through the same angle.

The results of the calculations are shown in Table IV. It is rather surprising and somewhat fortuitous that the various approximations do give tunneling times which bracket the characteristic time which would obtain if pseudorotation governed the slow exchange rate in PCl_5. The important conclusion to be drawn is simply that the hypothesis of pseudorotation in PF_5 and PCl_5 is consistent with the experimental data now available. Further experimentation is clearly necessary to confirm or reject the hypothesis.

Other related systems such as SF_4 and ClF_3 have been studied by Muetterties and Phillips.[20,21] It has been

[15] J. K. Wilmshurst and H. J. Bernstein, J. Chem. Phys. **27**, 661 (1957).
[16] M. Rouault, Ann. phys. **14**, 78 (1940).
[17] J. J. Downs and R. E. Johnson, J. Chem. Phys. **22**, 143 (1954).
[18] J. J. Downs and R. E. Johnson, J. Am. Chem. Soc. **77**, 2098 (1955).
[19] The author is indebted to Dr. F. T. Smith who first pointed out to him the existence of the pseudorotation operation of a trigonal bipyramid.
[20] E. L. Muetterties and W. D. Phillips, J. Am. Chem. Soc. **79**, 322 (1957).
[21] E. L. Muetterties and W. D. Phillips, J. Am. Chem. Soc. **81**, 1084 (1959).

pointed out that these compounds are capable of exhibiting pseudorotation,[22] and the results of NMR studies by Muetterties and Phillips[20,21] are consistent with this hypothesis. Chemical exchange is, however, at least as likely for these molecules.[23] Therefore we do not suggest that pseudorotation is necessarily the explanation for the observed line narrowings which appear as sample temperatures are increased. It is important, nonetheless, to note that the results of Muetterties and Phillips require that the pseudorotation times for SF_4 and ClF_3 be considerably longer than for PF_5. This is rationalized easily by the following argument. In PF_5, the phosphorus atom lies at the center of gravity and, therefore, need not move during the course of pseudorotation. Since SF_4[24,25] and ClF_3[26,27] are not symmetrical structures, the heavy atoms do not lie at the molecular centers of gravity and therefore must participate in pseudorotation. The large effective masses for motion along the tunneling coordinates would depress the tunneling rates, presumably by several orders of magnitude.

[22] R. S. Berry, Revs. Modern Phys. (to be published).
[23] M. T. Rogers and J. J. Katz, J. Am. Chem. Soc. **74**, 1375 (1952).
[24] Dodd, Woodward, and Roberts, Trans. Faraday Soc. **52**, 1052 (1955).
[25] Cotton, George, and Waugh, J. Chem. Phys. **28**, 994 (1958).
[26] R. D. Burbank and F. N. Bensey, J. Chem. Phys. **21**, 602 (1953).
[27] D. F. Smith, J. Chem. Phys. **21**, 609 (1953).

V. SUMMARY

A method has been presented whereby the tunneling frequencies ν for members of a homologous series of molecules may be estimated. The method depends on knowledge of the tunneling rate for one member of the series, and the vibrational frequencies and structure for this molecule and for any molecule whose tunneling frequency is desired. The method, useful only for finding orders of magnitude of ν, depends on the insensitivity of the tunneling frequency to barrier shape, and on the assumption that barrier shapes for the various members of the series are similar.

The method is applied to the NH_3-like molecules ND_3, NF_3, PH_3, and AsH_3. The ND_3 rate is close to the observed value if either a quadratic or cosine potential is assumed. The PH_3 rate is calculated to be of the order of 10 sec^{-1}, while the NF_3 and AsH_3 rates are of the order of 1 min^{-1}.

The method also is applied to correlate the rates of the hypothesized pseudorotation of PF_5 and PCl_5. If a characteristic time of 10^{-5} sec is assumed for PF_5, then the computed time for PCl_5 lies between $\frac{1}{2}$ min and 12 hrs. The hypothesis of pseudorotation therefore is consistent with the spectra and exchange experiments which have been performed on these two molecules.

ACKNOWLEDGMENT

The author would like to thank Professor R. B. Bernstein and Professor K. T. Hecht for their helpful comments.

Letters to the Editor

THE Letters to the Editor section is subdivided into three parts entitled Communications, Comments and Errata, and Notes. These three sections are all subject to the same limitations on length. The textual material of each Letter is limited to a number of words equal to 950 minus the following: (a) 200 words for each average-sized figure; (b) 50 words for each displayed equation; (c) 7 words for each line of table including headings and horizontal rulings. No proof will be sent to the authors of "Communications" and "Comments and Errata." Proof will be sent to the authors of "Notes." The publication charge for Letters is $30 per page, with a minimum of $30 per Letter. If honored, the Institution will be entitled to 100 reprints without covers. See issues of May–September, 1957, for descriptions of categories.

Communications

Critical Opalescence of Polystyrene Solutions*

P. DEBYE, H. COLL, AND D. WOERMANN

Cornell University, Ithaca, New York

(Received January 15, 1960)

IN a recent publication[1] on critical opalescence in liquid mixtures it was shown how the intensity of scattered light, measured under an angle θ with respect to the incident beam, can be related to the range of molecular forces characteristic for the components of the mixture. In the vicinity of the consolute point, for light vertically polarized with respect to the plane of observation, this relationship can be expressed in the simplified form[2]

$$I=\frac{CT/T_c}{(\Delta T/T_c)+(8\pi^2/3\lambda^2)l^2\sin^2\theta/2} \qquad (1)$$

I = intensity of scattered light
C = constant characteristic for the system
T = temperature, °K
T_c = critical (consolute) temperature, $\Delta T=T-T_c$
λ = wavelength of light in medium
l = average range of forces between component molecules
θ = angle of scattering.

Thus, a plot of $1/I$ *vs* $\sin^2\theta/2$ measured at various temperatures close to T_c should lead to parallel straight lines whose intercept is proportional to ΔT, provided the temperature range considered is small enough so that $T/T_c\cong 1$.

The validity of Eq. (1) has already been established for a system of small molecules, *viz.*, carbon tetrachloride-perfluoromethylcyclohexane.[3] We made the system polystyrene-cyclohexane the subject of our studies in order to show that polymer solutions exhibit an analogous behavior. Because of the expected larger values of the interaction range l in the case of polymers, angular dependence of I should be observable at much greater temperature distances from T_c than in the case of small molecules. From the experimental standpoint this advantage is offset by the range over which molecular weights usually distribute in polymer fractions. This may give rise to precipitation of high-molecular weight components already several degrees above the theoretical "average" consolute temperature.

In our experiments we used polystyrene samples of "narrow" molecular weight distribution which had been prepared by anionic polymerization of styrene.[4] The experimental results which we obtained with a particular fraction, $\bar{M}_n=147\,000$, $\bar{M}_w/\bar{M}_n=1.04$, may serve as an illustration.[5] It should be noted, however, that a quotient $\bar{M}_w/\bar{M}_n$ near unity still corresponds to an appreciable half-width of the distribution curve which in our particular case is 30% of the molecular weight at the maximum of this curve.

The critical concentration $(\phi_2)_{crit}$ of the polymer in cyclohexane was found by measuring the angular dissymmetry of scattered light as a function of concentration. At fixed temperatures of a few tenths of a degree above the experimentally determined point of incipient precipitation T_p, the curve goes through a pronounced maximum at $(\phi_2)_{crit}$, in our case equal to 5.0 vol % of polystyrene.[6] Figure 1 shows plots of $1/I$ *vs* $\sin^2\theta/2$ from data on a solution of critical concentration. The measurements were taken at several fixed temperatures between 0.6 and 1.3°C above T_c. The latter was calculated from the intercepts of Fig. 1.

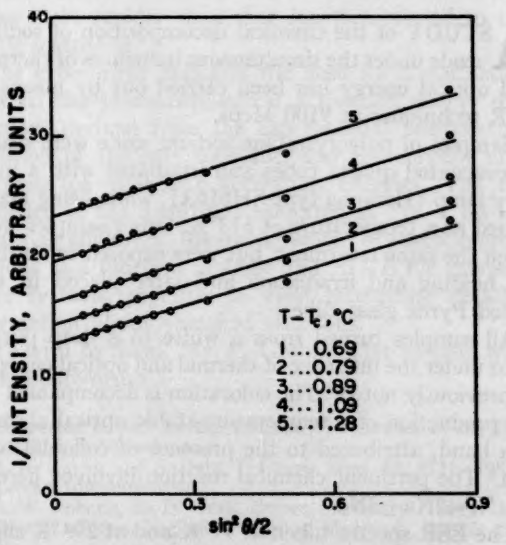

FIG. 1. Polystyrene ($\bar{M}_n=147\,000$) in cyclohexane. Reciprocal intensities as function of $\sin^2\theta/2$. $(\phi_2)_{crit}=5.0$ vol %, $T_c=23.1$°C, $\lambda(vac)=4360$ A.

The difference $T_p - T_c$ was found to be approximately 0.6 degree which is quite reasonable in view of the half-width of the molecular weight distribution in our sample. For the latter a range of T_c of approximately 1.2 degree can be calculated by a formula given by Shultz and Flory.[6]

The parameter l was calculated as 28 A. The end-to-end distance, $(\bar{R}^2)^{\frac{1}{2}}$, of the polymer coil at the theta point (calculated from $R^2=2Na^2$) should be 116 A. Applying the estimate[1] $l^2=R^2/6$ one should expect $l=47$ A, a value appreciably higher than our experimental result. Further work appears to be necessary to explain this small interaction range.

A more detailed report is to be published in the near future.

* This work was supported by grants from the National Science Foundation and the Office of Naval Research.

[1] P. Debye, J. Chem. Phys. **31**, 680 (1959).
[2] See reference 1, Eqs. (27) and (28).
[3] See reference 1, footnotes 5 and 6.
[4] Samples were obtained by courtesy of the Dow Chemical Company, Midland, Michigan.
[5] H. W. McCormick, Dow Chemical Company (private communication).
[6] This value is considerably higher than predicted by the Flory-Huggins theory; cf. A. R. Shultz and P. J. Flory, J. Am. Chem. Soc. **74**, 4760 (1952).

Electron Spin Resonance of Colloidal Sodium in Sodium Azide

G. J. KING, B. S. MILLER, F. F. CARLSON, AND R. C. MCMILLAN

Basic Research Group, Engineer Research and Development Laboratories, Fort Belvoir, Virginia

(Received January 13, 1960)

A STUDY of the chemical decomposition of sodium azide under the simultaneous influences of thermal and optical energy has been carried out by means of ESR techniques at 9100 Mcps.

Samples of polycrystalline sodium azide were sealed in evacuated quartz tubes and irradiated with a mercury lamp (Hanovia type SH616A), while being maintained at a temperature of 573°K. Other samples were given the same treatment, but were exposed to air during heating and irradiation and later placed in unsealed Pyrex glass tubes.

All samples turned from a white to a deep purple color under the influence of thermal and optical energies as previously noted.[1] The coloration is accompanied by the production of a temperature-stable optical absorption band, attributed to the presence of colloidal sodium.[2] The pertinent chemical reaction involved here is $2NaN_3 \rightarrow 2Na+3N_2$.

The ESR spectra taken at 77°K and at 293°K show a strong, highly symmetrical, single-line absorption which we attribute to the spin resonance of metallic sodium electrons. The characteristics of the resonance are given in Table I and are compared to the data of Feher and Kip[3] on colloidal sodium dispersed in oil by ultrasonic methods.

TABLE I. Comparison of data from this investigation with data of Feher and Kip.[a]

	Feher and Kip	This study
Line shape	Lorentzian	Lorentzian
g value (300°K)	2.0015 ± 0.0002	2.0017 ± 0.0002
Spin relaxation time (sec)	6×10^{-9}	7.4×10^{-9} (293°K) 23×10^{-9} (77°K)
Frequency	300 Mcps	9100 Mcps
Colloid size	5 μ	10 to 500 A (optical data)

[a] Reference 3.

The resonance absorption is independent of the presence of air during treatment of the samples thus precluding sodium oxygen interactions.

The g value determined here agrees with the theoretical value of 2.00164 given by Brooks[4] and also the value of 2.00193 given by Yafet.[5]

The decomposition of metal azides would appear to be a convenient method of producing colloidal metal particles of controllable size for ESR experiments. It should, however, be noted that many of the metal azides are highly explosive and poisonous.

The interest of Dr. Z. V. Harvalik in this work is gratefully acknowledged.

[1] Rosenwasser, Dreyfus, and Levy, J. Chem. Phys. **24**, 184 (1956).
[2] B. S. Miller (to be published).
[3] G. Feher and A. F. Kip, Phys. Rev. **98**, 337 (1955).
[4] H. Brooks, Phys. Rev. **94**, 1411 (A) (1954).
[5] Y. Yafet, Phys. Rev. **85**, 478 (1952).

Variation of a Chemical Reaction Cross Section with Energy*

E. F. GREENE, R. W. ROBERTS,† AND J. ROSS

Metcalf Chemical Laboratories, Brown University, Providence, Rhode Island

(Received January 6, 1960)

IN 1955 Taylor and Datz[1] studied the reaction $K+HBr \rightarrow KBr+H$ using molecular beam techniques. They were able to determine temperature-dependent chemical reaction cross sections by measuring the angular distribution of scattered KBr and K. From the variation of these cross sections with the temperature of the oven source they estimated an activation energy of 2.8 kcal/mole for this reaction.

We wish to report some initial results of a molecular beam experiment designed to measure the energy dependence of a chemical reaction cross section. The chem-

ical reaction was that of Taylor and Datz. Because the apparatus has been described elsewhere[2] only a few details will be mentioned here.

The potassium beam is formed by effusion from parallel canals[3] at the exit of a double chambered oven. The back chamber contains liquid potassium at a temperature of 626°K (equilibrium vapor pressure 1.2 mm), and the front chamber temperature, 654°K, determines the most probable speed of the K atoms in the thermal beam effusing from the oven. A velocity selector[4] transmits K atoms with a range of speeds; the half-width of the triangular distribution transmitted is 0.085 v_0, where v_0 is the central speed. The K beam at the detector is ribbon-shaped, 3 mm high and 0.76 mm wide. The scattering center is 68 cm from the exit of the K oven and 1.3 cm from the HBr oven. The HBr appears as a partially collimated effusive spray from a two chambered oven through a 3-mm hole which is covered with Ni mesh (46% transmission, 0.0005-in. thick, 0.0008-in. square holes). The back chamber was at 138°K for which the equilibrium vapor pressure is 1 mm, but the actual HBr pressure may be somewhat lower. The HBr beam is not velocity selected but has a thermal distribution with a most probable speed of 1.8×10^4 cm/sec corresponding to a front chamber temperature of 152°K. Although liquid nitrogen traps and cooled shields were used to maintain a high effective pumping speed for HBr, some HBr appeared throughout the vacuum chamber; we estimate that only 85% of the scattering occurred at the intersection of the two beams. The surface ionization detectors, like the ones used by Taylor and Datz, consisted of two heated wires, one tungsten and one an alloy, 92% Pt−8% W. The tungsten wire was ribbon-shaped with a 0.25-mm× 0.01-mm cross section and ionized both K and KBr, while the alloy wire (0.05-mm diam) ionized only K.

The ions were collected at a negative electrode connected to the input of a vibrating reed electrometer.

Figure 1 shows the ratio of K plus KBr flux to the K flux as a function of the relative initial kinetic energy (*RIKE*) at a scattering angle of 35° in laboratory coordinates. The values at low energy are not equal to unity because of geometrical restrictions on the detectors.

In the present experiment KBr may be formed in a number of final rotational and vibrational quantum states from HBr in a number of initial rotational states. The ordinate in Fig. 1 (minus unity and apparatus corrections) is therefore proportional to the ratio of a weighted sum of elementary differential chemical reaction cross sections to the differential elastic cross section for the scattering of K. The latter is expected to be a decreasing function of *RIKE* and this is confirmed by the dependence of $I_{Pt_{35}°}$ on *RIKE* which shows a decrease, with scatter, by a factor of 2.5 over the range of energies studied. The minimum molecular activation energy, i.e., threshold, for any one of the reaction cross

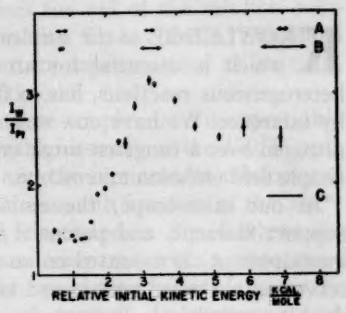

FIG. 1. I_W/I_{Pt} is the ratio of ion current from the W and W–Pt alloy surface ionization detectors, corrected for differences in ionization efficiency. The relative initial kinetic energy is $\frac{1}{2}\mu v_r^2$ where μ is the reduced mass, $m_K m_{HBr}/(m_K+m_{HBr})$, and v_r is the square root of the sum of the squares of the central speed of the K beam, and the most probable speed of the HBr beam. A: spread in *RIKE* corresponding to half-width of HBr energy distribution; B: spread in *RIKE* corresponding to half-width of triangular distribution of K-beam energy transmitted by selector; C: value of the ordinate for thermal K beam. Vertical lines through the points show the estimated reading error.

sections at a scattering angle of 35° is seen to be 1.4 kcal/mole. As the *RIKE* is increased up to 3.3 kcal/mole the percent yield of KBr is also increased. This may be because (a) more thresholds of elementary transitions may be reached, for instance, the molecular activation energy may depend on the quantum numbers J and M of HBr; or (b) each elementary cross section is not a step function of the *RIKE* but may well have a more complex energy dependence. A further increase in the *RIKE* brings a decline in the product formation which indicates that the potential energy surface related to the chemical reaction cross section varies more rapidly than that function related to the elastic scattering.

The experiment indicates the need for a distinction between the phenomenological activation energy of a reaction, derived from the experimental temperature variation of the rate constant, and the concept of a spectrum of molecular activation energies. The dependence of the quantities exhibited in Fig. 1 on the scattering angle, i.e., the measurement of reaction cross sections as a function of angle and *RIKE* for this and other systems, promises to yield interesting detailed information about chemical reactions.

We wish to thank Mr. P. Groblicki for helping with the measurements.

* Supported in part by the Division of Research of the U.S. Atomic Energy Commission.

[1] E. H. Taylor and S. Datz, J. Chem. Phys. 23, 1711 (1955); and private communication.

[2] R. W. Roberts, Ph.D. thesis, Brown University (1959).

† Present address: National Bureau of Standards, Washington, D. C.

[3] J. G. King and J. R. Zacharias, Advances in Electronics and Electron Phys. 8, 2 (1956).

[4] R. C. Miller and P. Kusch, Phys. Rev. 99, 1314 (1955); see also further references therein.

Surface Migration of Nitrogen on Tungsten

GERT EHRLICH AND F. G. HUDDA

General Electric Research Laboratory, Schenectady, New York

(Received January 15, 1960)

KNOWLEDGE of the surface diffusion of nitrogen, which is essential for an understanding of its heterogeneous reactions, has so far been attained only by inference. We have now examined the migration of nitrogen over a tungsten single crystal directly, using a simple field emission microscope.

In our microscope, the emitter assembly (point, support filament, and potential leads for temperature measurement) is mounted on an extended stem, which serves as a Dewar vessel, and is itself surrounded by double cylindrical Dewars in an arrangement resembling a low-temperature field ion microscope.[1] Aimed at the tungsten emitter is a tube which projects through the Dewars and is connected to a gas reservoir through a Granville-Phillips valve. The walls around the emitter are cooled with liquid hydrogen to trap molecules colliding with them; when the valve to the reservoir is opened, the point is exposed to a narrow beam of gas, and a localized deposit forms on one side.

Such a deposit of nitrogen around the 100 and 211 planes of a tungsten tip maintained at 290°K is shown in Fig. 1. This is stable and unchanging with temperature up to 400°K. The area encompassed between the 111 zone lines darkens slowly at ~425°K, and sharp boundaries form at the edges as these regions are filled

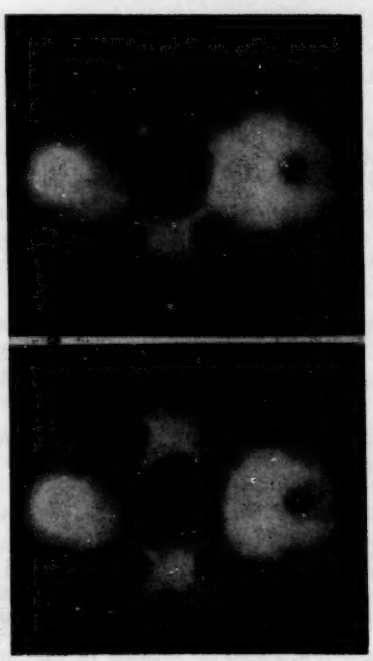

FIG. 1. Nitrogen deposit on W at $T=290$°K. Gas beam at 10 o'clock; (a) initial deposit; (b) deposit after spreading at $T=650$°K.

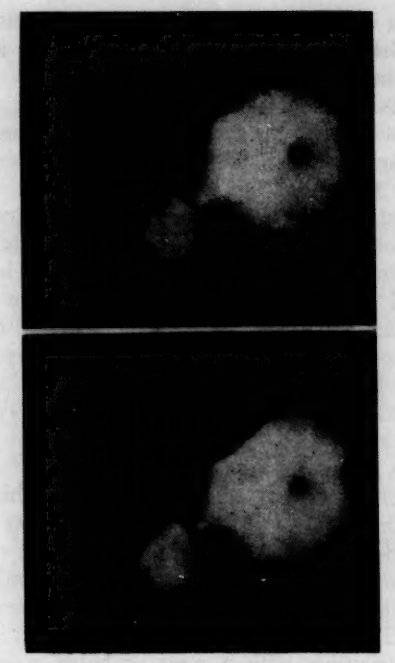

FIG. 2. Nitrogen deposit on W at $T=20$°K; (a) initial deposit; (b) deposit after equilibration at $T\sim45$°K.

by gas diffusing out of the deposit. Further changes can be brought about by raising the tip temperature to 650°K. The nitrogen then encroaches across the zone lines [Fig. 1(b)] and the bright emitting regions centered on the 100 poles gradually contract. At these temperatures the α state has evaporated, and the diffusing species must be nitrogen adatoms.[2] From the rates of migration across the 110 and 111 planes we estimate an activation barrier of ~20 kcal/mole. A much higher activation energy, $V_m\sim35$ kcal/mole, opposes the diffusion over the (116) and (120), which on an atomic model present deep holes to a nitrogen atom.

Deposits on an emitter initially at 77°K show essentially the same temperature behavior, as is expected from our picture of the γ state of nitrogen.[2] Shadowing of a point maintained at 20°K, however, results in a deposit with sharply defined borders [Fig. 2(a)]; small increases in temperature (to ~40°K) suffice to roll these borders toward the (100) [Fig. 2(b)]. Such diffusion is characteristic of two-layer systems in which mobile gas flows over the edge of an immobile layer and there chemisorbs.[3] In this second layer the activation energy for migration is $1.2<V_m<1.9$ kcal/mole, and it thus appears to be held by van der Waals forces only. This constitutes the fourth binding state for nitrogen so far isolated. The border adjacent to the 100 pole, which remains once the supply of physically bound nitrogen is exhausted, is stable to temperature increases even when the (111) regions have achieved their equilibrium gas distribution: It

disappears in the temperature range observed for the diffusion of the high-temperature deposit toward the (100), showing the same dependence of the jump frequency on surface structure. The activation energy χ for the desorption of nitrogen atoms from tungsten is $\sim$153 kcal/mole, and our diffusion experiments thus indicate $V_m/\chi \sim 0.23$. Despite the high valency of nitrogen atoms, this is in good agreement with the results for oxygen and hydrogen.[3]

[1] E. W. Müller, J. Appl. Phys. **28**, 1 (1957).
[2] G. Ehrlich, *Structure and Properties of Thin Films* (John Wiley & Sons, Inc., New York, 1959), p. 423.
[3] R. Gomer and J. K. Hulm, J. Chem. Phys. **27**, 1363 (1957).

Comments and Errata

Comments on "Thermoluminescent Properties of Calcite"

W. L. Medlin

Socony Mobil Oil Company, Inc., Field Research Laboratory, Dallas, Texas

(Received December 21, 1959)

THE results of a recent study of thermoluminescence in calcite showed that the presence of divalent manganese accounted for prominent peaks in the glow curve at 350°K and 470°K.[1] The efficiency of luminescence for the 350°K glow peak was found to be a predictable function of the Mn^{++} concentration but the results for the 470°K peak were erratic and did not fit a smooth curve. Since the intensities of both glow peaks were considerably enhanced by annealing (one hour at 550°C) there was reason to believe that the results were affected by lattice distortions produced during the precipitation and subsequent crystal growth of the samples.

This note describes a more recent investigation of the problem involving hydrothermal precipitation techniques. It has been found that a method which was originally developed for precipitating dolomite and magnesite from solution[2] can also be adapted to the precipitation of calcite. Briefly, the method consists of slowly raising the temperature of a slightly acidic $CaCl_2$ solution containing an appropriate concentration of urea to be about 200°C under 30–60 atmos of CO_2 pressure. At this elevated temperature the urea decomposes to NH_3 and CO_2 and raises the pH of the solution sufficiently to precipitate calcite. Traces of Mn^{++} included in the original solution are coprecipitated as impurity ions in the crystal lattice.

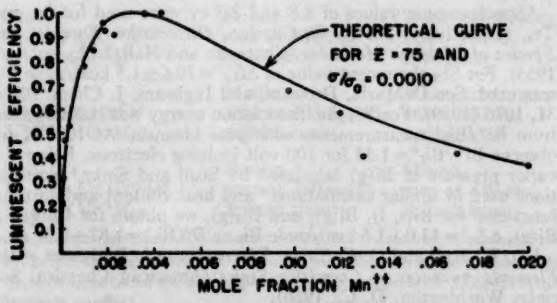

FIG. 1. Efficiency of luminescence as a function of concentration for the 470°K glow peak due to Mn^{++} in calcite.

The glow curves for these samples are not appreciably affected by annealing (the intensity of the 470°K peak is enhanced slightly) and the luminescent efficiency of the 470°K glow peak is a smooth function of the Mn^{++} concentration. This is illustrated in Fig. 1 where the experimental results are compared with a theoretical curve for concentration quenching.[3] The data for the 350°K glow peak are substantially in agreement with the results of the original work. The same values for the parameters Z and σ/σ_a appear to fit the data for both peaks, *viz.*, $Z=75$ and $\sigma/\sigma_a=0.001$. A glow peak which appeared at 200°K in the samples precipitated at room temperature does not appear in any of the samples precipitated at 200°C. This seems to confirm the association of this peak with a dislocation or other lattice distortion which could be removed by annealing.

All of these results confirm the original supposition that lattice imperfections incurred during the room temperature precipitations affect the intensity of the 470°K glow peak and account for the 200°K peak. Evidently, by carrying out the precipitations at elevated temperatures these imperfections are avoided.

[1] W. L. Medlin, J. Chem. Phys. **30**, 451 (1959).
[2] W. L. Medlin, Am. Mineral. **44**, 979 (1959).
[3] P. D. Johnson and F. E. Williams, J. Chem. Phys. **18**, 1477 (1950).

Notes

Stabilities of the Gaseous Molecules, BiSe, BiTe, and SbTe*

Richard F. Porter and C. W. Spencer

Departments of Chemistry and Metallurgical Engineering, Cornell University, Ithaca, New York

(Received November 16, 1959)

ALTHOUGH gaseous diatomic metal selenides and tellurides have been observed spectroscopically, there are few thermochemical data from which dissociation energies of these molecules may be obtained. Drowart and Goldfinger,[1] using a mass spectrometric technique, have found that the compounds CdSe and CdTe vaporize by decomposition to the gaseous ele-

TABLE I. Thermochemical data for reaction $M_2(g)+Y_2(g)=2MY(g)$.

System M—Y	Cell Temp. °K	K'[a]	$\Delta F_T°$ kcal/mole M_2	$\Delta S_T°$ cals/mole M_2/°K	$\Delta H_T°$ kcal/mole M_2	D_0 (MY) ev
Bi—Se	1050	40±10	−7.7±0.5	+4.0±0.2	−3.5±0.6	2.4
Bi-Te	1000	14±3	−5.3±0.4	+3.5±0.2	−1.8±0.5	2.1
Sb-Te	1000	0.8±0.3	+0.5±0.8	+3.3±0.2	+3.8±0.8	2.6
Te—Se	730	2.5±0.4	−1.3±0.2	+2.9±0.2	+0.8±0.3	2.5

[a] Ionizing electron energy=100 v.

ments, indicating low stabilities for the gaseous diatomic species, CdSe(g) or CdTe(g). Interest in the electrical properties of bismuth and antimony selenides and tellurides at high temperatures has led to the present investigation of the vaporization behavior of these materials.

The experimental method used here has been described in earlier publications[2] and involves the mass spectrometric identification of the vapor species escaping from an effusion cell in which condensed-vapor equilibrium is maintained. For these experiments a graphite cell was used. This was set into a heavy Inconel crucible to which a Pt-Pt 10% Rh thermocouple was securely fastened at the base. The crucible was heated by radiation from two surrounding tungsten filaments. Samples of Bi_2Se_3, Bi_2Te_3, and Sb_2Te_3 were crystalline and very near the stoichiometric composition M_2Y_3. Here we will use the notations M and Y to represent components. For experiments with Sb—Se and Te—Se systems mixtures of the pure components were used.

In the Bi—Se and Bi—Te systems ion currents of Bi_2^+, BiY^+, and Y_2^+ were observed in addition to Bi^+. On the basis of mass spectrometric work with selenide and telluride systems,[1] the known stabilities of $Bi_2(g)$ and $Y_2(g)$, the observed behavior in BiY^+ intensity with changes in Bi_2^+ and Y_2^+, we attribute the formation of these ions to processes of simple ionization by electron impact. For the Bi—Se system ion currents of Se_2^+ were quite high initially ($Se_2^+ > BiSe^+ \gg Bi_2^+$). As selenium was lost by evaporation, $BiSe^+$ became higher in intensity than Se_2^+ and after prolonged heating of the sample at a constant temperature, the intensity order was $Bi_2^+ > BiSe^+ \gg Se_2^+$. The Bi_2^+/Bi^+ ratio increased with time indicating that the melt was becoming richer in bismuth. Similar behavior was noted for the Bi—Te system.

For the reaction

$$M_2(g)+Y_2(g)=2MY(g), \qquad (1)$$

we have[3]

$$K_{eq} \simeq K' = (I_{MY^+})^2/(I_{M_2^+})(I_{Y_2^+}).$$

Experimental values of K' for several systems are given in Table I. Each values listed is an average of several determinations taken over a large range of condensed phase composition. For the Bi—Se system this corresponds to a change in the melt from selenium rich to bismuth rich. Values of ΔH for reaction (1) were determined from the free energy increments computed from K' and calculated values of ΔS. These latter values were obtained by assuming cancellation of vibrational and rotational terms (except for symmetry). The entropy increments thus contain only translation, symmetry and electronic terms. The latter were taken as $R\ln 3$ and $R\ln 2$ for $Y_2(g)$ and $MY(g)$, respectively. No electronic contribution was included for the Te—Se reaction. Dissociation energies for $MY(g)$ molecules have also been calculated by combining spectroscopic or thermochemical values[4] for $M_2(g)$ and $Y_2(g)$ with values of ΔH in Table I. It is to be noted that for all systems for which data have been obtained, the approximation $D_0(MY)=\frac{1}{2}D_0(M_2)+\frac{1}{2}D_0(Y_2)$ is good to within 0.1 ev.

The Sb—Se and Sb—Te systems were found to be considerably more complicated in their vaporization behavior due to the polyatomic species in high concentration (i.e., $Sb_4(g)$, Sb_2Se_2, or Sb_2Te_2). The thermochemical data for SbTe(g) in Table I are thus perhaps somewhat more uncertain than that for the other molecules since Sb_2^+ may originate partially by dissociative ionization of polymeric species. These systems will require extended investigations.

We wish to thank Mr. E. Zeller for assistance with these measurements.

* This research was supported by the United States Air Force through the Air Force Office of Scientific Research of the Air Research and Development Command under Contract No. AF 18(603)-1 and Contract No. AF 49(638)-480.

[1] J. Drowart and P. Goldfinger, J. Chim. Phys. **55**, 721 (1958).

[2] R. F. Porter and R. C. Schoonmaker, J. Phys. Chem. **62**, 234 (1958).

[3] R. C. Schoonmaker and R. F. Porter, J. Chem. Phys. **30**, 283 (1959).

[4] Spectroscopic values of 2.8 and 2.3 ev were used for Se_2 and Te_2, respectively. See A. G. Gaydon, *Dissociation Energies and Spectra of Diatomic Molecules* (Chapman and Hall, Ltd., London, 1953). For Sb_2 the recent value of $\Delta H_0° = 70.6 \pm 1.5$ kcal/mole Sb_2 was used. See DeMaria, Drowart, and Inghram, J. Chem. Phys. **31**, 1076 (1959). For Bi_2 the dissociation energy was redetermined from Bi^+/Bi_2^+ measurements with pure bismuth. At 1055°K we observe $Bi^+/Bi_2^+ = 1.33$ for 100-volt ionizing electrons. Using the vapor pressure of Bi(g) tabulated by Stull and Sinke,[5] assumptions used in similar calculations,[6] and heat content and entropy functions[5] for Bi(s, l), Bi(g), and $Bi_2(g)$, we obtain for $Bi_2(g)=2\,Bi(g)$, $\Delta E_0° = 43.0 \pm 1.5$ kcal/mole Bi_2 or $D°(Bi_2) = 1.87 \pm 0.07$ ev.

[5] D. R. Stull and G. C. Sinke, *Thermodynamic Properties of the Elements Advances in Chemistry Series* (American Chemical Society, Washington, D. C., 1956).

[6] R. F. Porter and R. C. Schoonmaker, J. Phys. Chem. **63**, 626 (1959).

Transient Species in the Flash Photolysis of Halogens in Solution*

N. K. BRIDGE†

Chemistry Division, Argonne National Laboratory, Lemont, Illinois

(Received November 2, 1959)

DURING a study of the radicals produced by flash photolysis of aqueous halate solution,[1] some very interesting, short-lived ($\lesssim 60$ μsec), and sometimes intense transients were detected on flashing the corresponding halogens separately in carbon tetrachloride, hexane, and normal sulfuric acid. They appear despite the fact that no permanent change can be detected in some cases (iodine in all solvents) and very little in other cases (bromine in CCl_4 and NH_2SO_4). Table I summarizes the results obtained.

Since, in addition, neither solvent or oxygen have a marked qualitative effect on the system it is difficult to decide which species produced can be absorbing light in this region of the spectrum. Solvent impurities seem unlikely as, in the case of the I_2 (Merck Reagent resublimed) in CCl_4 experiment, great care was taken to purify and introduce the iodine into the system before rigorous degassing according to the method described by Strong and Willard.[2] Solvent photolysis could not be detected and was in fact guarded against by interposing 1 cm of potassium acid phthalate filter solution[3] (cutoff 300 mμ).

It can be seen from the table that all the transients have the same general characteristic, namely, increased absorption in the region below approximately 350 mμ. In the case of Br_2 in N sulfuric acid and I_2 in hexane there are definitely peaks at 330 mμ and possible peaks in the same region for Br_2 in CCl_4, and in hexane (obscured, however, by the continuous absorption). The strongest transients were found in NH_2SO_4 and hexane for Br_2, and in hexane for I_2 though this is probably due in part to differences in halogen concentration.

These concentrations are approximately 10–100 times greater than those of Strong and Willard and, in addition, since, using the flash spectrophotometric technique, they observed only at the wavelength at which the halogen absorbs, it is not surprising that they did not detect these transients. The transient disappearance and reappearance of I_2 due to I-atom formation and recombination[2] was satisfactorily detected in all these solvents.

It was further found that flash wavelength altered the transient production in hexane; wavelengths of less than 410 mμ were less effective than those greater than 350 mμ. Hence the visible absorption bands ($^1\Sigma_g^+ \rightarrow {}^3\Pi_{1u}$, ${}^3\Pi_{0u}^+$) of the halogens are presumably responsible for the photoactivity. Using the technique of flash spectrophotometry,[1] the Br_2 in CCl_4 transient was followed at 313 mμ and found to last no longer than the flash ($\simeq 20$ μsec—although its peak lagged the flash peak by 6 μsec), and the transient from I_2 in hexane behaved similarly at 330 mμ (with a lag of $\simeq 8$ μsec). The NH_2SO_4 transients lasted longer—approximately 50 μsec.

The identification of these species is not obvious. The fact that they are so short-lived and appear when no reaction with the solvent is apparently taking place suggests that they are due to some modified halogen species. Perhaps under these conditions of intense irradiation they are an unusual halogen species such as X_2*[3] or X_3.[4,5] In the first case, it may be that a sufficient number of Br_2 or I_2 molecules are maintained in the excited ${}^3\Pi_{0u}^+$ state during the flash for their further transition to the higher ${}^3\Pi_{0u}^+$ state to be detected. This would correspond to an energy absorption of 29 318 cm^{-1},[6] i.e., 340 mμ, approximately the region observed. (Assuming the average rate of light absorption is at least 2×10^{-6} $Nh\nu$/μsec, then for 50 ml this corresponds to I_2* being produced at the rate of $4\times10^{-5}M$/μsec. For a 10^{-7} sec lifetime, the steady-state concentration would then be $4\times10^{-6}M$ and a molar extinction coefficient $\epsilon\sim10^3$ would be adequate.) The second possibility has been dis-

TABLE I. Changes in halogen solutions on flashing in air.

Solution	Unknown transient absorption		Halogen permanent change		Halogen transient change	
	Br_2	I_2	Br_2	I_2	Br_2	I_2
NH_2SO_4[a] $[Br_2]=2\times10^{-4}M$ $[I_2]=7\times10^{-5}M$	Strong, max at 330 mμ ≅70 μsec	Weak, continuous below 280 mμ ≅60 μsec	very small	none	obscured by transient	yes
CCl_4[b] $[Br_2]=5\times10^{-5}M$ $[I_2]=4\times10^{-4}M$	Medium, max at 305 mμ(?) ≅flash time	Weak, continuous below 280 mμ ≅flash time	medium	none	no	yes
Hexane[c] $[Br_2]=1.5\times10^{-3,4}M$ $[I_2]=8\times10^{-4}M$	Strong, max at 290 mμ? ≅flash time	Strong, max at 330 mμ ≅flash time	large	none	very doubtful	yes

[a] Br_2 in NH_2SO_4; saturation of the solution with N_2 or O_2 or rigorous degassing had qualitatively no effect.

[b] Cl_2 in CCl_4; no transient, marked permanent destruction of Cl_2. CCl_4 was Mallinckrodt AR low sulfur grade; saturating with O_2 or N_2 or rigorous degassing had qualitatively no effect.

[c] Hexane: spectroscopic grade.

cussed in detail recently by Bunker and Davidson.[5] In this case if we assume for a 3×10^{-4} M I_2 solution that of the molecules one-third on flashing are dissociated into I atoms, then the foregoing authors' equilibrium constant for I_3—obtained, however, in the gas phase—leads to an I_3 concentration of $6\times10^{-7}M$. To detect this, ϵ will be approximately 10^4. (I_2^- and I_3^- have values greater than this.) The fact that the transients in NH_2SO_4 last longer than the I-atom recombination time suggests that yet another species may be present here.

The foregoing observations, if substantiated, are clearly of importance since, taken in conjunction with the work on halogen atom recombination already referred to[2,4,5] they open up a new field of study for halogen atom or excited halogen molecule reactions in solution.

The author is greatly indebted to Dr. M. S. Matheson for helpful comments and the use of the flash photolysis apparatus, also to the British Rayon Research Association for giving him a leave of absence.

* Based on work performed under the auspices of the U. S. Atomic Energy Commission.

† Present address: British Rayon Research Association, Heald Green Laboratories, Wythenshawe, Manchester 22, England.

[1] N. K. Bridge and M. S. Matheson (to be published).

[2] R. L. Strong and J. E. Willard, J. Am. Chem. Soc. **79**, 2098 (1957).

[3] P. Pringsheim, *Fluorescence and Phosphorescence* (Interscience Publishers, Inc., New York, 1949), pp. 165, 212.

[4] D. L. Bunker and Davidson, J. Am. Chem. Soc. **80**, 5090 (1958).

[5] Christie, Harrison, Norrish, and Porter, Proc. Roy. Soc. (London) **A231**, 446 (1955).

[6] G. Herzberg, *Diatomic Molecules* (D. Van Nostrand Company, Inc., Princeton, New Jersey, 1950), second edition, p. 541.

Formation of Excited NO and N_2 by Wall Catalysis*

ROBERT R. REEVES, GENE MANNELLA, AND PAUL HARTECK

Chemistry Department, Rensselaer Polytechnic Institute, Troy, New York

(Received November 19, 1959)

NITROGEN, after passing through a condensed discharge, emits the well-known 1st positive system of the nitrogen afterglow. Similarly, dissociated oxygen, due to the presence of minute amounts of NO, will emit the oxygen afterglow. The kinetics of recombination and light-emission processes of both these species are known. Work has been under way in our laboratory to develop methods of determining N- or O-atom concentrations by titration methods.[1,2] A further refinement of these techniques permitted titration of N- and O-atom streams that were formed in separate discharges and then mixed. If this streaming mixture of N- and O-atoms (plus argon and undissociated N_2 and O_2) was passed over a small sheet of Ni, Co, or in some cases Ag, a bright reddish light emission was observed in the gas phase adjacent to the metal and extending out several millimeters. Decreasing the total pressure caused the glow to grow outward, indicating the active species were diffusing farther from the metal surface. The glow was about as bright as the discharge itself and much brighter than the N-atom or O-atom afterglows.

The light emission resembled a corona discharge in appearance†; however, no actual discharge existed. The color of this emission varied with N-atom to O-atom ratio: a high ratio gave a more reddish glow, while a low ratio gave a bluish glow. From observation of the thickness of the glow, the lifetime of the excited species was estimated to be 10^{-5} sec. Spectrographic analysis showed the 1st positive system of nitrogen and the β system of NO. However, the intensity distribution in the nitrogen spectrum observed was not the same as that occurring in the normal afterglow with no metal surface present. Also, only β bands of NO were observed whereas N-atoms and O-atoms recombining in the gas phase are observed to produce both β and γ bands.

This luminosity could not be produced with Ni or Ag using nitrogen atoms or oxygen atoms alone.‡ The emission began at once when both species were present and was observed for hours without any significant change in intensity. By observing the intensity of the normal afterglow upstream and downstream from the metal surface, it appeared that this luminosity did not consume a major fraction of the atoms, showing that this effect occurs with a substantial radiation efficiency.

Since the emissions required the presence of both N- and O-atoms, it appears that the O-atoms are not only required for the formation of NO, but are also involved in the emission by the nitrogen. The mechanism we favor is

$$N(^4S)+O(^3P)\rightarrow NO(B\,^2\Pi) \text{ forms on the wall and goes into the gas phase,} \quad (1)$$

$$NO(B\,^2\Pi)\rightarrow NO(X\,^2\Pi)+h\nu(\beta \text{ bands}), \quad (2a)$$

or

$$NO(B\,^2\Pi)+N(^4S)\rightarrow N_2(B^3\Pi g)+O(^3P), \quad (2b)$$

$$N_2(B\,^3\Pi g)\rightarrow N_2(A\,^3\Sigma_u^+)+h\nu(\text{1st. pos. system}). \quad (2c)$$

The upper energy level for $NO(B\,^2\Pi)$ is limited to the recombination energy of NO ($D_{NO}=6.5$ ev) minus the adsorption energy of the N- or O-atoms and the energy transfer to the wall. The most prominent bands of NO observed are from the $B^2\Pi$ state in the zero vibrational level, about 5.59 ev excitation. The calculation for the energy relations for

$$N(^4S)+NO(B\,^2\Pi)_{v=0}\rightarrow O(^3P)+N_2(B\,^3\Pi g)_{v=8} \quad (3)$$

gives an almost thermally neutral balance since the $N_2(B\,^3\Pi g)$ has 8.94 ev in the 8th vibrational level. Our spectrograms indicate that bands for the 8→5 (6469 A) and 8→4 (5959 A) transitions are the most intense. In

the normal afterglow, these bands are very weak and the 12→7 (5375 A), 11→7 (5804 A) and 11→6 (6252 A) are most prominent.

We therefore assume that primarily excited NO forms on Ni, Co, or Ag surfaces and that this NO ($B\,^2\Pi$) can either emit light or react with N atoms which will in turn emit light. It is very striking, that electronically excited systems are formed on the wall without becoming deactivated during the formation process. It should be mentioned that the luminosity produced by Ni, Co, and Ag are basically the same but somewhat different in color. This is possibly due to different energy transfer to the wall during the formation process.

To our knowledge, such an effect has not been reported in the available literature.

* The research reported in this document has been sponsored by the Geophysics Research Directorate of the Air Force Cambridge Research Center, Air Research and Development Command under Contract No. AF19(604)-2205.

[1] Harteck, Reeves, and Mannella, J. Chem. Phys. **29**, 608 (1958).

[2] Reeves, Manella, and Harteck, J. Chem. Phys. **32**, 632 (1960).

† Color photos are available to interested colleagues.

‡ A glow of lesser intensity was observed with Co in a stream of N atoms alone.

Proton and B^{11} Magnetic Resonance of Borazole

KAZUO ITO, HARUYUKI WATANABE, AND MASAJI KUBO

Chemistry Department, Nagoya University, Chikusa, Nagoya, Japan

(Received November 19, 1959)

THE proton and B^{11} magnetic resonance spectra of borazole prepared by the reduction of *B*-trichloroborazole with $NaBH_4$[1] were recorded by means of a JNR-3 high-resolution NMR spectrometer from Japan Electron Optics Laboratory Company operating at 40 and 12.6 Mcps. The proton spectrum obtained is shown in Fig. 1, in which chemical shifts defined by $\delta = 10^6(H_s - H_r)/H_r$ are plotted as abscissas. Here H_s denotes the applied magnetic field for the proton signal of the sample and H_r is that of cyclohexane used as an internal standard. Corrections for the bulk magnetic susceptibility of the sample were not made. Dilution with carbon tetrachloride did not affect the spectrum in an appreciable manner. The signal of cyclohexane was identified by the increase in its intensity on further addition of the standard.

The spectrum is comprised of a triplet centered at -4.0_5 and less intense broad peaks at 2.1_2, -1.3_4, and -8.2_6. The triplet was unequivocally assigned to the proton signal of $N^{14}H$ with a spin coupling constant $J(N^{14}H) = 56$ cps, because the signal is expected to split into three equally spaced peaks owing to the $2I+1$ orientations of an N^{14} spin with $I=1$. The spin coupling constant is of right order of magnitude, since the value for $N^{14}H_3$ is 46 cps.[2] Similarly, the proton signal of

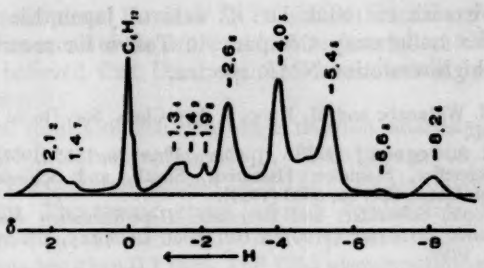

FIG. 1. Proton magnetic resonance spectrum of borazole.

$B^{11}H$ must split into four equally spaced peaks in accordance with the spin $I = \frac{3}{2}$ of B^{11} (abundance 81.17%). The separation, 3.4_6, between the two peaks at 2.1_2 and -1.3_4 is equal to half the difference 6.9_2 between those at -1.3_4 and -8.2_6, suggesting the presence of another peak at -4.8_0, which, although masked by the $N^{14}H$ triplet, appears as a hump between two peaks of the triplet. These four peaks complete the proton quartet of $B^{11}H$ with $J(B^{11}H) = 138$ cps. This assignment is also consistent with the B^{11} NMR spectrum of the same sample showing two peaks separated by 140 cps, in good agreement with 138 cps mentioned in the foregoing.

Two peaks at 1.4_7 and -1.4_9 were ascribed to spinning side bands, because they shifted depending on the spinning rate of the sample. The origin of other weak peaks at -1.9_8 and -6.6_8 is open to speculation. Although these bands might be due to the presence of some impurities in the sample, because borazole gradually decomposes even in a sealed tube,[3] a possible interpretation is afforded by the proton signal of $B^{10}H$. If the peak at -6.6_8 is assumed to be the outermost one of seven peaks predicted for the signal of protons bonded to B^{10} (abundance 18.83%), one obtains $J(B^{10}H) = 48$ cps in good agreement with 46 cps calculated from $J(B^{11}H)$ mentioned in the foregoing, and the peak at -1.9_8 may be considered to be another member of the septet. Three peaks between these two will escape detection owing to overlap with the strong $N^{14}H$ triplet. However, the last two peaks expected to appear at -0.7 and $+0.5$ have not been observed.

The proton chemical shifts -4.0_5 and -3.0_7 of NH and BH in borazole, as referred to cyclohexane, lead to about -0.7 and $+0.3$, respectively, referred to water as a standard.[4] The former differs definitely from the δ values 4.3–4.5 for secondary alkyl amines,[5] and is intermediate between about 2.0 for secondary aryl amines[5] and about -2.1 for pyrrole.[4] This is quite reasonable since nitrogen atoms in borazole assume sp^2 hybridization and π electrons are presumed to migrate to some extent from nitrogen to boron.[6] The chemical shift and the spin coupling constant $J(B^{11}H)$ of a BH proton, $+0.3$ and 138 cps, in borazole are closer to those of a terminal proton, $+2.0$ and 125 cps, in diborane, respectively, than those of a bridge proton, $+6.3$ and 43 cps, in the same molecule.[5]

We wish to thank Dr. T. Seki of Japan Electron Optics Laboratory Company in Tokyo for recording the high-resolution NMR spectra.

[1] H. Watanabe and M. Kubo, J. Am. Chem. Soc. (to be published).
[2] R. A. Ogg and J. D. Ray, J. Chem. Phys. **26**, 1515 (1957).
[3] Schaeffer, Steindler, Holnstedt, Smith, and Schlesinger, J. Am. Chem. Soc. **76**, 3303 (1954).
[4] Pople, Schneider, and Bernstein, *High-Resolution Nuclear Magnetic Resonance* (McGraw-Hill Book Company, Inc., New York, 1959).
[5] Meyer, Saika, and Gutowsky, J. Am. Chem. Soc. **75**, 4567 (1953).
[6] B. L. Crawford, Jr., and J. T. Edsall, J. Chem. Phys. **7**, 223 (1939); C. C. J. Roothaan and R. S. Mulliken, *ibid.* **16**, 118 (1948); Rector, Schaeffer, and Platt, *ibid.* **17**, 460 (1949).

Centrifugal Distortion in Symmetric Top Molecules*

MAURICE W. LONG

Georgia Institute of Technology, Atlanta, Georgia

(Received October 21, 1959)

EFFECTS of centrifugal distortion are expressed[1,2] by the distortion coefficients D_J and D_{JK} in

$$f/2(J+1)=B-D_{JK}K^2-2D_J(J+1)^2. \quad (1)$$

A recent investigation[3] of quadrupole interaction for three nuclei of spin $\frac{3}{2}$ has revealed that, for the $J=2\rightarrow3$ rotational transitions and $K=1$, 2, the D_{JK} of $CFCl_3^{35}$ and $CHCl_3^{35}$ are -196 ± 6 kc and -201 ± 3 kc, respectively. In addition, calculations based on the $K=1$ lines, the $J=1\rightarrow2$ data, and the $J=2\rightarrow3$ through $J=6\rightarrow7$ data for $CFCl_3$ yield for D_J the values -24 ± 2 kc, and -14 kc, -9 kc, -6 kc, and -4 kc with probable errors less than 1 kc. Similar calculations with the $J=1\rightarrow2$ and $J=2\rightarrow3$ data for $CHCl_3$ yield $D_J=-14.5\pm0.7$ kc; the $J=1\rightarrow2$ and $J=6\rightarrow7$ data for $CHCl_3$ yield $D_J=-1.8\pm0.1$ kc.

The sign of every D_{JK} given by Townes and Schawlow[2] for XYZ_3 molecules is positive and the sign of every D_{JK} given for XY_3 molecules is negative. The D_{JK} reported above for $CFCl_3^{35}$ and $CHCl_3^{35}$ are, however, negative. It is interesting that the centers of mass of the previously reported XYZ_3 molecules are outside the "umbrella" and the centers of mass of $CFCl_3$, $CHCl_3$, and XY_3 molecules are within the umbrella. The negative values of D_J for $CFCl_3^{35}$ and $CHCl_3^{35}$ are also interesting because previous investigations have yielded only positive values and some authors[2] have surmised that D_J must be positive.

Changes in the calculated D_J with J suggest a dependence of quadrupole coupling constant on J due to molecule distortion. However, relatively large changes in the quadrupole coupling constants would be required to produce substantial changes in D_J. Quadrupole coupling constants for both $CFCl_3$ and $CHCl_3$ were determined from the $J=1\rightarrow2$ and $J=2\rightarrow3$ spectra; no dependence on J was found. Because of the foregoing conditions, it was assumed that the quadrupole coupling constants are independent of J.

The rotational energy of a rigid symmetric rotor is given by

$$E=h[BJ(J+1)+(C-B)K^2], \quad (2)$$

where $C=h/(8\pi^2I_c)$ and $B=h/(8\pi^2I_b)$; I_c is the moment of inertia about the molecular symmetry axis and I_b is the moment of inertia about another principal axis. The result of using Eq. (2) with the selection rules $\Delta J=+1$, $\Delta K=0$ is

$$f/2(J+1)=B+\delta B[1+(J/2)]+[K^2/2(J+1)](\delta C-\delta B), \quad (3)$$

where $\delta B=B_{J+1}-B_J$ and $\delta C=C_{J+1}-C_J$. We expect δB to be negative because centrifugal distortion due to rotation about a given axis should tend to increase the moment of inertia about that axis. If D_J and D_{JK} are negative as determined experimentally for $CFCl_3$ and $CHCl_3$, $f/2(J+1)$ is greater than B. Then for $K=1$, 2 and $J\geq1$, $f/2(J+1)$ can be greater than B only if δC is positive. δC would be positive if I_c were reduced by an increase in the angular momentum perpendicular to the molecular symmetry axis (increase J, K fixed) by a reduction of the angle Cl—C—Cl and little increase in the C—Cl distance. This would be similar to reducing the moment of inertia about the symmetry axis of an umbrella by increasing angular momentum perpendicular to this axis. From Eq. (1) it may be seen that for K fixed a negative value of D_J is associated with an increase of $f/2(J+1)$ with J. Although δC and δB are expected to be functions of J, the factors $[1+(J/2)]$ and $1/(J+1)$ in Eq. (3) will tend to decrease D_J numerically with increase in J if D_J and D_{JK} are negative; this effect was observed for $CFCl_3$ and $CHCl_3$.

The XYZ_3 molecules $CFCl_3$ and $CHCl_3$ have negative values of D_{JK} and negative values of D_J. For XY_3 and XYZ_3 molecules, reported values of D_{JK} are negative for molecules with center of mass within the umbrella and are positive for molecules with center of mass outside the umbrella. D_J is generally called a centrifugal distortion constant but D_J depends on J for the low J-value data considered herein. It seems that the negative D_J values for $CFCl_3$ and $CHCl_3$ are caused by reduction of moment of inertia about the molecular symmetry axis with increased angular momentum J.

* Supported by the Office of Naval Research.
[1] Z. I. Slawsky and D. M. Dennison, J. Chem. Phys. **7**, 509 (1939).
[2] C. H. Townes and A. L. Schawlow, *Microwave Spectroscopy* (McGraw-Hill Book Company, Inc., New York, 1955). A typographical error exists in Tables 3–7 and Appendix VI in the sign of D_{JK} for AsF_3.
[3] M. W. Long, Technical Report No. 1, Contract No. Nonr-991(07), June, 1959; ASTIA No. AD 216 615.

Zone Refining and Chemical Analysis of KCl and KBr*

SCOTT ANDERSON, JOHN S. WILEY, AND LLOYD J. HENDRICKS

The Anderson Physical Laboratory, Champaign, Illinois

(Received October 13, 1959)

UPON initiation of our alkali halide purification program, we desired an accurate and complete chemical analysis of representative samples of the best salt commercially available. It was concluded that the most sensitive and probably most nearly complete technique is that provided by neutron activation. Therefore, Dr. G. W. Leddicotte of the Oak Ridge National Laboratories was asked to execute the analysis on samples of Harshaw KCl and KBr. Since Harshaw supplies much of the salt used in American laboratories, it is believed that Dr. Leddicotte's results will be of interest.

TABLE I. Results of neutron activation analysis.*

Element	KCl conc. ppm	KBr conc. ppm
Elements definitely present		
Br	72.5	...
Cs	<0.1	<0.1
Na	<0.1	<0.1
Ni	≦2	≦2
P	...	<0.1
Rb	<0.1	<0.1
S	1–2	1–2
Zn	0.46	0.45
Elements probably present in both KBr and KCl		
<0.1 ppm		
Ag, Si, Ta, W, Ti, Fe, Cr, Ga, Hf, In, Sc, Th, U, V, Y, Zr, Rare earths, Ca, Ba, Sr, Mg, P. (KCl only; for KBr P content see above.)		
Elements probably present in both KBr and KCl		
<0.01 ppm		
Cu, As, Au, Bi, Cd, Ge, Hg, Ir, Os, Re, Mo, Pd, Pt, Ru, Sb, Se, Te, Sn, Co, Mn.		

* Executed by Dr. G. W. Leddicotte, Oak Ridge National Laboratories.

The results of the neutron activation analyses are divided into two major groups. These groups are (1) elements definitely present; and (2) elements probably present. The second group is again divided into two subgroups: (2a) elements probably present in concentrations less than 0.1 ppm, and (2b) elements probably present in concentrations less than 0.01 ppm. The elements for which no analysis was made are Al, B, F, I, Li, Pb, and Tl. These data are presented in Table I.

Duerig and Markham[1] have reported some spectrochemical analyses on other samples of Harshaw salt. Their spectrochemical results are from 10 to 100 times that found by neutron activation. It may be said that the concentration of many elements varies between samples of Harshaw salt depending upon the region of the boule from which the samples are taken, but even so, their results are higher than the concentration of most impurities in salt currently available from Harshaw. Moreover, they point out that their values are only qualitative and that further analyses are required. Our own spectrochemical results with present-day Harshaw salts are more nearly in accord with the activation analysis.

In numerous zone-refining experiments, the only normal impurity elements in reagent grade KCl found to segregate well are Ag and Na. Analyses of two ingots of KCl are summarized in Table II. One ingot was subjected to two zone passes and the other to four zone passes. Spectrochemical analyses were performed on the first zone length, the 5th zone length, 9th and 10th zone lengths as a unit, the last $\frac{1}{3}$ of the 10th zone length, and the condensate on the walls of the container. The limit of sensitivity for Ag is 0.5 ppm. Consequently, after four zone passes, the only place Ag could be detected was in the last two zone lengths, but to the accuracy of these measurements 100% of this element was

TABLE II. Impurity concentration in zone refined reagent grade KCl. N.D. means impurity not detected; ... means no determination was made.

Element	No. zone passes	Original ppm	1st zone ppm	5th zone ppm	9th and 10th zones ppm	Last $\frac{1}{3}$ 10th zone ppm	Last $\frac{1}{3}$ 10th zone % total impurity	Condensate on wall ppm
Ag	2	2	N.D.	0.5	6	31	44	2
	4	2	N.D.	N.D.	7.5	56	93	
Na	2	250	150	300	550	...	...	375
	4	250	90	200	1500	...	...	
Cu	2	21	11	12	19	...	...	100
	4	21	16	19	10	...	...	
Fe	2	3	2	2	2	...	...	10
	4	3	2	2	2	...	...	
Al	2	8	2	1	N.D.	...	...	80
	4	8	...	...	...	...	...	

concentrated into these two zones and 93% was in the last $\frac{1}{3}$ of the last one. A practical segregation coefficient for Ag in KCl is 0.09.

Sodium moves less dramatically but very definitely by zone melting. As is evidenced by the increased concentration in the wall condensate some sodium is removed by evaporation. Due to this fact, it is difficult to calculate a practical segregation coefficient, but it is probably of the order of 0.4.

It is noted that in all sections the concentration of Cu, Al, and Fe is less after zone melting than originally, and that their concentrations in the wall condensate are very high. Evidently, these elements as well as sodium are removed from the boats by differential evaporation. Silver evaporates at about the same rate as the KCl.

* Work performed under the sponsorship of the U. S. Atomic Energy Commission.

[1] W. H. Duerig and J. J. Markham, Phys. Rev. 88, 1043 (1952).

Radiolysis and Bond Stability of Squalane

HIDEO YAMAZAKI AND SHOJI SHIDA

Laboratory of Physical Chemistry, Tokyo Institute of Technology, Ookayama, Meguro-ku, Tokyo, Japan

(Received October 26, 1959)

ALTHOUGH a number of investigations have been made on the radiolysis of liquid paraffins of low molecular weight[1] and that of high polymers such as polyethylene,[2] relatively few studies have been made of hydrocarbons of intermediate molecular weight. In view of the bond stability, the gaseous products from the radiolysis of squalane $C_{30}H_{62}$ were studied.

The pure squalane sample (made by the Riken Seiyu Company) used in this experiment showed no residual double bond absorption in its infrared spectrogram, and the molecular weight measured by boiling point elevation for benzene solution was 420±10. The samples were irradiated *in vacuo* by ^{60}Co γ rays with total dosage, $3\times10^6\sim3\times10^7$r, at a dosage rate of 6×10^3 r/min. The noncondensable gaseous products at liquid nitrogen temperature, hydrogen plus methane, were collected with a Toepler pump, measured by a micro gas burette, and analyzed by selective oxidation with a heated tube of cupric oxide. The condensable gases were passed into gas chromatographs. Each fraction showing a peak in the chromatogram was trapped separately and analyzed with a Hitachi RMU-5 type mass spectrometer. The G values and the relative retention time of the products identified are shown in Table I. As is shown in this table, the G value of hydrogen production is 3.4 at a dosage of 3×10^7r. However, a gradual increase was observed at lower dosages, as observed in the radiolysis of cyclohexane.[3] The G values of C_1, C_3, C_6, and C_8 products are larger than those of C_2, C_4, C_5, and C_9 products to the order of magnitude.

TABLE I. The G values and relative retention time of gaseous products in the radiolysis of squalane.

Products	G values	Relative retention time
hydrogen	3.4	...
methane	0.12	...
C_2	0.002	1.00[a]
propane	0.056	1.45[a]
propylene	0.050	1.65[a]
isobutane	0.015	2.11[a]
other C_4	0.002	3.0∼6.0[a]
pentane	0.023	1.00[b]
hexane	0.21	1.94[b]
octane	0.14	9.48[b]
octene	0.03	11.12[b]
nonane	0.01	16.78[b]

[a] Measurement made using a 10-m column with benzylether operated at room temperature.
[b] Measurement made using a 3-m column with high vacuum oil operated at 78°C.

The cracking pattern of the mass spectrogram of individual products indicated that the pentane, hexane, and octane in the products are 2-methylbutane, 2-methylpentane, and 2-methylheptane, respectively. If we consider the experimental facts that C_2 and C_7 fractions are negligibly small and that the structure of each product coincides with that of a corresponding part of the original molecule, the gaseous products may come simply from the fracture of the C—C bonds of squalane. Thus, production of these products by secondary reaction between free radicals may be ignored. As a theoretical approach to this problem, the bond energies in the squalane molecule were calculated by means of the Brown method.[4] The result is shown in Fig. 1 which indicates that the C—C bonds with lower bond energies are preferentially fractured and yield products of high G value. The formation of unsaturated products such as propylene and octene may result from the removal of hydrogen in the weaker C—H bond adjacent to the C—C bond fractured. The methane produced may come from eight methyl groups in a

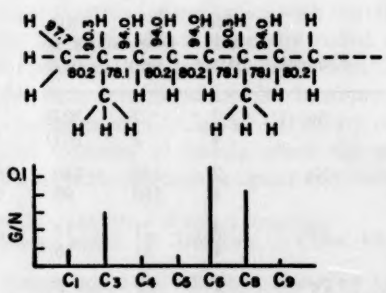

FIG. 1. Bond energies (kcal) of a part of a squalane molecule as calculated by the Brown method, and reduced G values G/N of the corresponding products. N denotes the number of C_n— groups in the squalane molecule.

squalane molecule, and the considerably large G value of this product is reasonable.

Apart from the mechanism in radiolysis, bond energy calculations show that a difference of only two kcal in bond energy is associated with a factor of ten in G value. A similar phenomenon was also observed in the case of the ionization of gases by electron impact.[5]

[1] H. A. Dewhurst, J. Phys. Chem. **61**, 1466 (1957); H. A. Dewhurst, J. Am. Chem. Soc. **80**, 5607 (1958).
[2] A. Charlesby, Proc. Roy. Soc. (London) **A215**, 187 (1952); A. Charlesby, *ibid.* **A222**, 542 (1954).
[3] Guentner, Hardwick, and Nejak, J. Chem. Phys. **30**, 601 (1959).
[4] R. D. Brown, J. Chem. Soc. **1953**, 2615.
[5] Wallenstein, Wahrhaftig, Rosenstock, and Eyring, *Symposium on Radiobiology* (John Wiley & Sons, Inc., New York, 1952), p. 70.

Paramagnetic Susceptibility of Polycrystalline Thulium from 300 to 1500°K

SIGURDS ARAJS

Edgar C. Bain Laboratory, for Fundamental Research, United States Steel Corporation Research Center, Monroeville, Pennsylvania

(Received October 26, 1959)

THE 4f electrons in the rare earth metals make them an attractive series for studying the relationship between the electronic structures and the physical properties. Much experimental work has been done on these metals at low temperatures. However, their high temperature properties have not been that completely explored. This note reports for the first time measurements on the magnetic susceptibility of thulium from about 300 to 1500°K.

Polycrystalline thulium (99.0+%) was purchased from the Lindsay Chemical Division of the American Potash and Chemical Corporation. According to the supplier, this material was 99.9% pure with respect to other rare earths and no iron was detected in it. The major impurities were tantalum, calcium, oxygen, and magnesium. Four samples, each having a mass of about 5g, were prepared from the polycrystalline material. Each sample was wrapped with a tantalum foil and enclosed in an evacuated silica capsule. The magnetic susceptibilities were measured using the Faraday method with an experimental error of about ±3%.

The inverse magnetic susceptibility *vs* temperature data (which have been corrected for the diamagnetism of the silica capsule and of Tm^{3+} ions) are shown in Fig. 1. The Weiss-Curie law, $\chi\,(T-17.4)=4.37\times10^{-2}$, where χ is the mass magnetic susceptibility and T the absolute temperature is satisfied between 300 and 1500°K. The paramagnetic Curie temperature $\theta_p=17.4\pm0.5$°K and the Curie constant $C=(4.37\pm0.13)\times10^{-2}$ cm³°K g^{-1} were determined from the experimental data using the method of least squares.

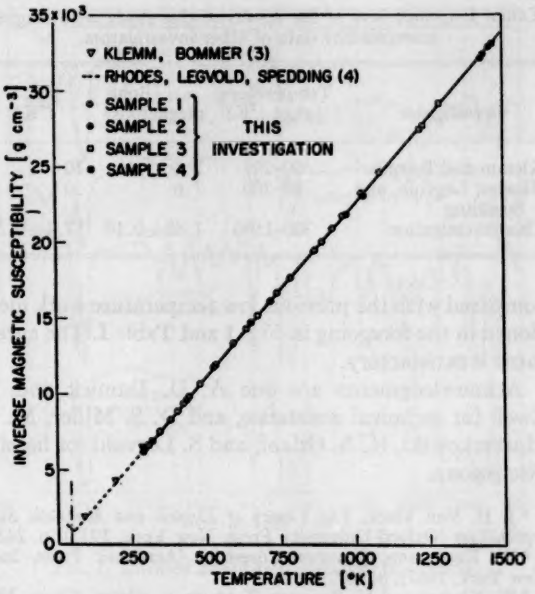

FIG. 1. Inverse paramagnetic susceptibility of Tm as a function of temperature.

The effective Bohr magneton number corresponding to the measured Curie constant C is $\mu_{eff}=7.68\pm0.10$. The magnetic moment of Tm^{3+} ion expressed in the Bohr magnetons with the electron configuration $4f^{12}$ in the ground state $^3H_6$ is 7.56.[1,2] Thus the tripositive ion model is a fairly good approximation for the paramagnetic behavior of metallic thulium. The unfilled 4f shell of a thulium atom apparently is not much disturbed by the surrounding atoms. Also the Tm^{3+} ions even at 1500°K are in the ground state $^3H_6$.

The only known previous work on the magnetic behavior of metallic thulium is due to Klemm and Bommer,[3] Rhodes *et al.*,[4] and Leipfinger.[5] Klemm and Bommer used a mixture of powdered Tm and KCl for their paramagnetic investigations covering temperatures between 90 to 291°K. Rhodes *et al.* studied polycrystalline thulium from liquid helium to room temperatures. They found that thulium is strictly paramagnetic from room temperatures down to 60°K and possibly antiferromagnetic below 51°K. From the fact that the 4.2°K magnetic isotherm fell below that at 20.4°K, they concluded that thulium does not become ferromagnetic. Leipfinger's work was also on polycrystalline thulium. He found that the magnetic isotherms between 2 and 20°K were similar to those of a normal ferromagnetic substance and hence he concluded that thulium is ferromagnetic at these temperatures. It appears that the question of the existence of ferromagnetism in thulium is not completely settled yet. It is possible that the discrepancies between the work of Rhodes *et al.* and of Leipfinger may be due to the influence of impurities at low temperatures on the crystalline field splitting.

The present investigation of the magnetic behavior of polycrystalline thulium above room temperature is

TABLE I. Comparison of the results of this study with magnetic susceptibility data of other investigators.

Investigator	Temperature range (°K)	μ_{eff} (Bohr magnetons)	θ_p (°K)
Klemm and Bommer[3]	90–291	7.6	10
Rhodes, Legvold, and Spedding[4]	60–300	7.6	20
This investigation	300–1500	7.68±0.10	17.4±0.5

compared with the previous low temperature work mentioned in the foregoing in Fig. 1 and Table I. The agreement is satisfactory.

Acknowledgments are due A. D. Damick and L. Zwell for technical assistance, and D. S. Miller, M. J. Marcinkowski, R. A. Oriani, and S. Legvold for helpful discussions.

[1] J. H. Van Vleck, *The Theory of Electric and Magnetic Susceptibilities* (Oxford University Press, New York, 1932), p. 243.
[2] W. Kauzmann, *Quantum Chemistry* (Academic Press, Inc., New York, 1957), p. 367.
[3] W. Klemm and H. Bommer, Z. anorg. u. allgem. Chem. **231**, 138 (1937).
[4] Rhodes, Legvold, and Spedding, Phys. Rev. **109**, 1547 (1958).
[5] H. Leipfinger, Z. Physik **150**, 415 (1958).

B^{11} Nuclear Magnetic Resonance Spectrum of the "Diammoniate of Diborane"

THOMAS P. ONAK* AND I. SHAPIRO†

Research Laboratory, Olin Mathieson Chemical Corporation, Pasadena, California

(Received November 3, 1959)

THE structure of the "diammoniate of diborane" has been the subject of much controversy.[1] Recently R. W. Parry and collaborators in a series of papers[1d] presented evidence in favor of structure I:

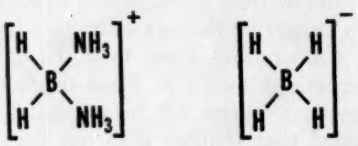

I

Since this structure requires two different types of boron atoms, chemical shifts would be expected to occur in the B^{11} NMR spectrum, along with splitting of the boron resonance lines due to B^{11}—H spin-spin coupling. In an effort to confirm its structure the "diammoniate of diborane" was prepared according to Parry and Shore[3d] and its spectrum in liquid ammonia solution (sealed tube) was taken immediately afterwards at room temperature with a Varian high-resolution NMR spectrometer operating at 12.83 Mc.

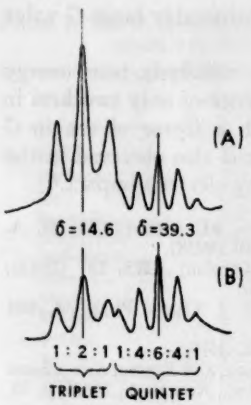

FIG. 1. The B^{11} NMR spectra of "diammoniate of diborane;" δ values relative to $BF_3 \cdot Et_2O$[2]. (A) partial saturation; (B) saturation minimized.

The B^{11} NMR spectrum of the "diammoniate of diborane" given in Fig. 1 is composed of a 1:2:1 triplet and a 1:4:6:4:1 quintet which can be established by use of a saturation technique. By changing the radio-frequency power to satisfy the conditions of partial saturation, one can diminish the signal intensity of the quintet relative to that of the triplet [Fig. 1(A)] because of the difference in relaxation times. At an optimum radio-frequency power [Fig. 1(B)] saturation effects are minimized and the signal intensities of the quintet and the triplet become nearly equivalent.

The spin coupling constant of the quintet, $J=80$ cps, is comparable to that of the borohydride ion (*viz.*, $NaBH_4$, $J=82$ cps; $LiBH_4$, $J=75$ cps),[2] and its chemical shift, $\delta=+39.3$,[3] also is in the region characteristic of borohydride ion (*viz.*, $NaBH_4$, aq soln, $\delta=+38.7$; $LiBH_4$, ether soln, $\delta=+38.2$).[2] The triplet, $J=120$ cps, is characteristic of a boron bonded to two hydrogens [BH_2 of tetraborane, $J=123$ cps[2,4]; $H_2BN(CH_3)_2$, $J=110$ cps]. The position of the triplet, $\delta=+14.6$, is adequately within the region assigned to the tetrahedral boron atom[2] and not unreasonable for $H_2B(NH_3)_2^+$ which would be expected to occur in the region of tetrahedral boron atoms with similar adjacent atoms, e.g., $H_3BNH(CH_3)_2$, $\delta=+15.1$; $H_2BN(CH_3)_2$ dimer, $\delta=-6.0$.

The above NMR data corroborate the presence of $H_2B(NH_3)_2^+$ and BH_4^- in a ratio of 1:1, and therefore substantiate structure I for the "diammoniate of diborane."

* Present address: Los Angeles State College, Los Angeles, California.
† Present address: Hughes Tool Company—Aircraft Division, Culver City, California.

[1] (a) H. I. Schlesinger and A. B. Burg, J. Am. Chem. Soc. **60**, 290 (1938); (b) A. B. Burg, *ibid.* **69**, 747 (1947); (c) Schaeffer, Adams, and Koenig, *ibid.* **78**, 725 (1956); (d) Parry in collaboration with Schultz, Shore, Girardot, and Kodama, *ibid.* **80**, 4–27 (1958); (e) Taylor, Schultz, and Emergy, *ibid.* **80**, 27 (1958).
[2] Onak, Landesman, Williams, and Shapiro, J. Phys. Chem. **63**, 1533 (1959).
[3] $\delta=(H_s-H_r)/H_r\times10^6$.
[4] Williams, Gibbins, and Shapiro, Abstracts of the 135th Meeting of the American Chemical Society, Boston, Massachusetts, April, 1959, 38M.

On the Radiation-Induced Gas-Phase Polymerizations of Acetylene and Benzene

A. Russell Jones

Oak Ridge National Laboratory, Chemistry Division, Oak Ridge, Tennessee*

(Received August 27, 1959)

ACETYLENE gas was polymerized by irradiation with 1-Mev electrons from a Van de Graaff generator, and the infrared spectrum of the fresh polymer (cuprene) was examined via the KBr-pressed-disk technique with a Perkin-Elmer Model 21 spectrophotometer.

The radiation-induced polymerization of acetylene to form cuprene was one of the earliest hydrocarbon radiolyses studied,[1] and it has since been investigated from many points of view.[2] The $-G_{C_2H_2}=72$ has been well established.[3] There is a linear relationship between the logarithm of the pressure of acetylene and the energy input over large pressure and dose-rate ranges. The reaction rate is relatively insensitive to impurities. The solid product is an almost-white, insoluble, infusible, and nonvolatile powder whose formula is reported to vary from $(C_2H_2)_x$ by less than 1% of hydrogen.[4] The only other characterization of the material to date has been the detection of crystallinity when the polymer is formed under special conditions.[5] As ordinarily formed (which includes the present work), the polymer appears amorphous.[5,6] Benzene which accounts for virtually all the remainder of the reacted acetylene, was produced with an initial $G=5$ in experiments in which the residual acetylene pressure was always at least 50 times as high as the amount of benzene formed.[3]

The infrared absorption spectrum of cuprene (Fig. 1) is largely characteristic of aromaticity, indicating that cyclization to form the aromatic nucleus is not an exclusive property of the reaction path leading to the formation of benzene. It has been suggested[7] from experiments on the rare-gas-sensitized radiolysis of acetylene that ionization of acetylene leads to polymerization, whereas cyclization requires electronic excitation of the acetylene, probably to a triplet state.

The assumption of a strong tendency for the growing chain of conjugated double bonds initiated by energetic (excited or ionized) C_2H_2 species to cyclize to form aromatic rings could explain much of the information. The polymer's lack of color-depth is clearly demonstrative of the absence of an extended, conjugated, aliphatic system of multiple bonds (cf. carotenoids). Its physical properties (insolubility, infusibility, and nonvolatility) and infrared absorption curve appear to describe cuprene as a three-dimensional network of benzenoid rings, probably joined by short, conjugated, aliphatic chains and acetylenic linkages, and appended by phenyl and HC≡C—groups. The aliphatic double and triple bonds would account for the large affinity

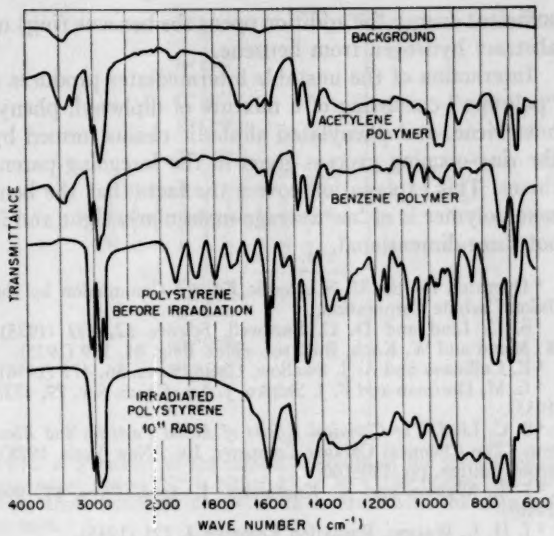

FIG. 1. Infrared absorption spectrum of cuprene.

which the polymer shows for oxygen (greater than 30 weight-percent up-take of the element within 12–15 days.[8]

The formation of only one, simple, organic compound (and that from the trimer stage of polymerization) is explainable on the basis that as the chain grows from one C_2H_2 unit through the trimer stage, a fraction of the latter in passing through a favorable configuration can cyclize without even rearrangement of a hydrogen atom. While the substance so produced, benzene, is not wholly inert under irradiation, its rate of disappearance from the gas phase is only $\frac{1}{15}$ that of acetylene.[9] This together with its low partial pressure in the initial stages of the reaction, would contribute to its accumulation.

Aromatic cyclization at a later stage of chain formation, for example the tetramer, could occur with migration of a hydrogen atom to produce, for example, styrene: a compound which would certainly polymerize or react with the ionic and free radical species produced by the irradiation of acetylene.

The electron irradiation of benzene vapor produced some acetylene and a polymer: yellow, sticky, sweet-smelling; average molecular weight reported[9] to be 330 in benzene solution. Its infrared absorption pattern resembled that of irradiated polystyrene.[10] The benzene polymer appears largely to involve monosubstituted benzene rings. Note the monosubstituted acetylenic structure evidenced near 3300 cm^{-1}. The absorption of energy appears to open the ring to form the aliphatic biradical —CH=CH—CH=CH—CH=CH— and/or its ion, sone of which depolymerizes to acetylene. In contrast to the situation during the irradiation of acetylene, this "acetylene trimer" is surrounded by the much more chemically inert molecules of benzene, hence a chain reaction does not occur. Those radicals and/or ions which do not recyclize add benzene (if they have

sufficient energy the addition opens the benzene ring) or abstract hydrogen from benzene.

Interaction of the unstable intermediates produces a "polymer" consisting of a mixture of diphenyl, phenyl hexatriene, and phenylated aliphatic chains formed by the ring-opening process given in the foregoing parentheses. This explanation covers the facts that the benzene polymer is of low average-molecular-weight and is not three-dimensional.

* Operated for the U. S. Atomic Energy Commission by the Union Carbide Corporation.

[1] S. C. Lind and D. C. Bardwell, Science **62**, 422 (1925); W. Mund and W. Koch, Bull. soc. chim. Belg. **34**, 119 (1925).
[2] E. Collinson and A. J. Swallow, Chem. Revs. **56**, 471 (1956).
[3] L. M. Dorfman and F. J. Shipko, J. Am. Chem. Soc. **77**, 4723 (1955).
[4] S. C. Lind, *The Chemical Effects of Alpha Particles and Electrons* (The Chemical Catalog Company, Inc., New York, 1928), second edition, pp. 159–160.
[5] J. L. Watson and K. Kaufmann, J. Appl. Phys. **17**, 996 (1946).
[6] J. H. L. Watson, Radiation Research **3**, 121 (1955).
[7] L. M. Dorfman and A. C. Wohl, Radiation Research **10**, 680 (1959).
[8] S. C. Lind and C. H. Shiflett, J. Am. Chem. Soc. **59**, 411 (1937).
[9] Henri, Maxwell, White, and Peterson, J. Phys. Chem. **56**, 153 (1952).
[10] Sample obtained through the courtesy of W. W. Parkinson, Oak Ridge National Laboratory.

Electron Spin Resonance Studies of the Oxygen Effect on Irradiated Polytetrafluoroethylene

TEIKICHI MATSUGASHITA* AND KENICHI SHINOHARA

Tokyo Laboratories, Japanese Association for Radiation Research on Polymers, 31, Kamifujimae, Bunkyo-ku, Tokyo, Japan

(Received October 14, 1959)

THE oxygen effect on irradiated polytetrafluoroethylene (PTFE) observed in electron spin resonance was studied by Rexroad and Gordy,[1] and other workers.[2,3] We have made a further investigation of this effect and have found some new phenomena.

The PTFE sample used was in powdered form. It was evacuated and sealed in a glass tube. The irradiation was carried out with gamma rays from a 1000 curies cobalt-60 source to a dose of 3×10^7 rads. The electron spin resonance spectra were observed at a frequency of 9400 Mc/sec.

The irradiated PTFE gave a spectrum composed of more than ten lines at room temperature (spectrum A). When air was admitted to the sample, the signal of the original PTFE radicals disappeared and an intense signal of the oxygenated radicals, which were stable in air, developed almost immediately (spectrum B). This was true also with a block sample although the change was slower than in the case of the powdered one. By reevacuation of this sample at room temperature, 11% of the signal disappeared in 15 min, and 25% in 24 hr (spectrum C). When, however, air was readmitted to the sample, the initial signal of the oxygenated radicals was immediately recovered. This disappearance and recovery of the signal were completely reversible. The intensity of the signal was found to depend on the pressure of air or oxygen.

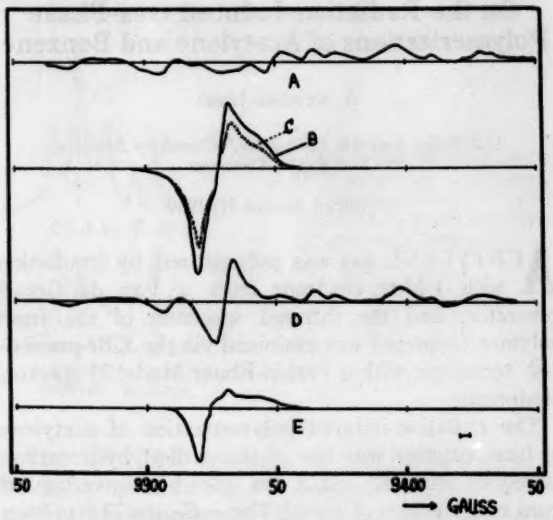

FIG. 1. Oxygen effect appearing in electron spin resonance spectra. (A) PTFE sample after irradiation in vacuo; (B) After admission of air into A; (C) After evacuation of B for 24 hr at room temperature; (D) After evacuation of B for 15 min at 150°C; (E) After evacuation of B for 15 min at 250°C followed by readmission of air.

The same experiment was repeated at high temperatures. When the oxygenated sample was evacuated for 15 min at 150°C, a larger decrease of the signal accompanied with some deformation and also with the recovery of the greater part of the signal of the original PTFE radicals was observed (spectrum D). It was likely that one component of the signal of the oxygenated radicals disappeared and another component remained after this treatment. (The former component is called, for convenience, component I and the latter, component II. With readmission of air to this sample, the signal of the oxygenated radicals was immediately recovered in complete form and this showed that the lost component I was recovered (spectrum B was recovered). This change was again found to be reversible. After evacuation of the oxygenated sample for 15 min at 250°C, a still higher temperature, the signal of the oxygenated radicals disappeared completely (both components I and II disappeared), and recovery of the signal of the original PTFE radicals was observed. However, when air was readmitted to this sample, spectrum E was obtained instead of B, showing that a large part of the component II did not recover in this case. (The signal of the oxygenated radicals in spectrum B seems to be composed of both components I and II, while that in spectrum E seems to be composed mainly of component I only.) Reevacuation of this

sample for 15 min at 250°C gave the signal of the original PTFE radicals again, but reevacuation at 150°C instead of 250°C gave a spectrum which is similar to D except that the signal of the oxygenated radicals was exceedingly weakened.

These results show that at least two kinds of radicals are formed, when air is admitted, in the irradiated PTFE. One of them liberates oxygen by evacuation at a relatively low temperature, and the other liberates at a high temperature accompanied by a rather quick decay.

* On leave from Asahi Chemical Industry Company, Ltd.

[1] H. N. Rexroad and W. Gordy, J. Chem. Phys. **30**, 399 (1959).
[2] Ohnishi, Kashiwagi, Ikeda, and Nitta, Isotopes and Radiation **1**, 210 (1958).
[3] R. J. Abraham and D. H. Whiffen, Trans. Faraday Soc. **54**, 1291 (1958).

EPR Characterization of Radicals in Irradiated Tetra-*n*-Butyl Ammonium Halides

E. J. Burrell, Jr.

Radiation Physics Laboratory, Engineering Department, E. I. du Pont de Nemours and Company, Inc., Wilmington, Delaware

(Received October 14, 1959)

In a number of compounds the electron paramagnetic resonance (EPR) spectrum of a single kind of radical is observed after irradiation of the parent compound with γ rays or high-energy electrons.[1-4] Two such compounds are presented here. Polycrystalline tetra-*n*-butyl ammonium iodide and tetra-*n*-butyl ammonium bromide were individually sealed off in tubes under 10^{-5} mm Hg vacuum. Each compound was irradiated with 2-Mev electrons from a General Electric Resonant Transformer at −80°C, warmed to 25°C, and the EPR spectrum taken immediately with a modified Varian Model V-4500 spectrometer.[5]

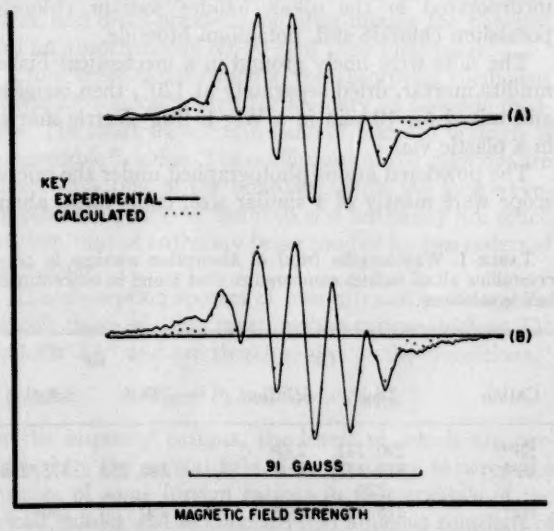

Fig. 1. First derivative of EPR absorption spectra of irradiated tetra-*n*-butyl ammonium iodide (A), and irradiated tetra-*n*-butyl ammonium bromide (B).

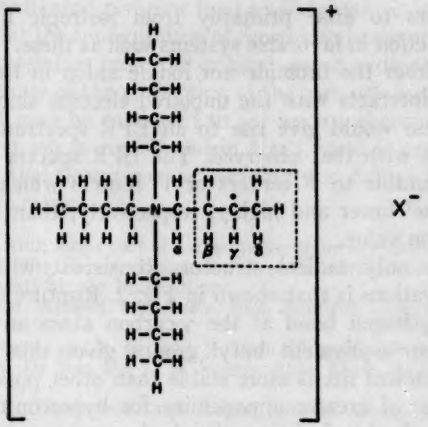

Fig. 2. Structure of the radical produced in the tetra-*n*-butyl ammonium cation. X^- is either I^- or Br^-. The dotted line encloses those hydrogen atoms which interact with the unpaired electron.

Irradiated tetra-*n*-butyl ammonium iodide gave a symmetrical, well-resolved seven-line EPR spectrum (Fig. 1). Irradiated tetra-*n*-butyl ammonium bromide showed an EPR spectrum virtually identical with that of the iodide (Fig. 1). The EPR signal of each was only slightly diminished after storage at 25°C for 24 hr. The spectroscopic splitting factor g for both irradiated compounds was found to be 2.0024 ± 0.0003, by comparison with 1,1-diphenyl-2-picrylhydrazyl. The total splitting between points of maximum slope for both compounds is about 91 gauss. The line width was found to be 10 gauss.

An IBM 650 digital computer was programed to calculate the EPR spectrum to be expected from a model which appeared to fit the experimental curve. The isotropic hyperfine peaks in the spectrum were assumed to have Gaussian line shape[6] and the relative peak heights were fixed at 1:6:15:20:15:6:1. The computer then adjusted the parameters for hyperfine splitting and the line widths of individual peaks so as to give a least squares fit between the assumed model and the experimental EPR spectrum.

For both tetra-*n*-butyl ammonium iodide and tetra-*n*-butyl ammonium bromide the calculated EPR spectrum shows a good fit to the experimental spectrum. The model is that of an unpaired electron in the environment of six equivalent hydrogen atoms. The value of $g=2.0024$ indicates very small spin-orbit coupling. Since this value of g is essentially that for a free electron ($g=2.0023$) the anisotropic environmental effects are minimized, a fact substantiated by the quantitative symmetry of each spectrum. Thus, the EPR spectrum

appears to arise primarily from isotropic hyperfine interaction in favorable systems such as these.

Neither the bromide nor iodide anion in these systems interacts with the unpaired electron since either of these would give rise to an EPR spectrum inconsistent with that observed. The EPR spectra are not attributable to F centers or V centers which show a g value[7] lower and higher, respectively, than the free electron value.

The only radical structure consistent with these observations is that shown in Fig. 2. Rupture of a carbon-hydrogen bond at the γ-carbon atom on any of the four equivalent butyl groups gives this radical. This radical site is more stable than other possibilities because of greater opportunity for hyperconjugation. Although the six interacting hydrogen atoms are not chemically equivalent, molecular orbital calculations for aliphatic radicals show that such atoms can manifest equivalent interactions with an unpaired electron.[8,9] Subsequent confirmation of this site, i.e., the carbon atom next to the end of the chain, was provided by the EPR spectrum of irradiated tetra-*n*-propylammonium bromide, $(C_3H_7)_4N^+Br^-$, which is essentially identical with the spectra of the butyl compounds.

The work of R. G. Bennett and D. W. Marquardt in setting up the computer program is gratefully acknowledged.

[1] W. Gordy and C. G. McCormick, J. Am. Chem. Soc. **78**, 3243 (1956); C. F. Luck and W. Gordy, J. Am. Chem. Soc. **78**, 3240 (1956).
[2] B. Smaller and M. S. Matheson, J. Chem. Phys. **28**, 1169 (1958).
[3] R. H. Luebbe and J. E. Willard, J. Am. Chem. Soc. **81**, 761 (1959).
[4] Bennett, McCarthy, Nolin, and Zimmerman, J. Chem. Phys. **29**, 249 (1958).
[5] Bennett, Hoell, and Schwenker, Rev. Sci. Instr. **29**, 659 (1958).
[6] D. J. E. Ingram, *Free Radicals as Studied by Electron Spin Resonance* (Academic Press, Inc., New York, 1958), p. 127.
[7] A. H. Kahn and C. Kittel, Phys. Rev. **89**, 315 (1953).
[8] D. B. Chestnut, J. Chem. Phys. **29**, 43 (1958).
[9] A. D. McLachlan, Mol. Phys. **1**, 233 (1958).

Absorption Spectra of Mercury, Bismuth, and Antimony Halides in Pressed Alkali Halide Disks

ABRAHAM GLASNER AND RENATA REISFELD*

Department of Inorganic and Analytical Chemistry, The Hebrew University, Jerusalem, Israel

(Received July 17, 1959)

IN previous publications[1,2] it has been shown that when pressed disks of potassium chloride to which thallium or lead chloride has been added are heated, they develop absorption spectra identical with those of unit crystals prepared from the melt, and it has been suggested that this phenomenon be utilized in the evaluation of diffusion constants in solids. On continuing these investigations, it was observed that a number of metal halides yield fully developed absorption spectra on being mixed with the alkali halide at room temperature.

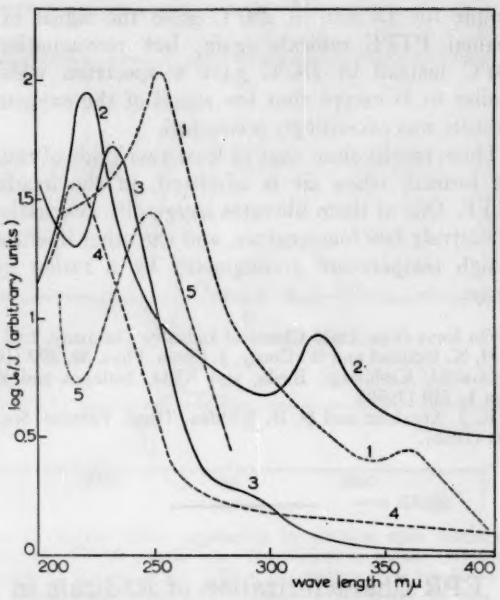

FIG. 1. Absorption spectra of polycrystalline alkali halide disks containing heavy cations. (1) KBr:$BiCl_3$ 0.049%, (2) KCl:$BiCl_3$ 0.08%, (3) KCl:$SbCl_3$ 0.14%, (4) KCl:$HgCl_2$ 0.018%, (5) KBr:$HgBr_2$ 0.042%.

Measurements on the spectra of three such cations are reported here, namely, mercuric chloride and bromide, antimonous chloride, and bismuth chloride, incorporated in the alkali halides sodium chloride, potassium chloride and, potassium bromide.

The salts were finely ground in a mechanical Fisher mullite mortar, dried separately at 120°, then weighed and mixed for 10 min in a Wig-L-Bug electric mortar in a plastic vial.

The powdered grains photographed under the microscope were mostly of a similar size, cubic form, about

TABLE I. Wavelengths (mμ) of absorption maxima in polycrystalline alkali halides compared to that found in concentrated halide solutions.

	Cl^-		Br^-	
Cation	Disk	Solution	Disk	Solution
Sb^{3+}	290, 231	230[a]		
Bi^{3+}	319–323, 220	327[b]	360, 255	375, 258[b]
Hg^{++}	215	230[b]	250	250[b]

[a] Reference 3.
[b] Reference 4.

20 μ on the edge. The concentration of the heavy metal salt in the alkali halide mixtures varied between 0.005–0.1% by weight. For pressing, a Hilger die ($\frac{1}{2}$-in. diam.) was used, and pressures of about 9 and 14 tons/cm^2 were applied on the potassium and sodium salts, respectively. The disks obtained were clear and transparent; the pure alkali halide disks transmitted more than 70% of light in the near ultraviolet and somewhat less at shorter wavelengths. The spectra were measured with a Beckman DU Spectrophotometer.

Figure 1 shows a few of the spectra obtained, and in Table I the position of the peaks of absorption are compared with those recorded in the literature[3,4] for concentrated halide solutions of the respective ions. In most cases the absorption bands seem to coincide in the two media, but there is sometimes a shift to shorter wavelengths in the polycrystalline disks. With bismuth and antimony two absorption bands were observed. To our knowledge, none of these spectra have previously been recorded in solid solutions. The cation of the alkali halide had only a slight influence on the position of the absorption bands, but on changing from chloride to bromide, an appreciable shift to longer wavelengths is observed.

It should be emphasized that unless diffusion and substitution has taken place, none of the heavy metal ions exhibit their characteristic spectra. This statement is confirmed by the observation that chlorides of a cation in potassium bromide have spectra characteristic for a bromide. It is therefore concluded that diffusion has actually taken place at room temperature. This remarkable fact is thought to be connected with the volatility and softness of the heavy metal halides.

The absorbancy of potassium bromide disks containing 0.005–0.02% mercuric chloride obeyed Beer's Law. As a rule, maximum absorption was obtained only a few days after the preparation of the powdered mixtures, and disks pressed soon after mixing the powders had an absorbance of 80–90% of their final value.

From these measurements, the absorption coefficient 1.35×10^5 was calculated for mercury in bromide medium. The short wavelength band of bismuth bromide is comparable in value. The coefficients of the chlorides are about 75% that of the bromides, while the long wavelength absorptions of bismuth and antimony are much weaker, that of antimony being smaller by two orders of magnitude.

The absorption spectra of bismuth and antimony resemble those of other mercury-like cations such as Tl^+ and Pb^{++} [5–7] and are therefore due to the transitions,

$$^1S_0 \rightarrow {}^1P_1 \text{ and } {}^1S_0 \rightarrow {}^3P_{0,1,2},$$

in the impurity cations, the levels of which are perturbed by the crystal field. The similarity between the spectra of some foreign cations in unit crystals of the alkali halides and in concentrated aqueous solutions of these halides has been noted long ago.[8,9] But this similarity cannot be considered as proof for the presence of a four coordinated complex in the solid state; it is more likely that the configuration of the anions in the strained lattice resembles more the original sexa coordination.

The cause of the absorption of the mercuric ion is less clear. It may be compared to the known absorption of the silver ion in AgCl[10] and in NaCl,[11] and is probably due to the transitions $5d^{10} \rightarrow 5d^9 6p$ (or $5d^9 6s$) in the mercuric cation.

* This work forms part of a dissertation to be submitted to the Senate of the Hebrew University in partial fulfillment of the requirements for the Ph.D. degree.

[1] Glasner, Reisfeld, and Adam, Bull. Research Council Israel **5A**, 219 (1956).
[2] A. Glasner and R. Reisfeld, J. Chem. Phys. **25**, 381–2 (1956).
[3] M. A. De Sesa and L. B. Rogers, Anal. Chim. Acta **6**, 534 (1952).
[4] Merrit, Hershenson, and Rogers, Analyt. Chem. **25**, 572 (1953).
[5] F. Seitz, J. Chem. Phys. **6**, 150 (1938).
[6] P. D. Johnson and F. E. Williams, J. Chem. Phys. **20**, 124 (1952); F. E. Williams, *ibid.* **19**, 457 (1951).
[7] Ch. B. Lushchik and N. E. Lushchik, Izvest. Akad. Nauk. S.S.S.R., Ser. Fiz. **22**, 1351–5 (1958).
[8] R. Hilsch, Proc. Phys. Soc. (London) **49**, 40 (1937); H. Fromherz, Z. Phys. **68**, 233–43 (1931).
[9] P. Pringsheim, Revs. Modern Phys. **14**, 132 (1942).
[10] F. Seitz, Revs. Modern Phys. **23**, 328 (1951).
[11] M. L. Kats, Optica i Spectroskopija **3**, 602–9 (1957).

Use of Constant-Boiling Systems in Calibration of Mass Spectrometers and Other Molecular Beam Instruments

ALAN W. SEARCY,* *Department of Mineral Technology, University of California, Berkeley, California*

WENDELL S. WILLIAMS, *Research Laboratory, National Carbon Company, Division of Union Carbide Corporation, Parma, Ohio*

AND

PAUL O. SCHISSEL, *Parma Research Laboratory, Union Carbide Corporation, Parma, Ohio*

(Received October 22, 1959)

IN measurements of lifetimes for excited particle states or of cross sections for reactions in a molecular beam, the concentrations of the vapor species must be known. Relative concentrations of fluxes are known immediately for vaporization from constant-boiling compounds. For such compounds at equilibrium, the flux ratio of component vapor species is the same as the composition ratio for these species in the condensed phase. If vaporization occurs by dissociation to two major gas species, only the formulas of these species and the composition of the constant-boiling compound need be determined in order to fix the flux ratio of these gas species.

Suppose, for example, that a solid is evaporated by the reaction $Q_aR_{cd}(s) = aQ_b(g) + cR_d(g)$, where Q and R are the components, a and c are the number of moles of gas produced, and b and d are the number of

atoms per gas molecule. If Q_aR_{cd} is a constant-boiling phase, for equilibrium vaporization in the molecular-flow range of pressures,

$$a/c=f_{Q_b}/f_{R_d}=\alpha_{Q_b}f^\circ_{Q_b}/\alpha_{R_d}f^\circ_{R_d}=\alpha_{Q_b}P_{Q_b}M_{R_d}^{\frac{1}{2}}/\alpha_{R_d}P_{R_d}M_{Q_b}^{\frac{1}{2}}, \quad (1)$$

where the f's are the evaporated components of the fluxes leaving a surface at equilibrium, the α's are evaporation coefficients, the f°'s are the fluxes striking the surface from the equilibrium vapor, the P's are equilibrium pressures, and the M's are molecular weights.

In most cases $\alpha_{Q_b}\cong\alpha_{R_d}$ so free surface evaporation will yield the flux ratio $f^\circ_{Q_b}/f^\circ_{R_d}=f_{Q_b}/f_{R_d}=a/c$. Thus the flux ratio and hence the composition of the solid will be the same as at equilibrium. However, if, as occasionally is found,[1] α_{Q_b} and α_{R_d} differ by orders of magnitude, all the terms in Eq. (1) (except the molecular weights) will change on going to the free surface experiment. The resulting difference in loss rate of the two components will shift the composition of the solid with corresponding changes in the pressures. Since the rate of change of pressure with composition is usually large for the small composition range called a compound, the foregoing pressure ratio can take on a new value such that the flux ratio from the surface is a'/c' where the primes refer to the slightly adjusted composition of the solid. But $a'/c'\cong a/c$ because of the small composition range of the compound, and experimentally the distinction is unimportant. With the foregoing qualifications, the flux ratio from a constant-boiling compound is essentially independent of whether the evaporation is equilibrium or free-surface. The constant-boiling composition is restricted to the narrow composition range for wide variations in temperature or pressure.

A simple rule for prediction of the existence of constant-boiling phases can be stated if the small effect of molecular weights is neglected: a phase for which the vapor pressure curves cross will generally contain a constant-boiling composition. A necessary thermodynamic condition is that the free energy of formation of a phase per mole of Q_b (the more volatile gas component) when subtracted from the free energy of formation of Q_b gas yields a number more positive than the free energy of formation of R_d gas.

A wide variety of constant-boiling compounds are available for study. Calcium, for example, should form constant-boiling compounds with zinc, tin, aluminum, cadmium, the oxygen family, the nitrogen family, and the halides.

For each of these compounds, except the calcium halides, vaporization can be expected to take place largely by dissociation. The presence of some molecules of the same formula as the condensed phase will not interfere with use of the method provided that species that vaporize by dissociation can be distinguished from fragments produced in the beam. Mixtures of component species such as S_2 and S particles require an independent equation for complete definition of the system.

The basic idea presented here was applied by two of us in a mass spectrometer analysis of the titanium-boron system.[2] Chupka *et al.* independently recognized the applicability of the method and used it in a study of the vaporization of BeO.[3]

Titanium diboride, because of the simplicity of its vapor species, provides a good illustration of the use of the constant-boiling property in obtaining relative atomic cross sections for ionization by electron impact. In the mass spectrometer, a Langmuir free surface was approximated by using an open TiB_2 cell in a tungsten jacket. Ions were formed using 40-ev electrons. Only Ti^+ and B^+ were observed. As expected, no significant temperature variation in the ratio was found, while I_{Ti} and I_B each changed by two orders of magnitude.

The observed intensity ratio can be used to compute relative ionization cross sections for atomic Ti and B providing the detector response is known. The mass spectrometer used employs an electron multiplier detector, whose response for ions in the kev range is approximately inversely proportional to the square root of the mass, but this term is canceled by a term from the equation relating flux to pressure. Hence, $\sigma_{Ti}/\sigma_B=I_{Ti}/I_B\times f_B/f_{Ti}$, where σ=cross section for ionization, I=measured intensity, and f=flux of atoms from the TiB_2 surface. The flux ratio for the constant-boiling compound TiB_2 equals 2. The average observed intensity ratio is 3.8 with an estimated uncertainty of $\pm 20\%$. Hence, the cross-section ratio according to Eq. (1) is 7.6 ± 1.5. The value obtained from the calculations of Otvos and Stevenson[4] is 7.3.

* Consultant to Parma Research Center, Union Carbide Corporation.

[1] Soulen, Sthapitanonda, and Margrave, J. Phys. Chem. **59**, 132 (1955).

[2] P. O. Schissel and W. S. Williams, Bull. Am. Phys. Soc. Ser. II, **4**, No. 3 (1959).

[3] Chupka, Berkowitz, and Giese, J. Chem. Phys. **30**, 827 (1959).

[4] J. W. Otvos and D. P. Stevenson, J. Am. Chem. Soc. **78**, 546 (1956).